

**GENERATION OF HIGHLY ELECTROPHILIC CATIONIC BORON  
COMPLEXES AND THEIR APPLICATION TOWARD FORMATION OF C–B  
BONDS**

by

Aleksandrs Prokofjevs

A dissertation submitted in partial fulfillment  
of the requirements for the degree of  
Doctor of Philosophy  
(Chemistry)  
in the University of Michigan  
2013

Doctoral Committee:

Professor Edwin Vedejs, Chair  
Professor Adam Matzger  
Professor John Montgomery  
Professor Robert Zand

© Aleksandrs Prokofjevs  
2013

## **Acknowledgements**

During my time here at the University of Michigan, I've had the honor of working with highly influential and inspiring mentors, students, and peers.

My utmost gratitude goes to my advisor, Professor Edwin Vedejs. Not only has his intellectual guidance and creativity been a driving force for this research, but also for my professional development. As a mentor, Ed has helped me grow as a researcher, an educator, and a person. The accomplishments of those who have had the privilege of working with him are a testimony to his commitment to the success of others. His dedication to science and loyalty to students have, and always will continue to inspire me.

Special thanks go to the members of my graduate committee, Professors Adam Matzger, John Montgomery and Robert Zand for helping me develop this thesis. I'm also indebted to the many professors here at the university that have taught me over the years. Additionally, Professor Dennis Curran from the University of Pittsburgh and his research group are acknowledged for helping to expand the scope of the project.

This research would not have been possible without the early work by Timothy DeVries. Furthermore, the support from the entire Vedejs group is deeply appreciated, especially Naresh, Clement, Janis, Bob, John, Val, Susan, Jiten, Andy and Effie.

Finally, I'm tremendously grateful for the continuous encouragement and care from my family and friends. Without them I could never have accomplished what I have today. Most importantly, I would like to thank my mom, my grandparents, my sister and my wife Alina for the strength and courage they have provided me with.

## Table of Contents

<b>Acknowledgements</b>	ii
<b>List of Figures</b>	v
<b>List of Schemes</b>	vi
<b>List of Tables</b>	vii
<b>List of Appendices</b>	viii
<b>Abstract</b>	ix
<b>Chapter 1. Toward Generation of Primary Borenium Ions</b>	1
Introduction—Boron Cation Overview	1
Electrophilic Activation of Lewis Base Borane Complexes	8
Reactions of L–BH <sub>3</sub> with Electrophiles Possessing Moderately Coordinating Counterions	9
Reactions of L–BH <sub>3</sub> with Electrophiles Possessing Weakly Coordinating Counterions	13
Experimental Evaluation of Borenium Lewis Acidity	27
Computational Studies on Lewis Acidity of Borenium Ions	30
Computational Details and Method Validation	32
Computational Evaluation of Borenium Lewis Acidity	36
Calculation of <sup>11</sup> B NMR Chemical Shifts of Cationic Boron Species	42
Summary	42
Experimental	44
Chapter 1 Bibliography	63

<b>Chapter 2. Electrophilic Borylation and Related Reactions of B–H Borenium Cations</b>	68
Introduction—C–H Borylation by Electrophilic Boron Complexes	68
Electrophilic Borylations Using Stoichiometric Electrophiles	69
Electrophilic Borylations Using Catalytic Electrophiles	78
Lewis Base Borane Complex Reactions with B(C <sub>6</sub> F <sub>5</sub> ) <sub>3</sub>	93
Hydroboration of Alkenes with Activated Lewis Base Borane Complexes	94
Summary	99
Experimental	100
Chapter 2 Bibliography	118
<b>Chapter 3. Borenium and Boronium Salts Derived from 9–BBN and Their Application toward Electrophilic Aromatic Borylation</b>	122
Introduction	122
Electrophilic Aromatic Borylation of Electron-Rich Arenes and Heteroarenes	123
Summary	134
Experimental	135
Chapter 3 Bibliography	145
<b>Appendices</b>	148

## List of Figures

Figure

1-1. Major boron cation classes	2
1-2. X-Ray structure of <b>24a</b> (cation only, 50% probability ellipsoids)	17
1-3. X-Ray structure of <b>37e</b> (dication only, 50% probability ellipsoids)	21
2-1. X-Ray structure of <b>4</b> (cation only, 50% probability ellipsoids)	75
2-2. Mechanistic Alternatives for the Catalytic C–H Borylation	91
3-1. X-Ray structure of <b>13</b> (cation only, 50% probability ellipsoids)	128
3-2. X-Ray structure of <b>23a</b> (50% probability ellipsoids)	133

## List of Schemes

### Scheme

1-1. Proposed Mechanism for the Electrophilic Ph <sub>3</sub> CH Degradation in CH <sub>2</sub> Cl <sub>2</sub>	15
1-2. Electrophilic activation of H-bridged borocations	26
2-1. The Stoichiometric Aromatic Borylation	69
2-2. Substrate Scope of the Stoichiometric Borylation	71
2-3. Stoichiometric Aliphatic Borylation	76
2-4. Stoichiometric Trityl Activation of <b>26</b>	78
2-5. Substrate Scope of the Catalytic Aromatic Borylation	82
2-6. Substrate Scope of the Catalytic Aliphatic Borylation	84
2-7. The Catalytic Borylation Mechanism. An Early Proposal	86
2-8. The Catalytic Borylation Mechanism Involving B–H Insertion	92
3-1. Formation of Boronium <b>13</b>	126
3-2. Generation of Borenium Salts from <b>6</b>	129

## List of Tables

### Table

1-1. $^{11}\text{B}$ and $^{19}\text{F}$ NMR Data for $\text{R}_3\text{N}-\text{BH}_2\text{NTf}_2$ Complexes <b>17</b> and <b>18</b>	11
1-2. Reaction Enthalpies Calculated Using W1BD and M06-2X Methods	35
1-3. Experimental and Calculated Dissociation Enthalpies of Amine Boranes	36
1-4. Calculated Borenium Geometries and $\text{NH}_3$ Affinities	40
2-1. Synthesis of $\text{C}_6\text{F}_5\text{BH}_2$ Complexes	94
2-2. Alkene Hydroboration Using Activated <b>82</b>	97
3-1. Borylation of Nitrogen Heterocycles Using <b>13</b>	131



## **List of Appendices**

### Appendix

A. X-ray Crystal Structures	148
B. Selected NMR Spectra	180

## Abstract

The focus of our research was to achieve better understanding of the processes underlining the chemistry of highly electrophilic boron cations, and to develop the applications of such cations to C–B bond formation. The reactions of Lewis base borane complexes with potent electrophiles such as the trityl cation, bistriflimide and tris(pentafluorophenyl)borane were explored, and the product structures were assigned based on the X-ray crystallographic and spectroscopic data. Hydride abstraction from Lewis base borane complexes by trityl cation was shown to be a viable method for generation of unstabilized primary borenium species, and several such  $L-BH_2^+$  cations were shown to exist in the condensed phase in the form of diborane(6)-type dicationic dimers. We also explored the aliphatic and aromatic borylation chemistry involving B–H borocations, and developed a procedure for the intramolecular C–H borylation of amine boranes that uses only a catalytic amount of a strong electrophile, and produces  $H_2$  gas as the sole byproduct.

Additionally, the methodology for generation of more substituted unstabilized borocations derived from 9-BBN was developed, and subsequently applied to the borylation of electron-rich heteroaromatic compounds. An unusually hindered boronium cation possessing a 9-BBN cage chelated by 1,8-bis(dimethylamino)naphthalene was structurally characterized and shown to be a potent borylating reagent.

## Chapter 1

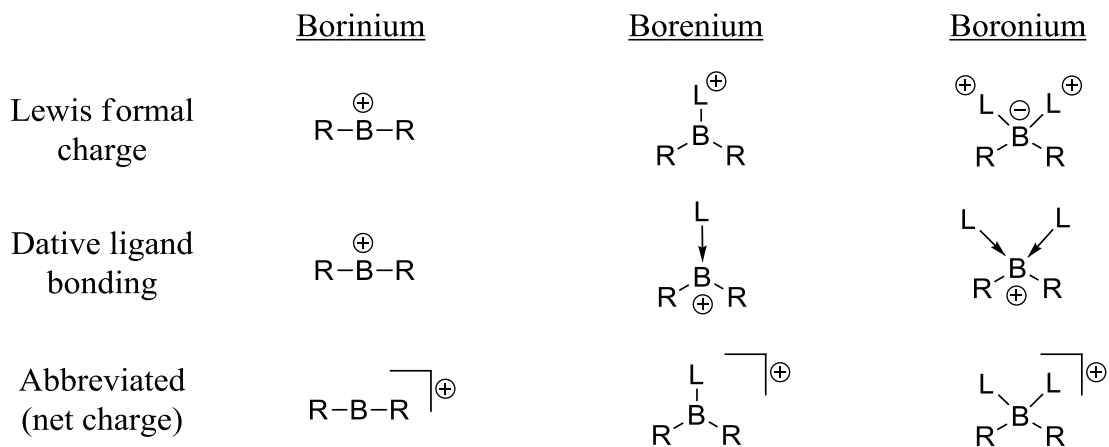
### Toward Generation of Primary Borenium Ions

#### Introduction—Boron Cation Overview

Cationic boron complexes have been known since 1906, when Diltthey *et al.* reported formation of salt-like boron compounds such as  $[(\text{acac})_2\text{B}]^+ [\text{FeCl}_4]^-$  (acac = 2,4-pentanedionate) upon treatment of 1,3-diketones with  $\text{BCl}_3$  followed by anion exchange.<sup>1</sup> The range of cationic boron species produced in the following 100 years is remarkable. Both extremely robust species surviving reflux in aqueous acids and transient cations existing only in the gas phase have been reported. In general, reactivity of boron compounds is influenced by the coordination number of the boron atom, its Lewis acidity, and both steric and electronic properties of the substituents. The same considerations apply to cationic boron complexes, with the coordination number arguably being the most important factor determining borocation reactivity. As proposed by Nöth, boron cations can be divided into three major groups based on their coordination number (Figure 1-1).<sup>2</sup>

This simple division scheme allows making some generalizations regarding the reactivity of boron cations, although it is important to keep in mind that no distinction is made about B–L and B–R bond orders and population of the formally vacant *p*-orbitals at boron. Thus, for a group of structurally related species, dicoordinate (borinium) cations can be expected to have higher reactivity toward external Lewis bases than the

**Figure 1-1.** Major boron cation classes<sup>a</sup>

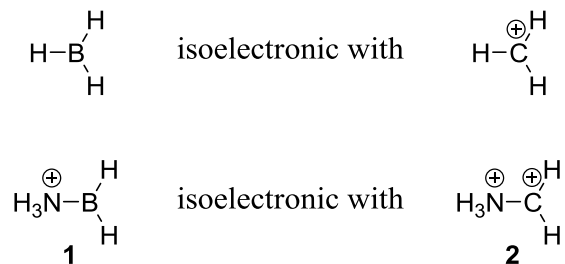


<sup>a</sup>L = neutral Lewis base ligand

corresponding tricoordinate (borenium) species. Tetracoordinate (boronium) cations, in turn, can be expected to have the lowest reactivity due to the absence of empty *p*-orbitals at boron. Also, the borinium-borenium-boronium nomenclature conveniently parallels the trends observed in the <sup>11</sup>B NMR chemical shifts of borocations, due to the substantial dependence of chemical shifts on the coordination number at boron, a topic that will be discussed later.

Figure 1-1 also serves to illustrate some shortcomings of the traditional Lewis structure drawings when applied to boron cations. Despite the absence of a formal positive charge at boron in Lewis structures, the reactivity of these compounds is best understood by assuming that the net positive charge of the cation mostly resides at the boron atom. In view of this, and also of the fact that multicenter bonds frequently encountered in boron compounds cannot be properly described by Lewis structures, both Lewis and abbreviated (net charge) structures will be used interchangeably throughout the text.

Some general understanding of the reactivity of boron cations can be gained from their isoelectronic relationship with carbenium ions. Thus, assuming that  $\text{BH}_3$  is isoelectronic with  $\text{CH}_3^+$ , primary borinium cation **1** can be considered to be isoelectronic with dication **2**. It is this isoelectronic relationship that allows classifying borinium cations as gtonic superelectrophiles according to Olah's terminology.<sup>3</sup>

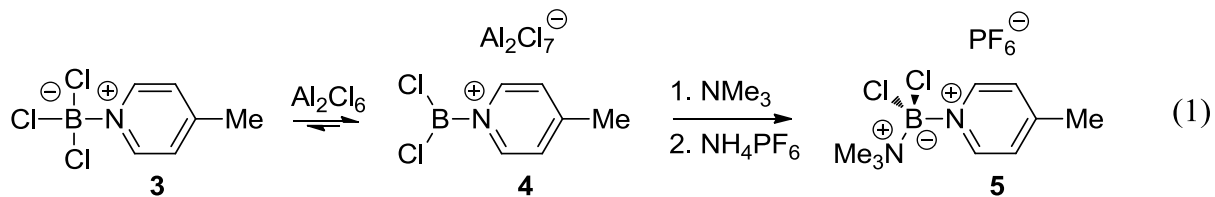


As with the isoelectronic carbenium counterparts, borinium and borinium structures are most easily accessible in those structural environments that allow efficient population of the *p*-orbital on the boron atom. Similarly to the widely encountered iminium and oxocarbenium structures in carbocation series, the vast majority of known borinium and borinium ions are stabilized by adjacent N and O atom lone pairs. Unstabilized borinium and borinium structures are exceedingly rare, however. Thus, the extremely reactive non-stabilized dicoordinate borinium cations have been generated exclusively in the gas phase,<sup>4</sup> while convincing evidence for the existence of non-stabilized tricoordinate borinium ions in the condensed phase was reported only very recently (Chapters 2, 3).<sup>5</sup>

Tricoordinate borinium cations hold the most promise for synthetic applications. This is due to their intermediate position between the rather unreactive tetracoordinate borinium species and the violently reactive dicoordinate borinium cations. Since the area of cationic boron complexes has been reviewed extensively,<sup>2,6</sup> we will only focus on

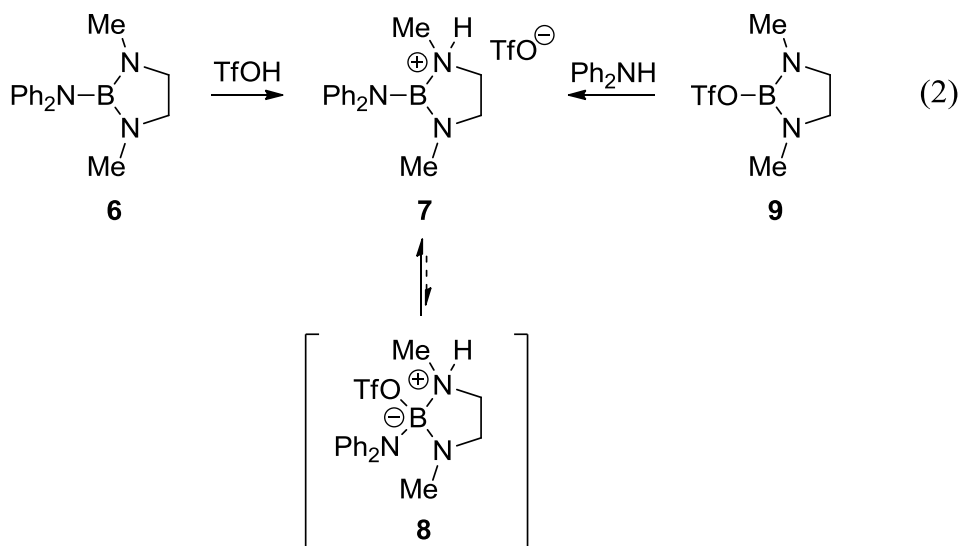
some of the major methods used for borenium generation, as well as selected synthetic applications.

Even though the first tricoordinate borenium species might have been encountered as early as in 1933,<sup>7</sup> it was not until the advent of <sup>11</sup>B NMR spectroscopy that their existence was unambiguously established. In 1970 Ryschkewitsch *et al.* reported formation of tricoordinate borenium ion **4** upon chloride abstraction from 4-picoline BCl<sub>3</sub> complex **3** (eq 1).<sup>8</sup> The tricoordinate nature of cation **4** was deduced from the prominent change in the <sup>11</sup>B chemical shift upon reaction of **3** with Al<sub>2</sub>Cl<sub>6</sub> (**3**, δ <sup>11</sup>B +8 ppm; **4**, δ <sup>11</sup>B +47 ppm). The chemical shift difference between tricoordinate salt **4** and tetracoordinate precursor **3** (39 ppm difference) illustrates the usefulness of <sup>11</sup>B NMR spectroscopy for determining the number of ligands at boron. Generally, tetracoordinate boron species give rise to signals anywhere between +20 and -60 ppm, while tricoordinate boron peaks are typically observed between +100 to +10 ppm.<sup>9</sup> The same study by Ryschkewitsch *et al.* also proved the existence of an equilibrium between **3** + Al<sub>2</sub>Cl<sub>6</sub> and **4** (*K*<sub>eq</sub> ≈ 20), confirming that tricoordinate cation **4** does not form by a spontaneous dissociation of **3**, but rather by interaction of **3** with a strong halophile. This equilibrium also suggests that **4** is a sufficiently strong halophile to partially compete for Cl<sup>-</sup> with strongly Lewis acidic Al<sub>2</sub>Cl<sub>6</sub>. Further support for the Lewis acidity of **4** comes from its reactivity with added Lewis bases, such as NMe<sub>3</sub> (eq 1) and Cl<sup>-</sup>.



Overall, formation of **4** from **3** represents a widely used approach for borenium generation, namely abstraction of an anionic fragment (in this case  $\text{Cl}^-$ ) from a tetracoordinate boron complex by a strong Lewis acid. Aside from halide abstraction by a halophile (eq 1), other variations of this general approach are known, such as hydride abstraction by a “hydridophile”, which is the focus of the following parts of this chapter.

Protonation of tricoordinate boron species possessing basic ligands at boron is the other commonly used approach for accessing borenium ions. This method is especially efficient for generation of tricoordinate boron cations from aminoboranes  $\text{R}_2\text{B}-\text{NR}'_2$ . In 1984 Narula and Nöth reported what might be the first convincing evidence for the formation of *n*-stabilized borenium structures upon protonation of aminoboranes (eq 2),<sup>10</sup> although such processes have been considered previously.<sup>11</sup> Despite the diminished basicity of the nitrogen lone pairs due to  $\pi$ -delocalization, protonation of diazaborolidine **6** with TfOH proceeds smoothly yielding borenium triflate **7**.



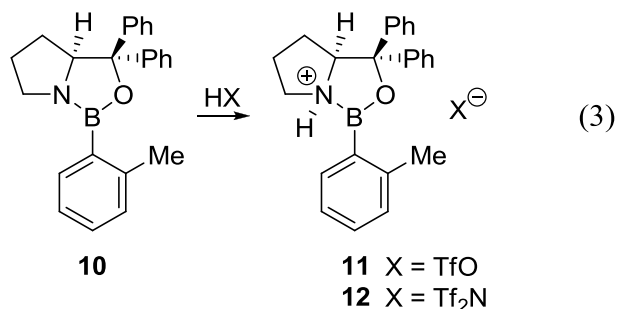
Several factors account for the existence of salt **7** in the tricoordinate borenium form as opposed to the tetracoordinate covalent adduct **8**. While the stability of the tricoordinate form is partially determined by the low coordinating ability of the triflate

anion, this by itself might not be sufficient to prevent formation of the covalent adduct. In fact, even the much less coordinating  $\text{Tf}_2\text{N}^-$  anion has been shown to form covalent adducts with tricoordinate boron cations in some circumstances (*vide infra*). The other factor determining the stability of the tricoordinate form of **7** is the population of the *p*-orbital on boron by the lone pair of the adjacent nitrogen atom. This iminium-type stabilization decreases Lewis acidity of the boron atom, thus preventing interaction with the weakly basic  $\text{TfO}^-$  anion.

An undisputable proof of the tricoordinate nature of borenium **7** in the solid state was obtained by a single crystal X-ray diffraction study.<sup>10</sup> To produce suitable quality crystals, salt **7** was prepared by an independent route starting from boron triflate **9** and diphenylamine (eq 2). The process apparently involves complexation of the amine to the Lewis acidic boron center, followed by the loss of triflate and a proton transfer. This nucleophilic addition–heterolysis approach represents another common method used to access borenium species, and will be discussed in more detail in Chapter 3.

Despite the long history of cationic boron compounds, they have seen relatively few synthetic applications. Arguably, the most widely known boreniums are the cationic oxazaborolidine catalysts developed by Corey *et al.*<sup>12</sup> The inherent Lewis acidity of the borenium unit constrained by the asymmetric prolinol backbone makes protonated oxazaborolidines a highly efficient class of chiral Lewis acids. A typical oxazaborolidine borenium preparation route involves protonation of the commercially available neutral aminoborane **10** with strong protic acids such as  $\text{TfOH}$  or  $\text{Tf}_2\text{NH}$  (eq 3).<sup>13</sup>





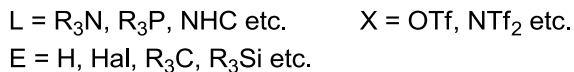
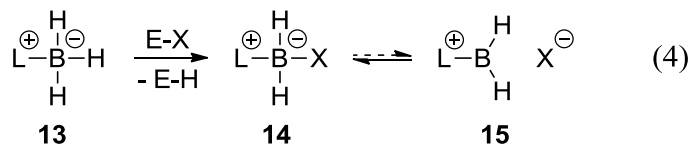
In view of the utility of ionic oxazaborolidine catalysts, it is surprising that little data is available to convincingly establish the degree of coordination around the B atom in protonated oxazaborolidines in solution. No <sup>11</sup>B NMR data has been reported, and the less informative <sup>1</sup>H NMR evidence suggests that salt **11** apparently exists in equilibrium with the corresponding covalent triflate adduct (*cf.* equilibrium between **7** and **8**). In general, the equilibria between tricoordinate boreniums and their corresponding neutral tetracoordinate counterion adducts are substantially affected by borenium structure and counterion coordinating ability, as well as smaller factors such as the solvent effect.

One of the major goals of our research is to develop boron reagents that are sufficiently electrophilic to interact with unactivated C–H bonds in both aromatic and aliphatic environments. Logical steps toward reaching this degree of electrophilicity in boron cations are to increase the Lewis acidity of the empty orbital at boron, and to decrease the coordinating ability of both the counterion and the solvent. The subsequent parts of this chapter will focus on preparation and properties of some of the most electrophilic boron species accessible in the condensed phase, while the following chapters mostly deal with applications of such species toward C–H bond functionalization.

## Electrophilic Activation of Lewis Base Borane Complexes

Development of highly electrophilic cationic boron reagents capable of interacting with weakly basic  $\sigma$ - and  $\pi$ -bonds crucially relies on the availability of tools and methods that could be used to regulate Lewis acidity of the boron atom. The coordinating properties of the medium in which such cations are generated must also be controlled tightly to ensure that the solvent and the counterion don't bind to the boron electrophile irreversibly. In our attempts to generate highly reactive borenium species we focused our attention on cations possessing exclusively  $\sigma$ -donor substituents at boron. In the absence of  $n$ - and  $\pi$ -donor ligands, hyperconjugation is expected to be the only substantial contributor of electron density to the vacant  $p$ -orbital at B. Because of this, the electron population of the  $p$ -orbital is expected to be noticeably lower than in the previously reported borenium salts. The degree of borenium stabilization can further be reduced by introducing H substituents at boron, thereby limiting the number of groups available for participation in hyperconjugative interactions. The subsequent sections of this chapter summarize our efforts toward the preparation of some of the least stabilized borenium species imaginable.

Lewis base borane complexes are well known to react with electrophiles.<sup>14</sup> In this process the starting borane complex **13** formally acts as a hydride source, while the electrophile acts as a “hydridophile” (eq 4). The choice of electrophile is virtually unlimited, given that the electrophile is sufficiently strong to make the process thermodynamically favorable.



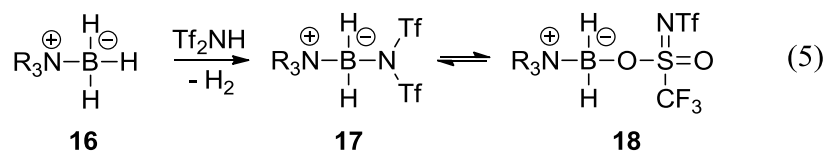
Depending on the leaving group ability and coordinating properties of X, the resulting B–X bond in complex **14** can be expected to have a variable degree of covalent character. In principle, in the case of a sufficiently weakly-coordinating X<sup>−</sup>, complex **14** can be reasonably expected to exist in the borenium form **15**, making the reaction between L–BH<sub>3</sub> and E–X a viable pathway for non-stabilized borenium generation. The exact position of the borderline between **14** and **15** was not known at the time this research project was initiated, however.

#### *Reactions of L–BH<sub>3</sub> with Electrophiles Possessing Moderately Coordinating Counterions*

Probably, the most desirable electrophiles for Lewis base borane complex activation are protic acids, since the only other product (E–H, eq 4) generated besides the desired **14** or **15** would be H<sub>2</sub> gas. Early attempts to use strong acids TfOH and Tf<sub>2</sub>NH (bistriflimide) in Et<sub>3</sub>N–BH<sub>3</sub> activations performed by Timothy DeVries led to the conclusion that tetravalent boron adducts **14** (L = Et<sub>3</sub>N, X = OTf and NTf<sub>2</sub>) are formed as dominant products.<sup>15</sup> No other structural features of these adducts besides coordination number at boron have been established, however. Further clarification of these features was the starting point for the studies presented below.

Treatment of a range of amine borane complexes **16** with 1 equiv of Tf<sub>2</sub>NH in CD<sub>2</sub>Cl<sub>2</sub>, *d*<sub>8</sub>-PhMe or *d*<sub>5</sub>-PhBr generally produced mixtures of two isomeric species (eq 5, Table 1-1). The reaction proceeded vigorously, and gas liberation ceased within seconds

at rt, indicating complete consumption of Tf<sub>2</sub>NH. The products were identified as N- and O-bound covalent boron bistriflimides **17** and **18** based on multinuclear NMR spectroscopy. Thus, both species could be reliably assigned as tetracoordinate boron complexes based on <sup>11</sup>B NMR data. From <sup>19</sup>F and <sup>13</sup>C NMR data it is also apparent that in one of the isomers both CF<sub>3</sub> groups are magnetically equivalent, as expected in the N-bound isomer **17**, but they are distinctly different in the O-bound isomer **18**. Bistriflimide connectivity isomerism has previously not been observed in boron compounds (very few boron sulfonylimides have been reported so far<sup>16</sup>), although it is a known phenomenon in Si bistriflimides.<sup>17</sup>

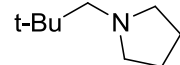


In most cases the ratio of **17** to **18** measured immediately following mixing **16** and Tf<sub>2</sub>NH was different from that observed after a few hours at room temperature, suggesting a kinetic preference for the formation of one of the isomers. Such kinetic product mixtures initially contained larger amounts of the O-bound isomer **18**, some of which gradually turned into **17** over time. Activation of Me<sub>3</sub>N–BH<sub>3</sub> (**16a**) with Tf<sub>2</sub>NH in *d*<sub>8</sub>-PhMe serves as a representative example where equilibration to the thermodynamic product ratio was observed to be particularly slow (hours at rt). To avoid discrepancies caused by slow kinetics, ratios of N- vs. O-bound products (**17** vs. **18**) summarized in Table 1-1 were confirmed to remain unchanged for days following the initial equilibration period. Product ratio (**17** vs. **18**) measured at equilibrium correlates reasonably well with steric properties of the amine fragment. Thus, while **17** is the thermodynamically preferred isomer in the relatively unhindered Me<sub>3</sub>N series (7:1

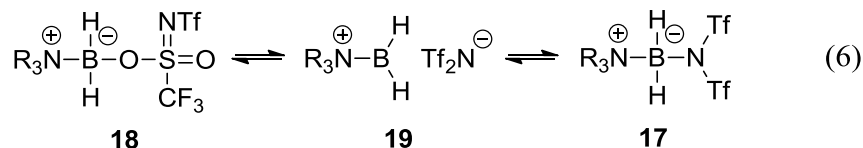
**17a:18a**), the O-bound isomer is clearly the dominant species in the far more hindered *i*-Pr<sub>2</sub>NEt derivatives (<1:25 **17c:18c**). Similar observations in Si bistriflimides have been rationalized based on lower steric demands of the bistriflimide fragment in the O-bound isomer,<sup>17</sup> and the same considerations apparently can be extended to boron compounds.

While the observed equilibration suggests facile interconversion of **17** and **18**, the exact mechanism of this process is unclear. The existing array of experimental data does not allow a clear distinction between the dissociative mechanism (which would involve primary borenium **19**, eq 6) and other alternatives, such as an S<sub>N</sub>2 process involving Tf<sub>2</sub>N<sup>-</sup> anion inevitably present in all Tf<sub>2</sub>NH activations, as suggested by <sup>19</sup>F NMR data.

**Table 1-1.** <sup>11</sup>B and <sup>19</sup>F NMR Data for R<sub>3</sub>N–BH<sub>2</sub>NTf<sub>2</sub> Complexes **17** and **18**<sup>a</sup>

Entry	R <sub>3</sub> N	δ <sup>11</sup> B, N-bound ( <b>17</b> )	δ <sup>11</sup> B, O-bound ( <b>18</b> )	δ <sup>19</sup> F, N-bound ( <b>17</b> )	δ <sup>19</sup> F, O-bound ( <b>18</b> )	N-/O-bound product ratio ( <b>17:18</b> ) at equilibrium <sup>b</sup>
<b>a</b>	Me <sub>3</sub> N	-3.7	4.0	-69.2	-77.6, -79.1	7:1
<b>b</b>	Et <sub>3</sub> N	-7.4	0.7	-68.9	-76.7, -79.1	1:4.7
<b>c</b>	( <i>i</i> -Pr) <sub>2</sub> NEt	ND	1.2	-68.4	-77.0, -79.1	<1:25
<b>d</b>	<i>p</i> -MeBnNMe <sub>2</sub>	-3.2	4.0	-69.0	-76.6, -79.1	4.2:1
<b>e</b>		-4.6 <sup>c</sup>	0.6 <sup>c</sup>	-69.2 <sup>c</sup>	-76.7 <sup>c</sup> , -78.7 <sup>c</sup>	1:2.6 <sup>c</sup>

<sup>a</sup>1:1 R<sub>3</sub>N–BH<sub>3</sub>:Tf<sub>2</sub>NH, CD<sub>2</sub>Cl<sub>2</sub>, rt. <sup>b</sup>monitored up to 2-14 days at rt. <sup>c</sup>in *d*<sub>8</sub>-PhMe.

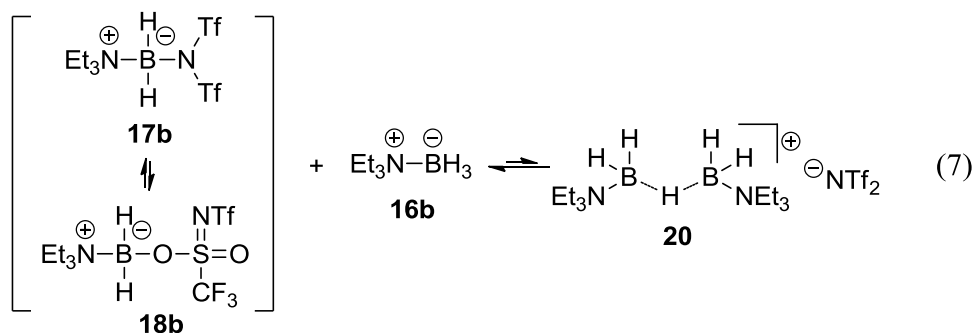


Similar mechanistic ambiguities represent a recurring theme throughout this work. As an example, reactions of **17/18** with nucleophiles can be imagined to proceed either by an S<sub>N</sub>1 pathway involving dissociation to **19** (as in eq 6), or by a direct S<sub>N</sub>2 displacement. To obscure issues even further, primary borenium **19** can potentially exist

as a weak complex with the solvent, a species that may also be capable of reacting by an  $S_N2$  pathway. While a careful kinetic study can distinguish between these mechanistic alternatives in theory, we chose not to focus on the fine mechanistic details, but rather to treat **17/18** and related highly reactive complexes as “equivalents” of **19**, making the distinction between these species only when reliable spectroscopic evidence is available. It should be noted, however, that the “equivalency” of **17/18** to **19** is only partial, since both species can still differ substantially in their reactivity. It is only their ability to serve as a source of the cationic  $[R_3N-BH_2]^+$  unit (**19**) in reactions with nucleophiles that is the real basis for their equivalency in our terms.

When activations of amine boranes were performed using only a substoichiometric amount of  $Tf_2NH$ , formation of an additional product was observed by NMR spectroscopy. Thus, when  $Et_3N-BH_3$  (**16b**) was treated with 0.5 equiv of  $Tf_2NH$  in  $CD_2Cl_2$ , NMR assay after 30 min at rt indicated the presence of three new compounds aside from unreacted **16b** (eq 7). While two of the products were found to be **17b** and **18b** in the same 1:4.7 ratio as in the stoichiometric  $Tf_2NH$  activation experiment (Table 1-1), the third product was assigned as the unusual H-bridged cationic boron complex **20** based on the similarity of the NMR data to that reported by Timothy DeVries for the corresponding  $[B(C_6F_5)_4]^-$  salt.<sup>15</sup> Structurally, cation **20** can be viewed as a complex between amine borane **16b** and the hypothetical primary borenium cation **19** ( $R = Et$ ), with the central  $3c2e$  B–H–B bond formed from the empty  $p$ -orbital of **19** ( $R = Et$ ) and the  $\sigma$ -basic B–H bond of **16b**. The observed ratio between **16b**, **17b**, **18b** and **20** (approx. 7.2:1.1:5.0:1.0 mol) thus suggests that B–H  $\sigma$ -bonds of  $Et_3N-BH_3$  are sufficiently basic to compete with  $Tf_2N^-$  for binding to **19** ( $R = Et$ ) in the thermodynamic

sense. The existence of a rapid equilibrium between **16b**, **17b/18b** and **20** is in line with the previous observations suggesting rapid formation of covalent boron bistriflimides upon treatment of independently generated  $[\text{B}(\text{C}_6\text{F}_5)_4]^-$  salt of the H-bridged cation **20** with the  $\text{Tf}_2\text{N}^-$  salt of a hindered pyridinium cation.<sup>15</sup>



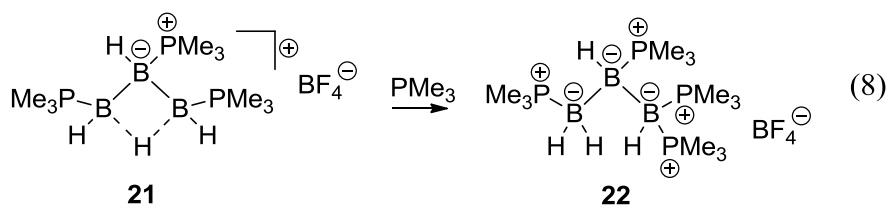
Despite the structural description of cation **20** as a complex between **16b** and **19** ( $\text{R} = \text{Et}$ ), the free borenium cation **19** ( $\text{R} = \text{Et}$ ) is not necessarily present at any stage of the reaction shown in eq 7, since both the forward and the reverse processes can also be envisioned as proceeding by  $\text{S}_{\text{N}}2$ -type displacements at B atoms of **17b** or **18b** (forward process) or **20** (reverse process). While the chemistry of such H-bridged cations occupying an intermediate position between borenium and boronium species will be discussed in more detail in the following section, it should be noted that eq 7 represents the borderline case for the formation of covalent counterion adducts of **19**. Any further decrease in the coordinating ability of the anion can be expected to favor formation of **20**.

#### *Reactions of $\text{L}-\text{BH}_3$ with Electrophiles Possessing Weakly Coordinating Counterions*

As was pointed out in the previous section, attempts to generate borenium ions in the presence of compounds possessing basic B–H bonds can lead to formation of H-bridged borocations when the coordinating ability of the counterion and the solvent is

sufficiently low. This section deals specifically with chemistry of such H-bridged boron cations, including their intermediate role in the generation of tricoordinate borenium ions.

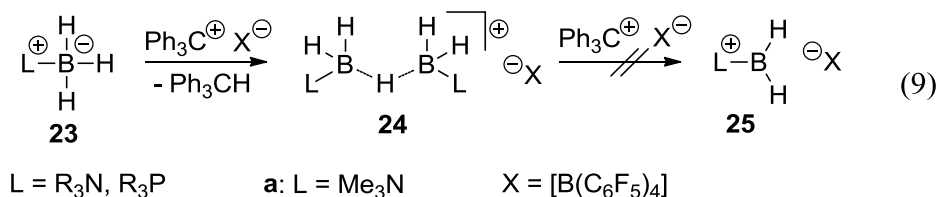
Cationic boron species possessing 3c2e B–H–B bonds are fairly uncommon, despite the wide abundance of multi-center bonds in both neutral and anionic boron compounds. In 1997 Kodama reported formation of triboron cation **21** upon treatment of  $B_2H_4(PMe_3)_2$  with  $Ph_3C^+ BF_4^-$ .<sup>18</sup> To the best of our knowledge, this is the first report on a borocation for which the existence of a B–H–B bridge can be reliably assigned based on multinuclear NMR data. Facile cleavage of the B–H–B bridge in **21** by  $PMe_3$  was also reported (eq 8).



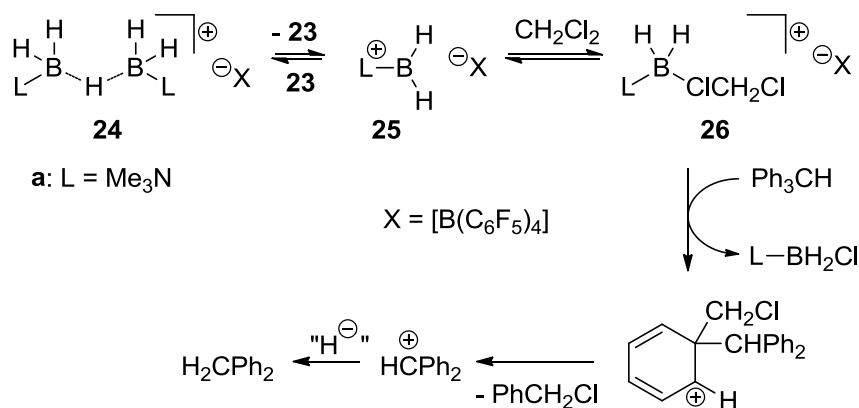
More intriguingly, formation of a cation tentatively assigned as  $[B_2H_5(PMe_3)_2]^+$  by hydride abstraction from  $Me_3P-BH_3$  with  $Ph_3C^+ BF_4^-$  was also reported in the same communication by Kodama,<sup>18</sup> although no structural or spectroscopic details were provided. Hydride abstractions from amine and phosphine borane complexes by  $Ph_3C^+$  salts were further studied in our group by Timothy DeVries, and it was concluded that when  $L-BH_3$  (**23**) and  $Ph_3C^+ [B(C_6F_5)_4]^-$  were mixed in a 1:1 ratio, hydride abstraction proceeded only to the stage of H-bridged intermediate **24**, leaving 50 mol% of  $Ph_3C^+$  intact (eq 9).<sup>15</sup> At that point it was also noted that when  $CH_2Cl_2$  solvent was used, extensive decomposition of  $Ph_3CH$  byproduct was taking place. This behavior was rationalized by Timothy DeVries by proposing facile dissociation of **24** to **25** and **23** at rt, followed by generation of the electrophilic  $CH_2Cl_2$  complex **26**, and subsequent reaction



of **26** with Ph<sub>3</sub>CH byproduct (Scheme 1-1). Fast reactions of **24** with other nucleophiles such as R<sub>3</sub>SiH were also proposed to proceed via generation of an equilibrium concentration of **25** by the spontaneous dissociation of **24**.



**Scheme 1-1.** Proposed Mechanism for the Electrophilic Ph<sub>3</sub>CH Degradation in CH<sub>2</sub>Cl<sub>2</sub><sup>15</sup>



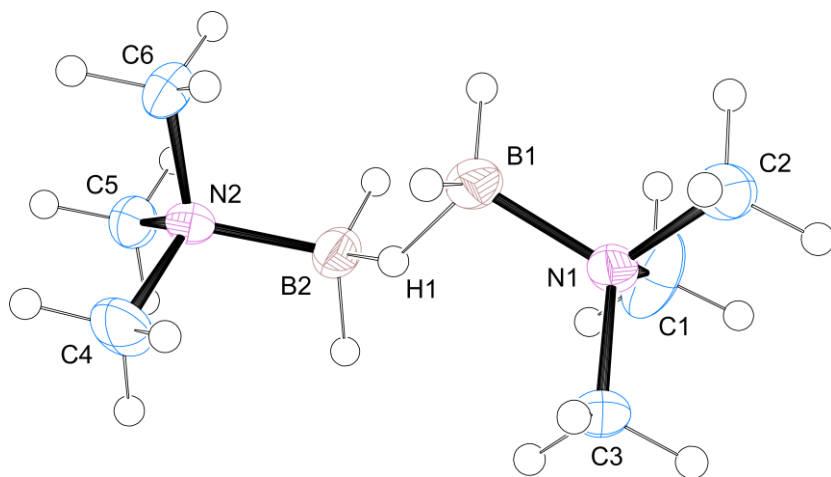
Our further exploration of the hydride abstraction from Lewis base borane complexes, however, raised the suspicion that the proposed dissociation of **24** to **25** and **23** may be somewhat less thermodynamically favorable than was suggested previously. For example, it was noticed that the stability of H-bridged dimers **24** in CD<sub>2</sub>Cl<sub>2</sub> solution containing Ph<sub>3</sub>CH depends rather strongly on whether additional Ph<sub>3</sub>C<sup>+</sup> is present in the solution or not. Thus, in the absence of Ph<sub>3</sub>C<sup>+</sup>, a 1:1 mixture of **24a** (**24**, L = Me<sub>3</sub>N) and Ph<sub>3</sub>CH in CD<sub>2</sub>Cl<sub>2</sub> does not show any traces of Ph<sub>3</sub>CH decomposition for weeks at rt, while in the presence of 1 eq Ph<sub>3</sub>C<sup>+</sup> substantial decomposition of **24a** and Ph<sub>3</sub>CH is evident after a mere 10 min at rt. The ability of cation **24** to generate **25** efficiently in a spontaneous dissociation event thus demands additional investigation. Importantly, the

hypothesis that **24** can produce **25** only under the influence of an added electrophile deserves close attention. The relevant issues of stability of H-bridged species **24** toward dissociation, as well as their thermal stability, will be discussed in more detail in Chapter 2.

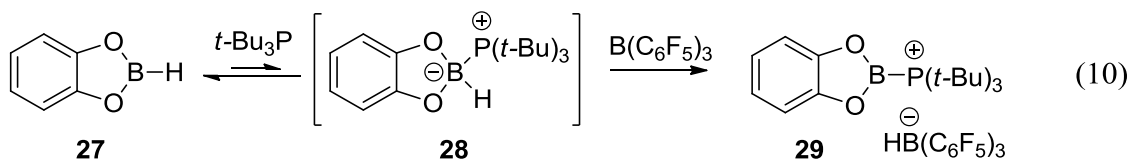
Unambiguous structural proof for cation **24a** was obtained by isolating the compound in the pure form, and confirming its structure by X-ray crystallography. Performing the reaction between  $\text{Me}_3\text{N-BH}_3$  (**23a**) and  $\text{Ph}_3\text{C}^+ [\text{B}(\text{C}_6\text{F}_5)_4]^-$  in PhH solvent allowed facile removal of  $\text{Ph}_3\text{CH}$  byproduct by separating layers of the biphasic reaction mixture, while X-ray quality single crystals of **24a** were produced by layering  $\text{CH}_2\text{Cl}_2$  solution of the product with hexanes. Crystallographic analysis confirmed the H-bridged nature of the cation (Figure 1-2, Appendix A), and allowed measuring some bonding parameters despite the fact that the part of the structure to the left of H1 in Figure 1-2 is disordered with the  $\text{Me}_3\text{N-BH}_2$  fragment occupying two different orientations. Comparison with the X-ray data<sup>19</sup> for  $\text{Me}_3\text{N-BH}_3$  reveals a ca. 0.04Å shorter B–N distance in **24a**, and distorted B–N–C bond angles. Thus, the B1–N1–C2 bond angle involving the methyl group (C2) antiperiplanar to the hydride bridge is ca. 6° smaller than the other two B–N–C angles, indicating hyperconjugative interaction between the filled orbital of N1–C2 bond with the antibonding orbital of the B–H–B bridge.

Having confirmed the H-bridged cationic structure of **24a**, we proceeded to investigate the possibility of generating unstabilized boreniums such as **25** by the stoichiometric trityl cation activation of Lewis base borane complexes. The existing data suggest that moderately to weakly stabilized tricoordinate borenium species can be accessed by the action of “hydridophiles” on tetracoordinate boron species possessing

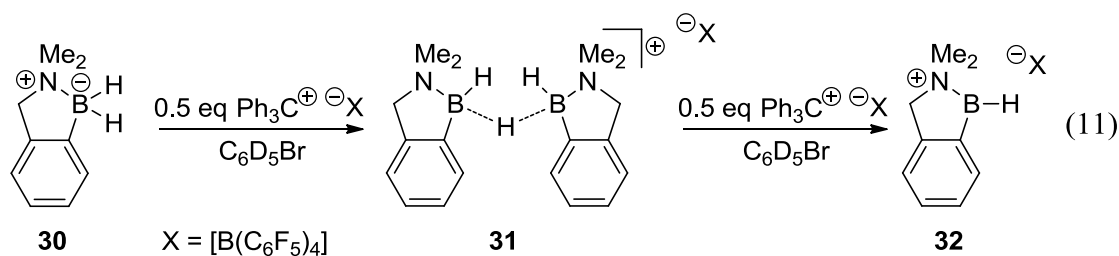
**Figure 1-2.** X-Ray structure of **24a** (cation only, 50% probability ellipsoids)



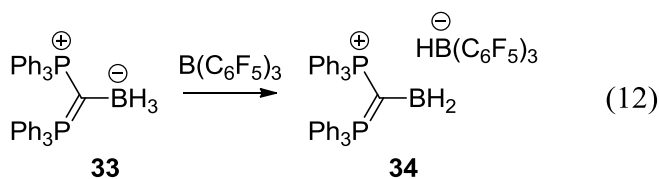
B–H bonds. Thus, Stephan *et al.* reported formation of borenium **29** upon treatment of catecholborane (**27**) with a “frustrated Lewis pair” composed of *t*-Bu<sub>3</sub>P and strongly electrophilic borane B(C<sub>6</sub>F<sub>5</sub>)<sub>3</sub> (eq 10).<sup>20</sup> The key step of the process apparently involves hydride abstraction from the transient tetracoordinate adduct **28**.



Additionally, reinvestigation of the previous results on hydride abstraction from cyclic amine borane complexes<sup>21</sup> by Timothy DeVries revealed that rather weakly stabilized bora-benzylic borenium cation **32** can be prepared by treating **30** with 1 equiv of Ph<sub>3</sub>C<sup>+</sup> [B(C<sub>6</sub>F<sub>5</sub>)<sub>4</sub>]<sup>−</sup> (eq 11).<sup>15</sup> Interestingly, in this case the H-bridged cation **31** was observed to be merely an intermediate on the way to tricoordinate species **32**, and not the ultimate trityl activation product.

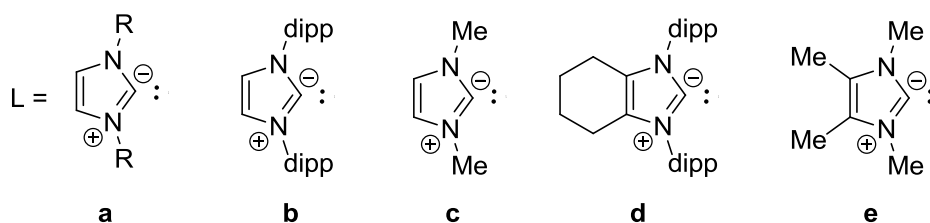
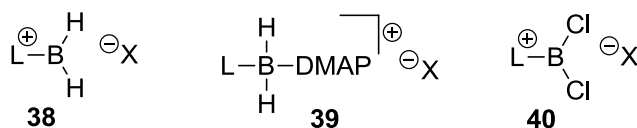
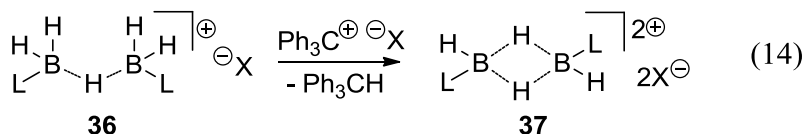
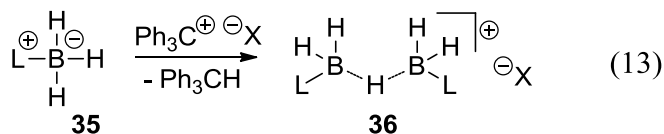


Finally, generation of a stabilized primary borenium salt **34** was reported very recently by Alcarazo *et al.*<sup>22</sup> In this case formation of a dihydrido borenium species upon  $\text{H}^-$  abstraction from complex **33** by  $\text{B}(\text{C}_6\text{F}_5)_3$  (eq 12) was possible due to strong  $\sigma$ - and  $\pi$ -donating properties of the carbodiphosphorane ligand.



We thus proceeded to explore the reactivity of Lewis base borane complexes with  $\text{Ph}_3\text{C}^+ [\text{B}(\text{C}_6\text{F}_5)_4]^-$  in  $d_5$ -PhBr solution at rt. Two different types of Lewis base complexes were used, namely amine and N-heterocyclic carbene (NHC) borane complexes.<sup>23,24</sup> Activation of NHC– $\text{BH}_3$  complexes **35a**, **35b** and **35c** with 0.5 equiv of the trityl salt predictably resulted in clean formation of H-bridged cations **36a**, **36b** and **36c**, respectively (eq 13). The product cations were identified based on their spectroscopic properties, featuring broad peaks in  $^{11}\text{B}$  NMR spectra downfield from the corresponding starting complexes **35** (**35a**  $\delta^{11}\text{B}$  –36.3 ppm, **36a**  $\delta^{11}\text{B}$  –24.6 ppm; **35b**  $\delta^{11}\text{B}$  –35.5 ppm, **36b**  $\delta^{11}\text{B}$  –24.6 ppm; **35c**  $\delta^{11}\text{B}$  –36.6 ppm, **36c**  $\delta^{11}\text{B}$  –22.1 ppm). The H-bridged nature of the product complexes was evident from the characteristic broad resonances in  $^1\text{H}$  NMR spectra (**36a**  $\delta^1\text{H}$  –2.6 ppm; **36b**  $\delta^1\text{H}$  –2.7 ppm; **36c**  $\delta^1\text{H}$  –3.0 ppm), paralleling observations in amine borane activation.<sup>15</sup> Additionally, H-bridged

cation **36c**  $[\text{B}(\text{C}_6\text{F}_5)_4]^-$  salt was prepared in PhH suspension, isolated as a sensitive crystalline solid in 97% yield and characterized by  $^1\text{H}$ ,  $^{11}\text{B}$ ,  $^{13}\text{C}$  and  $^{19}\text{F}$  NMR.



R = 2,6-Me<sub>2</sub>-4-*t*-BuC<sub>6</sub>H<sub>2</sub>

dipp = 2,6-(*i*-Pr)<sub>2</sub>C<sub>6</sub>H<sub>3</sub>

X =  $[\text{B}(\text{C}_6\text{F}_5)_4]^-$

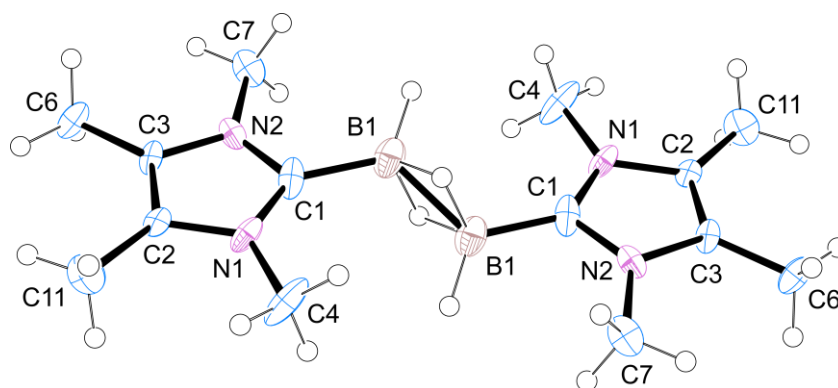
Subsequent addition of another 0.5 equiv of the trityl salt to the reaction mixture containing **36a** resulted in another hydride abstraction event, producing Ph<sub>3</sub>CH, and a new species **37a** giving rise to a  $^{11}\text{B}$  NMR signal at  $\delta$  +11.9 ppm. Formation of the new product was rather slow, taking a few hours at rt to reach completion. In contrast, a similar reaction involving the more substituted NHC borane **35d** proceeded noticeably faster, with full conversion of **36d** to the new product **37d** ( $\delta$   $^{11}\text{B}$  +8.0 ppm) reached in less than 10 min at rt. Intriguingly, the structural and reactivity data summarized below suggest that the product of the second hydride abstraction step is not the expected primary borenium **38**, but rather its dicationic dimer **37** (eq 14). Quenching the products **37** with 4-dimethylaminopyridine (DMAP) afforded isolable dihydridoboronium cations

**39** (quantitative by *in situ* NMR), while  $\text{BH}_4^-$  quench restored the starting carbene boranes **35** (>95% isolated yield). Analogously, reaction of **37** with **35** cleanly afforded the corresponding H-bridged cations **36** as single products according to NMR assay. No degradation of  $[\text{B}(\text{C}_6\text{F}_5)_4]^-$  counterion was observed by  $^{19}\text{F}$  NMR, so the composition of the NHC containing fragment could be formulated as “NHC– $\text{BH}_2^+$ ”. This structural assignment, however, does not explain the unusual  $^{11}\text{B}$  NMR chemical shift, which suggests that the product is unlikely to be a tricoordinate boron derivative. In principle, aside from the free cation structure **38**, under the reaction conditions the “NHC– $\text{BH}_2^+$ ” species could also exist as a base adduct, with the base being either the solvent, or the counterion, or the  $\text{Ph}_3\text{CH}$  byproduct. All of these possibilities, however, could be ruled out, since the chemical shift of the  $^{11}\text{B}$  NMR signal was observed to be fairly insensitive to the solvent ( $d_5\text{-PhBr}$  or  $\text{CD}_2\text{Cl}_2$ ) and the counterion ( $[\text{B}(\text{C}_6\text{F}_5)_4]^-$  or  $[\text{HCB}_{11}\text{Cl}_{11}]^-$ ) used, and did not depend on the presence of  $\text{Ph}_3\text{CH}$ . Even more puzzling for the “NHC– $\text{BH}_2^+$ ” species, the solubility of products **37** was found to be rather low. Thus, attempts to perform stoichiometric trityl activation of **35c** resulted in formation of a fine crystalline solid insoluble in both  $d_5\text{-PhBr}$  and  $\text{CD}_2\text{Cl}_2$ . Even the very lipophilic carbene complex **35d** upon activation with 1 equiv  $\text{Ph}_3\text{C}^+$  afforded a product (**37d**) that was only moderately soluble in  $d_5\text{-PhBr}$ , with excess product separating out as an oil.

The structure of the mysterious “NHC– $\text{BH}_2^+$ ” product **37** was unambiguously established by X-ray crystallography. The product derived from carbene borane **35e** was found to offer a nice balance between solubility and crystallinity, although the reaction conditions had to be optimized carefully to improve the crystal quality of the sensitive dication salt. Thus, competing formation of the dichlorinated cation **40e** (assigned based

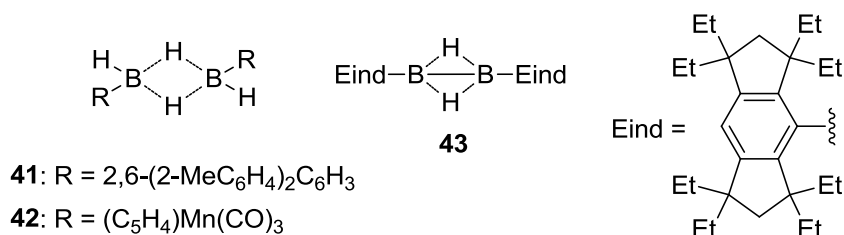
on a partially solved X-ray structure,  $\delta^{11}\text{B}$  +47.6 ppm) due to the reaction with the solvent prevented crystallization of **37e** salts from  $\text{CH}_2\text{Cl}_2$ , and the use of  $[\text{HCB}_{11}\text{Cl}_{11}]^-$  counterion in PhF resulted in heavily disordered crystal structures. Finally, suitable crystals of **37e** precipitated out of the reaction mixture upon allowing the stoichiometric mixture of  $\text{Ph}_3\text{C}^+ [\text{Al}_2\text{Br}_7]^-$  and **35e** to react in PhF solution at rt, again suggesting low solubility of the product in the relatively polar PhF solvent. Even in this case the crystal quality was found to deteriorate quickly with time, prompting immediate analysis after reasonable crystal size is reached.

**Figure 1-3.** X-Ray structure of **37e** (dication only, 50% probability ellipsoids)



The X-ray structure (Figure 1-3, Appendix A) serves as the key evidence suggesting the dicationic nature of **37e**. The dication conforms to the crystallographically imposed  $C_i$  symmetry, with the inversion center rendering both “ $\text{NHC-BH}_2^{+}$ ” subunits equivalent. The same symmetry considerations define the mutually parallel orientation of the mean planes of both 5-membered rings with interplane separation of 0.46Å. Another bonding parameter of interest is the C1–B1 bond distance of 1.58Å, which is only marginally shorter than the corresponding C–B bond in the starting carbene borane **35e** (1.59Å).<sup>25</sup> The most crucial bonding parameter, the B···B distance is 1.78Å which is very similar to B···B distances measured by X-ray crystallography in neutral  $\text{RBH}_2$

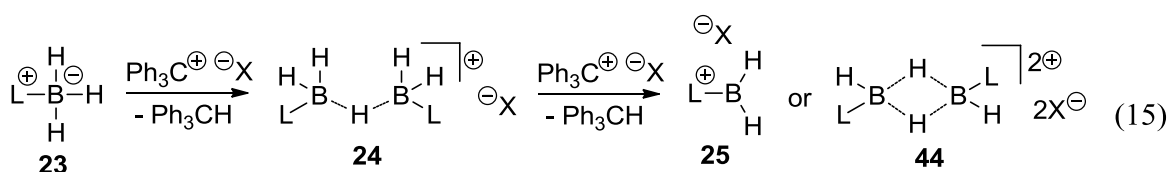
dimers **41** (1.79Å)<sup>26</sup> and **42** (1.78Å),<sup>27</sup> as well as the B···B distance determined by electron diffraction in the parent B<sub>2</sub>H<sub>6</sub> (1.77Å),<sup>28</sup> and substantially exceeds that determined in diborane(4) **43** (X-ray 1.49Å; neutron diffraction 1.48Å).<sup>29</sup> The hydrogen atoms at the central diboron fragment were located on difference Fourier maps and allowed to refine isotropically as independent atoms. A minor ambiguity about the number of H atoms at borons might still persist, however, due to the inherently low contribution of hydrogens to the electron density map. Therefore, while X-ray structure refinement clearly favors the diborane(6)-type structure, other evidence would only serve to strengthen this structural assignment. To this end, the B···B distance taken together with the results of the quenching experiments suggesting “NHC–BH<sub>2</sub><sup>+</sup>” composition of the crystalline solid serve as the key evidence supporting the diborane(6)-type structure of **37e**. Most importantly, the products that are formed quantitatively upon quenching solid **37e** with nucleophiles such as **35e** or DMAP suggest that the solid, for a selected crystal of which the X-ray analysis was performed, must contain one BH<sub>2</sub> unit per each NHC fragment.



The same dicationic dimer structure **37** is apparently also preserved in the solution phase, explaining the unusual chemical shifts of ca.  $\delta$  +8–12 ppm in the <sup>11</sup>B NMR spectrum. Further justification for the chemical shift value was gained by GIAO (gauge-independent atomic orbital) calculations for **37e** in dichloromethane solution. The predicted value of  $\delta$  <sup>11</sup>B +10.8 ppm is in a good agreement with the observed chemical



shift of 10.7 ppm, suggesting that the structural assignment is reasonable (method details summarized in the computational section of this chapter). It should be emphasized that dimerization of the extremely Lewis acidic cation **38** to form **37** is preferred over complexation with weakly basic species such as  $\text{Ph}_3\text{CH}$ ,  $\text{CD}_2\text{Cl}_2$ ,  $d_5\text{-PhBr}$ ,  $[\text{Al}_2\text{Br}_7]^-$  or  $[\text{B}(\text{C}_6\text{F}_5)_4]^-$ , suggesting that the  $\sigma$ -basicity of B–H bonds of **38** is sufficiently high to overcome electrostatic repulsion of the two cationic fragments. The preference for the dicationic structure is even more surprising given the possibility of benzylic-type stabilization of the empty orbital at boron by the  $\pi$ -system of the heterocyclic ring in **38**, but not in **37**.

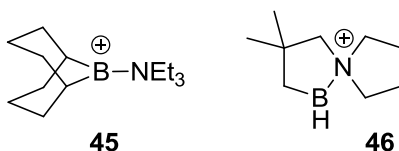


**a:** L =  $\text{Me}_3\text{N}$   
**b:** L =  $i\text{-Pr}_2\text{NEt}$

X =  $[\text{B}(\text{C}_6\text{F}_5)_4]^-$

Having established the behavior of NHC borane complexes upon hydride abstraction, we turned our attention to amine borane complexes, hoping to gain insight into their reactivity in the electrophilic activation beyond formation of H-bridged monocations **24**. Amine boranes ( $i\text{Pr}$ )<sub>2</sub>EtN–BH<sub>3</sub> (DIEA–BH<sub>3</sub>, **23b**) and Me<sub>3</sub>N–BH<sub>3</sub> (**23a**) were tested in the reaction with  $\text{Ph}_3\text{C}^+ [\text{B}(\text{C}_6\text{F}_5)_4]^-$  in  $d_5\text{-PhBr}$  at rt, giving rise to markedly different observations (eq 15). Thus, treatment of the more hindered **23b** with 1 equiv of the trityl salt resulted in immediate formation of two new boron species as evidenced by NMR spectra. While the major new product can be assigned as **24b** ( $\delta^{11}\text{B}$  –0.5 ppm; bridging H  $\delta^1\text{H}$  –2.8 ppm), the other product ( $\delta^{11}\text{B}$  +53.9 ppm) is clearly a tricoordinate boron cation. The observation of a broad resonance around  $\delta^1\text{H}$  4.8 ppm

typical for B–H resonances in tricoordinate boron species allows us to postulate that the signal at  $\delta^{11}\text{B} +53.9$  ppm might be due to the primary borenium ion **25b**. It should be noted here that formation of other unidentified species starts to interfere within minutes following the mixing of reagents, and decomposition results in complete consumption of  $\text{Ph}_3\text{CH}$  and partial degradation of  $[\text{B}(\text{C}_6\text{F}_5)_4]^-$  in 2h at rt as evidenced by  $^1\text{H}$  and  $^{19}\text{F}$  NMR data. The observed  $^{11}\text{B}$  chemical shift of +53.9 ppm for **25b** (in  $d_5$ -PhBr) can be reasonably rationalized based on the comparison with  $^{11}\text{B}$  spectra of boreniums **45** ( $\delta^{11}\text{B} +85.1$  ppm in  $\text{CD}_2\text{Cl}_2$ ) and **46** ( $\delta^{11}\text{B} +71.1$  ppm in  $\text{CD}_2\text{Cl}_2$ , +69.5 ppm in  $d_5$ -PhBr), which will be covered in more detail in the following chapters. Since it is reasonable to expect that most of the  $^{11}\text{B}$  chemical shift difference between **45** and **46** arises from the differences in substituents directly attached to B, it could be proposed that replacing an alkyl group at B in a non-stabilized borenium with a hydrogen atom shifts the  $^{11}\text{B}$  NMR signal upfield by ca. 14 ppm. Further extrapolation of this effect suggests a chemical shift of ca. +57 ppm for a primary borenium species, which is sufficiently close to the observed value of +53.9 ppm for what could be **25b**. Also, the  $^{11}\text{B}$  chemical shift of **25b** (+55.8 ppm in  $d_5$ -PhBr, method details summarized in the computational section of this chapter) as calculated by GIAO can be taken as further evidence for the formation of a primary borenium cation in the stoichiometric  $\text{Ph}_3\text{C}^+$  activation of **23b**.

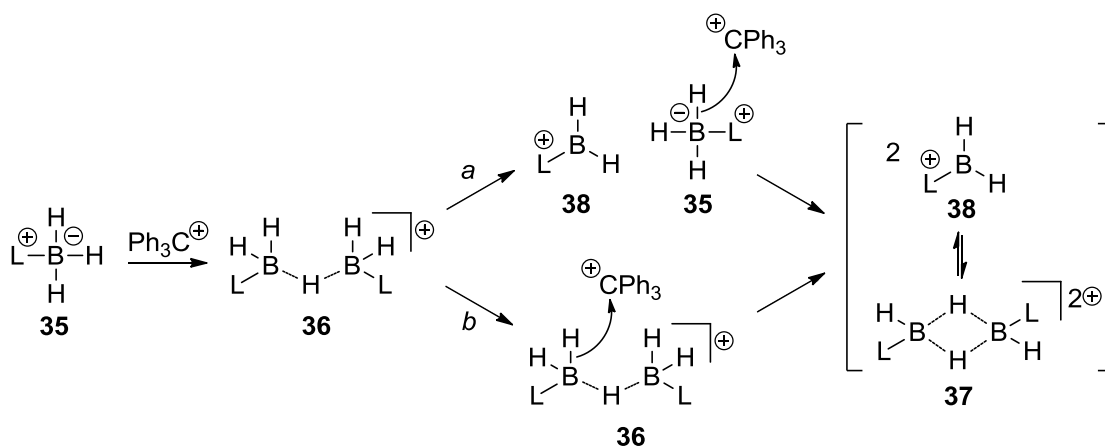


Behavior of the less hindered trimethylamine borane (**23a**) under the same activation conditions was noticeably different, however. While little reactivity beyond generation of **24a** was observed after 10 min at rt, formation of a new product **44a** ( $\delta^{11}\text{B}$

+12.9 ppm) was evident, reaching roughly a 1:3 **44a:24a** ratio ( $^{11}\text{B}$  NMR peak intensity) after 2h at rt. Judging from the detection limits based on  $^1\text{H}$  and  $^{19}\text{F}$  NMR data, essentially no  $\text{Ph}_3\text{CH}$  or counterion degradation had occurred at this point, and the subsequent quenching experiments were thus performed at the relatively low conversion. Even after 24h at rt, with **44a** being the dominant component of the mixture (2.5:1 **44a:24a**,  $^{11}\text{B}$  NMR peak intensity), species originating from decomposition processes constituted only a minor fraction of the B containing products. While our attempts to obtain X-ray quality crystals of **44a** have not been successful, the apparent similarity between this process and formation of the NHC-derived dicationic dimers **37** allows us to postulate that the product of the reaction of **24a** with trityl cation is also a dicationic dimer. This tentative assignment is substantiated by quenching experiments, which suggest “ $\text{Me}_3\text{N}-\text{BH}_2^+$ ” stoichiometry of **44a**. Thus, when the reaction mixture containing **44a** and **24a** in a 1:3 ratio (1:1 mixture of **23a** and  $\text{Ph}_3\text{C}^+ [\text{B}(\text{C}_6\text{F}_5)_4]^-$  in  $d_5\text{-PhBr}$  after 2h at rt) was treated with a slight excess of trimethylamine borane (**23a**), the resulting solution was found to contain exclusively **24a** (as  $[\text{B}(\text{C}_6\text{F}_5)_4]^-$  salt) and  $\text{Ph}_3\text{CH}$ , aside from excess **23a**. The quenching experiment was performed at the same low conversion to **44a** as mentioned above to ensure high quality of the  $^1\text{H}$  and  $^{11}\text{B}$  NMR data, which allowed making a clear conclusion that **44a** reacts with trimethylamine borane (**23a**) forming **24a**. While the possibility that the peak at  $\delta^{11}\text{B} +12.9$  ppm might arise from  $\text{Me}_3\text{N}-\text{BH}_2-\text{L}^+$  ( $\text{L} =$  counterion,  $\text{Ph}_3\text{CH}$  or  $d_5\text{-PhBr}$ ) type of species cannot be excluded as rigorously as in the case of NHC boreniums **37**, no peaks that could be attributed to complexed L were identified in  $^1\text{H}$ ,  $^{11}\text{B}$ ,  $^{13}\text{C}$  and  $^{19}\text{F}$  spectra of the reaction mixtures containing **44a**. As an additional consistency proof, the observed chemical shift of  $\delta^{11}\text{B}$

+12.9 ppm is in a reasonable agreement with the calculated shift of  $\delta^{11}\text{B}$  17.0 ppm for **44a** (see computational section for details). The above structural assignment suggests that the differences in  $^{11}\text{B}$  chemical shift and stability of the products derived from amine boranes **23a** and **23b** might arise from the differences in the coordination environment at boron, since the tricoordinate B atom in borenium **25b** can reasonably be expected to be both more deshielded and more reactive than B atoms in the bridged dication **44a**.

**Scheme 1-2.** Electrophilic activation of H-bridged borocations



Two limiting mechanistic alternatives for the formation of H-bridged dications **37** (or **44** in the amine case) are summarized in Scheme 1-2. Depending on the ability of the H-bridged cations **36** to dissociate to **38** and **35** to a sufficient extent at rt, the second step of the electrophilic activation can either follow path *a* or *b*. While path *a* might seem more intuitive due to the facility of the hydride abstraction from **35**, path *b* might still operate in case dissociation of **36** is thermodynamically unfavorable. Even though path *b* necessarily involves the electrostatically unfavorable interaction between positively charged **36** and  $\text{Ph}_3\text{C}^+$ , such interactions are rather well preceded in superelectrophile chemistry.<sup>3</sup> Ultimate formation of dicationic product **37** can also serve as an indirect evidence suggesting that cation-cation repulsion can be overcome in such systems by

other stabilizing factors, such as 3c2e bonding. Therefore, it is also plausible that multi-center multi-electron interactions can lower the barrier for the formation of the doubly charged transition structure from two monocationic species in the hydride abstraction from **36** (path *b*).

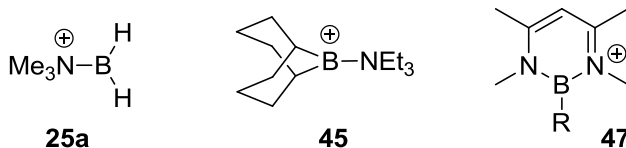
If the assignment of species **25b** and **44** is correct, then dissociation of dicationic dimers **37** and **44** to their corresponding monomers should be relatively facile, since the differences in the amine fragments of **23a** and **23b** are sufficient to determine the preference for monocationic vs. dicationic structure. It should be noted, however, that in contrast to amine borane derivatives, even the extremely hindered NHC borane complexes **35b** and **35d** (eq 13, 14) still form the dicationic dimers rather than the corresponding primary borenium cations, a result that can be rationalized by the relatively higher  $\sigma$ -basicity of B–H bonds in the strongly  $\sigma$ -donating NHC environment.

The results presented up to this point suggest that some borenium cations are potent Lewis acid. Thus, the extremely high electronic demand of the empty *p*-orbital at B in unstabilized primary borenium cations determines the ability of such species to covalently bind weak nucleophiles such as  $\text{Tf}_2\text{N}^-$ , as well as to form 3c2e bonds with B–H bonds of other boron species including another primary borenium cation. It was thus of interest for us to perform a more systematic analysis of known borenium cations with the aim of establishing the effects of the structure on their Lewis acidity.

### Experimental Evaluation of Borenium Lewis Acidity

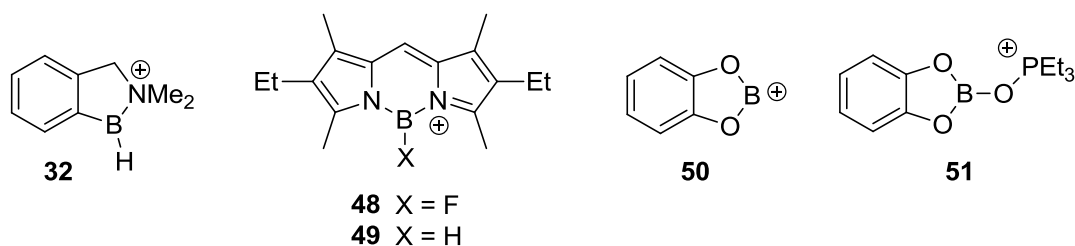
Borenium ions are stronger Lewis acids compared to typical boranes due the combined effect of the net positive charge and a formally vacant *p*-orbital at tricoordinate boron, but how much stronger are they? There is no simple way to answer this question.

Judging from the experimental data available in the literature, the degree of Lewis acidity of borenium ions spans a rather wide range, depending on the nature of substituents attached to boron. Thus, if the ability to form covalent bonds to counterions is used as a rough measure of Lewis acidity, then the two representative limiting cases would be (1) the aromatic cation **47** which resists complexation with the relatively nucleophilic chloride anion,<sup>30</sup> and (2) the powerful electrophile  $\text{H}_2\text{B}-\text{NMe}_3^+$  (**25a**) that covalently binds even to the weakly coordinating bistriflimidate anion to form the neutral adduct **14b** ( $\text{L} = \text{Me}_3\text{N}$ ; eq 4). However, the Lewis acidity of borenium ions depends on the steric as well as the electronic availability of the vacant *p*-orbital on boron. Thus, the borenium cation **45** does not bind the bistriflimidate counterion even though it lacks stabilizing  $\pi$  or *n* electron donors, nor does it bind excess added triethylamine (Chapter 3).<sup>5</sup> The more highly substituted **45** would have additional stabilizing hyperconjugative interactions with proximal  $\sigma$ -bonds compared to **25a**, but severe steric crowding is a major factor that makes **45** a weaker Lewis acid than **25a**. In contrast, the previously studied relatively unhindered borenium cation **47**<sup>30</sup> is unlikely to interfere sterically with an incoming nucleophile such as chloride ion, but **47** does not undergo conversion to the tetracoordinate boron adduct because the boron *p*-orbital is strongly populated by involvement in the aromatic  $\pi$ -system. In this case, electronic factors are dominant.



While most reports on borenium ion chemistry contain qualitative descriptors of Lewis acidity (such as the ability to coordinate counterions or other Lewis bases),

systematic comparisons of borenium Lewis acidities have been rare. Such comparisons would be informative if performed using the same reference Lewis base to probe the equilibrium between tricoordinate and tetracoordinate boron species, but the literature data are very limited, while data obtained using spectroscopic evaluation of tetracoordinate boron adducts are also limited and rather difficult to compare. Estimates of Lewis acidity for borenium ions based on NMR methods have been reported in some cases. Thus, Piers *et al.* investigated the effect of complexation by borenium species **48** and **49** on the  $^1\text{H}$  chemical shift for the  $\beta$ -proton of crotonaldehyde (Child's test), and concluded that the Lewis acidities of **48** and **49** are mutually close and comparable to those of  $\text{Et}_2\text{AlCl}$  and  $\text{BF}_3$ .<sup>31</sup> In a somewhat different test involving non-equilibrium conditions, Ingleson *et al.* assessed the Lewis acidity of the hypothetical cation **50** by measuring the  $^{31}\text{P}$  chemical shift of the  $\text{Et}_3\text{PO}$  adduct **51** ( $\delta$  106.9 ppm) and comparing this chemical shift with the corresponding values for the  $\text{Et}_3\text{PO}$  adducts of several reference Lewis acids including  $(\text{C}_6\text{F}_5)_3\text{B}$  ( $\delta$  76.6 ppm),  $\text{AlCl}_3$  ( $\delta$  80.3 ppm), and  $\text{BBr}_3$  ( $\delta$  91.2 ppm).<sup>32</sup> The chemical shifts for the three reference Lewis acids increased in the same order as their Lewis acidity determined from earlier studies using Child's test. This correlation suggests that the non-equilibrium  $^{31}\text{P}$  chemical shifts may also be used to estimate relative Lewis acidities. Unfortunately, the standard Child's test (complex formation with crotonaldehyde in  $\text{CD}_2\text{Cl}_2$ ) could not be performed with **50** due to its incompatibility with the solvent. This problem was avoided in  $\text{C}_6\text{D}_6$  solution, but the crotonaldehyde chemical shift data obtained for **50** in  $\text{C}_6\text{D}_6$  did not show a simple correlation with the reference data in  $\text{CD}_2\text{Cl}_2$ , and correlation data for the same solvent were not reported.



The simpler test based on the  $^{31}\text{P}$  chemical shift of **51** is consistent with the notion that **50** is a very powerful Lewis acid that is probably more potent than the neutral boron Lewis acids  $\text{B}(\text{C}_6\text{F}_5)_3$  and  $\text{BBr}_3$ . On the other hand, Lewis acidity estimates based on the  $^{31}\text{P}$  chemical shift criterion would be influenced by other factors resulting from structural changes near the boron subunit. Thus, the  $^{31}\text{P}$  chemical shifts for the  $\text{Et}_3\text{PO}$  adducts corresponding to the hypothetical, non-stabilized borenium cation  $\text{H}_2\text{BNMe}_3^+$  (**25a**) and the observable  $\pi$ -stabilized "borabenzyl" cation **32**<sup>15</sup> happen to be identical ( $\delta$  85.7 ppm in  $\text{CD}_2\text{Cl}_2$ ) despite the apparent difference in stabilization (see experimental section for details). In view of these findings, more definitive experimental methods to probe the Lewis acidity of borenium species are needed, and remain to be developed.

### Computational Studies on Lewis Acidity of Borenium Ions

The experimental challenges associated with handling highly reactive boron cations prompted us to use modern electronic structure methods as a means for getting additional insight into both the structural features and reactivity of such species. Besides the quantitative results summarized in this section, the use of computational tools throughout the project served to outline additional areas where experimental efforts should be directed. This section primarily deals with choosing appropriate methods for modeling cationic boron complexes, as well as with predicting the NMR properties and estimating the Lewis acidity of such species. The computational results relevant to the



reactivity of borocations are mostly treated in the computational section of the next chapter.

Closed shell boron compounds belong to the “easy cases” for *ab initio* electronic structure methods and can generally be modeled by post-Hartree–Fock methods with high accuracy. The size of the systems of interest to our research, however, and unfavorable scaling properties of electron-correlated *ab initio* methods made us consider a suitable density functional theory (DFT) method instead. Surprisingly enough, most widely used DFT functionals perform rather poorly in modeling even the simplest Lewis base complexes of boron Lewis acids. Thus, B3LYP and PBE functionals famous for their excellent performance in typical problems of interest to organic chemistry fail to reproduce experimentally determined dissociation enthalpies of simple amine borane complexes. As an example, the B–N bond dissociation enthalpy of Me<sub>3</sub>N–BMe<sub>3</sub> calculated at B3LYP/6-311++G(3df,2p)//B3LYP/6-311++G(3df,2p) level of theory is only –2.4 kcal/mol,<sup>33</sup> which is over 15 kcal/mol off from the experimentally determined enthalpy of –17.6 kcal/mol.<sup>34</sup> Perhaps more disturbing is the observation that the accuracy of the dissociation enthalpies predicted by this method varies substantially among a range of Me<sub>n</sub>H<sub>3–n</sub>N–BMe<sub>3</sub> complexes,<sup>33</sup> rendering systematic error correction impossible. Overall, the poor performance of most widely used DFT functionals appears to be traceable to their inability to reproduce the effects of non-bonding interactions. This is further substantiated by the fact that the performance of the PBE functional can be noticeably improved by including the empirical dispersion correction.<sup>33</sup>

The recently developed “Minnesota” family of parametrized functionals introduced by Truhlar *et al.* represents a significant milestone in the development of DFT

functionals suitable for use in systems with substantial contribution from non-bonding interactions.<sup>35</sup> Thus, mean absolute error (MAE) for a range of B–N bond dissociation enthalpies calculated using M06-2X functional with a large basis set is only 0.3 kcal/mol, as compared to the MAE of 10.8 kcal/mol for B3LYP functional with the same basis set.<sup>33</sup> A prohibitively expensive basis set (6-311++G(3df,2p)) was used for geometry optimization and frequency calculation, however, so a less computationally demanding method had to be established and validated for our systems. Calculating single point energies at a high level of theory using the molecular geometries from a lower level of theory is a common method for reducing computational effort without significant loss in accuracy.<sup>36</sup> The relatively inexpensive 6-31+G(d,p) basis set was thus chosen for geometry optimizations and frequency calculations, while single point energies were determined using a large 6-311++G(3df,2p) basis set.

The scarcity of high quality experimental thermochemical data for boron Lewis acid complexes is a substantial obstacle for validating the chosen computational method, however. To an extent, this could be compensated for by using highly accurate composite methods to generate a set of reference energy values. Taking the accuracy of the reference method to the extreme, W1BD composite *ab initio* method was used.<sup>37</sup> A member of the “Weizmann” family offering sub-kcal/mol accuracy in atomization energies, this outrageously demanding method can only be used on species containing just a few non-H atoms.

### *Computational Details and Method Validation*

The following methodology was used to obtain the results summarized in this section, as well as the computational results presented in the following chapters.

All calculations were performed using the Gaussian 09 suite of computational programs.<sup>38</sup> Gas-phase W1BD calculations were performed as implemented in the software; tight geometry optimization criteria were used, and the use of symmetry was enabled for larger systems. All other calculations were performed at M06-2X/6-311++G(3df,2p)//M06-2X/6-31+G(d,p) level of theory. Unless specified explicitly, calculations were performed in the gas phase, and stationary points at the potential energy surface (PES) were confirmed by calculating vibrational frequencies. Counterions were not considered in the calculations performed on cationic species. Tight optimization criteria (opt=tight) and ultrafine integration grids (int=ultrafine) were used in all DFT calculations. A scaling factor of 0.97 was used for the thermochemical analysis. Counterpoise correction for the basis set superposition error was applied to single point energies where specified explicitly. Extensive conformational search was not performed, so some of the structures presented below and in the following chapters might not be the lowest energy conformers. For the structures for which no X-ray crystallographic data exist, a few arbitrarily chosen conformations were tested, and the lowest energy conformation was used to gather the actual data. This is not expected to be a major complication, since the nature of the results was mostly intended to be qualitative rather than quantitative. As will be mentioned further, in some cases the condensed phase effects could not be neglected, such as when modeling processes involving dicationic species. In those cases the solution phase was modeled using the SMD method.<sup>39</sup> It should be noted, however, that the accuracy of the currently available methods for solution phase modeling is only moderate, and thus only rough conclusions can be drawn. The choice of the solvation method is somewhat arbitrary in the absence

of experimental thermochemical data on borenium ions, but Truhlar's SM methods are typically known to perform better than other continuum solvation models.<sup>40</sup> In the cases where solution modeling was employed, all steps of the calculation (geometry optimization, frequency calculation, single point energy calculation, NMR properties calculation) were performed using the same solvation model. Methods and reference compounds for calculating <sup>11</sup>B NMR chemical shifts are discussed further in the last section of this chapter.

Table 1-2 presents a set of gas-phase thermodynamic values for model reactions calculated at both W1BD and M06-2X/6-311++G(3df,2p)//M06-2X/6-31+G(d,p) levels of theory. The test set of enthalpies involves Lewis base affinities of BH<sub>3</sub> and a few selected boron cations, as well as the affinity of simple boreniums for the shared electron pair of B–H bonds in ammonia and phosphine BH<sub>3</sub> complexes (i.e. 3c2e bond formation). As can be seen from the table, in general the agreement between the two methods is excellent, with MAE (mean absolute error) being 0.6 kcal/mol. It is important to emphasize that both methods are fundamentally different from the theoretical perspective, and the good agreement between methods differing substantially in their weaknesses can be taken as a further evidence for the accuracy of the results.

**Table 1-2.** Reaction Enthalpies Calculated Using W1BD and M06-2X Methods

Reaction	$\Delta H_{298}$ , W1BD, kcal/mol <sup>a</sup>	$\Delta H_{298}$ , M06-2X, kcal/mol <sup>b</sup>
$[\text{BH}_2(\text{H}_2)]^+ \rightarrow \text{BH}_2^+ + \text{H}_2$	16.8	15.8
$[\text{H}_3\text{NBH}_2(\text{H}_2)]^+ \rightarrow [\text{H}_3\text{NBH}_2]^+ + \text{H}_2$	7.2	7.1
$[\text{H}_3\text{PBH}_2(\text{H}_2)]^+ \rightarrow [\text{H}_3\text{PBH}_2]^+ + \text{H}_2$	13.4	13.2
$[\text{H}_3\text{NBH}_2]^+ \rightarrow \text{H}_3\text{N} + \text{BH}_2^+$	91.4	91.0
$[\text{H}_3\text{PBH}_2]^+ \rightarrow \text{H}_3\text{P} + \text{BH}_2^+$	71.6	69.9
$[\text{H}_2\text{OBH}_2]^+ \rightarrow \text{H}_2\text{O} + \text{BH}_2^+$	74.9	76.1
$[\text{H}_2\text{SBH}_2]^+ \rightarrow \text{H}_2\text{S} + \text{BH}_2^+$	63.3	61.8
$[\text{HFBH}_2]^+ \rightarrow \text{HF} + \text{BH}_2^+$	35.5	36.5
$[\text{H}_3\text{NBH}_2\text{NH}_3]^+ \rightarrow [\text{H}_3\text{NBH}_2]^+ + \text{H}_3\text{N}$	55.8	55.9
$[\text{H}_3\text{NBH}_2\text{PH}_3]^+ \rightarrow [\text{H}_3\text{NBH}_2]^+ + \text{H}_3\text{P}$	41.6	40.8
$[\text{H}_3\text{NBH}_2\text{OH}_2]^+ \rightarrow [\text{H}_3\text{NBH}_2]^+ + \text{H}_2\text{O}$	37.8	39.2
$[\text{H}_3\text{NBH}_2\text{SH}_2]^+ \rightarrow [\text{H}_3\text{NBH}_2]^+ + \text{H}_2\text{S}$	31.2	31.0
$[\text{H}_3\text{NBH}_2\text{FH}]^+ \rightarrow [\text{H}_3\text{NBH}_2]^+ + \text{HF}$	15.5	16.8
$[\text{H}_3\text{NBH}_2\text{PH}_3]^+ \rightarrow [\text{H}_3\text{PBH}_2]^+ + \text{H}_3\text{N}$	61.4	61.9
$[\text{H}_3\text{NBH}_2\text{OH}_2]^+ \rightarrow [\text{H}_2\text{OBH}_2]^+ + \text{H}_3\text{N}$	54.3	54.2
$[\text{H}_3\text{NBH}_2\text{SH}_2]^+ \rightarrow [\text{H}_2\text{SBH}_2]^+ + \text{H}_3\text{N}$	59.3	60.2
$[\text{H}_3\text{NBH}_2\text{FH}]^+ \rightarrow [\text{HFBH}_2]^+ + \text{H}_3\text{N}$	71.3	71.2
$\text{H}_3\text{NBH}_3 \rightarrow \text{H}_3\text{N} + \text{BH}_3$	28.1	28.2
$\text{H}_3\text{PBH}_3 \rightarrow \text{H}_3\text{P} + \text{BH}_3$	22.7	22.3
$\text{H}_2\text{SBH}_3 \rightarrow \text{H}_2\text{S} + \text{BH}_3$	12.4	12.6
$\text{H}_2\text{OBH}_3 \rightarrow \text{H}_2\text{O} + \text{BH}_3$	11.6	12.5
$[\text{H}_3\text{NBH}_2\text{-H-BH}_2\text{NH}_3]^+ \rightarrow [\text{H}_3\text{NBH}_2]^+ + \text{H}_3\text{BNH}_3$	48.9	48.8
$[\text{H}_3\text{PBH}_2\text{-H-BH}_2\text{PH}_3]^+ \rightarrow [\text{H}_3\text{PBH}_2]^+ + \text{H}_3\text{PNH}_3$	47.3	46.9

<sup>a</sup>Gas-phase enthalpies (298.15K) determined using W1BD method as described above.

<sup>b</sup>Gas-phase enthalpies (298.15K) determined using M06-2X/6-311++G(3df,2p)//M06-2X/6-31+G(d,p) level of theory. No counterpoise correction applied.

Additional support for the validity of the chosen DFT method comes from the comparison of the calculated B–N dissociation enthalpies with the available experimental data (Table 1-3).<sup>34</sup> Since the importance of BSSE (basis set superposition error) correction in predicting accurate dissociation enthalpies of amine boranes has been previously emphasized in the literature, counterpoise correction for BSSE was employed to calculate enthalpies summarized in Table 1-3.<sup>33</sup> Note that in this case the dissociation enthalpies were calculated at 373K to match the available experimental data. While the

limited data set does not allow drawing statistically rigorous conclusions, the experimental enthalpies were reproduced with MAE of only 0.4 kcal/mol.

**Table 1-3.** Experimental and Calculated Dissociation Enthalpies of Amine Boranes

Amine-borane	$\Delta H_{373}$ , experimental, kcal/mol	$\Delta H_{373}$ , calculated, kcal/mol
H <sub>3</sub> N–BMe <sub>3</sub>	13.8	14.3
MeNH <sub>2</sub> –BMe <sub>3</sub>	17.6	18.5
Me <sub>2</sub> NH–BMe <sub>3</sub>	19.3	19.3
Me <sub>3</sub> N–BMe <sub>3</sub>	17.6	17.9

#### *Computational Evaluation of Borenium Lewis Acidity*

In an early computational attempt to gain insight regarding the factors that influence the bonding, stability, and Lewis acidity of boron cations, Nöth, Bursten *et al.* studied a series of cations R<sub>2</sub>BL<sup>+</sup> (R = H, NH<sub>2</sub>; L = H<sub>2</sub>O, pyridine, NH<sub>3</sub>, etc.) using *ab initio* methods.<sup>41</sup> Two different geometries were compared for the L = pyridine case, and the fully planar structure was found to be favored by 12.6 kcal/mol compared to the geometry having the pyridine ring turned perpendicular to the plane of the boron  $\sigma$ -bonds. This energy difference was associated with a  $\pi$ -delocalization effect, the same stabilizing interaction involving delocalization between the pyridine ring with the boron *p*-orbital that had been deduced in earlier studies.<sup>2</sup> The *ab initio* investigation also explored the dissociation of the borenium cation H<sub>3</sub>N–BH<sub>2</sub><sup>+</sup> (**1**) into the simple components (the borinium ion H<sub>2</sub>B<sup>+</sup> and ammonia).<sup>41</sup> This conversion was discussed in the context of heterolytic bond dissociation, a process that reflects the enthalpic component for B–N bond formation in the reverse reaction (ammonia + H<sub>2</sub>B<sup>+</sup> as the Lewis acid), corresponding to the ammonia affinity of H<sub>2</sub>B<sup>+</sup>. Subject to the usual caveats regarding the evaluation of condensed phase phenomena using computed gas phase energies, this general approach offers a potential way to estimate NH<sub>3</sub> affinities of other

boron cations, including labile borenium ions that are difficult to compare under standardized solution conditions.

An extrapolation from the above precedent has been performed with the goal of ranking a series of borenium ions according to their gas phase NH<sub>3</sub> affinities. The range of borenium ions studied (Table 1-4) includes several structures of synthetic interest (Lewis acid catalysts; electrophilic borylating agents). It also represents various bonding environments for boron, and includes most borenium examples characterized by X-ray crystallography during the past decade to allow the comparison of computed and experimental geometries. While the calculations disregard additional factors such as solvation, ion pairing, and conformational effects, a qualitative comparison of borenium Lewis acidities should still be possible. The data presented in Table 1-4 show that in the cases where reliable X-ray crystallographic data are available, the calculated bond lengths are in reasonable agreement with the experiment. Only qualitative enthalpies can be obtained from these computational results, but some trends deserve attention. Thus, Piers' borenium ions **48** and **49** are predicted to have comparable Lewis acidities, well in accord with the reported data.<sup>31</sup> Moreover, the NH<sub>3</sub> affinities of **48** and **49** are close to the NH<sub>3</sub> affinity of BF<sub>3</sub> calculated using the same method ( $\Delta H = -20.4$  kcal/mol), consistent with the Lewis acidities determined by Piers using Child's test.<sup>31</sup> As expected, borenium ions **25a** or **1** having the highest NH<sub>3</sub> affinity are sterically unhindered, and experience relatively little electronic stabilization by the ligands due to the absence of *n*- or  $\pi$ -donors (entries 13, 14). The 9-BBN-derived cation **45** also lacks *n*- or  $\pi$ -donors, but the calculated NH<sub>3</sub> affinity is rather modest (entry 4). The explanation for this contrast lies partly in the greater degree of boron substitution in **45** and the resulting hyperconjugative

stabilization compared to **25a**, but steric hindrance may be even more important. One consequence of the highly hindered environment is apparent in the substantially longer B–NEt<sub>3</sub> bond compared to the B–NH<sub>3</sub> bond in the ammonia adduct, evidence that the larger ligand encounters severe steric strain. More generally, the above example reflects the elongation of bonds to the boron atom that occurs upon complexation with the Lewis base, and the pronounced moderating effect of steric hindrance on borenium NH<sub>3</sub> affinity.

Nitrogen *n*-donor substituents at boron substantially decrease the NH<sub>3</sub> affinity of borenium ions, as exemplified by structure **7** (entry 1). Related borenium cations possessing oxygen *n*-donors such as cation **29** (entry 6) or Corey's Diels-Alder catalyst **12** (entry 10) are somewhat more Lewis acidic, apparently due to the increased electronegativity of oxygen compared to nitrogen. The substantial difference between **29** and **12** in terms of NH<sub>3</sub> affinity remains unexplained, but **12** clearly is a potent Lewis acid, as also expected from its catalytic reactivity. Similar oxygen electronegativity effects on NH<sub>3</sub> binding energies were noted for dicoordinate boron cations (borinium ions) by Nöth, Bursten *et al.* in their computational study,<sup>41</sup> and the general trends were recognized in earlier experimental work.<sup>2</sup>

Increased NH<sub>3</sub> affinity also correlates with the presence of a larger number of electronegative atoms in the conjugated  $\pi$ -systems attached to boron (entries 7, 8, 11), but other factors are difficult to evaluate in these more complex examples. Thus, cations **49** and **48** (entries 7, 8) are formally antiaromatic 12 $\pi$  electron systems, a factor that should also enhance NH<sub>3</sub> affinity. However, Piers *et al.* found no evidence for substantial antiaromaticity using the nucleus-independent chemical shift criterion NICS(1),<sup>31</sup>

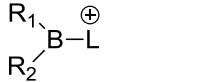
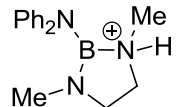
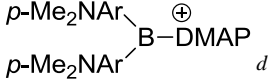
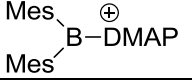
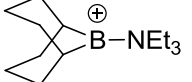
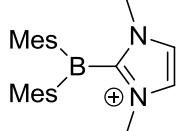
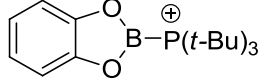
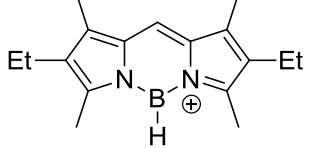
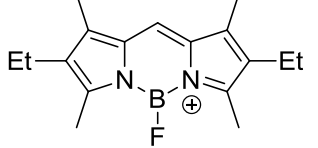


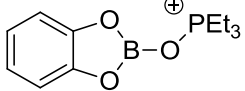
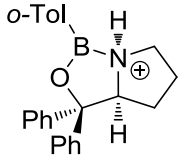
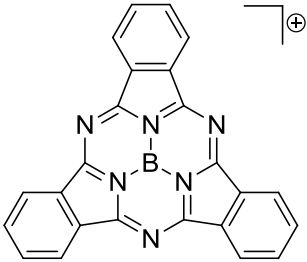
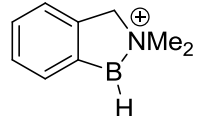
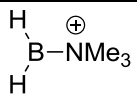
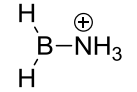
precluding the unambiguous assessment of antiaromaticity and electronegativity vs. simple *n*-delocalization from the nitrogen substituent attached to B in cations **48** and **49**.

The calculated NH<sub>3</sub> affinities are generally consistent with the empirical comparisons of borenium Lewis acidities as discussed earlier in this chapter. To a first approximation, the ordering of calculated NH<sub>3</sub> affinities may reflect the Lewis acidities of borenium ions toward other nucleophiles, provided that they are relatively unhindered. However, the structure of the test nucleophile is certainly important. One telling observation is the fact that **45** does not form an adduct with triethylamine (See Chapter 3 for details). If triethylamine had been selected as the test nucleophile for Table 1-4, then **45** would have to be classified as a weak Lewis acid, a ranking that would be somewhat at odds with the observed reactivity, as discussed in Chapter 3.

The most striking feature of Table 1-4 is the broad range of  $\Delta H$  values, differing by >50 kcal/mol from the weakest to the strongest Lewis acid (from entry 1 to entry 14). By comparison, the NH<sub>3</sub> affinities for simple borane derivatives (tricoordinate boron lacking any formally positive substituent) span a much narrower range. Thus, the same computational approach gave the following NH<sub>3</sub> affinities for several boranes: BMe<sub>3</sub> ( $\Delta H = -14.3$  kcal/mol), BF<sub>3</sub> ( $\Delta H = -20.4$  kcal/mol), BCl<sub>3</sub> ( $\Delta H = -25.3$  kcal/mol), BH<sub>3</sub> ( $\Delta H = -27.9$  kcal/mol), values that are in good agreement with earlier computational and experimental studies.<sup>33,34</sup> Because the inherent NH<sub>3</sub> affinities are much larger for borenium ions compared to boranes, the moderating effect of stabilizing substituents is also larger, and this trend is evident in Table 1-4.

**Table 1-4.** Calculated Borenium Geometries and NH<sub>3</sub> Affinities<sup>a,b</sup>

Entry	Structure		Borenium cation			NH <sub>3</sub> adduct R <sub>1</sub> R <sub>2</sub> B(L)NH <sub>3</sub>				ΔH <sup>c</sup>
			B-R <sub>1</sub> , Å	B-R <sub>2</sub> , Å	B-L, Å	B-R <sub>1</sub> , Å	B-R <sub>2</sub> , Å	B-L, Å	B-NH <sub>3</sub> , Å	
1	<b>7</b> <sup>10</sup>		1.408 <b>1.412</b>	1.395 <b>1.386</b>	1.576 <b>1.547</b>	1.489	1.469	1.659	1.706	-2.3
2	<b>52</b> <sup>42</sup>		1.541 <b>1.550</b>	1.541 <b>1.532</b>	1.533 <b>1.501</b>	1.616	1.620	1.619	1.689	-9.2
3	<b>53</b> <sup>42</sup>		1.553 <b>1.560</b>	1.553 <b>1.570</b>	1.517 <b>1.480</b>	1.626	1.623	1.610	1.682	-13.3
4	<b>45</b> <sup>5</sup>		1.559	1.555	1.571	1.618	1.621	1.712	1.660	-13.6
5	<b>54</b> <sup>43</sup>		1.551 <b>1.562</b>	1.551 <b>1.560</b>	1.602 <b>1.579</b>	1.636	1.631	1.648	1.688	-15.1
6	<b>29</b> <sup>20</sup>		1.368 <b>1.369</b>	1.369 <b>1.373</b>	1.945 <b>1.933</b>	1.438	1.440	2.015	1.665	-17.4
7	<b>49</b> <sup>31</sup>		1.438 <b>1.404<sup>e</sup></b>	1.181	1.438 <b>1.402<sup>e</sup></b>	1.522	1.196	1.520	1.664	-18.8
8	<b>48</b> <sup>31</sup>		1.439 <b>1.429<sup>e</sup></b>	1.323 <b>1.414<sup>e</sup></b>	1.439 <b>1.430<sup>e</sup></b>	1.520	1.379	1.520	1.659	-18.9

9	<b>51</b> <sup>32</sup>		1.377 <b>1.381</b>	1.360 <b>1.372</b>	1.386 <b>1.374</b>	1.443	1.438	1.474	1.631	-23.6
10	<b>12</b> <sup>13</sup>		1.534	1.340	1.576	1.592	1.423	1.664	1.659	-25.5
11	<b>55</b> <sup>44</sup>		1.385 <b>1.380</b>	1.385 <b>1.380</b>	1.385 <b>1.380</b>	1.466	1.466	1.466	1.650	-27.6
12	<b>32</b> <sup>15</sup>		1.504	1.183	1.559	1.587	1.199	1.627	1.633	-34.8
13	<b>25a</b>		1.181	1.181	1.528	1.198	1.198	1.604	1.620	-48.8
14	<b>1</b>		1.178	1.178	1.554	1.194	1.194	1.615	1.615	-55.6

<sup>a</sup>Gas-phase counterpoise-corrected heterolytic association enthalpies (298.15K) determined using M06-2X/6-311++G(3df,2p)//M06-2X/6-31+G(d,p) level of theory. <sup>b</sup>Bold numbers indicate bond lengths taken from X-ray crystal structure determination as cited. <sup>c</sup> $\Delta H$  corresponds to the enthalpy for [(cation + NH<sub>3</sub>) → (ammonia adduct)] in kcal/mol. <sup>d</sup>Ar = 2,6-di-Me-C<sub>6</sub>H<sub>2</sub>. <sup>e</sup>X-ray data for **48** and **49** may be imprecise due to disorder as reported by Piers *et al.*<sup>31</sup>

### *Calculation of $^{11}\text{B}$ NMR Chemical Shifts of Cationic Boron Species*

The structures of the very unusual cationic boron species presented in this chapter were largely deduced from their multinuclear NMR spectra, and only in a few cases was X-ray crystallographic analysis feasible. While good agreement between different sets of spectroscopic data was achieved, pointing at the consistency of the structural assignments, an independent prediction of spectroscopic properties, most importantly  $^{11}\text{B}$  NMR chemical shifts, is still highly desirable. To this end, we calculated  $^{11}\text{B}$  chemical shifts of cations **25b**, **37e** and **44a** using GIAO method at M06-2X/6-311++G(3df,2p)//M06-2X/6-31+G(d,p) level of theory using SMD solvation model as described above. Since the main goal of the study was to generate a reasonably good estimate of the  $^{11}\text{B}$  chemical shift of a given borocation, different reference molecules were employed for each cation. Thus, tricoordinate B–H cation **46** (described in detail in Chapter 2) was used as a reference molecule for predicting the chemical shift of another tricoordinate B–H cation **25b**, while  $\text{B}_2\text{H}_6$  was used as a reference molecule for dications **37e** and **44a** containing formal diborane(6) units.

### **Summary**

To summarize, electrophilic activation of Lewis base borane complexes under weakly nucleophilic conditions leads to formation of a range of structurally different species depending on the nature of the substrate and the electrophile. In terms of their reactivity with nucleophiles, all of these species can be generalized as being equivalent to the corresponding primary borenium cations  $\text{L–BH}_2^+$ . Depending on the stoichiometry, amine borane complex activation with  $\text{Tf}_2\text{NH}$  can lead either to neutral  $\text{R}_3\text{NBH}_2\text{–NTf}_2$  species (as a mixture of  $\text{Tf}_2\text{N}^-$  connectivity isomers), or to H-bridged cations such as **20**

(eq 7). Depending on the ratio of the reactants, the reaction of Lewis base borane complexes with the strongly electrophilic  $\text{Ph}_3\text{C}^+ [\text{B}(\text{C}_6\text{F}_5)_4]^-$  affords either monocationic H-bridged species, or their further activation products. The structure of the unusual H-bridged cation **24a** was confirmed by X-ray crystallography, and clear NMR evidence for the formation of the amine-based unstabilized primary borenium **25b** was obtained. Surprisingly, several other primary borenium species prefer to exist in the form of dicationic dimers such as **37**. The dicationic structure of **37** was established based on X-ray crystallography and quenching experiments.

## Experimental

**General Methods.** All reactions were performed at room temperature (unless otherwise stated), under an atmosphere of dry nitrogen, either in a glovebox, or using standard Schlenk techniques. Nuclear magnetic resonance experiments were performed on Varian Inova 700, Varian Inova 500 and Inova 400 spectrometers at the following frequencies:  $^1\text{H}$  700 MHz, 500 MHz or 400 MHz;  $^{11}\text{B}$  and  $^{11}\text{B}\{^1\text{H}\}$  225 MHz, 160 MHz or 128 MHz;  $^{13}\text{C}\{^1\text{H}\}$  176 MHz, 126 MHz or 101 MHz;  $^{19}\text{F}$  471 MHz or 377 MHz;  $^{31}\text{P}$  162 MHz. All spectra were recorded in  $\text{CDCl}_3$ ,  $\text{CD}_2\text{Cl}_2$ ,  $d_5\text{-PhBr}$ , or  $d_8\text{-PhMe}$  and referenced to the  $^1\text{H}$  signal of internal  $\text{Me}_4\text{Si}$  according to IUPAC recommendations,<sup>45</sup> using a  $\mathcal{E}$  (referencing parameter) of 32.083974 for  $\text{BF}_3\cdot\text{OEt}_2$  ( $^{11}\text{B}$ ), a  $\mathcal{E}$  of 25.145020 for  $\text{Me}_4\text{Si}$  ( $^{13}\text{C}$ ), a  $\mathcal{E}$  of 94.094011 for  $\text{CCl}_3\text{F}$  ( $^{19}\text{F}$ ), and a  $\mathcal{E}$  of 40.480742 for  $\text{H}_3\text{PO}_4$  ( $^{31}\text{P}$ ). When the internal  $\text{Me}_4\text{Si}$  reference could not be used, residual solvent peaks in  $^1\text{H}$  NMR spectra were referenced instead. Toluene was distilled over  $\text{CaH}_2$ ;  $\text{CH}_2\text{Cl}_2$ , THF and hexanes were dried by passing through a column of activated alumina. Toluene,  $\text{CH}_2\text{Cl}_2$  and hexanes used in sensitive reactions were further dried by storing over activated 3 Å molecular sieves in the glovebox. Commercially available NMR grade deuterated solvents (Cambridge Isotope Laboratories), as well as benzene and fluorobenzene were not distilled; instead they were simply dried over a large amount of activated 3 Å molecular sieves in the glovebox. All other reagents were used as received from commercial suppliers. NHC borane complexes **35a-d** were prepared in Prof. Curran's group at the University of Pittsburgh by following published procedures.<sup>24</sup>

### Procedure for Tf<sub>2</sub>NH Activations of Amine Borane Complexes. Formation of 17/18

*General Procedure.* Every possible effort was made to protect the reaction mixtures from exposure to air and moisture. The reactions were set up in dry J. Young NMR tubes under N<sub>2</sub> atmosphere in a glovebox. The NMR tubes were dried in a heating oven at ca. 200 °C overnight, and the fitted Teflon valves were dried in a dessicator over Drierite. Commercial grade Tf<sub>2</sub>NH and amine boranes (Me<sub>3</sub>N–BH<sub>3</sub> (**16a**), Et<sub>3</sub>N–BH<sub>3</sub> (**16b**) and (*i*Pr)<sub>2</sub>EtN–BH<sub>3</sub> (**16c**)) were used without further purification. Benzylic amine borane *p*-MeC<sub>6</sub>H<sub>4</sub>CH<sub>2</sub>NMe<sub>2</sub>–BH<sub>3</sub> was prepared as reported previously.<sup>15</sup> 1-Neopentylpyrrolidine borane was prepared as described in Chapter 2. Commercial grade CD<sub>2</sub>Cl<sub>2</sub> and *d*<sub>8</sub>-PhMe (Cambridge Isotope Laboratories) were not distilled, but rather simply dried with freshly activated molecular sieves in the glovebox.

When solid amine boranes were used (**16a**, *p*-MeC<sub>6</sub>H<sub>4</sub>CH<sub>2</sub>NMe<sub>2</sub>–BH<sub>3</sub> (**16d**), 1-neopentylpyrrolidine borane (**16e**)), the reaction tube was charged with a mixture of solid Tf<sub>2</sub>NH and the corresponding amine borane. The solid mixture was dissolved by adding the solvent (either 0.6 mL CD<sub>2</sub>Cl<sub>2</sub> or 0.8 mL *d*<sub>8</sub>-PhMe) to the tube in one portion at rt. Gas liberation was observed, although no substantial exotherm was noted, potentially due to the small scale of the reaction. The tube was sealed with the fitted Teflon valve, and then shaken vigorously for ca. 1 min. The amounts of the reagents used in each particular case are listed below.

When liquid amine boranes were used (Et<sub>3</sub>N–BH<sub>3</sub> (**16b**) and (*i*Pr)<sub>2</sub>EtN–BH<sub>3</sub> (**16c**)), the reaction tube was charged with a solution of Tf<sub>2</sub>NH in 0.6 mL of CD<sub>2</sub>Cl<sub>2</sub>. Neat amine borane was then added to the solution via a microsyringe at rt, causing intense gas liberation, although no substantial exotherm was noted, potentially due to the

small scale of the reaction. The tube was sealed with the fitted Teflon valve, and then shaken vigorously for ca. 1 min. The amounts of the reagents used in each particular case are listed below.

The ratios of N-/O-bound isomers of the products were measured by NMR after the initial equilibration had completed, and were confirmed to remain stable for 2-14 days at rt.

**17a:18a**, 7:1 ratio after equilibration. The following reagents were used: trimethylamine borane (**16a**) (8.0 mg, 0.109 mmol), Tf<sub>2</sub>NH (30.7 mg, 0.109 mmol), CD<sub>2</sub>Cl<sub>2</sub> (0.6 mL).

**17a**: <sup>1</sup>H NMR (500 MHz, CD<sub>2</sub>Cl<sub>2</sub>): δ 3.2-1.9 (br m, 2H), 2.65 ppm (s, 9H). <sup>11</sup>B NMR (160 MHz, CD<sub>2</sub>Cl<sub>2</sub>): δ -3.7 ppm (t, J = 115 Hz). <sup>13</sup>C NMR (126 MHz, CD<sub>2</sub>Cl<sub>2</sub>): δ 119.6 (q, J<sub>C-F</sub> = 326 Hz), 51.8 ppm. <sup>19</sup>F NMR (471 MHz, CD<sub>2</sub>Cl<sub>2</sub>): δ -69.2 ppm (s).

**18a**: <sup>1</sup>H NMR (500 MHz, CD<sub>2</sub>Cl<sub>2</sub>): δ 3.2-1.9 (br m, 2H), 2.69 ppm (s, 9H). <sup>11</sup>B NMR (160 MHz, CD<sub>2</sub>Cl<sub>2</sub>): δ 4.0 ppm (t, J = 120 Hz). <sup>13</sup>C NMR (126 MHz, CD<sub>2</sub>Cl<sub>2</sub>): δ 119.1 (q, J<sub>C-F</sub> = 320 Hz), 118.7 (q, J<sub>C-F</sub> = 321 Hz), 49.7 ppm. <sup>19</sup>F NMR (471 MHz, CD<sub>2</sub>Cl<sub>2</sub>): δ -76.6 (s), -79.1 ppm (s).

**17b:18b**, 1:4.7 ratio after equilibration. The following reagents were used: triethylamine borane (**16b**) (13.3 μL, 90.7 μmol), Tf<sub>2</sub>NH (25.5 mg, 90.7 μmol), CD<sub>2</sub>Cl<sub>2</sub> (0.6 mL).

**17b**: <sup>1</sup>H NMR (500 MHz, CD<sub>2</sub>Cl<sub>2</sub>): δ 3.4-1.9 (br m, 2H), 2.88 (q, J = 7.2 Hz, 6H), 1.21 ppm (t, J = 7.2 Hz, 9H). <sup>11</sup>B NMR (160 MHz, CD<sub>2</sub>Cl<sub>2</sub>): δ -7.4 ppm (unres t). <sup>13</sup>C NMR (126 MHz, CD<sub>2</sub>Cl<sub>2</sub>): δ 119.6 (q, J<sub>C-F</sub> = 327 Hz), 49.8, 8.2 ppm. <sup>19</sup>F NMR (471 MHz, CD<sub>2</sub>Cl<sub>2</sub>): δ -68.9 ppm (s).



**18b:**  $^1\text{H}$  NMR (500 MHz,  $\text{CD}_2\text{Cl}_2$ ):  $\delta$  3.4-1.9 (br m, 2H), 2.90 (q,  $J = 7.2$  Hz, 6H), 1.21 ppm (t,  $J = 7.2$  Hz, 9H).  $^{11}\text{B}$  NMR (160 MHz,  $\text{CD}_2\text{Cl}_2$ ):  $\delta$  0.7 ppm (unres t).  $^{13}\text{C}$  NMR (126 MHz,  $\text{CD}_2\text{Cl}_2$ ):  $\delta$  119.2 (q,  $J_{\text{C-F}} = 320$  Hz), 118.7 (q,  $J_{\text{C-F}} = 321$  Hz), 49.2, 7.5 ppm.  $^{19}\text{F}$  NMR (471 MHz,  $\text{CD}_2\text{Cl}_2$ ):  $\delta$  -76.7 (s), -79.1 ppm (s).

**17c:18c**, <1:25 ratio after equilibration. The following reagents were used:  $(i\text{Pr})_2\text{EtN-BH}_3$  (**16c**) (26.7  $\mu\text{L}$ , 0.153 mmol),  $\text{Tf}_2\text{NH}$  (43.0 mg, 0.153 mmol),  $\text{CD}_2\text{Cl}_2$  (0.6 mL). Due to the low concentration of the N-bound isomer **17c** in solution, only  $^{19}\text{F}$  signals were assigned.

**17c:**  $^{19}\text{F}$  NMR (471 MHz,  $\text{CD}_2\text{Cl}_2$ ):  $\delta$  -68.4 ppm (s).

**18c:**  $^1\text{H}$  NMR (500 MHz,  $\text{CD}_2\text{Cl}_2$ ):  $\delta$  3.70-3.60 (m, 2H), 3.4-2.1 (br m, 2H), 3.01 (q,  $J = 7.3$  Hz, 2H), 1.37-1.33 (m, 12H), 1.26 ppm (t,  $J = 7.3$  Hz, 3H).  $^{11}\text{B}$  NMR (160 MHz,  $\text{CD}_2\text{Cl}_2$ ):  $\delta$  1.2 ppm (unres t).  $^{13}\text{C}$  NMR (126 MHz,  $\text{CD}_2\text{Cl}_2$ ):  $\delta$  119.2 (q,  $J_{\text{C-F}} = 321$  Hz), 118.7 (q,  $J_{\text{C-F}} = 321$  Hz), 56.7, 56.6, 45.3, 18.3 (overlapping s), 9.5 ppm.  $^{19}\text{F}$  NMR (471 MHz,  $\text{CD}_2\text{Cl}_2$ ):  $\delta$  -77.0 (s), -79.1 ppm (s).

**17d:18d**, 4.2:1 ratio after equilibration. The following reagents were used:  $p\text{-MeC}_6\text{H}_4\text{CH}_2\text{NMe}_2\text{-BH}_3$  (**16d**) (23.0 mg, 0.141 mmol),  $\text{Tf}_2\text{NH}$  (39.6 mg, 0.141 mmol),  $\text{CD}_2\text{Cl}_2$  (0.6 mL).

**17d:**  $^1\text{H}$  NMR (500 MHz,  $\text{CD}_2\text{Cl}_2$ ):  $\delta$  7.30-7.17 (m, 4H), 3.96 (s, 2H), 3.3-2.0 (br m, 2H), 2.48 (s, 6H), 2.39 ppm (s, 3H).  $^{11}\text{B}$  NMR (160 MHz,  $\text{CD}_2\text{Cl}_2$ ):  $\delta$  -3.2 ppm (unres t).  $^{13}\text{C}$  NMR (126 MHz,  $\text{CD}_2\text{Cl}_2$ ):  $\delta$  140.0, 132.5, 129.4, 125.5, 119.7 (q,  $J_{\text{C-F}} = 326$  Hz), 64.9, 46.8, 20.9 ppm.  $^{19}\text{F}$  NMR (471 MHz,  $\text{CD}_2\text{Cl}_2$ ):  $\delta$  -69.0 ppm (s).

**18d:**  $^1\text{H}$  NMR (500 MHz,  $\text{CD}_2\text{Cl}_2$ ):  $\delta$  7.30-7.17 (m, 4H), 3.99-3.97 (m, 2H), 3.3-2.0 (br m, 2H), 2.54 (s, 3H), 2.53 (s, 3H), 2.39 ppm (s, 3H).  $^{11}\text{B}$  NMR (160 MHz,  $\text{CD}_2\text{Cl}_2$ ):  $\delta$  4.0 ppm (unres t).  $^{13}\text{C}$  NMR (126 MHz,  $\text{CD}_2\text{Cl}_2$ ):  $\delta$  140.3, 132.3, 129.5, 125.1, 119.2 (q,  $J_{\text{C-F}} = 321$  Hz), 118.8 (q,  $J_{\text{C-F}} = 321$  Hz), 63.5, 45.5, 45.4, 20.9 ppm.  $^{19}\text{F}$  NMR (471 MHz,  $\text{CD}_2\text{Cl}_2$ ):  $\delta$  -76.6 (s), -79.1 ppm (s).

**17e:18e**, 1:2.6 ratio after equilibration. The following reagents were used: 1-neopentylpyrrolidine borane (**16e**) (10.9 mg, 70.3  $\mu\text{mol}$ ),  $\text{Tf}_2\text{NH}$  (19.8 mg, 70.3  $\mu\text{mol}$ ),  $d_8$ -PhMe (0.8 mL).

**17e:**  $^1\text{H}$  NMR (700 MHz,  $d_8$ -PhMe):  $\delta$  3.2-2.3 (br m, 2H), 3.01-2.94 (m, 2H), 2.60-2.55 (m, 2H), 2.44 (s, 2H), 1.57-1.42 (m, 2H), 1.22-1.11 (m, 2H), 0.73 ppm (s, 9H).  $^{11}\text{B}$  NMR (225 MHz,  $d_8$ -PhMe):  $\delta$  -4.6 ppm (unres t).  $^{13}\text{C}$  NMR (176 MHz,  $d_8$ -PhMe):  $\delta$  120.5 (q,  $J_{\text{C-F}} = 327$  Hz), 68.8, 57.8, 33.0, 30.3, 22.0 ppm.  $^{19}\text{F}$  NMR (471 MHz,  $d_8$ -PhMe):  $\delta$  -69.2 ppm (s).

**18e:**  $^1\text{H}$  NMR (700 MHz,  $d_8$ -PhMe):  $\delta$  3.2-2.3 (br m, 2H), 3.01-2.94 (m, 1H), 2.79-2.74 (m, 1H), 2.33 (d,  $J = 13.7$  Hz, 1H), 2.08 (d,  $J = 13.7$  Hz, 1H), 1.98-1.93 (m, 1H), 1.93-1.86 (m, 1H), 1.57-1.42 (m, 2H), 1.22-1.11 (m, 2H), 0.78 ppm (s, 9H).  $^{11}\text{B}$  NMR (225 MHz,  $d_8$ -PhMe):  $\delta$  0.6 ppm (unres t).  $^{13}\text{C}$  NMR (176 MHz,  $d_8$ -PhMe):  $\delta$  120.2 (q,  $J_{\text{C-F}} = 320$  Hz), 119.6 (q,  $J_{\text{C-F}} = 320$  Hz), 72.2, 60.4, 59.4, 33.1, 29.7, 22.6, 22.1 ppm.  $^{19}\text{F}$  NMR (471 MHz,  $d_8$ -PhMe):  $\delta$  -76.7 (s), -78.7 ppm (s).

### Isolation of 24a

Every possible effort was made to protect the reaction mixture from the exposure to air and moisture. The reaction was performed under  $\text{N}_2$  atmosphere in a glovebox.

Disposable glassware flame-dried at the glass softening temperature was used. Commercial grade  $\text{Ph}_3\text{C}^+ [\text{B}(\text{C}_6\text{F}_5)_4]^-$  (Strem) and  $\text{Me}_3\text{N}-\text{BH}_3$  (**23a**) (Aldrich) were used without further purification. Commercial grade anhydrous benzene (Aldrich) was additionally dried with freshly activated molecular sieves in the glovebox. Solid  $\text{Ph}_3\text{C}^+ [\text{B}(\text{C}_6\text{F}_5)_4]^-$  (80.0 mg, 86.7  $\mu\text{mol}$ ) was added in portions to a stirred solution of  $\text{Me}_3\text{N}-\text{BH}_3$  (**23a**) (24.0 mg, 0.329 mmol) in 1 mL of dry PhH at rt. No substantial exotherm was observed, potentially due to the small scale of the reaction. After stirring for ca. 30 min at room temperature, the two-layer mixture was diluted with 1 mL of dry hexanes. The clear top layer contained triphenylmethane and was discarded, and the dark bottom layer of the crude product was washed with 3x1.5 mL PhH. The product crystallized on trituration with 1 mL of hexanes. Drying in the glovebox produced 59 mg (83%) of **24a** as a white solid. The NMR spectroscopic data matched those reported previously.<sup>15,46</sup> Solutions of the product in  $\text{CD}_2\text{Cl}_2$  protected from air and moisture showed no indications of decomposition after storing for ca. 3 days at rt, as evidenced by NMR spectroscopy. Layering  $\text{CH}_2\text{Cl}_2$  solution of the product with hexanes at room temperature produced X-ray quality crystals as colorless needles. X-ray crystallographic study confirmed the proposed structure of **24a** (see Appendix A for details).

### Generation of Unstabilized Primary Borenium Cation **25b**

Every possible effort was made to protect the reaction mixture from exposure to air and moisture. The reaction was set up in a dry J. Young NMR tube under  $\text{N}_2$  atmosphere in a glovebox. The NMR tube was dried in a heating oven at ca. 200 °C overnight, and the fitted Teflon valve was dried in a dessicator over Drierite. Commercial grade  $(i\text{Pr})_2\text{EtN}-\text{BH}_3$  (**23b**) was used without further purification.

Commercial grade  $d_5$ -PhBr (Cambridge Isotope Laboratories) was not distilled, but rather simply dried with freshly activated molecular sieves in the glovebox. The reaction tube was charged with a solution of  $\text{Ph}_3\text{C}^+ [\text{B}(\text{C}_6\text{F}_5)_4]^-$  (48.0 mg, 52.0  $\mu\text{mol}$ ) in 0.6 mL  $d_5$ -PhBr. To this solution neat  $(i\text{Pr})_2\text{EtN}-\text{BH}_3$  (**23b**) (9.1  $\mu\text{L}$ , 52.0  $\mu\text{mol}$ ) was added via a microsyringe in one portion. No substantial exotherm was observed, potentially due to the small scale of the reaction. The tube was immediately sealed with the fitted Teflon valve, and then shaken vigorously for ca. 1 min. Since primary borenium **25b** is very unstable under the reaction conditions, all NMR spectra had to be acquired within the first 10 minutes following mixing the reagents to obtain reasonable quality data. The following NMR spectra were acquired: (1)  $^1\text{H}$  NMR (ca. 3 sec total acquisition time) at 3 min counting from the moment of addition of **23b** to the solution of the trityl reagent; (2)  $^{11}\text{B}$  NMR (ca. 7 min total acquisition time) at 3–10 min counting from the moment addition of **23b** to the solution of the trityl reagent.

While overlaps in the  $^1\text{H}$  spectrum did not allow to fully assign the peaks of the  $(i\text{Pr})_2\text{EtN}$  fragment, observation of a broad signal at  $\delta$  5.2–4.3 ppm serves as a clear indication for the formation of a tricoordinate B–H species in the course of the reaction. To illustrate the reasoning behind this assignment, the  $^1\text{H}$  NMR B–H signal of tricoordinate borenium **46** also appears as a broad peak around  $\delta$  5.2–4.3 ppm (in  $d_5$ -PhBr), while the B–H signals of other plausible species with larger coordination numbers at B appear noticeably upfield from that (cf.  $\delta$   $^1\text{H}$  3.5–2.7 ppm for dication **44a** in  $d_5$ -PhBr). Integration of the peaks at  $\delta$  5.2–4.3 ppm ( $\text{BH}_2$  of **25b**) and –2.8 (bridging H of **24b**) in the  $^1\text{H}$  spectrum suggests a ca. 3.9:1 molar ratio of **24b** and **25b**. The molar ratio of **24b** to **25b** determined by the integration of peaks at  $\delta$  –0.5 and +53.9 ppm,

respectively, in the  $^{11}\text{B}$  NMR is comparable (4.3:1), supporting the assignment of the peak at  $\delta^{11}\text{B} +53.9$  ppm as the primary borenium species. The  $^{11}\text{B}$  NMR spectrum at that time also showed two minor peaks at  $\delta +19.1$  and  $+15.0$  ppm whose intensity gradually increased along with the disappearance of **25b**. Monitoring the progress of the reaction over time suggests that these two peaks apparently correspond to some unidentified decomposition products. Aside from the integration, the gradual disappearance of the peak at  $\delta^{11}\text{B} +53.9$  ppm due to decomposition appears to parallel the disappearance of the broad peak at  $\delta^1\text{H} 5.2\text{--}4.3$  ppm, suggesting that the two peaks likely arise from the same compound. The spectral data summarized below lists only those peaks that can be reasonably assigned as arising from the cation of **25b**. The signals corresponding to  $\text{Ph}_3\text{CH}$ ,  $\text{Ph}_3\text{C}^+$ , **24b** and  $[\text{B}(\text{C}_6\text{F}_5)_4]^-$  counterion are omitted.

$^1\text{H}$  NMR (700 MHz,  $d_5$ -PhBr):  $\delta$  5.2-4.3 ppm (br m, 2H).  $^{11}\text{B}$  NMR (225 MHz,  $d_5$ -PhBr):  $\delta$  +53.9 ppm.

### Preparation of **35e**

A solution of  $\text{LiN}(\text{SiMe}_3)_2$  (7.06 g, 42.2 mmol) in 20 mL of dry THF was cannulated to a slurry of thoroughly dried 1,3,4,5-tetramethylimidazolium iodide (9.68g, 38.4 mmol) in 20 mL of dry THF at  $-78$  °C. After stirring at  $-78$  °C for 1 h, neat  $\text{Me}_2\text{S-BH}_3$  (4.3 mL, 42.2 mmol) was added dropwise, and the resulting mixture was allowed to warm up to rt. The resulting clear yellowish solution was stirred at rt for 1 h, during which time it developed a white precipitate. Following careful quenching with 100 mL of brine (frothing!) the reaction mixture was extracted with  $\text{CH}_2\text{Cl}_2$  (1x70 mL, then 2x40 mL). The combined organic extracts were dried with  $\text{MgSO}_4$ , then filtered and concentrated. Crystallization of the resulting solid from hexanes/ $\text{CHCl}_3$  mixture

provided 4.94g (93%) of **35e** as an off-white crystalline solid in two crops. The product was additionally recrystallized from hexanes/ $\text{CHCl}_3$  before use in sensitive electrophilic activations.

$^1\text{H}$  NMR (700 MHz,  $\text{CDCl}_3$ ):  $\delta$  3.62 (s, 6H), 2.12 (s, 6H), 1.3-0.8 ppm (m, 3H).  $^{11}\text{B}$  NMR (225 MHz,  $\text{CDCl}_3$ ):  $\delta$  -36.9 ppm (q,  $J = 86$  Hz).  $^{13}\text{C}$  NMR (176 MHz,  $\text{CDCl}_3$ ):  $\delta$  169.7-168.6 (m), 123.0, 32.4, 8.7 ppm. HRMS (EI+):  $m/z$  calculated for  $\text{C}_9\text{H}_{22}\text{BNNa}$   $[\text{M}-\text{H}]^+$  137.1250, found 137.1257 (+5 ppm).

### Generation of Cations **36**

Every possible effort was made to protect the reaction mixtures from exposure to air and moisture. The reactions were set up in dry J. Young NMR tubes under  $\text{N}_2$  atmosphere in a glovebox. The NMR tubes were dried in a heating oven at ca. 200 °C overnight, and the fitted Teflon valves were dried in a dessicator over Drierite.  $\text{Ph}_3\text{C}^+ [\text{B}(\text{C}_6\text{F}_5)_4]^-$  (Strem) was used without further purification. Commercial grade  $d_5$ -PhBr and  $\text{CD}_2\text{Cl}_2$  (Cambridge Isotope Laboratories) were not distilled, but rather simply dried with freshly activated molecular sieves in the glovebox.

*General Procedure.* The reaction tube was charged with a mixture of solid NHC borane and  $\text{Ph}_3\text{C}^+ [\text{B}(\text{C}_6\text{F}_5)_4]^-$ . The solid mixture was then dissolved by adding 0.6 mL of solvent to the tube in one portion at rt. No substantial exotherm was observed, potentially due to the small scale of the reaction. The tube was immediately sealed with the fitted Teflon valve, and then shaken vigorously for ca. 1 min.

**36a:** The reaction was performed in  $d_5$ -PhBr solvent (0.6 mL). The following reagents were used: **35a** (25.0 mg, 62.1  $\mu\text{mol}$ ),  $\text{Ph}_3\text{C}^+ [\text{B}(\text{C}_6\text{F}_5)_4]^-$  (28.7 mg, 31.1  $\mu\text{mol}$ ). NMR

assay shortly following the mixing of reagents indicated clean formation of H-bridged cation **36a** ( $[\text{B}(\text{C}_6\text{F}_5)_4]^-$  salt) along with  $\text{Ph}_3\text{CH}$  byproduct.  $^{11}\text{B}$  NMR (225 MHz,  $d_5$ -PhBr):  $\delta$  -16.1 (s), -24.6 ppm (br s).

**36b** (in  $d_5$ -PhBr): The reaction was performed in  $d_5$ -PhBr solvent (0.6 mL). The following reagents were used: **35b** (27.4 mg, 68.1  $\mu\text{mol}$ ),  $\text{Ph}_3\text{C}^+ [\text{B}(\text{C}_6\text{F}_5)_4]^-$  (31.4 mg, 34.0  $\mu\text{mol}$ ). NMR assay shortly following the mixing of reagents indicated clean formation of H-bridged cation **36b** ( $[\text{B}(\text{C}_6\text{F}_5)_4]^-$  salt) along with  $\text{Ph}_3\text{CH}$  byproduct.  $^{11}\text{B}$  NMR (225 MHz,  $d_5$ -PhBr):  $\delta$  -16.1 (s), -24.6 ppm (br s).

**36b** (in  $\text{CD}_2\text{Cl}_2$ ): The reaction was performed in  $\text{CD}_2\text{Cl}_2$  solvent (0.6 mL). The following reagents were used: **35b** (24.9 mg, 61.9  $\mu\text{mol}$ ),  $\text{Ph}_3\text{C}^+ [\text{B}(\text{C}_6\text{F}_5)_4]^-$  (28.6 mg, 31.0  $\mu\text{mol}$ ). NMR assay shortly following the mixing of reagents indicated clean formation of H-bridged cation **36b** ( $[\text{B}(\text{C}_6\text{F}_5)_4]^-$  salt) along with  $\text{Ph}_3\text{CH}$  byproduct.  $^{11}\text{B}$  NMR (128 MHz,  $\text{CD}_2\text{Cl}_2$ ):  $\delta$  -16.7 (s), -24.6 ppm (br s).

### Isolation of **36c**

Every possible effort was made to protect the reaction mixture from exposure to air and moisture. The reaction was performed under  $\text{N}_2$  atmosphere in a glovebox. Disposable glassware flame-dried at the glass softening temperature was used. Commercial grade  $\text{Ph}_3\text{C}^+ [\text{B}(\text{C}_6\text{F}_5)_4]^-$  (Strem) was used without further purification. Commercial grade anhydrous benzene (Aldrich) was additionally dried with freshly activated molecular sieves in the glovebox. To a mixture of solid  $\text{Ph}_3\text{C}^+ [\text{B}(\text{C}_6\text{F}_5)_4]^-$  (0.461 g, 0.500 mmol) and **35c** (0.115 g, 1.05 mmol) 2 mL of dry PhH was added at rt, which resulted in formation of a two-layer liquid. No substantial exotherm was observed,

potentially due to the small scale of the reaction. After stirring for ca. 10 min at room temperature, the two-layer mixture was diluted with 2 mL of dry hexanes. The clear top layer contained triphenylmethane and was discarded, and the bottom layer of the crude product was washed with 4x2 mL of dry hexanes. The crude product crystallized on trituration with hexanes. Drying in the glovebox produced 0.437 g (97%) of **36c** as a white solid. Layering CH<sub>2</sub>Cl<sub>2</sub> solution of the product with hexanes at room temperature produced single crystals suitable for X-ray crystallographic analysis. X-ray crystallography confirmed the proposed connectivity in the cation, although severe disorder did not allow to solve the structure fully.

<sup>1</sup>H NMR (700 MHz, *d*<sub>5</sub>-PhBr): δ 6.29 (s, 4H), 3.26 (s, 12H), 2.7-1.6 (br m, 4H), -2.2--3.8 ppm (br s, 1H). <sup>11</sup>B NMR (225 MHz, *d*<sub>5</sub>-PhBr): δ -16.2 (s), -22.1 ppm (br m). <sup>13</sup>C NMR (176 MHz, *d*<sub>5</sub>-PhBr): δ 158.1-156.1 (br m), 149.7-147.5 (m), 139.4-137.5 (m), 137.5-135.5 (m), 125.2-123.7 (m), 121.7, 35.4 ppm. <sup>19</sup>F NMR (471 MHz, *d*<sub>5</sub>-PhBr): δ -131.8 (m), -162.0 (t, J = 20.9 Hz), -166.0 ppm (m).

### Generation of Dications **37**

Every possible effort was made to protect the reaction mixtures from exposure to air and moisture. The reactions were set up in dry J. Young NMR tubes under N<sub>2</sub> atmosphere in a glovebox. The NMR tubes were dried in a heating oven at ca. 200 °C overnight, and the fitted Teflon valves were dried in a dessicator over Drierite. Ph<sub>3</sub>C<sup>+</sup> [B(C<sub>6</sub>F<sub>5</sub>)<sub>4</sub>]<sup>-</sup> (Strem) was used without further purification. Commercial grade *d*<sub>5</sub>-PhBr and CD<sub>2</sub>Cl<sub>2</sub> (Cambridge Isotope Laboratories) were not distilled, but rather simply dried with freshly activated molecular sieves in the glovebox.



*General Procedure.* The reaction tube was charged with a mixture of solid NHC borane and  $\text{Ph}_3\text{C}^+ [\text{B}(\text{C}_6\text{F}_5)_4]^-$ . The solid mixture was then dissolved by adding 0.6 mL of solvent to the tube in one portion at rt. No substantial exotherm was observed, potentially due to the small scale of the reaction. The tube was immediately sealed with the fitted Teflon valve, and then shaken vigorously for ca. 1 min.

**37a** (in  $d_5$ -PhBr): The reaction was performed in  $d_5$ -PhBr solvent (1.0 mL). The following reagents were used: **35a** (25.0 mg, 62.1  $\mu\text{mol}$ ),  $\text{Ph}_3\text{C}^+ [\text{B}(\text{C}_6\text{F}_5)_4]^-$  (57.3 mg, 62.1  $\mu\text{mol}$ ). Formation of dication **37a** was found to be somewhat slow. Thus, after ca. 1.5 h at rt following the mixing of reagents the reaction mixture was found to contain **36a** and **37a** ( $[\text{B}(\text{C}_6\text{F}_5)_4]^-$  salts) in a ca. 1:1.4 ratio, along with  $\text{Ph}_3\text{CH}$  byproduct and unreacted  $\text{Ph}_3\text{C}^+$ . After 17 h at rt  $^{11}\text{B}$  NMR assay indicated clean formation of **37a**.  $^{11}\text{B}$  NMR (128 MHz,  $d_5$ -PhBr):  $\delta$  11.9 (br s),  $-16.2$  ppm (s).

**37a** (in  $\text{CD}_2\text{Cl}_2$ ): The reaction was performed in  $\text{CD}_2\text{Cl}_2$  solvent (0.6 mL). The following reagents were used: **35a** (30.8 mg, 76.5  $\mu\text{mol}$ ),  $\text{Ph}_3\text{C}^+ [\text{B}(\text{C}_6\text{F}_5)_4]^-$  (66.8 mg, 72.4  $\mu\text{mol}$ ). Formation of dication **37a** was found to be somewhat slow. Thus, after 15 min at rt following the mixing of reagents the reaction mixture was found to contain **36a** and **37a** ( $[\text{B}(\text{C}_6\text{F}_5)_4]^-$  salts) in a ca. 1.5:1 ratio, along with  $\text{Ph}_3\text{CH}$  byproduct and unreacted  $\text{Ph}_3\text{C}^+$ . After 26 h at rt  $^{11}\text{B}$  NMR assay indicated clean formation of **37a**.  $^{11}\text{B}$  NMR (225 MHz,  $\text{CD}_2\text{Cl}_2$ ):  $\delta$  12.4 (br s),  $-16.7$  ppm (s).

**37d** (in  $d_5$ -PhBr): The reaction was performed in  $d_5$ -PhBr solvent (0.6 mL). The following reagents were used: **35d** (20.6 mg, 45.1  $\mu\text{mol}$ ),  $\text{Ph}_3\text{C}^+ [\text{B}(\text{C}_6\text{F}_5)_4]^-$  (41.6 mg, 45.1  $\mu\text{mol}$ ). NMR assay shortly following the mixing of reagents indicated clean

formation of dication **37d** ( $[\text{B}(\text{C}_6\text{F}_5)_4]^-$  salt) along with  $\text{Ph}_3\text{CH}$  byproduct.  $^{11}\text{B}$  NMR (225 MHz,  $d_5$ -PhBr):  $\delta$  8.0 (br s),  $-16.1$  ppm (s).

**37d** (in  $\text{CD}_2\text{Cl}_2$ ): The reaction was performed in  $\text{CD}_2\text{Cl}_2$  solvent (0.6 mL). The following reagents were used: **35d** (20.6 mg, 45.1  $\mu\text{mol}$ ),  $\text{Ph}_3\text{C}^+ [\text{B}(\text{C}_6\text{F}_5)_4]^-$  (46.8 mg, 50.7  $\mu\text{mol}$ ). NMR assay shortly following the mixing of reagents indicated clean formation of dication **37d** ( $[\text{B}(\text{C}_6\text{F}_5)_4]^-$  salt) along with  $\text{Ph}_3\text{CH}$  byproduct. Some unreacted  $\text{Ph}_3\text{C}^+$  was also observed.  $^{11}\text{B}$  NMR (225 MHz,  $\text{CD}_2\text{Cl}_2$ ):  $\delta$  9.9 (br s),  $-16.7$  ppm (s).

**37e**: The reaction was performed in  $\text{CD}_2\text{Cl}_2$  solvent (0.6 mL). The following reagents were used: **35e** (9.9 mg, 71.7  $\mu\text{mol}$ ),  $\text{Ph}_3\text{C}^+ [\text{B}(\text{C}_6\text{F}_5)_4]^-$  (66.1 mg, 71.7  $\mu\text{mol}$ ). Addition of the solvent to the solid mixture produced a clear solution, which turned into a slush of fine crystals within ca. 1 min at rt. NMR assay shortly following the mixing of reagents indicated clean formation of dication **37e** ( $[\text{B}(\text{C}_6\text{F}_5)_4]^-$  salt) along with  $\text{Ph}_3\text{CH}$  byproduct.  $^{11}\text{B}$  NMR (225 MHz,  $\text{CD}_2\text{Cl}_2$ ):  $\delta$  10.6 (br s),  $-16.7$  ppm (s).

#### Quenching of **37e** with 4-(Dimethylamino)pyridine (DMAP)

Every possible effort was made to protect the reaction mixture from exposure to air and moisture. The reaction was set up in dry J. Young NMR tubes under  $\text{N}_2$  atmosphere in a glovebox. The NMR tube was dried in a heating oven at ca. 200  $^\circ\text{C}$  overnight, and the fitted Teflon valve was dried in a desiccator over Drierite.  $\text{Ph}_3\text{C}^+ [\text{B}(\text{C}_6\text{F}_5)_4]^-$  (Strem) was used without further purification. Commercial grade  $d_5$ -PhBr (Cambridge Isotope Laboratories) was not distilled, but rather simply dried with freshly activated molecular sieves in the glovebox. The reaction tube was charged with a mixture of solid **35e** (8.3 mg, 60.1  $\mu\text{mol}$ ) and  $\text{Ph}_3\text{C}^+ [\text{B}(\text{C}_6\text{F}_5)_4]^-$  (55.4 mg, 60.1  $\mu\text{mol}$ ).

The solid mixture was then dissolved by adding anhydrous  $d_5$ -PhBr (1.0 mL) to the tube in one portion at rt. No substantial exotherm was observed, potentially due to the small scale of the reaction. The tube was immediately sealed with the fitted Teflon valve, and then shaken vigorously for ca. 1 min. Formation of dication **37e**  $[\text{B}(\text{C}_6\text{F}_5)_4]^-$  salt was evident from the formation of a fine crystalline precipitate in the reaction tube (*vide supra*, *in situ* generation of **37e**). Addition of excess DMAP (ca. 1.5 equiv) along with ca. 1 mL  $d_5$ -PhBr resulted in dissolution of the crystalline solid.  $^{11}\text{B}$  NMR assay indicated clean formation of boronium salt **39e** ( $\delta$  -14.7 ppm, compared to an independently prepared sample).

### Isolation of **37e**

This procedure describes preparation of crystalline  $[\text{Al}_2\text{Br}_7]^-$  salt of the dication for the X-ray crystallographic study. For other applications such as the quenching experiments,  $[\text{B}(\text{C}_6\text{F}_5)_4]^-$  salts of **37e** were generated *in situ* as described in the next section. Every possible effort was made to protect the reaction mixture from exposure to air and moisture. The reaction was performed under  $\text{N}_2$  atmosphere in a glovebox. Disposable glassware flame-dried at the glass softening temperature was used. Commercial grade  $\text{Al}_2\text{Br}_6$  (Aldrich) and  $\text{Ph}_3\text{CBr}$  were used without further purification. Commercial grade fluorobenzene (Acros) was not distilled, but rather simply dried with freshly activated molecular sieves in the glovebox. The starting NHC borane **35e** was prepared as described above, crystallized from hexanes/ $\text{CHCl}_3$ , and dried in high vacuum before transferring into the glovebox. In a dry 4 mL scintillation vial a mixture of solid  $\text{Al}_2\text{Br}_6$  (96.0 mg, 0.180 mmol) and  $\text{Ph}_3\text{CBr}$  (58.2 mg, 0.180 mmol) was dissolved in 1 mL of dry PhF at rt. No substantial exotherm was observed, potentially due to the small scale

of the reaction. The resulting intensively colored red-orange solution was allowed to stand at rt for 20 min, and then it was carefully layered with a solution of **35e** (24.8 mg, 0.180 mmol) in 0.5 mL of dry PhF. On standing overnight at rt in the sealed vial the reaction mixture developed a substantial amount of X-ray quality crystalline material. The quality of the crystals was found to deteriorate quickly with time, prompting immediate crystallographic analysis as soon as the sufficient crystal size is reached. X-ray crystallographic study (Appendix A) confirmed the proposed dicationic structure of **37e**.

### Generation of Dication **44a**

Every possible effort was made to protect the reaction mixture from exposure to air and moisture. The reaction was set up in a dry J. Young NMR tube under N<sub>2</sub> atmosphere in a glovebox. The NMR tube was dried in a heating oven at ca. 200 °C overnight, and the fitted Teflon valve was dried in a dessicator over Drierite. Commercial grade Me<sub>3</sub>N–BH<sub>3</sub> (**23a**) (Aldrich) was used without further purification. Commercial grade *d*<sub>5</sub>-PhBr (Cambridge Isotope Laboratories) was not distilled, but rather simply dried with freshly activated molecular sieves in the glovebox. The reaction tube was charged with a mixture of solid **23a** (3.4 mg, 48.0 μmol) and Ph<sub>3</sub>C<sup>+</sup> [B(C<sub>6</sub>F<sub>5</sub>)<sub>4</sub>]<sup>-</sup> (44.3 mg, 48.0 μmol). The solid mixture was then dissolved by adding 0.6 mL of anhydrous *d*<sub>5</sub>-PhBr to the tube in one portion at rt. No substantial exotherm was observed, potentially due to the small scale of the reaction. The tube was immediately sealed with the fitted Teflon valve, and then shaken vigorously for ca. 1 min. After 2.5–3 h at rt a ca. 3:1 ratio of **24a:44a** was reached as evidenced by <sup>11</sup>B NMR (peaks at δ -0.4 and +12.9 ppm, respectively). At this point only Ph<sub>3</sub>CH, unreacted Ph<sub>3</sub>C<sup>+</sup>, **24a** and **44a** were

present in the reaction mixture according to  $^1\text{H}$  NMR data. After 24h following mixing the reagents the molar ratio of 1:2.4 (**24a:44a**) was reached. At this point a minor peak (<5% of the combined intensity of the peaks assigned as **44a** and **24a**) of an unidentified product at  $\delta$  +4.8 ppm was also apparent in  $^{11}\text{B}$  NMR. The spectral data summarized below are for the dication of **44a** only. The signals corresponding to  $\text{Ph}_3\text{CH}$ ,  $\text{Ph}_3\text{C}^+$ , **24a** and  $[\text{B}(\text{C}_6\text{F}_5)_4]^-$  counterion are omitted.

$^1\text{H}$  NMR (700 MHz,  $d_5$ -PhBr):  $\delta$  3.6-2.7 (br m, 2H), 2.08 ppm (s, 9H).  $^{11}\text{B}$  NMR (225 MHz,  $d_5$ -PhBr):  $\delta$  12.9 ppm (unres m).  $^{13}\text{C}$  NMR (176 MHz,  $d_5$ -PhBr):  $\delta$  50.3 ppm.

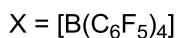
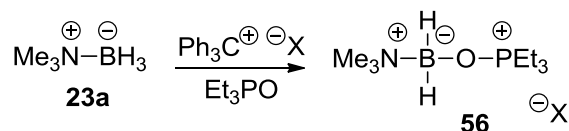
### Quenching Dication **44a** with Trimethylamine Borane (**23a**)

Every possible effort was made to protect the reaction mixture from exposure to air and moisture. The reaction was set up in a dry J. Young NMR tube under  $\text{N}_2$  atmosphere in a glovebox. The NMR tube was dried in a heating oven at ca. 200 °C overnight, and the fitted Teflon valve was dried in a dessicator over Drierite. Commercial grade  $\text{Me}_3\text{N}-\text{BH}_3$  (**23a**) (Aldrich) was used without further purification. Commercial grade  $d_5$ -PhBr (Cambridge Isotope Laboratories) was not distilled, but rather simply dried with freshly activated molecular sieves in the glovebox. The reaction tube was charged with a mixture of solid **23a** (7.4 mg, 0.102 mmol) and  $\text{Ph}_3\text{C}^+ [\text{B}(\text{C}_6\text{F}_5)_4]^-$  (93.9 mg, 0.102 mmol). The solid mixture was then dissolved by adding 0.6 mL of anhydrous  $d_5$ -PhBr to the tube in one portion at rt. No substantial exotherm was observed, potentially due to the small scale of the reaction. The tube was immediately sealed with the fitted Teflon valve, and then shaken vigorously for ca. 1 min. After 2 h at rt ca. 3:1 ratio of **24a:44a** was reached as evidenced by  $^{11}\text{B}$  NMR (peaks at  $\delta$  -0.4 and +12.9 ppm, respectively). At this point only  $\text{Ph}_3\text{CH}$ , unreacted  $\text{Ph}_3\text{C}^+$ , **24a** and **44a** were

present in the reaction mixture according to  $^1\text{H}$  NMR data. The reaction tube was opened in the glovebox, and solid **23a** (12.5 mg, 0.171 mmol) was added in one portion. The reaction tube was immediately sealed, and then shaken vigorously for ca. 1 min. According to the high quality  $^1\text{H}$  and  $^{11}\text{B}$  NMR spectra acquired shortly after the addition of **23a**, the only species present in the reaction mixture at that time were  $\text{Ph}_3\text{CH}$ , excess **23a** and **24a** in a ca. 1:1.5 molar ratio, as well as  $[\text{B}(\text{C}_6\text{F}_5)_4]^-$  counterion. No other signals were detected.

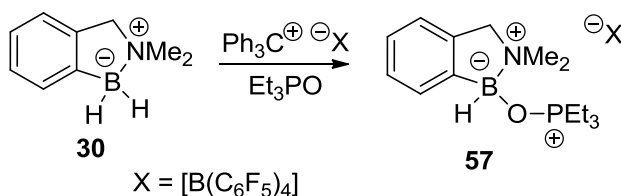
### **Attempted Assessment of Lewis Acidity of Boreniums 25a and 32 by $^{31}\text{P}$ NMR Chemical Shifts of Their Complexes with $\text{Et}_3\text{PO}$ . Boronium Cations 56 and 57**

The following experiments serve to illustrate some of the shortcomings of estimating Lewis acidity of borocations from the NMR properties of their  $\text{Et}_3\text{PO}$  adducts. As can be concluded from the spectroscopic data presented below,  $^{31}\text{P}$  chemical shifts of the two complexes match despite the substantial difference in the stabilization of boreniums **25a** and **32**. Every possible effort was made to protect the reaction mixtures from exposure to air and moisture. The reactions were performed under  $\text{N}_2$  atmosphere in a glovebox. Disposable glassware flame-dried at the glass softening temperature was used. Commercial grade  $\text{Ph}_3\text{C}^+ [\text{B}(\text{C}_6\text{F}_5)_4]^-$  (Strem),  $\text{Me}_3\text{N}-\text{BH}_3$  (**23a**) (Aldrich) and  $\text{Et}_3\text{PO}$  were used without further purification. Cyclic amine borane **30** was prepared as described in Chapter 2 and crystallized from hexanes. Commercial grade fluorobenzene (Acros) was not distilled, but rather simply dried with freshly activated molecular sieves in the glovebox.



*Et*<sub>3</sub>*PO* adduct of **25a** (**56**). A dry 4 mL scintillation vial was charged with a mixture of solid **23a** (7.3 mg, 0.100 mmol), Et<sub>3</sub>PO (13.4 mg, 0.100 mmol) and Ph<sub>3</sub>C<sup>+</sup> [B(C<sub>6</sub>F<sub>5</sub>)<sub>4</sub>]<sup>-</sup> (92.2 mg, 0.100 mmol). The solid mixture was then dissolved by adding 1 mL of dry PhF at rt. The characteristic color of Ph<sub>3</sub>C<sup>+</sup> vanished almost immediately. No substantial exotherm was observed, potentially due to the small scale of the reaction. After a few minutes at rt the solution was diluted with dry hexanes (3 mL), causing precipitation of an oil. The top layer containing triphenylmethane was removed and discarded, and the bottom layer was washed with 2x1 mL of hexanes, which induced crystallization. Following decantation of the solvent, the brownish powder of the product was dried in the glovebox. Yield was not determined.

<sup>1</sup>H NMR (400 MHz, CD<sub>2</sub>Cl<sub>2</sub>): δ 2.9-1.6 (br m, 2H), 2.58 (s, 9H), 2.09 (dq, J = 12.0, 7.7 Hz, 6H), 1.25 ppm (dt, J = 18.4, 7.7 Hz, 9H). <sup>11</sup>B NMR (128 MHz, CD<sub>2</sub>Cl<sub>2</sub>): δ 1.5 (t, J = 115 Hz), -16.7 ppm (s). <sup>13</sup>C NMR (101 MHz, CD<sub>2</sub>Cl<sub>2</sub>): δ 149.7-146.3 (m), 140.0-136.4 (m), 138.0-134.5 (m), 125.5-122.0 (br m), 49.1, 16.1 (d, J = 64 Hz), 4.7 ppm (d, J = 4.7 Hz). <sup>19</sup>F NMR (377 MHz, CD<sub>2</sub>Cl<sub>2</sub>): δ -133.2 (m), -163.7 (t, J = 20.4 Hz), -167.6 ppm (m). <sup>31</sup>P NMR (162 MHz, CD<sub>2</sub>Cl<sub>2</sub>): δ 85.7 ppm.



*Et<sub>3</sub>PO adduct of 32. (57)* The same procedure was followed to prepare Et<sub>3</sub>PO adduct of **32**. Instead of Me<sub>3</sub>N–BH<sub>3</sub> (**23a**), cyclic amine borane **30** (14.7 mg, 0.100 mmol) was used. Yield was not determined.

<sup>1</sup>H NMR (400 MHz, CD<sub>2</sub>Cl<sub>2</sub>): δ 7.44-7.39 (m, 1H), 7.35-7.26 (m, 2H), 7.23-7.18 (m, 1H), 4.32 (d, J = 14.0 Hz, 1H), 4.03 (d, J = 14.0 Hz, 1H), 3.9-2.5 (br m, 1H), 2.76 (s, 3H), 2.65 (s, 3H), 2.07 (dq, J = 12.0, 7.7 Hz, 6H), 1.16 ppm (dt, J = 18.6, 7.7 Hz, 9H). <sup>11</sup>B NMR (128 MHz, CD<sub>2</sub>Cl<sub>2</sub>): δ 6.5 (d, J = 105 Hz), -16.7 ppm (s). <sup>13</sup>C NMR (126 MHz, CD<sub>2</sub>Cl<sub>2</sub>): δ 149.6-146.6 (m), 144.6-142.6 (br m), 139.9, 139.5-136.7 (m), 137.7-134.8 (m), 130.0, 128.7, 128.0, 125.0-122.6 (br m), 123.2, 67.5, 49.0, 45.4, 16.8 (d, J = 64 Hz), 4.7 ppm (unres d). <sup>19</sup>F NMR (377 MHz, CD<sub>2</sub>Cl<sub>2</sub>): δ -133.1 (m), -163.7 (t, J = 20.4 Hz), -167.6 ppm (m). <sup>31</sup>P NMR (162 MHz, CD<sub>2</sub>Cl<sub>2</sub>): δ 85.7 ppm.



## Chapter 1 Bibliography

1. Dilthey, W.; Eduardoff, F.; Schumacher, F. J. "Ueber Siliconium-, Boronium- und Titanoniumsalze." *Liebigs Ann. Chem.* **1906**, 344, 300.
2. Kölle, P.; Nöth, H. "The Chemistry of Borinium and Borenium Ions." *Chem. Rev.* **1985**, 85, 399.
3. Olah, G.; Klumpp, D. A. *Superelectrophiles and their chemistry*; Wiley-Interscience: Hoboken N.J., 2008.
4. DePuy, C. H.; Gareyev, R.; Hankin, J.; Davico, G. E.; Krempp, M.; Damrauer, R. "The Gas Phase Ion Chemistry of  $\text{BH}_2^+$ ." *J. Am. Chem. Soc.* **1998**, 120, 5086.
5. Prokofjevs, A.; Kampf, J. W.; Vedejs, E. "A Boronium Ion with Exceptional Electrophilicity." *Angew. Chem. Int. Ed.* **2011**, 50, 2098.
6. (a) Piers, W. E.; Bourke, S. C.; Conroy, K. D. "Borinium, Borenium, and Boronium Ions: Synthesis, Reactivity, and Applications." *Angew. Chem. Int. Ed.* **2005**, 44, 5016. (b) De Vries, T. S.; Prokofjevs, A.; Vedejs, E. "Cationic Tricoordinate Boron Intermediates: Borenium Chemistry from the Organic Perspective." *Chem. Rev.* **2012**, 112, 4246.
7. (a) Wiberg, E.; Schuster, K. "Zur Kenntnis der Verbindungsreihe  $\text{BCl}_{3-n}[\text{N}(\text{CH}_3)_2]_n$  (Über dimethylamino-substituierte Borchloride)." *Z. Anorg. Allg. Chem.* **1933**, 213, 77. (b) Wiberg, E.; Schuster, K. "Über zwei physikalisch und chemisch verschiedene Verbindungen der Zusammensetzung  $\text{BCl}_2 \cdot \text{N}(\text{CH}_3)_2$ ." *Z. Anorg. Allg. Chem.* **1933**, 213, 89.
8. Ryschkewitsch, G. E.; Wiggins, J. W. "A Trigonal Boron Cation." *J. Am. Chem. Soc.* **1970**, 92, 1790.
9. Nöth, H.; Wrackmeyer, B. *Nuclear Magnetic Resonance Spectroscopy of Boron Compounds*; Springer: Berlin, 1978.
10. Narula, C. K.; Nöth, H. "Preparation and Characterization of Salts Containing Cations of Tricoordinate Boron." *Inorg. Chem.* **1984**, 23, 4147.
11. Nöth, H.; Fritz, P. "Beiträge zur Chemie des Bors. XX. Zur Kenntnis von Alkylbis(dimethylamino)-boranen." *Z. Anorg. Allg. Chem.* **1963**, 322, 297.
12. Corey, E. J. "Enantioselective Catalysis Based on Cationic Oxazaborolidines." *Angew. Chem. Int. Ed.* **2009**, 48, 2100.

13. Ryu, D. H.; Corey, E. J. "Triflimide Activation of a Chiral Oxazaborolidine Leads to a More General Catalytic System for Enantioselective Diels–Alder Addition." *J. Am. Chem. Soc.* **2003**, *125*, 6388.
14. For a recent review see: Staubitz, A.; Robertson, A. P. M.; Sloan, M. E.; Manners, I. "Amine- and Phosphine-Borane Adducts: New Interest in Old Molecules." *Chem. Rev.* **2010**, *110*, 4023.
15. DeVries, T. S. Ph.D. Thesis, University of Michigan, Ann Arbor, MI, 2008.
16. Wirth, A.; Moers, O.; Blaschette, A.; Jones, P. G. "Die ersten Bor(III)-di(organosulfonyl)amide: Ein neuartiger B(OS)<sub>2</sub>N-Sechsring und zwei Aminoboran-Strukturen mit langen B–N-Bindungen." *Z. Anorg. Allg. Chem.* **1998**, *624*, 991.
17. Simchen, G.; Jonas, S. "Hochreaktive Trialkylsilylierungsreagentien aus Bis(trifluormethansulfonyl)imid – Silylierung von funktionellen Gruppen, alkinen und reaktiven Aromaten." *J. Prakt. Chem.* **1998**, *340*, 506.
18. Kameda, M.; Kodama, G. "Synthesis of the Tris(trimethylphosphine)tetrahydrotriboron(1+) Cation." *Inorg. Chem.* **1997**, *36*, 4369.
19. Aldridge, S.; Downs, A. J.; Tang, C. Y.; Parsons, S.; Clarke, M. C.; Johnstone, R. D. L.; Robertson, H. E.; Rankin, D. W. H.; Wann, D. A. "Structures and Aggregation of the Methylamine–Borane Molecules, Me<sub>n</sub>H<sub>3–n</sub>N·BH<sub>3</sub> (n = 1–3), Studied by X-ray Diffraction, Gas-Phase Electron Diffraction, and Quantum Chemical Calculations." *J. Am. Chem. Soc.* **2009**, *131*, 2231.
20. Dureen, M. A.; Lough, A.; Gilbert, T. M.; Stephan, D. W. "B–H Activation by Frustrated Lewis Pairs: Borenium or Boryl Phosponium Cation?" *Chem. Commun.* **2008**, 4303.
21. Vedejs, E.; Nguyen, T.; Powell, D. R.; Schrimpf, M. R. "Generation of Reactive Borenium Ions in the 2,3-Benzazaborolidine Series." *Chem. Commun.* **1996**, 2721.
22. Inés, B.; Patil, M.; Carreras, J.; Goddard, R.; Thiel, W.; Alcarazo, M. "Synthesis, Structure, and Reactivity of a Dihydrido Borenium Cation." *Angew. Chem. Int. Ed.* **2011**, *50*, 8400.
23. Our work on the electrophilic activation of NHC–BH<sub>3</sub> complexes was initiated following a private communication from Curran and Solovyev suggesting that NHC–BH<sub>3</sub> complexes react with Al<sub>2</sub>Cl<sub>6</sub> to form unidentified cationic boron species characterized by a signal with an unusual chemical shift of δ <sup>11</sup>B +12 ppm. See: Solovyev, A. Ph.D. Thesis, University of Pittsburgh, Pittsburgh, PA, 2012.
24. Makhlof Brahmi, M.; Monot, J.; Desage-El Murr, M.; Curran, D. P.; Fensterbank, L.; Lacôte, E.; Malacria, M. "Preparation of NHC Borane

- Complexes by Lewis Base Exchange with Amine- and Phosphine-Boranes.” *J. Org. Chem.* **2010**, *75*, 6983.
25. Adolf, A.; Vogel, U.; Zabel, M.; Timoshkin, A. Y.; Scheer, M. “N-Heterocyclic Carbenes in Lewis Acid/Base Stabilised Phosphanylboranes.” *Eur. J. Inorg. Chem.* **2008**, 3482.
  26. Wehmschulte, R. J.; Diaz, A. A.; Khan, M. A. “Unsymmetrical 9-Borafluorenes via Low-Temperature C–H Activation of m-Terphenylboranes.” *Organometallics* **2003**, *22*, 83.
  27. Eckensberger, U. D.; Weber, M.; Wildt, J.; Bolte, M.; Lerner, H.-W.; Wagner, M. “Reactivity of [(C<sub>5</sub>Me<sub>5</sub>)Fe(C<sub>5</sub>H<sub>4</sub>BBr<sub>2</sub>)] and [(OC)<sub>3</sub>Mn(C<sub>5</sub>H<sub>4</sub>BBr<sub>2</sub>)] toward Et<sub>3</sub>SiH: Facile Access to [(OC)<sub>3</sub>Mn(C<sub>5</sub>H<sub>4</sub>BH<sub>2</sub>)]<sub>2</sub> and to Boron-Bridged Dinuclear Organometallics.” *Organometallics* **2010**, *29*, 5301.
  28. Hedberg, K.; Shomaker, V. “A Reinvestigation of the Structures of Diborane and Ethane by Electron Diffraction.” *J. Am. Chem. Soc.* **1951**, *73*, 1482.
  29. (a) Shoji, Y.; Matsuo, T.; Hashizume, D.; Fueno, H.; Tanaka, K.; Tamao, K. “A Stable Doubly Hydrogen-Bridged Butterfly-Shaped Diborane(4) Compound.” *J. Am. Chem. Soc.* **2010**, *132*, 8258. (b) Shoji, Y.; Matsuo, T.; Hashizume, D.; Gutmann, M. J.; Fueno, H.; Tanaka, K.; Tamao, K. “Boron–Boron  $\sigma$ -Bond Formation by Two-Electron Reduction of a H-Bridged Dimer of Monoborane.” *J. Am. Chem. Soc.* **2011**, *133*, 11058.
  30. (a) Kuhn, N.; Kuhn, A.; Lewandowski, J.; Speis, M. “1,3,2-Diazaborinium-Verbindungen — neue Heteroaren-Kationen des Bors.” *Chem. Ber.* **1991**, *124*, 2197. (b) Qian, B.; Baek, S. W.; Smith, M. R. III. “Synthesis, Structure and Reactivity of  $\beta$ -Diketimate Boron(III) Complexes.” *Polyhedron* **1999**, *18*, 2405. (c) Cowley, A. H.; Lu, Z.; Jones, J. N.; Moore, J. A. “Synthesis and Structure of a Boron Cation Supported by a  $\beta$ -Diketimate Ligand.” *J. Organomet. Chem.* **2004**, *689*, 2562.
  31. (a) Bonnier, C.; Piers, W. E.; Parvez, M.; Sorensen, T. S. “Borenium Cations Derived from BODIPY Dyes.” *Chem. Commun.* **2008**, 4593. (b) Bonnier, C.; Piers, W. E.; Parvez, M. “Isomeric Dipyrrinato and Dipyrrromethanato Boranes.” *Organometallics* **2011**, *30*, 1067.
  32. Del Grosso, A.; Pritchard, R. G.; Muryn, C. A.; Ingleson, M. J. “Chelate Restrained Boron Cations for Intermolecular Electrophilic Arene Borylation.” *Organometallics* **2010**, *29*, 241.
  33. (a) Gilbert, T. M. “Tests of the MP2 Model and Various DFT Models in Predicting the Structures and B–N Bond Dissociation Energies of Amine–Boranes (X<sub>3</sub>C)<sub>m</sub>H<sub>3–m</sub>B–N(CH<sub>3</sub>)<sub>n</sub>H<sub>3–n</sub> (X = H, F; m = 0–3; n = 0–3): Poor Performance of the B3LYP Approach for Dative B–N Bonds.” *J. Phys. Chem. A* **2004**, *108*, 2550. (b) Plumley, J. A.; Evanseck, J. D. “Hybrid Meta-Generalized

- Gradient Functional Modeling of Boron–Nitrogen Coordinate Covalent Bonds.” *J. Chem. Theory Comput.* **2008**, *4*, 1249. (c) Janesko, B. G. “Using Nonempirical Semilocal Density Functionals and Empirical Dispersion Corrections to Model Dative Bonding in Substituted Boranes.” *J. Chem. Theory Comput.* **2010**, *6*, 1825.
34. Brown, H. C.; Bartholomay, H.; Taylor, M. D. “Acid-Base Studies in Gaseous Systems. II. The Anomalous Base Strength of the Methylamines; A New Manifestation of Steric Strain.” *J. Am. Chem. Soc.* **1944**, *66*, 435.
  35. Zhao, Y.; Truhlar, D. G. “The M06 Suite of Density Functionals for Main Group Thermochemistry, Thermochemical Kinetics, Noncovalent Interactions, Excited States, and Transition Elements: Two New Functionals and Systematic Testing of Four M06-Class Functionals and 12 Other Functionals.” *Theor. Chem. Acc.* **2008**, *120*, 215.
  36. Foresman, J. B.; Frisch, Æ. *Exploring Chemistry with Electronic Structure Methods*; Gaussian, Inc.: Pittsburgh, P.A., 1996.
  37. Barnes, E. C.; Petersson, G. A.; Montgomery, J. A. Jr.; Frisch, M. J.; Martin, J. M. L. “Unrestricted Coupled Cluster and Brueckner Doubles Variations of W1 Theory.” *J. Chem. Theory Comput.* **2009**, *5*, 2687.
  38. Gaussian 09, Revision A.02. M. J. Frisch, G. W. Trucks, H. B. Schlegel, G. E. Scuseria, M. A. Robb, J. R. Cheeseman, G. Scalmani, V. Barone, B. Mennucci, G. A. Petersson, H. Nakatsuji, M. Caricato, X. Li, H. P. Hratchian, A. F. Izmaylov, J. Bloino, G. Zheng, J. L. Sonnenberg, M. Hada, M. Ehara, K. Toyota, R. Fukuda, J. Hasegawa, M. Ishida, T. Nakajima, Y. Honda, O. Kitao, H. Nakai, T. Vreven, J. A. Montgomery, Jr., J. E. Peralta, F. Ogliaro, M. Bearpark, J. J. Heyd, E. Brothers, K. N. Kudin, V. N. Staroverov, R. Kobayashi, J. Normand, K. Raghavachari, A. Rendell, J. C. Burant, S. S. Iyengar, J. Tomasi, M. Cossi, N. Rega, J. M. Millam, M. Klene, J. E. Knox, J. B. Cross, V. Bakken, C. Adamo, J. Jaramillo, R. Gomperts, R. E. Stratmann, O. Yazyev, A. J. Austin, R. Cammi, C. Pomelli, J. W. Ochterski, R. L. Martin, K. Morokuma, V. G. Zakrzewski, G. A. Voth, P. Salvador, J. J. Dannenberg, S. Dapprich, A. D. Daniels, O. Farkas, J. B. Foresman, J. V. Ortiz, J. Cioslowski, and D. J. Fox, Gaussian, Inc., Wallingford CT, 2009.
  39. Marenich, A. V.; Cramer, C. J.; Truhlar, D. G. “Universal Solvation Model Based on Solute Electron Density and on a Continuum Model of the Solvent Defined by the Bulk Dielectric Constant and Atomic Surface Tensions.” *J. Phys. Chem. B* **2009**, *113*, 6378.
  40. Bachrach, S. M. *Computational Organic Chemistry*; Wiley-Interscience: Hoboken N.J., 2007.
  41. Schneider, W. F.; Narula, C. K.; Nöth, H.; Bursten, B. E. “Structure and Bonding Trends in Two- and Three-Coordinate Boron Cations.” *Inorg. Chem.* **1991**, *30*, 3919.

42. Chiu, C.-W.; Gabbai, F. P. "Diarylboronium Cations: Synthesis, Structure, and Electrochemistry." *Organometallics* **2008**, *27*, 1657.
43. Matsumoto, T.; Gabbai, F. P. "A Boronium Cation Stabilized by an N-Heterocyclic Carbene Ligand." *Organometallics* **2009**, *28*, 4252.
44. Kato, T.; Tham, F. S.; Boyd, P. D. W.; Reed, C. A. "Synthesis and structure of the coordinatively unsaturated boron subphthalocyanine cation, [B(SubPc)]<sup>+</sup>." *Heteroatom Chem.* **2006**, *17*, 209.
45. Harris, R. K.; Becker, E. D.; Cabral de Menezes, S. M.; Goodfellow, R.; Granger, P. "NMR Nomenclature. Nuclear Spin Properties and Conventions for Chemical Shifts." *Pure Appl. Chem.* **2001**, *73*, 1795.
46. DeVries, T. S.; Vedejs, E. "Electrophilic Activation of Lewis Base Complexes of Borane with Trityl Tetrakis(pentafluorophenyl)borate." *Organometallics* **2007**, *26*, 3079.

## Chapter 2

### Electrophilic Borylation and Related Reactions of B–H Borenium Cations

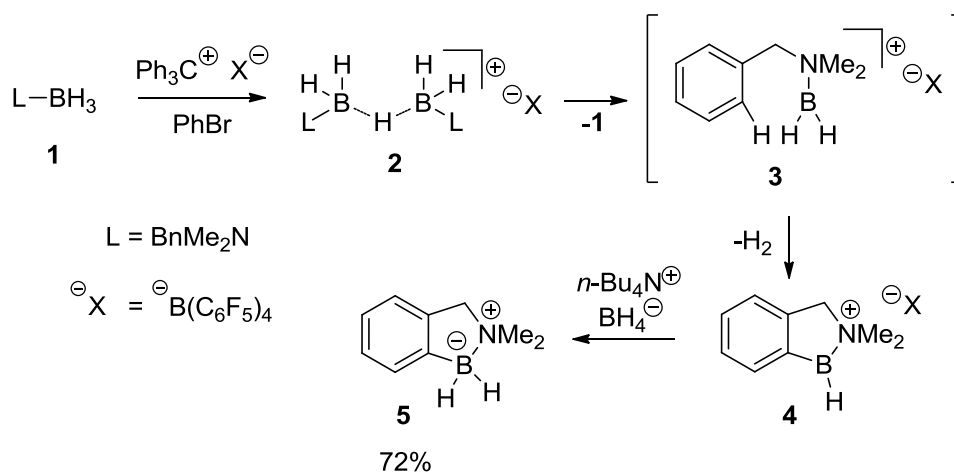
#### Introduction—C–H Borylation by Electrophilic Boron Complexes

Tricoordinate boron inserts into C–H bonds upon heating.<sup>1-5</sup> In the first report, Hurd studied the reaction of B<sub>2</sub>H<sub>6</sub> with several substrates including benzene (100 °C) and methane (180 °C), and found evidence for the formation of phenylboron compounds and, indirectly, of methylboron species, respectively.<sup>1</sup> Related intramolecular C–H insertion reactions were subsequently identified,<sup>2,3</sup> and were explored in depth by Köster et al.<sup>3</sup> However, typically extreme conditions (ca. 200-300 °C), variable regioselectivity, and substrate limitations may have discouraged further development. According to computational evaluation, the borylation of aliphatic C–H bonds involves a 4-center mechanism.<sup>6,7</sup> Related C–H insertion may also take place in the gas phase reactions of simple alkanes with cationic, dicoordinate boron intermediates (borinium cations) under flowing afterglow conditions.<sup>8</sup>

Some of the relatively facile electrophilic borylations of aromatic substrates by tethered tricoordinate boron species may also follow a C–H insertion pathway. Timothy DeVries in our group previously studied the intramolecular borylation of N,N-dimethylbenzylamine borane (**1**) activated with a stoichiometric amount of Ph<sub>3</sub>C<sup>+</sup> [B(C<sub>6</sub>F<sub>5</sub>)<sub>4</sub>]<sup>−</sup> (Scheme 2-1). The structures of the crucial intermediates **2** and **4** were convincingly established using <sup>11</sup>B and <sup>1</sup>H NMR spectroscopy, and a C–H insertion step

in the hypothetical tricoordinate borenium **3** was proposed to rationalize the formation of the observable cation **4**. Since a full equivalent of the cationic trityl reagent was used, a hydride quench was necessary to convert **4** to the isolable amine borane **5**. The C–B bond forming event was proposed to occur via a concerted insertion mechanism based on the substantial kinetic isotope effect associated with the loss of the aromatic proton, although an electrophilic aromatic substitution mechanism still remains a plausible alternative.<sup>4,5</sup>

**Scheme 2-1.** The Stoichiometric Aromatic Borylation



### Electrophilic Borylations Using Stoichiometric Electrophiles

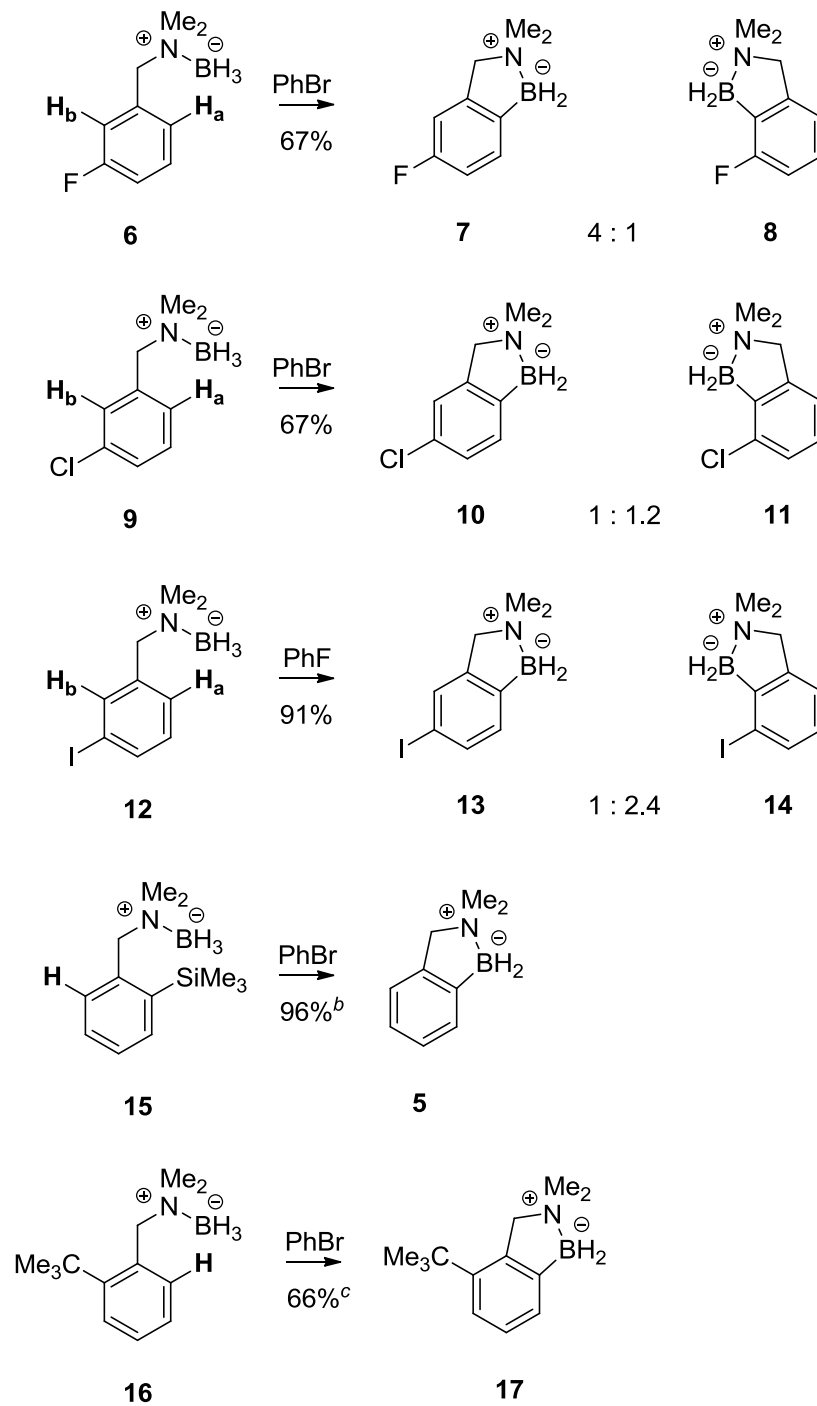
The previous work<sup>4,5</sup> on the directed electrophilic aromatic borylation using stoichiometric trityl activation clearly outlined the possibility of C–H insertions in reactive B–H borenium cations, and we continued this research in order to get a deeper insight into this intriguing transformation. The initial mechanistic proposal considered spontaneous dissociation of the H-bridged cation **2**, followed by a rate-limiting C–H insertion step. The kinetic isotope effect served as good evidence for the rate-limiting C–H borylation, although little experimental evidence was available to support the

spontaneous generation of the primary borenium cation **3** from **2**. We thus proceeded to explore the effects of the variations in the **1**:Ph<sub>3</sub>C<sup>+</sup> stoichiometry on the progress of the reaction by *in situ* NMR experiments. If activated with <50 mol% of Ph<sub>3</sub>C<sup>+</sup> [B(C<sub>6</sub>F<sub>5</sub>)<sub>4</sub>]<sup>-</sup>, the solutions of amine borane **1** showed exclusive formation of the H-bridged cation **2** ( $\delta$  <sup>11</sup>B 0.0 ppm), with no traces of the expected cyclization product **4**. No NMR signals attributable to the borylation product **4** were detected even after multiple days at rt, or after heating to 50 °C for 28 h. Addition of another 0.5 equiv Ph<sub>3</sub>C<sup>+</sup> [B(C<sub>6</sub>F<sub>5</sub>)<sub>4</sub>]<sup>-</sup>, however, induced a rapid aromatic borylation reaction which reached a ca. 50% conversion to **4** ( $\delta$  <sup>11</sup>B 59 ppm) in 25 min at rt. This observation suggests that the additional trityl cation is necessary for efficient progress of the reaction beyond formation of the H-bridged dimer **2**. The room temperature intramolecular borylation of **1** thus demands the use of a full equivalent of the trityl reagent.

Having established the trityl stoichiometry required for borylation reactivity at room temperature we turned our attention to expanding the substrate scope of this reaction (Scheme 2-2). The reactions were performed using 0.9 equiv of Ph<sub>3</sub>C<sup>+</sup> [B(C<sub>6</sub>F<sub>5</sub>)<sub>4</sub>]<sup>-</sup> in either PhBr or PhF solutions at rt. A small excess of the amine borane substrates was used because this stoichiometry leads to a slight improvement in the purity of the crude reaction mixture, as observed empirically in the previous study.<sup>4,5</sup> Since the reactions were performed using roughly stoichiometric trityl activation, a hydride quench with *n*-Bu<sub>4</sub>NBH<sub>4</sub> was essential to generate the isolable cyclic arylboranes.



**Scheme 2-2.** Substrate Scope of the Stoichiometric Borylation<sup>a</sup>



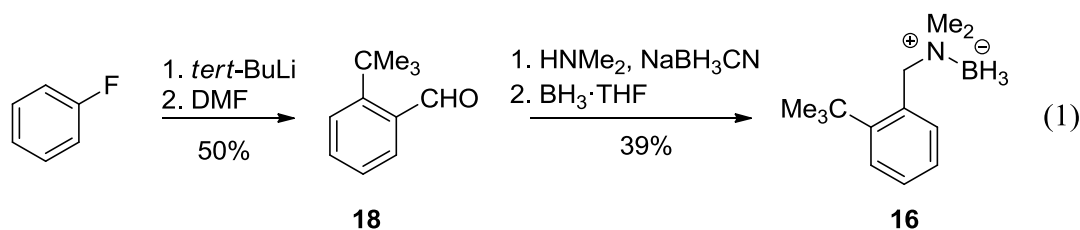
<sup>a</sup>1:0.9 L-BH<sub>3</sub>:Ph<sub>3</sub>C<sup>+</sup> [B(C<sub>6</sub>F<sub>5</sub>)<sub>4</sub>]<sup>-</sup>, rt, 4 h; quenched with excess *n*-Bu<sub>4</sub>NBH<sub>4</sub>. <sup>b</sup>5 min at rt.

<sup>c</sup>2 h at rt

The regiochemistry of the borylation was explored using *m*-halogenated benzylamine substrates **6**, **9** and **12**, and in all cases negligible selectivity was observed. While the fluorinated substrate **6** mostly undergoes borylation at the *para*-position relative to the halogen substituent, borylation at the *ortho*-position is marginally preferred in the iodinated amine borane **12**. The chlorinated substrate **9**, in turn, occupies an intermediate position, leading to roughly equal amounts of the *ortho*- and *para*-borylation products **10** and **11**. As discussed later, however, the borylation selectivity of amine boranes **6**, **9** and **12** can be noticeably improved by using an alternative protocol employing a catalytic electrophile at high temperatures.

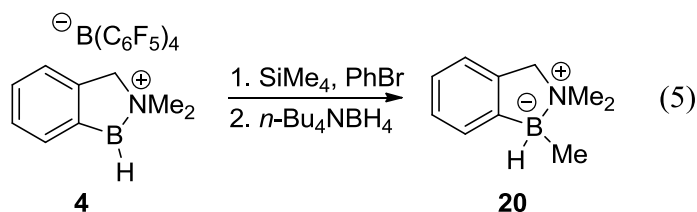
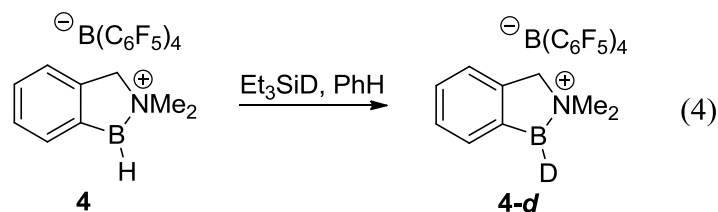
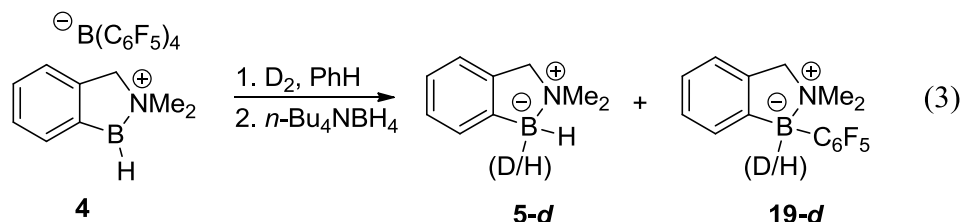
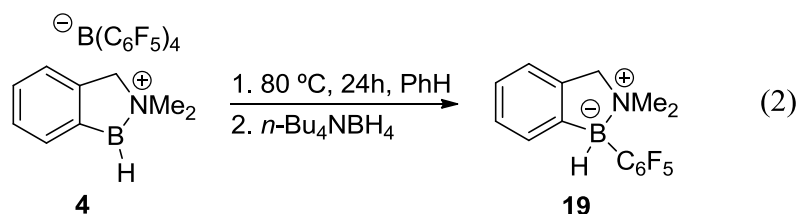
Prior literature indicates that the trimethylsilyl group, as well as the *tert*-butyl group are easily displaced in the electrophilic aromatic substitution,<sup>9</sup> resulting in an *ipso*-substitution pathway. In order to test whether *ipso*-substitution is feasible in the borylation reaction, substrates **15** and **16** were prepared. While the amine core of the silylated substrate **15** was prepared in a straightforward route involving *ortho*-lithiation of *N,N*-dimethylbenzylamine followed by Me<sub>3</sub>SiCl quench,<sup>10</sup> the preparation of the butylated substrate **16** required a more sophisticated approach (eq 1). Inspired by the literature reports on organolithium addition to benzyne intermediates,<sup>11</sup> we envisioned that a convenient aldehyde intermediate **18** can be prepared in one step from fluorobenzene, *tert*-butyllithium (*tert*-BuLi) and *N,N*-dimethylformamide (DMF). Indeed, addition of 4 equiv of *tert*-BuLi to a solution of fluorobenzene in Et<sub>2</sub>O at -78 °C, followed by stirring the reaction mixture at -55 °C for 3h, generated *o*-(*tert*-Bu)C<sub>6</sub>H<sub>4</sub>Li, which was subsequently quenched with DMF to afford **18** after a mildly acidic aqueous workup and chromatographic purification. While the reductive amination of the hindered

aldehyde **18** was somewhat sluggish, the overall sequence of eq 1 allowed a straightforward access to the substituted amine borane **16**.



The performance of **15** and **16** upon trityl activation, however, was noticeably different. Thus, the activation of the silylated substrate **15** resulted in a very rapid formation of the *ipso*-substituted product **5** after a hydride quench. The closely related amine borane **16**, however, underwent a clean cyclization to **17**. No trace of the product arising from loss of the *tert*-butyl group (**5**) was observed in the crude  $^1\text{H}$  NMR spectrum.

The cyclic cation **4** is a representative of the rare B–H borenium class,<sup>4,5,12</sup> and shares a structural analogy with the hypothetical cation **3**, so its reactivity demanded a closer investigation. Since the cyclization of **1** produces minor impurities aside from the desired **4**, a pure sample of **4** was prepared by the alternative route of hydride abstraction from **5** with  $\text{Ph}_3\text{C}^+ [\text{B}(\text{C}_6\text{F}_5)_4]^-$ . The borenium salt **4** was isolated as a pure solid by performing the trityl activation of **5** in anhydrous benzene, which allowed complete removal of the triphenylmethane byproduct. Surprisingly, while not affected by  $\text{CD}_2\text{Cl}_2$  and  $d_5$ -PhBr solvents, solutions of the borenium salt **4** underwent a slow decomposition at rt involving a pentafluorophenyl group abstraction from the counterion. The counterion decomposition was substantially accelerated by heating, which allowed a preparative access to the substituted amine borane **19** (eq 2). Similar dearylation of  $[\text{B}(\text{C}_6\text{F}_5)_4]^-$  by potent cationic Zr and Al electrophiles was reported in the literature.<sup>13</sup>

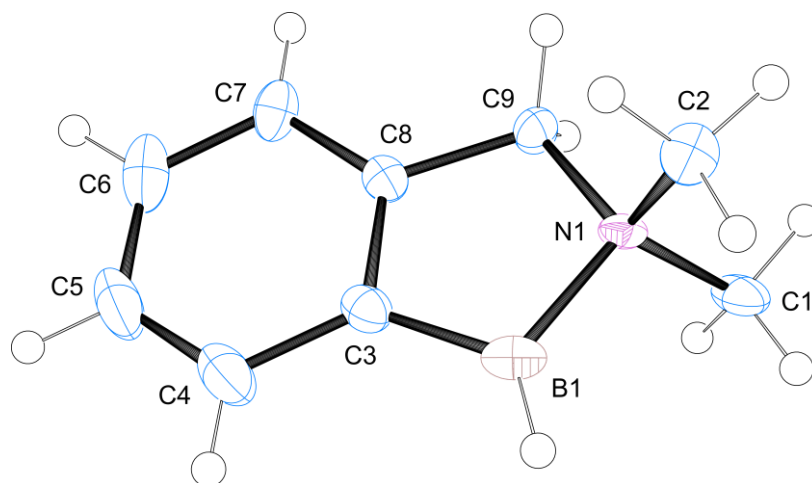


As expected from the C–H borylating reactivity of weakly stabilized B–H boreniums, cation **4** reacts with  $\sigma$ -bond nucleophiles, such as  $\text{D}_2$  gas and silanes. Thus, stirring the suspension of **4** in PhH under  $\text{D}_2$  (ca. 2–3 atm) for 15–30 days at rt followed by quenching the heterogeneous reaction mixture with  $n\text{-Bu}_4\text{NBH}_4$  provided mixtures of **5** and **19** with variable deuterium incorporation (**5-d** and **19-d**, eq 3). Some caution must be used while interpreting the deuterium incorporation results, since the byproduct of the counterion decomposition is the strongly electrophilic  $\text{B}(\text{C}_6\text{F}_5)_3$ , which is a part of the known protocol for molecular  $\text{H}_2$  activation.<sup>14</sup> Additionally, cation **4** inserts into Si–D and Si–C bonds of  $\text{Et}_3\text{SiD}$  (eq 4) and  $\text{Me}_4\text{Si}$  (eq 5), respectively. Thus, stirring the

suspension of **4** in benzene with excess  $\text{Et}_3\text{SiD}$  for 10 min at rt, followed by a hexane wash to remove the silicon reagent, afforded a sample of **4-d** with only 8% residual intensity of the B–H peak in the  $^1\text{H}$  NMR spectrum. The methylated amine borane **20** (eq 5) was first identified among decomposition products of **4** in a  $d_5$ -PhBr solution containing  $\text{Me}_4\text{Si}$  NMR reference. Repeating the experiment in a preparative fashion using large excess of  $\text{Me}_4\text{Si}$  afforded **20** in 31% yield after chromatography.

Finally, X-ray crystallographic analysis of **4** was performed, this time using a salt with the more robust  $[\text{HCB}_{11}\text{Cl}_{11}]^-$  anion (Figure 2-1). The X-ray quality crystals were grown in a glovebox at rt by layering a solution of **4** in  $\text{CH}_2\text{Cl}_2$  with hexanes. Additional details are provided in the experimental section, as well as in Appendix A.

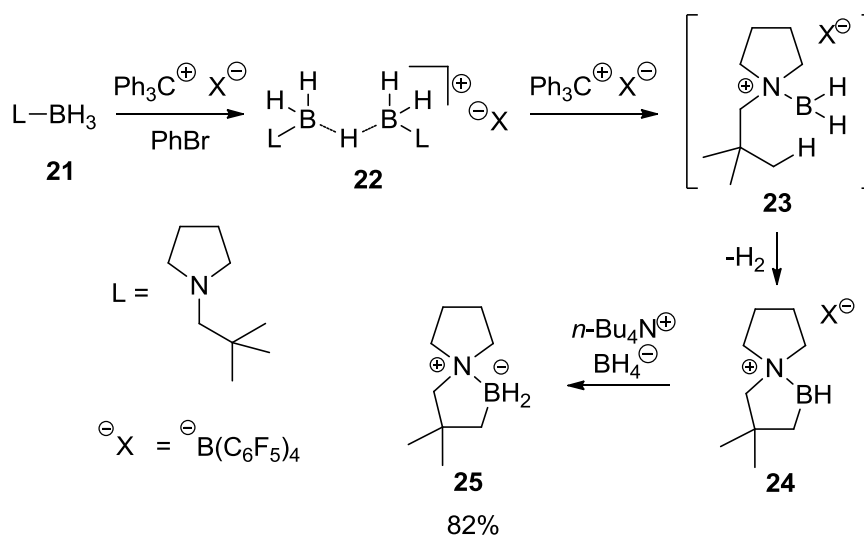
**Figure 2-1.** X-Ray structure of **4** (cation only, 50% probability ellipsoids)



In view of the reactivity of **4** with  $\sigma$ -bond nucleophiles, the possibility of aliphatic C–H borylation seemed plausible. Treating a hindered amine borane complex **21** with 50 mol% of the strong electrophile  $\text{Ph}_3\text{C}^+ [\text{B}(\text{C}_6\text{F}_5)_4]^-$  predictably resulted in formation of an H-bridged cationic boron intermediate **22**,  $\delta^{11}\text{B} = -1.1$  ppm in  $d_5$ -PhBr (Scheme 2-3).<sup>15</sup> Further addition of the electrophilic trityl salt induced rapid formation of a tricoordinate boron species, as evidenced by a broad signal at  $\delta +69.3$  ppm in the  $^{11}\text{B}$  NMR spectrum

within 10 minutes at room temperature.<sup>16</sup> Over the same timescale, the <sup>1</sup>H NMR spectrum showed disappearance of the *tert*-Bu singlet of **22** ( $\delta$  <sup>1</sup>H = 0.86 ppm), while two new singlets appeared ( $\delta$  <sup>1</sup>H = 0.64 and 1.27 ppm; 6:2 integral ratio). Together with the substantial downfield shift of the broad B–H resonance ( $\delta$  <sup>1</sup>H = 4.8 ppm) and liberation of H<sub>2</sub>, these and other spectroscopic data (see experimental section) are consistent with the spirocyclic borenium structure **24**. At no time was the open-chain borenium cation **23** detected. Interestingly, **24** constitutes a rare example of a tricoordinate boron cation lacking stabilizing *n*- or  $\pi$ -donor groups.<sup>16</sup> Additionally, **24** is a representative of the uncommon B–H borenium ion class; only a few such compounds have been reported to date.<sup>4,5,12</sup> Borenium salt **24** was also isolated and characterized in pure form by treating **21** with the trityl reagent, followed by precipitation of the product with hexanes. Single crystals of **24** were grown by layering a CH<sub>2</sub>Cl<sub>2</sub> solution of the borenium salt with hexanes. X-ray crystallography confirmed the proposed connectivity of the cation, although a severe disorder in the crystal prevented reliable determination of the bonding parameters.

### Scheme 2-3. Stoichiometric Aliphatic Borylation

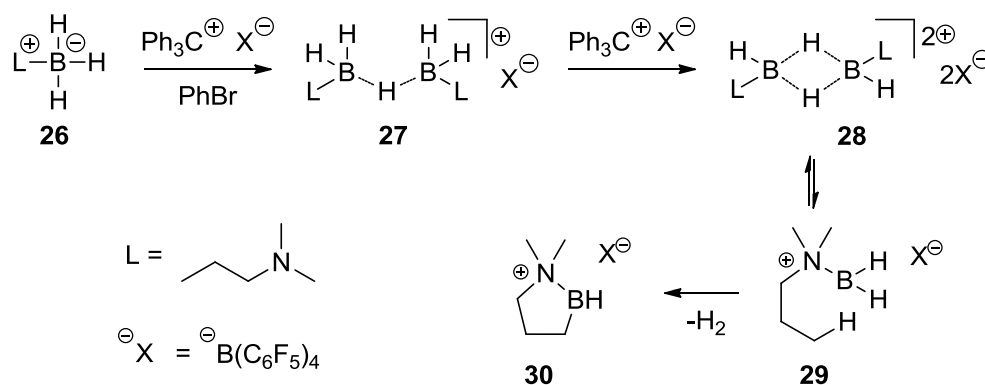


Hydride quench with *n*-Bu<sub>4</sub>NBH<sub>4</sub> converted **24** to the isolable amine borane **25** (82% yield), readily identified by the broad CH<sub>2</sub>B <sup>1</sup>H and <sup>13</sup>C NMR signals ( $\delta$  0.75 ppm and 31 ppm, respectively, in CDCl<sub>3</sub>), and an H-coupled triplet at  $\delta$  -4.2 ppm in the <sup>11</sup>B NMR spectrum.

In contrast to the stoichiometric trityl activation of the sterically hindered amine borane **21**, intramolecular borylation of N,N-dimethylpropanamine borane (**26**) was noticeably less efficient under the same conditions (Scheme 2-4). Thus, essentially no cyclic cation **30** was observed in the reaction mixture by *in situ* <sup>11</sup>B and <sup>1</sup>H NMR even after 2 h at rt. Instead, the major boron species observed besides the complex borate anion were the incomplete activation product **27**, as well as the unprecedented dicationic dimer **28**, tentatively evidenced by the peaks at  $\delta$  <sup>11</sup>B -0.9 ppm and  $\delta$  <sup>11</sup>B +13.2 ppm, respectively, and supported by analogies to be discussed later. While after 48 h at rt the cyclic cation **29** was found to be the dominant species in the reaction mixture, small amounts of **27** and **28** were still observed by <sup>11</sup>B NMR. This behavior contrasts the cyclization of **21**, where exclusive formation of the cyclization product **24** ( $\delta$  <sup>11</sup>B +69.3 ppm) was observed after only 10 min at rt. The difference in the cyclization rates of amine boranes **21** and **26** might simply reflect the difference in the energy barriers associated with the actual C-H insertion step, but the data presented in Chapter 1 suggest an additional possibility. In principle, the observed dissimilarities in the behavior of the activated complexes **21** and **26** might also be caused by the differences in the processes leading to generation of the primary boreniums **23** and **29**, respectively. While multiple factors might be involved, the existence of the primary borenium **29** in the form

of the dicationic dimer **28** may be one of the reasons responsible for the difference in the cyclization rates of **21** and **26**.

**Scheme 2-4.** Stoichiometric Trityl Activation of **26**



The trityl activations of complexes **21** and **26** are reminiscent of the activations of  $\text{Me}_3\text{N-BH}_3$  and  $(i\text{Pr})_2\text{EtN-BH}_3$  presented in Chapter 1. Thus, the stoichiometric trityl activation of the unhindered trimethylamine borane proceeded slowly at rt, leading to buildup of the corresponding dicationic dimer, with relatively little decomposition observed even after 24h at rt. In contrast, activation of the bulky  $(i\text{Pr})_2\text{EtN-BH}_3$  led to formation of the observable primary borenium cation in solution, and very rapid degradation of  $\text{Ph}_3\text{CH}$  and  $[\text{B}(\text{C}_6\text{F}_5)_4]^-$  was observed. Since the most plausible explanation suggests that it is the primary borenium cation that is responsible for the observed borylation and decomposition processes, it is likely that the high reactivity of the hindered amine boranes upon activation is in part due to the instability of the corresponding dicationic dimers.

### Electrophilic Borylations Using Catalytic Electrophiles

The experimental data summarized in the previous section suggest that a stoichiometric amount of the trityl cation is required in order to induce the electrophilic



borylation in **1** (Scheme 2-1) at rt. In accord with the observations presented in Chapter 1, this suggests that the H-bridged monocations **2** apparently are not very efficient sources of the free primary borenium cations at rt. On the other hand, it is possible that the free borenium ion **3** can be generated along with the starting amine borane **1** in the thermal dissociation of **2**. To test this possibility, a solution of N,N-dimethylbenzylamine borane (**1**) in *d*<sub>5</sub>-PhBr was activated with ca. 4 mol% of Ph<sub>3</sub>C<sup>+</sup>[B(C<sub>6</sub>F<sub>5</sub>)<sub>4</sub>]<sup>-</sup>, resulting in partial formation of the H-bridged cation **2** as the sole intermediate detected. Heating the reaction mixture at 120 °C caused rapid disappearance of **2**, and formation of the cyclization product **5** along with H<sub>2</sub> gas, as evidenced by NMR. The reaction was found to be rather slow at 120 °C, reaching ca. 60% conversion after 44 h of heating.

Intrigued by this observation, we attempted to perform the same transformation using a range of other strongly electrophilic catalysts, such as Ph<sub>3</sub>C<sup>+</sup>[*closo*-HCB<sub>11</sub>H<sub>5</sub>Br<sub>6</sub>]<sup>-</sup>, Tf<sub>2</sub>NH, B(C<sub>6</sub>F<sub>5</sub>)<sub>3</sub>, AgNTf<sub>2</sub>, TfOH and Li[B(C<sub>6</sub>F<sub>5</sub>)<sub>4</sub>] (Et<sub>2</sub>O complex). Interestingly, formation of the H-bridged dimer **2** was observed upon treating the solutions of **1** with catalytic amounts of the first three electrophiles (Ph<sub>3</sub>C<sup>+</sup>[*closo*-HB<sub>11</sub>H<sub>5</sub>Br<sub>6</sub>]<sup>-</sup>, Tf<sub>2</sub>NH and B(C<sub>6</sub>F<sub>5</sub>)<sub>3</sub>), and clean formation of the cyclization product **5** was observed in these cases upon heating the reaction mixtures to 120 °C. In contrast, the use of TfOH and Li[B(C<sub>6</sub>F<sub>5</sub>)<sub>4</sub>] catalysts did not produce **2** upon activation, and did not result in borylation upon heating. Formation of colloidal Ag metal prevented a clear conclusion about the nature of the intermediates formed upon treating a solution of **1** with AgNTf<sub>2</sub> at rt, although in this case the high-temperature borylation was also successful. The seeming insensitivity of the borylation reaction to the nature of the electrophilic

catalyst introduced to the reaction mixture suggests that the activated intermediate sustaining the catalytic cycle is a boron species, potentially related to the H-bridged dimer **2**.

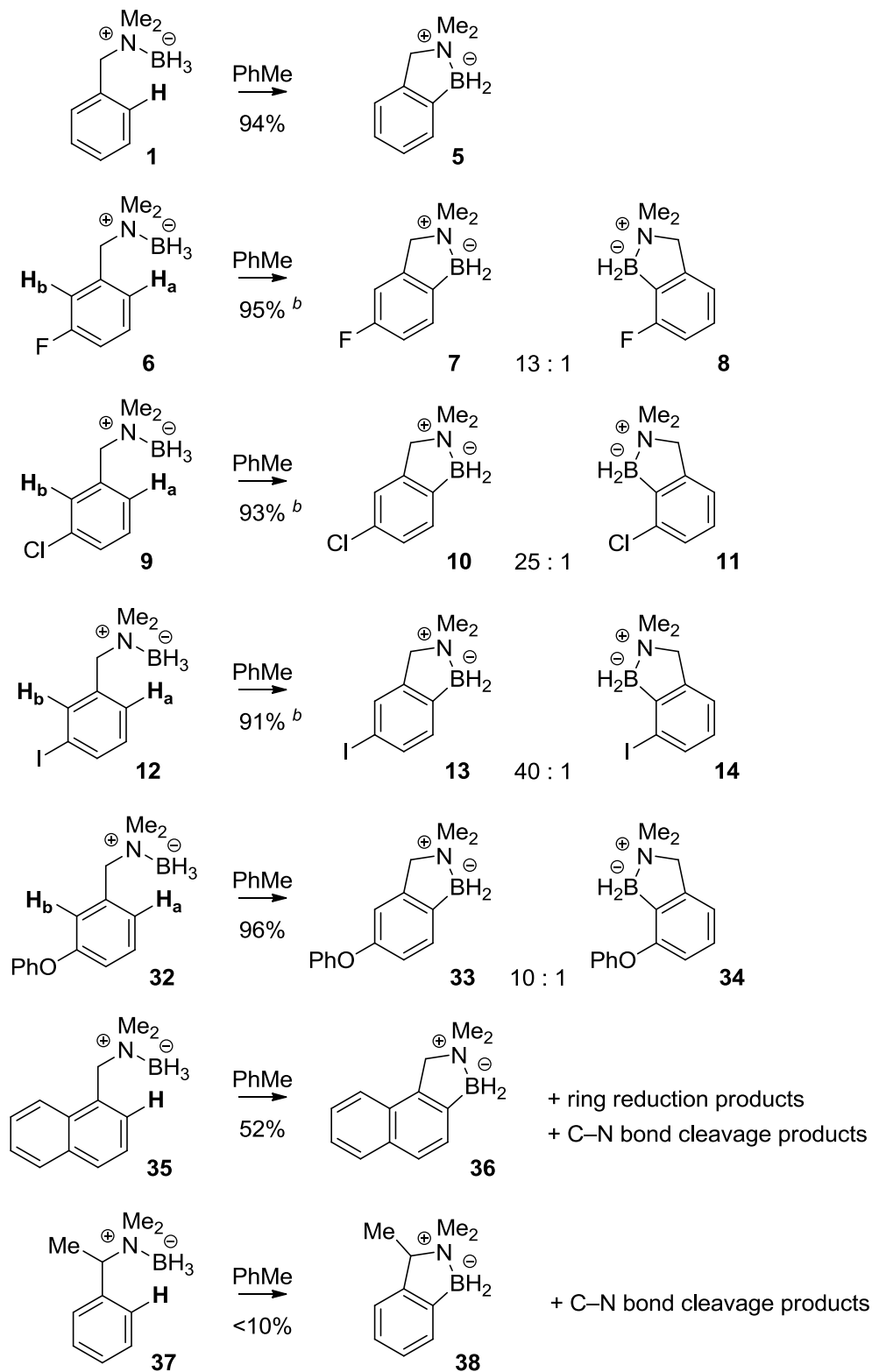
Seeking further improvement of the protocol, Tf<sub>2</sub>NH “hydridophile” was evaluated more thoroughly, this time in *d*<sub>8</sub>-PhMe, which was expected to simplify the product isolation. The composition of the activated intermediates was greatly influenced by the solvent and by the ratio of **1** and Tf<sub>2</sub>NH, as described in more detail for other amine boranes in Chapter 1. Thus, the stoichiometric reaction between **1** and Tf<sub>2</sub>NH afforded the covalent adduct BnMe<sub>2</sub>N–BH<sub>2</sub>–NTf<sub>2</sub> (**31**) as a mixture of N- and O-bound isomers. The same adduct **31** was seen in *d*<sub>8</sub>-PhMe using 5 mol% of Tf<sub>2</sub>NH for activation, but the H-bridged cation **2** was also detected as the activated species in CD<sub>2</sub>Cl<sub>2</sub>. Subsequent events were also influenced by the ratio of Tf<sub>2</sub>NH and N,N-dimethylbenzylamine borane (**1**). Using 5 mol% of Tf<sub>2</sub>NH in toluene, clean catalytic cyclization to **5** and H<sub>2</sub> was observed above 120 °C. In contrast, heating the covalent adduct **31** under the same conditions afforded essentially no cyclization product.

The high stability of the bistriflimide anion paired with good solubility of its derivatives in aromatic solvents allowed developing a simple catalytic procedure that could be used with a range of substrates, both aromatic and aliphatic (Schemes 2-5 and 2-6). The same 5% loading of the catalyst Tf<sub>2</sub>NH was used in all cases, and the reactions were performed in toluene, fluorobenzene or benzene in sealed thick-walled tubes at 160 °C without attempting to define the threshold temperatures for each example. After quenching with *n*-Bu<sub>4</sub>NBH<sub>4</sub> (to slightly increase the reaction yields), simple filtration through silica gel to retain polar bistriflimide-containing byproducts gave clean products

or isomer mixtures. The isomer mixtures were further separated by crystallization or chromatography, and structures of all compounds were assigned by multinuclear NMR spectroscopy and HRMS (see experimental section).

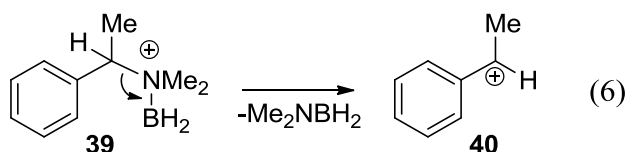
Besides the unsubstituted benzylic amine borane **1**, the catalytic borylation protocol also works well for the substituted analogs, provided that the substituent is sufficiently stable under the reaction conditions. The functional group tolerance is fairly limited due to the highly electrophilic (and, to some extent, reducing) nature of the activated amine borane solution, although the presence of halogen (**6**, **9**, **12**) and 3-PhO (**32**) substituents presented no complications. The borylation regioselectivity in substituted benzylic amine boranes **6**, **9**, **12**, **32** is very good, favoring *p*-borylation relative to the ring substituent in all cases. This selectivity sharply contrasts that observed in the stoichiometric borylations described earlier in this chapter, and will be discussed in more detail later. The observed regioselectivity and functional group tolerance in some cases appears to be complementary to other widely used borylation protocols, namely transition metal-catalyzed borylation,<sup>17</sup> and C–H lithiation followed by Li to B exchange. Thus, the iodinated substrate **12** can be imagined to be a challenging substrate for both approaches due to the high lability of the iodine substituent, while lithiation of 1-(dimethylamino)naphthalene was previously shown to favor the C8 atom of the naphthalene backbone.<sup>18</sup>

**Scheme 2-5.** Substrate Scope of the Catalytic Aromatic Borylation<sup>a</sup>



<sup>a</sup>5 mol% Tf<sub>2</sub>NH, 160 °C, sealed tube, 14 h; quenched with 5-10 mol% *n*-Bu<sub>4</sub>NBH<sub>4</sub>. <sup>b</sup>24h

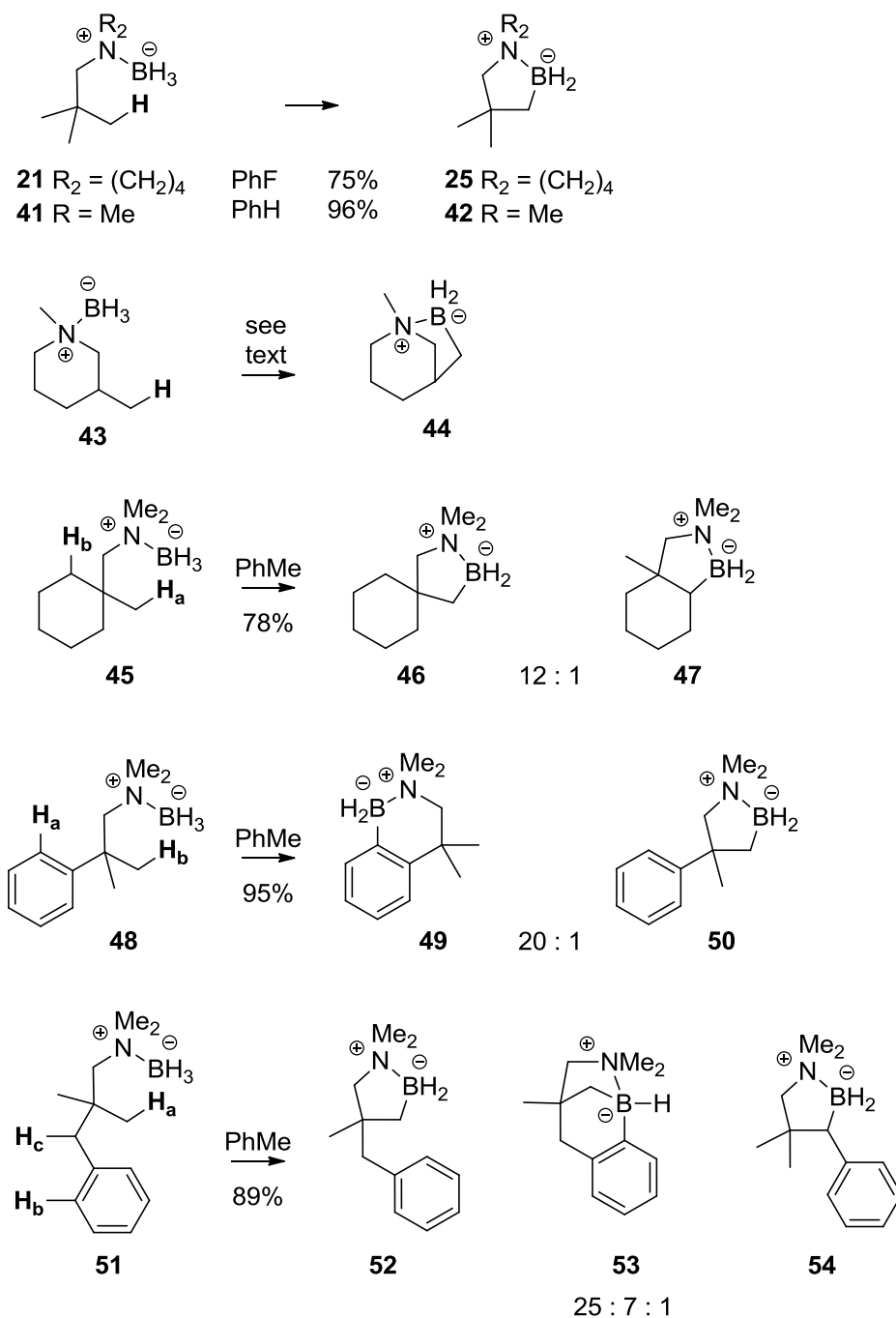
Amine borane **37** presented a more unusual limitation to the substrate scope. Here, apparently, the facile cleavage of the C–N bond in an activated intermediate<sup>5</sup> produced  $\alpha$ -phenethyl cation **40**, which was then quenched by a hydridic B–H, regenerating a reactive boron species (eq 6). The exact species undergoing the C–N bond cleavage is unknown, and eq 6 shows **39** as a plausible candidate for that role, although a wide variety of other activated derivatives of **37** can be reasonably imagined to decompose in the same fashion. Overall, the major reaction pathway for the  $\alpha$ -substituted amine borane **37** thus amounts to decomposition to ethylbenzene and Me<sub>2</sub>NBH<sub>2</sub> dimer. A similar degradation pathway apparently also complicates the cyclization of **35**, since 1-methylnaphthalene byproduct was observed in the reaction mixture by GC-MS. Overall, it appears that the fragmentation interferes most in those cases where a reasonably stable carbocation can be formed upon the C–N bond cleavage.



A range of substrates possessing suitably placed aliphatic C–H bonds was also screened in the same high-temperature catalytic protocol (Scheme 2-6). The intramolecular borylation method is particularly efficient for forming aliphatic C–B bonds next to quaternary centers in hindered amine boranes, furnishing organoboron structures not available via the conventional hydroboration route. Thus, amine boranes **21** and **41** cleanly formed products **25** and **42**, respectively. In contrast, a similar process involving substrate **43** stalled at 20% conversion. It remains to be seen whether the low conversion in this difficult case reflects thermodynamic or kinetic complications in the

catalytic cycle, or whether the unfavorable 1,3-diaxial arrangement of the N–B and C–CH<sub>3</sub> bonds impedes cyclization.

**Scheme 2-6.** Substrate Scope of the Catalytic Aliphatic Borylation<sup>a</sup>



<sup>a</sup>5 mol% Tf<sub>2</sub>NH, 160 °C, sealed tube, 14 h; quenched with 5-10 mol% *n*-Bu<sub>4</sub>NBH<sub>4</sub>.

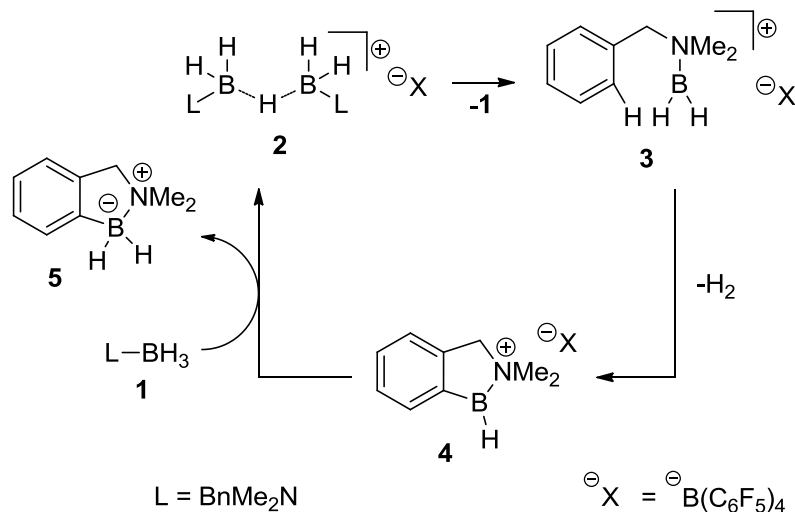
Cyclization of the aliphatic amine borane **45** afforded spirocycle **46** as the major product, revealing the preferred C–H insertion reactivity as methyl > methylene. Due to difficulties in isomer separation, the minor product **47** was characterized as an enriched mixture.

To further address regioselectivity, substrate **48** was tested under the catalytic conditions. The aromatic borylation product **49** was found to predominate, although the minor aliphatic borylation product **50** was also detected.<sup>19</sup> The cyclization of a related substrate **51** was more complex, although the major product **52** was formed by a similar preference for borylation at methyl over methylene C–H as seen with **45**. The minor product **54** also contains a new aliphatic C–B bond, while the unusual tricyclic product **53** contains aryl as well as aliphatic C–B bonds, apparently due to a second borylation event with loss of H<sub>2</sub>. As evidenced by *in situ* NMR spectroscopy between 120-160 °C, the formation of **53** begins only after most of **51** has been converted to **52**, suggesting that the aromatic borylation event leading to **53** is the slower cyclization step in this sequence.

The initial studies on the catalytic borylation were based on the rationale that the dissociation of **2** to the borenium **3** and the amine borane **1** might be possible under the thermal conditions (Scheme 2-7). In this catalytic cycle, the crucial C–H borylation step (**3** to **4**) is expected to be the same as in the stoichiometric experiment. To confirm the feasibility of the hydride transfer step (regeneration of **2**), a solution of **4** was treated with **1**, and the subsequent NMR assay indicated formation of **2** among other reaction products. The only step of the proposed catalytic cycle that lacked a clear precedent was the dissociation of **2** to **3** and **1**, and the success of the catalytic reaction was initially interpreted as an indication for the formation of **3** at a high temperature. While this

mechanism does not include a role for the dimeric dications discussed in the context of stoichiometric borylations, the significance of such species under the catalytic conditions can be expected to be low, since the concentration of **3** available for dimerization in the presence of a stronger  $\sigma$ -donor **1** might be too small.

**Scheme 2-7.** The Catalytic Borylation Mechanism. An Early Proposal



At the present time, however, the real reaction mechanism remains unclear. The most striking difference between the catalytic and stoichiometric borylation processes is in the opposite trends in regioselectivity for the halogenated amine boranes **6**, **9** and **12**. While in the catalytic process the *p*-/*o*-selectivity gradually increases in the F–Cl–I series from 13:1 (**6**) to 40:1 (**12**), in the stoichiometric trityl borylations in the same series the selectivity gradually decreases from 4:1 (**6**) to 1:2.4 (**12**). It is tempting to propose that the differences in the product ratios arise from thermodynamic equilibration under the high-temperature conditions, but so far all indications have suggested that the catalytic borylations are a kinetic process. Thus, the product regioisomer ratios do not change throughout the reaction process, and the isolated borylation products were shown not to undergo equilibration under the reaction conditions.



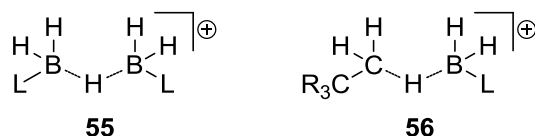
The following experiments were performed to confirm the stability of the products **10** and **11** under the reaction conditions. Each of the isolated isomers was activated with 5 mol% Tf<sub>2</sub>NH in *d*<sub>8</sub>-PhMe, and the resulting solutions were heated at 120 °C. No equilibration of pure **10** or **11** to the isomer mixture was observed, although the catalytic activation of **9** under the same conditions led to a ca. 25:1 mixture of **10** and **11**.

Since it can be argued that the catalytic activation of the products **10** or **11** does not exactly mimic the borylation conditions, a slightly modified set of experiments was also performed. Thus, mixtures of 0.1 equiv of either **10** or **11** with 1 equiv of **1** in toluene were activated with 5 mol% Tf<sub>2</sub>NH, and then heated in sealed tubes at 160 °C. Under the reaction conditions, full conversion of **1** to **5** was observed (after a borohydride quench), although compounds **10** and **11** were recovered unchanged. In a control experiment, 0.1 equiv of **9** and 1 equiv of **1** were used. This time, a mixture of the cyclized products **5**, **10** and **11** was formed, and the ratio of **10** and **11** was found to be the same as in the cyclization of **9** with no **1** present (ca. 25:1 **10**:**11**). This suggests that while under the explored conditions the starting amine borane **9** cyclizes to form a mixture of **10** and **11**, the interconversion of the two isomers does not occur. In this series of experiments, the cyclization of **1** to **5** serves not only to reproduce the actual cyclization conditions, but also as a probe confirming that in a particular experiment such conditions were indeed available.

In view of these observations, the dissociation of **2** to generate the primary borenium **3** appears unlikely, since in this case the selectivity determining step would be the very same C–H insertion process as in the stoichiometric reaction, and both processes

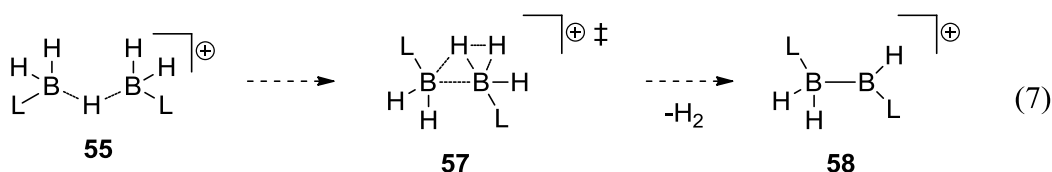
would be expected to provide the same regioselectivity corrected for the difference in the reaction temperatures.

Interestingly, the rate determining step in the catalytic borylation appears to be mostly insensitive to the electronic effects in the substrate, since a competition experiment showed that the cyclization rates of **1** and **32** are essentially equal, despite the presence of the activating 3-phenoxy substituent in the latter. This is consistent with the C–B bond forming event being a concerted C–H insertion step, and thus the possibilities of other insertion mechanisms not involving the primary borenium **3** were explored computationally.



Intriguingly, aside from the dissociation discussed above, there exists another reasonable mechanism by which tricoordinate boron species capable of inserting into C–H bonds might be generated from the H-bridged cations such as **2**. A closer look at the generic 3c2e B–H–B cation **55** reveals that this cation is formally isoelectronic with the alkane borenium complex **56**, which is a logical intermediate in the borenium C–H insertion step. Comparing the structures **55** and **56** reveals that while **56** appears to be pre-organized for a C–H insertion step resulting in formation of a new C–B bond, the isoelectronic structure **55** clearly has potential for undergoing a B–H insertion (**57**, eq 7) leading to formation of a new B–B bond. This insertion can be expected to produce a molecule of H<sub>2</sub> along with the tricoordinate diboron cation **58**. It should be noted here that the insertion of tricoordinate boron hydrides into B–H bonds accompanied by the

loss of H<sub>2</sub> is among the most important reactions in the field of polyhedral boron complexes.<sup>20</sup>

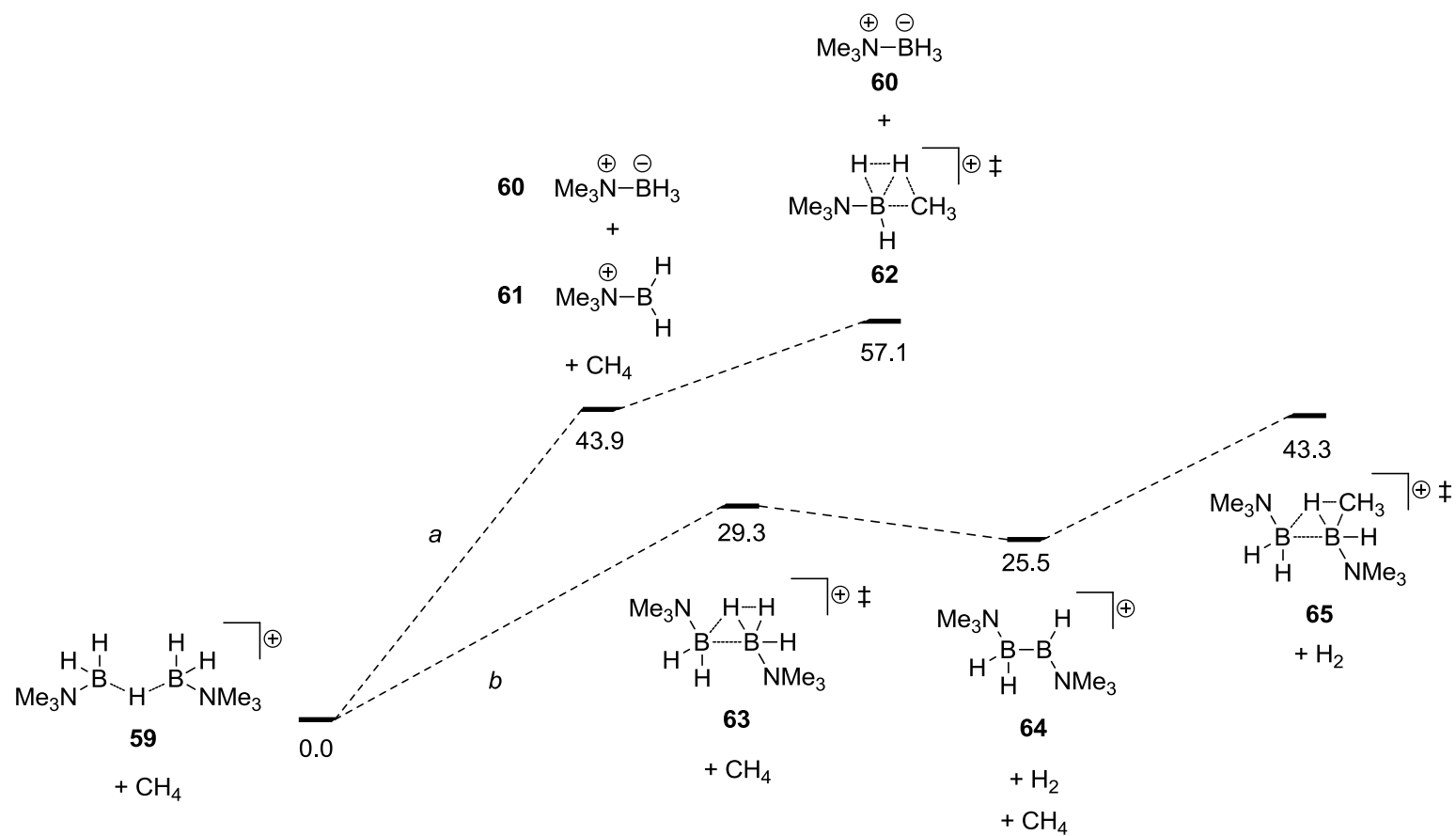


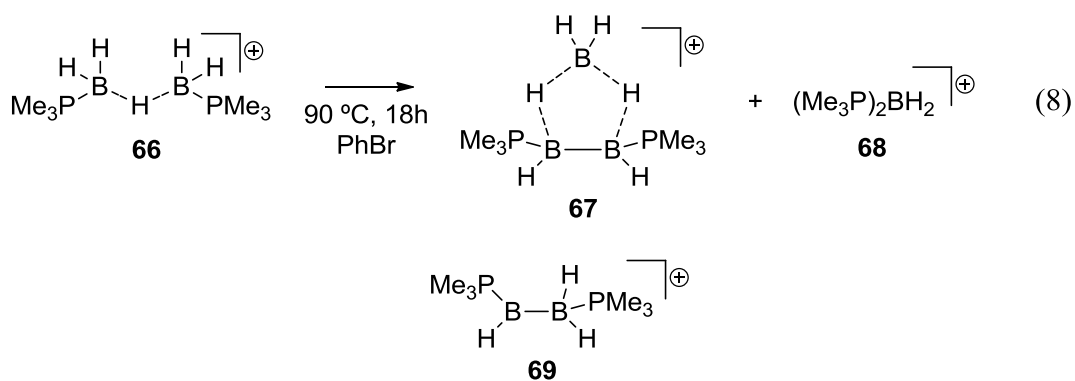
The two possible pathways of the catalytic process were explored using the same M06-2X/6-311++G(3df,2p)//M06-2X/6-31+G(d,p) method as described in Chapter 1. Figure 2-2 summarizes the gas-phase enthalpies (kcal/mol) of selected structures corresponding to the critical points on the potential energy surface. A few structures of no direct significance to the discussion presented below, such as the weak complex between **61** and CH<sub>4</sub>, have been omitted from the scheme. The enthalpies shown in Figure 2-2 were calculated at 298.15 K, using a scaling factor of 0.97 in the thermochemical analysis. To reduce the computational effort, the calculations were performed using simplified models of both the H-bridged cation (**59**), and the aliphatic C–H fragment undergoing borylation (CH<sub>4</sub>). Figure 2-2 shows two hypothetical reaction pathways (*a* and *b*) shown up to the highest energy transition states (**62** and **65**, respectively). In pathway *a*, the initial event is the dissociation of the H-bridged cation **59** to the amine borane **60** and the primary borenium **61**, which is calculated to be enthalpically unfavorable by 43.9 kcal/mol. The rate limiting step in this sequence is predicted to be the C–H borylation proceeding via the transition state **62** (57.1 kcal/mol above the starting **59** and CH<sub>4</sub>), ultimately forming H<sub>2</sub> byproduct and a new C–B bond. Pathway *b*, however, starts with a lower energy B–H insertion step **63** (29.3 kcal/mol), which produces a molecule of H<sub>2</sub>, as well as the tricoordinate cation **64** possessing a covalent B–B bond. The diboron cation **64** (25.5 kcal/mol) is calculated to be the

reactive borylating agent in this pathway, which is illustrated by its reaction with CH<sub>4</sub> in the transition state **65**. Interestingly, the C–H borylation of CH<sub>4</sub> in **65** does not produce H<sub>2</sub>, since the C–H hydrogen ultimately gets captured by the B–B bond of **64** in the form of a 3c2e B–H–B bond.

The most important message delivered by the computational results summarized in Figure 2-2 is that there apparently exists a lower energy pathway for the C–H borylation starting with H-bridged monocations such as **59**, which does not involve generation of the primary borenium species such as **61**. While the initial results suggesting that the catalytic borylation process might begin with a B–H insertion step were purely computational, we were delighted to find an experimental result supporting the theoretical predictions. Thus, heating a solution of the phosphine-based H-bridged cation **66** ([B(C<sub>6</sub>F<sub>5</sub>)<sub>4</sub>]<sup>−</sup> salt) in *d*<sub>5</sub>-PhBr at 90 °C for 18 h resulted in clean formation of the complex triborane cation **67**, and the boronium byproduct **68** in 1:1 ratio, as shown by multinuclear NMR experiments (eq 8). Formally, the known cation **67**<sup>21</sup> can be viewed as the adduct between a BH<sub>3</sub> molecule and the tricoordinate diboron cation **69**, although this formalism may not necessarily reflect the actual structure of **67**. While formation of **67** serves as a clear indication for the formation of covalently bound B–B species in the decomposition of H-bridged cations, it also introduces some additional ambiguity to the reaction mechanism. Thus, while it is reasonable that species like **69** can react with the suitably placed C–H bonds before the formation of **67**, cation **67** can also be expected to lose H<sub>2</sub> under the thermal conditions. This would inevitably lead to formation of other weakly stabilized tricoordinate boron cations, further complicating the mechanistic pathways.

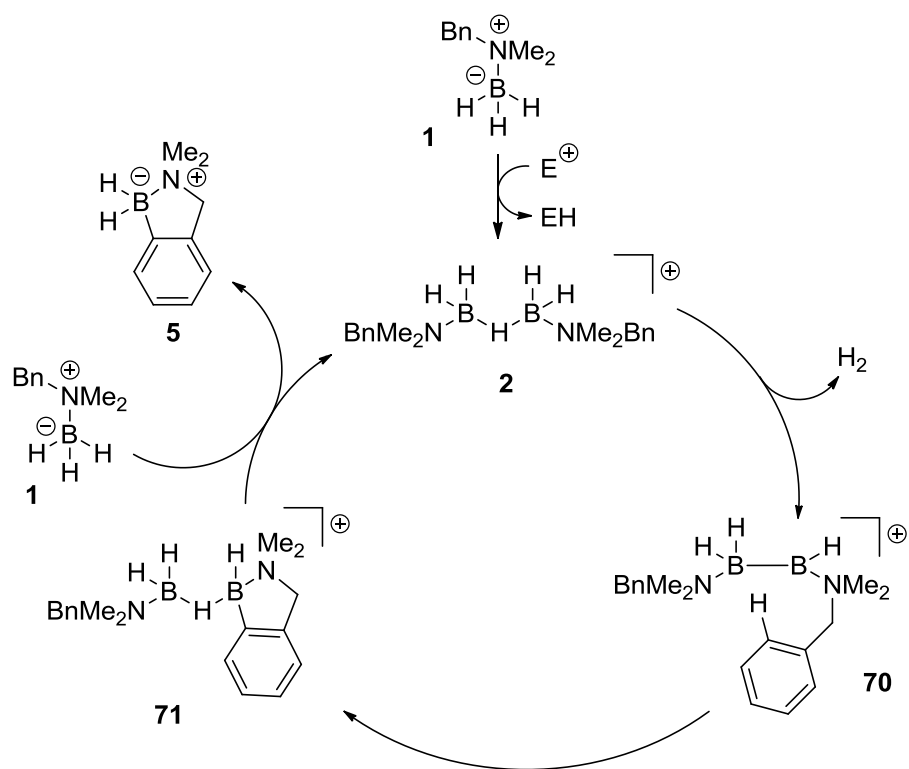
**Figure 2-2.** Mechanistic Alternatives for the Catalytic C–H Borylation





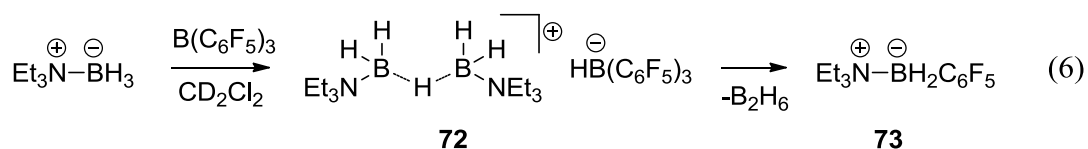
With the above B–H insertion mechanism, a plausible catalytic cycle can be drawn for the borylation of **1** (Scheme 2-8). Under the thermal conditions, loss of H<sub>2</sub> from the H-bridged cation **2** might lead to tricoordinate diboron cation **70**, which then isomerizes to the H-bridged species **71** via a C–H insertion. Interaction with another molecule of the starting amine borane **1** is then expected to regenerate **2**, displacing the product **5** from the H-bridged dimer **71**.

**Scheme 2-8.** The Catalytic Borylation Mechanism Involving B–H Insertion



## Lewis Base Borane Complex Reactions with B(C<sub>6</sub>F<sub>5</sub>)<sub>3</sub>

The successful performance of B(C<sub>6</sub>F<sub>5</sub>)<sub>3</sub> in the catalytic borylation chemistry briefly mentioned in this chapter demanded a closer investigation of the reactivity of this highly Lewis acidic compound with amine boranes. Addition of triethylamine borane to a solution of 0.5 equiv of B(C<sub>6</sub>F<sub>5</sub>)<sub>3</sub> in CD<sub>2</sub>Cl<sub>2</sub> at rt resulted in a rapid hydride abstraction and formation of the H-bridged cation **72**, as evidenced by <sup>1</sup>H and <sup>11</sup>B NMR (eq 6). Unlike in the trityl activation experiments described in Chapter 1, the other product of the hydride abstraction was not a mere spectator, but rather the weakly coordinating [HB(C<sub>6</sub>F<sub>5</sub>)<sub>3</sub>]<sup>-</sup> counterion. Additionally, the difference in the counterion structure and stability was found to have a prominent effect on the subsequent events. Thus, even at rt degradation of the H-bridged cation **72** was evident, and the process was substantially accelerated by heating the sealed reaction tube to 40 °C. At this point the <sup>11</sup>B NMR analysis indicated formation of B<sub>2</sub>H<sub>6</sub>, and another compound identified as **73** upon isolation. Formation of **73** is apparently a result of some disproportionation process involving a [HB(C<sub>6</sub>F<sub>5</sub>)<sub>3</sub>]<sup>-</sup> derivative, and despite the 1:1.5 “R<sub>3</sub>N–BH<sub>3</sub>”：“–C<sub>6</sub>F<sub>5</sub>” reaction stoichiometry, only C<sub>6</sub>F<sub>5</sub>BH<sub>2</sub> complexes were formed.



The reaction was further developed to a preparative protocol, optimized with respect to decreasing the amount of the expensive B(C<sub>6</sub>F<sub>5</sub>)<sub>3</sub> used, and simplified product isolation. Consequently, the optimized procedure requires only a slight excess (0.36 equiv vs. theoretical 0.33 equiv) of the fluorinated borane, and the product isolation in most cases is accomplished by a simple filtration of the reaction mixture through a plug

of silica gel, followed by concentration of the solution. The results listed in Table 2-1 suggest that this method can be conveniently used to access pentafluorophenylborane complexes of simple tertiary amines and phosphines. Very recently, a similar method for accessing related dimethylsulfide complexes was reported in the literature.<sup>22</sup>

**Table 2-1.** Synthesis of C<sub>6</sub>F<sub>5</sub>BH<sub>2</sub> Complexes<sup>a</sup>

Entry	Substrate	Solvent	Temp	Time	Product	Yield
1	Me <sub>3</sub> N–BH <sub>3</sub>	CH <sub>2</sub> Cl <sub>2</sub>	50 °C	1 h	Me <sub>3</sub> N–BH <sub>2</sub> C <sub>6</sub> F <sub>5</sub> ( <b>74</b> )	97%
2	Et <sub>3</sub> N–BH <sub>3</sub>	PhF	50 °C	3 h	Et <sub>3</sub> N–BH <sub>2</sub> C <sub>6</sub> F <sub>5</sub> ( <b>73</b> )	quant
3	BnMe <sub>2</sub> N–BH <sub>3</sub>	PhF	50 °C	1 h	BnMe <sub>2</sub> N–BH <sub>2</sub> C <sub>6</sub> F <sub>5</sub> ( <b>75</b> )	quant
4	Ph <sub>3</sub> P–BH <sub>3</sub>	CH <sub>2</sub> Cl <sub>2</sub>	40 °C	1 h	Ph <sub>3</sub> P–BH <sub>2</sub> C <sub>6</sub> F <sub>5</sub> ( <b>76</b> )	71%

<sup>a</sup>0.36:1 B(C<sub>6</sub>F<sub>5</sub>)<sub>3</sub>:L–BH<sub>3</sub>; the reaction performed in sealed vials

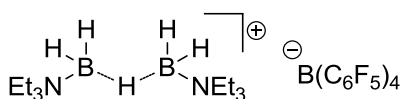
### Hydroboration of Alkenes with Activated Lewis Base Borane Complexes

The high electrophilicity of activated Lewis base borane complexes evident from their reactivity with weak nucleophiles such as the aliphatic C–H bonds suggests that they can also be useful for other types of synthetic transformations. Indeed, the foundations of the C–H borylation project in our research group were laid while developing the methodology for alkene hydroboration using activated borane complexes.<sup>23</sup> Some aspects of alkene hydroboration by amine and phosphine borane complexes under Ph<sub>3</sub>C<sup>+</sup> [B(C<sub>6</sub>F<sub>5</sub>)<sub>4</sub>]<sup>–</sup> activation conditions were previously explored in our group by Timothy DeVries,<sup>5</sup> and thus the initial goals of this study were to expand the potential applications of this chemistry to other classes of substrates and borane complexes.

Drawing some parallels to the *ipso*-substitution of silyl groups in the electrophilic aromatic borylation described in the beginning of this chapter, we proceeded to explore hydroboration of silylated alkenes using activated triethylamine borane. The

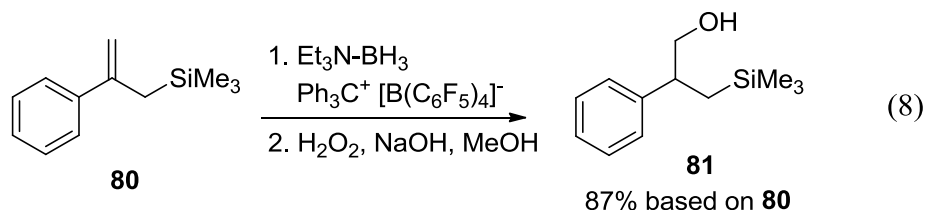
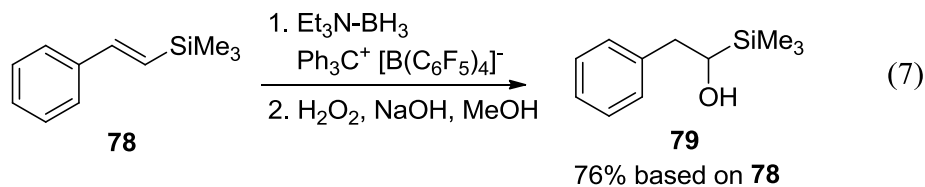


hydroborations were performed using the H-bridged cation **77** generated from 1:2 mixture of  $\text{Ph}_3\text{C}^+ [\text{B}(\text{C}_6\text{F}_5)_4]^-$  and  $\text{Et}_3\text{N}-\text{BH}_3$  in PhMe, and the hydroboration products were isolated as the corresponding alcohols following the oxidative workup. As the substrates for hydroboration we chose to use alkenylsilane **78** (eq 7) and allylsilane **80** (eq 8), mainly due to the differences in the relative position of the silyl groups to the double bonds in these compounds.

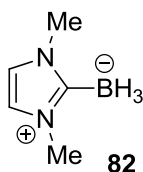


**77**

Interestingly, despite the high electrophilicity of the reaction medium, in both cases the major products retained the C–Si bonds. Furthermore, the hydroboration regiochemistry in the case of **78** was strongly influenced by the presence of the trimethylsilyl group in the substrate, since no trace of the regioisomeric benzylic alcohol was observed in the  $^1\text{H}$  NMR spectrum of the crude reaction mixture. The directing effect of the silyl group in hydroboration reactions using  $\text{BH}_3\cdot\text{THF}$  and  $\text{Br}_2\text{BH}\cdot\text{SMe}_2$  was previously described in the literature,<sup>24</sup> and appears to operate under the current hydroboration conditions as well. The effect of the more remote trimethylsilyl group in the alkene **80**, however, was not sufficient to override the inherent preference for hydroboration at the least hindered position. It should be emphasized that in both cases the isolated yields of the alcohols are sufficiently high to suggest that at least two H atoms of **77** can be used in the hydroboration process.



We also explored the applicability of the trityl activation protocol to hydroborations using NHC boranes. Without activation, such complexes do not hydroborate alkenes even at very high temperatures,<sup>25</sup> which is explained by the very strong (in the heterolytic sense) bonding between the NHC unit and BH<sub>3</sub>. Electrophilic activation of such complexes, however, opens up the possibility of performing hydroborations without breaking the strong bond between the NHC fragment and the boron atom.



In accord with our expectations based on the analogy to other Lewis base borane complexes, the electrophilic activation approach to hydroborations using NHC boranes was found to be successful. The reactions summarized in Table 2-2 were performed using the relatively unhindered 1,3-dimethyl-2-ylidene borane (**82**), although the feasibility of hydroboration reactions using more hindered carbene borane complexes was established by *in situ* NMR experiments. The reaction protocol involved activation of **82** in CH<sub>2</sub>Cl<sub>2</sub> solution with an electrophile (5 mol% of either Ph<sub>3</sub>C<sup>+</sup> [B(C<sub>6</sub>F<sub>5</sub>)<sub>4</sub>]<sup>-</sup> or Tf<sub>2</sub>NH),

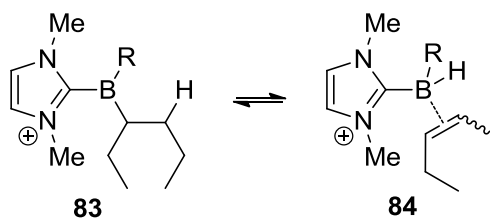
followed by addition of excess alkene. The oxidative workup using a H<sub>2</sub>O<sub>2</sub>/NaOH/MeOH mixture was much slower than in conventional hydroborations using BH<sub>3</sub>·THF, although full conversion to the alcohol products was still achieved in ca. 16 h at rt. The product yields summarized in Table 2-2 were determined by <sup>1</sup>H NMR analysis using PhMe as the internal reference.

**Table 2-2.** Alkene Hydroboration Using Activated **82**<sup>a,b</sup>

Entry	Substrate	Time	Temp	% C <sub>α</sub> OH (unrearr)	% C <sub>β</sub> OH (unrearr)	% rearranged products
1 <sup>c</sup>	(E)-3-hexene	1.5 h	25 °C	3-hexanol (5%)	–	1-hexanol (2%) 2-hexanol (71%)
2 <sup>d</sup>	(E)-3-hexene	1.5 h	25 °C	3-hexanol (5%)	–	1-hexanol (3%) 2-hexanol (72%)
3 <sup>c</sup>	(E)-3-hexene	20 min	25 °C	3-hexanol (68%)	–	2-hexanol (7%)
4 <sup>c</sup>	(E)-3-hexene	4 h	50 °C	3-hexanol (6%)	–	1-hexanol (16%) 2-hexanol (68%)
5 <sup>c</sup>	1-octene	1.5 h	25 °C	1-octanol (94%)	2-octanol (5%)	–
6 <sup>c</sup>	(E)-2-octene	1.5 h	25 °C	2-octanol (85%)	3-octanol (5%)	1-octanol (tr) 4-octanol (tr)
7 <sup>c</sup>	(E)-3-octene	1.5 h	25 °C	3-octanol (8%)	4-octanol (9%)	1-octanol (tr) 2-octanol (74%)
8 <sup>c</sup>	(E)-3-octene	19 h	25 °C	3-octanol (5%)	4-octanol (5%)	1-octanol (31%) 2-octanol (57%)
9 <sup>e</sup>	(E)-3-octene	2 h	50 °C	–	4-octanol (tr)	1-octanol (61%) 2-octanol (15%)
10 <sup>e</sup>	(E)-4-octene	1.5 h	25 °C	–	4-octanol (8%)	1-octanol (15%) 2-octanol (65%) 3-octanol (7%)
11 <sup>e</sup>	(E)-4-octene	2 h	50 °C	–	4-octanol (7%)	1-octanol (62%) 2-octanol (25%) 3-octanol (tr%)
12 <sup>e</sup>	(Z)-4-octene	2 h	50 °C	–	4-octanol (tr)	1-octanol (32%) 2-octanol (21%) 3-octanol (tr)

<sup>a</sup>3.5:1 alkene:**82**. <sup>b</sup>Product yields as determined by <sup>1</sup>H NMR using an internal reference; 2:1 alkene:**82** hydroboration ratio assumed for calculating the theoretical yield. <sup>c</sup>5 mol% Tf<sub>2</sub>NH used as the catalyst. <sup>d</sup>5 mol% Ph<sub>3</sub>C<sup>+</sup> [B(C<sub>6</sub>F<sub>5</sub>)<sub>4</sub>]<sup>–</sup> used as the catalyst. <sup>e</sup>30 mol% Tf<sub>2</sub>NH used as the catalyst.

To our surprise, the major product of the (E)-3-hexene hydroboration after 1.5 h at rt (entry 1) was found to be 2-hexanol. The expected 3-hexanol was found to be only a minor component of the reaction mixture (14:1 2-hexanol:3-hexanol), and a trace of 1-hexanol was also detected. A similar experiment quenched after 20 min at rt gave a different product ratio, this time favoring 3-hexanol (entry 3). The experiment performed for a longer period of time (4 h) at 50 °C (entry 4), however, provided a mixture containing a larger amount of 1-hexanol, although 2-hexanol was still found to be the dominant product. Similar reactivity patterns were also observed using octene substrates (entries 5–12), and a substantial selectivity for the C2 migration product in (E)-3-octene hydroboration was achieved after 1.5 h at rt (entry 7). Somewhat larger loadings of the bistriflimide catalyst (30 mol%) were necessary for the efficient conversion of (E)- and (Z)-4-octenes (entries 10–12), and under these conditions 1- and 2-octanols were found to predominate among the reaction products.



The above results are best rationalized by the existence of a low energy barrier for the reversible conversion between dialkylborenium cation **83** and the corresponding alkene  $\pi$ -complexes such as **84**. While alkylboranes are well known to undergo rearrangements at high temperatures (typically above 150 °C),<sup>26</sup> the C–B bond migrations in the NHC borane derivatives appear to be unusually facile. Another surprising aspect of the hydroborations by activated NHC boranes is the apparent kinetic selectivity for the C2 rearranged products in 3-hexene and 3-octene hydroborations. This suggests higher

thermodynamic stability of the secondary alkyl C2 isomer vs. secondary alkyl C3 isomer, as well as the lower kinetic barrier for the C3/C2 rearrangement as compared to C2/C1 rearrangement.

### Summary

To summarize, we explored a range of reactions involving Lewis base borane complexes activated with potent electrophiles. The scope of C–H insertion reactions of unstabilized primary borenium cations was expanded to include aliphatic substrates, and convenient C–H borylation protocols using only catalytic amounts of strong electrophiles were developed. Additionally, weakly stabilized B–H borenium ions **4** and **24** were isolated, and characterized by multinuclear NMR spectroscopy, as well as X-ray crystallography in the case of compound **4**. A protocol for electrophile-catalyzed hydroboration using NHC borane **82** was developed, and was found to offer unusual hydroboration products arising from facile C–B bond migration under the reaction conditions.

## Experimental

**General Methods.** All reactions were performed at room temperature (unless otherwise stated), under an atmosphere of dry nitrogen, either in a glovebox, or using standard Schlenk techniques. Nuclear magnetic resonance experiments were performed on Varian Inova 700, Varian Inova 500 and Inova 400 spectrometers at the following frequencies:  $^1\text{H}$  700 MHz, 500 MHz or 400 MHz;  $^{11}\text{B}$  and  $^{11}\text{B}\{^1\text{H}\}$  225 MHz, 160 MHz or 128 MHz;  $^{13}\text{C}\{^1\text{H}\}$  176 MHz, 126 MHz or 101 MHz;  $^{19}\text{F}$  471 MHz or 377 MHz;  $^{31}\text{P}$  162 MHz. All spectra were recorded in  $\text{CDCl}_3$ ,  $\text{CD}_2\text{Cl}_2$ ,  $d_5$ -PhBr, or  $d_8$ -PhMe and referenced to the  $^1\text{H}$  signal of internal  $\text{Me}_4\text{Si}$  according to IUPAC recommendations,<sup>27</sup> using a  $\mathcal{E}$  (referencing parameter) of 32.083974 for  $\text{BF}_3\cdot\text{OEt}_2$  ( $^{11}\text{B}$ ), a  $\mathcal{E}$  of 25.145020 for  $\text{Me}_4\text{Si}$  ( $^{13}\text{C}$ ), a  $\mathcal{E}$  of 94.094011 for  $\text{CCl}_3\text{F}$  ( $^{19}\text{F}$ ), and a  $\mathcal{E}$  of 40.480742 for  $\text{H}_3\text{PO}_4$  ( $^{31}\text{P}$ ). When the internal  $\text{Me}_4\text{Si}$  reference could not be used, residual solvent peaks in  $^1\text{H}$  NMR spectra were referenced instead. Toluene was distilled over  $\text{CaH}_2$ ;  $\text{CH}_2\text{Cl}_2$ , THF and hexanes were dried by passing through a column of activated alumina. Toluene,  $\text{CH}_2\text{Cl}_2$  and hexanes used in sensitive reactions were further dried by storing over activated 3 Å molecular sieves in the glovebox. Commercially available NMR grade deuterated solvents (Cambridge Isotope Laboratories), as well as benzene and fluorobenzene were not distilled; instead they were simply dried over a large amount of activated 3 Å molecular sieves in the glovebox. All other reagents were used as received from commercial suppliers.

## Preparation of Borylation Substrates

### 1-Neopentylpyrrolidine Borane (21)

A solution of pivalyl chloride (2.5 mL, 2.5 g, 21 mmol) in 10 mL of anhydrous  $\text{CH}_2\text{Cl}_2$  was added slowly to a stirred solution of pyrrolidine (5.0 mL, 4.4 g, 62 mmol) in 15 mL  $\text{CH}_2\text{Cl}_2$  (exotherm!). The resulting mixture was stirred at room temperature for 1 h, and then washed with 25 mL 10% aqueous NaOH solution. The organic layer was separated, the aqueous layer was extracted with 2x25 mL  $\text{CH}_2\text{Cl}_2$ , and the combined  $\text{CH}_2\text{Cl}_2$  phases were dried with  $\text{MgSO}_4$ . Filtration and concentration of the solution provided a white solid, which was dissolved in 20 mL of anhydrous THF. Treatment of the solution with  $\text{Me}_2\text{S-BH}_3$  (3.5 mL, 35 mmol) resulted in an exothermic reaction after a short induction period. After the exothermic reaction had ceased, the reaction mixture was refluxed for 1h, and then filtered through a pad of silica gel (eluted with  $\text{CH}_2\text{Cl}_2$ ) to decompose residual  $\text{Me}_2\text{S-BH}_3$ . Aqueous workup can also be used at this stage. Crystallization from hexanes provided 2.2 g (67%) of white crystals.

$^1\text{H}$  NMR (500 MHz,  $\text{CDCl}_3$ ):  $\delta$  = 3.38-3.32 (m, 2H), 2.73 (s, 2H), 2.73-2.66 (m, 2H), 2.29-2.18 (m, 2H), 1.90-1.80 (m, 2H), 2.1-1.3 (br m, 3H), 1.18 ppm (s, 9H).  $^{11}\text{B}$  NMR (128 MHz,  $\text{CDCl}_3$ ):  $\delta$  -12.0 ppm (q, J = 96 Hz).  $^{13}\text{C}$  NMR (101 MHz,  $\text{CDCl}_3$ ):  $\delta$  76.5, 63.8, 33.7, 30.5, 22.6 ppm. HRMS (ES<sup>+</sup>): m/z calculated for  $\text{C}_9\text{H}_{22}\text{BNNa}$  [ $\text{M}+\text{Na}$ ]<sup>+</sup> 178.1735, found 178.1743 (+4 ppm). IR ( $\text{CDCl}_3$ , NaCl): 2962, 2388, 1460, 1370, 1166, 1093  $\text{cm}^{-1}$ . m.p. 78-79 °C (from hexanes).

### N,N-Dimethylneopentylamine Borane (41)

Neat pivalyl chloride (5.0 mL, 4.9 g, 41 mmol) was added slowly to 40% aqueous HNMe<sub>2</sub> (50 mL, 0.41 mol) while keeping the solution at an ambient temperature (exothermic reaction!). The amide was isolated and converted to **41** as described in the preparative procedure for compound **21**.

<sup>1</sup>H NMR (400 MHz, CDCl<sub>3</sub>): δ = 2.85 (s, 2H), 2.74 (s, 6H), 2.3-1.2 (br m, 3H), 1.13 ppm (s, 9H). <sup>11</sup>B NMR (128 MHz, CDCl<sub>3</sub>): δ -6.8 ppm (q, J = 97 Hz). <sup>13</sup>C NMR (101 MHz, CDCl<sub>3</sub>): δ 74.5, 52.2, 33.8, 30.5 ppm. HRMS (ES<sup>+</sup>): m/z calculated for C<sub>7</sub>H<sub>20</sub>BNNa [M+Na]<sup>+</sup> 152.1586, found 152.1579 (-5 ppm). IR (CDCl<sub>3</sub>, NaCl): 2964, 2375, 2324, 1487, 1465, 1370, 1168, 1005 cm<sup>-1</sup>. m.p. 32 °C (after vacuum distillation).

### **N,3-Dimethylpiperidine Borane (43)**

To a solution of *N*,3-dimethylpyridinium iodide (10.3 g, 43.9 mmol) in MeOH (50 mL) was added PtO<sub>2</sub> hydrate (200 mg), and the mixture was shaken in a Parr vessel under H<sub>2</sub> atmosphere (5 bar) overnight. Following filtration, the solution was concentrated in vacuum, producing a yellowish solid. The solid was treated with 10% aqueous NaOH (40 mL), and the resulting two-layer mixture was extracted with CH<sub>2</sub>Cl<sub>2</sub> (3x40 mL). The combined extracts were dried with MgSO<sub>4</sub>, filtered, and then treated with neat Me<sub>2</sub>S-BH<sub>3</sub> (4.4 mL, 44 mmol) at room temperature. After stirring for 5 min, the solvent was removed in vacuum. The crude product was then dissolved in hexanes (25 mL), filtered, and left at -20 °C for 2 days. The product crystals were filtered out, and then washed with cold hexanes (10 mL). The procedure afforded 3.81 g (68%) of the product after prompt vacuum drying. NMR assay indicated that the product was obtained as a single diastereomer (Diastereomer 1). The pure diastereomer can be converted to a roughly 1:1 diastereomer mixture upon thermal equilibration.



Diastereomer 1:  $^1\text{H}$  NMR (500 MHz,  $\text{CDCl}_3$ ):  $\delta$  = 3.08-2.98 (m, 1H), 2.98-2.91 (m, 1H), 2.60 (s, 3H), 2.45-2.34 (m, 1H), 2.34-2.23 (m, 2H), 2.0-1.2 (br m, 3H), 1.94 (t,  $J$  = 11.6 Hz, 1H), 1.87-1.80 (m, 1H), 1.59-1.49 (m, 1H), 0.90-0.80 (m, 1H), 0.85 ppm (d,  $J$  = 6.7 Hz, 3H).  $^{11}\text{B}$  NMR (128 MHz,  $\text{CDCl}_3$ ):  $\delta$  -13.0 ppm (q,  $J$  = 96 Hz).  $^{13}\text{C}$  NMR (101 MHz,  $\text{CDCl}_3$ ):  $\delta$  67.9, 60.7, 56.6, 31.9, 26.8, 21.8, 19.4 ppm. HRMS (EI+ 70 eV):  $m/z$  calculated for  $\text{C}_7\text{H}_{17}\text{BN}$   $[\text{M}-\text{H}]^+$  126.1454, found 126.1452 (-2 ppm). IR ( $\text{CDCl}_3$ , NaCl): 2962, 2378, 2339, 1470, 1454, 1198, 1178, 1160  $\text{cm}^{-1}$ .

Diastereomer 2 (Not separated; signals determined in the 1:1 mixture):  $^1\text{H}$  NMR (700 MHz,  $\text{CDCl}_3$ ):  $\delta$  = 2.98-2.92 (m, 1H), 2.90-2.81 (m, 2H), 2.58 (s, 3H), 2.52 (t,  $J$  = 13.0, 1H), 2.0-1.2 (br m, 3H), 1.84-1.77 (m, 2H), 1.76-1.67 (m, 1H), 1.63-1.58 (m, 1H), 0.96 (dd,  $J$  = 13.6, 4.2 Hz, 1H), 0.88 ppm (d,  $J$  = 6.3 Hz, 3H).  $^{11}\text{B}$  NMR (225 MHz,  $\text{CDCl}_3$ ):  $\delta$  -8.0 ppm (q,  $J$  = 97 Hz).  $^{13}\text{C}$  NMR (176 MHz,  $\text{CDCl}_3$ ):  $\delta$  65.8, 58.7, 44.9, 31.4, 25.7, 20.4, 19.3 ppm.

#### **N,N-Dimethyl-1-(1-methylcyclohexyl)methanamine Borane (45)**

1-Methyl-1-cyclohexanecarboxylic acid (3.02 g, 21.2 mmol) was added in portions to  $\text{SOCl}_2$  (15 ml, 25 g, 0.21 mol), and the resulting solution was refluxed for 2 hours. Excess  $\text{SOCl}_2$  was distilled off, and the remaining liquid was added slowly to 40% aqueous  $\text{HNMe}_2$  (27 ml, 0.21 mol) while keeping the solution at an ambient temperature (exothermic reaction!). After stirring the solution for 1h at room temperature, the amide was isolated and converted to **42** as described above for the preparation of **21**. The procedure afforded 2.58 g (72%) of a colorless oil after vacuum distillation.

$^1\text{H}$  NMR (500 MHz,  $\text{CDCl}_3$ ):  $\delta$  = 2.85 (s, 2H), 2.76 (s, 6H), 2.2-1.4 (br m, 3H), 1.59-1.35 (m, 9H), 1.30-1.21 (m, 1H), 1.20 ppm (s, 3H).  $^{11}\text{B}$  NMR (128 MHz,  $\text{CDCl}_3$ ):  $\delta$  -6.6 ppm (q,  $J$  = 97 Hz).  $^{13}\text{C}$  NMR (101 MHz,  $\text{CDCl}_3$ ):  $\delta$  75.0, 52.7, 38.1, 36.4, 25.9, 24.1, 21.5 ppm. HRMS (EI+ 70 eV): no  $\text{M}^+$  observed, only  $[\text{M}-3\text{H}]^+$ . IR (neat, NaCl): 2930, 2861, 2374, 2321, 2274, 1458, 1168, 1015, 1004, 798  $\text{cm}^{-1}$ .

### **Preparation of *N,N*,2-trimethyl-2-phenylpropanamide**

2-Methyl-2-phenylpropanoic acid (2.23 g, 15.4 mmol) was added in portions to  $\text{SOCl}_2$  (15 mL, 25 g, 0.21 mol), and the resulting solution was refluxed for 5 h. Excess  $\text{SOCl}_2$  was distilled off, the residue was dissolved in 10 mL  $\text{CH}_2\text{Cl}_2$ , and the solution was added slowly to 40% aqueous  $\text{HNMe}_2$  (20 mL, 0.16 mol) (exothermic reaction!). After stirring at room temperature for 1h, the organic phase was separated, and the aqueous phase was extracted with  $\text{CH}_2\text{Cl}_2$ . The combined extracts were washed with 1M aqueous NaOH solution, then dried with  $\text{MgSO}_4$ , filtered and concentrated, providing 2.72 g (92%) of a brown oil.

$^1\text{H}$  NMR (500 MHz,  $\text{CDCl}_3$ ):  $\delta$  = 7.35-7.30 (m, 2H), 7.24-7.19 (m, 3H), 2.93 (br s, 3H), 2.50 (br s, 3H), 1.54 ppm (s, 6H).  $^{13}\text{C}$  NMR (101 MHz,  $\text{CDCl}_3$ ):  $\delta$  176.2, 146.6, 128.9, 126.2, 124.8, 47.0, 38.1, 37.2, 28.2 ppm. HRMS (EI+ 70 eV):  $m/z$  calculated for  $\text{C}_{12}\text{H}_{17}\text{NO} [\text{M}]^+$  191.1310, found 191.1319 (+5 ppm). IR (neat, NaCl): 2976, 2929, 1629, 1496, 1447, 1391, 1262, 1116, 1096, 771, 703, 616  $\text{cm}^{-1}$ .

### ***N,N*,2-Trimethyl-2-phenylpropan-1-amine Borane (48)**

The compound was prepared starting with *N,N*,2-trimethyl-2-phenylpropanamide (2.58 g, 13.5 mmol) and  $\text{Me}_2\text{S-BH}_3$  (2.3 mL, 23 mmol) as described above for the

preparation of **21**. The crude product was crystallized from hexanes to obtain 1.42 g (55%) of a white solid.

$^1\text{H}$  NMR (500 MHz,  $\text{CDCl}_3$ ):  $\delta$  = 7.42-7.38 (m, 2H), 7.37-7.32 (m, 2H), 7.26-7.21 (m, 1H), 3.35 (s, 2H), 2.35 (s, 6H), 2.1-1.2 (br m, 3H), 1.49 ppm (s, 6H).  $^{11}\text{B}$  NMR (128 MHz,  $\text{CDCl}_3$ ):  $\delta$  -6.3 ppm (q,  $J$  = 93 Hz).  $^{13}\text{C}$  NMR (101 MHz,  $\text{CDCl}_3$ ):  $\delta$  146.1, 128.6, 126.5, 125.9, 73.8, 51.7, 39.5, 30.2 ppm. HRMS (ES<sup>+</sup>):  $m/z$  calculated for  $\text{C}_{12}\text{H}_{22}\text{BNNa}$   $[\text{M}+\text{Na}]^+$  214.1743, found 214.1739 (-2 ppm). IR ( $\text{CDCl}_3$ , NaCl): 2972, 2376, 2322, 1462, 1168, 1027  $\text{cm}^{-1}$ . m.p. 76 °C (from hexanes).

### Preparation of *N,N,2,2*-tetramethyl-3-phenylpropanamide

Neat *N,N*-dimethylisobutyramide (1.0 mL, 0.90 g, 7.8 mmol) was added dropwise to a solution of 8.6 mmol lithium diisopropylamide in 15 mL of anhydrous THF at -30 °C. No significant exotherm was observed. The mixture was warmed up to 0 °C, stirred at that temperature for 2 h, and then cooled to -50 °C. Then, benzyl bromide (1.0 mL, 1.5 g, 8.6 mmol) was added dropwise. Again, no substantial exotherm was observed. The reaction mixture was warmed up to room temperature, and then stirred overnight. Concentration and purification by flash chromatography (2/1 Hexanes/EtOAc, 200 mL silica gel) afforded 0.926 g (58%) of a pale yellow oil.

$^1\text{H}$  NMR (500 MHz,  $\text{CDCl}_3$ ):  $\delta$  = 7.28-7.23 (m, 2H), 7.23-7.18 (m, 1H), 7.13-7.09 (m, 2H), 3.04 (s, 6H), 2.94 (s, 2H), 1.27 ppm (s, 6H).  $^{13}\text{C}$  NMR (101 MHz,  $\text{CDCl}_3$ ):  $\delta$  176.5, 138.2, 130.1, 128.0, 126.4, 46.0, 43.6, 38.6, 26.5 ppm. HRMS (EI+ 70 eV):  $m/z$  calculated for  $\text{C}_{13}\text{H}_{19}\text{NO}$   $[\text{M}]^+$  205.1467, found 205.1472 (+2 ppm). IR (neat, NaCl): 2969, 2930, 1628, 1495, 1473, 1391, 1364, 1251, 1102, 763, 740, 702  $\text{cm}^{-1}$ .

### **N,N,2,2-Tetramethyl-3-phenylpropan-1-amine Borane (51)**

The compound was prepared in the manner described above for the preparation of **21** using 0.904 g (4.40 mmol) of *N,N,2,2*-tetramethyl-3-phenylpropanamide. Yield of the product after crystallization from hexanes: 0.760 g (84%).

$^1\text{H}$  NMR (500 MHz,  $\text{CDCl}_3$ ):  $\delta = 7.32\text{-}7.21$  (m, 3H), 7.16-7.12 (m, 2H), 2.93 (s, 2H), 2.77 (s, 6H), 2.69 (s, 2H), 2.2-1.4 (br m, 3H), 1.13 ppm (s, 6H).  $^{11}\text{B}$  NMR (128 MHz,  $\text{CDCl}_3$ ):  $\delta -7.0$  ppm (br q,  $J = 94$  Hz).  $^{13}\text{C}$  NMR (101 MHz,  $\text{CDCl}_3$ ):  $\delta 137.4, 130.9, 127.9, 126.4, 74.2, 53.0, 49.4, 37.3, 27.1$  ppm. HRMS (ES+):  $m/z$  calculated for  $\text{C}_{13}\text{H}_{24}\text{BNNa}$   $[\text{M}+\text{Na}]^+$  228.1899, found 228.1904 (+2 ppm). IR ( $\text{CDCl}_3$ , NaCl): 2963, 2380, 2325, 1455, 1168, 1029, 1009  $\text{cm}^{-1}$ . m.p. 48 °C (from hexanes).

### **Intramolecular Borylation of 21 Using Stoichiometric $\text{Ph}_3\text{C}^+ [\text{B}(\text{C}_6\text{F}_5)_4]^-$**

A dry J. Young NMR tube was charged with a solution of **21** (9.2 mg, 59  $\mu\text{mol}$ ) in 0.6 mL  $\text{C}_6\text{D}_5\text{Br}$ , followed by a solution of  $\text{Ph}_3\text{C}^+ [\text{B}(\text{C}_6\text{F}_5)_4]^-$  (28 mg, 30  $\mu\text{mol}$ ) in 2x0.2 mL  $\text{C}_6\text{D}_5\text{Br}$ . NMR assay after thorough shaking of the tube indicated clean formation of *H*-bridged cation **22** and  $\text{Ph}_3\text{CH}$ .

**22**:  $^1\text{H}$  NMR (700 MHz,  $\text{CDCl}_3$ ):  $\delta = 3.2\text{-}2.0$  (br m, 4H), 2.92-2.85 (m, 4H), 2.62-2.55 (m, 4H), 2.45 (s, 4H), 1.71-1.62 (m, 4H), 1.61-1.51 (m, 4H), 0.86 (s, 18H), -2.27 ppm (br s, 1H).  $^{11}\text{B}$  NMR (225 MHz,  $\text{CDCl}_3$ ):  $\delta -1.1$  ppm (br s,  $\text{whh} = 700$  Hz), -16.1 ppm (s).

To the solution, another portion of  $\text{Ph}_3\text{C}^+ [\text{B}(\text{C}_6\text{F}_5)_4]^-$  (28 mg, 30  $\mu\text{mol}$ ) in 2x0.2 mL  $\text{C}_6\text{D}_5\text{Br}$  was added, gas liberation was observed. After 10 minutes at room temperature NMR assay indicated essentially complete conversion to the cyclic cation salt **24**,  $\text{Ph}_3\text{CH}$  and  $\text{H}_2$ .

**24:**  $^1\text{H}$  NMR (700 MHz,  $\text{CDCl}_3$ ):  $\delta$  = 5.3-4.2 (br m, 1H), 2.78-2.71 (m, 2H), 2.59 (s, 2H), 2.49-2.42 (m, 2H), 1.65-1.68 (m, 2H), 1.52-1.45 (m, 2H), 1.27 (s, 2H), 0.64 ppm (s, 6H).  
 $^{11}\text{B}$  NMR (225 MHz,  $\text{CDCl}_3$ ):  $\delta$  69.3 ppm (br s, whh = 690 Hz), -16.2 ppm (s).

Quenching the reaction mixture with excess  $n\text{-Bu}_4\text{NBH}_4$  resulted in clean formation of the cyclic amine borane **25**, consistent with the NMR data presented below.

In a separate preparative experiment, a mixture of solid **21** (19.2 mg, 0.124 mmol) and  $\text{Ph}_3\text{C}^+ [\text{B}(\text{C}_6\text{F}_5)_4]^-$  (0.103 g, 0.112 mmol) was dissolved in 1 mL PhF. After 1 h at room temperature the reaction mixture was quenched by adding excess of solid  $n\text{-Bu}_4\text{NBH}_4$  under  $\text{N}_2$  atmosphere. The mixture was then filtered through a short plug of silica, eluting with  $\text{CHCl}_3$ . The crude product was first purified by preparative TLC (1/1  $\text{CH}_2\text{Cl}_2$ /Hexanes), followed by flash chromatography (3/1 Hexanes/ $\text{CHCl}_3$ ), affording 14.1 mg (82%) of the desired cyclic amine borane as a colorless oil. The theoretical yield of the product was calculated based on the amount of  $[\text{Ph}_3\text{C}][\text{B}(\text{C}_6\text{F}_5)_4]$  used (0.9 equiv).

### **Intramolecular Borylation Using Catalytic $\text{Tf}_2\text{NH}$ . A General Procedure**

A dry 12 mL thick-walled Schlenk tube fitted with a teflon stopper was charged with a mixture of solid amine borane (1.32 mmol) and  $\text{Tf}_2\text{NH}$  (18.6 mg, 66.2  $\mu\text{mol}$ ). Solvent (3 mL) was then added, and some minor frothing due to gas formation was observed. The gas formed during the initial activation stage was identified as  $\text{H}_2$  in an *in situ* NMR study. After  $\text{H}_2$  liberation ceased, and the gas was allowed to escape the reaction vessel, the tube was sealed and heated at 160  $^\circ\text{C}$  (bath) for the indicated time. When liquid amine borane complexes were used, the substrate was first dissolved in 1 mL of the solvent, and then  $\text{Tf}_2\text{NH}$  and the additional solvent were added. The reaction mixture was quenched by adding solid  $n\text{-Bu}_4\text{NBH}_4$  (~30 mg) under  $\text{N}_2$  atmosphere. The

mixture was then diluted with CH<sub>2</sub>Cl<sub>2</sub>, and filtered through a short plug of silica, eluting with CH<sub>2</sub>Cl<sub>2</sub> or CHCl<sub>3</sub>. The products were isolated by concentrating the solution.

#### **Borylation of 21. 3,3-Dimethyl-5-aza-1-borasp[4.4]nonane (25)**

PhH solvent, 14 h reaction time. The product was isolated as a colorless oil in 75% yield after flash chromatography (2/1 Hexanes/EtOAc, 30 mL silica gel) to remove traces of unreacted **21**.

<sup>1</sup>H NMR (500 MHz, CDCl<sub>3</sub>): δ = 3.32-3.23 (m, 2H), 2.76-2.68 (m, 2H), 2.71 (s, 2H), 2.4-1.6 (br m, 2H), 2.15-2.04 (m, 2H), 1.93-1.82 (m, 2H), 1.12 (s, 6H), 0.75 ppm (t, J = 5.7 Hz, 2H). <sup>11</sup>B NMR (128 MHz, CDCl<sub>3</sub>): δ -4.2 ppm (t, J = 96 Hz). <sup>13</sup>C NMR (101 MHz, CDCl<sub>3</sub>): δ 75.7, 61.7, 37.7, 32.4-30.1 (br m), 31.8, 22.7 ppm. HRMS (EI+ 70 eV): m/z calculated for C<sub>9</sub>H<sub>19</sub>BN [M-H]<sup>+</sup> 152.1611, found 152.1616 (+3 ppm). IR (neat, NaCl): 2954, 2338, 1459, 1362, 1310, 1236, 1193, 1137, 1063, 870 cm<sup>-1</sup>.

#### **Borylation of 41. 1,1,4,4-Tetramethyl-1,2-azaborolidine (42)**

PhH solvent, 14 h reaction time. Colorless oil, 96% yield.

<sup>1</sup>H NMR (400 MHz, CDCl<sub>3</sub>): δ = 2.64 (s, 6H), 2.63 (s, 2H), 2.5-1.5 (br m, 2H), 1.14 (s, 6H), 0.80 ppm (t, J = 5.6 Hz, 2H). <sup>11</sup>B NMR (128 MHz, CDCl<sub>3</sub>): δ -2.9 ppm (t, J = 97 Hz). <sup>13</sup>C NMR (101 MHz, CDCl<sub>3</sub>): δ 77.7, 52.4, 38.7, 33.0-30.3 (br m), 32.6 ppm. HRMS (EI+ 70 eV): m/z calculated for C<sub>7</sub>H<sub>17</sub>BN [M-H]<sup>+</sup> 126.1454, found 126.1450 (-3 ppm). IR (neat, NaCl): 2949, 2338, 1460, 1361, 1248, 1175, 1192, 1141, 1103, 1071, 1001, 851, 758 cm<sup>-1</sup>.

#### **Borylation of 43. 1-Methyl-1-aza-7-borabicyclo[3.2.1]octane (44)**

PhF solvent, 14 h reaction time. ~20% conversion according to crude  $^1\text{H}$  NMR. The product was isolated as a white solid in 14% yield after flash chromatography (benzene, 30 mL silica gel, long column), 63% of the starting material recovered. 37% yield based on recovered starting material.

The results of the above experiment were essentially the same no matter whether a pure diastereomer or a 1:1 mixture of diastereomers of **43** was used. In all cases the starting material was recovered as a mixture of diastereomers, suggesting fast equilibration under the reaction conditions. Extended reaction times and higher  $\text{Tf}_2\text{NH}$  loadings did not improve the yield of the borylation product. The amounts of the recovered starting material were lower, however.

In an attempt to improve the yield of the borylation product, the following experiments were performed starting with a single diastereomer of **43**. Two identical reactions were performed in parallel as described in the general procedure, using PhF solvent and 10 mol% of  $\text{Tf}_2\text{NH}$ . During the course of the reaction (60.5 h at 160 °C) one of the two vessels was periodically cooled to room temperature, then vented and flushed with nitrogen in a glovebox to remove  $\text{H}_2$  byproduct (vented 4 times total). The other reaction vessel was identically cooled and heated, although never vented before the completion of the reaction time. The isolated yield of the borylation product in the former experiment (with periodic  $\text{H}_2$  removal) was 25% (35% of **43** recovered), as compared to 13% in the latter case (45% of **43** recovered).

$^1\text{H}$  NMR (700 MHz,  $\text{CDCl}_3$ ):  $\delta$  = 2.92-2.88 (m, 1H), 2.88-2.85 (m, 1H), 2.59 (s, 3H), 2.60-2.51 (m, 1H), 2.47-2.42 (m, 1H), 2.39-2.34 (m, 1H), 2.34-2.26 (m, 1H), 2.3-1.5 (br m, 2H), 1.54-1.46 (m, 2H), 1.43-1.36 (m, 1H), 1.11-1.03 (m, 1H), 0.48-0.42 (m, 1H).  $^{11}\text{B}$

NMR (225 MHz, CDCl<sub>3</sub>):  $\delta$  -5.0 ppm (t, J = 97 Hz). <sup>13</sup>C NMR (176 MHz, CDCl<sub>3</sub>):  $\delta$  67.8, 61.9, 50.7, 35.1, 30.2, 19.7, 19.4-18.2 ppm (br m). HRMS (ES<sup>+</sup>): m/z calculated for C<sub>7</sub>H<sub>15</sub>BN [M-H]<sup>+</sup> 124.1292, found 124.1291 (-1 ppm). IR (CDCl<sub>3</sub>, NaCl): 2914, 2319, 1455, 1200, 1155, 1135, 1110, 1003 cm<sup>-1</sup>.

### **Borylation of 45**

PhMe solvent, 14 h reaction time. A mixture of isomeric products **46** and **47** was isolated in 78% yield after flash chromatography to remove traces of unreacted **45**. An analytical sample of the major product (**46**) was isolated by repeated crystallization of the crude mixture from hexanes at -78 °C. The mother liquor after several successive crystallizations of **46** served as an enriched sample for **47** characterization.

### **2,2-Dimethyl-2-aza-3-borasp[iro[4.5]decane (46)**

<sup>1</sup>H NMR (700 MHz, CDCl<sub>3</sub>):  $\delta$  = 2.64 (s, 2H), 2.63 (s, 6H), 2.3-1.7 (br m, 2H), 1.61-1.54 (m, 2H), 1.54-1.49 (m, 2H), 1.46-1.31 (m, 5H), 1.31-1.23 (m, 1H), 0.76 (t, J = 5.5 Hz, 2H). <sup>11</sup>B NMR (225 MHz, CDCl<sub>3</sub>):  $\delta$  -3.5 ppm (t, J = 96 Hz). <sup>13</sup>C NMR (176 MHz, CDCl<sub>3</sub>):  $\delta$  76.9 (from gHSQCAD), 52.3, 42.6, 41.0, 28.3-26.7 (br m), 26.0, 23.6 ppm. HRMS (EI+ 70 eV): m/z calculated for C<sub>10</sub>H<sub>21</sub>BN [M-H]<sup>+</sup> 166.1767, found 166.1760 (-4 ppm). IR (CDCl<sub>3</sub>, NaCl): 2924, 2838, 2328, 1463, 1448, 1207, 1187, 1162, 1118, 1096, 1022 cm<sup>-1</sup>.

### **2,2,3a-trimethyloctahydro-1H-benzo[c][1,2]-1,2-azaborole (47)**

<sup>1</sup>H NMR (700 MHz, CDCl<sub>3</sub>):  $\delta$  = 2.89 (d, J = 12.5 Hz, 1H), 2.72 (s, 3H), 2.66 (s, 3H), 2.61 (d, J = 12.6 Hz, 1H), 2.5-1.7 (br m, 2H), 1.84 (td, J = 10.4, 4.3 Hz, 1H), 1.7-1.2 (m,



6H), 1.17-1.13 (m, 1H), 1.10 (s, 3H), 1.05 (m, 1H).  $^{11}\text{B}$  NMR (225 MHz,  $\text{CDCl}_3$ ):  $\delta$  -0.6 ppm (t,  $J = 96$  Hz).  $^{13}\text{C}$  NMR (176 MHz,  $\text{CDCl}_3$ ):  $\delta$  78.0, 56.4, 56.2, 41.8, 37.1-35.7 (br m), 35.3, 27.6, 25.6, 23.6, 23.3 ppm.

### **Borylation of 48**

PhMe solvent, 14 h reaction time. A mixture of isomeric products **49** and **50** (20:1) was isolated in 95% yield. An analytical sample of the major product (**49**) was isolated by crystallization of the crude mixture from hexanes. The minor product (**50**) was isolated from the mother liquor by repeated preparative TLC (9/1 Hexanes/EtOAc, followed by 2/1 Hexanes/ $\text{CH}_2\text{Cl}_2$ ).

### **2,2,4,4-Tetramethyl-2,1-benzazaborinane (49)**

$^1\text{H}$  NMR (500 MHz,  $\text{CDCl}_3$ ):  $\delta = 7.30$ -7.26 (m, 1H), 7.25-7.22 (m, 1H), 7.15-7.08 (m, 2H), 2.95 (s, 2H), 2.9-2.2 (br m, 2H), 2.68 (s, 6H), 1.41 (s, 6H).  $^{11}\text{B}$  NMR (128 MHz,  $\text{CDCl}_3$ ):  $\delta$  -4.8 ppm (t,  $J = 94$  Hz).  $^{13}\text{C}$  NMR (101 MHz,  $\text{CDCl}_3$ ):  $\delta$  147.1-144.4 (br m), 144.1, 133.1, 125.3, 125.2, 124.6, 72.6, 52.1, 36.8, 33.0 ppm. HRMS (EI+ 70 eV):  $m/z$  calculated for  $\text{C}_{12}\text{H}_{19}\text{BN}$   $[\text{M}-\text{H}]^+$  188.1611, found 188.1613 (+1 ppm). IR ( $\text{CDCl}_3$ , NaCl): 3051, 2962, 2940, 2329, 1481, 1458, 1249, 1199, 1171, 1130, 1090, 855  $\text{cm}^{-1}$ .

### **1,1,4-Trimethyl-4-Phenyl-1,2-azaborolidine (50)**

$^1\text{H}$  NMR (500 MHz,  $\text{CDCl}_3$ ):  $\delta = 7.44$ -7.40 (m, 2H), 7.33-7.28 (m, 2H), 7.17-7.14 (m, 1H), 3.33 (d,  $J = 11.9$ , 1H), 3.03 (d,  $J = 11.9$ , 1H), 2.75 (s, 3H), 2.6-1.7 (br m, 2H), 2.44 (s, 3H), 1.61-1.52 (m, 1H), 1.45 (s, 3H), 1.09 (ddd,  $J = 2.6, 5.6, 13.6$  Hz, 1H).  $^{11}\text{B}$  NMR (128 MHz,  $\text{CDCl}_3$ ):  $\delta$  -2.8 ppm (t,  $J = 96$  Hz).  $^{13}\text{C}$  NMR (101 MHz,  $\text{CDCl}_3$ ):  $\delta$  152.4,

128.2, 125.9, 125.4, 76.9, 53.4, 52.3, 47.0, 34.2, 30.4-28.0 (br m) ppm. HRMS (EI+ 70 eV): m/z calculated for C<sub>12</sub>H<sub>19</sub>BN [M-H]<sup>+</sup> 188.1611, found 188.1612 (+1 ppm). IR (CDCl<sub>3</sub>, NaCl): 2952, 2338, 1465, 1215, 1098 cm<sup>-1</sup>.

### **Borylation of 51**

PhMe solvent, 14 h reaction time. A mixture of isomeric products **52**, **53** and **54** (25:6.8:1) was isolated in 89% yield. Analytical samples of the major (**52**) and tricyclic (**53**) products were isolated by repeated flash chromatography (9/1 Hexanes/EtOAc). The minor product (**54**) was isolated by preparative TLC (9/1 Hexanes/EtOAc) of the overlapping fractions.

### **4-Benzyl-1,1,4-trimethyl -1,2-azaborolidine (52)**

<sup>1</sup>H NMR (500 MHz, CDCl<sub>3</sub>): δ = 7.29-7.25 (m, 3H), 7.23-7.26 (m, 2H), 2.89 (d, J = 12.3 Hz, 1H), 2.76 (d, J = 13.1 Hz, 1H), 2.68 (d, J = 13.1 Hz, 1H), 2.64 (s, 3H), 2.56 (s, 3H), 2.49 (d, J = 12.3 Hz, 1H), 2.4-1.6 (br m, 2H), 1.14 (s, 3H), 1.03 (td, J = 6.1, 13.6 Hz, 1H), 0.69 ppm (td, J = 4.9, 13.6 Hz, 1H). <sup>11</sup>B NMR (128 MHz, CDCl<sub>3</sub>): δ -3.2 ppm (t, J = 92 Hz). <sup>13</sup>C NMR (101 MHz, CDCl<sub>3</sub>): δ 139.7, 130.6, 127.8, 125.9, 75.4, 52.9, 52.7, 50.3, 43.2, 30.5-28.8 (br m), 29.9 ppm. HRMS (EI+ 70 eV): m/z calculated for C<sub>13</sub>H<sub>21</sub>BN [M-H]<sup>+</sup> 202.1767, found 202.1772 (+2 ppm). IR (neat, NaCl): 3026, 2950, 2921, 2339, 1602, 1495, 1461, 1373, 1246, 1197, 1132, 1099, 1000, 853, 755, 704 cm<sup>-1</sup>.

### **Tricyclic product 53**

<sup>1</sup>H NMR (500 MHz, CDCl<sub>3</sub>): δ = 7.34 (dd, J = 1.1, 7.0 Hz, 1H), 7.13-7.09 (m, 1H), 7.08-7.04 (m, 1H), 7.01-6.98 (m, 1H), 2.95 (d, J = 16.7 Hz, 1H), 3.0-2.0 (br m, 1H), 2.75-2.71

(m, 4H), 2.69-2.62 (m, 2H), 2.22 (s, 3H), 1.20 (s, 3H), 1.07-1.01 (m, 1H), 0.74 (d, J = 12.8 Hz, 1H).  $^{11}\text{B}$  NMR (128 MHz,  $\text{CDCl}_3$ ):  $\delta$  1.9 ppm (d, J = 95 Hz).  $^{13}\text{C}$  NMR (101 MHz,  $\text{CDCl}_3$ ):  $\delta$  149.0-146.6 (br m), 141.1, 135.8, 127.7, 126.2, 124.6, 75.1, 53.7, 50.4, 49.7, 42.1, 31.4-29.4 (br s), 30.7 ppm. HRMS (EI+ 70 eV): m/z calculated for  $\text{C}_{13}\text{H}_{20}\text{BN}$   $[\text{M}]^+$  201.1689, found 201.1692 (+1 ppm). IR ( $\text{CDCl}_3$ , NaCl): 3022, 2950, 2917, 2366, 2347, 1463, 1242, 1180, 1078, 1039, 854  $\text{cm}^{-1}$ .

#### **1,1,4,4-Tetramethyl-3-phenyl-1,2-azaborolidine (54)**

$^1\text{H}$  NMR (500 MHz,  $\text{CDCl}_3$ ):  $\delta$  = 7.31-7.27 (m, 2H), 7.23-7.18 (m, 2H), 7.12-7.07 (m, 1H), 2.93 (d, J = 12.3 Hz, 1H), 2.82 (d, J = 12.3 Hz, 1H), 2.78 (s, 3H), 2.75 (s, 3H), 2.7-1.8 (m, 2H), 2.38 (dd, J = 5.4, 9.2 Hz, 1H), 1.06 (s, 3H), 0.85 (s, 3H).  $^{11}\text{B}$  NMR (128 MHz,  $\text{CDCl}_3$ ):  $\delta$  -1.6 ppm (br t, J = 85 Hz).  $^{13}\text{C}$  NMR (101 MHz,  $\text{CDCl}_3$ ):  $\delta$  143.8, 131.0, 127.3, 124.5, 79.0, 54.9, 54.7, 49.2-47.3 (br m), 42.3, 30.4, 25.7 ppm. HRMS (EI+ 70 eV): m/z calculated for  $\text{C}_{13}\text{H}_{21}\text{BN}$   $[\text{M}-\text{H}]^+$  202.1767, found 202.1763 (-2 ppm). IR ( $\text{CDCl}_3$ , NaCl): 3022, 2948, 2355, 1463, 1384, 1245, 1094  $\text{cm}^{-1}$ .

#### **Reaction of Triethylamine Borane with $\text{B}(\text{C}_6\text{F}_5)_3$ . *In Situ* NMR Study**

Every possible effort was made to protect the reaction mixture from exposure to air and moisture. The reaction was set up in a dry J. Young NMR tube under  $\text{N}_2$  atmosphere in a glovebox. The NMR tube was dried in a heating oven at ca. 200  $^\circ\text{C}$  overnight, and the fitted Teflon valve was dried in a desiccator over Drierite. Commercial grade  $\text{B}(\text{C}_6\text{F}_5)_3$  and  $\text{Et}_3\text{N}-\text{BH}_3$  were used without further purification. Commercial grade  $\text{CD}_2\text{Cl}_2$  (Cambridge Isotope Laboratories) was not distilled, but rather simply dried with freshly activated molecular sieves in the glovebox.

The reaction tube was charged with a solution of  $B(C_6F_5)_3$  (27.0 mg, 52.7  $\mu\text{mol}$ ) in 0.6 mL  $CD_2Cl_2$ . To this solution neat  $Et_3N-BH_3$  (14.7  $\mu\text{L}$ , 0.100 mmol) was added via a microsyringe in one portion. No substantial exotherm was observed, potentially due to the small scale of the reaction. The tube was immediately sealed with the fitted Teflon valve, and then shaken vigorously for ca. 1 min. The NMR assay performed within the first 30 minutes following mixing the reagents indicated clean formation of salt **72**. The sealed reaction tube was then heated at 40 °C for 1 h. Formation of disproportionation product **73** was observed according to  $^{11}\text{B}$  NMR assay.

**72**:  $^1\text{H}$  NMR (400 MHz,  $CD_2Cl_2$ ):  $\delta$  4.1-1.9 (br m, 5H), 2.93 (q,  $J = 7.3$  Hz, 12H), 1.23 (t,  $J = 7.3$  Hz, 17H), -2.0–-3.3 ppm (br s, 1H).  $^{11}\text{B}$  NMR (128 MHz,  $CD_2Cl_2$ ):  $\delta$  -3.0 (unres t), -25.4 ppm (d,  $J = 80$  Hz).  $^{13}\text{C}$  NMR (101 MHz,  $CD_2Cl_2$ ):  $\delta$  150.3-146.9 (m), 140.2-136.6 (m), 138.6-135.2 (m), 127.1-123.7 (br m), 52.4, 8.3 ppm.  $^{19}\text{F}$  NMR (377 MHz,  $CD_2Cl_2$ ):  $\delta$  -134.0 (s), -164.7 (s), -167.6 ppm (s).

### **Preparation of Amine and Phosphine Pentafluorophenylborane Complexes**

*General Procedure.* Every possible effort was made to protect the reaction mixtures from exposure to air and moisture. The reactions were performed under  $N_2$  atmosphere in a glovebox. Disposable glassware flame-dried at the glass softening temperature was used. Commercial grade  $B(C_6F_5)_3$  (Aldrich) was used without further purification. Methylene chloride was dried by passing through a column of activated alumina, and then further dried with freshly activated molecular sieves in the glovebox. Fluorobenzene was not distilled; instead it was simply dried over a large amount of activated molecular sieves in the glovebox.

In the glovebox, a dry 4 mL scintillation vial was charged with a mixture of solid amine borane or phosphine borane and  $B(C_6F_5)_3$ . The solid mixture was then dissolved by adding the specified solvent to the vial in one portion at rt, the vial was sealed and then heated as indicated below. No special precautions were necessary when isolating the products, since they were found to be reasonably stable to both air and moisture. Passing the reaction mixture through a short (3-4 cm) plug of silica while flushing with  $CHCl_3$  afforded pure products in all cases except when  $Ph_3P-BH_3$  was used as the starting material. In that case the product was purified as indicated below.

**74:** Prepared following the general procedure using  $B(C_6F_5)_3$  (0.211 g, 0.412 mmol) and  $Me_3N-BH_3$  (83.2 mg, 1.14 mmol) in 1 mL of anhydrous  $CH_2Cl_2$ . Heated in a sealed vial at 50 °C for 1 h. Isolated as described above providing 0.264 g (97%) of a white solid.

$^1H$  NMR (400 MHz,  $CDCl_3$ ):  $\delta$  3.0-1.8 (br m, 2H), 2.62 ppm (s, 9H).  $^{11}B$  NMR (128 MHz,  $CDCl_3$ ):  $\delta$  -9.6 ppm (t,  $J = 100$  Hz).  $^{13}C$  NMR (101 MHz,  $CDCl_3$ ):  $\delta$  150.3-147.0 (m), 141.7-138.5 (m), 138.5-135.2 (m), 117.8-115.3 (br m), 52.4 ppm.  $^{19}F$  NMR (377 MHz,  $CDCl_3$ ):  $\delta$  -129.6 (m), -157.5 (m), -164.0 ppm (m). HRMS (EI+):  $m/z$  calculated for  $C_9H_{10}BF_5N [M-H]^+$  238.0826, found 238.0829 (+1 ppm). IR( $CDCl_3$ , NaCl): 2418, 2358, 1641, 1483, 1466, 1283, 1150, 1101, 1085  $cm^{-1}$ . m.p. 99 °C (from  $CH_2Cl_2$ ).

**73:** Prepared following the general procedure using  $B(C_6F_5)_3$  (43.0 mg, 84.0  $\mu$ mol) and  $Et_3N-BH_3$  (34.4  $\mu$ L, 0.233 mmol) in 0.5 mL of anhydrous PhF. Since  $Et_3N-BH_3$  is a liquid at rt, it was added via a microsyringe to the solution of  $B(C_6F_5)_3$ . Heated in a sealed vial at 50 °C for 3 h. Isolated as described above providing a colorless oil in quantitative yield.

$^1\text{H}$  NMR (400 MHz,  $\text{CDCl}_3$ ):  $\delta$  2.9-1.7 (br m, 2H), 2.76 (q,  $J = 7.2$  Hz, 6H), 1.26 ppm (t,  $J = 7.2$  Hz, 9H).  $^{11}\text{B}$  NMR (128 MHz,  $\text{CDCl}_3$ ):  $\delta$  -14.2 ppm (t,  $J = 100$  Hz).  $^{13}\text{C}$  NMR (101 MHz,  $\text{CDCl}_3$ ):  $\delta$  150.7-147.8 (m), 141.3-137.8 (m), 138.8-135.4 (m), 118.5-115.7 (br m), 50.5, 8.4 ppm.  $^{19}\text{F}$  NMR (377 MHz,  $\text{CDCl}_3$ ):  $\delta$  -128.4 (m), -158.0 (t,  $J = 20$  Hz), -164.2 ppm (m). HRMS (EI+):  $m/z$  calculated for  $\text{C}_{12}\text{H}_{16}\text{BF}_5\text{N}$   $[\text{M}-\text{H}]^+$  280.1296, found 280.1295 (0 ppm). IR( $\text{CDCl}_3$ , NaCl): 2990, 2431, 2383, 1641, 1512, 1394, 1281, 1131, 1085  $\text{cm}^{-1}$ .

**75:** Prepared following the general procedure using  $\text{B}(\text{C}_6\text{F}_5)_3$  (43.0 mg, 84.0  $\mu\text{mol}$ ) and  $\text{BnMe}_2\text{N}-\text{BH}_3$  (34.7 mg, 0.233 mmol) in 0.5 mL of anhydrous PhF. Heated in a sealed vial at 50  $^\circ\text{C}$  for 1 h. Isolated as described above providing a white solid in quantitative yield.

$^1\text{H}$  NMR (500 MHz,  $\text{CDCl}_3$ ):  $\delta$  7.45-7.38 (m, 3H), 7.30-7.24 (m, 2H), 4.00 (s, 2H), 3.0-2.0 (br m, 2H), 2.45 ppm (s, 6H).  $^{11}\text{B}$  NMR (128 MHz,  $\text{CDCl}_3$ ):  $\delta$  -8.8 ppm (unres t).  $^{13}\text{C}$  NMR (101 MHz,  $\text{CDCl}_3$ ):  $\delta$  150.4-147.2 (m), 141.7-138.6 (m), 138.6-135.4 (m), 132.4, 130.1, 129.4, 128.7, 117.7-115.3 (br m), 65.9, 47.4 ppm.  $^{19}\text{F}$  NMR (377 MHz,  $\text{CDCl}_3$ ):  $\delta$  -129.0 (m), -157.2 (t,  $J = 20$  Hz), -163.8 ppm (m). HRMS (EI+): dissociates to  $\text{BnNMe}_2$  and  $\text{C}_6\text{F}_5\text{BH}_2$  under EI-MS conditions.  $m/z$  calculated for  $\text{C}_6\text{F}_5\text{BH}_2$   $[\text{M}]^+$  180.0170, found 180.0163 (-4 ppm);  $m/z$  calculated for  $\text{C}_9\text{H}_{13}\text{N}$   $[\text{M}]^+$  135.1048, found 135.1042 (-4 ppm). IR( $\text{CDCl}_3$ , NaCl): 3010, 2957, 2418, 2358, 1641, 1513, 1466, 1283, 1155, 1086, 1036  $\text{cm}^{-1}$ . m.p. 79  $^\circ\text{C}$  (from  $\text{CH}_2\text{Cl}_2$ ).

**76:** Prepared following the general procedure using  $\text{B}(\text{C}_6\text{F}_5)_3$  (43.0 mg, 84.0  $\mu\text{mol}$ ) and  $\text{Ph}_3\text{P}-\text{BH}_3$  (64.3 mg, 0.233 mmol) in 0.5 mL of anhydrous  $\text{CH}_2\text{Cl}_2$ . Heated in a sealed

vial at 40 °C for 1 h. The reaction mixture was passed through a short plug of silica gel while eluting with CHCl<sub>3</sub>. Concentration of the solution provided the crude product as a white solid. Double crystallization from cyclohexane provided 73 mg (71%) of a white crystalline solid.

<sup>1</sup>H NMR (500 MHz, CDCl<sub>3</sub>): δ 7.65-7.48 (m, 9H), 7.46-7.41 (m, 6H), 3.2-2.2 ppm (br m, 2H). <sup>11</sup>B NMR (128 MHz, CDCl<sub>3</sub>): δ -31.3 ppm (m). <sup>13</sup>C NMR (101 MHz, CDCl<sub>3</sub>): δ 150.0-146.6 (m), 140.6-137.4 (m), 138.4-135.1 (m), 133.4 (d, J = 9 Hz), 131.7, 128.9 (d, J = 10 Hz), 127.0 (d, J = 59 Hz), 116.5-114.2 ppm (br m). <sup>19</sup>F NMR (377 MHz, CDCl<sub>3</sub>): δ -128.1 (m), -159.5 (dt, J = 6.8, 20 Hz), -164.7 ppm (m). <sup>31</sup>P NMR (162 MHz, CDCl<sub>3</sub>): δ 12.8 ppm. HRMS (EI+): m/z calculated for C<sub>24</sub>H<sub>16</sub>BF<sub>5</sub>P [M-H]<sup>+</sup> 441.1003, found 441.1001 (0 ppm). IR(CDCl<sub>3</sub>, NaCl): 2420, 2394, 2253, 1511, 1470 cm<sup>-1</sup>.

## Chapter 2 Bibliography

1. Hurd, D. T. "The Reactions of Diborane with Hydrocarbons." *J. Am. Chem. Soc.* **1948**, *70*, 2053.
2. (a) Winternitz, P. F.; Carotti, A. A. "The Thermal Decomposition of Trialkylboranes." *J. Am. Chem. Soc.* **1960**, *82*, 2430. (b) Logan, T. J.; Flautt, T. J. "The Reaction of Diborane with Di-*t*-butylethylene and Di-*t*-acetylene." *J. Am. Chem. Soc.* **1960**, *82*, 3446. (c) Brown, H. C.; Murray, K. J.; Müller, H.; Zweifel, G. "Organoboranes. V. The Thermal Cyclization of Dialkylboranes. A Convenient Synthesis of 2,4,4-Trimethyl-1,5-pentanediol and Related 1,5-diols." *J. Am. Chem. Soc.* **1966**, *88*, 1443. (d) Abruscato, G. J.; Tidwell, T. T. "Steric Crowding in Organic Chemistry. VI. Reactivity of Tri-*tert*-butylethylene and Related Compounds." *J. Org. Chem.* **1972**, *37*, 4151. (e) Varela, J. A.; Peña, D.; Goldfuss, B.; Denisenko, D.; Kulhanek, J.; Polborn, K.; Knochel, P. "Diastereoselective Remote C–H Activation by Hydroboration." *Chem. Eur. J.* **2004**, *10*, 4252 and references therein.
3. (a) Köster, R.; Reinert, K. "Synthesen neuartiger Bor-Heterocyclen." *Angew. Chem.* **1959**, *71*, 521. (b) Köster, R.; Larbig, W.; Rotermund, G. W. "Borverbindungen, VIII. Pyrolyse von Alkyl- und Cycloalkylboranen." *Justus Liebigs Ann. Chem.* **1965**, *682*, 21. (c) Köster, R.; Benedikt, G.; Fenzl, W.; Reinert, K. "Borverbindungen, XI. Pyrolyseprodukte einiger Alkyl- und Arylborane." *Justus Liebigs Ann. Chem.* **1967**, *702*, 197.
4. De Vries, T. S.; Prokofjevs, A.; Harvey, J. N.; Vedejs, E. "Superelectrophilic Intermediates in Nitrogen-Directed Aromatic Borylation." *J. Am. Chem. Soc.* **2009**, *131*, 14679 and references therein.
5. DeVries, T. S. Ph.D. Thesis, University of Michigan, Ann Arbor, MI, 2008.
6. Goldfuss, B.; Knochel, P.; Bromm, L. O.; Knapp, K. "C–H Activation by Direct Borane-Hydrocarbon Dehydrogenation: Kinetic and Thermodynamic Aspects." *Angew. Chem. Int. Ed.* **2000**, *39*, 4136.
7. (a) Goldfuss, B. "C–H Functionalizations by Means of Direct Borane-Hydrocarbon Dehydrogenations and Dehydrocarbonations." *Chem. Eur. J.* **2009**, *15*, 12856. (b) Swinnen, S.; Nguyen, V. S.; Sakai, S.; Nguyen, M. T. "Production of Hydrogen from Reactions of Methane with Boranes." *Phys. Chem. Chem. Phys.* **2009**, *11*, 9703.
8. DePuy, C. H.; Gareyev, R.; Hankin, J., Davico, G. E.; Krempp, M.; Damrauer, R. "The Gas Phase Ion Chemistry of  $\text{BH}_2^+$ ." *J. Am. Chem. Soc.* **1998**, *120*, 5086.



9. For a representative review, see: Bennetau, B.; Dunogues, J. "Unusual Electrophilic Substitution in the Aromatic Series via Organosilicon Intermediates." *Synlett* **1993**, 171.
10. (a) Slocum, D. W.; Book, G.; Jennings, C. A. "Rate and Orientation Effect of TMEDA on Directed Lithiation Reactions." *Tetrahedron Lett.* **1970**, *11*, 3443. (b) Müller, P.; Bernardinelli, G.; Jacquier, Y. "Organometallic Derivatives of Cyclopropenes." *Helv. Chim. Acta* **1992**, *75*, 1995.
11. Pansegrau, P. D.; Rieker, W. F.; Meyers, A. I. "The Oxazoline–Benzyne Route to 1,2,3-Trisubstituted Benzenes. Tandem Addition of Organolithiums, Organocuprates, and  $\alpha$ -Lithionitriles to Benzynes." *J. Am. Chem. Soc.* **1988**, *110*, 7178.
12. (a) Bonnier, C.; Piers, W. E.; Parvez, M.; Sorensen, T. S. "Borenium Cations Derived from BODIPY Dyes." *Chem. Commun.* **2008**, 4593. (b) Bonnier, C.; Piers, W. E.; Parvez, M. "Isomeric Dipyrinato and Dipyrromethanato Boranes." *Organometallics* **2011**, *30*, 1067. (c) Inés, B.; Patil, M.; Carreras, J.; Goddard, R.; Thiel, W.; Alcarazo, M. "Synthesis, Structure, and Reactivity of a Dihydrido Borenium Cation." *Angew. Chem. Int. Ed.* **2011**, *50*, 8400.
13. (a) Gómez, R.; Green, M. L. H.; Haggitt, J. L. "Unexpected Reactions of Pentafluorophenyl Boron Compounds with  $\eta$ -Cyclopentadienyl(benzamidinato)-zirconium Derivatives." *J. Chem. Soc., Dalton Trans.* **1996**, 939. (b) Bochmann, M.; Sarsfield, M. J. "Reaction of  $AlR_3$  with  $[CPh_3][B(C_6F_5)_4]$ : Facile Degradation of  $[B(C_6F_5)_4]^-$  by Transient " $[AlR_2]^+$ "." *Organometallics* **1998**, *17*, 5908. (c) Korolev, A. V.; Ihara, E.; Guzei, I. A.; Young, V. G., Jr.; Jordan, R. F. "Cationic Aluminum Alkyl Complexes Incorporating Aminotroponimate Ligands." *J. Am. Chem. Soc.* **2001**, *123*, 8291.
14. (a) Welch, G. C.; San Juan, R. R.; Masuda, J. D.; Stephan, D. W. "Reversible, Metal-Free Hydrogen Activation." *Science* **2006**, *314*, 1124. (b) Stephan, D. W.; Erker, G. "Frustrated Lewis Pairs: Metal-Free Hydrogen Activation and More." *Angew. Chem. Int. Ed.* **2010**, *49*, 46 and references therein.
15. DeVries, T. S.; Vedejs, E. "Electrophilic Activation of Lewis Base Complexes of Borane with Trityl Tetrakis(pentafluorophenyl)borate." *Organometallics* **2007**, *26*, 3079.
16. Prokofjevs, A.; Kampf, J. W.; Vedejs, E. "A Boronium Ion with Exceptional Electrophilicity." *Angew. Chem. Int. Ed.* **2011**, *50*, 2098.
17. (a) Cho, J.-Y.; Iverson, C. N.; Smith, M. R., III. "Steric and Chelate Directing Effects in Aromatic Borylation." *J. Am. Chem. Soc.* **2000**, *122*, 12868. (b) Vanchura, B. A., II.; Preshlock, S. M.; Roosen, P. C.; Kallepalli, V. A.; Staples, R. J.; Maleczka, R. E., Jr.; Singleton, D. A.; Smith, M. R., III. "Electronic Effects in Iridium C–H Borylations: Insights from Unencumbered Substrates and Variation of Boryl Ligand Substituents." *Chem. Commun.* **2010**, *46*, 7724 and

- references therein. (c) Mkhaliid, I. A. I.; Barnard, J. H.; Marder, T. B.; Murphy, J. M.; Hartwig, J. F. "C–H Activation for the Construction of C–B bonds." *Chem. Rev.* **2010**, *110*, 890.
18. Gay, R. L.; Hauser, C. R. "Lithiations of  $\alpha$ - and  $\beta$ -Dimethylaminomethylnaphthalenes with *n*-Butyllithium and Condensations with Benzophenone. Some Related Results." *J. Am. Chem. Soc.* **1967**, *89*, 2297.
19. For recent reports of electrophilic aromatic borylation, see: (a) Del Grosso, A.; Pritchard, R. G.; Muryn, C. A.; Ingleson, M. J. "Chelate Restrained Boron Cations for Intermolecular Electrophilic Arene Borylation." *Organometallics* **2010**, *29*, 241. (b) Ishida, N.; Moriya, T.; Goya, T.; Murakami, M. "Synthesis of Pyridine–Borane Complexes via Electrophilic Aromatic Borylation." *J. Org. Chem.* **2010**, *75*, 8709. (c) Del Grosso, A.; Singleton, P. J.; Muryn, C. A.; Ingleson, M. J. "Pinacol Boronates by Direct Arene Borylation with Borenium Cations." *Angew. Chem. Int. Ed.* **2011**, *50*, 2102.
20. For representative reviews mentioning borane cage expansion with BH<sub>3</sub>, see: (a) Sivaev, I. B.; Bregadze, V. I.; Sjöberg, S. "Chemistry of *closo*-Dodecaborate Anion [B<sub>12</sub>H<sub>12</sub>]<sup>2-</sup>: a Review." *Collect. Czech. Chem. Commun.* **2002**, *67*, 679. (b) Kaszynski, P. "Four Decades of Organic Chemistry of *closo*-Boranes: a Synthetic Toolbox for Constructing Liquid Crystal Materials. A Review." *Collect. Czech. Chem. Commun.* **1999**, *64*, 895.
21. Kameda, M.; Kodama, G. "Unsymmetrical Cleavage of Boranes by Bis(trimethylphosphine)–Diborane(4). Formation of a Triboron Cation." *J. Am. Chem. Soc.* **1980**, *102*, 3647.
22. Fuller, A.-M.; Hughes, D. L.; Lancaster, S. J.; White, C. M. "Synthesis and Structure of the Dimethyl Sulfide Adducts of Mono- and Bis(pentafluorophenyl)-borane." *Organometallics* **2010**, *29*, 2194.
23. (a) Scheideman, M.; Shapland, P.; Vedejs, E. "A Mechanistic Alternative for the Intramolecular Hydroboration of Homoallylic Amine and Phosphine Borane Complexes." *J. Am. Chem. Soc.* **2003**, *125*, 10502. (b) Shapland, P.; Vedejs, E. "Intramolecular Hydroboration of Unsaturated Phosphine Boranes." *J. Org. Chem.* **2004**, *69*, 4094. (c) Clay, J. M.; Vedejs, E. "Hydroboration with Pyridine Borane at Room Temperature." *J. Am. Chem. Soc.* **2005**, *127*, 5766. (d) Shapland, P.; Vedejs, E. "Isopinocampheylborane Derivatives with >99% ee via the DMAP Complex." *J. Org. Chem.* **2006**, *71*, 6666. (e) Karatjas, A. G.; Vedejs, E. "Formation of Pinacol Boronate Esters via Pyridine Iodoborane Hydroboration." *J. Org. Chem.* **2008**, *73*, 9508. (f) Scheideman, M.; Wang, G.; Vedejs, E. "Amine-Directed Hydroboration: Scope and Limitations." *J. Am. Chem. Soc.* **2008**, *130*, 8669. (g) Rarig, R.-A. F.; Scheideman, M.; Vedejs, E. "Oxygen-Directed Intramolecular Hydroboration." *J. Am. Chem. Soc.* **2008**, *130*, 9182.

24. (a) Soderquist, J. A.; Brown, H. C. "Hydroboration. 56. Convenient and Regiospecific Route to Functionalized Organosilanes through the Hydroboration of Alkenylsilanes." *J. Org. Chem.* **1980**, *45*, 3571. (b) Bhat, N. G.; Garza, A. "A Simple Synthesis of B-2-(1-trimethylsilyl-1-alkyl)-1,3,2-dioxaborinanes. Isolation and Selective Oxidation to 1-Trimethylsilyl-1-alkanols." *Tetrahedron Lett.* **2003**, *44*, 6833.
25. Curran, D. P.; Solovyev, A.; Makhlof Brahmi, M.; Fensterbank, L.; Malacria, M.; Lacôte, E. "Synthesis and Reactions of N-Heterocyclic Carbene Boranes." *Angew. Chem. Int. Ed.* **2011**, *50*, 10294.
26. (a) Brown, H. C.; Knights, E. F.; Scouten, C. G. "Hydroboration. XXXVI. A Direct Route to 9-Borabicyclo[3.3.1]nonane via the Cyclic Hydroboration of 1,5-Cyclooctadiene. 9-Borabicyclo[3.3.1]nonane as a Uniquely Selective Reagent for the Hydroboration of Olefins." *J. Am. Chem. Soc.* **1974**, *96*, 7765. (b) Brown, H. C.; Bhatt, M. V. "Organoboranes. IV. The Displacement Reaction with Organoboranes Derived from the Hydroboration of Branched-Chain Olefins. A Contrathermodynamic Isomerization of Olefins." *J. Am. Chem. Soc.* **1966**, *88*, 1440. (c) Rickborn, B.; Wood, S. E. "Cleavage of Cyclopropanes by Diborane." *J. Am. Chem. Soc.* **1971**, *93*, 3940. (d) Parks, D. J.; Piers, W. E.; Yap, G. P. A. "Synthesis, Properties and Hydroboration Activity of the Highly Electrophilic Borane Bis(pentafluorophenyl)borane,  $\text{HB}(\text{C}_6\text{F}_5)_2$ ." *Organometallics* **1998**, *17*, 5492.
27. Harris, R. K.; Becker, E. D.; Cabral de Menezes, S. M.; Goodfellow, R.; Granger, P. "NMR Nomenclature. Nuclear Spin Properties and Conventions for Chemical Shifts." *Pure Appl. Chem.* **2001**, *73*, 1795.

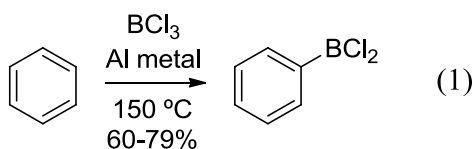
## Chapter 3

# Borenium and Boronium Salts Derived from 9-BBN and Their Application toward Electrophilic Aromatic Borylation

### Introduction

The borylation reactions of tricoordinate B–H borenium ions discussed in the previous chapter are most reasonably rationalized as occurring via a C–H insertion mechanism. This mechanism suggests that in the C–B bond forming process the formally empty *p*-orbital at boron acts as the acceptor of the electron pair of the C–H bond, while the H atom at B acts as a base responsible for scavenging the C–H hydrogen atom. In other cases, such as in the classical Friedel–Crafts reaction, the attack of the Lewis acid on the substrate and the C–H deprotonation step are performed by two different species. A brief survey of C–H borylations reported in the literature reveals that at least in some cases, such as in the classical study on borylation of benzene with BCl<sub>3</sub> in presence of Al metal reported by Muetterties in 1960 some variations of the Friedel–Crafts mechanism might operate (eq 1).<sup>1</sup> This methodology has seen relatively little development until very recently, however. The main reasons for that include limited electrophilicity of boron compounds,<sup>2</sup> but more importantly the instability of the borylation products under the typical electrophilic aromatic substitution conditions. The reverse of the electrophilic aromatic borylation reaction, protodeboration, is typically very facile under the reaction conditions due to the formation of the acid byproduct, which must be neutralized

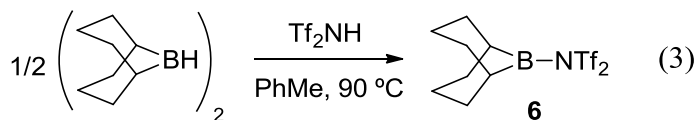
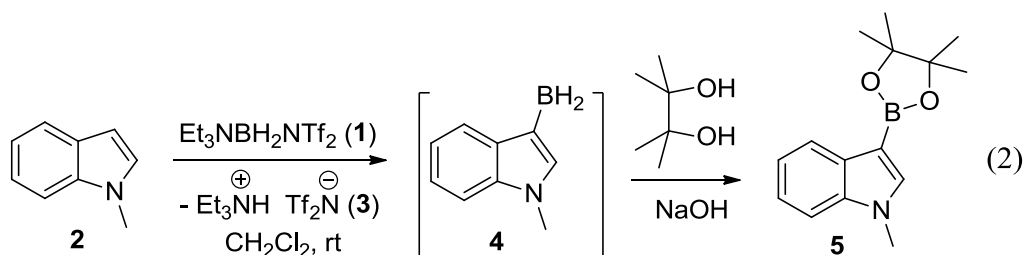
in some way to drive the reaction toward the borylated compound. On the other hand, neutralization of the acid byproduct without deactivation of the boron electrophile becomes challenging, which explains the unusual choice of Al metal as the acid scavenger in the Muetterties protocol.<sup>1</sup>



### Electrophilic Aromatic Borylation of Electron-Rich Arenes and Heteroarenes

During our studies on amine borane activation with Tf<sub>2</sub>NH we noticed that boron bistriflimide **1** (as a mixture of N- and O-bound species, see Chapter 1) is sufficiently electrophilic to react with electron-rich heteroarenes such as N-methylindole (**2**) (eq 2). Interestingly, while the reaction between **1** and N-methylindole (**2**) led to the formation of a new C–B bond, the byproduct of the transformation was found to be the triethylammonium salt **3** rather than H<sub>2</sub> gas as detected by <sup>1</sup>H NMR, which sharply contrasts with the borylation processes described in Chapter 2. While the exact structure of the borylation product arising from **1** and **2** is unknown, the stoichiometry of the reaction suggests that a BH fragment is delivered to **2** during the course of the reaction, and thus the product structure was tentatively assigned as **4**. The regiochemistry of the borylation reaction was established by converting **4** to the isolable boronic ester **5**, although the efficiency of the process was found to be rather low (ca. 20-30% isolated yield of **5**), and a substantial amount of the starting indole **2** was recovered. Since *in situ* NMR experiments indicated full consumption of **2** in the initial borylation step, the low yield of the isolated product **5** is apparently explained by the facile protodeboration of

borylated indoles under the quenching conditions. Additionally, NMR monitoring of the reaction progress suggested that disproportionation processes leading to products with multiple indole units connected to a single B atom might be taking place under the reaction conditions. Since the disproportionation process presents a major complication on the way to improving the yields of the borylated indole **5**, the reactivity of B-substituted analogs of **1** was explored.



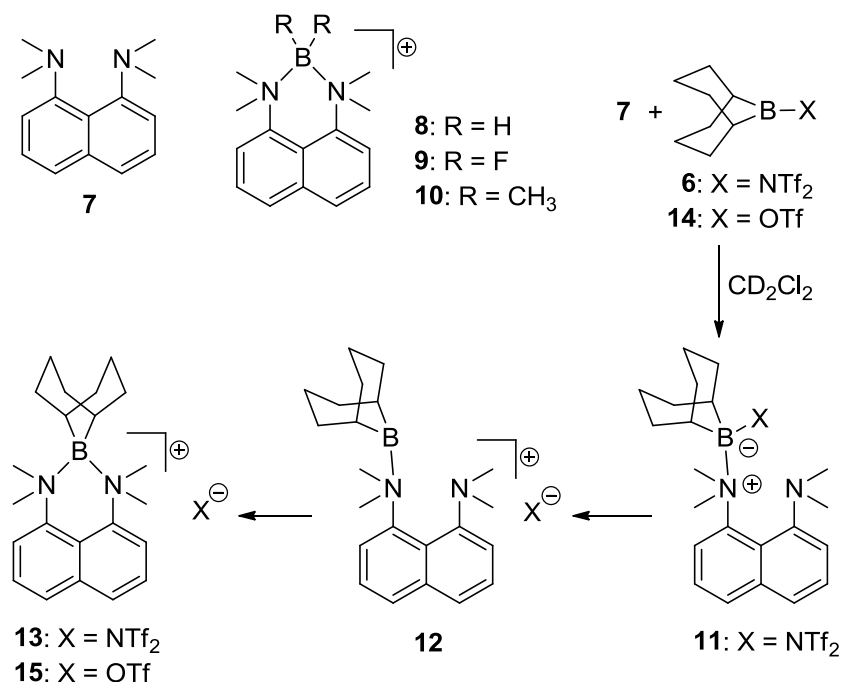
In our search for a more reliable protocol for the electrophilic borylation of electron-rich substrates, the previously unreported boron bistriflimide **6** was prepared in one step from commercially available 9-borabicyclo[3.3.1]nonane (9-BBN) and Tf<sub>2</sub>NH (eq 3) upon heating in toluene. Unlike amine adduct **1**, tricoordinate boron bistriflimide **6** possesses no built-in basic fragment, and thus an external non-nucleophilic base is necessary. In principle, a suitable base might be 1,8-bis(dimethylamino)naphthalene (**7**), a hindered and exceptionally basic aniline that finds numerous applications as a basic catalyst or reagent due to its legendary lack of nucleophilicity.<sup>3,4</sup> Strong electrophiles interact weakly, if at all, with the amine nitrogens, and very few examples are known where stable bonds to nitrogen can be formed between **7** and electrophilic groups larger

than hydrogen.<sup>3,5-8</sup> Among these exceptional cases, cyclic boronium structures **8** and **9** are relatively stable because the subunits BH<sub>2</sub> and BF<sub>2</sub> have minimal steric requirements, and while the BCl<sub>2</sub> analog has been claimed, no definitive evidence has been reported.<sup>6</sup> However, the more hindered BMe<sub>2</sub> derivative **10** has not been detected and no analogous BR<sub>2</sub> structures are known.<sup>6a</sup> In view of this long history, we were somewhat surprised to find that an adduct is readily formed simply upon mixing **7** with the 9-BBN bistriflimide reagent **6** despite the transannular steric demands of the 9-BBN core and the need to form adjacent quaternary bonds to boron as well as nitrogen.<sup>9,10</sup>

Combination of the bulky tricoordinate boron reagent **6** with a stoichiometric amount of **7** in CD<sub>2</sub>Cl<sub>2</sub> at room temperature formed a deep red solution that turned colorless within seconds of mixing the reagents. Analysis of the resulting solution by <sup>11</sup>B NMR spectroscopy revealed a signal at  $\delta$  16.2 ppm, suggesting that a single tetracoordinate<sup>11</sup> boron atom is present in the product. The <sup>19</sup>F NMR spectrum showed a single peak at  $\delta$  -79.4 ppm ( $\delta$  -79.4 ppm at -80 °C), which is characteristic of bistriflimide anion,<sup>12</sup> so the boron-containing fragment was thus identified to be a cation. For comparison, the covalent bistriflimide **6** gives rise to a signal at  $\delta$  -70.0 ppm. The <sup>1</sup>H NMR spectrum suggested that the solution structure of the cation is highly symmetrical on the NMR timescale at room temperature. Only four groups of protons corresponding to the diamine subunit **7** were observed, including one sharp singlet for all four methyl groups, and a well-resolved (at 500 MHz) AMX system for the aromatic protons. Other peaks in the <sup>1</sup>H and <sup>13</sup>C NMR spectra were also consistent with a symmetrical time-averaged structure for the cation (for example, a single <sup>13</sup>C methyl peak at  $\delta$  57.1 ppm, and only 3 peaks for the 9-BBN cage carbons). Since the covalent adduct

**11** is ruled by observation of the bistriflimide anion, and the tricoordinate cationic borenium structure **12** is not consistent with the observed  $^{11}\text{B}$  NMR chemical shift, the most plausible structure for the species formed from **6** and **7** is the exceptionally hindered boronium salt **13**. Several mechanistic alternatives for the formation of **13** may be possible, such as the logical sequence in Scheme 3-1, an equivalent electron transfer process, a process involving dicoordinate borinium intermediates, or a direct displacement mechanism from **6** and **7** via a transition state that resembles **12**. Formation of >95% **13** depends on the low nucleophilicity of the counterion, and only partial conversion to the boronium ion was observed when **14** was used instead of **6**. Thus, when equimolar **7** and the triflate reagent **14** were mixed in  $\text{CD}_2\text{Cl}_2$ , the resulting solution showed both the starting **7** and the product **15** (ca. 1.2:1 ratio by  $^1\text{H}$  NMR assay).

**Scheme 3-1.** Formation of Boronium **13**



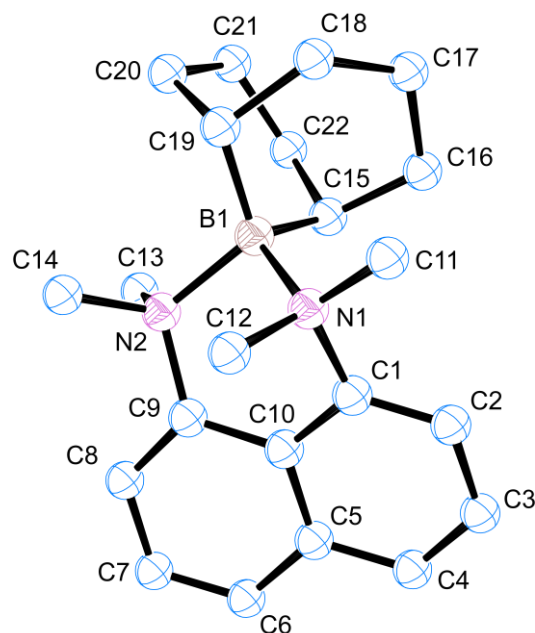
The low temperature  $^1\text{H}$  NMR behavior of **13** in  $\text{CD}_2\text{Cl}_2$  is complex and indicates the presence of unsymmetrical species. Decreasing the temperature broadens the



$^1\text{H}$  NMR singlet corresponding to the N-methyl groups, until it turns into a broad set of at least three maxima that are not fully resolved even at  $-80^\circ\text{C}$ . Additional information about the solution structure is provided by the very different shielding of the two bridgehead hydrogen atoms of the 9-BBN cage observed in the low temperature  $^1\text{H}$  NMR spectra. While the spectrum taken at room temperature shows only one peak for both bridgehead protons, two distinct resonances are observed at  $-80^\circ\text{C}$ . One of the bridgehead hydrogens gives rise to a peak at an unremarkable  $\delta$  1.57 ppm, while the other hydrogen appears at  $\delta$  0.33 ppm. Such prominent shielding by the aromatic ring is consistent with the 9-BBN cage being tilted toward one side of the naphthalene plane to place the shielded proton above the aromatic  $\pi$ -system.

Slow cooling of the solution of **13** in a mixture of  $\text{CH}_2\text{Cl}_2$  and hexanes produced large platelike crystals, suitable for X-ray diffraction studies (see Appendix A). Due to strain imposed by the hindered environment, the structure of **13** is non-symmetrical, the B–N bonds are very long, and both the 9-BBN cage and the bis(dimethylamino)naphthalene unit are severely twisted. While the C15–B1–C19 angle ( $106^\circ$ ) and C–B bond lengths (1.63 Å, B1–C15; 1.61 Å, B1–C19) are within the expected range for 9-BBN derivatives,<sup>9a,13</sup> the C20–C19–C15–C22 and C18–C19–C15–C16 dihedral angles are in excess of  $10^\circ$ . Furthermore, strong distortion of the diamine base is evidenced by the N2–C9–C1–N1 dihedral angle of  $28.9^\circ$ , compared to  $20.3^\circ$  in **7**.<sup>14</sup> On the other hand, the aniline N $\cdots$ N distance in **13** (2.65 Å) is substantially shorter than that reported for **7** (2.79 Å), and only slightly exceeds that in salts of protonated **7**, such as the sulfonimide salt **7**·HNMs<sub>2</sub> (2.60 Å).<sup>15</sup>

**Figure 3-1.** X-Ray structure of **13** (cation only, 50% probability ellipsoids)



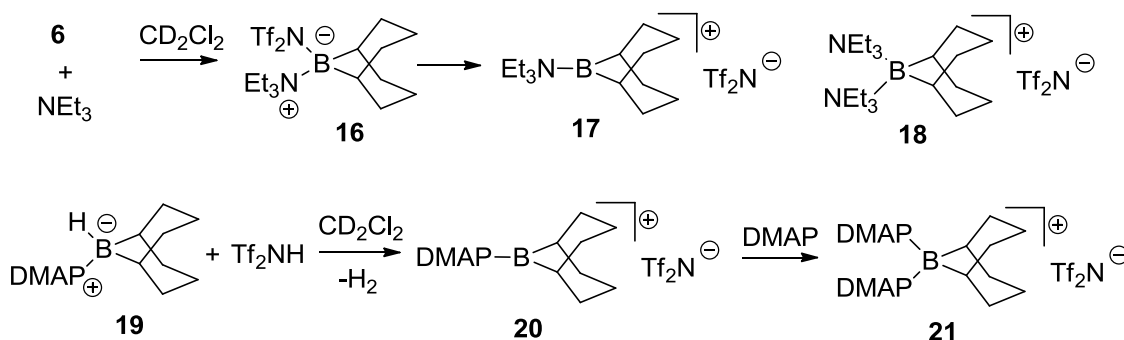
The arrangement of the 9-BBN cage in crystals of **13** is also noteworthy. The bridgehead carbons C15 and C19 are quite distinct, and C15 is pseudo-axial with respect to the distorted half-chair boron heterocycle. This places C15–H above the aromatic  $\pi$ -system, consistent with the low temperature  $^1\text{H}$  NMR result indicating substantial shielding of one of the bridgehead protons. Another prominent structural detail is the length of the B–N bonds (B1–N1 1.72 Å; B1–N2 1.73 Å), compared to values of 1.58–1.60 Å in simpler boronium cations such as  $[\text{H}_2\text{B}(\text{NMe}_3)(\text{MeIm})]^+$  or  $[\text{H}_2\text{B}(\text{NH}_2\text{Me})(\text{MeIm})]^+$  (MeIm = 1-methylimidazole).<sup>16,17</sup> Since the 1.72–1.73 Å distance greatly exceeds the sum of covalent radii for B and N atoms (1.55 Å),<sup>18</sup> the calculated Pauling bond order for both B–N bonds in **13** is only ca. 0.55.<sup>19</sup>

The unusual structural features prompted computational modeling of the cation **13**.<sup>20</sup> Gas phase geometry optimization at the M06-2X/6-31G(d,p) level produced a structure that is in close agreement with the X-ray data (for example, B–N bond lengths

are within 0.01 Å of the experimental values). NBO analysis<sup>20c</sup> performed on the optimized structure indicates that the boron atom carries the bulk of the positive charge (NBO charge 0.97), and Wiberg bond orders of the two B–N bonds are 0.52 and 0.53.

It was also of interest to compare the interactions of other amines with the potent Lewis acid **6** in solution. When triethylamine was combined with **6** in CD<sub>2</sub>Cl<sub>2</sub>, clean formation of the borenium ion **17** was observed (Scheme 3-2). No evidence for a boronium structure **18** was detected, even when excess triethylamine was used. The borenium character of **17** is substantiated by a strongly deshielded <sup>11</sup>B NMR peak at δ 85.1 ppm, as well as the bistriflimide anion peak at δ –79.5 ppm in the <sup>19</sup>F NMR spectrum,<sup>12</sup> evidence that rules out the alternative structure **16**. For simplicity, **16** is tentatively shown as a precursor of **17**, although direct conversion from **6** is not ruled out.

**Scheme 3-2.** Generation of Borenium Salts from **6**



In contrast to triethylamine, 4-(dimethylamino)pyridine (DMAP) reacted with a stoichiometric amount of **6** to afford mostly the isolable boronium cation **21** according to the <sup>11</sup>B NMR shift of δ 3.0 ppm (CD<sub>2</sub>Cl<sub>2</sub>, rt) along with traces of the borenium cation **20** (δ 66.5 ppm).<sup>21</sup> A much better way to generate **20** *in situ* was to protonate the amine borane complex **19** with Tf<sub>2</sub>NH. This method confirmed the chemical shift of **20** and afforded solutions also containing relatively minor amounts of the boronium salt **21** (ca.

7-11:1 **20:21**). However, the more hindered 2,6-di-*tert*-butyl-4-methylpyridine did not interact with **6** at room temperature according to  $^1\text{H}$  and  $^{11}\text{B}$  NMR assay.

The most remarkable feature of the boronium salt **17** is the absence of any stabilizing  $\pi$ -donor or *n*-donor substituents at boron, in contrast to **20** and to all previously reported persistent boronium ions generated in the condensed phase.<sup>22</sup> A comparison of  $^{11}\text{B}$  NMR shifts for **17** ( $\delta$  85.1 ppm) and **20** ( $\delta$  66.5 ppm) indicates extensive cation stabilization by  $\pi$  delocalization between DMAP and the boron atom. Other  $\pi$ -stabilized boronium cations have been observed in the  $^{11}\text{B}$  chemical shift range of  $\delta$  58.2 to 66 ppm,<sup>22</sup> suggesting that **17** may be an exceptionally electrophilic member of the boronium family of structures.

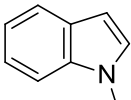
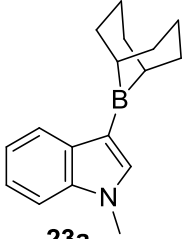
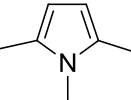
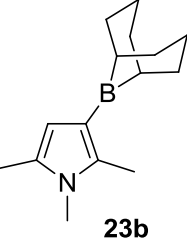
High electrophilicity of boron cations is crucial for potential applications in electrophilic aromatic borylation.<sup>22,23</sup> Thus, different combinations of the bistriflimide **6** with basic amines generated reagents that react with electron-rich heterocycles to provide B-heteroaryl 9-BBN derivatives along with the protonated amines. The reagent consisting of **6** and the non-complexing 2,6-di-*tert*-butyl-4-methylpyridine was the most reactive, and borylated N-methylindole in seconds at room temperature to afford **23a** (>95% conversion by NMR spectroscopy), while the cationic reagents **13** and **17** required several hours at 50 °C for similar conversion. No added base was needed with **13** or **17** because both reagents already contain a “built-in” base (proton sponge **7** and triethylamine, respectively) to neutralize the HNTf<sub>2</sub> that forms during borylation. On the other hand, neither **20** nor **21** reacted with N-methylindole under these conditions.

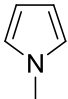
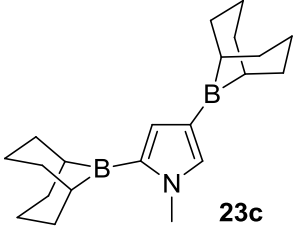
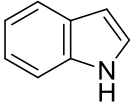
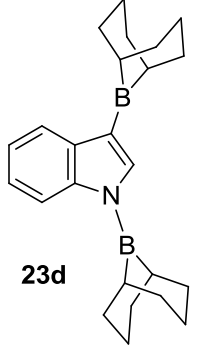
While the boronium salt **13** is less potent than the reagent from **6** and 2,6-di-*tert*-butyl-4-methylpyridine, **13** is a far more convenient borylating agent. Practical access to

**13** on gram scale is possible using a one-pot procedure from 9-BBN, **7**, and HNTf<sub>2</sub> without having to isolate the highly sensitive **6** (see Experimental). Crystallized **13** is much easier to handle compared to **6**, and even survives up to a month of exposure to dry air (desiccator over Drierite), in contrast to **6** or **17**. Furthermore, the aromatic borylation products obtained using **13** are easy to isolate (eq 4, Table 3-1). Crystalline products **23a–d** were obtained in high purity simply by extracting the reaction mixtures with hexanes, where neither the unreacted **13** nor the byproduct **7·HNTf<sub>2</sub>** is soluble, followed by solvent evaporation. This procedure minimizes the risk of competing protodeboration using **13**, but it is not feasible with the reagent from **6** and 2,6-di-*tert*-butyl-4-methylpyridine due to differences in reagent solubility.



**Table 3-1.** Borylation of Nitrogen Heterocycles Using **13**<sup>a</sup>

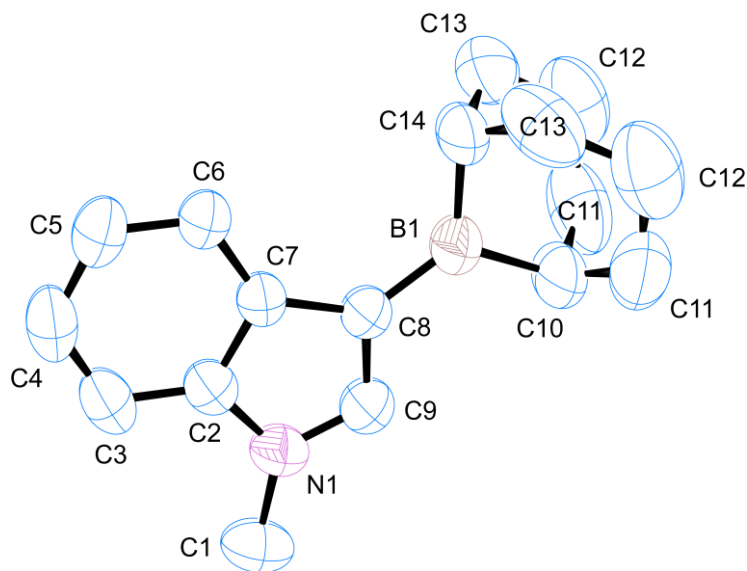
Het-H	Product, Het-BBN	Time	Yield, %
 <p><b>22a</b></p>	 <p><b>23a</b></p>	1.5 h	96
 <p><b>22b</b></p>	 <p><b>23b</b></p>	1.5 h	98

 <p><b>22c</b></p>	 <p><b>23c</b></p>	3.5 h	97 <sup>b</sup>
 <p><b>22d</b></p>	 <p><b>23d</b></p>	5.5 d	97 <sup>b</sup>

<sup>a</sup>1.05 equiv of **13**; CH<sub>2</sub>Cl<sub>2</sub>; 50 °C. <sup>b</sup>2.10 equiv of **13**

The structures of boranes **23a-d** were established by multinuclear NMR spectroscopy, as well as X-ray crystallography in the case of **23a** (Figure 3-2, also see Appendix A). Borylation of N-methylindole afforded exclusively the 3-substituted regioisomer, in sharp contrast to the previously reported reaction with B(C<sub>6</sub>F<sub>5</sub>)<sub>3</sub>, which produces the 2-borylated N-methylindole.<sup>24</sup> Pyrrole **22c** gave a mixture of mono-borylated regioisomers along with some of the diborylated **23c** using one equivalent of **13** (ca. 80% conversion of **22c**), but two equivalents of the borylating agent cleanly produced the diborylated pyrrole **23c**. In the reaction with unsubstituted indole, the known N-borylation product was produced first,<sup>25</sup> followed by much slower C3-borylation to afford **23d**.

**Figure 3-2.** X-Ray structure of **23a** (50% probability ellipsoids)



Several reactions of **13** suggest that it is in equilibrium with the starting **6** and **7**. Thus, equimolar **13** and  $\text{Tf}_2\text{NH}$  produced the protonated diamine ( $\mathbf{7}\cdot\text{HNTf}_2$ ) and released **6** (NMR assay). Furthermore, reaction of **13** with triethylammonium bistriflimide ( $\text{Et}_3\text{NH}^+ \text{Tf}_2\text{N}^-$ ) yielded  $\mathbf{7}\cdot\text{HNTf}_2$  and the tricoordinate cation **17**, representing an unusual route from boronium to borenium ions involving the formal migration of the 9-BBN fragment to a different amine. These events can be understood if dissociation of **13** to **6** + **7** is the first step. The same dissociative mechanism may also help explain the borylations of Table 3-1, although the identity of the key boron electrophile is not clear. Depending on the timing of bond dissociation and borylation events, a role for the tricoordinate borenium ion **12** or even a dicoordinate borinium ion<sup>23</sup> cannot be ruled out at this point. The equilibrium between **23** and **6** + **7** is not directly observable by  $^1\text{H}$  NMR spectroscopy, but the analogous process does occur in the related system **15** and **7** + **14**, containing the more nucleophilic triflate anion (*vide supra*).

The hindered boronium salt **13** cautions against interpreting the name “proton sponge” too literally: in fact, this study proves that **7** can act as a chelating ligand for species much larger than a proton. Also, the unusual structure of **13** raises a rhetorical question: is there a distinct boundary between the cationic species called “boronium” (tetra-substituted B), “borenium” (tri-substituted B), and “borinium” (di-substituted B), according to Nöth's terminology?<sup>22a</sup> While **13** should be most appropriately called a boronium salt, the long B-N distances increase the “borinium-like” character, and the unusual reactivity adds a small hint of a borenium ion (**12**). Aside from the structural features of **13**, the chemoselectivity of its formation also deserves attention. In view of earlier reports that strong electrophiles attack the aromatic system of **7**<sup>2</sup> or abstract hydride from one of the *N*-methyl groups,<sup>2a,26</sup> it is quite intriguing that the reaction between **6** and **7** proceeds to form **13**, the most hindered of all plausible products.

### Summary

To summarize, the covalent boron bistriflimide **6** was used to access the unusual boron salts **13** and **17**, as well as borenium **20** by exploiting the excellent leaving group ability of bistriflimide anion. The structure of the hindered boronium **13** was established using X-ray crystallography. The triethylamine-derived **17** expands the range of borenium salts observed in the condensed phase, proving that resonance delocalization of the positive charge is not required for a persistent borenium cation. Amine-based borocations **13** and **17**, as well as the combination of **6** with 2,6-di-*tert*-butyl-4-methylpyridine serve as potent borylating agents, capable of reacting with electron-rich aromatic systems.



## Experimental

**General Methods.** All reactions were performed at room temperature (unless otherwise stated), under an atmosphere of dry nitrogen, either in a glovebox, or using standard Schlenk techniques. Nuclear magnetic resonance experiments were performed on Varian Inova 500 and Inova 400 spectrometers at the following frequencies:  $^1\text{H}$  500 MHz or 400 MHz;  $^{11}\text{B}$  and  $^{11}\text{B}\{^1\text{H}\}$  128 MHz;  $^{13}\text{C}\{^1\text{H}\}$  101 MHz;  $^{19}\text{F}$  377 MHz. All spectra were recorded in  $\text{CD}_2\text{Cl}_2$  and referenced to the  $^1\text{H}$  signal of internal  $\text{Me}_4\text{Si}$  according to IUPAC recommendations,<sup>27</sup> using a  $\mathcal{E}$  (referencing parameter) of 32.083974 for  $\text{BF}_3\cdot\text{OEt}_2$  ( $^{11}\text{B}$ ), a  $\mathcal{E}$  of 25.145020 for  $\text{Me}_4\text{Si}$  ( $^{13}\text{C}$ ), and a  $\mathcal{E}$  of 94.094011 for  $\text{CCl}_3\text{F}$  ( $^{19}\text{F}$ ). IR spectra were acquired in  $\text{CCl}_4$  or  $\text{CD}_2\text{Cl}_2$  solutions using a  $\text{CaF}_2$  cell. UV spectra were acquired using a Shimadzu UV-1601 spectrophotometer. Toluene and  $\text{Et}_3\text{N}$  were distilled over  $\text{CaH}_2$ ;  $\text{CH}_2\text{Cl}_2$  and hexanes were dried by passing through a column of activated alumina. Then, the solvents and  $\text{Et}_3\text{N}$  were further dried by storing over activated 3Å molecular sieves in the glovebox. Commercially available NMR grade  $\text{CD}_2\text{Cl}_2$  (Cambridge Isotope Laboratories) was not distilled; instead it was simply dried over a large amount of activated 3Å molecular sieves in the glovebox. All other reagents were used as received from commercial suppliers.

### Preparation of 9-BBN Bistriflimide 6

Every possible effort was made to protect the reaction mixture from exposure to air and moisture. The glassware used in this experiment was dried in a heating oven at ca. 200 °C overnight. Toluene was distilled over  $\text{CaH}_2$ , and then further dried by storing over activated 3Å molecular sieves in the glovebox. In the glovebox, a dry round-bottom

flask fitted with a reflux condenser was charged with a mixture of solid 9-borabicyclo[3.3.1]nonane dimer (0.868 g, 7.11 mmol of the monomer) and bis(trifluoromethanesulfonyl)imide (2.00 g, 7.11 mmol). Dry toluene (1 mL) was added to the solid mixture at rt, the apparatus was capped with a rubber septum, removed from the glovebox, and connected to a nitrogen line. The reaction mixture was then heated at 90 °C for 40 min. Intensive gas liberation was observed while heating (adequate venting must be provided), and a clear solution was formed. The resulting solution was distilled in vacuum, and a fraction boiling at 108 °C (1.5 Torr) was collected. Boron bistriflimide **6** is a very dense ( $d = 1.49 \text{ g/cm}^3$ ), viscous liquid and is highly air-sensitive.

$^1\text{H}$  NMR (400 MHz,  $\text{CD}_2\text{Cl}_2$ ):  $\delta$  2.07-1.81 (m, 10H), 1.59-1.52 (m, 2H), 1.52-1.42 ppm (m, 2H).  $^{11}\text{B}$  NMR (128 MHz,  $\text{CD}_2\text{Cl}_2$ ):  $\delta$  59.2 ppm (s).  $^{13}\text{C}$  NMR (101 MHz,  $\text{CD}_2\text{Cl}_2$ ):  $\delta$  119.4 (q,  $J_{\text{C-F}} = 325 \text{ Hz}$ ), 33.6, 29.6-28.0 (m), 22.9 ppm.  $^{19}\text{F}$  NMR (377 MHz,  $\text{CD}_2\text{Cl}_2$ ):  $\delta$  -70.0 ppm (br s). HRMS (EI+):  $m/z$  calculated for  $\text{C}_{10}\text{H}_{14}\text{BF}_6\text{NO}_4\text{S}_2$   $[\text{M}]^+$  401.0362, found 401.0347 (-4 ppm). IR ( $\text{CCl}_4$ ,  $\text{CaF}_2$ ): 1437, 1417, 1359, 1325, 1121  $\text{cm}^{-1}$ .

### Preparation of Boronium Salt 13

Every possible effort was made to protect the reaction mixtures from exposure to air and moisture. The glassware used in this experiment was either dried in a heating oven at ca. 200 °C overnight (for *method A*), or disposable glassware flame-dried at the glass softening temperature was used (for *method B*). Toluene was distilled over  $\text{CaH}_2$ , and hexanes were dried by passing through a column of activated alumina. The solvents were further dried by storing over activated 3Å molecular sieves in the glovebox before use.

*Method A.* In the glovebox, a dry round-bottom flask fitted with a reflux condenser was charged with a mixture of solid 9-borabicyclo[3.3.1]nonane dimer (0.461 g, 3.78 mmol of the monomer) and bis(trifluoromethanesulfonyl)imide (0.966 g, 3.44 mmol). Dry toluene (5 mL) was added to the solid mixture at rt, the apparatus was capped with a rubber septum, removed from the glovebox, and connected to a nitrogen line. The reaction mixture was then heated at reflux for 1 h under nitrogen atmosphere. Intensive gas liberation was observed while heating (adequate venting must be provided), and a clear solution was formed. The reaction apparatus was transferred back into the glovebox, where the reaction mixture along with 2x1 mL of dry toluene was slowly added to a solution of 1,8-bis(dimethylamino)naphthalene (0.737 g, 3.44 mmol) in 3 mL of dry toluene at rt. Upon mixing the reagents the reaction mixture developed a striking red color that persisted for a few seconds. A small exotherm was observed, and precipitation of a pale yellow oil began immediately. The oil crystallized within a few minutes of stirring at rt, the resulting crystals were isolated by filtration, and then washed with 2x1 mL of dry toluene followed by 2 mL of dry hexanes. Drying the resulting solid in the glovebox yielded 2.04 g (96%) of the desired product. The resulting crystals of **13** if thoroughly dried are very stable in dry air, although solutions of the product are very sensitive.

*Method B.* Alternatively, the boronium salt **13** was prepared by mixing equimolar amounts of the boron bistriflimide reagent **6** and 1,8-bis(dimethylamino)-naphthalene in dry CH<sub>2</sub>Cl<sub>2</sub> followed by evaporation of the solvent. The reaction was essentially instantaneous, but the product prepared in this manner was contaminated with the

bis(trifluoromethanesulfonyl)imide salt of 1,8-bis(dimethylamino)naphthalene due to Tf<sub>2</sub>NH impurity in the boron reagent **6**.

<sup>1</sup>H NMR (500 MHz, CD<sub>2</sub>Cl<sub>2</sub>): δ 8.01 (dd, J = 8.3 Hz, 0.5 Hz, 2H), 7.90 (dd, J = 8.0 Hz, 0.5 Hz, 2H), 7.74 (t, J = 8.0 Hz, 2H), 3.48 (s, 12H), 2.31-2.13 (m, 4H), 2.19-2.05 (m, 2H), 1.81-1.67 (m, 6H), 1.02-0.91 ppm (br s, 2H). <sup>11</sup>B NMR (128 MHz, CD<sub>2</sub>Cl<sub>2</sub>): δ 16.2 ppm (s). <sup>13</sup>C NMR (101 MHz, CD<sub>2</sub>Cl<sub>2</sub>): δ 142.9, 135.0, 129.5, 127.7, 120.3 (q, J<sub>C-F</sub> = 322 Hz), 120.1, 119.7, 57.1, 34.6, 21.0-19.9 (m), 20.3 ppm. <sup>19</sup>F NMR (377 MHz, CD<sub>2</sub>Cl<sub>2</sub>): δ -79.4 ppm (s). HRMS (ES<sup>+</sup>): m/z calculated for C<sub>22</sub>H<sub>32</sub>BN<sub>2</sub> [M]<sup>+</sup> 335.2653, found 355.3655 (+1 ppm). IR(CD<sub>2</sub>Cl<sub>2</sub>, CaF<sub>2</sub>): 2874, 1603, 1576, 1492, 1435, 1342, 1142 cm<sup>-1</sup>. m.p. 128 °C (sealed capillary); decomposition begins ca. 100 °C.

### Generation of Borenium Salt **17**

Every possible effort was made to protect the reaction mixtures from exposure to air and moisture. The reaction was set up in a dry J. Young NMR tube under N<sub>2</sub> atmosphere in a glovebox. Commercially available NMR grade CD<sub>2</sub>Cl<sub>2</sub> was dried over a large amount of activated 3Å molecular sieves in the glovebox. Triethylamine was distilled over CaH<sub>2</sub>, and then further dried by storing over activated 3Å molecular sieves in the glovebox. The NMR tube was dried in a heating oven at ca. 200 °C overnight, and the fitted Teflon valve was dried in a dessicator over Drierite. The reaction tube was charged with a solution of boron bistriflimide **6** (30.0 μL, 0.111 mmol) in 0.6 mL of dry CD<sub>2</sub>Cl<sub>2</sub>. Neat triethylamine (15.5 μL, 0.112 mmol) was added via a microsyringe in one portion at rt. The tube was immediately sealed with the fitted Teflon valve, and then

shaken vigorously for ca. 1 min. NMR analysis indicated clean formation of borenium salt **17**.

$^1\text{H}$  NMR (400 MHz,  $\text{CD}_2\text{Cl}_2$ ):  $\delta$  3.51 (q,  $J = 7.4$  Hz, 6H), 2.35-2.26 (m, 4H), 2.25-2.12 (m, 2H), 2.07-1.94 (m, 4H), 1.87-1.80 (m, 2H), 1.66-1.56 (m, 2H), 1.35 ppm (t,  $J = 7.4$  Hz, 9H).  $^{11}\text{B}$  NMR (128 MHz,  $\text{CD}_2\text{Cl}_2$ ):  $\delta$  85.1 ppm (s).  $^{13}\text{C}$  NMR (101 MHz,  $\text{CD}_2\text{Cl}_2$ ):  $\delta$  120.4 (q,  $J_{\text{C-F}} = 322$  Hz), 50.0, 36.3, 30.4-29.1 (m), 22.5, 9.6 ppm.  $^{19}\text{F}$  NMR (377 MHz,  $\text{CD}_2\text{Cl}_2$ ):  $\delta$  -79.5 ppm (s).

### Preparation of Amine Borane **19**

The reaction was performed under  $\text{N}_2$  atmosphere in a glovebox. In a dry 4 mL scintillation vial a mixture of solid 9-borabicyclo[3.3.1]nonane dimer (82.2 mg, 0.674 mmol of the monomer) and 4-(dimethylamino)pyridine (82.3 mg, 0.674 mmol) was dissolved in 1 mL of anhydrous  $\text{CH}_2\text{Cl}_2$ , and the resulting clear solution was stirred at rt overnight. A white precipitate appeared on stirring, and the slurry was concentrated to afford **19** as a white solid in quantitative yield.

$^1\text{H}$  NMR (500 MHz,  $\text{CD}_2\text{Cl}_2$ ):  $\delta$  8.11-8.06 (m, 2H), 6.62-6.58 (m, 2H), 3.09 (s, 6H), 2.77-2.00 (m, 1H), 1.96-1.72 (m, 6H), 1.56-1.48 (m, 3H), 1.48-1.39 (m, 2H), 1.29-1.21 (m, 1H), 1.13-1.04 ppm (m, 2H).  $^{11}\text{B}$  NMR (128 MHz,  $\text{CD}_2\text{Cl}_2$ ):  $\delta$  -3.2 ppm (d,  $J_{\text{B-H}} = 60$  Hz).  $^{13}\text{C}$  NMR (101 MHz,  $\text{CD}_2\text{Cl}_2$ ):  $\delta$  155.1, 144.8, 106.9, 39.6, 35.4, 29.5, 25.9, 25.5, 24.6-23.0 ppm (m). IR( $\text{CD}_2\text{Cl}_2$ ,  $\text{CaF}_2$ ): 2269, 2239, 1635, 1547, 1444, 1344, 1229, 1202  $\text{cm}^{-1}$ . The compound has no distinct melting point; partial melting ca. 163  $^\circ\text{C}$  (sealed capillary) with decomposition.

### Generation of Borenium Salt **20** and Boronium Salt **21**

Every possible effort was made to protect the reaction mixtures from exposure to air and moisture. The reactions were performed under N<sub>2</sub> atmosphere in a glovebox. Commercially available NMR grade CD<sub>2</sub>Cl<sub>2</sub> was dried over a large amount of activated 3Å molecular sieves in the glovebox. The NMR tube was dried in a heating oven at ca. 200 °C overnight, and the fitted Teflon valve was dried in a dessicator over Drierite. Other glassware was flame-dried at the glass softening temperature.

Solid bis(trifluoromethanesulfonyl)imide (23.8 mg, 84.8 μmol) was added in small portions to a stirred solution of amine-borane complex **19** (20.7 mg, 84.8 μmol) in 1 mL of dry CD<sub>2</sub>Cl<sub>2</sub>. Intensive gas liberation was observed. The resulting clear solution was then transferred to a dry J. Young NMR tube. NMR assay of the solution showed formation of borenium salt **20**, along with minor amounts of the boronium salt **21** and DMAP·HNTf<sub>2</sub> (typically 7-11:1 **20:21**). Addition of an extra equivalent of 4-(dimethylamino)pyridine (10.4 mg, 84.8 μmol) cleanly produced boronium salt **21**, as evidenced by NMR spectroscopy.

Alternatively, complex **21** was prepared by carefully treating a solution of 4-(dimethylamino)pyridine (27.1 mg, 0.222 mmol) in 0.5 mL of anhydrous CH<sub>2</sub>Cl<sub>2</sub> with neat boron bistriflimide **6** (30.0 μL, 0.111 mmol). Concentration of the resulting solution afforded a white crystalline solid in quantitative yield.

**20**: <sup>1</sup>H NMR (500 MHz, CD<sub>2</sub>Cl<sub>2</sub>): δ 8.37-8.33 (m, 2H), 6.99-6.95 (m, 2H), 3.37 (s, 6H), 2.14-1.98 (m, 8H), 1.93-1.84 (m, 4H), 1.45-1.37 ppm (m, 2H). <sup>11</sup>B NMR (128 MHz, CD<sub>2</sub>Cl<sub>2</sub>): δ 66.5 ppm (s). <sup>13</sup>C NMR (101 MHz, CD<sub>2</sub>Cl<sub>2</sub>): δ 159.2, 142.6, 120.3 (q, J<sub>C-F</sub> = 322 Hz), 108.8, 41.2, 34.4, 28.0-26.2 (m), 23.2 ppm. <sup>19</sup>F NMR (377 MHz, CD<sub>2</sub>Cl<sub>2</sub>): δ -79.4 ppm (s).

**21:**  $^1\text{H}$  NMR (500 MHz,  $\text{CD}_2\text{Cl}_2$ ):  $\delta$  8.07-8.03 (m, 4H), 6.69-6.65 (m, 4H), 3.11 (s, 12H), 1.97-1.85 (m, 2H), 1.85-1.78 (m, 4H), 1.62-1.58 (m, 2H), 1.58-1.48 (m, 4H), 1.38-1.31 ppm (m, 2H).  $^{11}\text{B}$  NMR (128 MHz,  $\text{CD}_2\text{Cl}_2$ ):  $\delta$  3.0 ppm (s).  $^{13}\text{C}$  NMR (101 MHz,  $\text{CD}_2\text{Cl}_2$ ):  $\delta$  156.3, 142.8, 120.4 (q,  $J_{\text{C-F}} = 322$  Hz), 108.1, 39.9, 30.4, 23.7, 21.5-20.5 ppm (m).  $^{19}\text{F}$  NMR (377 MHz,  $\text{CD}_2\text{Cl}_2$ ):  $\delta$  -79.5 ppm (s). HRMS (ES<sup>+</sup>): m/z calculated for  $\text{C}_{22}\text{H}_{34}\text{BN}_4$   $[\text{M}]^+$  365.2871, found 365.2873 (+1 ppm). IR( $\text{CD}_2\text{Cl}_2$ ,  $\text{CaF}_2$ ): 2891, 2851, 1635, 1557, 1444, 1350, 1138  $\text{cm}^{-1}$ . The compound has no distinct melting point; partial melting ca. 208 °C (sealed capillary) with decomposition. UV/Vis ( $\text{CH}_2\text{Cl}_2$ ):  $\lambda_{\text{max}}(\epsilon) = 295$  (24000), 283 nm (21000).

### Indole and Pyrrole Borylation with **13**

Every possible effort was made to protect the reaction mixtures from exposure to air and moisture. The reactions were performed under  $\text{N}_2$  atmosphere in a glovebox. Disposable glassware flame-dried at the glass softening temperature was used.

*Small Scale Procedure.* In the glovebox, a dry 4 mL scintillation vial was charged with a solution of the desired substrate (0.16-0.17 mmol) and boronium salt **13** (1.05 equivalents per each 9-BBN unit introduced) in dry  $\text{CH}_2\text{Cl}_2$  (0.5 mL per each 9-BBN unit introduced). The reaction vessel was sealed and heated at 50 °C for the amount of time indicated below. The reaction mixture was then diluted with dry hexanes (1 mL per each 9-BBN unit introduced) and left at rt for 1–2 hours to allow the byproduct to precipitate. Following decantation of supernatant, the solids were washed with 4x0.5 mL of dry hexanes, and the combined solutions were evaporated to dryness to give crude material. The pure product was obtained by extracting the crude material with 4x0.5 mL of dry hexanes followed by concentration of the extracts. All of the resulting borylated

heterocycles were found to be extremely sensitive to water and air. UV spectra of the borylated heterocycles were acquired in 0.83% (v/v) solution of NEt<sub>3</sub> in hexanes. Very rapid protodeboronation precludes acquisition of UV spectra in the absence of NEt<sub>3</sub>.

*Large Scale Procedure.* Compound **23a** was also prepared on a larger scale using a modified procedure. A dry 12 mL thick-walled Schlenk tube (dried in a heating oven at ca. 200 °C overnight) fitted with a teflon stopper was charged with a mixture of N-methylindole (206 μL, 0.218 g, 1.66 mmol) and boronium salt **13** (1.07 g, 1.74 mmol) in 3 mL of dry CH<sub>2</sub>Cl<sub>2</sub>. The reaction vessel was sealed and then heated at 50 °C for 2 h. The reaction mixture was then diluted with 5 mL of dry hexanes and left at room temperature for 1-2 hours to allow the byproduct to precipitate. Following decantation of supernatant, the solids were washed with 3x1 mL of dry hexanes, and the combined extracts were evaporated to dryness to give crude material. The pure product (0.415 g) was obtained in essentially quantitative yield by extracting the crude material with 5 portions of dry hexanes (total solvent volume 12 mL) followed by concentration of the extracts.

**23a**: Reaction time 1.5 hours, 96% yield of a colorless crystalline solid. <sup>1</sup>H NMR (500 MHz, CD<sub>2</sub>Cl<sub>2</sub>): δ 8.04 (d, J = 8.0 Hz, 1H), 7.74 (s, 1H), 7.37 (d, J = 8.0 Hz, 1H), 7.27-7.23 (m, 1H), 7.20-7.16 (m, 1H), 3.83 (s, 3H), 2.38-2.29 (m, 2H), 2.07-1.95 (m, 6H), 1.94-1.82 (m, 4H), 1.40-1.31 ppm (m, 2H). <sup>11</sup>B NMR (128 MHz, CD<sub>2</sub>Cl<sub>2</sub>): δ 72.6 ppm (s). <sup>13</sup>C NMR (101 MHz, CD<sub>2</sub>Cl<sub>2</sub>): δ 141.7, 139.8, 133.5, 122.9, 122.2, 121.2, 116.2-114.9 (m), 110.0, 34.3, 33.5, 30.0-28.8 (m), 24.0 ppm. HRMS (EI+ 70 eV): m/z calculated for C<sub>17</sub>H<sub>22</sub>BN [M]<sup>+</sup> 251.1845, found 251.1850 (+2 ppm). IR(CCl<sub>4</sub>, CaF<sub>2</sub>):



1675, 1511, 1465, 1421, 1364, 1333, 1159, 1132, 1109  $\text{cm}^{-1}$ . m.p. 106-108 °C (sealed capillary). UV/Vis (0.83% v/v  $\text{NEt}_3$  in hexanes):  $\lambda_{\text{max}}(\epsilon) = 291 \text{ nm}$  (15000).

**23b:** Reaction time 1.5 hours, 98% yield of a colorless crystalline solid.  $^1\text{H}$  NMR (500 MHz):  $\delta$  6.21 (q,  $J = 0.9 \text{ Hz}$ , 1H), 3.41 (s, 3H), 2.43 (s, 3H), 2.20 (s, 3H), 2.11-2.05 (m, 2H), 2.01-1.86 (m, 6H), 1.82-1.73 (m, 4H), 1.35-1.25 ppm (m, 2H).  $^{11}\text{B}$  NMR (128 MHz,  $\text{CD}_2\text{Cl}_2$ ):  $\delta$  72.2 ppm (s).  $^{13}\text{C}$  NMR (101 MHz,  $\text{CD}_2\text{Cl}_2$ ):  $\delta$  140.5, 129.0, 120.0-118.3 (m), 112.7, 34.2, 30.6, 29.8-29.0 (m), 24.0, 13.4, 12.6 ppm. HRMS (EI+ 70 eV):  $m/z$  calculated for  $\text{C}_{15}\text{H}_{24}\text{BN} [\text{M}]^+$  229.2002, found 229.2002 (0 ppm). IR( $\text{CCl}_4$ ,  $\text{CaF}_2$ ): 2915, 2837, 1503, 1433, 1405, 1372, 1350, 1172, 1115  $\text{cm}^{-1}$ . m.p. 120 °C (sealed capillary). UV/Vis (0.83% v/v  $\text{NEt}_3$  in hexanes):  $\lambda_{\text{max}}(\epsilon) = 286 \text{ nm}$  (6100).

**23c:** Reaction time 3.5 hours, 97% yield of a colorless crystalline solid.  $^1\text{H}$  NMR (500 MHz,  $\text{CD}_2\text{Cl}_2$ ):  $\delta$  7.60 (d,  $J = 1.6 \text{ Hz}$ , 1H), 7.55 (dd,  $J = 1.6 \text{ Hz}$ , 0.4 Hz, 1H), 3.92 (t,  $J = 0.4 \text{ Hz}$ , 3H), 2.23-2.18 (m, 2H), 2.08-1.90 (m, 14H), 1.90-1.73 (m, 8H), 1.41-1.25 ppm (m, 4H).  $^{11}\text{B}$  NMR (128 MHz,  $\text{CD}_2\text{Cl}_2$ ):  $\delta$  73.0 (s), 70.2 ppm (s).  $^{13}\text{C}$  NMR (101 MHz,  $\text{CD}_2\text{Cl}_2$ ):  $\delta$  142.8, 141.2-140.0 (m), 134.4, 124.0-123.1 (m), 38.4, 34.4, 34.3, 29.9-29.1(m), 29.1-28.3 (m), 24.0, 23.8 ppm. HRMS (EI+ 70 eV):  $m/z$  calculated for  $\text{C}_{21}\text{H}_{33}\text{B}_2\text{N} [\text{M}]^+$  321.2799, found 321.2811 (+4 ppm). IR( $\text{CCl}_4$ ,  $\text{CaF}_2$ ): 1656, 1486, 1450, 1422, 1362, 1325, 1150, 1112  $\text{cm}^{-1}$ . m.p. 133-135 °C (sealed capillary). UV/Vis (0.83% v/v  $\text{NEt}_3$  in hexanes):  $\lambda_{\text{max}}(\epsilon) = 290 \text{ nm}$  (22000).

**23d:** Reaction time 5.5 days, 97% yield of a colorless crystalline solid.  $^1\text{H}$  NMR (500 MHz,  $\text{CD}_2\text{Cl}_2$ ):  $\delta$  8.22 (s, 1H), 8.03-7.99 (m, 1H), 7.93-7.88 (m, 1H), 7.28-7.23 (m, 2H), 2.70-2.21 (m, 4H), 2.16-1.83 (m, 20H), 1.50-1.41 (m, 2H), 1.41-1.32 ppm (m, 2H).  $^{11}\text{B}$

NMR (128 MHz, CD<sub>2</sub>Cl<sub>2</sub>): δ 75.7 (s), 62.0 ppm (s). <sup>13</sup>C NMR (101 MHz, CD<sub>2</sub>Cl<sub>2</sub>): δ 143.5, 143.3, 137.4, 123.5, 123.2, 122.9, 122.7-122.0 (m), 116.0, 34.3, 34.1, 30.7-29.6 (m), 28.2-26.3 (m), 23.9, 23.5 ppm. HRMS (EI+ 70 eV): m/z calculated for C<sub>24</sub>H<sub>33</sub>B<sub>2</sub>N [M]<sup>+</sup> 357.2799, found 357.2814 (+4 ppm). IR(CCl<sub>4</sub>, CaF<sub>2</sub>): 1694, 1487, 1471, 1449, 1405, 1334, 1292, 1135, 1108 cm<sup>-1</sup>. m.p. 204-206 °C (sealed capillary).

### Chapter 3 Bibliography

1. Muetterties, E. L. "Synthesis of Organoboranes." *J. Am. Chem. Soc.* **1960**, *82*, 4163.
2. Intermediates in the Muetterties borylation protocol apparently involve superelectrophilic species: Olah, G.; Klumpp, D. A. *Superelectrophiles and their chemistry*; Wiley-Interscience: Hoboken N.J., 2008.
3. Alder, R. W.; Bowman, P. S.; Steele, W. R. S.; Winterman, D. R. "The Remarkable Basicity of 1,8-Bis(dimethylamino)naphthalene." *Chem. Commun.* **1968**, 723.
4. Reviews: (a) Barner, B. A.; Faler, C. A.; Joullié, M. M. *1,8-Bis(dimethylamino)naphthalene. e-EROS Encyclopedia of Reagents for Organic Synthesis*; DOI 10.1002/047084289X.rb144.pub2, and references therein. (b) Pozharskii, A. F.; Ozeryanskii, V. A. *The Chemistry of Anilines, Part 1*; John Wiley & Sons Ltd: Chichester, 2007.
5. N-Monomethylation of 1,8-bis(dimethylamino)naphthalene: Alder, R. W.; Goode, N. C. "A Case of Kinetic N- and Equilibrium C-Protonation in Strong Acids." *J. Chem. Soc., Chem. Commun.* **1976**, 108.
6. (a) Axtell, D. D.; Cambell, A. C.; Keller, P. C.; Rund, J. V. "The Behavior of Rigid and Semi-Rigid Bidentate Donor Molecules toward Some Simple Boron Acceptors." *J. Coord. Chem.* **1976**, *5*, 129. (b) Onak, T.; Rosendo, H.; Siwapinyoyos, G.; Kubo, R.; Liauw, L. "Reaction of 1,8-Bis(dimethylamino)naphthalene, a Highly Basic and Weakly Nucleophilic Amine, with Several Polyboranes and with Boron Trifluoride." *Inorg. Chem.* **1979**, *18*, 2943. (c) Keller, P. C.; Rund, J. V. "Reactions of Diborane with Some Chelating Bidentate Ligands. A One-Step Synthesis of [(LL)BH<sub>2</sub>]<sub>2</sub>B<sub>2</sub>H<sub>7</sub> Salts." *Inorg. Chem.* **1979**, *18*, 3197. (d) Hartman, J. S.; Shoemaker, J. A. W. "Chelated Fluoroboron Cations II. Synthesis and NMR Studies Involving Aromatic Chelating Ligands." *Polyhedron* **2000**, *19*, 165.
7. Only one transition metal complex of 1,8-bis(dimethylamino)naphthalene has been structurally characterized: Yamasaki, T.; Ozaki, N.; Saika, Y.; Ohta, K.; Goboh, K.; Nakamura, F.; Hashimoto, M.; Okeya, S. "First Transition Metal Complex of 1,8-Bis(dimethylamino)naphthalene (Proton Sponge)." *Chem. Lett.* **2004**, *33*, 928.
8. 1,8-Bis(dimethylamino)naphthalene as a proposed ligand for metals: (a) Lucht, B. L.; Bernstein, M. P.; Remenar, J. F.; Collum, D. B. *J. Am. Chem. Soc.* **1996**, *118*, 10707. (b) Farzaneh, F.; Majidian, M.; Ghandi, M. *J. Mol. Catal. A: Chem.* **1999**, *148*, 227. (c) Collman, J. P.; Zhong, M.; Zhang, C.; Costanzo, S. *J. Org. Chem.* **2001**, *66*, 7892.

9. For 9-BBN-derived boronium salts containing relatively non-hindered pyridine ligands, see: (a) Ma, K.; Bats, J. W.; Wagner, M. "(2,2'-Bipyridyl-N,N')(bicyclo[3.3.1]nonane-C<sup>1</sup>,C<sup>5</sup>)boronium Trifluoromethanesulfonate." *Acta Crystallogr., Sect. E: Struct. Rep. Online* **2001**, E57, o846. (b) Köster, R.; Grassberger, M. A. "Halogen-organoborane durch katalytische Komproportionierung von Trihalogenboranen und Organoboranen." *Justus Liebigs Ann. Chem.* **1968**, 719, 169. (c) Hünig, S.; Wehner, I. "Two Step Redox Systems LII: 2,2'-Bipyridylboronium Salts." *Heterocycles* **1989**, 28, 359.
10. Cyclic aminoboranes derived from 1,8-diaminonaphthalene and 9-BBN: (a) Bar-Haim, G.; Kol, M. "Selective Synthesis of N-Monoalkyl and N,N'-Dialkyl Derivatives of 1,8-Diaminonaphthalene-9-BBN as an Activating and Directing Group." *J. Org. Chem.* **1997**, 62, 6682. (b) Bar-Haim, G. Shach, R.; Kol, M. "A Novel Diaminoborate Ligand System Derived from 1,8-Diaminonaphthalene and 9-BBN: Preparation of Titanium and Zirconium Complexes and Crystal Structure of the Titanium Complex." *Chem. Commun.* **1997**, 229.
11. Nöth, H.; Wrackmeyer, B. *Nuclear Magnetic Resonance Spectroscopy of Boron Compounds*; Springer: Berlin, 1978.
12. Tf<sub>2</sub>N<sup>-</sup> salts: Arvai, R.; Toulgoat, F.; Langlois, B. R.; Sanchez, J.-Y.; Médebielle, M. *Tetrahedron* **2009**, 65, 5361.
13. (a) Yalpani, M.; Boese, R.; Köster, R. *Chem. Ber.* **1990**, 123, 1275. (b) Brock, C. P.; Fu, Y.; Niedenzu, K.; Nöth, H. *Main Group Met. Chem.* **1992**, 15, 53. (c) Wrackmeyer, B.; Schwarze, B.; Milius, W. *J. Organomet. Chem.* **1995**, 489, 201.
14. Einspahr, H.; Robert, J.-B.; Marsh, R. E.; Roberts, J. D. *Acta Crystallogr., Sect. B: Struct. Crystallogr. Cryst. Chem.* **1973**, 29, 1611.
15. Henschel, D.; Moers, O.; Lange, I.; Blaschette, A.; Jones, P. G. *Z. Naturforsch., B: J. Chem. Sci.* **2002**, 57b, 777.
16. (a) Fox, P. A.; Griffin, S. T.; Reichert, W. M.; Salter, E. A.; Smith, A. B.; Tickell, M. D.; Wicker, B. F.; Cioffi, E. A.; Davis, J. H. Jr.; Rogers, R. D.; Wierzbicki, A. *Chem. Commun.* **2005**, 3679. (b) Soutullo, M. D.; Odom, C. I.; Smith, A. B.; McCreary, D. R.; Sykora, R. E.; Salter, E. A.; Wierzbicki, A.; Davis, J. H. Jr. *Inorg. Chim. Acta* **2007**, 360, 3099.
17. A B–N bond distance of 1.61 Å has been reported for a 9-BBN-derived boronium ion with bipyridyl as the nitrogen ligand (ref. 9a).
18. B. Cordero, V. Gómez, A. E. Platero-Prats, M. Revés, J. Echeverría, E. Cremades, F. Barragán, S. Alvarez, *Dalton Trans.* **2008**, 2832
19. L. Pauling, *J. Am. Chem. Soc.* **1947**, 69, 542

20. (a) Gaussian 09, Revision A.02. M. J. Frisch, G. W. Trucks, H. B. Schlegel, G. E. Scuseria, M. A. Robb, J. R. Cheeseman, G. Scalmani, V. Barone, B. Mennucci, G. A. Petersson, H. Nakatsuji, M. Caricato, X. Li, H. P. Hratchian, A. F. Izmaylov, J. Bloino, G. Zheng, J. L. Sonnenberg, M. Hada, M. Ehara, K. Toyota, R. Fukuda, J. Hasegawa, M. Ishida, T. Nakajima, Y. Honda, O. Kitao, H. Nakai, T. Vreven, J. A. Montgomery, Jr., J. E. Peralta, F. Ogliaro, M. Bearpark, J. J. Heyd, E. Brothers, K. N. Kudin, V. N. Staroverov, R. Kobayashi, J. Normand, K. Raghavachari, A. Rendell, J. C. Burant, S. S. Iyengar, J. Tomasi, M. Cossi, N. Rega, J. M. Millam, M. Klene, J. E. Knox, J. B. Cross, V. Bakken, C. Adamo, J. Jaramillo, R. Gomperts, R. E. Stratmann, O. Yazyev, A. J. Austin, R. Cammi, C. Pomelli, J. W. Ochterski, R. L. Martin, K. Morokuma, V. G. Zakrzewski, G. A. Voth, P. Salvador, J. J. Dannenberg, S. Dapprich, A. D. Daniels, O. Farkas, J. B. Foresman, J. V. Ortiz, J. Cioslowski, and D. J. Fox, Gaussian, Inc., Wallingford CT, 2009. (b) Zhao, Y.; Truhlar, D. G. "The M06 Suite of Density Functionals for Main Group Thermochemistry, Thermochemical Kinetics, Noncovalent Interactions, Excited States, and Transition Elements: Two New Functionals and Systematic Testing of Four M06-Class Functionals and 12 Other Functionals." *Theor. Chem. Acc.* **2008**, *120*, 215. (c) NBO Version 3.1. Glendening, E. D.; Reed, A. E.; Carpenter, J. E.; Weinhold, F.
21. Narula, C. K.; Nöth, H. *Inorg. Chem.* **1985**, *24*, 2532.
22. (a) Kölle, P.; Nöth, H. "The Chemistry of Borinium and Borenum Ions." *Chem. Rev.* **1985**, *85*, 399. (b) Piers, W. E.; Bourke, S. C.; Conroy, K. D. "Borinium, Borenum, and Boronium Ions: Synthesis, Reactivity, and Applications." *Angew. Chem. Int. Ed.* **2005**, *44*, 5016. (c) De Vries, T. S.; Prokofjevs, A.; Vedejs, E. "Cationic Tricoordinate Boron Intermediates: Borenum Chemistry from the Organic Perspective." *Chem. Rev.* **2012**, *112*, 4246.
23. Del Grosso, A.; Pritchard, R. G.; Muryn, C. A.; Ingleson, M. J. *Organometallics* **2010**, *29*, 241.
24. F. Focante, I. Camurati, D. Nanni, R. Leardini, L. Resconi, *Organometallics* **2004**, *23*, 5135.
25. B. Wrackmeyer, H. E. Maisel, B. Schwarze, W. Milius, R. Köster, *J. Organomet. Chem.* **1997**, *541*, 97-107; B. Wrackmeyer, B. Schwarze, *J. Organomet. Chem.* **1997**, *534*, 207.
26. Harris, R. K.; Becker, E. D.; Cabral de Menezes, S. M.; Goodfellow, R.; Granger, P. "NMR Nomenclature. Nuclear Spin Properties and Conventions for Chemical Shifts." *Pure Appl. Chem.* **2001**, *73*, 1795.

**Appendix A**  
**X-Ray Crystal Structures**

### X-Ray Structure of **1-24a** ( $[\text{B}(\text{C}_6\text{F}_5)_4]^-$ salt)

See Figure 1-2 for an ORTEP plot of **1-24a**. A crystal of dimensions 0.44x0.14x0.12 mm was mounted on a Bruker SMART APEX CCD-based X-ray diffractometer equipped with a low temperature device and fine focus Mo-target X-ray tube ( $\lambda = 0.71073 \text{ \AA}$ ) operated at 1500 W power (50 kV, 30 mA). The X-ray intensities were measured at 85(1) K; the detector was placed at a distance 5.055 cm from the crystal. A total of 5190 frames were collected with a scan width of  $0.5^\circ$  in  $\omega$  and  $0.45^\circ$  in  $\phi$  with an exposure time of 25 s/frame. The integration of the data yielded a total of 76588 reflections to a maximum  $2\theta$  value of  $56.74^\circ$  of which 8372 were independent and 7015 were greater than  $2\sigma(I)$ . The final cell constants (triclinic,  $a = 10.3435(9) \text{ \AA}$ ;  $\alpha = 76.7247(13)^\circ$ ;  $b = 12.4348(11) \text{ \AA}$ ;  $\beta = 81.6108(13)^\circ$ ;  $c = 13.7303(12) \text{ \AA}$ ;  $\gamma = 78.5633(13)^\circ$ ;  $V = 1675.3(3) \text{ \AA}^3$ ) were based on the xyz centroids of 9736 reflections above  $10\sigma(I)$ . Analysis of the data showed negligible decay during data collection; the data were processed with SADABS and corrected for absorption. The structure was solved and refined with the Bruker SHELXTL (version 2008/3) software package, using the space group  $P\bar{1}$  with  $Z = 2$  for the formula  $\text{C}_{30}\text{H}_{23}\text{B}_3\text{N}_2\text{F}_{20}$ . All non-hydrogen atoms were refined anisotropically with the hydrogen atoms placed in idealized or refined positions. The cation is partially disordered with a  $(\text{CH}_3)_3\text{NBH}_2$  fragment occupying two orientations. Full matrix least-squares refinement based on  $F^2$  converged at  $R1 = 0.0371$  and  $wR2 = 0.0968$  [based on  $I > 2\sigma(I)$ ],  $R1 = 0.0451$  and  $wR2 = 0.1025$  for all data.

Sheldrick, G.M. SHELXTL, v. 2008/3; Bruker Analytical X-ray, Madison, WI, 2008; Sheldrick, G.M. SADABS, v. 2008/1. Program for Empirical Absorption

Correction of Area Detector Data, University of Gottingen: Gottingen, Germany, 2008;  
 Saint Plus, v. 7.53a, Bruker Analytical X-ray, Madison, WI, 2008.

Table 1. Crystal data and structure refinement for **1-24a**.

Empirical formula	C <sub>30</sub> H <sub>23</sub> B <sub>3</sub> F <sub>20</sub> N <sub>2</sub>
Formula weight	823.93
Temperature	85(2) K
Wavelength	0.71073 Å
Crystal system, space group	Triclinic, P-1
Unit cell dimensions	a = 10.3435(9) Å, α = 76.7247(13)°. b = 12.4348(11) Å, β = 81.6108(13)°. c = 13.7303(12) Å, γ = 78.5633(13)°.
Volume	1675.3(3) Å <sup>3</sup>
Z, Calculated density	2, 1.633 Mg/m <sup>3</sup>
Absorption coefficient	0.173 mm <sup>-1</sup>
F(000)	824
Crystal size	0.44 x 0.14 x 0.12 mm
Theta range for data collection	1.53 to 28.36°.
Limiting indices	-13<=h<=13, -16<=k<=16, -18<=l<=18
Reflections collected / unique	76588 / 8372 [R(int) = 0.0293]
Completeness to θ = 28.36	99.7 %
Absorption correction	Semi-empirical from equivalents
Max. and min. transmission	0.9795 and 0.9278
Refinement method	Full-matrix least-squares on F <sup>2</sup>
Data / restraints / parameters	8372 / 8 / 578
Goodness-of-fit on F <sup>2</sup>	1.033
Final R indices [I>2σ(I)]	R1 = 0.0371, wR2 = 0.0968
R indices (all data)	R1 = 0.0451, wR2 = 0.1025
Largest diff. peak and hole	0.444 and -0.315 e·Å <sup>-3</sup>



Table 2. Atomic coordinates ( $\times 10^4$ ) and equivalent isotropic displacement parameters ( $\text{\AA}^2 \times 10^3$ ) for **1-24a**.  
 $U(\text{eq})$  is defined as one third of the trace of the orthogonalized  $U_{ij}$  tensor.

	x	y	z	U(eq)
F(1)	7197(1)	2952(1)	4231(1)	33(1)
F(2)	8292(1)	4431(1)	4812(1)	49(1)
F(3)	10005(1)	5622(1)	3491(1)	52(1)
F(4)	10561(1)	5284(1)	1568(1)	43(1)
F(5)	9445(1)	3865(1)	959(1)	30(1)
F(6)	6644(1)	4349(1)	820(1)	28(1)
F(7)	6570(1)	4561(1)	-1140(1)	38(1)
F(8)	7515(1)	2767(1)	-2037(1)	45(1)
F(9)	8475(1)	745(1)	-881(1)	43(1)
F(10)	8487(1)	496(1)	1078(1)	30(1)
F(11)	10234(1)	1398(1)	1870(1)	26(1)
F(12)	11612(1)	-446(1)	2920(1)	31(1)
F(13)	10470(1)	-1606(1)	4652(1)	37(1)
F(14)	7870(1)	-901(1)	5280(1)	38(1)
F(15)	6441(1)	829(1)	4208(1)	32(1)
F(16)	5830(1)	834(1)	2200(1)	31(1)
F(17)	3204(1)	1050(1)	2546(1)	42(1)
F(18)	1730(1)	2913(1)	3123(1)	43(1)
F(19)	2975(1)	4597(1)	3292(1)	38(1)
F(20)	5568(1)	4438(1)	2892(1)	33(1)
N(1)	5532(1)	7584(1)	3651(1)	26(1)
N(2)	7252(2)	7654(2)	435(2)	27(1)
N(2A)	7236(10)	7758(6)	462(5)	27(4)
C(1)	5205(2)	6448(2)	3781(2)	58(1)
C(2)	5945(2)	7690(2)	4609(1)	55(1)
C(3)	4334(2)	8430(1)	3415(1)	40(1)
C(4)	6528(2)	8790(2)	2(2)	43(1)
C(5)	7433(2)	6924(2)	-320(1)	33(1)
C(6)	8589(3)	7781(5)	643(3)	32(2)
C(6A)	8598(13)	7848(17)	649(16)	37(8)
C(7)	8217(1)	3342(1)	2557(1)	23(1)
C(8)	8022(1)	3525(1)	3534(1)	27(1)
C(9)	8586(1)	4279(1)	3860(1)	35(1)
C(10)	9435(1)	4890(1)	3195(1)	36(1)
C(11)	9700(1)	4723(1)	2227(1)	32(1)
C(12)	9099(1)	3965(1)	1929(1)	26(1)
C(13)	7616(1)	2425(1)	1061(1)	22(1)
C(14)	7119(1)	3428(1)	426(1)	24(1)
C(15)	7068(1)	3562(1)	-593(1)	29(1)
C(16)	7538(1)	2660(1)	-1045(1)	33(1)
C(17)	8024(1)	1642(1)	-457(1)	31(1)
C(18)	8039(1)	1543(1)	569(1)	25(1)
C(19)	8247(1)	1207(1)	2950(1)	21(1)
C(20)	9589(1)	827(1)	2696(1)	22(1)
C(21)	10336(1)	-111(1)	3234(1)	24(1)
C(22)	9760(1)	-706(1)	4107(1)	27(1)
C(23)	8449(1)	-354(1)	4414(1)	27(1)
C(24)	7729(1)	573(1)	3834(1)	25(1)
C(25)	5867(1)	2599(1)	2565(1)	22(1)
C(26)	5162(1)	1790(1)	2479(1)	25(1)
C(27)	3805(1)	1874(1)	2656(1)	30(1)
C(28)	3053(1)	2823(1)	2936(1)	31(1)
C(29)	3680(1)	3670(1)	3011(1)	29(1)
C(30)	5055(1)	3550(1)	2814(1)	25(1)
B(1)	6745(2)	7776(2)	2824(1)	31(1)
B(2)	6450(2)	7055(2)	1405(2)	31(1)
B(2A)	6068(8)	8341(7)	1143(6)	31(2)
C(4A)	7006(8)	8322(7)	-601(5)	38(2)
C(5A)	7155(8)	6543(6)	586(6)	36(2)
B(3)	7495(1)	2392(1)	2282(1)	21(1)

Table 3. Bond lengths [Å] and angles [°] for **1-24a**.

---

F (1)-C (8)	1.3570 (16)
F (2)-C (9)	1.3457 (18)
F (3)-C (10)	1.3380 (16)
F (4)-C (11)	1.3489 (18)
F (5)-C (12)	1.3554 (16)
F (6)-C (14)	1.3521 (15)
F (7)-C (15)	1.3430 (16)
F (8)-C (16)	1.3411 (16)
F (9)-C (17)	1.3468 (16)
F (10)-C (18)	1.3542 (15)
F (11)-C (20)	1.3532 (14)
F (12)-C (21)	1.3419 (14)
F (13)-C (22)	1.3426 (14)
F (14)-C (23)	1.3483 (15)
F (15)-C (24)	1.3588 (14)
F (16)-C (26)	1.3579 (15)
F (17)-C (27)	1.3457 (17)
F (18)-C (28)	1.3428 (15)
F (19)-C (29)	1.3418 (15)
F (20)-C (30)	1.3472 (16)
N (1)-C (3)	1.4802 (17)
N (1)-C (1)	1.482 (2)
N (1)-C (2)	1.482 (2)
N (1)-B (1)	1.581 (2)
N (2)-C (4)	1.495 (2)
N (2)-C (6)	1.497 (2)
N (2)-C (5)	1.497 (3)
N (2)-B (2)	1.575 (3)
N (2A)-C (4A)	1.498 (4)
N (2A)-C (6A)	1.499 (4)
N (2A)-C (5A)	1.499 (4)
N (2A)-B (2A)	1.579 (5)
C (1)-H (1A)	0.9800
C (1)-H (1B)	0.9800
C (1)-H (1C)	0.9800
C (2)-H (2A)	0.9800
C (2)-H (2B)	0.9800
C (2)-H (2C)	0.9800
C (3)-H (3A)	0.9800
C (3)-H (3B)	0.9800
C (3)-H (3C)	0.9800
C (4)-H (4A)	0.9800
C (4)-H (4B)	0.9800
C (4)-H (4C)	0.9800
C (5)-H (5A)	0.9800
C (5)-H (5B)	0.9800
C (5)-H (5C)	0.9800
C (6)-H (6A)	0.9800
C (6)-H (6B)	0.9800
C (6)-H (6C)	0.9800
C (6A)-H (6D)	0.9800
C (6A)-H (6E)	0.9800
C (6A)-H (6F)	0.9800
C (7)-C (12)	1.3854 (18)
C (7)-C (8)	1.3915 (19)
C (7)-B (3)	1.6528 (19)
C (8)-C (9)	1.381 (2)
C (9)-C (10)	1.377 (2)
C (10)-C (11)	1.373 (2)
C (11)-C (12)	1.3881 (19)
C (13)-C (18)	1.3838 (18)
C (13)-C (14)	1.3987 (17)
C (13)-B (3)	1.6542 (19)
C (14)-C (15)	1.3783 (19)
C (15)-C (16)	1.377 (2)
C (16)-C (17)	1.380 (2)
C (17)-C (18)	1.3882 (19)

C (19) -C (24)	1.3851 (18)
C (19) -C (20)	1.3954 (17)
C (19) -B (3)	1.6585 (17)
C (20) -C (21)	1.3846 (17)
C (21) -C (22)	1.3776 (19)
C (22) -C (23)	1.3747 (19)
C (23) -C (24)	1.3894 (17)
C (25) -C (26)	1.3887 (18)
C (25) -C (30)	1.3891 (17)
C (25) -B (3)	1.6541 (18)
C (26) -C (27)	1.3769 (18)
C (27) -C (28)	1.379 (2)
C (28) -C (29)	1.371 (2)
C (29) -C (30)	1.3922 (18)
B (1) -H (1)	1.296 (17)
B (1) -H (1D)	1.10 (2)
B (1) -H (1E)	1.07 (2)
B (2) -H (1)	1.295 (15)
B (2) -H (2D)	1.05 (2)
B (2) -H (2E)	1.10 (3)
B (2A) -H (1)	1.287 (15)
B (2A) -H (2F)	1.25 (9)
B (2A) -H (2G)	0.98 (9)
C (4A) -H (4D)	0.9800
C (4A) -H (4E)	0.9800
C (4A) -H (4F)	0.9800
C (5A) -H (5D)	0.9800
C (5A) -H (5E)	0.9800
C (5A) -H (5F)	0.9800
C (3) -N (1) -C (1)	109.09 (14)
C (3) -N (1) -C (2)	108.89 (12)
C (1) -N (1) -C (2)	108.59 (15)
C (3) -N (1) -B (1)	112.05 (11)
C (1) -N (1) -B (1)	111.65 (12)
C (2) -N (1) -B (1)	106.47 (12)
C (4) -N (2) -C (6)	108.2 (3)
C (4) -N (2) -C (5)	109.09 (18)
C (6) -N (2) -C (5)	108.8 (2)
C (4) -N (2) -B (2)	112.06 (19)
C (6) -N (2) -B (2)	111.9 (2)
C (5) -N (2) -B (2)	106.67 (19)
C (4A) -N (2A) -C (6A)	109.4 (10)
C (4A) -N (2A) -C (5A)	107.7 (7)
C (6A) -N (2A) -C (5A)	108.7 (10)
C (4A) -N (2A) -B (2A)	105.7 (7)
C (6A) -N (2A) -B (2A)	114.8 (11)
C (5A) -N (2A) -B (2A)	110.3 (7)
N (1) -C (1) -H (1A)	109.5
N (1) -C (1) -H (1B)	109.5
H (1A) -C (1) -H (1B)	109.5
N (1) -C (1) -H (1C)	109.5
H (1A) -C (1) -H (1C)	109.5
H (1B) -C (1) -H (1C)	109.5
N (1) -C (2) -H (2A)	109.5
N (1) -C (2) -H (2B)	109.5
H (2A) -C (2) -H (2B)	109.5
N (1) -C (2) -H (2C)	109.5
H (2A) -C (2) -H (2C)	109.5
H (2B) -C (2) -H (2C)	109.5
N (1) -C (3) -H (3A)	109.5
N (1) -C (3) -H (3B)	109.5
H (3A) -C (3) -H (3B)	109.5
N (1) -C (3) -H (3C)	109.5
H (3A) -C (3) -H (3C)	109.5
H (3B) -C (3) -H (3C)	109.5
N (2) -C (4) -H (4A)	109.5
N (2) -C (4) -H (4B)	109.5
H (4A) -C (4) -H (4B)	109.5
N (2) -C (4) -H (4C)	109.5
H (4A) -C (4) -H (4C)	109.5

H (4B) -C (4) -H (4C)	109.5
N (2) -C (4) -H (2G)	93 (3)
H (4A) -C (4) -H (2G)	127.7
H (4C) -C (4) -H (2G)	105.9
N (2) -C (5) -H (5A)	109.5
N (2) -C (5) -H (5B)	109.5
H (5A) -C (5) -H (5B)	109.5
N (2) -C (5) -H (5C)	109.5
H (5A) -C (5) -H (5C)	109.5
H (5B) -C (5) -H (5C)	109.5
N (2A) -C (6A) -H (6D)	109.5
N (2A) -C (6A) -H (6E)	109.5
H (6D) -C (6A) -H (6E)	109.5
N (2A) -C (6A) -H (6F)	109.5
H (6D) -C (6A) -H (6F)	109.5
H (6E) -C (6A) -H (6F)	109.5
C (12) -C (7) -C (8)	113.13 (12)
C (12) -C (7) -B (3)	127.35 (12)
C (8) -C (7) -B (3)	119.39 (11)
F (1) -C (8) -C (9)	115.96 (13)
F (1) -C (8) -C (7)	119.14 (12)
C (9) -C (8) -C (7)	124.88 (14)
F (2) -C (9) -C (10)	120.25 (14)
F (2) -C (9) -C (8)	120.50 (15)
C (10) -C (9) -C (8)	119.24 (14)
F (3) -C (10) -C (11)	120.67 (15)
F (3) -C (10) -C (9)	120.66 (15)
C (11) -C (10) -C (9)	118.67 (13)
F (4) -C (11) -C (10)	119.97 (13)
F (4) -C (11) -C (12)	119.91 (14)
C (10) -C (11) -C (12)	120.11 (14)
F (5) -C (12) -C (7)	121.30 (12)
F (5) -C (12) -C (11)	114.78 (12)
C (7) -C (12) -C (11)	123.93 (13)
C (18) -C (13) -C (14)	113.23 (12)
C (18) -C (13) -B (3)	128.16 (11)
C (14) -C (13) -B (3)	118.28 (11)
F (6) -C (14) -C (15)	116.02 (11)
F (6) -C (14) -C (13)	119.11 (11)
C (15) -C (14) -C (13)	124.87 (12)
F (7) -C (15) -C (16)	120.29 (13)
F (7) -C (15) -C (14)	120.48 (13)
C (16) -C (15) -C (14)	119.23 (13)
F (8) -C (16) -C (15)	120.65 (14)
F (8) -C (16) -C (17)	120.63 (14)
C (15) -C (16) -C (17)	118.71 (13)
F (9) -C (17) -C (16)	119.78 (13)
F (9) -C (17) -C (18)	120.20 (13)
C (16) -C (17) -C (18)	120.02 (13)
F (10) -C (18) -C (13)	121.14 (12)
F (10) -C (18) -C (17)	114.96 (12)
C (13) -C (18) -C (17)	123.89 (12)
C (24) -C (19) -C (20)	113.07 (11)
C (24) -C (19) -B (3)	127.00 (11)
C (20) -C (19) -B (3)	119.54 (11)
F (11) -C (20) -C (21)	116.24 (11)
F (11) -C (20) -C (19)	119.24 (10)
C (21) -C (20) -C (19)	124.52 (12)
F (12) -C (21) -C (22)	119.59 (11)
F (12) -C (21) -C (20)	120.95 (12)
C (22) -C (21) -C (20)	119.46 (12)
F (13) -C (22) -C (23)	120.67 (12)
F (13) -C (22) -C (21)	120.54 (12)
C (23) -C (22) -C (21)	118.78 (11)
F (14) -C (23) -C (22)	120.09 (11)
F (14) -C (23) -C (24)	120.20 (12)
C (22) -C (23) -C (24)	119.71 (12)
F (15) -C (24) -C (19)	121.36 (11)
F (15) -C (24) -C (23)	114.24 (11)
C (19) -C (24) -C (23)	124.40 (12)
C (26) -C (25) -C (30)	113.00 (11)

C (26) -C (25) -B (3)	118.96 (11)
C (30) -C (25) -B (3)	127.82 (11)
F (16) -C (26) -C (27)	115.80 (12)
F (16) -C (26) -C (25)	119.28 (11)
C (27) -C (26) -C (25)	124.91 (12)
F (17) -C (27) -C (26)	120.84 (13)
F (17) -C (27) -C (28)	119.75 (12)
C (26) -C (27) -C (28)	119.41 (13)
F (18) -C (28) -C (29)	120.94 (13)
F (18) -C (28) -C (27)	120.18 (14)
C (29) -C (28) -C (27)	118.87 (12)
F (19) -C (29) -C (28)	120.12 (12)
F (19) -C (29) -C (30)	120.29 (13)
C (28) -C (29) -C (30)	119.57 (12)
F (20) -C (30) -C (25)	121.04 (11)
F (20) -C (30) -C (29)	114.80 (11)
C (25) -C (30) -C (29)	124.15 (13)
N (1) -B (1) -H (1)	101.1 (8)
N (1) -B (1) -H (1D)	112.6 (10)
H (1) -B (1) -H (1D)	102.1 (11)
N (1) -B (1) -H (1E)	112.2 (11)
H (1) -B (1) -H (1E)	110.1 (12)
H (1D) -B (1) -H (1E)	117.0 (15)
N (2) -B (2) -H (1)	105.2 (7)
N (2) -B (2) -H (2D)	110.5 (12)
H (1) -B (2) -H (2D)	112.6 (13)
N (2) -B (2) -H (2E)	108.5 (13)
H (1) -B (2) -H (2E)	99.5 (15)
H (2D) -B (2) -H (2E)	119.2 (18)
N (2A) -B (2A) -H (1)	101.7 (8)
N (2A) -B (2A) -H (2F)	109 (4)
H (1) -B (2A) -H (2F)	96 (4)
N (2A) -B (2A) -H (2G)	105 (5)
H (1) -B (2A) -H (2G)	117 (5)
H (2F) -B (2A) -H (2G)	125 (7)
N (2A) -C (4A) -H (4D)	109.5
N (2A) -C (4A) -H (4E)	109.5
H (4D) -C (4A) -H (4E)	109.5
N (2A) -C (4A) -H (4F)	109.5
H (4D) -C (4A) -H (4F)	109.5
H (4E) -C (4A) -H (4F)	109.5
N (2A) -C (5A) -H (2D)	97.5 (10)
N (2A) -C (5A) -H (5D)	109.5
N (2A) -C (5A) -H (5E)	109.5
H (5D) -C (5A) -H (5E)	109.5
N (2A) -C (5A) -H (5F)	109.5
H (5D) -C (5A) -H (5F)	109.5
H (5E) -C (5A) -H (5F)	109.5
C (7) -B (3) -C (25)	113.39 (10)
C (7) -B (3) -C (13)	113.29 (10)
C (25) -B (3) -C (13)	101.31 (9)
C (7) -B (3) -C (19)	102.36 (9)
C (25) -B (3) -C (19)	112.69 (10)
C (13) -B (3) -C (19)	114.30 (10)

---

Symmetry transformations used to generate equivalent atoms:

Table 4. Anisotropic displacement parameters ( $\text{\AA}^2 \times 10^3$ ) for **1-24a**.  
The anisotropic displacement factor exponent takes the form:  
 $-2 \pi^2 [ h^2 a^{*2} U_{11} + \dots + 2 h k a^* b^* U_{12} ]$

	U11	U22	U33	U23	U13	U12
F(1)	31(1)	38(1)	27(1)	-8(1)	-2(1)	0(1)
F(2)	43(1)	61(1)	51(1)	-36(1)	-16(1)	6(1)
F(3)	35(1)	40(1)	94(1)	-35(1)	-26(1)	1(1)
F(4)	28(1)	28(1)	74(1)	-3(1)	-9(1)	-10(1)
F(5)	26(1)	29(1)	33(1)	0(1)	-1(1)	-7(1)
F(6)	28(1)	19(1)	31(1)	0(1)	-4(1)	2(1)
F(7)	35(1)	41(1)	30(1)	9(1)	-9(1)	-1(1)
F(8)	47(1)	65(1)	24(1)	-9(1)	-6(1)	-11(1)
F(9)	49(1)	45(1)	40(1)	-24(1)	-2(1)	-5(1)
F(10)	32(1)	21(1)	36(1)	-9(1)	-5(1)	1(1)
F(11)	20(1)	24(1)	30(1)	-2(1)	1(1)	-2(1)
F(12)	18(1)	26(1)	46(1)	-8(1)	-7(1)	4(1)
F(13)	33(1)	24(1)	47(1)	6(1)	-18(1)	3(1)
F(14)	35(1)	37(1)	32(1)	12(1)	-5(1)	-7(1)
F(15)	22(1)	34(1)	31(1)	4(1)	2(1)	1(1)
F(16)	23(1)	18(1)	50(1)	-6(1)	-5(1)	-1(1)
F(17)	24(1)	29(1)	69(1)	6(1)	-12(1)	-8(1)
F(18)	16(1)	46(1)	51(1)	12(1)	-1(1)	5(1)
F(19)	31(1)	38(1)	36(1)	-9(1)	-1(1)	17(1)
F(20)	30(1)	25(1)	44(1)	-14(1)	-8(1)	6(1)
N(1)	26(1)	21(1)	26(1)	-4(1)	-4(1)	4(1)
N(2)	22(2)	25(1)	29(2)	-3(1)	-4(1)	3(1)
N(2A)	39(9)	30(6)	17(6)	-15(5)	7(5)	-15(5)
C(1)	73(1)	31(1)	62(1)	-12(1)	29(1)	-16(1)
C(2)	32(1)	101(2)	32(1)	-26(1)	-7(1)	8(1)
C(3)	27(1)	43(1)	36(1)	0(1)	-2(1)	13(1)
C(4)	45(1)	34(1)	39(1)	-2(1)	-8(1)	12(1)
C(5)	34(1)	37(1)	27(1)	-9(1)	0(1)	-3(1)
C(6)	28(3)	37(3)	30(2)	-9(2)	5(2)	-8(2)
C(6A)	23(10)	17(7)	66(14)	11(7)	-27(8)	0(6)
C(7)	20(1)	17(1)	29(1)	-4(1)	-6(1)	2(1)
C(8)	23(1)	25(1)	33(1)	-7(1)	-7(1)	4(1)
C(9)	29(1)	34(1)	44(1)	-20(1)	-14(1)	9(1)
C(10)	24(1)	25(1)	66(1)	-20(1)	-20(1)	5(1)
C(11)	20(1)	18(1)	56(1)	-4(1)	-11(1)	0(1)
C(12)	21(1)	19(1)	34(1)	-3(1)	-7(1)	2(1)
C(13)	17(1)	20(1)	26(1)	-3(1)	-2(1)	-2(1)
C(14)	20(1)	23(1)	27(1)	-3(1)	-2(1)	-2(1)
C(15)	23(1)	33(1)	28(1)	2(1)	-5(1)	-4(1)
C(16)	30(1)	47(1)	22(1)	-6(1)	-3(1)	-10(1)
C(17)	28(1)	36(1)	32(1)	-15(1)	-1(1)	-6(1)
C(18)	21(1)	24(1)	29(1)	-5(1)	-2(1)	-3(1)
C(19)	20(1)	16(1)	26(1)	-3(1)	-4(1)	0(1)
C(20)	21(1)	18(1)	26(1)	-3(1)	-2(1)	-3(1)
C(21)	18(1)	21(1)	35(1)	-7(1)	-6(1)	1(1)
C(22)	27(1)	18(1)	34(1)	1(1)	-13(1)	1(1)
C(23)	29(1)	24(1)	27(1)	3(1)	-5(1)	-5(1)
C(24)	19(1)	23(1)	29(1)	-2(1)	-2(1)	-1(1)
C(25)	20(1)	19(1)	22(1)	0(1)	-2(1)	2(1)
C(26)	21(1)	18(1)	32(1)	1(1)	-4(1)	2(1)
C(27)	22(1)	24(1)	37(1)	7(1)	-6(1)	-3(1)
C(28)	16(1)	34(1)	31(1)	8(1)	-1(1)	4(1)
C(29)	24(1)	28(1)	25(1)	-1(1)	-1(1)	11(1)
C(30)	25(1)	22(1)	25(1)	-3(1)	-4(1)	3(1)
B(1)	25(1)	34(1)	32(1)	-9(1)	-2(1)	2(1)
B(2)	27(1)	37(1)	28(1)	-9(1)	1(1)	-6(1)
B(2A)	26(4)	26(4)	36(4)	-5(3)	-3(3)	5(3)
C(4A)	36(4)	50(5)	27(4)	-6(3)	2(3)	-12(3)
C(5A)	35(4)	26(4)	45(4)	-9(3)	6(3)	-4(3)
B(3)	19(1)	15(1)	25(1)	-2(1)	-2(1)	1(1)

Table 5. Hydrogen coordinates ( $\times 10^4$ ) and isotropic displacement parameters ( $\text{\AA}^2 \times 10^3$ ) for **1-24a**.

	x	y	z	U (eq)
H (1A)	4513	6330	4345	86
H (1B)	6000	5885	3921	86
H (1C)	4885	6380	3164	86
H (2A)	5243	7530	5156	83
H (2B)	6105	8455	4549	83
H (2C)	6761	7156	4756	83
H (3A)	4057	8370	2780	59
H (3B)	4535	9182	3353	59
H (3C)	3617	8299	3957	59
H (4A)	7068	9140	-588	64
H (4B)	6357	9257	508	64
H (4C)	5683	8717	-199	64
H (5A)	7932	7265	-938	50
H (5B)	6563	6848	-472	50
H (5C)	7922	6182	-44	50
H (6A)	9085	8094	13	47
H (6B)	9074	7045	940	47
H (6C)	8481	8285	1114	47
H (6D)	9261	7430	225	56
H (6E)	8723	7533	1359	56
H (6F)	8702	8638	487	56
H (1)	6250 (17)	7732 (8)	2022 (13)	35 (4)
H (1D)	6930 (19)	8647 (17)	2657 (15)	45 (5)
H (1E)	7580 (20)	7123 (17)	2956 (15)	47 (5)
H (2D)	6990 (20)	6264 (18)	1701 (16)	34 (6)
H (2E)	5420 (20)	7120 (20)	1242 (18)	46 (6)
H (2F)	5020 (90)	8030 (80)	1070 (70)	30 (20)
H (2G)	6200 (80)	9120 (70)	1020 (60)	30 (20)
H (4D)	7680	7968	-1063	56
H (4E)	7065	9118	-706	56
H (4F)	6123	8248	-729	56
H (5D)	6285	6475	428	54
H (5E)	7276	6156	1282	54
H (5F)	7851	6202	129	54

### X-Ray Structure of **1-37e** ( $[\text{Al}_2\text{Br}_7]^-$ salt)

See Figure 1-3 for an ORTEP plot of **1-37e**. A crystal of dimensions 0.14x0.10x0.10 mm was mounted on a Rigaku AFC10K Saturn 944+ CCD-based X-ray diffractometer equipped with a low temperature device and Micromax-007HF Cu-target micro-focus rotating anode ( $\lambda = 1.54187 \text{ \AA}$ ) operated at 1.2 kW power (40 kV, 30 mA). The X-ray intensities were measured at 85(1) K with the detector placed at a distance 42.00 mm from the crystal. A total of 3750 images were collected with an oscillation

width of  $1.0^\circ$  in  $\omega$ . The exposure time was 2 sec. for the low angle images, 6 sec. for high angle. The integration of the data yielded a total of 26707 reflections to a maximum  $2\theta$  value of  $136.46^\circ$  of which 3680 were independent and 3490 were greater than  $2\sigma(I)$ . The final cell constants (Table 1) were based on the xyz centroids of 17391 reflections above  $10\sigma(I)$ . Analysis of the data showed negligible decay during data collection; the data were processed with CrystalClear 2.0 and corrected for absorption. The structure was solved and refined with the Bruker SHELXTL (version 2008/4) software package, using the space group  $P\bar{1}$  with  $Z = 2$  for the formula  $C_{14}H_{28}B_2N_4Al_4Br_{14}$ . Full matrix least-squares refinement based on  $F^2$  converged at  $R1 = 0.0371$  and  $wR2 = 0.0909$  [based on  $I > 2\sigma(I)$ ],  $R1 = 0.0394$  and  $wR2 = 0.0926$  for all data. Additional details are presented in Table 1.

Sheldrick, G.M. SHELXTL, v. 2008/4; Bruker Analytical X-ray, Madison, WI, 2008. CrystalClear Expert 2.0 r12, Rigaku Americas and Rigaku Corporation (2011), Rigaku Americas, 9009, TX, USA 77381-5209, Rigaku Tokyo, 196-8666, Japan.

Table 1. Crystal data and structure refinement for **1-37e**.

Empirical formula	$C_{14}H_{28}Al_4B_2Br_{14}N_4$
Formula weight	1500.68
Temperature	85(2) K
Wavelength	1.54178 Å
Crystal system, space group	Triclinic, $P\bar{1}$
Unit cell dimensions	a = 9.4348(2) Å, $\alpha = 98.386(7)^\circ$ . b = 9.4885(2) Å, $\beta = 92.646(7)^\circ$ . c = 11.5808(8) Å, $\gamma = 93.785(7)^\circ$ .
Volume	1021.78(8) Å <sup>3</sup>
Z, Calculated density	1, 2.439 Mg/m <sup>3</sup>
Absorption coefficient	17.238 mm <sup>-1</sup>
F(000)	692



Crystal size	0.14 x 0.10 x 0.10 mm
Theta range for data collection	4.70 to 68.23°.
Limiting indices	-11<=h<=11, -11<=k<=11, -13<=l<=13
Reflections collected / unique	26707 / 3680 [R(int) = 0.0745]
Completeness to theta = 68.23	98.2%
Absorption correction	Semi-empirical from equivalents
Max. and min. transmission	0.2775 and 0.1964
Refinement method	Full-matrix least-squares on F <sup>2</sup>
Data / restraints / parameters	3680 / 0 / 184
Goodness-of-fit on F <sup>2</sup>	1.085
Final R indices [I>2σ(I)]	R1 = 0.0371, wR2 = 0.0909
R indices (all data)	R1 = 0.0394, wR2 = 0.0927
Largest diff. peak and hole	1.132 and -0.818 e·Å <sup>-3</sup>

Table 2. Atomic coordinates (x 10<sup>4</sup>) and equivalent isotropic displacement parameters (Å<sup>2</sup> x 10<sup>3</sup>) for **1-37e**. U(eq) is defined as one third of the trace of the orthogonalized U<sub>ij</sub> tensor.

	x	y	z	U(eq)
Br (1)	697 (1)	6078 (1)	2111 (1)	23 (1)
Br (2)	2526 (1)	3062 (1)	493 (1)	30 (1)
Br (3)	3305 (1)	4037 (1)	3761 (1)	21 (1)
Br (4)	4648 (1)	6274 (1)	1535 (1)	17 (1)
Br (5)	4736 (1)	10223 (1)	1873 (1)	27 (1)
Br (6)	7610 (1)	8378 (1)	3280 (1)	23 (1)
Br (7)	3862 (1)	8258 (1)	4448 (1)	23 (1)
Al (1)	2656 (1)	4816 (2)	2071 (1)	14 (1)
Al (2)	5237 (1)	8457 (2)	2928 (1)	14 (1)
N (1)	1533 (4)	-2114 (5)	-1629 (4)	22 (1)
N (2)	22 (4)	-1339 (5)	-2789 (4)	21 (1)
C (1)	523 (5)	-1161 (6)	-1681 (5)	26 (1)
C (2)	1650 (5)	-2883 (5)	-2722 (4)	17 (1)
C (3)	690 (5)	-2386 (6)	-3448 (4)	17 (1)
C (4)	2367 (7)	-2307 (9)	-583 (5)	42 (2)
C (6)	365 (6)	-2853 (7)	-4731 (5)	26 (1)
C (7)	-1095 (6)	-534 (6)	-3295 (6)	29 (1)
C (11)	2662 (6)	-3988 (7)	-2960 (6)	31 (1)
B (1)	-9 (7)	57 (8)	-760 (6)	31 (2)

Table 3. Bond lengths [Å] and angles [°] for **1-37e**.

Br (1)-Al (1)	2.2662 (16)
Br (2)-Al (1)	2.2778 (14)
Br (3)-Al (1)	2.2635 (16)
Br (4)-Al (1)	2.4178 (14)
Br (4)-Al (2)	2.4479 (14)
Br (5)-Al (2)	2.2742 (17)

Br (6) -Al (2)	2.2656 (14)
Br (7) -Al (2)	2.2564 (14)
N (1) -C (1)	1.361 (8)
N (1) -C (2)	1.379 (6)
N (1) -C (4)	1.455 (8)
N (2) -C (1)	1.330 (8)
N (2) -C (3)	1.368 (6)
N (2) -C (7)	1.489 (8)
C (1) -B (1)	1.579 (8)
C (2) -C (3)	1.360 (8)
C (2) -C (11)	1.470 (8)
C (3) -C (6)	1.499 (7)
C (4) -H (4A)	0.9800
C (4) -H (4B)	0.9800
C (4) -H (4C)	0.9800
C (6) -H (6A)	0.9800
C (6) -H (6B)	0.9800
C (6) -H (6C)	0.9800
C (7) -H (7A)	0.9800
C (7) -H (7B)	0.9800
C (7) -H (7C)	0.9800
C (11) -H (11A)	0.9800
C (11) -H (11B)	0.9800
C (11) -H (11C)	0.9800
B (1) -B (1) #1	1.778 (14)
B (1) -H (1A)	1.25 (6)
B (1) -H (1B)	1.20 (7)
Al (1) -Br (4) -Al (2)	113.27 (5)
Br (3) -Al (1) -Br (1)	115.82 (6)
Br (3) -Al (1) -Br (2)	113.04 (7)
Br (1) -Al (1) -Br (2)	111.26 (6)
Br (3) -Al (1) -Br (4)	107.72 (6)
Br (1) -Al (1) -Br (4)	108.99 (6)
Br (2) -Al (1) -Br (4)	98.44 (5)
Br (7) -Al (2) -Br (6)	116.47 (7)
Br (7) -Al (2) -Br (5)	115.56 (6)
Br (6) -Al (2) -Br (5)	111.75 (6)
Br (7) -Al (2) -Br (4)	105.52 (5)
Br (6) -Al (2) -Br (4)	102.09 (6)
Br (5) -Al (2) -Br (4)	103.30 (6)
C (1) -N (1) -C (2)	109.8 (4)
C (1) -N (1) -C (4)	125.6 (5)
C (2) -N (1) -C (4)	124.6 (5)
C (1) -N (2) -C (3)	110.6 (5)
C (1) -N (2) -C (7)	126.8 (5)
C (3) -N (2) -C (7)	122.6 (5)
N (2) -C (1) -N (1)	106.1 (4)
N (2) -C (1) -B (1)	120.3 (6)
N (1) -C (1) -B (1)	133.4 (5)
C (3) -C (2) -N (1)	106.2 (4)
C (3) -C (2) -C (11)	130.7 (5)
N (1) -C (2) -C (11)	123.1 (5)
C (2) -C (3) -N (2)	107.3 (4)
C (2) -C (3) -C (6)	128.7 (5)
N (2) -C (3) -C (6)	124.0 (5)
N (1) -C (4) -H (4A)	109.5
N (1) -C (4) -H (4B)	109.5
H (4A) -C (4) -H (4B)	109.5
N (1) -C (4) -H (4C)	109.5
H (4A) -C (4) -H (4C)	109.5
H (4B) -C (4) -H (4C)	109.5
C (3) -C (6) -H (6A)	109.5
C (3) -C (6) -H (6B)	109.5
H (6A) -C (6) -H (6B)	109.5
C (3) -C (6) -H (6C)	109.5
H (6A) -C (6) -H (6C)	109.5
H (6B) -C (6) -H (6C)	109.5
N (2) -C (7) -H (7A)	109.5
N (2) -C (7) -H (7B)	109.5
H (7A) -C (7) -H (7B)	109.5

N(2)-C(7)-H(7C)	109.5
H(7A)-C(7)-H(7C)	109.5
H(7B)-C(7)-H(7C)	109.5
C(2)-C(11)-H(11A)	109.5
C(2)-C(11)-H(11B)	109.5
H(11A)-C(11)-H(11B)	109.5
C(2)-C(11)-H(11C)	109.5
H(11A)-C(11)-H(11C)	109.5
H(11B)-C(11)-H(11C)	109.5
C(1)-B(1)-B(1)#1	122.3(8)
C(1)-B(1)-H(1A)	108(3)
B(1)#1-B(1)-H(1A)	44(3)
C(1)-B(1)-H(1B)	121(3)
B(1)#1-B(1)-H(1B)	116(3)
H(1A)-B(1)-H(1B)	110(4)

Symmetry transformations used to generate equivalent atoms:  
 #1 -x, -y, -z

Table 4. Anisotropic displacement parameters ( $\text{\AA}^2 \times 10^3$ ) for **1-37e**.  
 The anisotropic displacement factor exponent takes the form:  
 $-2 \pi^2 [ h^2 a^{*2} U_{11} + \dots + 2 h k a^* b^* U_{12} ]$

	U11	U22	U33	U23	U13	U12
Br(1)	11(1)	35(1)	24(1)	7(1)	6(1)	3(1)
Br(2)	35(1)	27(1)	23(1)	-11(1)	12(1)	-17(1)
Br(3)	19(1)	27(1)	19(1)	7(1)	5(1)	0(1)
Br(4)	12(1)	22(1)	14(1)	-2(1)	5(1)	-7(1)
Br(5)	26(1)	24(1)	31(1)	9(1)	0(1)	-1(1)
Br(6)	8(1)	32(1)	27(1)	-4(1)	-2(1)	-3(1)
Br(7)	20(1)	26(1)	20(1)	-5(1)	9(1)	-8(1)
Al(1)	10(1)	18(1)	14(1)	-1(1)	4(1)	-4(1)
Al(2)	8(1)	18(1)	16(1)	2(1)	1(1)	-2(1)
N(1)	15(2)	38(3)	13(2)	4(2)	2(2)	-10(2)
N(2)	14(2)	15(2)	32(3)	-1(2)	9(2)	-2(2)
C(1)	17(2)	31(3)	24(3)	-9(2)	8(2)	-12(2)
C(2)	11(2)	21(3)	17(2)	3(2)	5(2)	-8(2)
C(3)	8(2)	26(3)	17(2)	-2(2)	7(2)	-6(2)
C(4)	28(3)	82(5)	15(3)	13(3)	-2(2)	-4(3)
C(6)	17(2)	46(4)	16(3)	6(2)	2(2)	1(2)
C(7)	18(3)	27(3)	41(3)	-1(3)	4(2)	1(2)
C(11)	19(3)	34(3)	39(3)	3(3)	-1(2)	7(2)
B(1)	24(3)	42(4)	26(3)	1(3)	8(3)	-2(3)

Table 5. Hydrogen coordinates ( $\times 10^4$ ) and isotropic displacement parameters ( $\text{\AA}^2 \times 10^3$ ) for **1-37e**.

	x	y	z	U(eq)
H(4A)	2689	-1371	-141	63
H(4B)	3195	-2835	-807	63
H(4C)	1780	-2845	-96	63
H(6A)	986	-3600	-5017	40
H(6B)	527	-2035	-5149	40
H(6C)	-631	-3229	-4866	40
H(7A)	-1989	-694	-2918	44
H(7B)	-1237	-867	-4137	44
H(7C)	-795	487	-3163	44

H(11A)	2553	-4408	-3787	46
H(11B)	2473	-4735	-2473	46
H(11C)	3635	-3559	-2779	46
H(1A)	-810 (60)	-520 (60)	-100 (50)	26 (16)
H(1B)	-540 (80)	1070 (80)	-1060 (60)	40 (20)

---

### X-Ray Structure of 2-4

See Figure 2-1 for an ORTEP plot of **2-4**. A crystal of dimensions 0.23x0.19x0.19 mm was mounted on a Bruker SMART APEX CCD-based X-ray diffractometer equipped with a low temperature device and fine focus Mo-target X-ray tube ( $\lambda = 0.71073 \text{ \AA}$ ) operated at 1500 W power (50 kV, 30 mA). The X-ray intensities were measured at 85(1) K; the detector was placed at a distance 5.055 cm from the crystal. A total of 5190 frames were collected with a scan width of  $0.5^\circ$  in  $\omega$  and  $0.45^\circ$  in  $\phi$  with an exposure time of 10 s/frame. The integration of the data yielded a total of 151618 reflections to a maximum  $2\theta$  value of  $72.76^\circ$  of which 6882 were independent and 5395 were greater than  $2\sigma(I)$ . The final cell constants (Table 1) were based on the xyz centroids of 9701 reflections above  $10\sigma(I)$ . Analysis of the data showed negligible decay during data collection; the data were processed with SADABS and corrected for absorption. The structure was solved and refined with the Bruker SHELXTL (version 2008/4) software package, using the space group Pbam with  $Z = 4$  for the formula  $C_{10}H_{15}B_{12}NCl$ . All non-hydrogen atoms were refined anisotropically with the hydrogen atoms placed in a mix of idealized and refined positions. Both the borolidine cation and carba-*closo*-dodecaborate anion lie on mirror planes in the crystal lattice. The borolidine cation is disordered. Full matrix least-squares refinement based on  $F^2$  converged at  $R1 = 0.0398$  and  $wR2 = 0.0923$  [based on  $I > 2\sigma(I)$ ],  $R1 = 0.0570$  and  $wR2 = 0.1005$  for all data. Additional details are presented in Table 1.

Sheldrick, G.M. SHELXTL, v. 2008/4; Bruker Analytical X-ray, Madison, WI, 2008. Saint Plus, v. 7.60A, Bruker Analytical X-ray, Madison, WI, 2009. Sheldrick, G.M. SADABS, v. 2008/1. Program for Empirical Absorption Correction of Area Detector Data, University of Gottingen: Gottingen, Germany, 2008.

Table 1. Crystal data and structure refinement for **2-4**.

Empirical formula	C <sub>10</sub> H <sub>14</sub> B <sub>12</sub> Cl <sub>11</sub> N
Formula weight	667.89
Temperature	85(2) K
Wavelength	0.71073 Å
Crystal system, space group	Orthorhombic, Pbam
Unit cell dimensions	a = 14.1671(3) Å, α = 90°. b = 20.0121(5) Å, β = 90°. c = 9.5338(2) Å, γ = 90°.
Volume	2702.96(11) Å <sup>3</sup>
Z, Calculated density	4, 1.641 Mg/m <sup>3</sup>
Absorption coefficient	1.137 mm <sup>-1</sup>
F(000)	1312
Crystal size	0.23 x 0.19 x 0.19 mm
Theta range for data collection	1.76 to 36.38°.
Limiting indices	-23<=h<=23, -33<=k<=33, -15<=l<=15
Reflections collected / unique	151618 / 6882 [R(int) = 0.0574]
Completeness to θ = 36.38	99.9 %
Absorption correction	Semi-empirical from equivalents
Max. and min. transmission	0.8130 and 0.7800
Refinement method	Full-matrix least-squares on F <sup>2</sup>
Data / restraints / parameters	6882 / 86 / 219
Goodness-of-fit on F <sup>2</sup>	1.039
Final R indices [I>2σ(I)]	R1 = 0.0398, wR2 = 0.0923
R indices (all data)	R1 = 0.0570, wR2 = 0.1005
Largest diff. peak and hole	0.816 and -0.367 e·Å <sup>-3</sup>

Table 2. Atomic coordinates ( $\times 10^4$ ) and equivalent isotropic displacement parameters ( $\text{\AA}^2 \times 10^3$ ) for **2-4**.  
 $U(\text{eq})$  is defined as one third of the trace of the orthogonalized  $U_{ij}$  tensor.

	x	y	z	U(eq)
N(1)	1614(1)	3919(1)	5111(2)	17(1)
C(1)	1004(1)	3309(1)	5006(8)	27(1)
C(2)	1021(1)	4539(1)	4936(6)	26(1)
B(1)	2359(2)	3928(1)	3881(2)	26(1)
C(3)	3300(1)	4008(1)	4575(2)	22(1)
C(4)	4221(2)	4057(1)	4014(3)	36(1)
C(5)	4966(1)	4133(1)	4918(6)	40(1)
C(6)	4810(1)	4188(1)	6372(3)	37(1)
C(7)	3906(1)	4146(1)	6944(2)	26(1)
C(8)	3165(1)	4042(1)	6020(2)	19(1)
C(9)	2155(1)	3945(1)	6442(2)	21(1)
C(10)	3802(1)	1966(1)	0	18(1)
Cl(1)	2748(1)	3281(1)	0	26(1)
Cl(2)	1004(1)	2226(1)	1910(1)	26(1)
Cl(3)	793(1)	640(1)	0	28(1)
Cl(4)	3127(1)	-173(1)	0	23(1)
Cl(5)	4792(1)	946(1)	1836(1)	25(1)
Cl(6)	3528(1)	2384(1)	3039(1)	25(1)
Cl(7)	2336(1)	740(1)	3124(1)	25(1)
B(2)	2762(1)	2400(1)	0	18(1)
B(3)	1961(1)	1881(1)	941(1)	18(1)
B(4)	1856(1)	1107(1)	0	18(1)
B(5)	2991(1)	706(1)	0	16(1)
B(6)	3781(1)	1233(1)	933(1)	18(1)
B(7)	3152(1)	1955(1)	1521(1)	18(1)
B(8)	2600(1)	1156(1)	1521(1)	18(1)

Table 3. Bond lengths [ $\text{\AA}$ ] and angles [ $^\circ$ ] for **2-4**.

N(1)-C(9)	1.483(3)
N(1)-C(1)	1.4988(18)
N(1)-C(2)	1.5082(18)
N(1)-B(1)	1.577(3)
B(1)-C(3)	1.497(3)
C(3)-C(8)	1.392(3)
C(3)-C(4)	1.413(3)
C(4)-C(5)	1.370(4)
C(5)-C(6)	1.408(6)
C(6)-C(7)	1.394(3)
C(7)-C(8)	1.387(3)
C(8)-C(9)	1.498(3)
C(10)-B(2)	1.7093(18)
C(10)-B(6)#1	1.7155(13)
C(10)-B(6)	1.7156(13)
C(10)-B(7)#1	1.7173(11)
C(10)-B(7)	1.7173(11)
Cl(1)-B(2)	1.7647(13)
Cl(2)-B(3)	1.7792(9)
Cl(3)-B(4)	1.7712(13)
Cl(4)-B(5)	1.7698(12)
Cl(5)-B(6)	1.7677(9)
Cl(6)-B(7)	1.7663(10)
Cl(7)-B(8)	1.7791(10)
B(2)-B(3)#1	1.7809(15)
B(2)-B(3)	1.7809(15)
B(2)-B(7)	1.7885(12)
B(2)-B(7)#1	1.7886(12)

B (3) -B (7)	1.7822 (13)
B (3) -B (3) #1	1.7940 (19)
B (3) -B (4)	1.7961 (14)
B (3) -B (8)	1.7987 (13)
B (4) -B (3) #1	1.7962 (14)
B (4) -B (8)	1.7963 (12)
B (4) -B (8) #1	1.7963 (12)
B (4) -B (5)	1.7972 (18)
B (5) -B (6)	1.7771 (14)
B (5) -B (6) #1	1.7771 (14)
B (5) -B (8)	1.7941 (12)
B (5) -B (8) #1	1.7941 (12)
B (6) -B (8)	1.7711 (13)
B (6) -B (6) #1	1.7790 (19)
B (6) -B (7)	1.7869 (13)
B (7) -B (8)	1.7805 (13)

C (9) -N (1) -C (1)	112.6 (3)
C (9) -N (1) -C (2)	110.7 (2)
C (1) -N (1) -C (2)	109.92 (12)
C (9) -N (1) -B (1)	106.87 (14)
C (1) -N (1) -B (1)	110.2 (3)
C (2) -N (1) -B (1)	106.3 (2)
C (3) -B (1) -N (1)	105.59 (16)
C (8) -C (3) -C (4)	119.85 (19)
C (8) -C (3) -B (1)	108.62 (17)
C (4) -C (3) -B (1)	131.53 (19)
C (5) -C (4) -C (3)	118.7 (3)
C (4) -C (5) -C (6)	120.4 (2)
C (7) -C (6) -C (5)	121.7 (2)
C (8) -C (7) -C (6)	117.1 (2)
C (7) -C (8) -C (3)	122.11 (17)
C (7) -C (8) -C (9)	124.85 (18)
C (3) -C (8) -C (9)	113.03 (17)
N (1) -C (9) -C (8)	105.52 (15)
B (2) -C (10) -B (6) #1	114.78 (7)
B (2) -C (10) -B (6)	114.78 (7)
B (6) #1 -C (10) -B (6)	62.46 (7)
B (2) -C (10) -B (7) #1	62.93 (5)
B (6) #1 -C (10) -B (7) #1	62.73 (5)
B (6) -C (10) -B (7) #1	114.66 (7)
B (2) -C (10) -B (7)	62.93 (5)
B (6) #1 -C (10) -B (7)	114.66 (7)
B (6) -C (10) -B (7)	62.74 (5)
B (7) #1 -C (10) -B (7)	115.16 (9)
C (10) -B (2) -C1 (1)	121.13 (9)
C (10) -B (2) -B (3) #1	104.69 (7)
C1 (1) -B (2) -B (3) #1	125.15 (7)
C (10) -B (2) -B (3)	104.69 (7)
C1 (1) -B (2) -B (3)	125.15 (7)
B (3) #1 -B (2) -B (3)	60.49 (8)
C (10) -B (2) -B (7)	58.76 (5)
C1 (1) -B (2) -B (7)	120.07 (5)
B (3) #1 -B (2) -B (7)	108.37 (8)
B (3) -B (2) -B (7)	59.91 (5)
C (10) -B (2) -B (7) #1	58.76 (5)
C1 (1) -B (2) -B (7) #1	120.07 (5)
B (3) #1 -B (2) -B (7) #1	59.91 (5)
B (3) -B (2) -B (7) #1	108.37 (8)
B (7) -B (2) -B (7) #1	108.30 (9)
C1 (2) -B (3) -B (2)	121.40 (6)
C1 (2) -B (3) -B (7)	121.87 (6)
B (2) -B (3) -B (7)	60.26 (5)
C1 (2) -B (3) -B (3) #1	121.27 (3)
B (2) -B (3) -B (3) #1	59.76 (4)
B (7) -B (3) -B (3) #1	108.07 (4)
C1 (2) -B (3) -B (4)	122.05 (7)
B (2) -B (3) -B (4)	107.70 (6)
B (7) -B (3) -B (4)	107.76 (7)
B (3) #1 -B (3) -B (4)	60.04 (4)
C1 (2) -B (3) -B (8)	122.48 (6)

B (2) -B (3) -B (8)	107.71 (7)
B (7) -B (3) -B (8)	59.63 (5)
B (3) #1 -B (3) -B (8)	107.93 (4)
B (4) -B (3) -B (8)	59.96 (5)
Cl (3) -B (4) -B (3)	121.67 (7)
Cl (3) -B (4) -B (3) #1	121.67 (7)
B (3) -B (4) -B (3) #1	59.92 (7)
Cl (3) -B (4) -B (8)	121.85 (5)
B (3) -B (4) -B (8)	60.09 (5)
B (3) #1 -B (4) -B (8)	107.93 (8)
Cl (3) -B (4) -B (8) #1	121.85 (5)
B (3) -B (4) -B (8) #1	107.93 (8)
B (3) #1 -B (4) -B (8) #1	60.09 (5)
B (8) -B (4) -B (8) #1	107.70 (9)
Cl (3) -B (4) -B (5)	121.67 (8)
B (3) -B (4) -B (5)	108.11 (7)
B (3) #1 -B (4) -B (5)	108.11 (7)
B (8) -B (4) -B (5)	59.90 (5)
B (8) #1 -B (4) -B (5)	59.90 (5)
Cl (4) -B (5) -B (6)	121.44 (7)
Cl (4) -B (5) -B (6) #1	121.44 (7)
B (6) -B (5) -B (6) #1	60.07 (7)
Cl (4) -B (5) -B (8)	122.14 (5)
B (6) -B (5) -B (8)	59.46 (5)
B (6) #1 -B (5) -B (8)	107.53 (7)
Cl (4) -B (5) -B (8) #1	122.14 (5)
B (6) -B (5) -B (8) #1	107.53 (7)
B (6) #1 -B (5) -B (8) #1	59.46 (5)
B (8) -B (5) -B (8) #1	107.89 (9)
Cl (4) -B (5) -B (4)	122.76 (8)
B (6) -B (5) -B (4)	107.38 (7)
B (6) #1 -B (5) -B (4)	107.38 (7)
B (8) -B (5) -B (4)	60.02 (5)
B (8) #1 -B (5) -B (4)	60.02 (5)
C (10) -B (6) -Cl (5)	121.09 (6)
C (10) -B (6) -B (8)	104.81 (7)
Cl (5) -B (6) -B (8)	125.64 (6)
C (10) -B (6) -B (5)	105.00 (6)
Cl (5) -B (6) -B (5)	124.18 (6)
B (8) -B (6) -B (5)	60.75 (5)
C (10) -B (6) -B (6) #1	58.77 (4)
Cl (5) -B (6) -B (6) #1	119.17 (3)
B (8) -B (6) -B (6) #1	108.47 (4)
B (5) -B (6) -B (6) #1	59.97 (4)
C (10) -B (6) -B (7)	58.68 (5)
Cl (5) -B (6) -B (7)	120.92 (6)
B (8) -B (6) -B (7)	60.05 (5)
B (5) -B (6) -B (7)	108.82 (7)
B (6) #1 -B (6) -B (7)	108.27 (4)
C (10) -B (7) -Cl (6)	121.61 (6)
C (10) -B (7) -B (8)	104.33 (7)
Cl (6) -B (7) -B (8)	124.70 (6)
C (10) -B (7) -B (3)	104.29 (7)
Cl (6) -B (7) -B (3)	125.47 (6)
B (8) -B (7) -B (3)	60.64 (5)
C (10) -B (7) -B (6)	58.58 (6)
Cl (6) -B (7) -B (6)	120.00 (6)
B (8) -B (7) -B (6)	59.53 (5)
B (3) -B (7) -B (6)	107.93 (6)
C (10) -B (7) -B (2)	58.32 (6)
Cl (6) -B (7) -B (2)	121.02 (6)
B (8) -B (7) -B (2)	108.18 (7)
B (3) -B (7) -B (2)	59.83 (6)
B (6) -B (7) -B (2)	107.58 (7)
B (6) -B (8) -Cl (7)	120.81 (6)
B (6) -B (8) -B (7)	60.41 (5)
Cl (7) -B (8) -B (7)	120.82 (6)
B (6) -B (8) -B (5)	59.79 (6)
Cl (7) -B (8) -B (5)	121.69 (6)
B (7) -B (8) -B (5)	108.35 (7)
B (6) -B (8) -B (4)	107.68 (7)



Cl(7)-B(8)-B(4)	122.99(6)
B(7)-B(8)-B(4)	107.83(7)
B(5)-B(8)-B(4)	60.07(6)
B(6)-B(8)-B(3)	107.90(6)
Cl(7)-B(8)-B(3)	122.34(6)
B(7)-B(8)-B(3)	59.73(5)
B(5)-B(8)-B(3)	108.13(7)
B(4)-B(8)-B(3)	59.95(6)

Symmetry transformations used to generate equivalent atoms:  
#1 x,y,-z

Table 4. Anisotropic displacement parameters ( $\text{\AA}^2 \times 10^3$ ) for **2-4**.  
The anisotropic displacement factor exponent takes the form:  
 $-2 \pi^2 [ h^2 a^2 U_{11} + \dots + 2 h k a^* b^* U_{12} ]$

	U11	U22	U33	U23	U13	U12
N(1)	21(1)	20(1)	10(1)	-2(1)	1(1)	2(1)
C(1)	32(1)	19(1)	29(1)	-9(2)	11(2)	-3(1)
C(2)	27(1)	20(1)	30(1)	3(2)	-4(2)	2(1)
B(1)	36(1)	23(1)	18(1)	-4(1)	2(1)	3(1)
C(3)	24(1)	19(1)	24(1)	-1(1)	5(1)	1(1)
C(4)	32(1)	30(1)	46(1)	-4(1)	17(1)	0(1)
C(5)	23(1)	39(1)	57(1)	1(2)	15(2)	-1(1)
C(6)	22(1)	31(1)	59(1)	11(1)	-5(1)	-4(1)
C(7)	22(1)	22(1)	34(1)	6(1)	-6(1)	-4(1)
C(8)	20(1)	14(1)	23(1)	2(1)	2(1)	2(1)
C(9)	19(1)	26(1)	17(1)	0(1)	-2(1)	-1(1)
C(10)	18(1)	14(1)	21(1)	0	0	-2(1)
Cl(1)	38(1)	12(1)	28(1)	0	0	3(1)
Cl(2)	24(1)	26(1)	27(1)	-3(1)	6(1)	8(1)
Cl(3)	19(1)	26(1)	38(1)	0	0	-7(1)
Cl(4)	28(1)	11(1)	30(1)	0	0	1(1)
Cl(5)	22(1)	25(1)	29(1)	1(1)	-7(1)	4(1)
Cl(6)	31(1)	23(1)	22(1)	-7(1)	-4(1)	0(1)
Cl(7)	28(1)	26(1)	22(1)	8(1)	4(1)	2(1)
B(2)	23(1)	13(1)	19(1)	0	0	2(1)
B(3)	18(1)	16(1)	20(1)	-1(1)	1(1)	2(1)
B(4)	18(1)	16(1)	21(1)	0	0	-2(1)
B(5)	18(1)	12(1)	19(1)	0	0	1(1)
B(6)	18(1)	15(1)	20(1)	0(1)	-2(1)	1(1)
B(7)	21(1)	15(1)	18(1)	-1(1)	0(1)	1(1)
B(8)	20(1)	15(1)	18(1)	2(1)	2(1)	0(1)

Table 5. Hydrogen coordinates ( $\times 10^4$ ) and isotropic displacement parameters ( $\text{\AA}^2 \times 10^3$ ) for **2-4**.

	x	y	z	U(eq)
H(1A)	528	3318	5751	40
H(1B)	1396	2908	5107	40
H(1C)	690	3302	4090	40
H(2A)	778	4559	3974	38
H(2B)	1408	4935	5123	38
H(2C)	491	4526	5596	38
H(1)	2236	3891	2905	31
H(4)	4322	4038	3030	43
H(5)	5591	4148	4560	47

H (6)	5333	4255	6978	45
H (7)	3803	4186	7925	31
H (9A)	2079	3524	6976	25
H (9B)	1937	4322	7033	25
H (10)	4359 (12)	2229 (9)	0	25 (4)

---

### X-Ray Structure of 3-13

See Figure 3-1 for an ORTEP plot of **3-13**. A crystal of dimensions 0.37x0.37x0.025 mm was mounted on a Bruker SMART APEX CCD-based X-ray diffractometer equipped with a low temperature device and fine focus Mo-target X-ray tube ( $\lambda = 0.71073 \text{ \AA}$ ) operated at 1500 W power (50 kV, 30 mA). The X-ray intensities were measured at 85(1) K; the detector was placed at a distance 5.055 cm from the crystal. A total of 2790 frames were collected with a scan width of  $0.5^\circ$  in  $\omega$  and  $0.45^\circ$  in  $\phi$  with an exposure time of 25 s/frame. The integration of the data yielded a total of 61663 reflections to a maximum  $2\theta$  value of  $56.58^\circ$  of which 6437 were independent and 5096 were greater than  $2\sigma(I)$ . The final cell constants (Table 1) were based on the xyz centroids of 9873 reflections above  $10\sigma(I)$ . Analysis of the data showed negligible decay during data collection; the data were processed with SADABS and corrected for absorption. The structure was solved and refined with the Bruker SHELXTL (version 2008/3) software package, using the space group  $P2_1/c$  with  $Z = 4$  for the formula  $C_{24}H_{32}BF_6N_3O_4S_2$ . All non-hydrogen atoms were refined anisotropically with the hydrogen atoms placed in idealized positions. Full matrix least-squares refinement based on  $F^2$  converged at  $R1 = 0.0493$  and  $wR2 = 0.1158$  [based on  $I > 2\sigma(I)$ ],  $R1 = 0.0671$  and  $wR2 = 0.1255$  for all data. Additional details are presented in Table 1

Sheldrick, G.M. SHELXTL, v. 2008/3; Bruker Analytical X-ray, Madison, WI, 2008. Sheldrick, G.M. SADABS, v. 2008/1. Program for Empirical Absorption Correction of Area Detector Data, University of Gottingen: Gottingen, Germany, 2008. Saint Plus, v. 7.53a, Bruker Analytical X-ray, Madison, WI, 2008.

Table 1. Crystal data and structure refinement for **3-13**.

Empirical formula	C <sub>24</sub> H <sub>32</sub> BF <sub>6</sub> N <sub>3</sub> O <sub>4</sub> S <sub>2</sub>
Formula weight	615.46
Temperature	85(2) K
Wavelength	0.71073 Å
Crystal system, space group	Monoclinic, P2(1)/c
Unit cell dimensions	a = 12.0734(12) Å, α = 90°. b = 26.951(3) Å, β = 100.946(2)°. c = 8.1362(8) Å, γ = 90°.
Volume	2599.2(4) Å <sup>3</sup>
Z, Calculated density	4, 1.573 Mg/m <sup>3</sup>
Absorption coefficient	0.287 mm <sup>-1</sup>
F(000)	1280
Crystal size	0.37 x 0.37 x 0.03 mm
Theta range for data collection	1.72 to 28.29°.
Limiting indices	-16<=h<=16, -35<=k<=35, -10<=l<=10
Reflections collected / unique	61663 / 6437 [R(int) = 0.0771]
Completeness to θ = 28.29	99.8 %
Absorption correction	Semi-empirical from equivalents
Max. and min. transmission	0.9929 and 0.9013
Refinement method	Full-matrix least-squares on F <sup>2</sup>
Data / restraints / parameters	6437 / 0 / 365
Goodness-of-fit on F <sup>2</sup>	1.067
Final R indices [I>2σ(I)]	R1 = 0.0493, wR2 = 0.1158
R indices (all data)	R1 = 0.0671, wR2 = 0.1255
Largest diff. peak and hole	0.695 and -0.454 e·Å <sup>-3</sup>

Table 2. Atomic coordinates ( $\times 10^4$ ) and equivalent isotropic displacement parameters ( $\text{\AA}^2 \times 10^3$ ) for **3-13**.  
 $U(\text{eq})$  is defined as one third of the trace of the orthogonalized  $U_{ij}$  tensor.

	x	y	z	U(eq)
B(1)	2703(2)	782(1)	5262(3)	17(1)
N(1)	3823(1)	1025(1)	4493(2)	17(1)
N(2)	1618(1)	899(1)	3584(2)	16(1)
N(3)	8030(1)	1207(1)	10503(2)	22(1)
C(1)	3649(2)	1568(1)	4388(2)	17(1)
C(2)	4444(2)	1906(1)	5094(2)	22(1)
C(3)	4273(2)	2417(1)	4738(3)	25(1)
C(4)	3353(2)	2573(1)	3620(3)	24(1)
C(5)	2503(2)	2232(1)	2887(2)	21(1)
C(6)	1569(2)	2382(1)	1651(3)	24(1)
C(7)	790(2)	2041(1)	917(3)	23(1)
C(8)	846(2)	1547(1)	1488(2)	20(1)
C(9)	1710(2)	1393(1)	2739(2)	16(1)
C(10)	2613(2)	1723(1)	3375(2)	18(1)
C(11)	5003(2)	896(1)	5391(2)	21(1)
C(12)	3874(2)	846(1)	2732(2)	20(1)
C(13)	498(2)	948(1)	4178(3)	21(1)
C(14)	1418(2)	475(1)	2330(2)	20(1)
C(15)	2497(2)	1067(1)	6947(2)	17(1)
C(16)	3602(2)	1062(1)	8257(2)	19(1)
C(17)	4047(2)	533(1)	8717(2)	20(1)
C(18)	3893(2)	138(1)	7297(2)	19(1)
C(19)	2894(2)	206(1)	5770(2)	18(1)
C(20)	1827(2)	-16(1)	6307(3)	21(1)
C(21)	1526(2)	251(1)	7832(3)	22(1)
C(22)	1571(2)	824(1)	7797(2)	20(1)
C(23)	7562(2)	2013(1)	11951(3)	25(1)
C(24)	8154(2)	1307(1)	7216(3)	22(1)
S(1)	6923(1)	1442(1)	10981(1)	21(1)
S(2)	8030(1)	873(1)	8924(1)	19(1)
F(1)	7968(1)	2293(1)	10859(2)	37(1)
F(2)	6772(1)	2274(1)	12521(2)	36(1)
F(3)	8399(1)	1919(1)	13232(2)	34(1)
F(4)	8288(1)	1048(1)	5868(2)	35(1)
F(5)	9052(1)	1600(1)	7644(2)	30(1)
F(6)	7251(1)	1594(1)	6796(2)	31(1)
O(1)	6568(1)	1181(1)	12322(2)	34(1)
O(2)	6078(1)	1601(1)	9601(2)	32(1)
O(3)	9089(1)	613(1)	9156(2)	23(1)
O(4)	7010(1)	602(1)	8327(2)	23(1)

Table 3. Bond lengths [ $\text{\AA}$ ] and angles [ $^\circ$ ] for **3-13**.

B(1)-C(19)	1.612(3)
B(1)-C(15)	1.631(3)
B(1)-N(1)	1.724(3)
B(1)-N(2)	1.732(3)
N(1)-C(1)	1.477(3)
N(1)-C(11)	1.513(2)
N(1)-C(12)	1.523(2)
N(2)-C(9)	1.511(3)
N(2)-C(14)	1.522(2)
N(2)-C(13)	1.525(2)
N(3)-S(2)	1.5690(18)
N(3)-S(1)	1.5923(18)
C(1)-C(2)	1.370(3)
C(1)-C(10)	1.423(3)

C (2) -C (3)	1.413 (3)
C (3) -C (4)	1.362 (3)
C (4) -C (5)	1.421 (3)
C (5) -C (6)	1.419 (3)
C (5) -C (10)	1.429 (3)
C (6) -C (7)	1.368 (3)
C (7) -C (8)	1.408 (3)
C (8) -C (9)	1.376 (3)
C (9) -C (10)	1.426 (3)
C (15) -C (16)	1.542 (3)
C (15) -C (22)	1.565 (3)
C (16) -C (17)	1.543 (3)
C (17) -C (18)	1.556 (3)
C (18) -C (19)	1.570 (3)
C (19) -C (20)	1.555 (3)
C (20) -C (21)	1.537 (3)
C (21) -C (22)	1.543 (3)
C (23) -F (1)	1.328 (3)
C (23) -F (3)	1.331 (2)
C (23) -F (2)	1.337 (2)
C (23) -S (1)	1.831 (2)
C (24) -F (6)	1.328 (2)
C (24) -F (5)	1.333 (2)
C (24) -F (4)	1.336 (2)
C (24) -S (2)	1.844 (2)
S (1) -O (1)	1.4311 (17)
S (1) -O (2)	1.4319 (16)
S (2) -O (4)	1.4357 (15)
S (2) -O (3)	1.4384 (15)

C (19) -B (1) -C (15)	106.00 (15)
C (19) -B (1) -N (1)	112.06 (16)
C (15) -B (1) -N (1)	112.40 (16)
C (19) -B (1) -N (2)	115.36 (16)
C (15) -B (1) -N (2)	111.28 (15)
N (1) -B (1) -N (2)	99.91 (13)
C (1) -N (1) -C (11)	111.39 (15)
C (1) -N (1) -C (12)	106.81 (15)
C (11) -N (1) -C (12)	100.32 (14)
C (1) -N (1) -B (1)	106.55 (14)
C (11) -N (1) -B (1)	118.00 (15)
C (12) -N (1) -B (1)	113.31 (14)
C (9) -N (2) -C (14)	111.87 (15)
C (9) -N (2) -C (13)	102.43 (15)
C (14) -N (2) -C (13)	103.89 (15)
C (9) -N (2) -B (1)	114.19 (14)
C (14) -N (2) -B (1)	112.98 (15)
C (13) -N (2) -B (1)	110.42 (14)
S (2) -N (3) -S (1)	123.98 (11)
C (2) -C (1) -C (10)	121.05 (19)
C (2) -C (1) -N (1)	123.71 (18)
C (10) -C (1) -N (1)	115.07 (17)
C (1) -C (2) -C (3)	119.97 (19)
C (4) -C (3) -C (2)	120.4 (2)
C (3) -C (4) -C (5)	120.9 (2)
C (6) -C (5) -C (4)	121.9 (2)
C (6) -C (5) -C (10)	119.30 (19)
C (4) -C (5) -C (10)	118.82 (19)
C (7) -C (6) -C (5)	120.4 (2)
C (6) -C (7) -C (8)	120.33 (19)
C (9) -C (8) -C (7)	120.78 (19)
C (8) -C (9) -C (10)	120.02 (18)
C (8) -C (9) -N (2)	119.42 (17)
C (10) -C (9) -N (2)	120.08 (16)
C (1) -C (10) -C (9)	123.64 (19)
C (1) -C (10) -C (5)	117.95 (18)
C (9) -C (10) -C (5)	118.29 (18)
C (16) -C (15) -C (22)	106.72 (16)
C (16) -C (15) -B (1)	109.06 (16)
C (22) -C (15) -B (1)	114.17 (16)
C (15) -C (16) -C (17)	113.07 (17)

C (16)-C (17)-C (18)	117.65 (16)
C (17)-C (18)-C (19)	118.33 (16)
C (20)-C (19)-C (18)	106.63 (15)
C (20)-C (19)-B (1)	110.84 (16)
C (18)-C (19)-B (1)	111.40 (16)
C (21)-C (20)-C (19)	112.51 (17)
C (20)-C (21)-C (22)	116.00 (17)
C (21)-C (22)-C (15)	117.23 (17)
F (1)-C (23)-F (3)	108.08 (18)
F (1)-C (23)-F (2)	108.12 (19)
F (3)-C (23)-F (2)	108.31 (18)
F (1)-C (23)-S (1)	111.61 (15)
F (3)-C (23)-S (1)	111.86 (16)
F (2)-C (23)-S (1)	108.74 (15)
F (6)-C (24)-F (5)	108.09 (18)
F (6)-C (24)-F (4)	108.31 (17)
F (5)-C (24)-F (4)	107.72 (17)
F (6)-C (24)-S (2)	112.58 (15)
F (5)-C (24)-S (2)	110.91 (14)
F (4)-C (24)-S (2)	109.10 (15)
O (1)-S (1)-O (2)	118.22 (11)
O (1)-S (1)-N (3)	112.11 (10)
O (2)-S (1)-N (3)	115.72 (10)
O (1)-S (1)-C (23)	104.34 (11)
O (2)-S (1)-C (23)	105.43 (10)
N (3)-S (1)-C (23)	97.78 (10)
O (4)-S (2)-O (3)	118.77 (9)
O (4)-S (2)-N (3)	115.79 (9)
O (3)-S (2)-N (3)	108.08 (9)
O (4)-S (2)-C (24)	104.77 (9)
O (3)-S (2)-C (24)	102.18 (9)
N (3)-S (2)-C (24)	105.42 (10)

---

Symmetry transformations used to generate equivalent atoms:

Table 4. Anisotropic displacement parameters ( $\text{\AA}^2 \times 10^3$ ) for **3-13**.  
The anisotropic displacement factor exponent takes the form:  
 $-2 \pi^2 [ h^2 a^{*2} U_{11} + \dots + 2 h k a^* b^* U_{12} ]$

---

	U11	U22	U33	U23	U13	U12
B (1)	11 (1)	26 (1)	12 (1)	1 (1)	2 (1)	-1 (1)
N (1)	11 (1)	28 (1)	12 (1)	0 (1)	3 (1)	0 (1)
N (2)	13 (1)	24 (1)	13 (1)	-1 (1)	3 (1)	0 (1)
N (3)	13 (1)	34 (1)	19 (1)	-4 (1)	4 (1)	2 (1)
C (1)	14 (1)	27 (1)	12 (1)	1 (1)	6 (1)	-2 (1)
C (2)	15 (1)	34 (1)	17 (1)	1 (1)	1 (1)	-3 (1)
C (3)	23 (1)	30 (1)	21 (1)	-1 (1)	2 (1)	-9 (1)
C (4)	25 (1)	25 (1)	23 (1)	3 (1)	3 (1)	-4 (1)
C (5)	19 (1)	28 (1)	16 (1)	1 (1)	4 (1)	-2 (1)
C (6)	23 (1)	25 (1)	22 (1)	4 (1)	4 (1)	2 (1)
C (7)	18 (1)	34 (1)	17 (1)	4 (1)	0 (1)	2 (1)
C (8)	15 (1)	28 (1)	18 (1)	-1 (1)	4 (1)	-1 (1)
C (9)	15 (1)	22 (1)	14 (1)	0 (1)	6 (1)	1 (1)
C (10)	14 (1)	27 (1)	13 (1)	1 (1)	5 (1)	0 (1)
C (11)	12 (1)	33 (1)	17 (1)	2 (1)	3 (1)	2 (1)
C (12)	16 (1)	31 (1)	13 (1)	-1 (1)	6 (1)	1 (1)
C (13)	11 (1)	32 (1)	20 (1)	2 (1)	6 (1)	-1 (1)
C (14)	18 (1)	27 (1)	14 (1)	-4 (1)	0 (1)	-2 (1)
C (15)	14 (1)	23 (1)	14 (1)	0 (1)	5 (1)	0 (1)
C (16)	19 (1)	26 (1)	12 (1)	-2 (1)	4 (1)	0 (1)
C (17)	18 (1)	29 (1)	12 (1)	1 (1)	2 (1)	0 (1)
C (18)	17 (1)	25 (1)	15 (1)	2 (1)	2 (1)	3 (1)
C (19)	15 (1)	25 (1)	12 (1)	-1 (1)	3 (1)	1 (1)

C(20)	18(1)	25(1)	19(1)	2(1)	4(1)	-2(1)
C(21)	19(1)	30(1)	20(1)	2(1)	8(1)	-2(1)
C(22)	18(1)	28(1)	15(1)	0(1)	8(1)	1(1)
C(23)	18(1)	32(1)	25(1)	-2(1)	4(1)	2(1)
C(24)	16(1)	31(1)	19(1)	-2(1)	1(1)	0(1)
S(1)	14(1)	28(1)	23(1)	-3(1)	6(1)	0(1)
S(2)	13(1)	26(1)	16(1)	-1(1)	2(1)	1(1)
F(1)	35(1)	35(1)	42(1)	7(1)	10(1)	-6(1)
F(2)	28(1)	42(1)	40(1)	-16(1)	7(1)	7(1)
F(3)	26(1)	46(1)	26(1)	-9(1)	-4(1)	5(1)
F(4)	42(1)	45(1)	18(1)	-3(1)	10(1)	1(1)
F(5)	21(1)	39(1)	30(1)	5(1)	4(1)	-7(1)
F(6)	20(1)	38(1)	32(1)	10(1)	0(1)	4(1)
O(1)	30(1)	36(1)	42(1)	6(1)	23(1)	0(1)
O(2)	16(1)	46(1)	32(1)	-10(1)	-1(1)	7(1)
O(3)	15(1)	31(1)	22(1)	-1(1)	4(1)	4(1)
O(4)	15(1)	29(1)	24(1)	-2(1)	1(1)	-2(1)

Table 5. Hydrogen coordinates ( $\times 10^4$ ) and isotropic displacement parameters ( $\text{\AA}^2 \times 10^3$ ) for **3-13**.

	x	y	z	U (eq)
H(2A)	5111	1798	5822	26
H(3B)	4803	2653	5283	30
H(4A)	3279	2914	3326	29
H(6A)	1484	2721	1333	28
H(7A)	209	2138	16	28
H(8A)	281	1317	1004	24
H(11A)	5553	1086	4900	31
H(11B)	5136	541	5273	31
H(11C)	5085	980	6580	31
H(12A)	3217	972	1945	29
H(12B)	3871	483	2710	29
H(12C)	4566	970	2410	29
H(13A)	505	1251	4847	31
H(13B)	391	659	4864	31
H(13C)	-120	965	3207	31
H(14A)	785	557	1427	30
H(14B)	1243	172	2895	30
H(14C)	2099	422	1861	30
H(15A)	2280	1419	6658	20
H(16A)	3474	1231	9283	23
H(16B)	4185	1250	7813	23
H(17A)	3670	408	9614	24
H(17B)	4863	558	9195	24
H(18A)	3801	-189	7808	23
H(18B)	4602	125	6856	23
H(19A)	3061	15	4790	21
H(20A)	1181	8	5358	25
H(20B)	1959	-372	6578	25
H(21A)	2048	135	8847	27
H(21B)	754	150	7940	27
H(22A)	1683	944	8966	24
H(22B)	826	946	7214	24

### X-Ray Structure of 3-23a

See Figure 3-2 for an ORTEP plot of **3-23a**. A crystal of dimensions 0.37x0.24x0.24 mm was mounted on a standard Bruker SMART-APEX CCD-based X-ray diffractometer equipped with a low temperature device and fine focus Mo-target X-ray tube ( $\lambda = 0.71073$  Å) operated at 1500 W power (50 kV, 30 mA). The X-ray intensities were measured at 85(2) K; the detector was placed at a distance 5.055 cm from the crystal. A total of 2333 frames were collected with a scan width of  $0.5^\circ$  in  $\omega$  and  $0.45^\circ$  in  $\phi$  with an exposure time of 25 s/frame. The frames were integrated with the Bruker SAINT software package with a narrow frame algorithm. The integration of the data yielded a total of 19089 reflections to a maximum  $2\theta$  value of  $48.34^\circ$  of which 2510 were independent and 2007 were greater than  $2\sigma(I)$ . The final cell constants (Table 1) were based on the xyz centroids of 7767 reflections above  $10\sigma(I)$ . Analysis of the data showed negligible decay during data collection; the data were processed with SADABS and corrected for absorption. The structure was solved and refined with the Bruker SHELXTL (version 2008/4) software package, using the space group C2/m with  $Z = 8$  for the formula  $C_{17}H_{22}BN$ . All non-hydrogen atoms were refined anisotropically with the hydrogen atoms placed in idealized positions. There are two crystallographically independent molecules in the asymmetric unit, each lying on a mirror plane. Full-matrix least-squares refinement based on  $F^2$  converged at  $R1 = 0.0579$  and  $wR2 = 0.1697$  [based on  $I > 2\sigma(I)$ ],  $R1 = 0.0705$  and  $wR2 = 0.1822$  for all data. Additional details are presented in Table 1.

Sheldrick, G.M. SHELXTL, v. 2008/4; Bruker Analytical X-ray, Madison, WI, 2008. Saint Plus, v. 7.60A, Bruker Analytical X-ray, Madison, WI, 2009. Sheldrick,



G.M. SADABS, v. 2008/1. Program for Empirical Absorption Correction of Area  
 Detector Data, University of Gottingen: Gottingen, Germany, 2008.

Table 1. Crystal data and structure refinement for **3-23a**.

Empirical formula	C <sub>17</sub> H <sub>22</sub> BN
Formula weight	251.17
Temperature	250 (2) K
Wavelength	0.71073 Å
Crystal system, space group	Monoclinic, C2/m
Unit cell dimensions	a = 20.122 (2) Å, α = 90°. b = 7.1578 (8) Å, β = 115.372 (6)°. c = 22.560 (2) Å, γ = 90°.
Volume	2935.9 (5) Å <sup>3</sup>
Z, Calculated density	8, 1.136 Mg/m <sup>3</sup>
Absorption coefficient	0.064 mm <sup>-1</sup>
F(000)	1088
Crystal size	0.37 x 0.24 x 0.24 mm
Theta range for data collection	2.24 to 24.17°.
Limiting indices	-22<=h<=22, -8<=k<=8, -25<=l<=25
Reflections collected / unique	19089 / 2510 [R(int) = 0.0269]
Completeness to θ = 24.17	97.8 %
Absorption correction	Semi-empirical from equivalents
Max. and min. transmission	0.9848 and 0.9767
Refinement method	Full-matrix least-squares on F <sup>2</sup>
Data / restraints / parameters	2510 / 0 / 213
Goodness-of-fit on F <sup>2</sup>	1.039
Final R indices [I>2σ(I)]	R1 = 0.0579, wR2 = 0.1697
R indices (all data)	R1 = 0.0705, wR2 = 0.1822
Largest diff. peak and hole	0.240 and -0.154 e·Å <sup>-3</sup>

Table 2. Atomic coordinates ( $\times 10^4$ ) and equivalent isotropic displacement parameters ( $\text{\AA}^2 \times 10^3$ ) for **3-23a**.  
 $U(\text{eq})$  is defined as one third of the trace of the orthogonalized  $U_{ij}$  tensor.

	x	y	z	U(eq)
N(1)	7474(1)	10000	5411(1)	66(1)
N(2)	1943(1)	0	-496(1)	64(1)
C(1)	7875(2)	10000	6126(1)	84(1)
C(2)	7792(1)	10000	4974(1)	60(1)
C(3)	8533(2)	10000	5102(2)	77(1)
C(4)	8704(2)	10000	4578(2)	88(1)
C(5)	8155(2)	10000	3938(2)	80(1)
C(6)	7422(1)	10000	3811(1)	64(1)
C(7)	7225(1)	10000	4337(1)	55(1)
C(8)	6524(1)	10000	4390(1)	61(1)
C(9)	6739(2)	10000	5061(1)	69(1)
C(10)	5045(2)	10000	4051(2)	102(1)
C(11)	4604(2)	8203(5)	3764(2)	129(1)
C(12)	4393(2)	7865(5)	3049(2)	126(1)
C(13)	5000(2)	8198(5)	2845(1)	112(1)
C(14)	5445(2)	10000	3116(2)	89(1)
C(15)	1615(2)	0	-1213(1)	83(1)
C(16)	2691(2)	0	-91(1)	56(1)
C(17)	3279(2)	0	-260(2)	73(1)
C(18)	3976(2)	0	243(2)	79(1)
C(19)	4087(2)	0	889(2)	75(1)
C(20)	3500(1)	0	1059(1)	64(1)
C(21)	2786(1)	0	567(1)	53(1)
C(22)	2051(1)	0	554(1)	54(1)
C(23)	1586(2)	0	-111(1)	62(1)
C(24)	2281(2)	0	1849(1)	91(1)
C(25)	2134(2)	1790(5)	2142(1)	118(1)
C(26)	1341(2)	2133(5)	1988(2)	125(1)
C(27)	818(2)	1800(5)	1277(2)	113(1)
C(28)	957(2)	0	974(2)	81(1)
B(1)	5730(2)	10000	3880(2)	70(1)
B(2)	1788(2)	0	1092(2)	61(1)

Table 3. Bond lengths [ $\text{\AA}$ ] and angles [ $^\circ$ ] for **3-23a**.

N(1)-C(9)	1.345(4)
N(1)-C(2)	1.388(4)
N(1)-C(1)	1.460(3)
N(2)-C(23)	1.343(4)
N(2)-C(16)	1.386(3)
N(2)-C(15)	1.462(3)
C(2)-C(3)	1.391(4)
C(2)-C(7)	1.401(4)
C(3)-C(4)	1.366(5)
C(4)-C(5)	1.393(5)
C(5)-C(6)	1.378(4)
C(6)-C(7)	1.403(4)
C(7)-C(8)	1.467(4)
C(8)-C(9)	1.384(4)
C(8)-B(1)	1.516(4)
C(10)-C(11)#1	1.539(4)
C(10)-C(11)	1.539(4)
C(10)-B(1)	1.583(5)
C(11)-C(12)	1.501(4)
C(12)-C(13)	1.499(4)
C(13)-C(14)	1.539(3)
C(14)-C(13)#1	1.539(3)

C (14) -B (1)	1.566 (5)
C (16) -C (17)	1.391 (4)
C (16) -C (21)	1.414 (4)
C (17) -C (18)	1.375 (4)
C (18) -C (19)	1.376 (4)
C (19) -C (20)	1.390 (4)
C (20) -C (21)	1.390 (4)
C (21) -C (22)	1.466 (3)
C (22) -C (23)	1.387 (4)
C (22) -B (2)	1.518 (4)
C (24) -C (25) #2	1.528 (4)
C (24) -C (25)	1.528 (4)
C (24) -B (2)	1.564 (4)
C (25) -C (26)	1.500 (4)
C (26) -C (27)	1.513 (4)
C (27) -C (28)	1.539 (3)
C (28) -C (27) #2	1.539 (3)
C (28) -B (2)	1.576 (4)
C (9) -N (1) -C (2)	107.9 (2)
C (9) -N (1) -C (1)	126.6 (3)
C (2) -N (1) -C (1)	125.5 (2)
C (23) -N (2) -C (16)	107.8 (2)
C (23) -N (2) -C (15)	127.0 (3)
C (16) -N (2) -C (15)	125.2 (3)
N (1) -C (2) -C (3)	129.1 (3)
N (1) -C (2) -C (7)	108.0 (2)
C (3) -C (2) -C (7)	122.9 (3)
C (4) -C (3) -C (2)	117.7 (3)
C (3) -C (4) -C (5)	121.1 (3)
C (6) -C (5) -C (4)	121.2 (3)
C (5) -C (6) -C (7)	119.3 (3)
C (2) -C (7) -C (6)	117.8 (2)
C (2) -C (7) -C (8)	107.8 (2)
C (6) -C (7) -C (8)	134.4 (2)
C (9) -C (8) -C (7)	103.2 (2)
C (9) -C (8) -B (1)	124.4 (3)
C (7) -C (8) -B (1)	132.4 (2)
N (1) -C (9) -C (8)	113.2 (3)
C (11) #1-C (10) -C (11)	113.4 (3)
C (11) #1-C (10) -B (1)	107.6 (2)
C (11) -C (10) -B (1)	107.6 (2)
C (12) -C (11) -C (10)	115.7 (3)
C (13) -C (12) -C (11)	114.3 (2)
C (12) -C (13) -C (14)	115.1 (3)
C (13) #1-C (14) -C (13)	113.8 (3)
C (13) #1-C (14) -B (1)	108.26 (19)
C (13) -C (14) -B (1)	108.26 (19)
N (2) -C (16) -C (17)	129.2 (3)
N (2) -C (16) -C (21)	108.1 (2)
C (17) -C (16) -C (21)	122.7 (3)
C (18) -C (17) -C (16)	117.4 (3)
C (17) -C (18) -C (19)	121.3 (3)
C (18) -C (19) -C (20)	121.5 (3)
C (21) -C (20) -C (19)	119.3 (3)
C (20) -C (21) -C (16)	117.9 (2)
C (20) -C (21) -C (22)	134.8 (2)
C (16) -C (21) -C (22)	107.3 (2)
C (23) -C (22) -C (21)	103.2 (2)
C (23) -C (22) -B (2)	124.1 (2)
C (21) -C (22) -B (2)	132.6 (2)
N (2) -C (23) -C (22)	113.5 (2)
C (25) #2-C (24) -C (25)	114.0 (3)
C (25) #2-C (24) -B (2)	108.83 (18)
C (25) -C (24) -B (2)	108.83 (18)
C (26) -C (25) -C (24)	114.9 (2)
C (25) -C (26) -C (27)	114.0 (2)
C (26) -C (27) -C (28)	115.2 (2)
C (27) -C (28) -C (27) #2	113.7 (3)
C (27) -C (28) -B (2)	107.84 (17)
C (27) #2-C (28) -B (2)	107.84 (17)

C(8)-B(1)-C(14)	127.3(3)
C(8)-B(1)-C(10)	123.9(3)
C(14)-B(1)-C(10)	108.8(3)
C(22)-B(2)-C(24)	126.7(2)
C(22)-B(2)-C(28)	124.9(3)
C(24)-B(2)-C(28)	108.4(3)

Symmetry transformations used to generate equivalent atoms:  
 #1 x,-y+2,z #2 x,-y,z

Table 4. Anisotropic displacement parameters ( $\text{\AA}^2 \times 10^3$ ) for **3-23a**.  
 The anisotropic displacement factor exponent takes the form:  
 $-2 \pi^2 [ h^2 a^{*2} U_{11} + \dots + 2 h k a^* b^* U_{12} ]$

	U11	U22	U33	U23	U13	U12
N(1)	65(1)	76(2)	50(1)	0	20(1)	0
N(2)	73(1)	60(1)	57(1)	0	28(1)	0
C(1)	97(2)	88(2)	52(2)	0	17(2)	0
C(2)	53(1)	63(2)	59(2)	0	20(1)	0
C(3)	49(2)	87(2)	80(2)	0	13(2)	0
C(4)	50(2)	109(3)	106(3)	0	35(2)	0
C(5)	65(2)	96(2)	92(2)	0	48(2)	0
C(6)	53(1)	82(2)	62(2)	0	28(1)	0
C(7)	46(1)	63(2)	56(1)	0	22(1)	0
C(8)	51(1)	82(2)	52(1)	0	25(1)	0
C(9)	61(2)	92(2)	59(2)	0	30(1)	0
C(10)	56(2)	183(4)	75(2)	0	36(2)	0
C(11)	74(2)	159(3)	153(3)	60(2)	47(2)	-1(2)
C(12)	89(2)	90(2)	171(3)	0(2)	30(2)	-8(2)
C(13)	86(2)	128(2)	98(2)	-20(2)	17(1)	28(2)
C(14)	47(2)	157(4)	65(2)	0	25(1)	0
C(15)	105(2)	83(2)	53(2)	0	26(2)	0
C(16)	68(2)	43(1)	66(2)	0	38(1)	0
C(17)	90(2)	67(2)	81(2)	0	55(2)	0
C(18)	71(2)	83(2)	100(2)	0	53(2)	0
C(19)	53(2)	82(2)	95(2)	0	37(2)	0
C(20)	57(2)	67(2)	68(2)	0	28(1)	0
C(21)	56(1)	42(1)	63(2)	0	28(1)	0
C(22)	51(1)	56(2)	54(1)	0	22(1)	0
C(23)	59(2)	63(2)	64(2)	0	26(1)	0
C(24)	51(2)	169(4)	58(2)	0	28(1)	0
C(25)	134(2)	147(3)	89(2)	-33(2)	62(2)	-60(2)
C(26)	174(3)	90(2)	152(3)	-24(2)	110(2)	-3(2)
C(27)	108(2)	127(2)	131(2)	38(2)	77(2)	47(2)
C(28)	50(2)	132(3)	65(2)	0	26(1)	0
B(1)	54(2)	96(3)	67(2)	0	31(2)	0
B(2)	51(2)	73(2)	61(2)	0	25(1)	0

Table 5. Hydrogen coordinates ( $\times 10^4$ ) and isotropic displacement parameters ( $\text{\AA}^2 \times 10^3$ ) for **3-23a**.

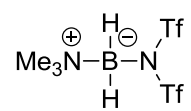
	x	y	z	U(eq)
H(1A)	8091	8778	6273	126
H(1B)	7538	10287	6318	126
H(1C)	8261	10935	6259	126
H(3A)	8903	10000	5535	92
H(4A)	9200	10000	4651	105

H (5A)	8288	10000	3586	95
H (6A)	7057	10000	3376	77
H (9A)	6406	10000	5252	83
H (10A)	5220	10000	4533	122
H (11A)	4895	7135	4013	155
H (11B)	4154	8243	3831	155
H (12A)	4224	6571	2945	151
H (12B)	3978	8682	2791	151
H (13A)	4787	8240	2365	134
H (13B)	5338	7133	2988	134
H (14A)	5874	10000	3009	107
H (15A)	1101	-355	-1381	124
H (15B)	1873	-886	-1364	124
H (15C)	1652	1240	-1369	124
H (17A)	3204	0	-701	87
H (18A)	4385	0	144	95
H (19A)	4570	0	1222	90
H (20A)	3585	0	1503	77
H (23A)	1070	0	-277	74
H (24A)	2803	0	1923	109
H (25A)	2416	1742	2620	142
H (25B)	2317	2853	1982	142
H (26A)	1286	3427	2102	149
H (26B)	1201	1314	2264	149
H (27A)	850	2866	1018	136
H (27B)	316	1761	1241	136
H (28A)	639	0	496	98

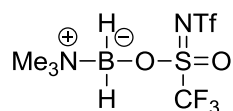
---

**Appendix B**  
**Selected NMR Spectra**

$^1\text{H}$  NMR (500 MHz),  
 $\text{CD}_2\text{Cl}_2$

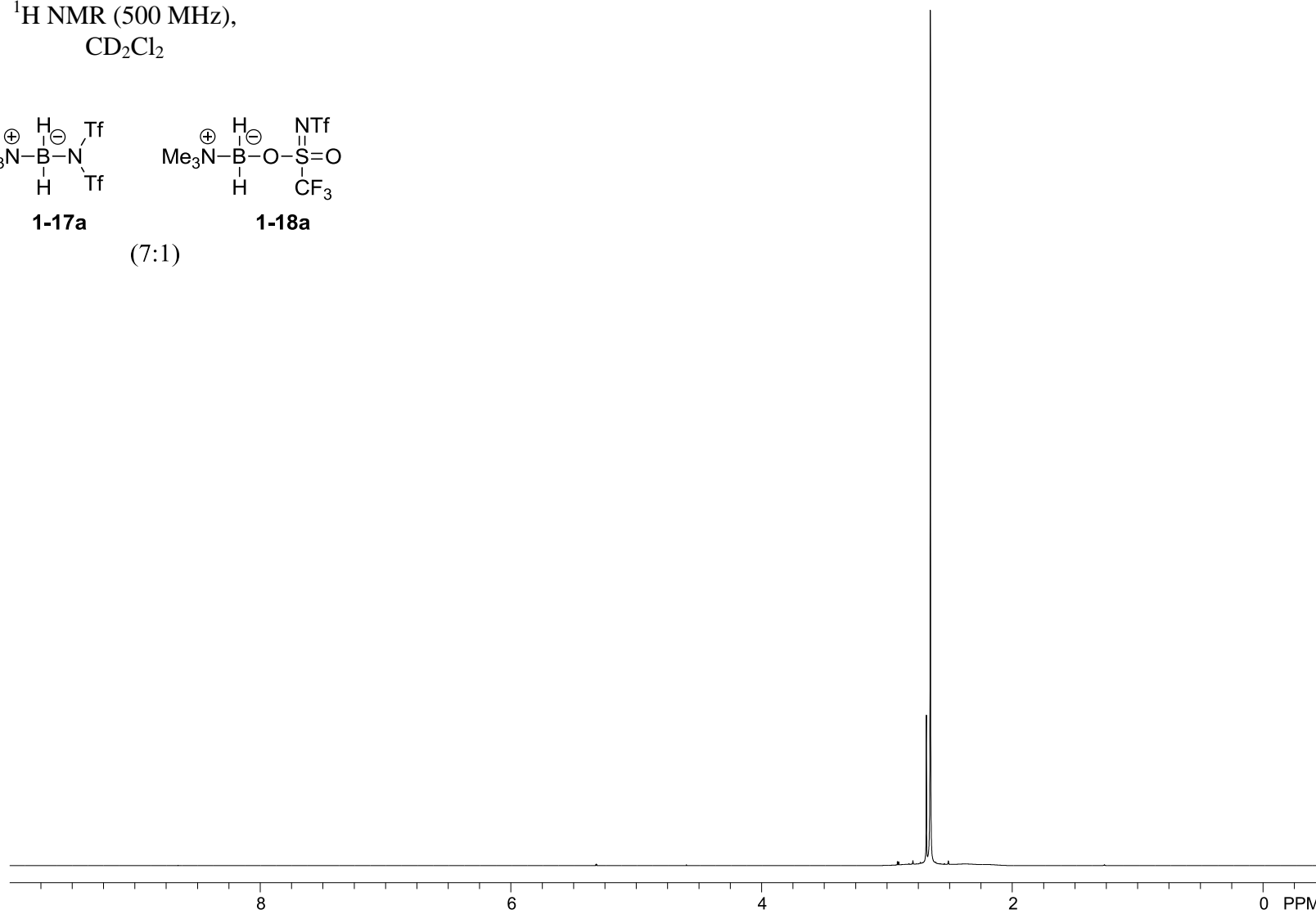


**1-17a**

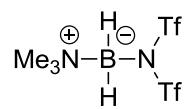


**1-18a**

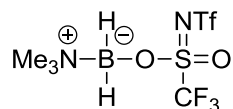
(7:1)



$^{11}\text{B}$  NMR (160 MHz),  
 $\text{CD}_2\text{Cl}_2$

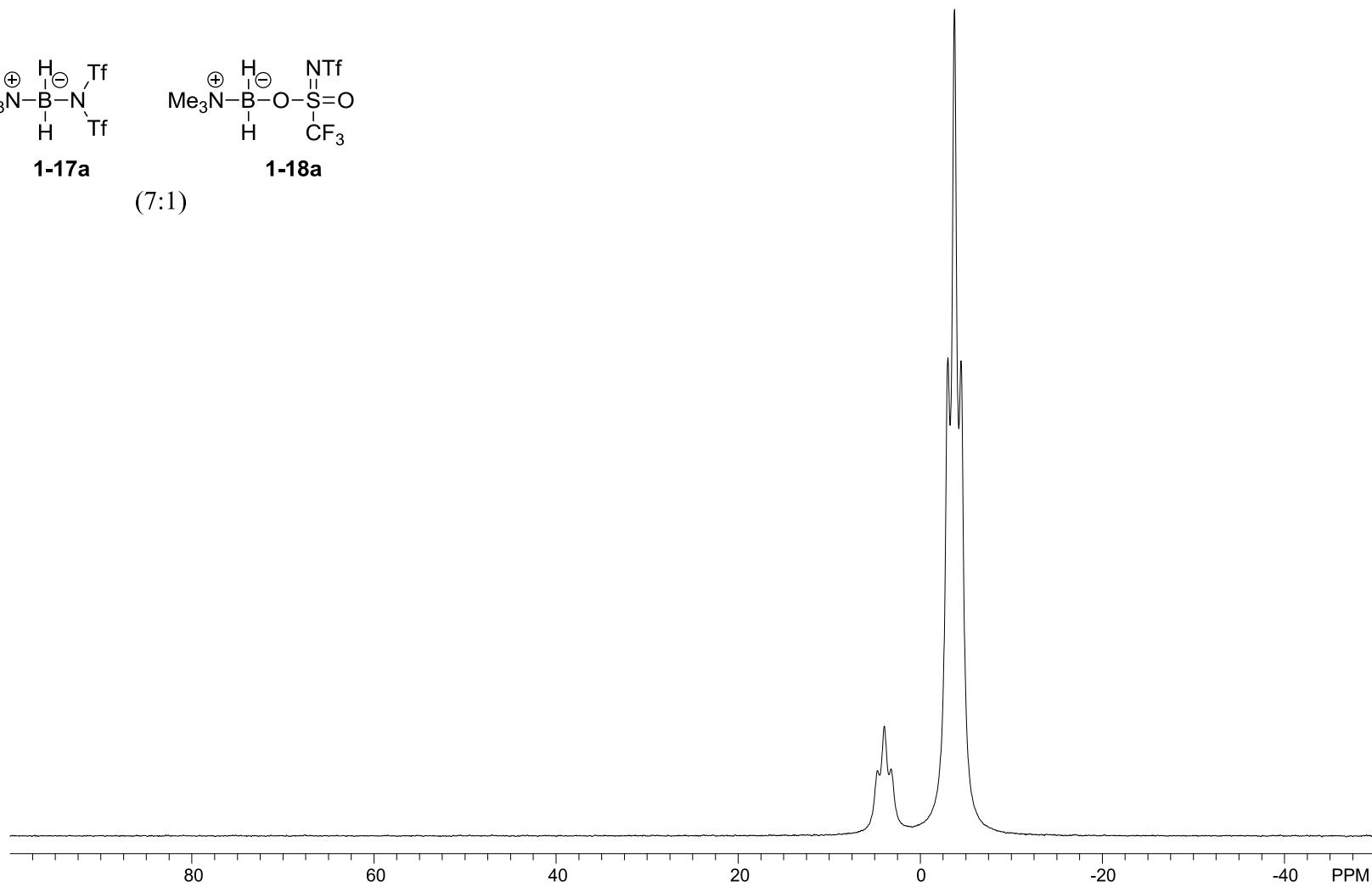


**1-17a**



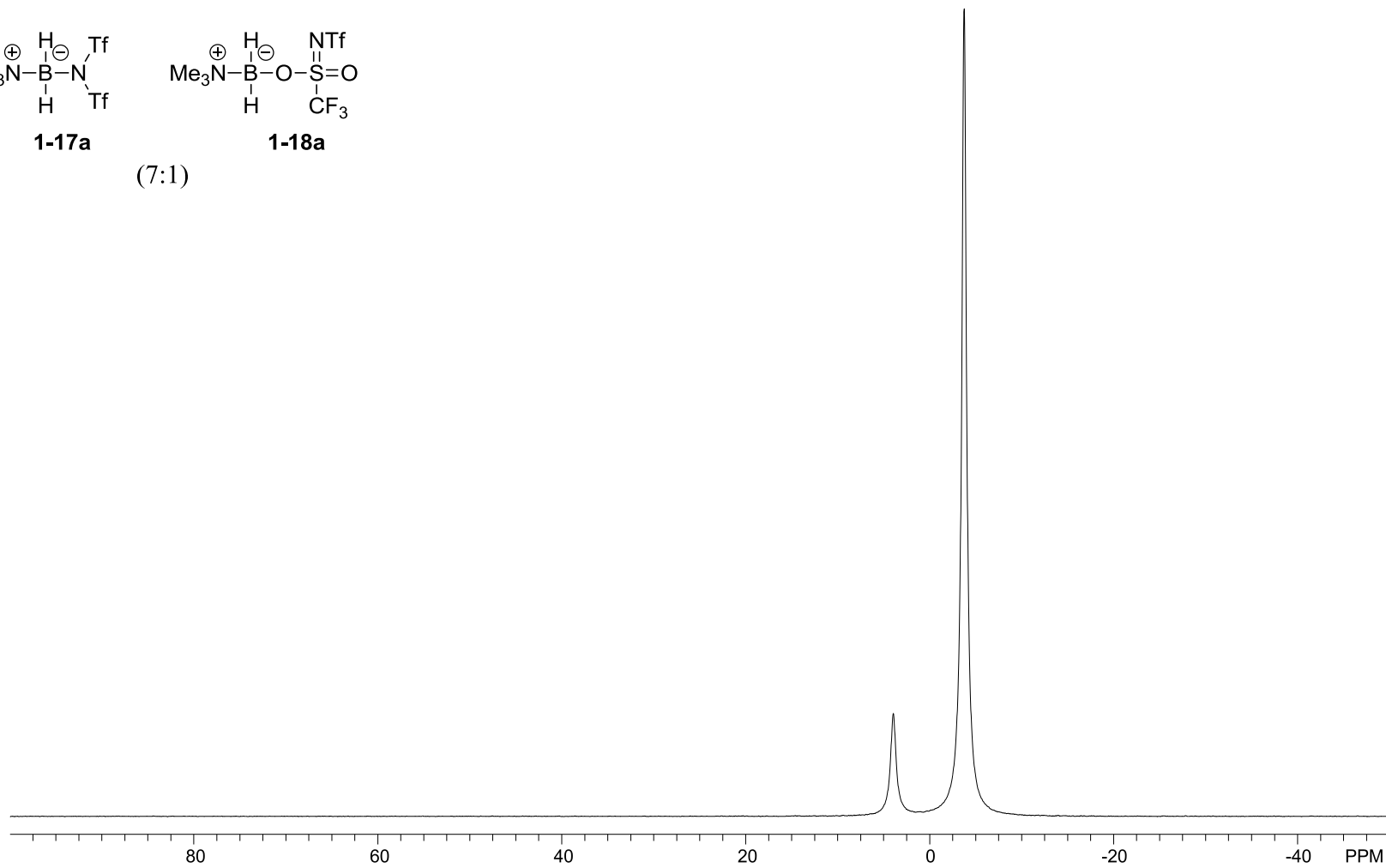
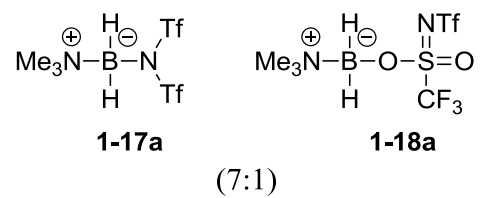
**1-18a**

(7:1)

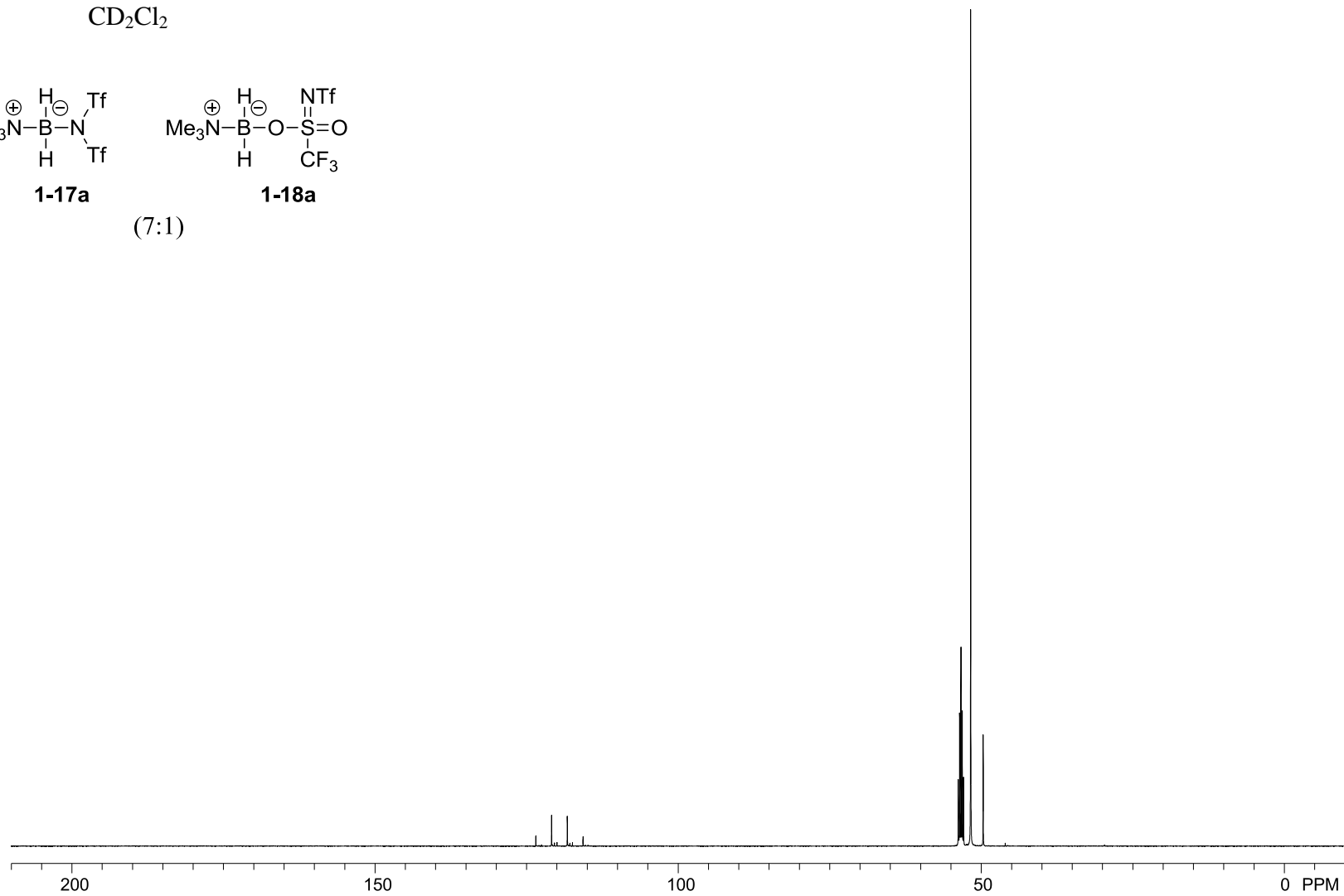
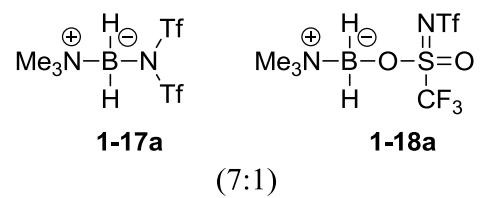




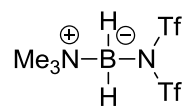
$^{11}\text{B}\{^1\text{H}\}$  NMR (160 MHz),  
 $\text{CD}_2\text{Cl}_2$



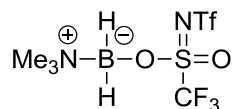
$^{13}\text{C}\{^1\text{H}\}$  NMR (126 MHz),  
 $\text{CD}_2\text{Cl}_2$



$^{19}\text{F}$  NMR (471 MHz),  
 $\text{CD}_2\text{Cl}_2$

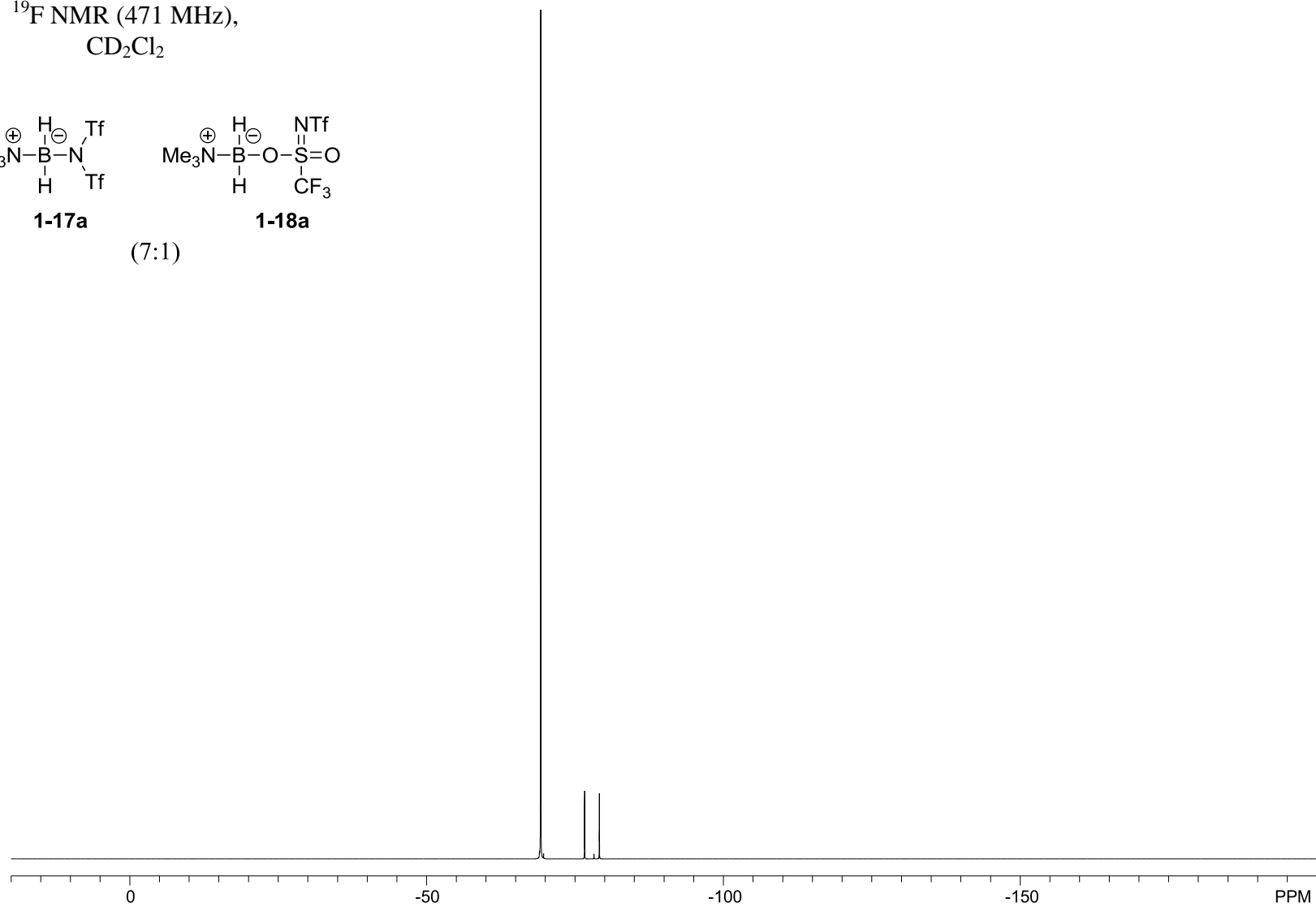


**1-17a**

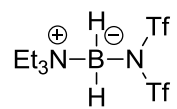


**1-18a**

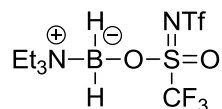
(7:1)



$^1\text{H}$  NMR (500 MHz),  
 $\text{CD}_2\text{Cl}_2$

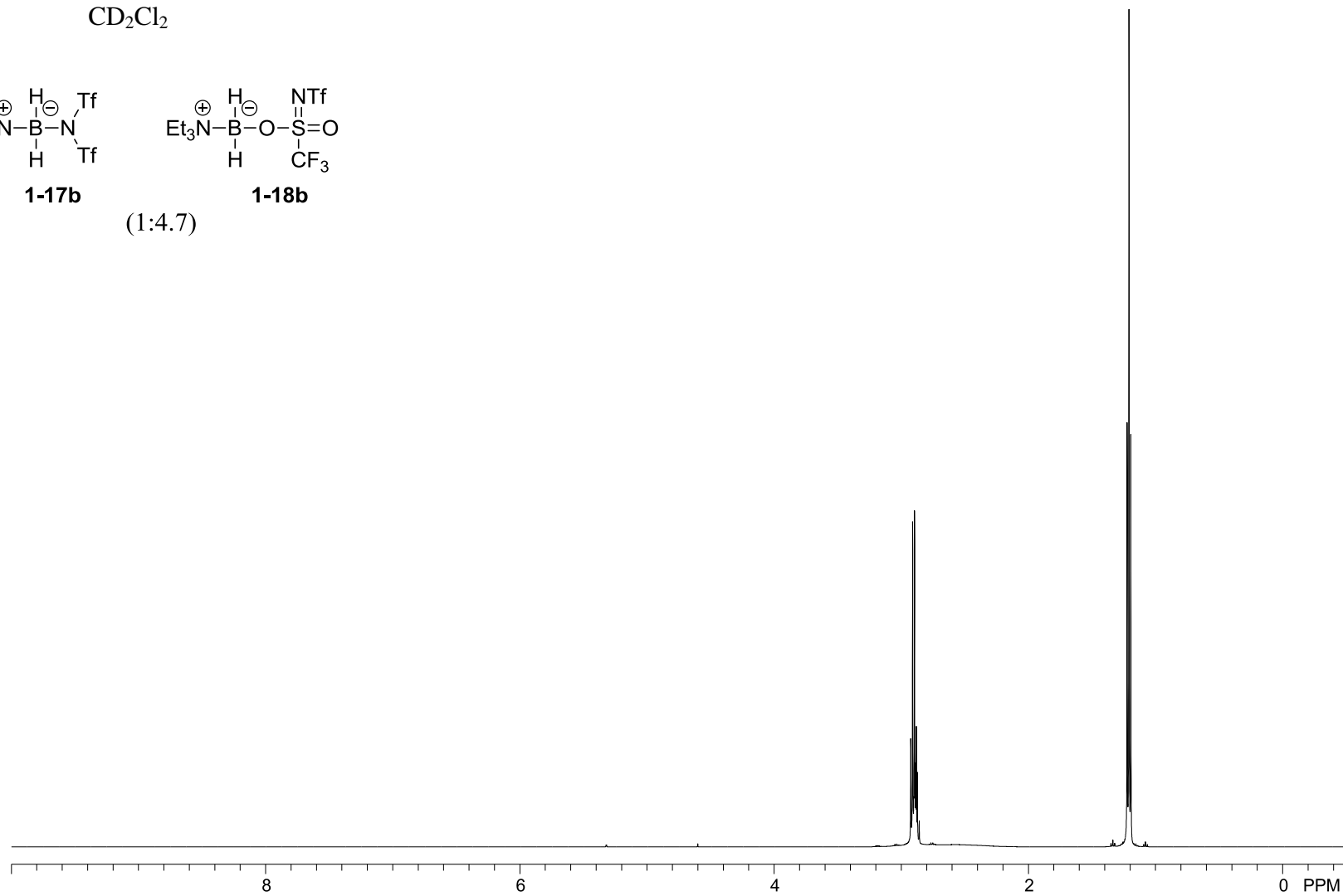


**1-17b**

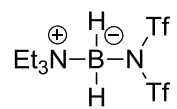


**1-18b**

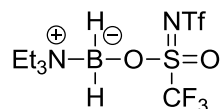
(1:4.7)



$^{11}\text{B}$  NMR (160 MHz),  
 $\text{CD}_2\text{Cl}_2$

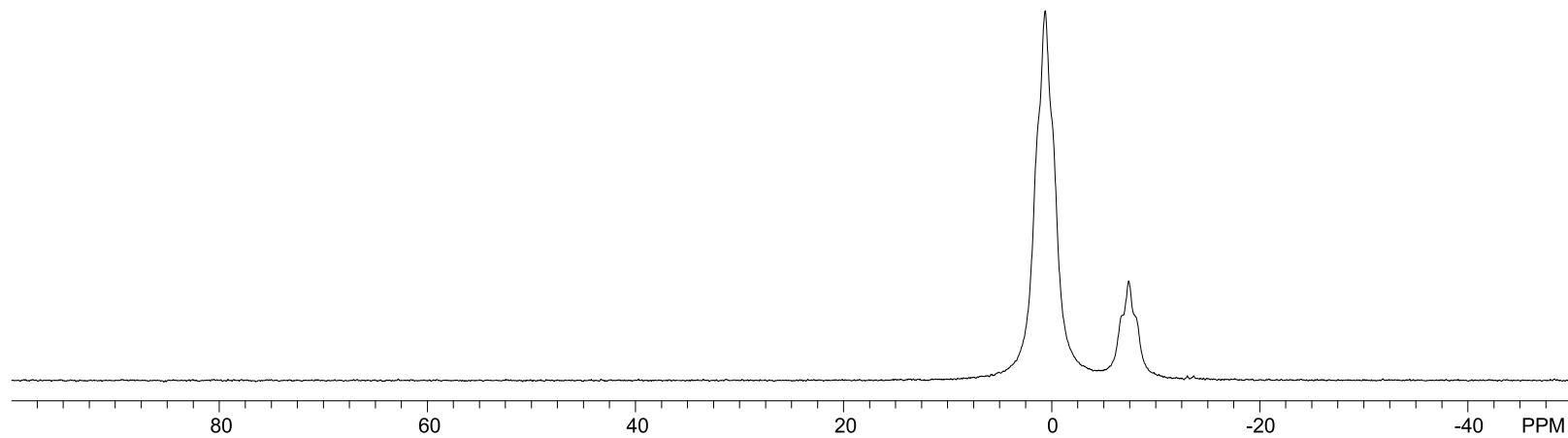


**1-17b**

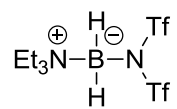


**1-18b**

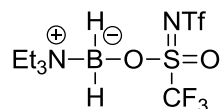
(1:4.7)



$^{11}\text{B}\{^1\text{H}\}$  NMR (160 MHz),  
 $\text{CD}_2\text{Cl}_2$

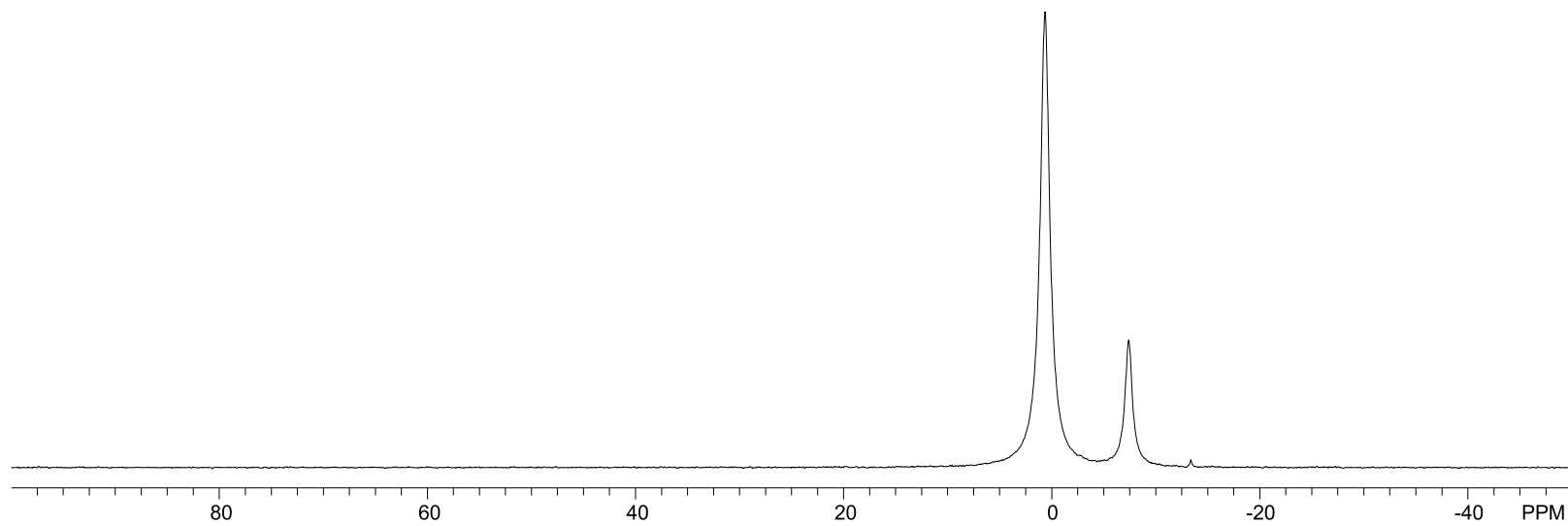


**1-17b**

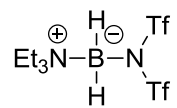


**1-18b**

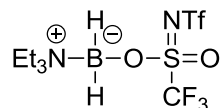
(1:4.7)



$^{13}\text{C}\{^1\text{H}\}$  NMR (126 MHz),  
 $\text{CD}_2\text{Cl}_2$

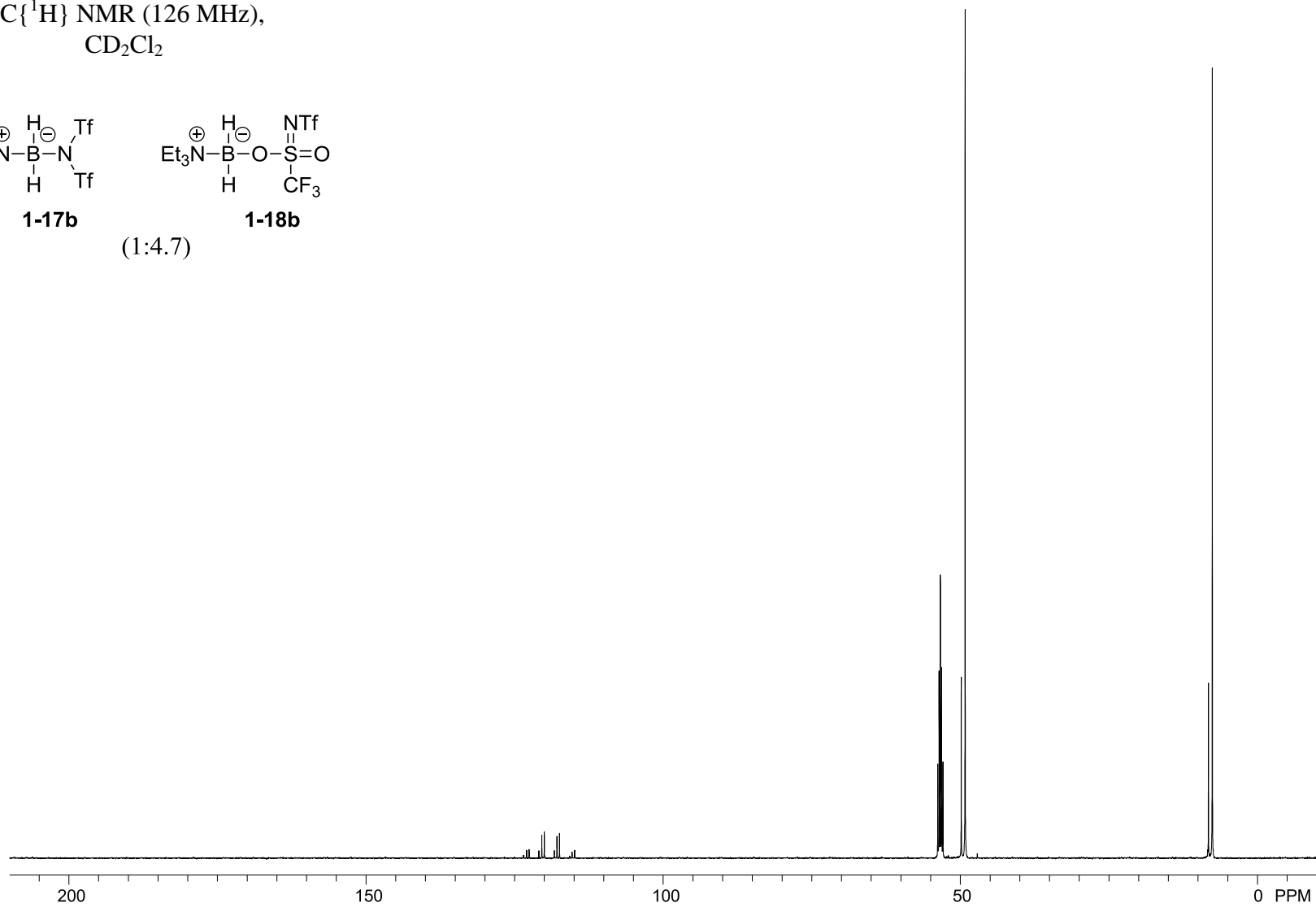


**1-17b**

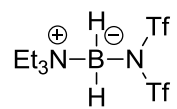


**1-18b**

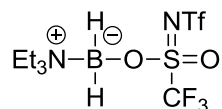
(1:4.7)



$^{19}\text{F}$  NMR (471 MHz),  
 $\text{CD}_2\text{Cl}_2$

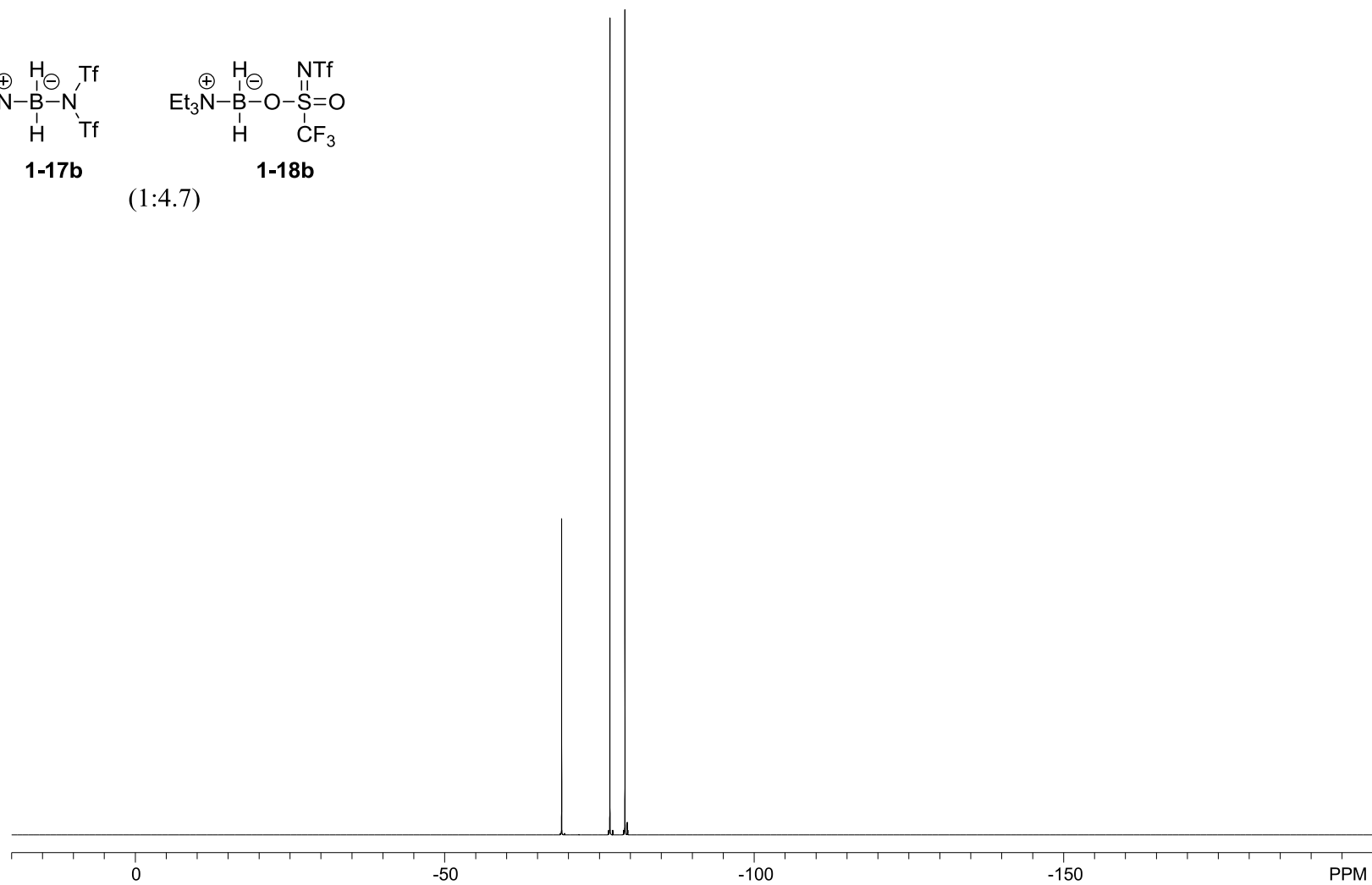


**1-17b**



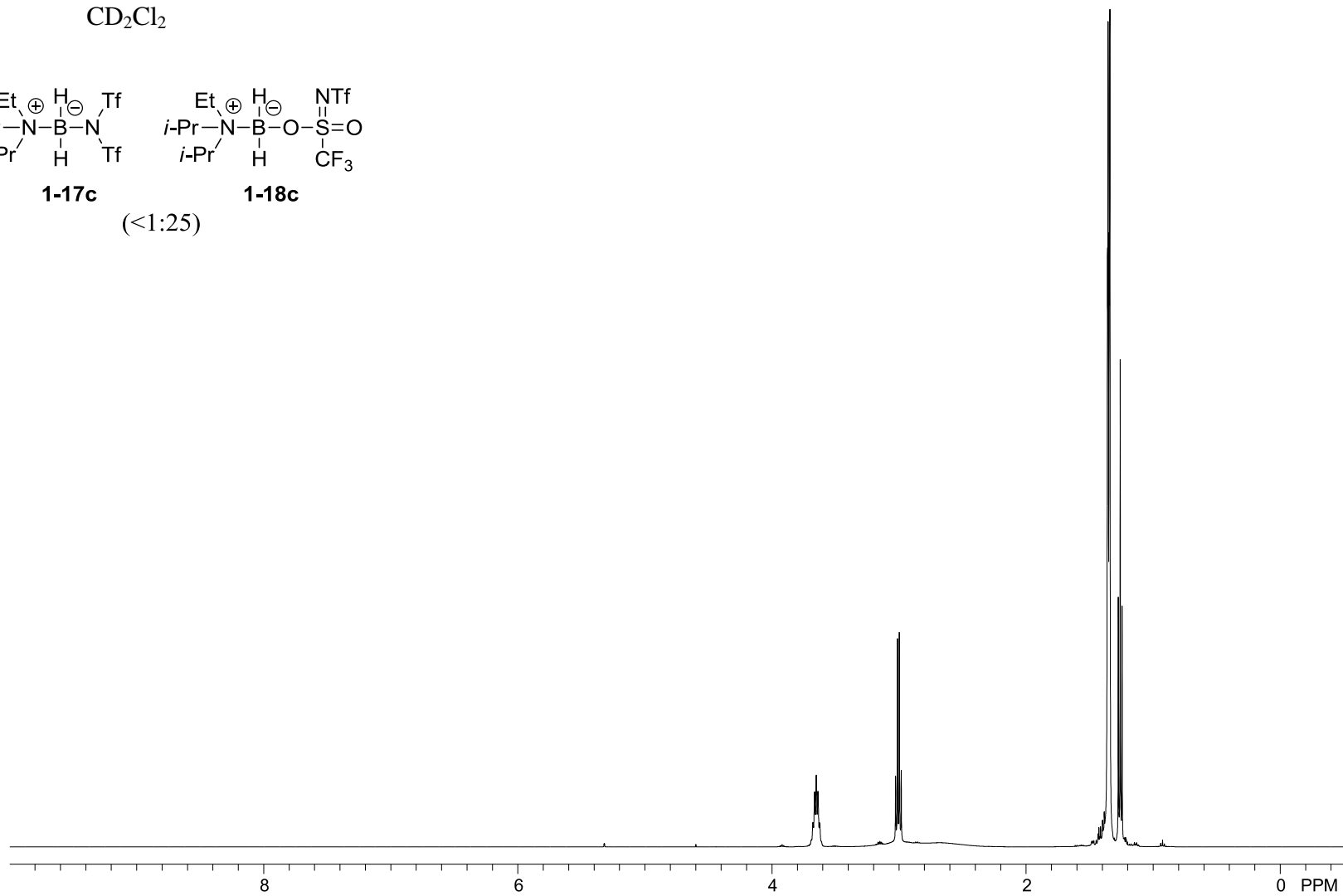
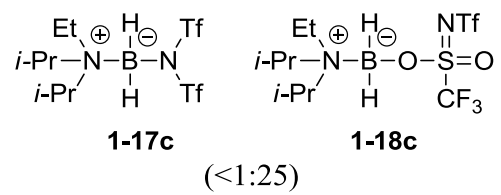
**1-18b**

(1:4.7)

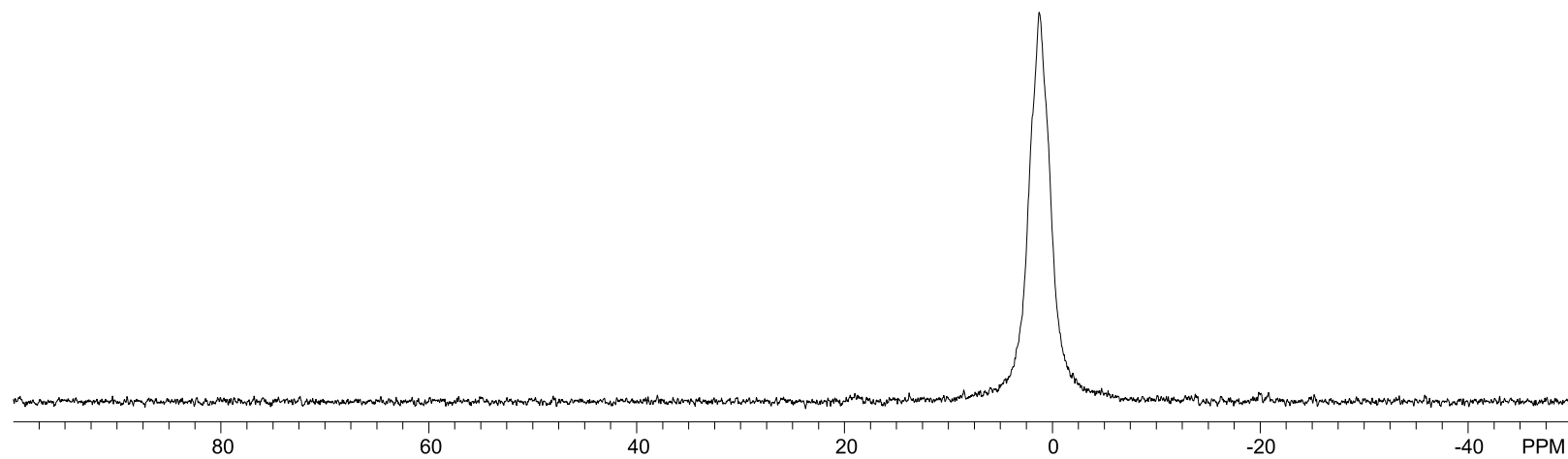
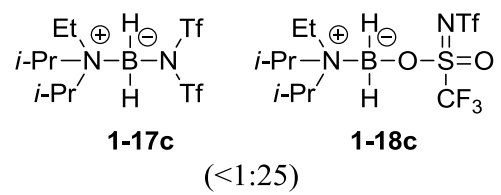




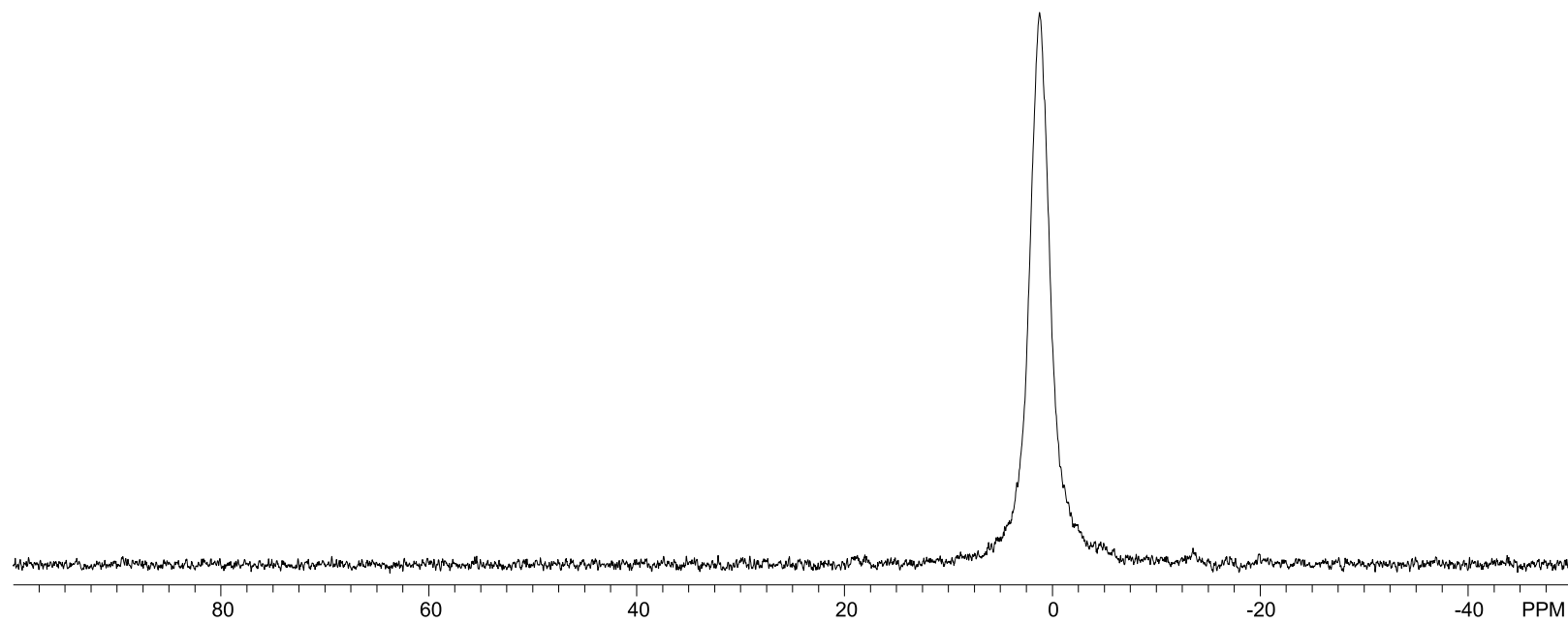
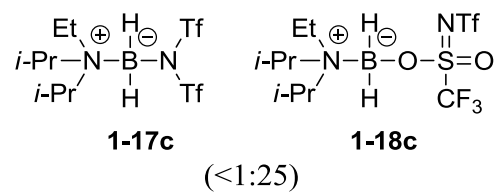
$^1\text{H}$  NMR (500 MHz),  
 $\text{CD}_2\text{Cl}_2$



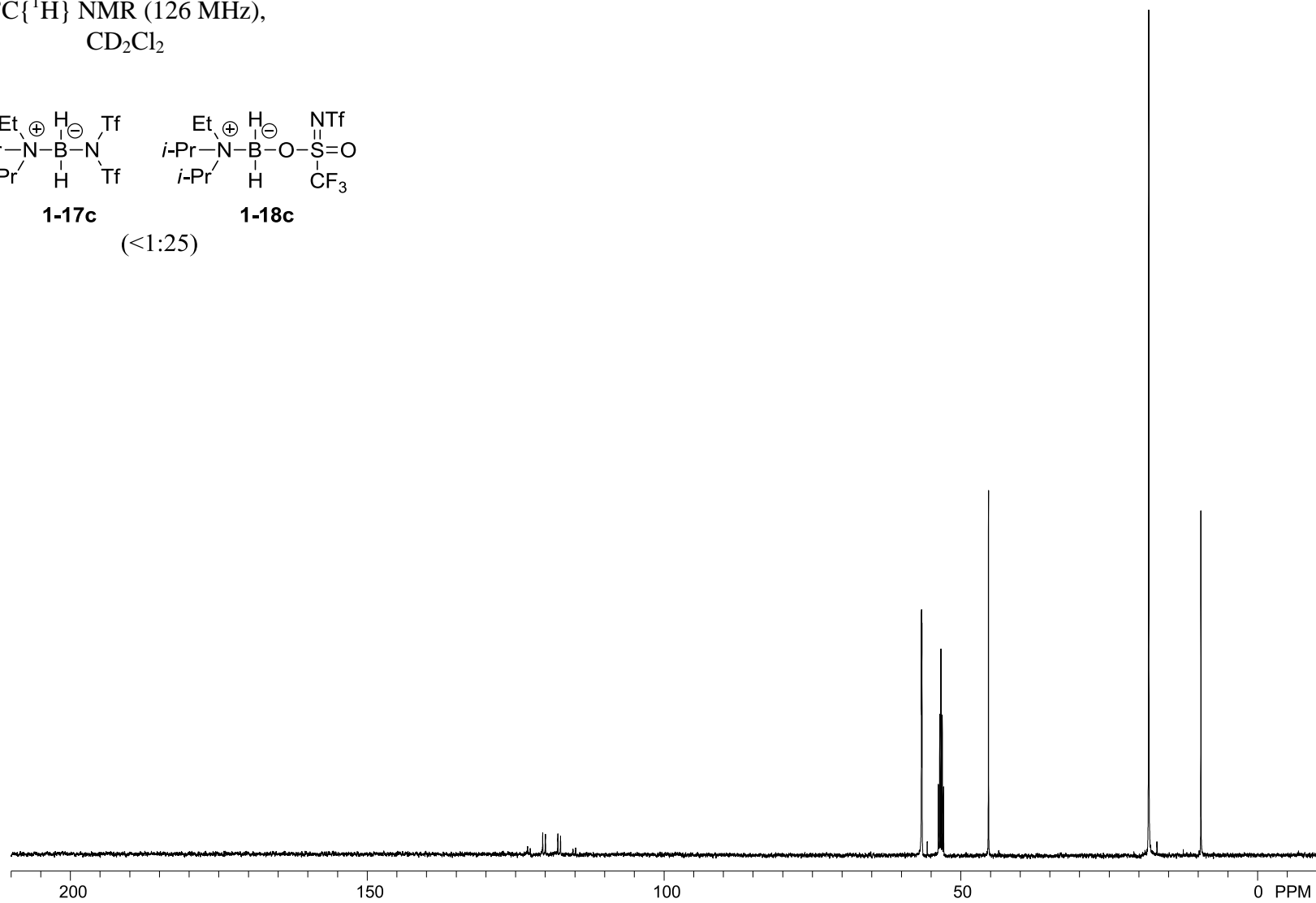
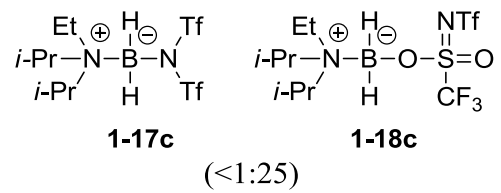
$^{11}\text{B}$  NMR (160 MHz),  
 $\text{CD}_2\text{Cl}_2$



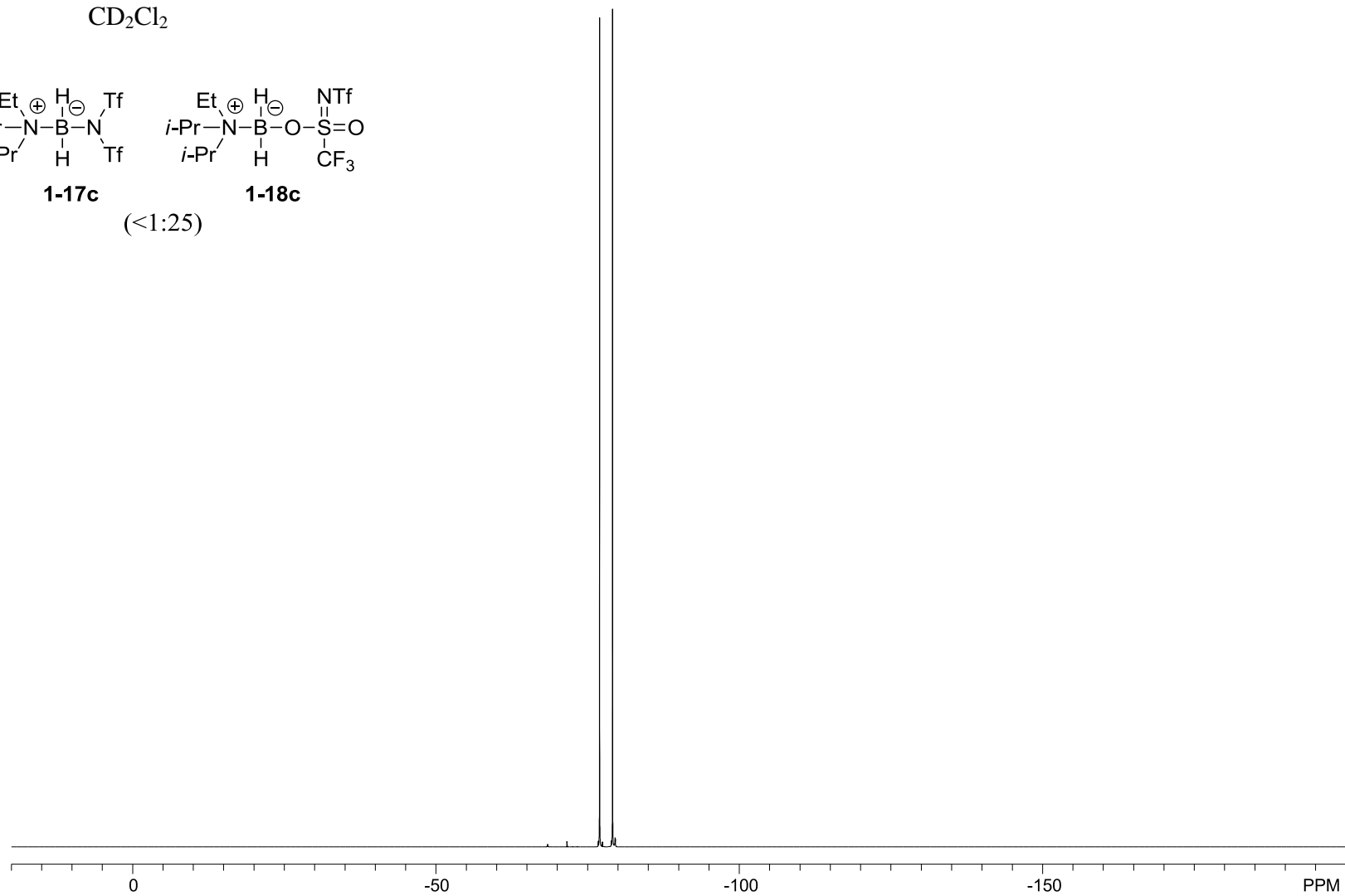
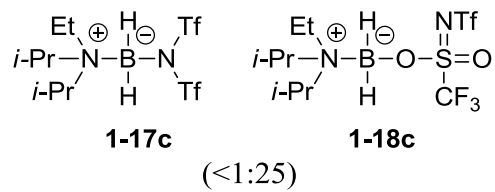
$^{11}\text{B}\{^1\text{H}\}$  NMR (160 MHz),  
 $\text{CD}_2\text{Cl}_2$



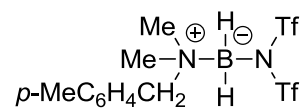
$^{13}\text{C}\{^1\text{H}\}$  NMR (126 MHz),  
 $\text{CD}_2\text{Cl}_2$



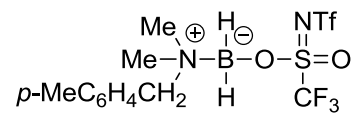
$^{19}\text{F}$  NMR (471 MHz),  
 $\text{CD}_2\text{Cl}_2$



$^1\text{H}$  NMR (500 MHz),  
 $\text{CD}_2\text{Cl}_2$

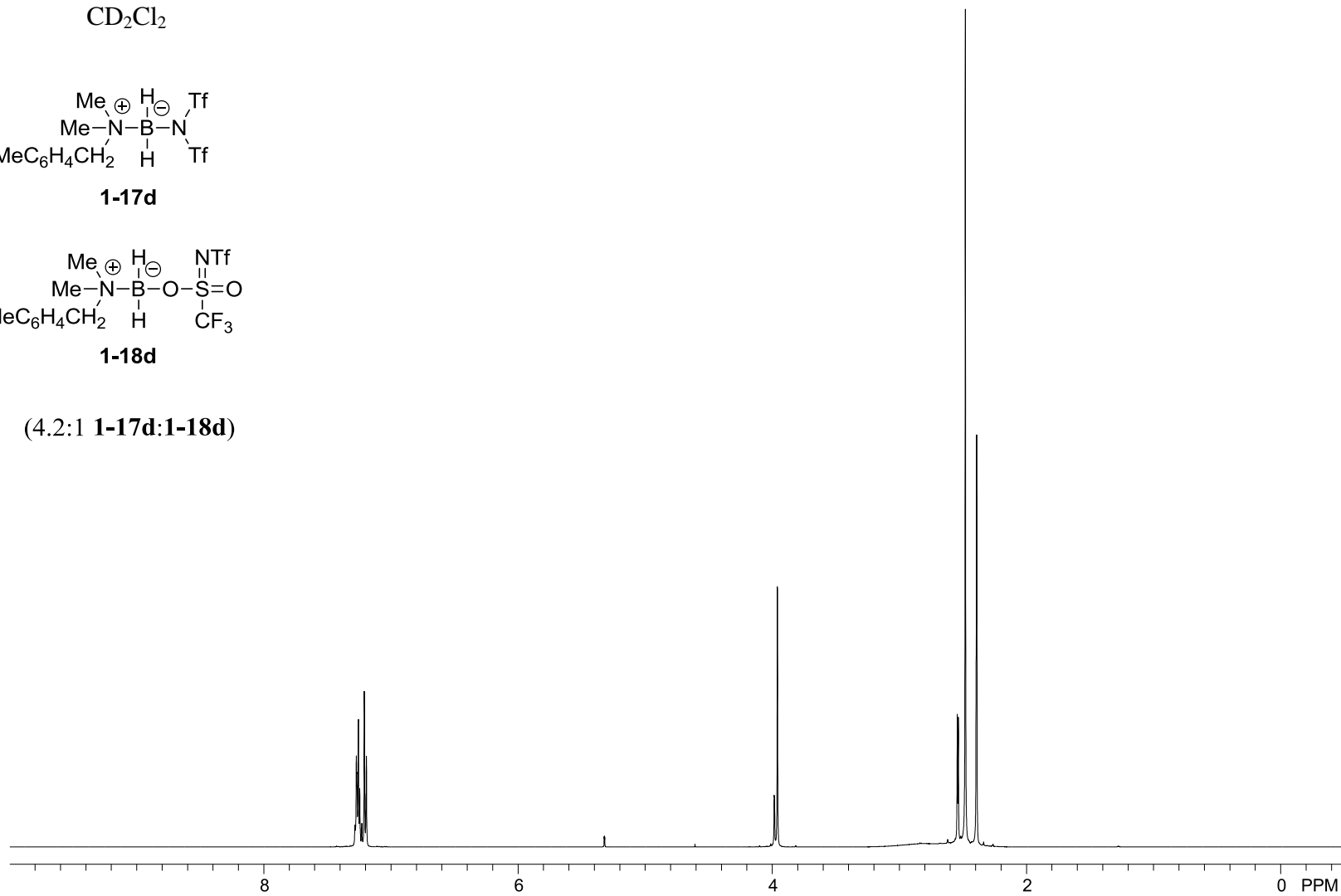


**1-17d**

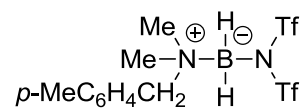


**1-18d**

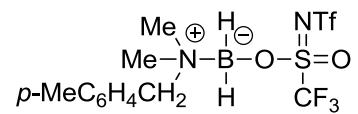
(4.2:1 **1-17d**:**1-18d**)



$^{11}\text{B}$  NMR (160 MHz),  
 $\text{CD}_2\text{Cl}_2$

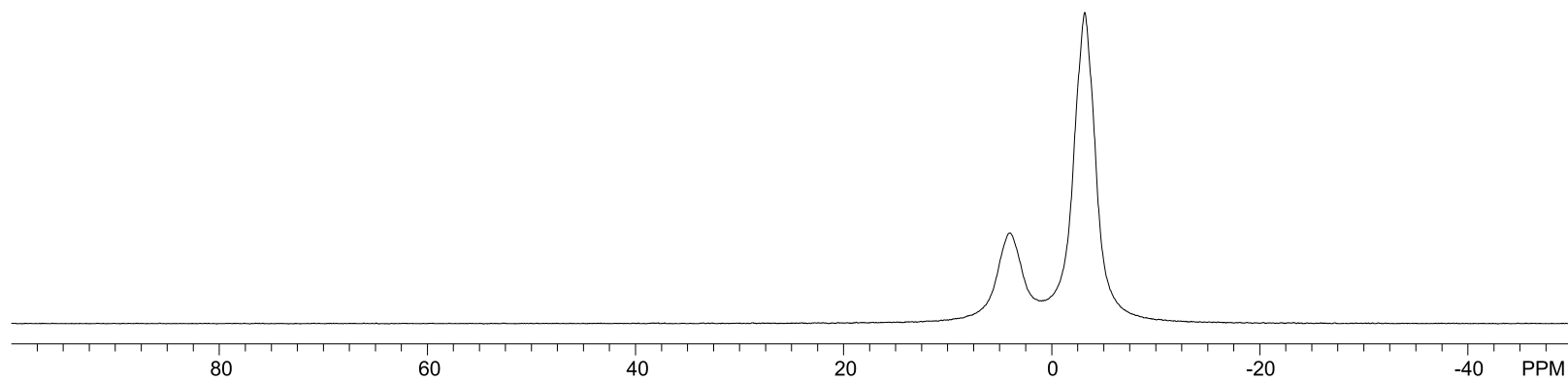


**1-17d**

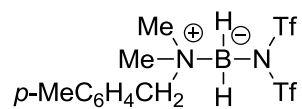


**1-18d**

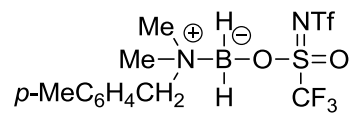
(4.2:1 **1-17d**:**1-18d**)



$^{11}\text{B}\{^1\text{H}\}$  NMR (160 MHz),  
 $\text{CD}_2\text{Cl}_2$

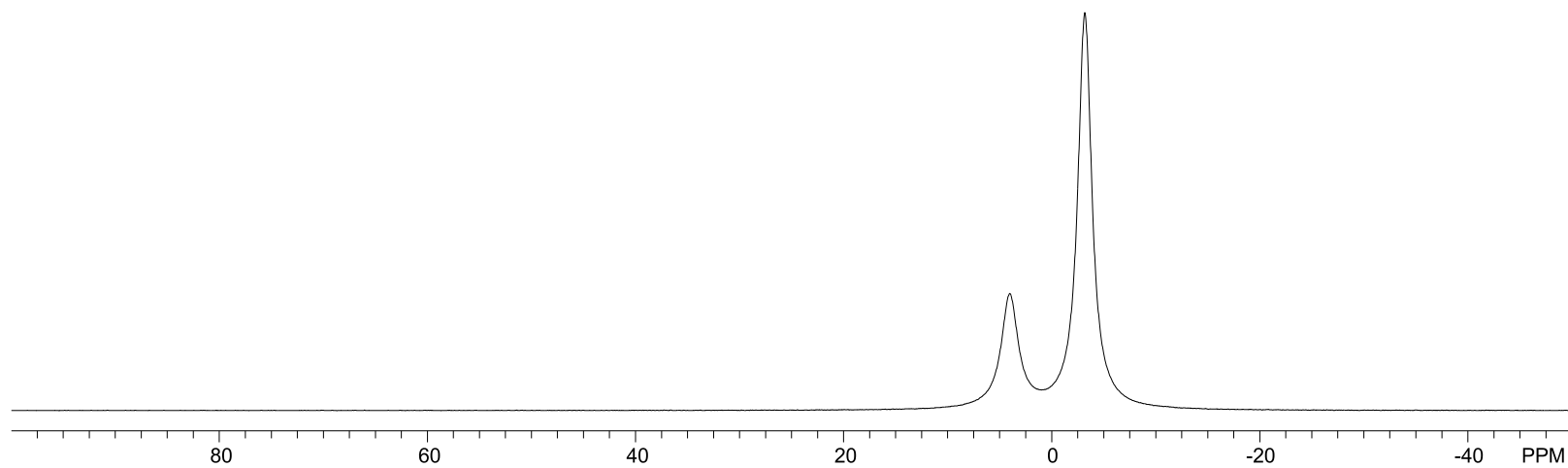


**1-17d**



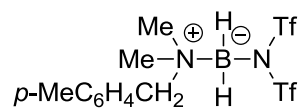
**1-18d**

(4.2:1 **1-17d**:**1-18d**)

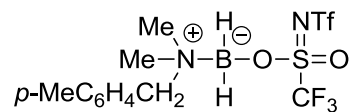




$^{13}\text{C}\{^1\text{H}\}$  NMR (126 MHz),  
 $\text{CD}_2\text{Cl}_2$

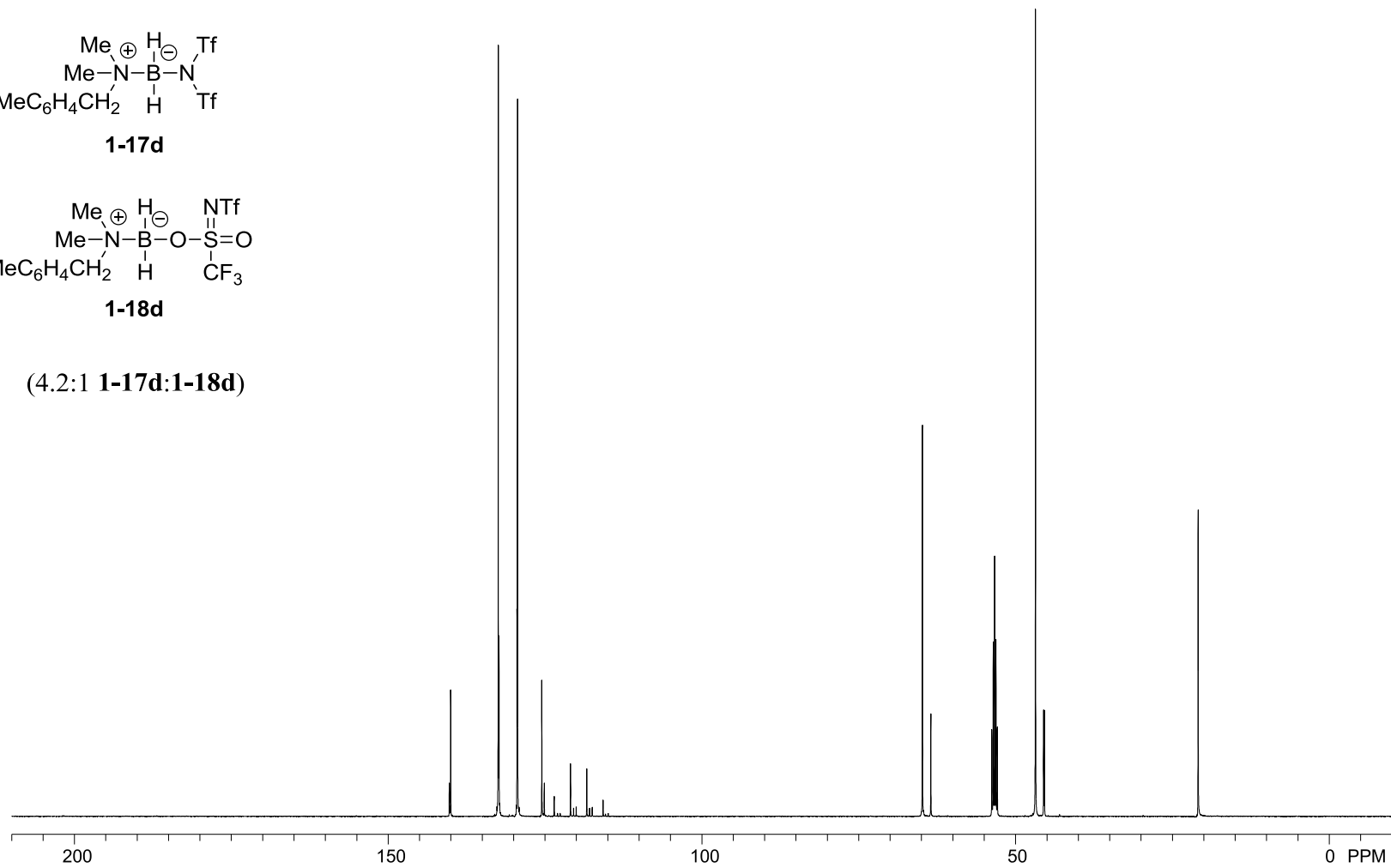


**1-17d**

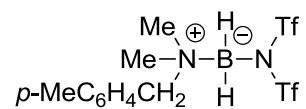


**1-18d**

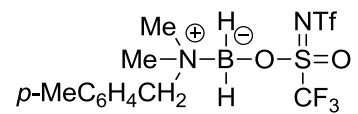
(4.2:1 **1-17d**:**1-18d**)



$^{19}\text{F}$  NMR (471 MHz),  
 $\text{CD}_2\text{Cl}_2$

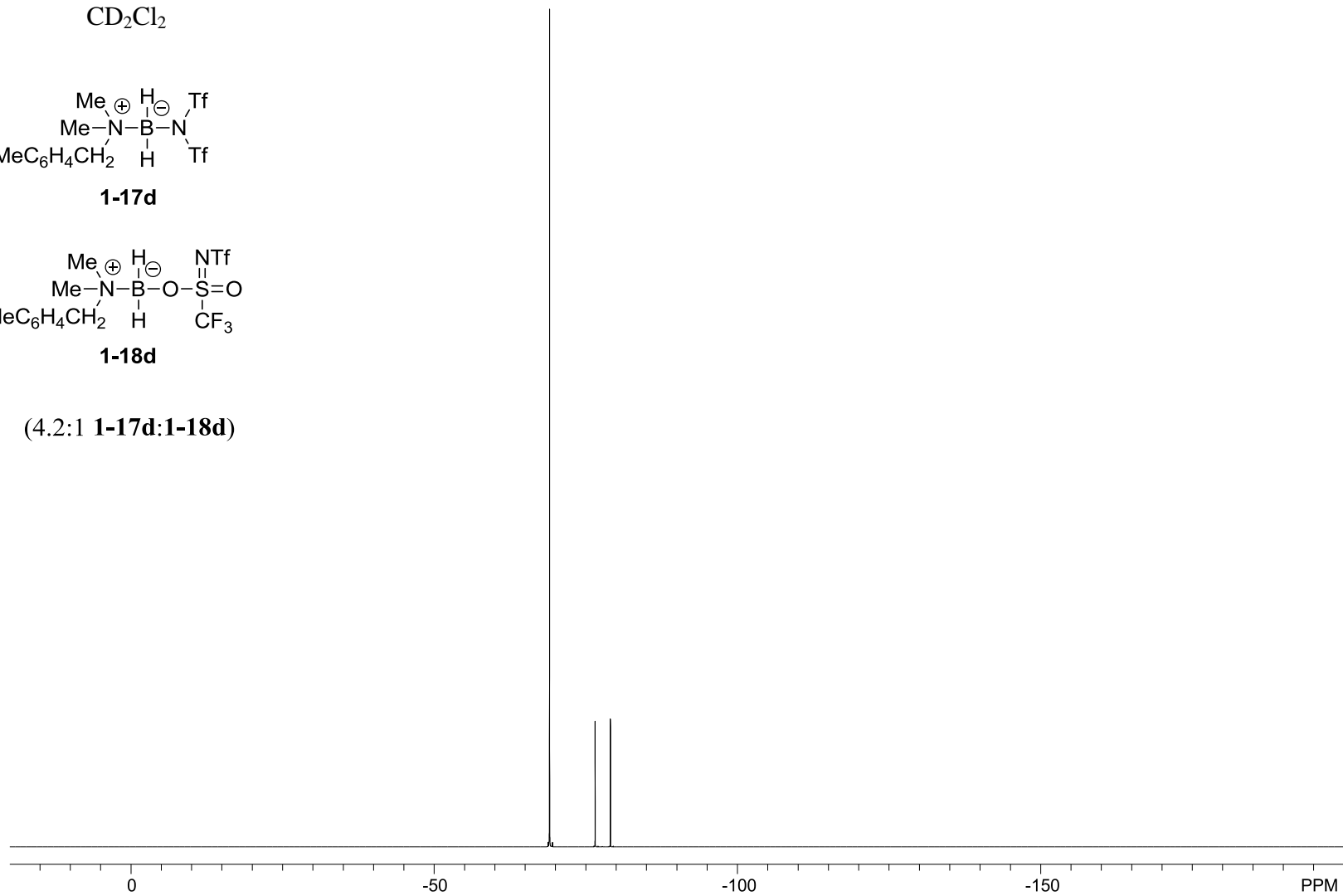


**1-17d**

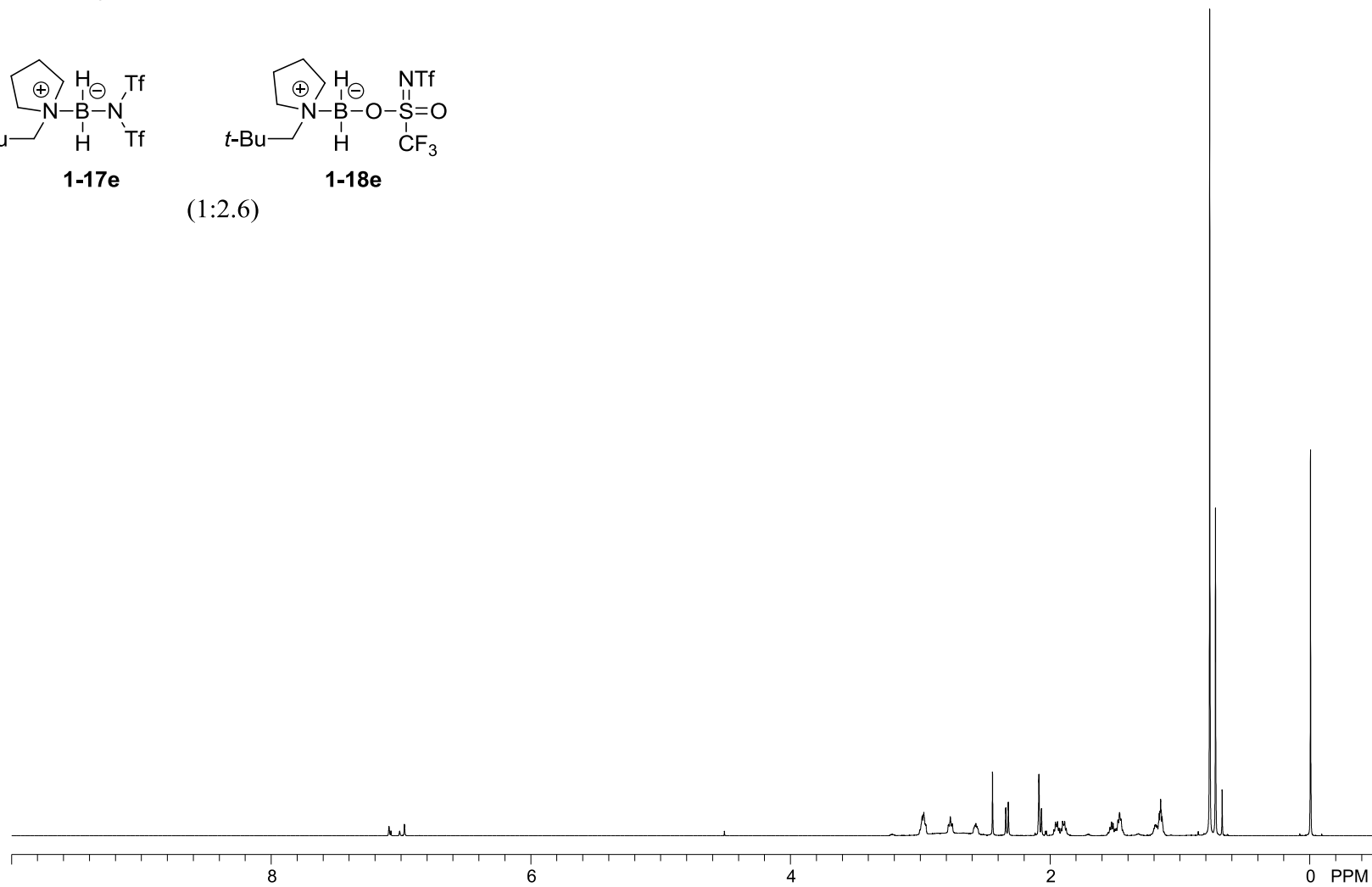
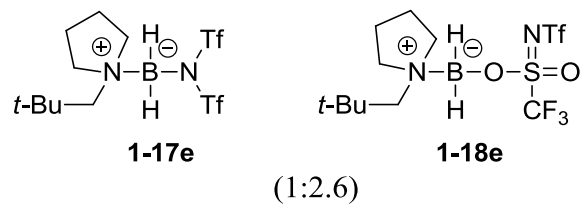


**1-18d**

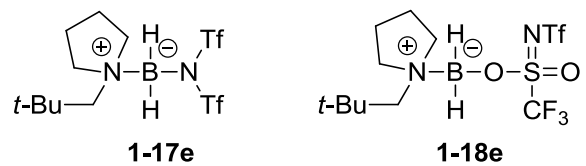
(4.2:1 **1-17d**:**1-18d**)



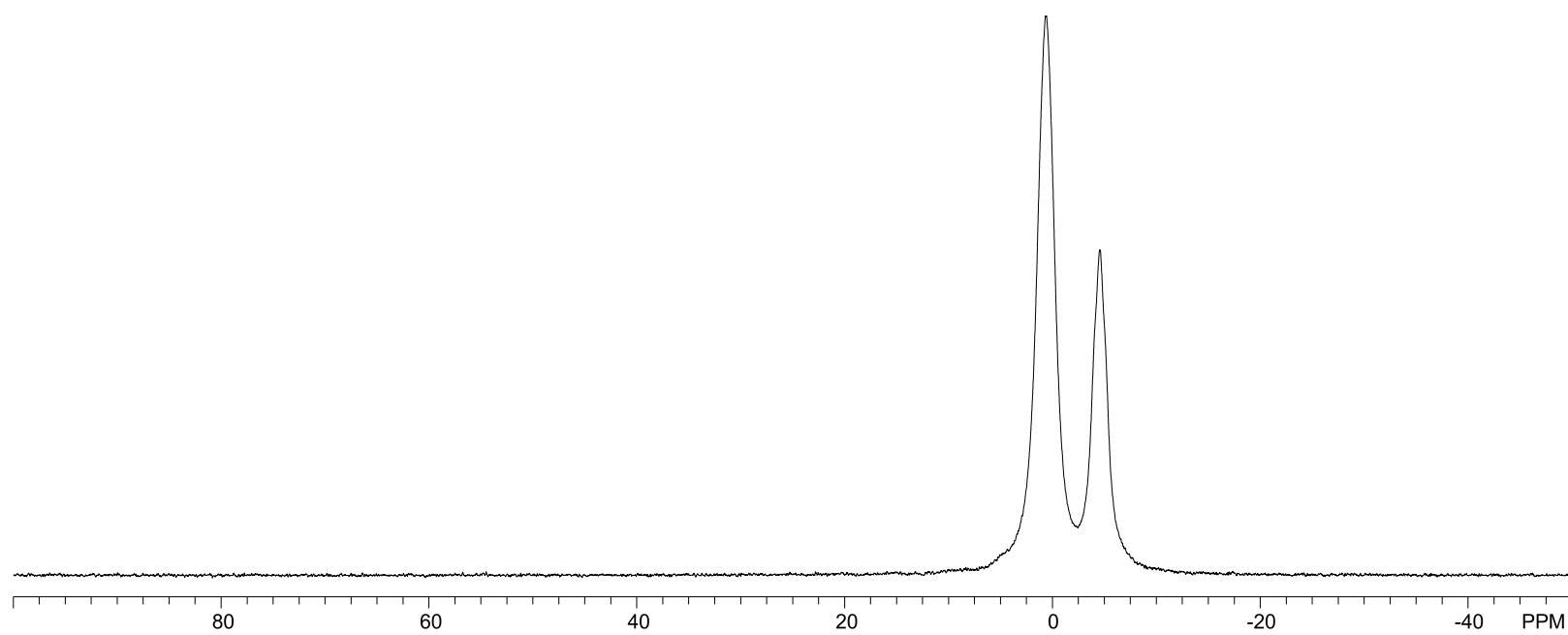
$^1\text{H}$  NMR (700 MHz),  
 $d_8$ -PhMe



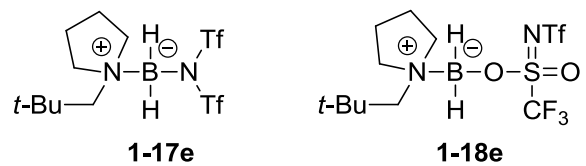
$^{11}\text{B}$  NMR (225 MHz),  
 $d_8\text{-PhMe}$



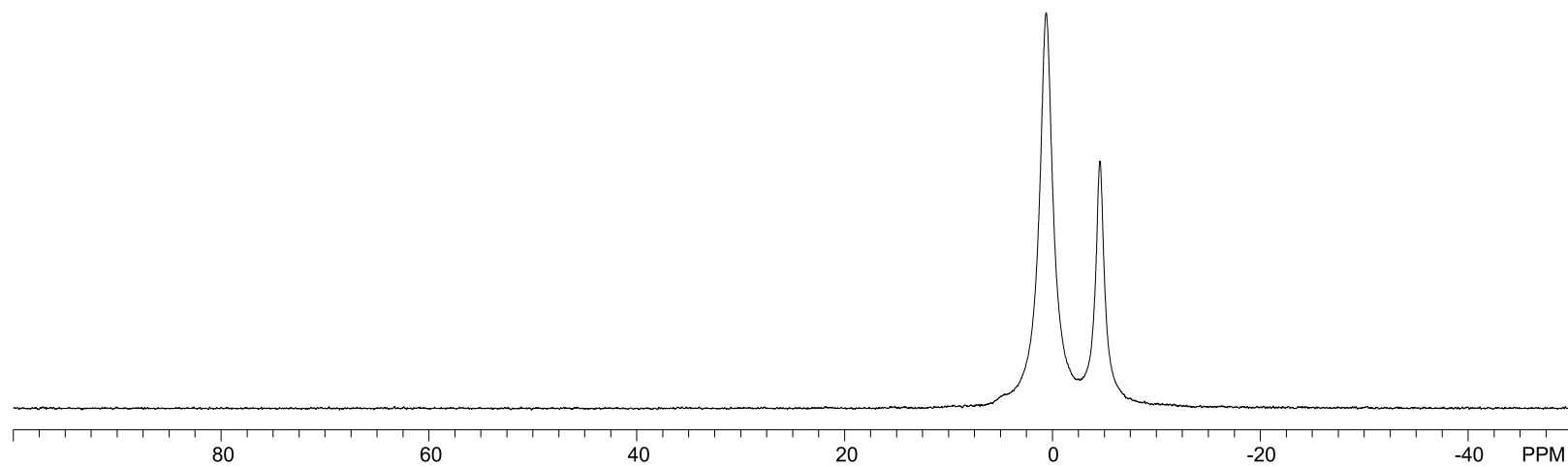
(1:2.6)



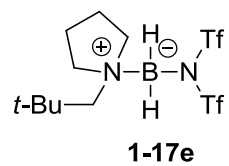
$^{11}\text{B}\{^1\text{H}\}$  NMR (225 MHz),  
 $d_8\text{-PhMe}$



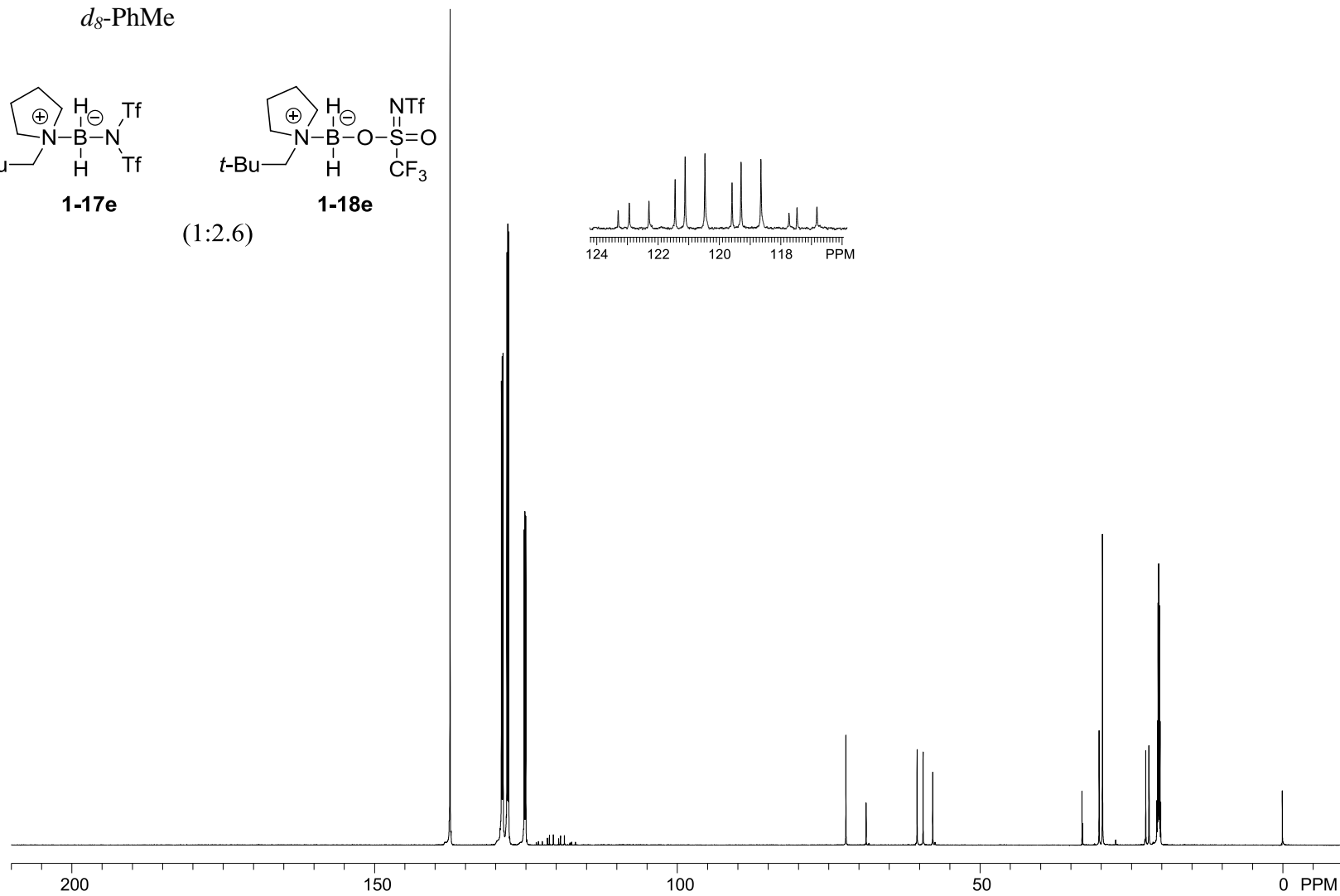
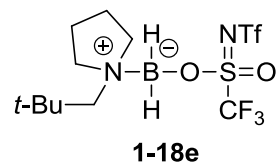
(1:2.6)



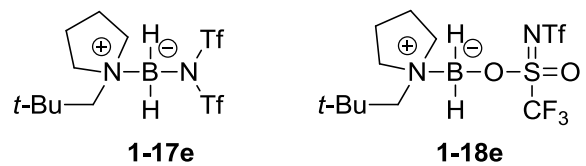
$^{13}\text{C}\{^1\text{H}\}$  NMR (176 MHz),  
 $d_8\text{-PhMe}$



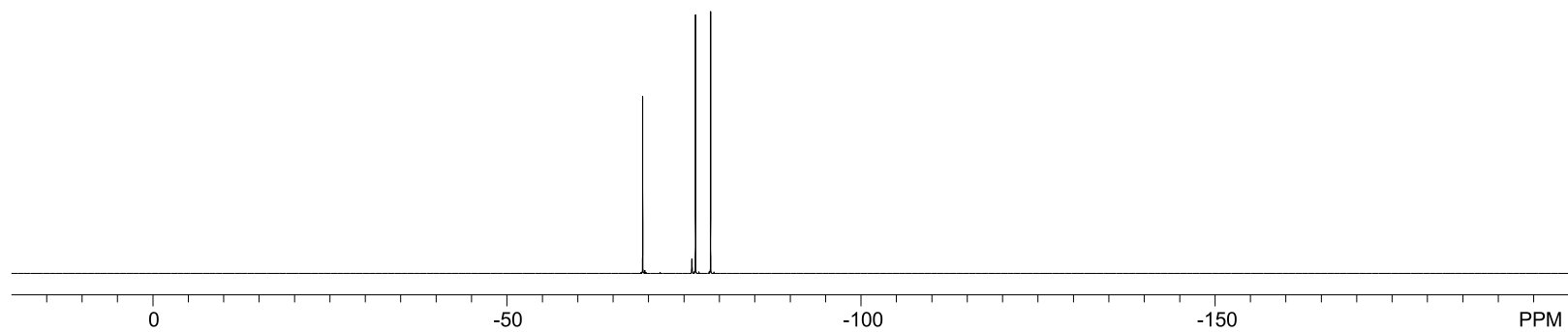
(1:2.6)



$^{19}\text{F}$  NMR (471 MHz),  
 $d_8\text{-PhMe}$

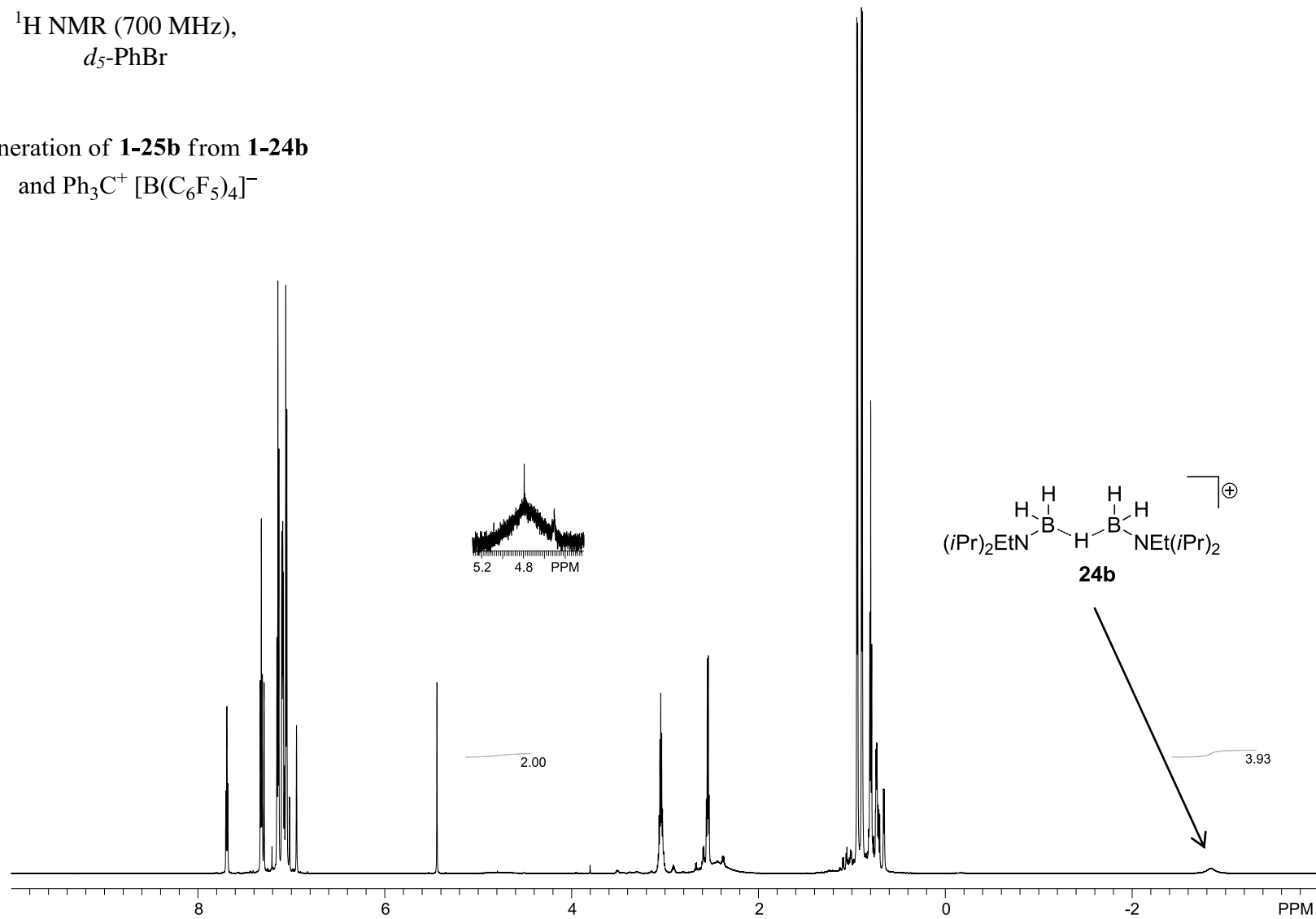


(1:2.6)



$^1\text{H}$  NMR (700 MHz),  
 $d_5$ -PhBr

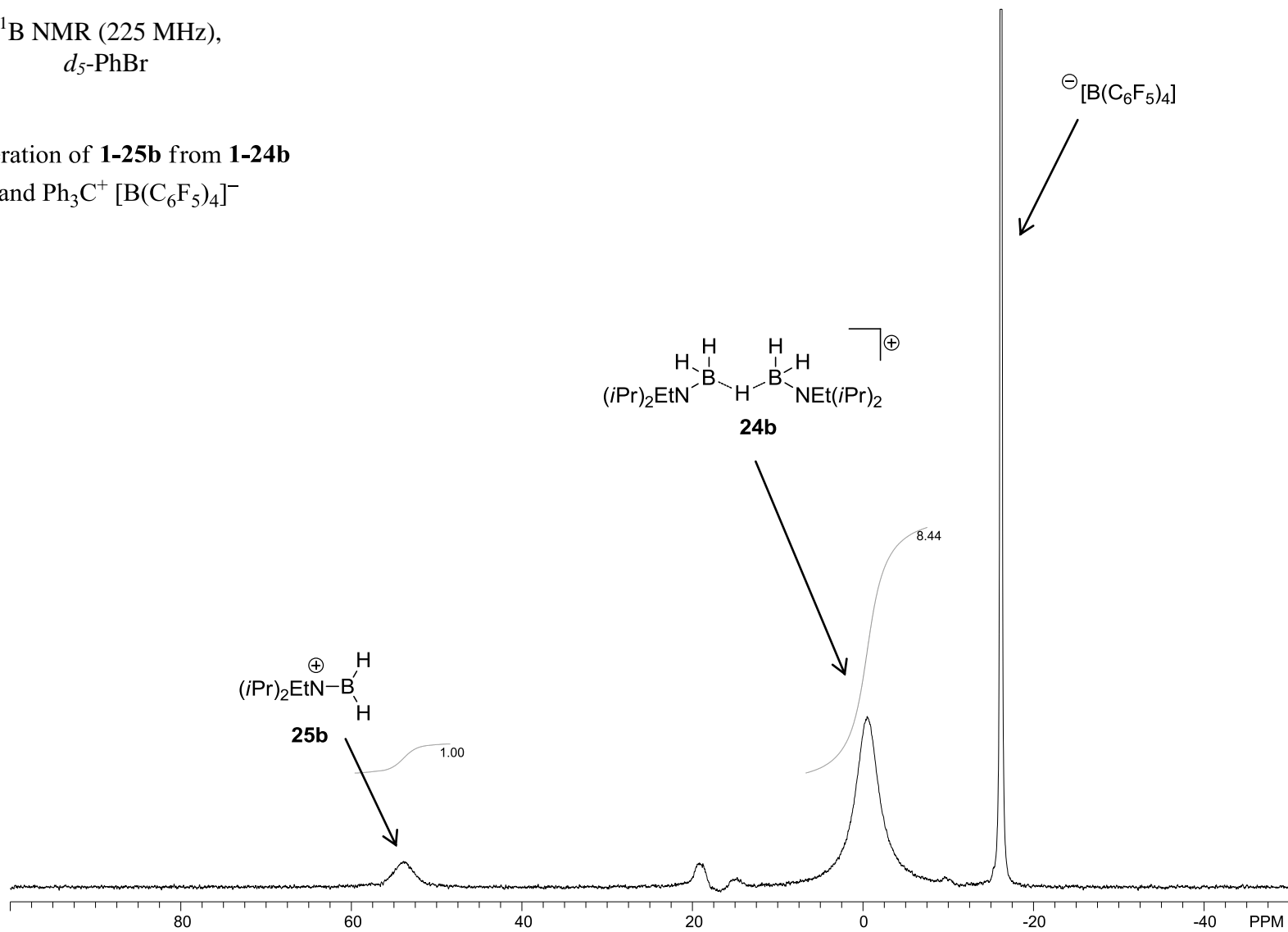
Generation of **1-25b** from **1-24b**  
and  $\text{Ph}_3\text{C}^+ [\text{B}(\text{C}_6\text{F}_5)_4]^-$





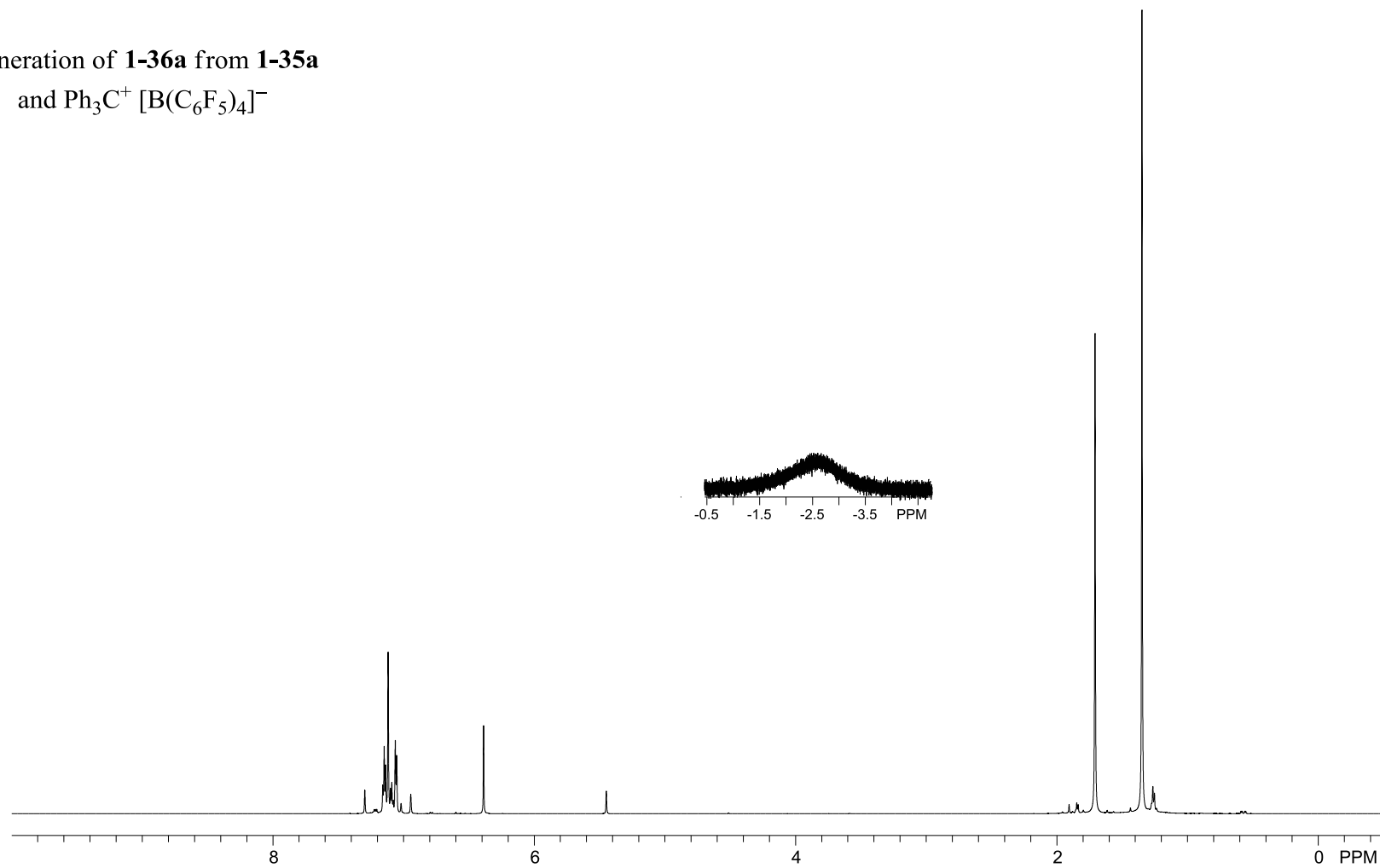
$^{11}\text{B}$  NMR (225 MHz),  
 $d_5$ -PhBr

Generation of **1-25b** from **1-24b**  
and  $\text{Ph}_3\text{C}^+ [\text{B}(\text{C}_6\text{F}_5)_4]^-$



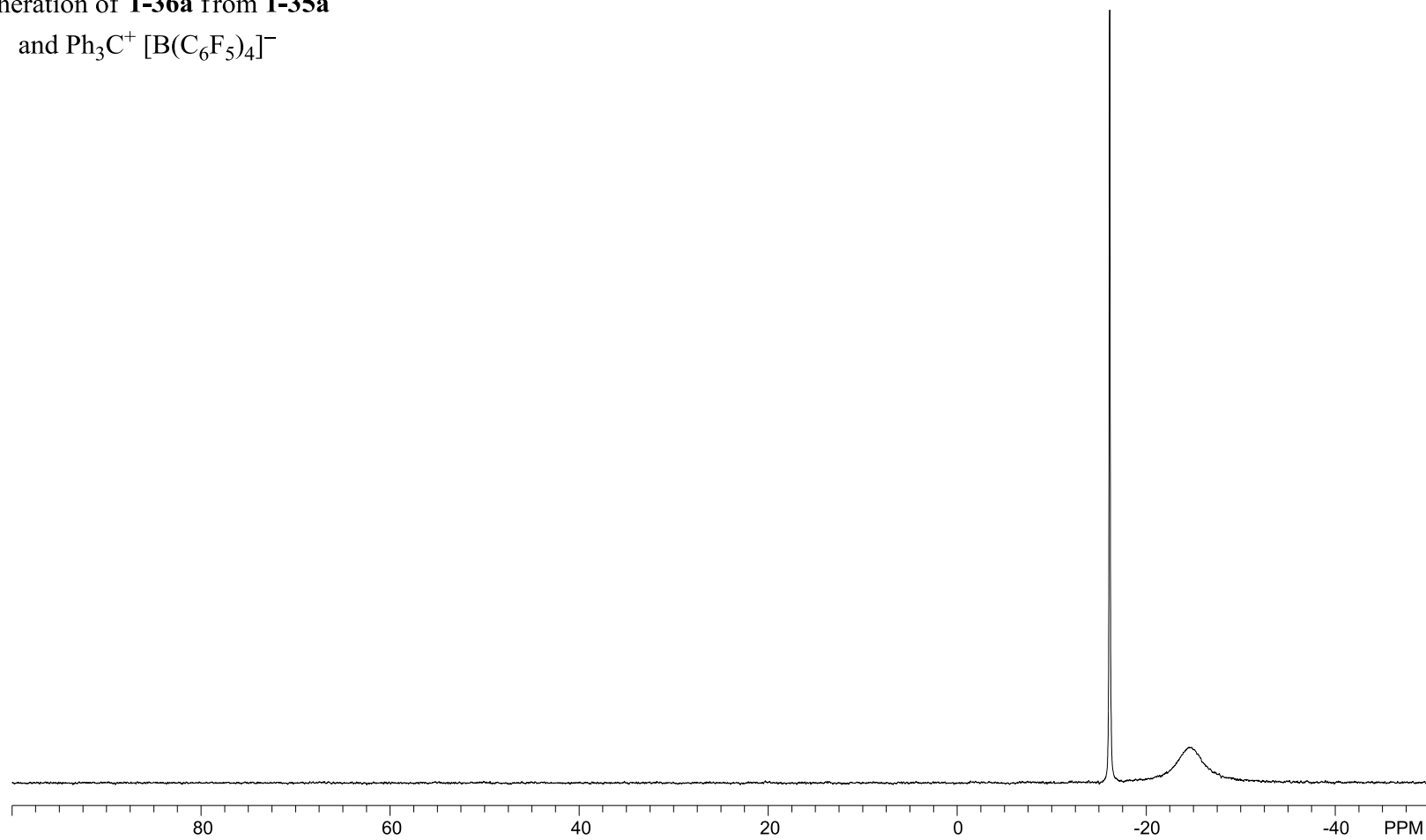
$^1\text{H}$  NMR (700 MHz),  
 $d_5$ -PhBr

Generation of **1-36a** from **1-35a**  
and  $\text{Ph}_3\text{C}^+ [\text{B}(\text{C}_6\text{F}_5)_4]^-$



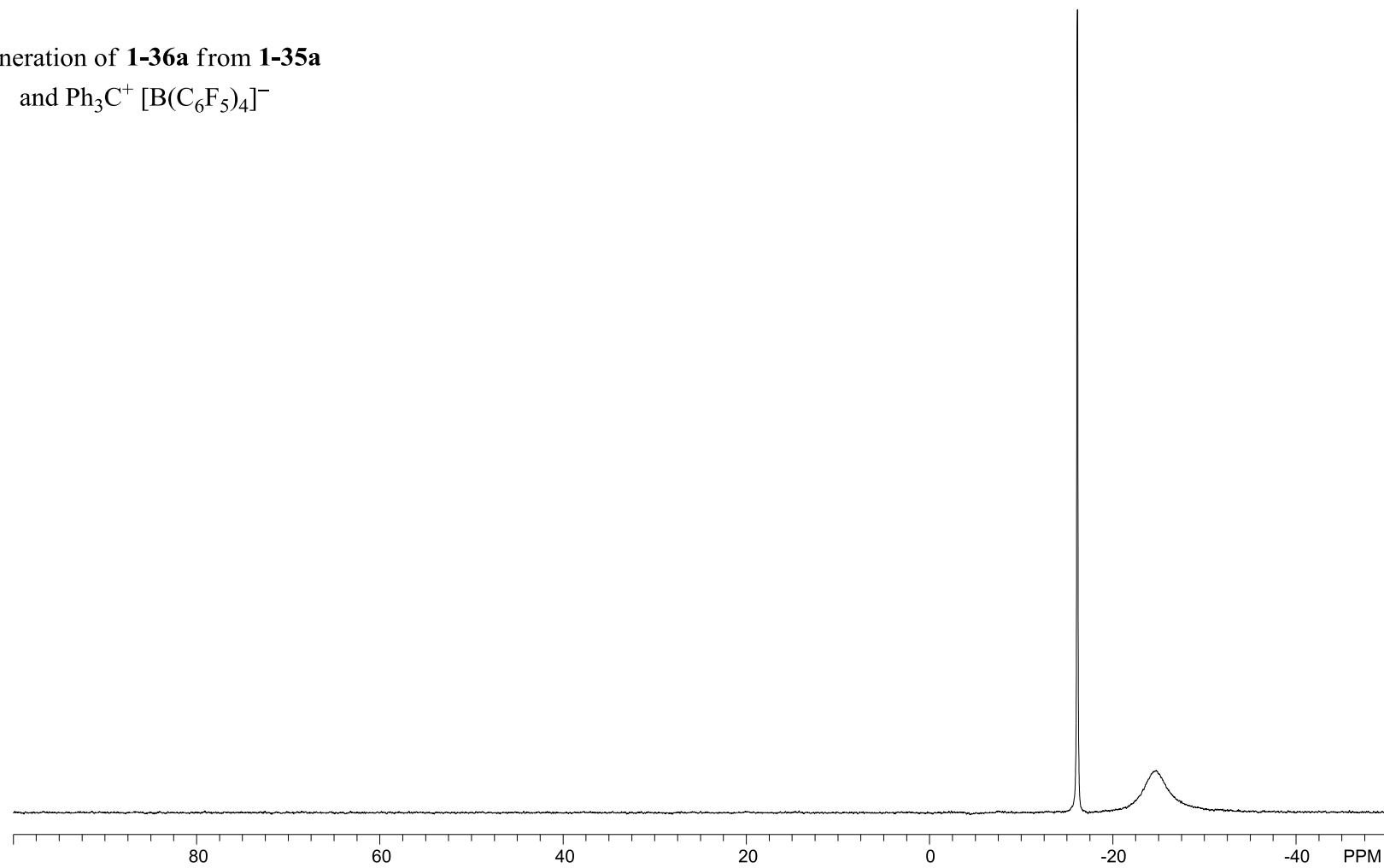
$^{11}\text{B}$  NMR (225 MHz),  
 $d_5\text{-PhBr}$

Generation of **1-36a** from **1-35a**  
and  $\text{Ph}_3\text{C}^+ [\text{B}(\text{C}_6\text{F}_5)_4]^-$



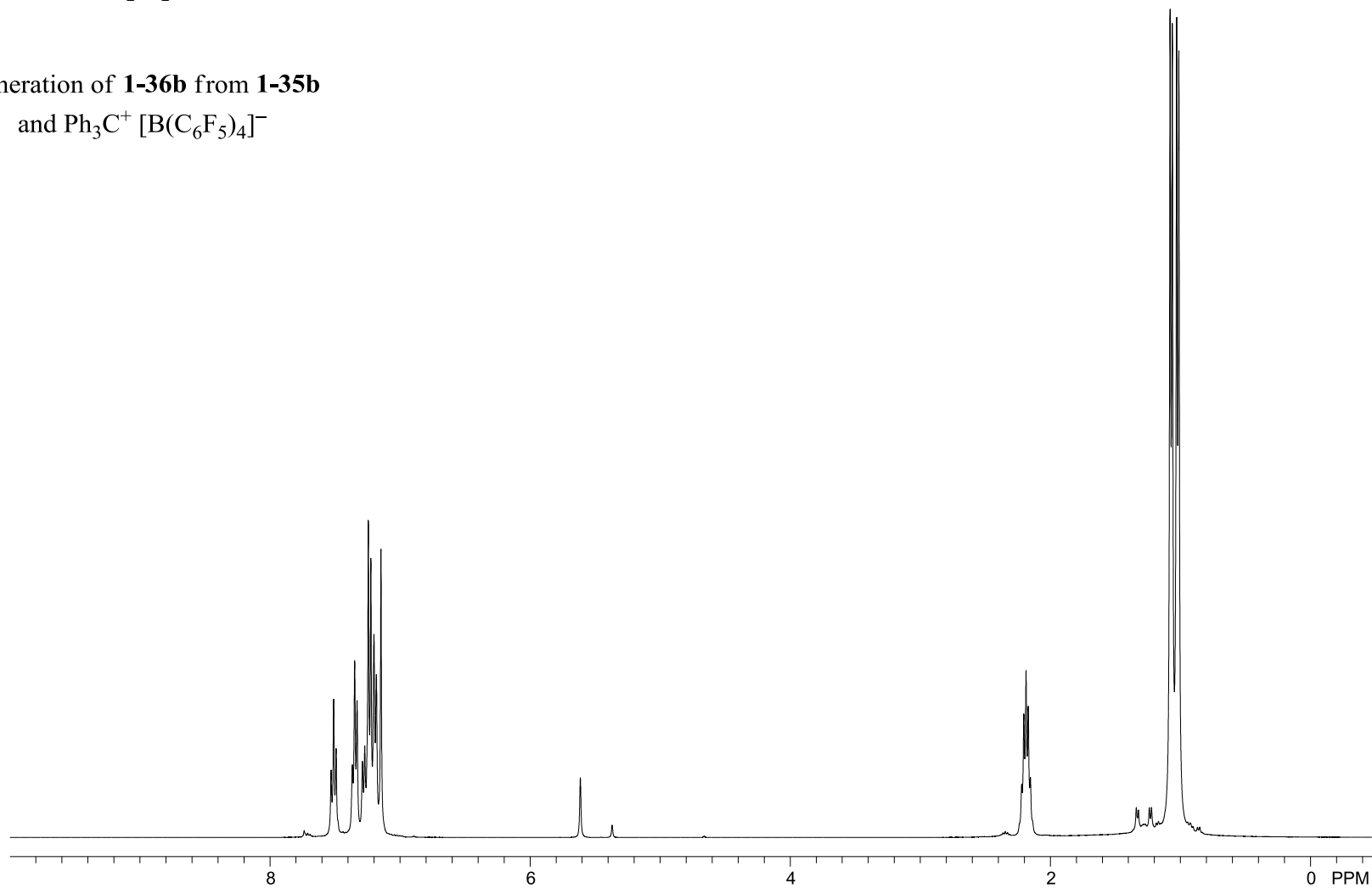
$^{11}\text{B}\{^1\text{H}\}$  NMR (225 MHz),  
 $d_5\text{-PhBr}$

Generation of **1-36a** from **1-35a**  
and  $\text{Ph}_3\text{C}^+ [\text{B}(\text{C}_6\text{F}_5)_4]^-$



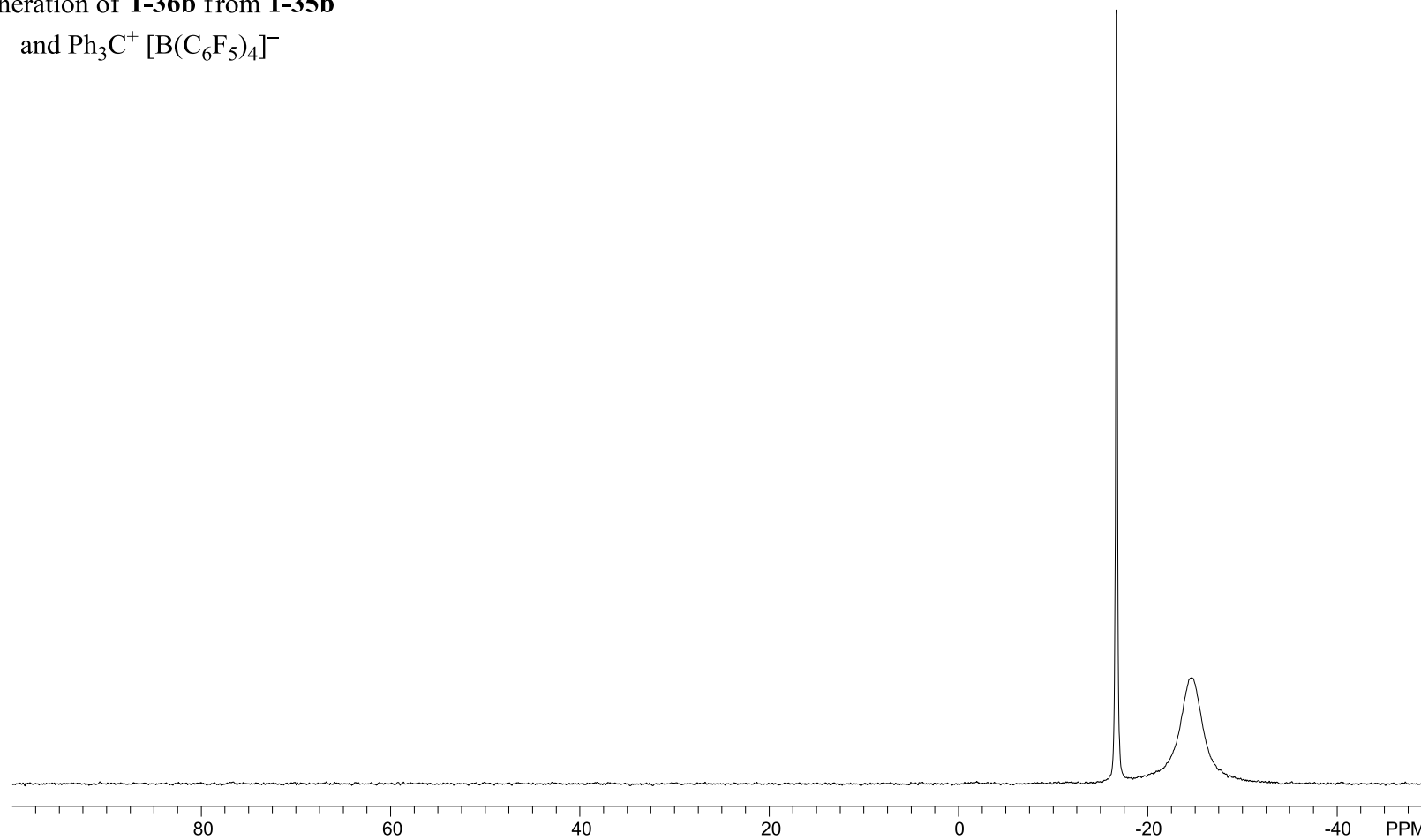
$^1\text{H}$  NMR (400 MHz),  
 $\text{CD}_2\text{Cl}_2$

Generation of **1-36b** from **1-35b**  
and  $\text{Ph}_3\text{C}^+ [\text{B}(\text{C}_6\text{F}_5)_4]^-$



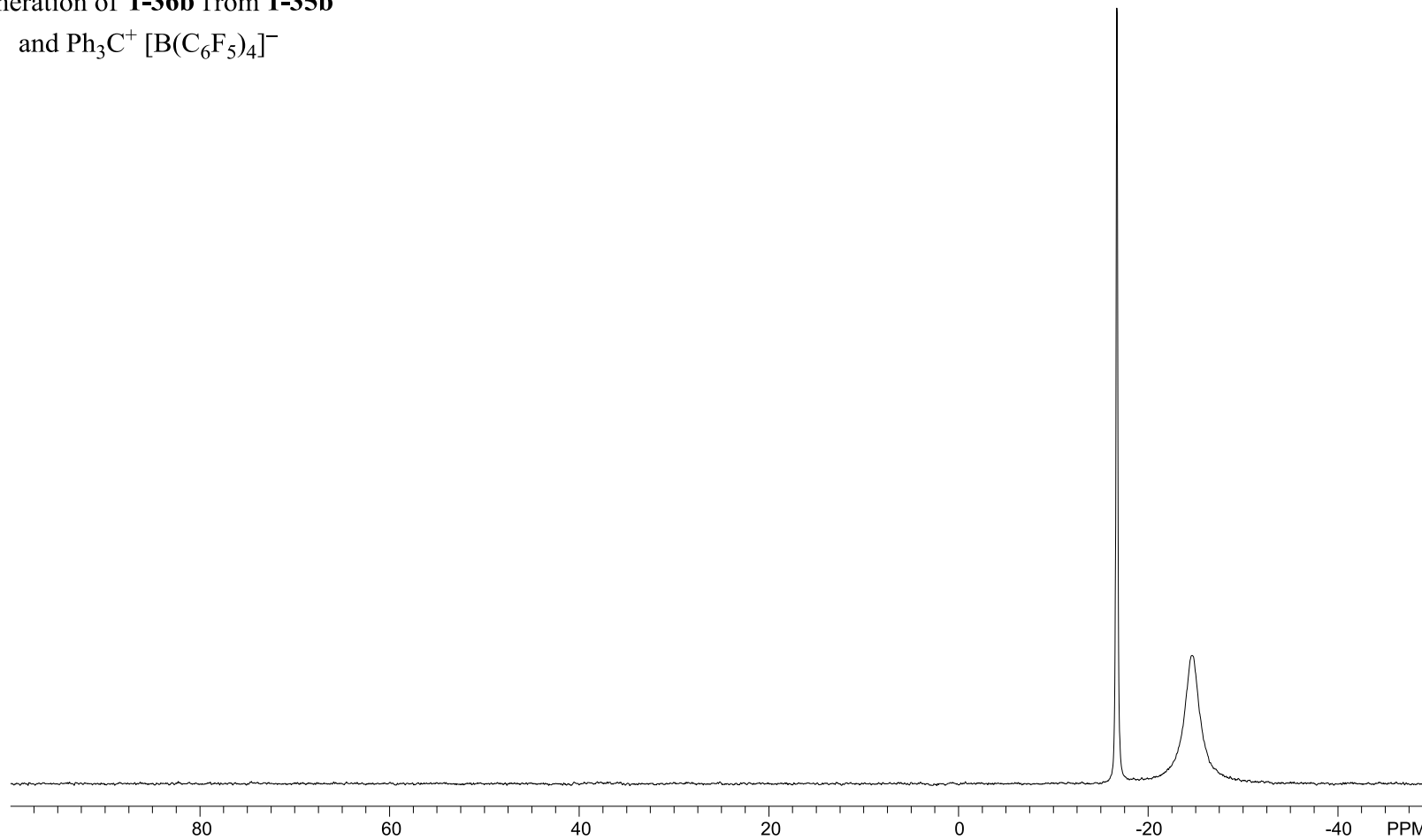
$^{11}\text{B}$  NMR (128 MHz),  
 $\text{CD}_2\text{Cl}_2$

Generation of **1-36b** from **1-35b**  
and  $\text{Ph}_3\text{C}^+ [\text{B}(\text{C}_6\text{F}_5)_4]^-$

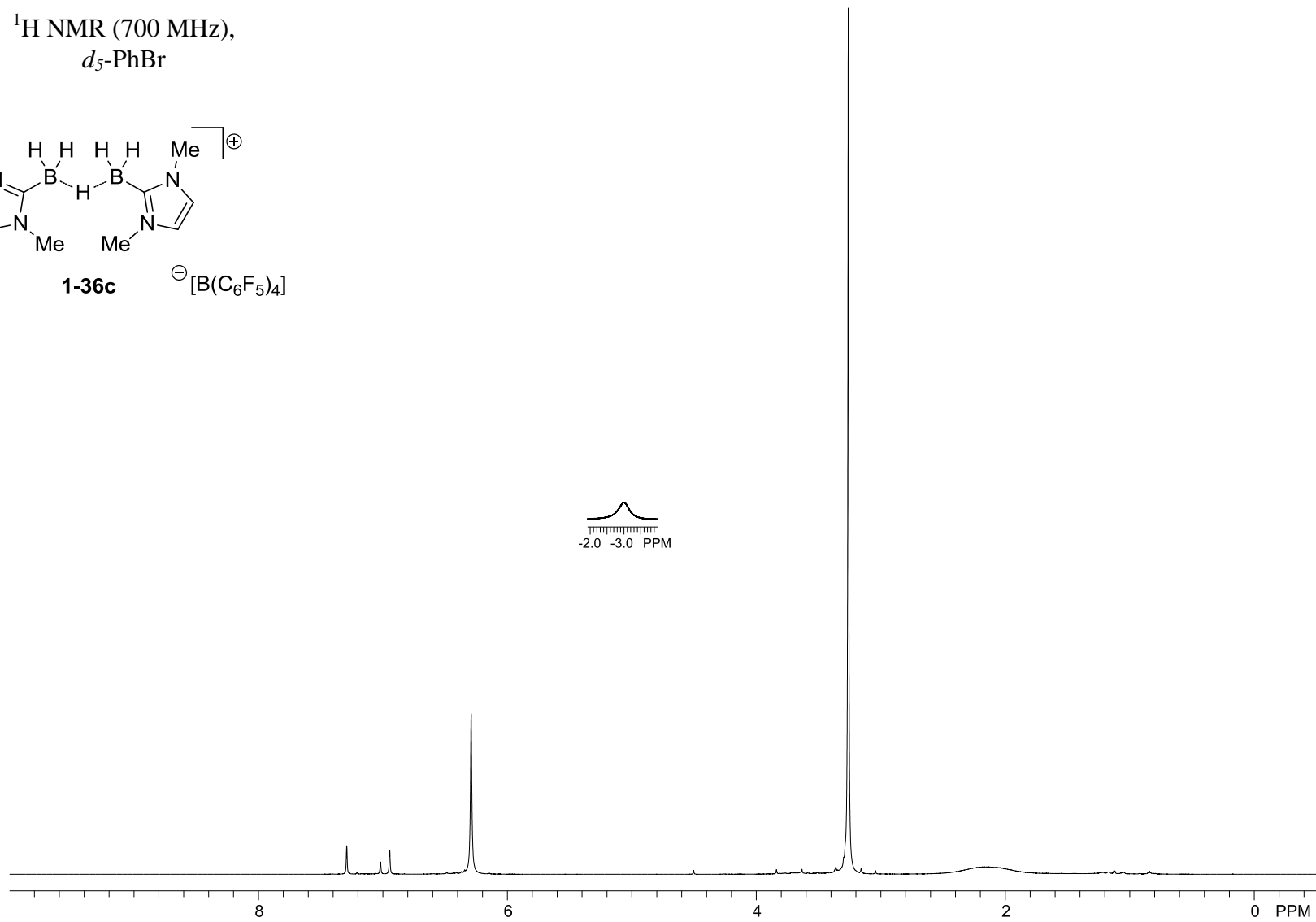
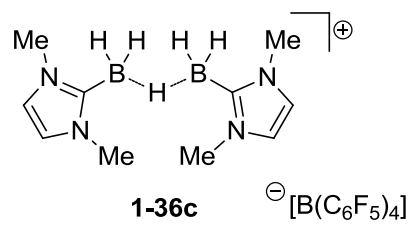


$^{11}\text{B}\{^1\text{H}\}$  NMR (128 MHz),  
 $\text{CD}_2\text{Cl}_2$

Generation of **1-36b** from **1-35b**  
and  $\text{Ph}_3\text{C}^+ [\text{B}(\text{C}_6\text{F}_5)_4]^-$

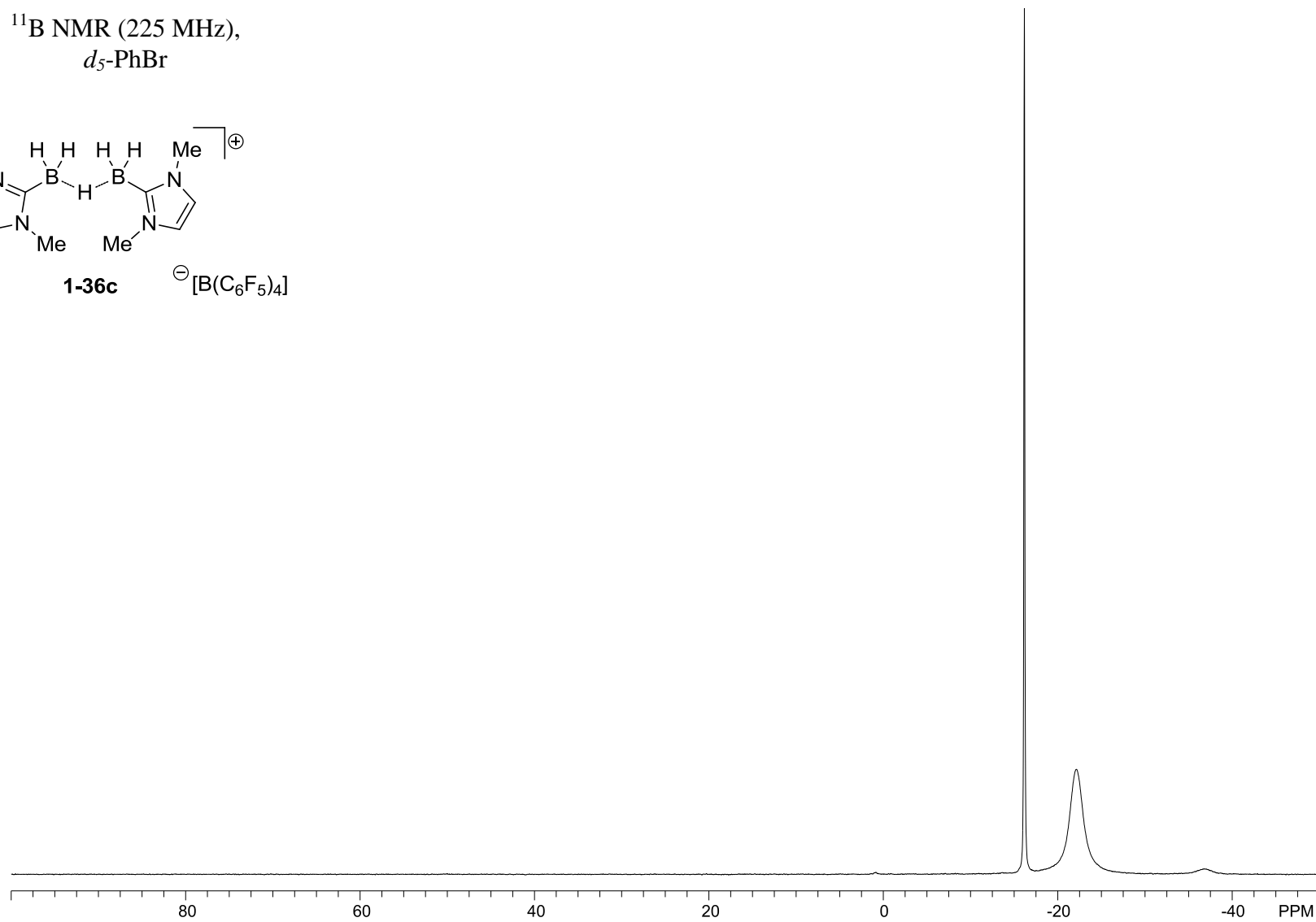
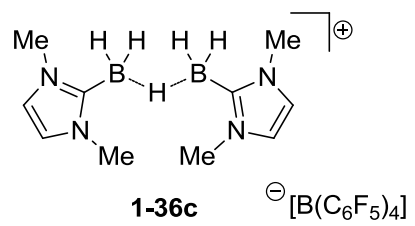


$^1\text{H}$  NMR (700 MHz),  
 $d_5$ -PhBr

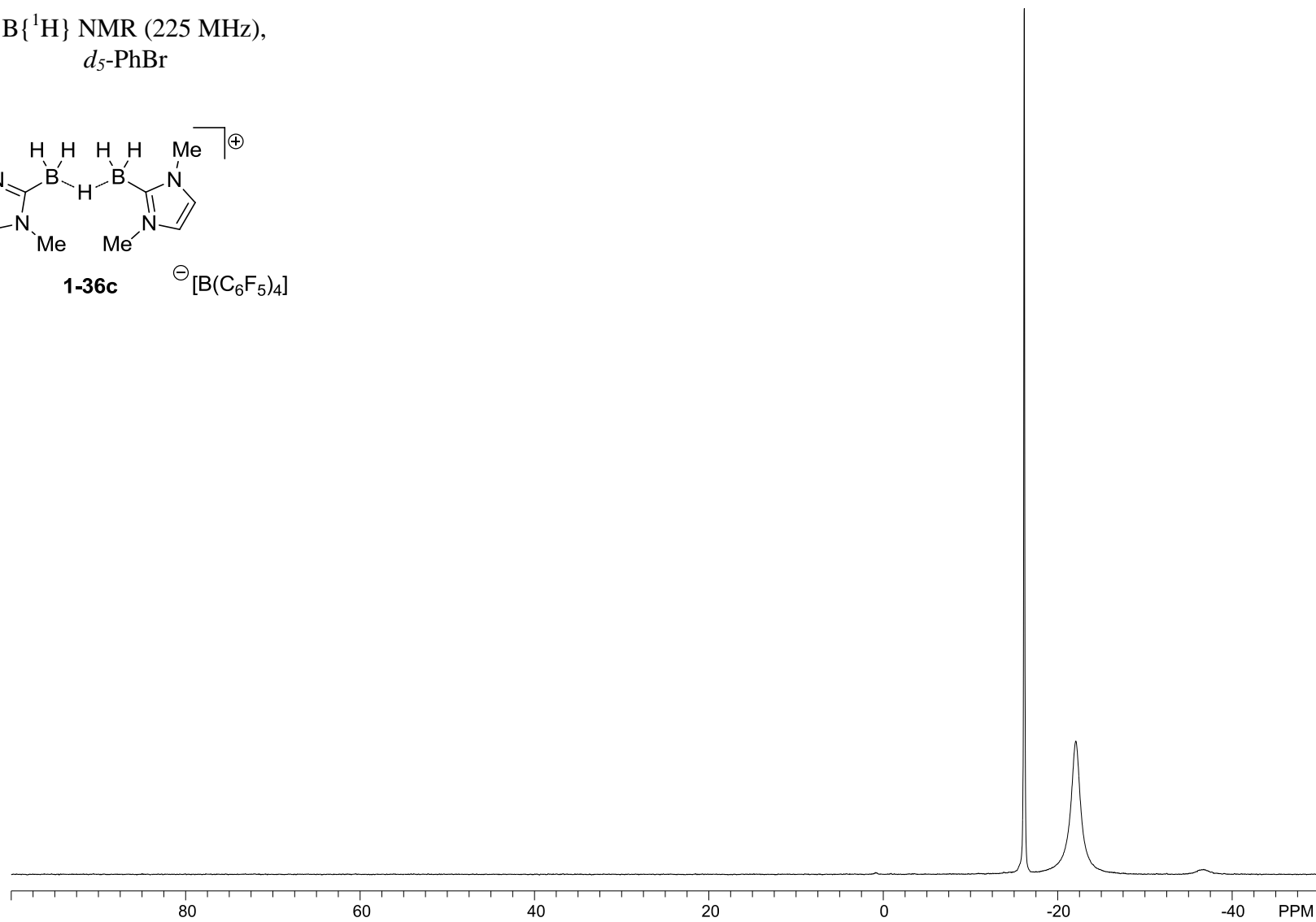
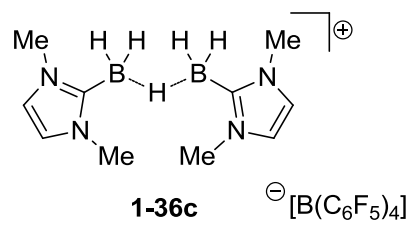




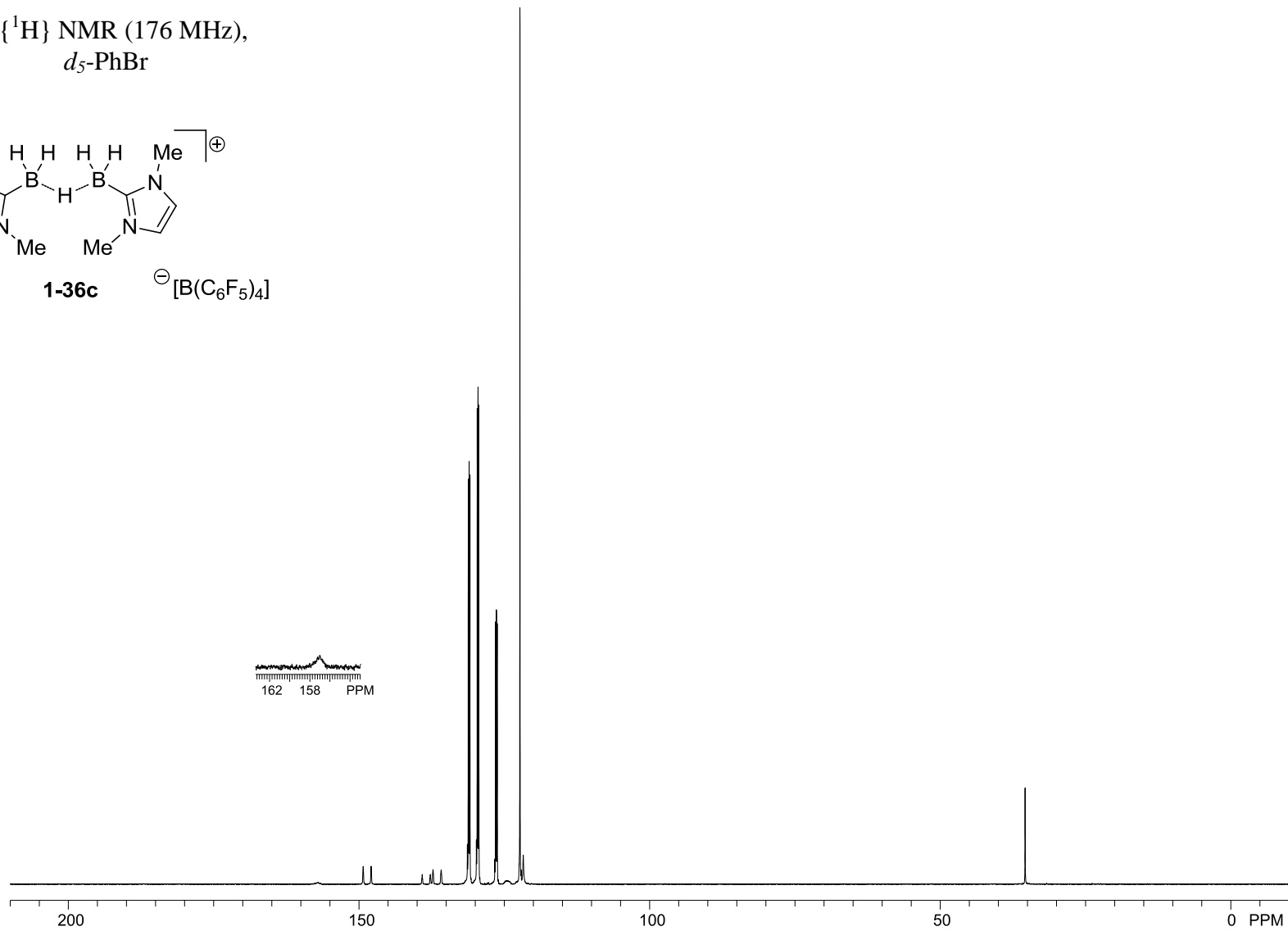
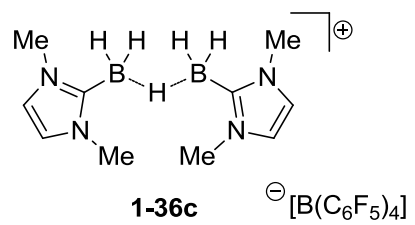
$^{11}\text{B}$  NMR (225 MHz),  
 $d_5\text{-PhBr}$



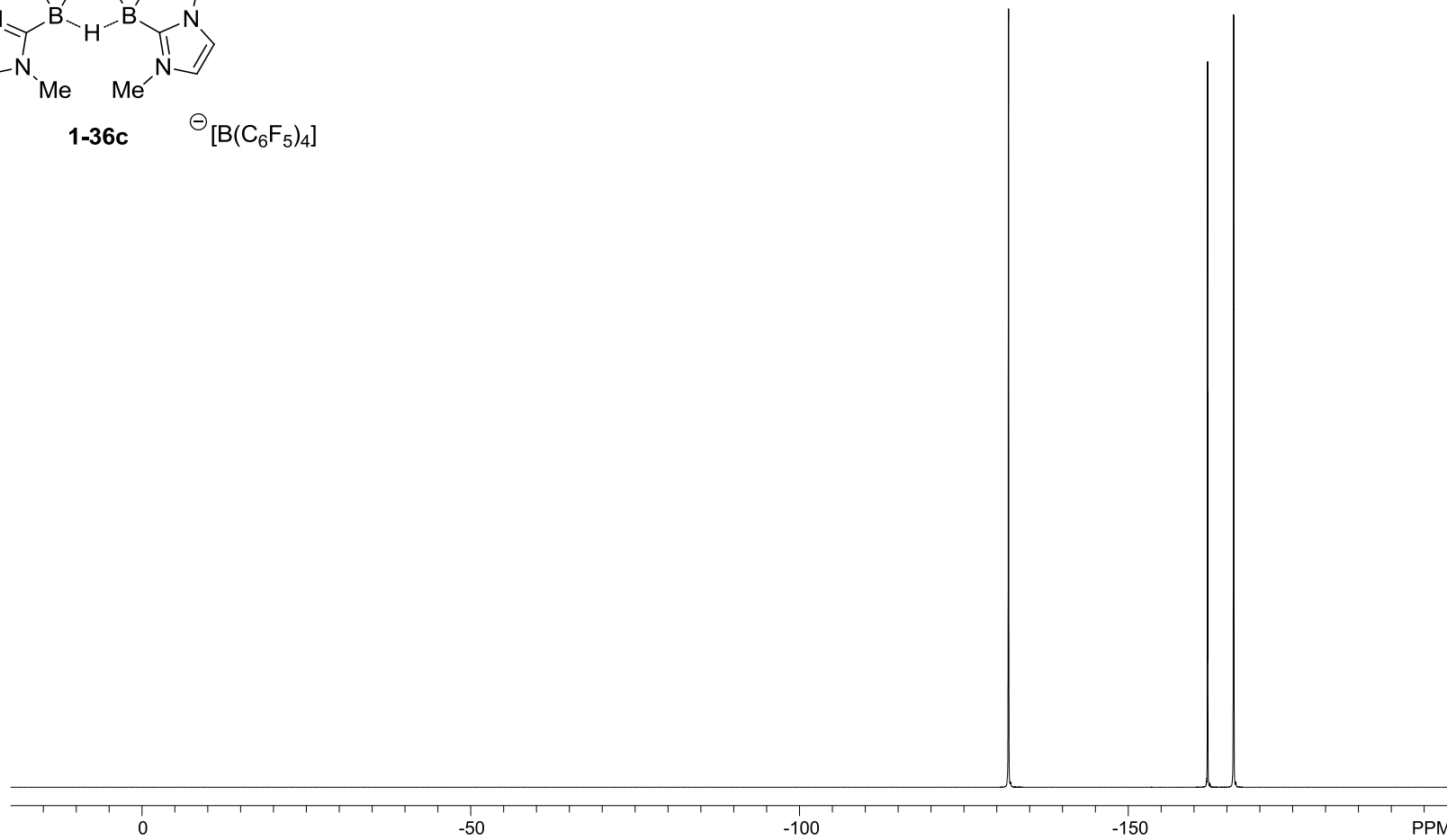
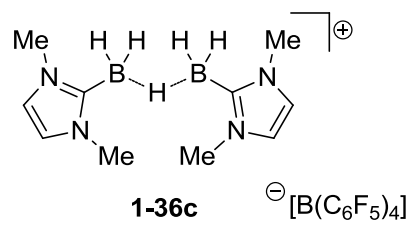
$^{11}\text{B}\{^1\text{H}\}$  NMR (225 MHz),  
 $d_5\text{-PhBr}$



$^{13}\text{C}\{^1\text{H}\}$  NMR (176 MHz),  
 $d_5\text{-PhBr}$

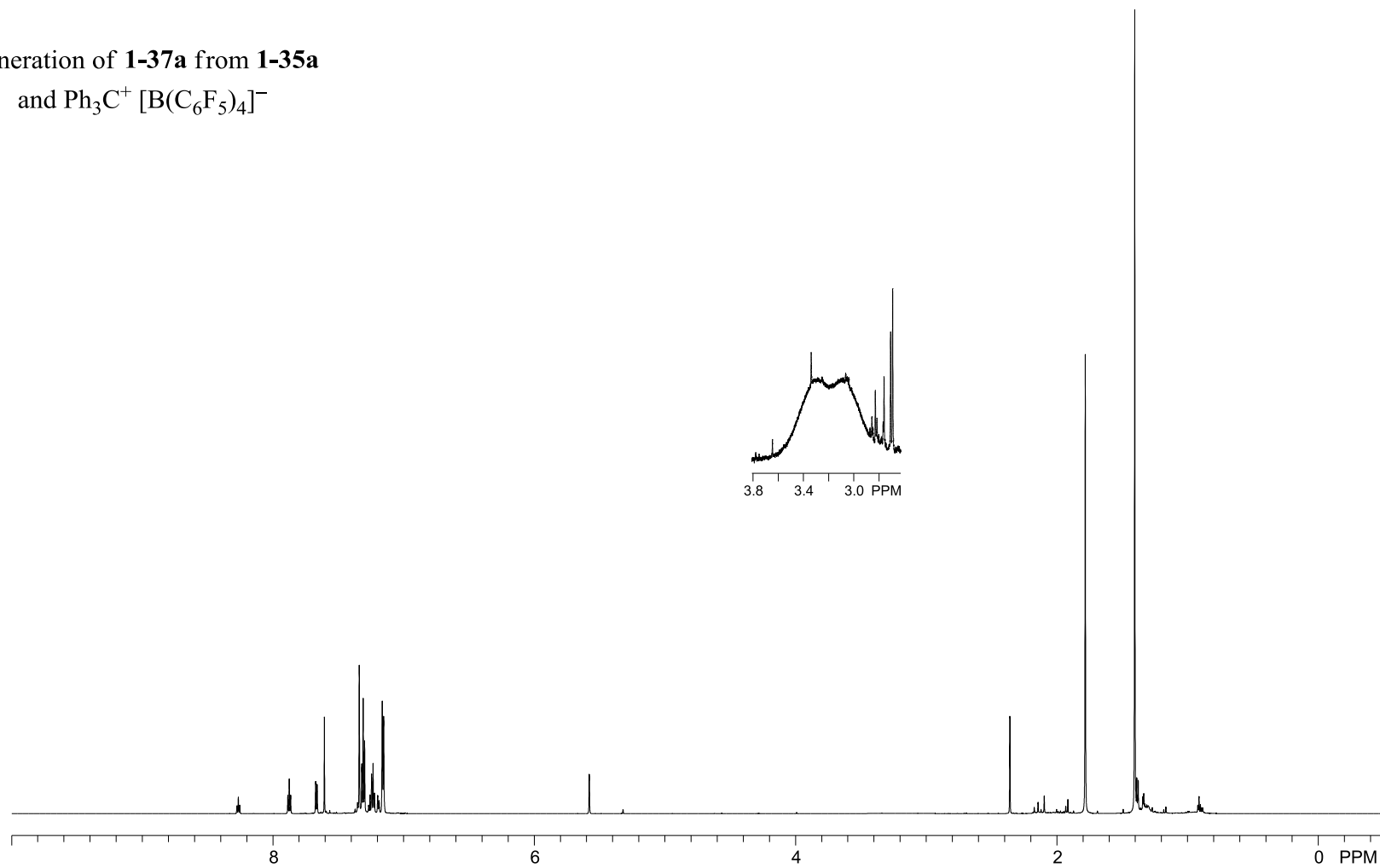


$^{19}\text{F}$  NMR (471 MHz),  
 $d_5\text{-PhBr}$



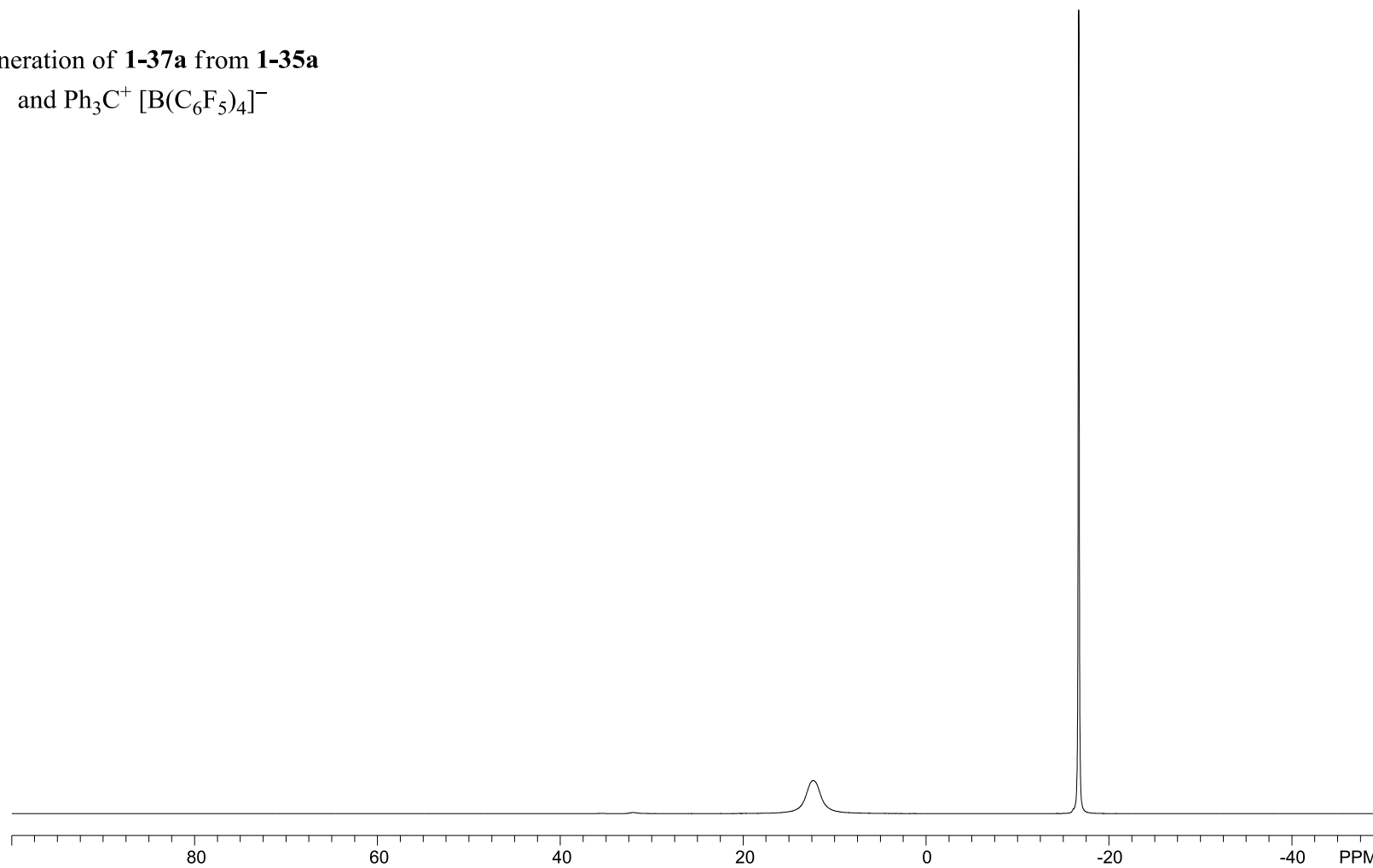
$^1\text{H}$  NMR (700 MHz),  
 $\text{CD}_2\text{Cl}_2$

Generation of **1-37a** from **1-35a**  
and  $\text{Ph}_3\text{C}^+ [\text{B}(\text{C}_6\text{F}_5)_4]^-$



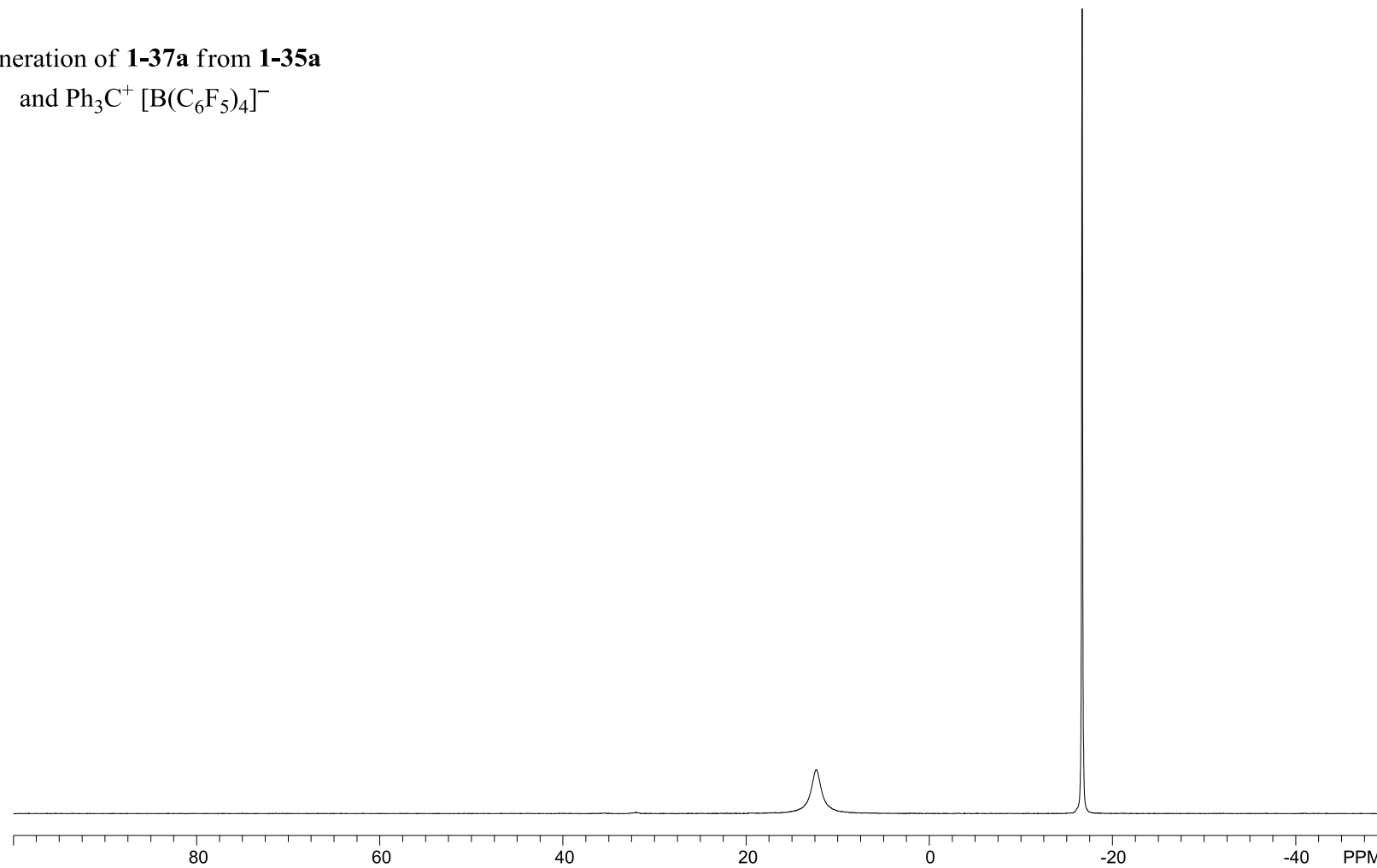
$^{11}\text{B}$  NMR (225 MHz),  
 $\text{CD}_2\text{Cl}_2$

Generation of **1-37a** from **1-35a**  
and  $\text{Ph}_3\text{C}^+ [\text{B}(\text{C}_6\text{F}_5)_4]^-$



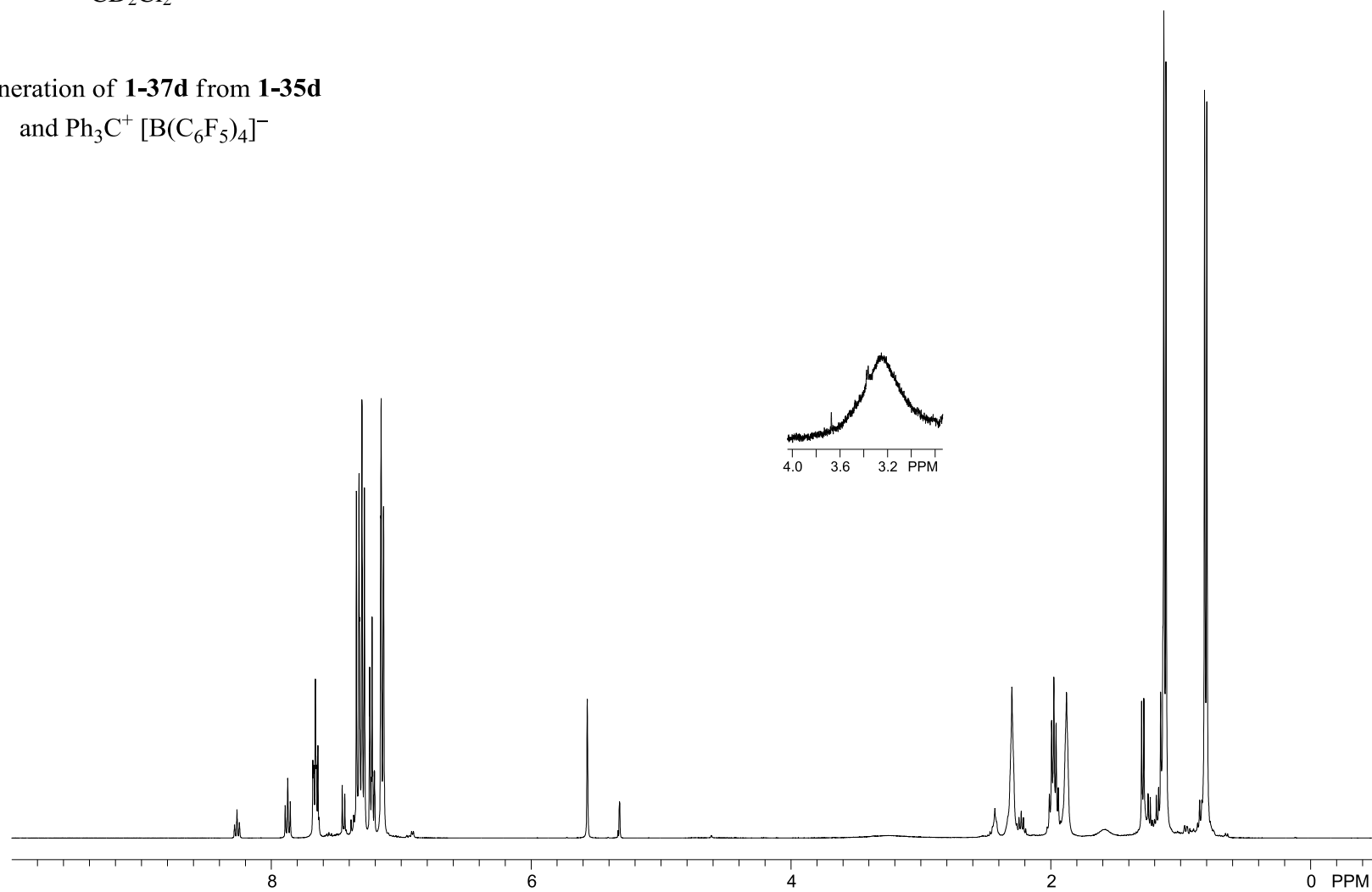
$^{11}\text{B}\{^1\text{H}\}$  NMR (225 MHz),  
 $\text{CD}_2\text{Cl}_2$

Generation of **1-37a** from **1-35a**  
and  $\text{Ph}_3\text{C}^+ [\text{B}(\text{C}_6\text{F}_5)_4]^-$



$^1\text{H}$  NMR (400 MHz),  
 $\text{CD}_2\text{Cl}_2$

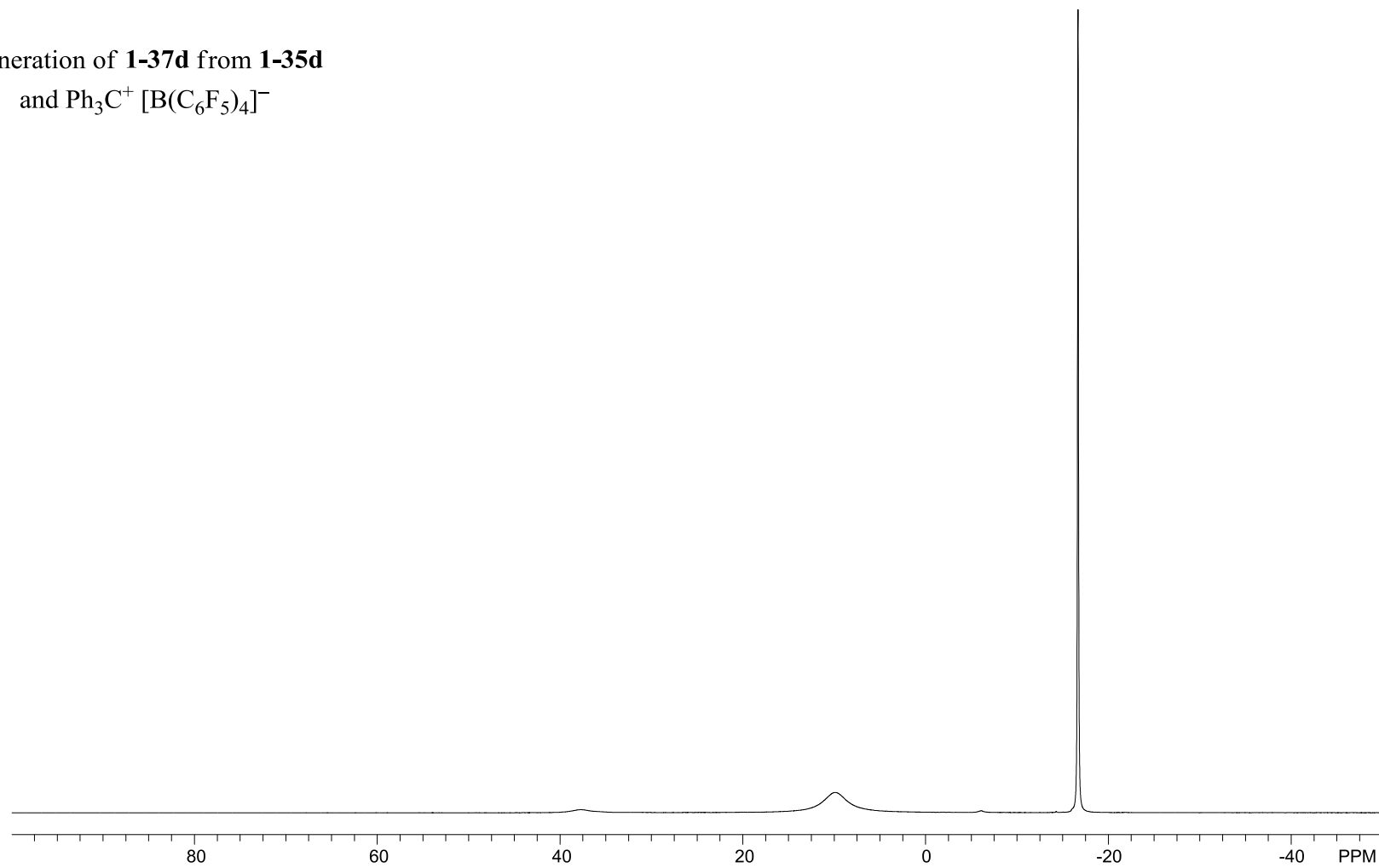
Generation of **1-37d** from **1-35d**  
and  $\text{Ph}_3\text{C}^+ [\text{B}(\text{C}_6\text{F}_5)_4]^-$





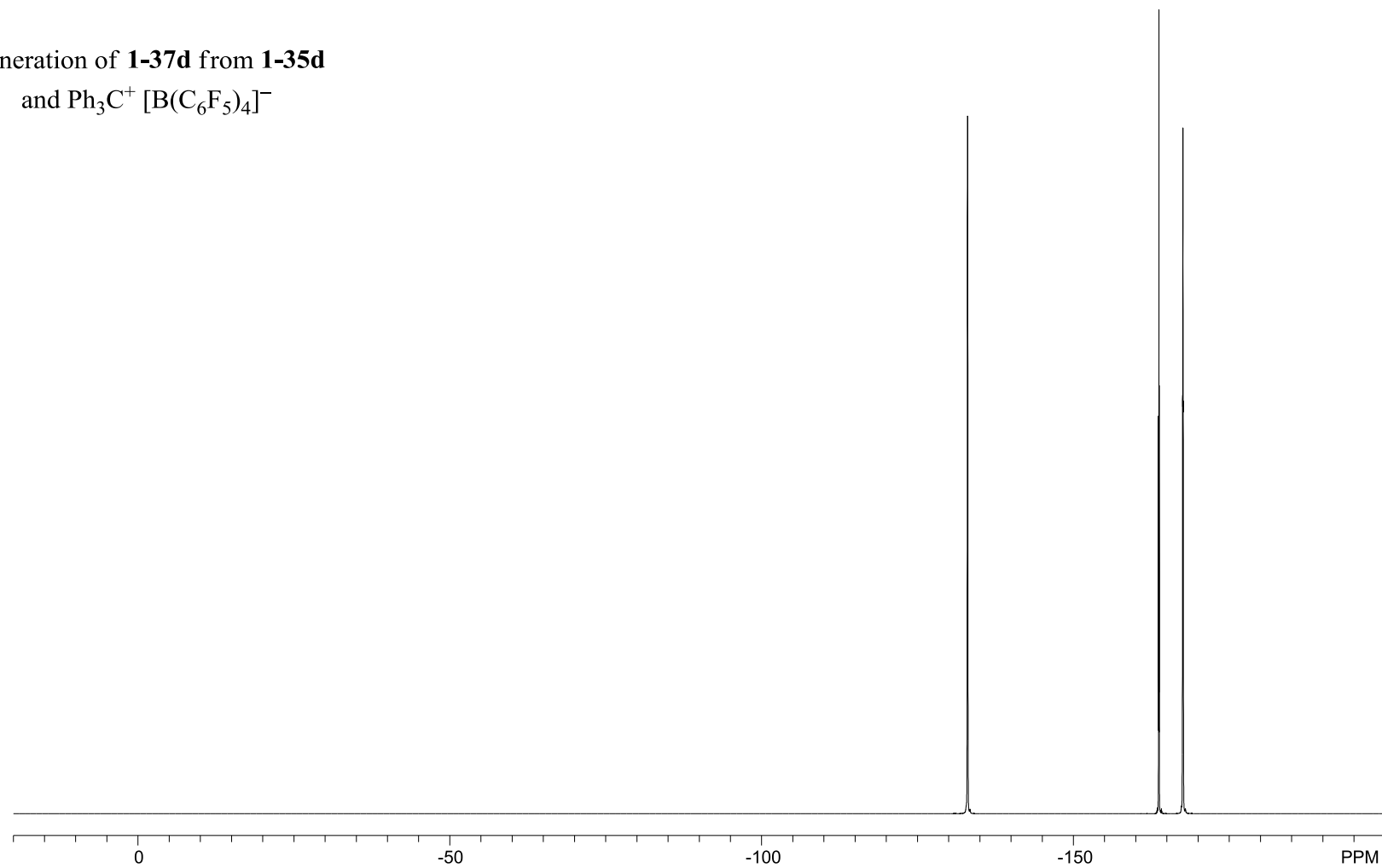
$^{11}\text{B}\{^1\text{H}\}$  NMR (225 MHz),  
 $\text{CD}_2\text{Cl}_2$

Generation of **1-37d** from **1-35d**  
and  $\text{Ph}_3\text{C}^+ [\text{B}(\text{C}_6\text{F}_5)_4]^-$



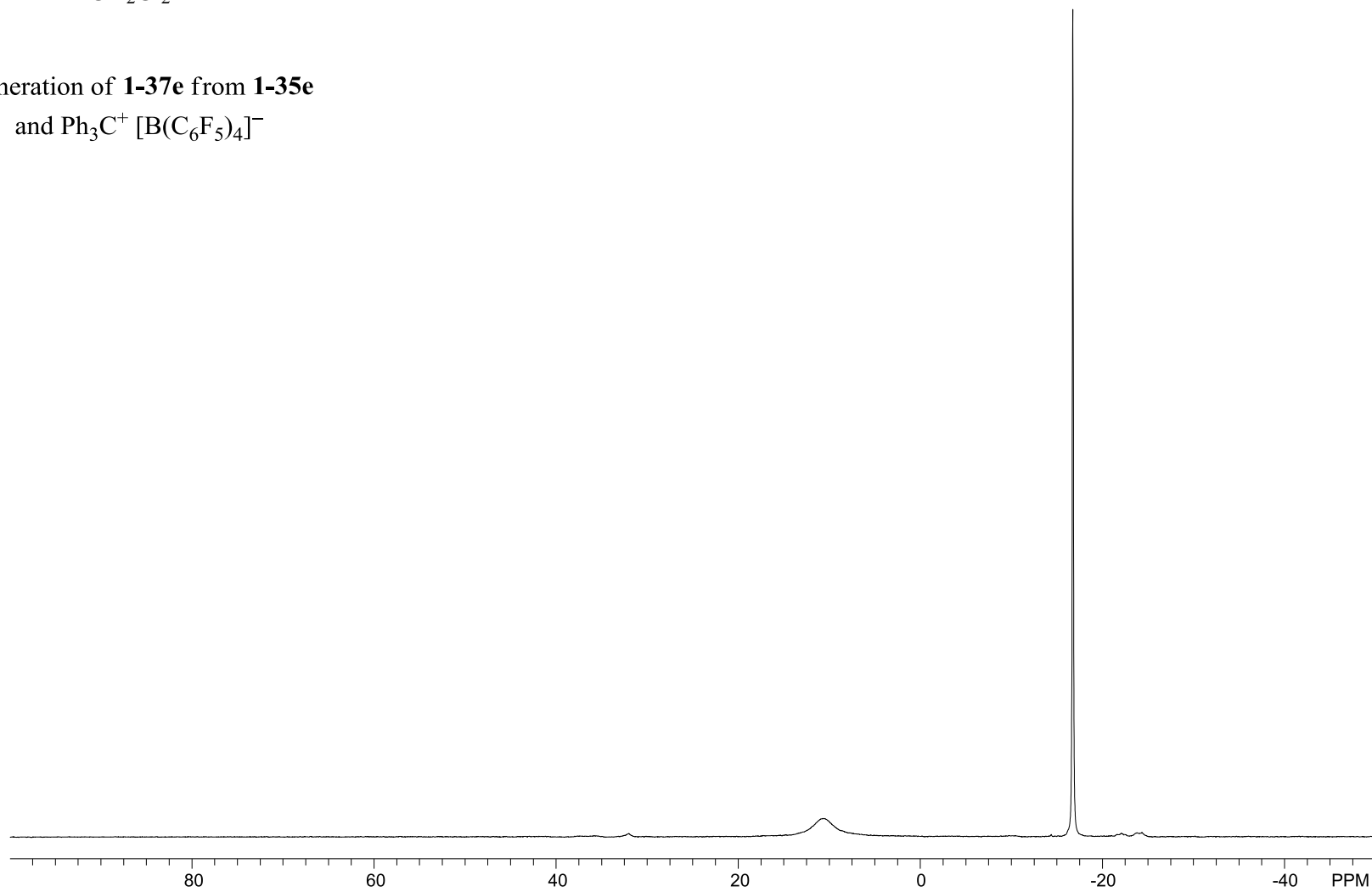
$^{19}\text{F}$  NMR (376 MHz),  
 $\text{CD}_2\text{Cl}_2$

Generation of **1-37d** from **1-35d**  
and  $\text{Ph}_3\text{C}^+ [\text{B}(\text{C}_6\text{F}_5)_4]^-$



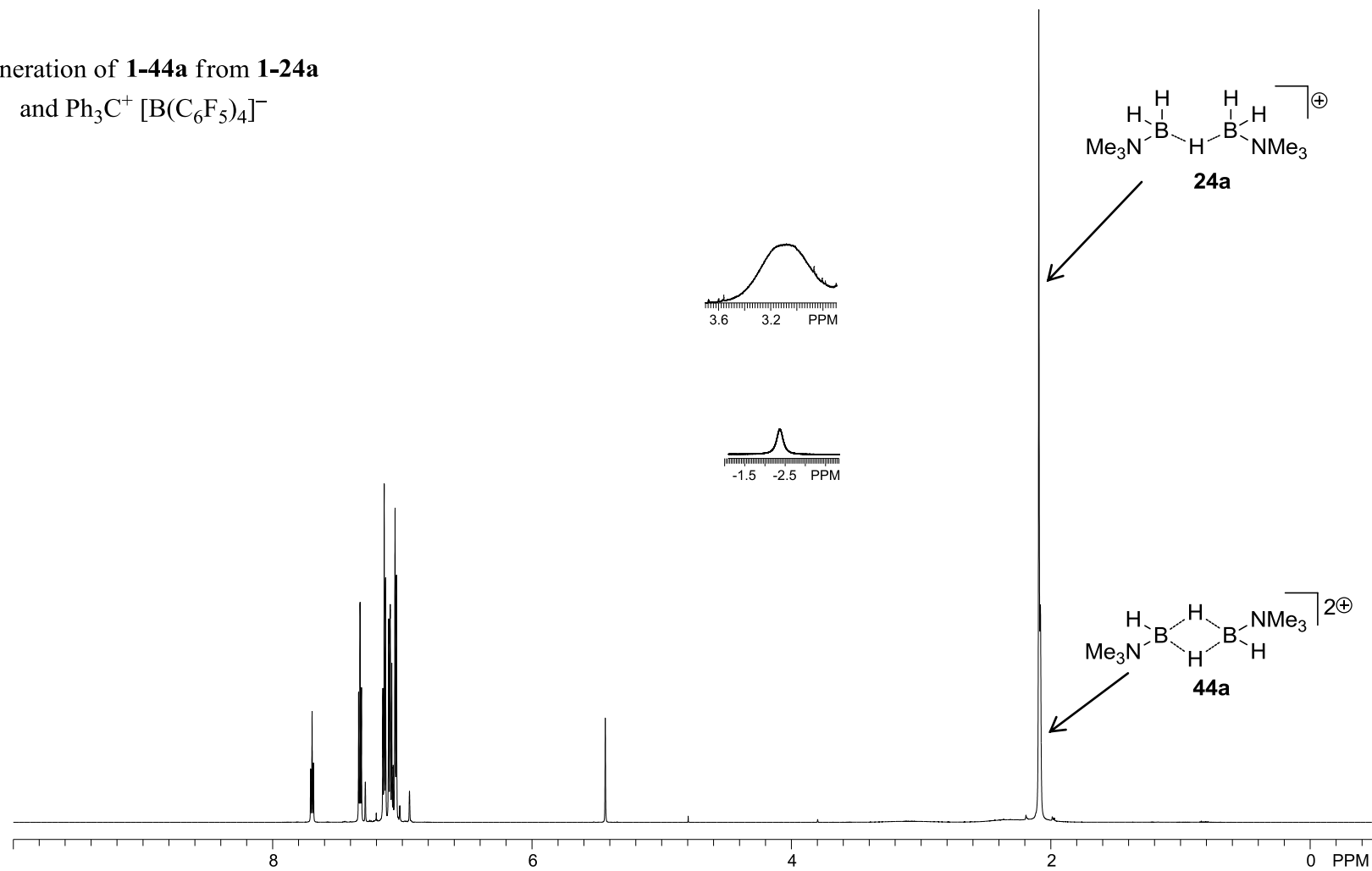
$^{11}\text{B}$  NMR (225 MHz),  
 $\text{CD}_2\text{Cl}_2$

Generation of **1-37e** from **1-35e**  
and  $\text{Ph}_3\text{C}^+ [\text{B}(\text{C}_6\text{F}_5)_4]^-$



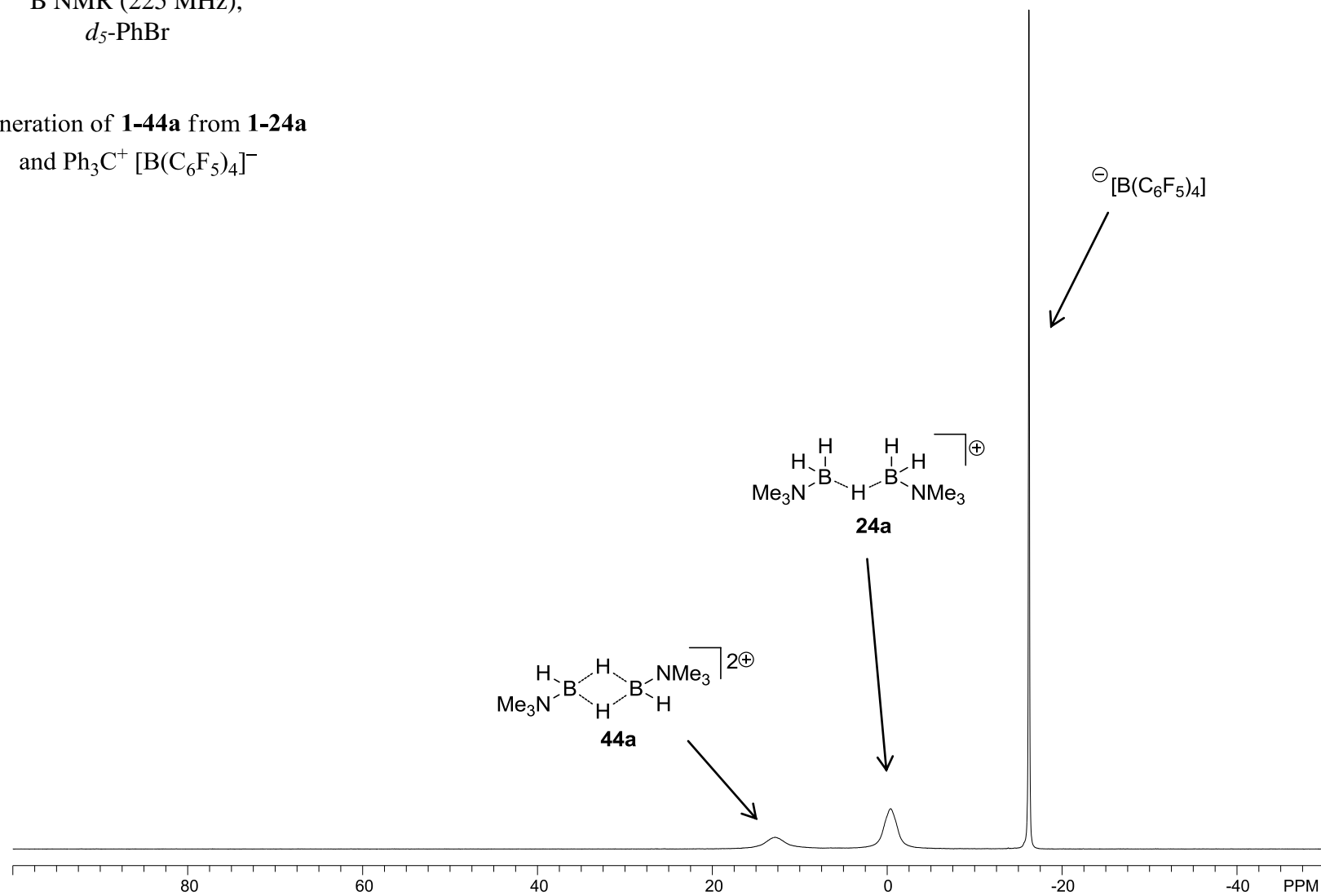
$^1\text{H}$  NMR (700 MHz),  
 $d_5$ -PhBr

Generation of **1-44a** from **1-24a**  
and  $\text{Ph}_3\text{C}^+ [\text{B}(\text{C}_6\text{F}_5)_4]^-$



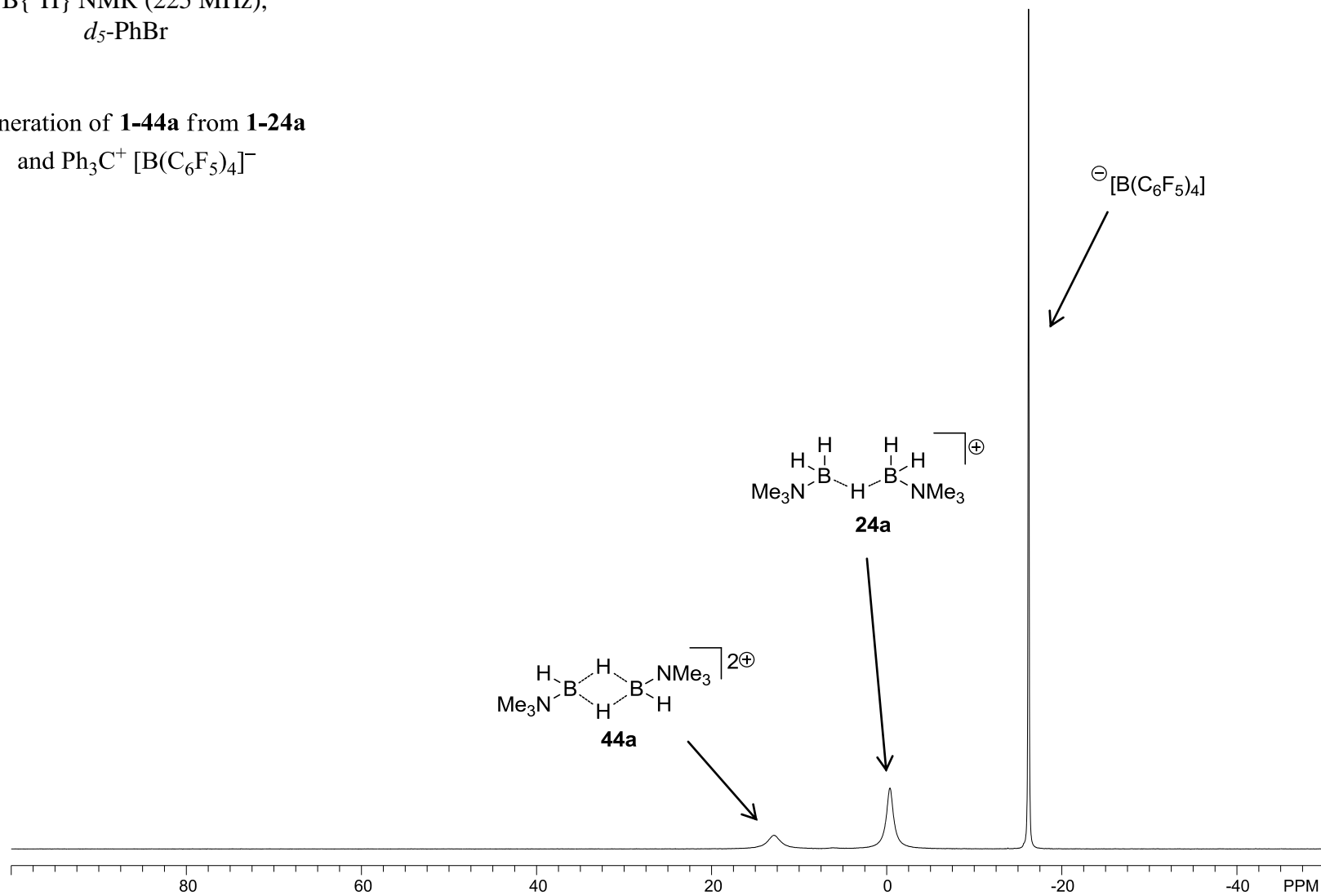
$^{11}\text{B}$  NMR (225 MHz),  
 $d_5\text{-PhBr}$

Generation of **1-44a** from **1-24a**  
and  $\text{Ph}_3\text{C}^+ [\text{B}(\text{C}_6\text{F}_5)_4]^-$



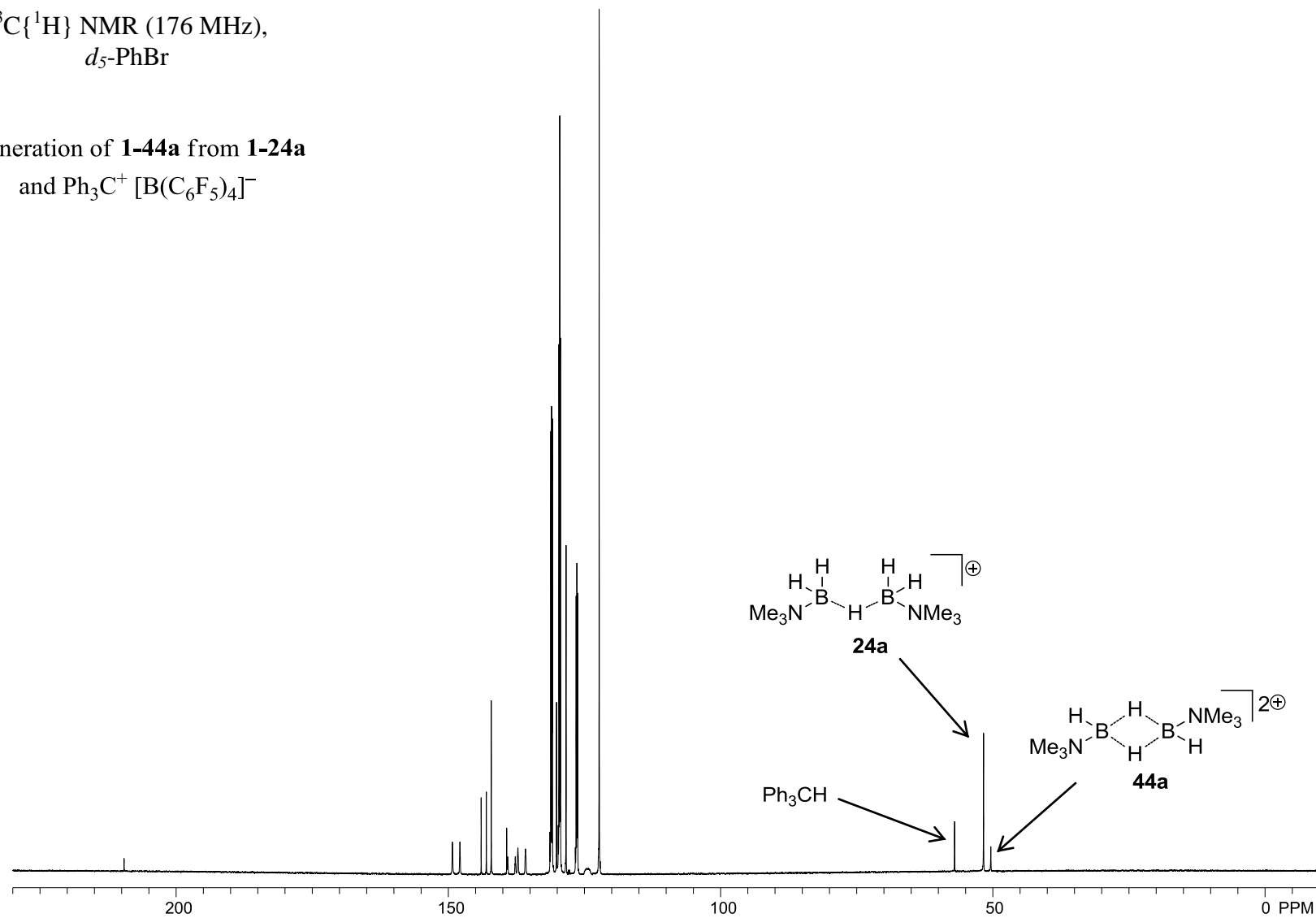
$^{11}\text{B}\{^1\text{H}\}$  NMR (225 MHz),  
 $d_5\text{-PhBr}$

Generation of **1-44a** from **1-24a**  
and  $\text{Ph}_3\text{C}^+ [\text{B}(\text{C}_6\text{F}_5)_4]^-$

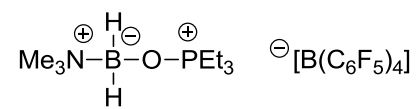


$^{13}\text{C}\{^1\text{H}\}$  NMR (176 MHz),  
 $d_5$ -PhBr

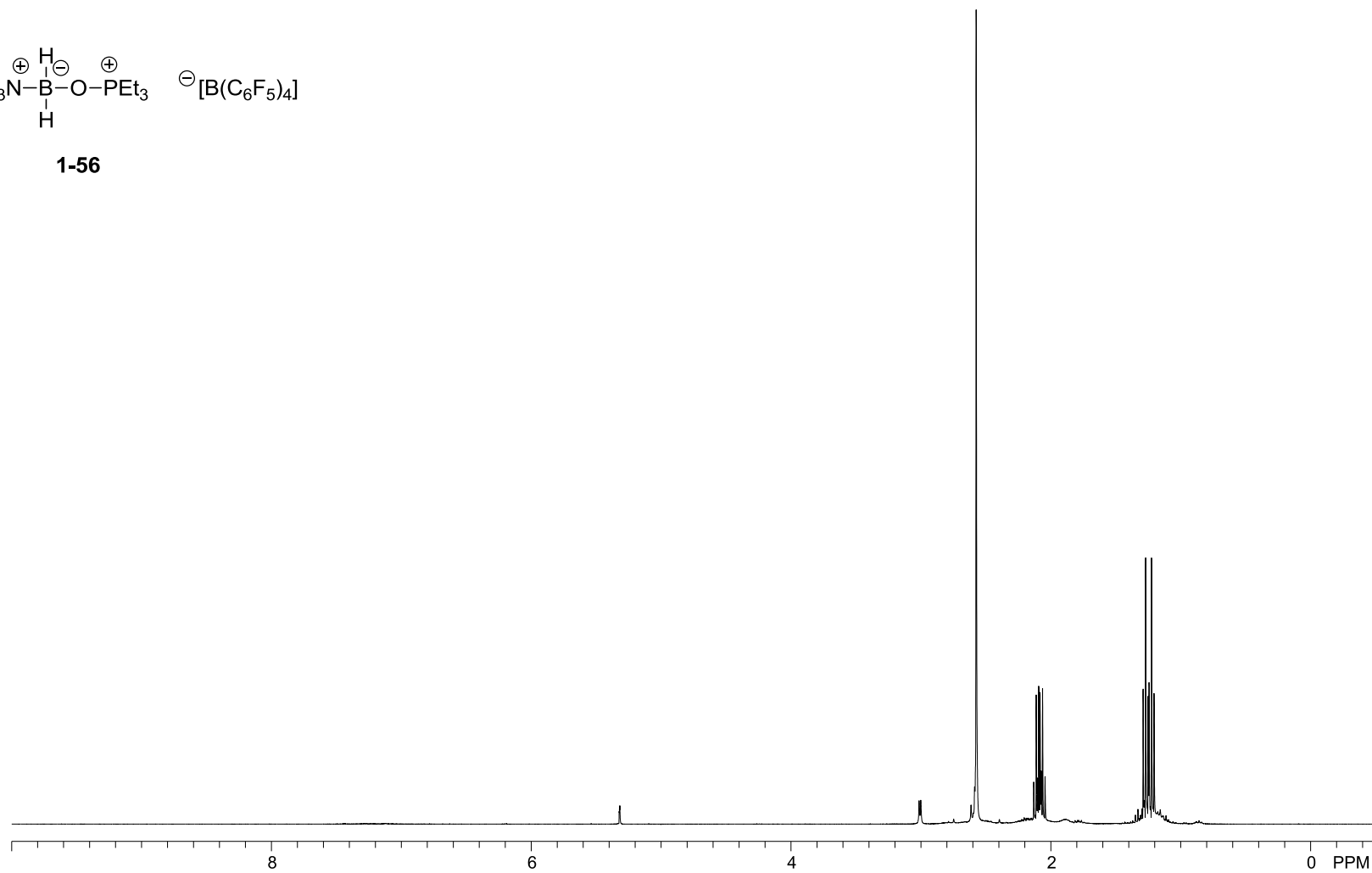
Generation of **1-44a** from **1-24a**  
and  $\text{Ph}_3\text{C}^+ [\text{B}(\text{C}_6\text{F}_5)_4]^-$



$^1\text{H}$  NMR (400 MHz),  
 $\text{CD}_2\text{Cl}_2$

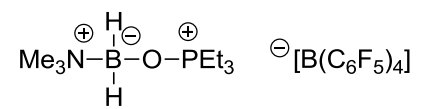


**1-56**

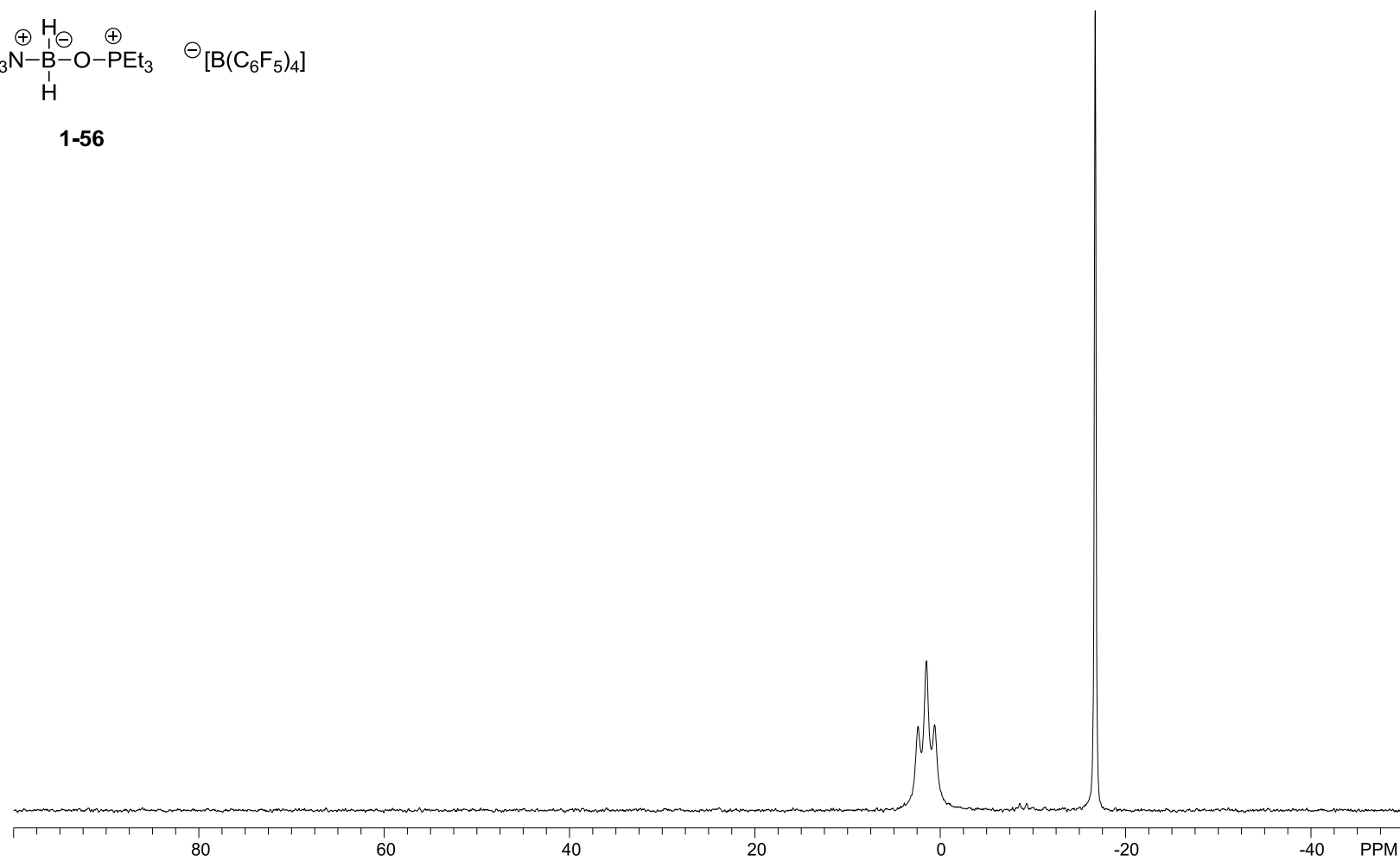




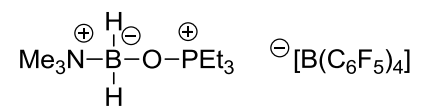
$^{11}\text{B}$  NMR (128 MHz),  
 $\text{CD}_2\text{Cl}_2$



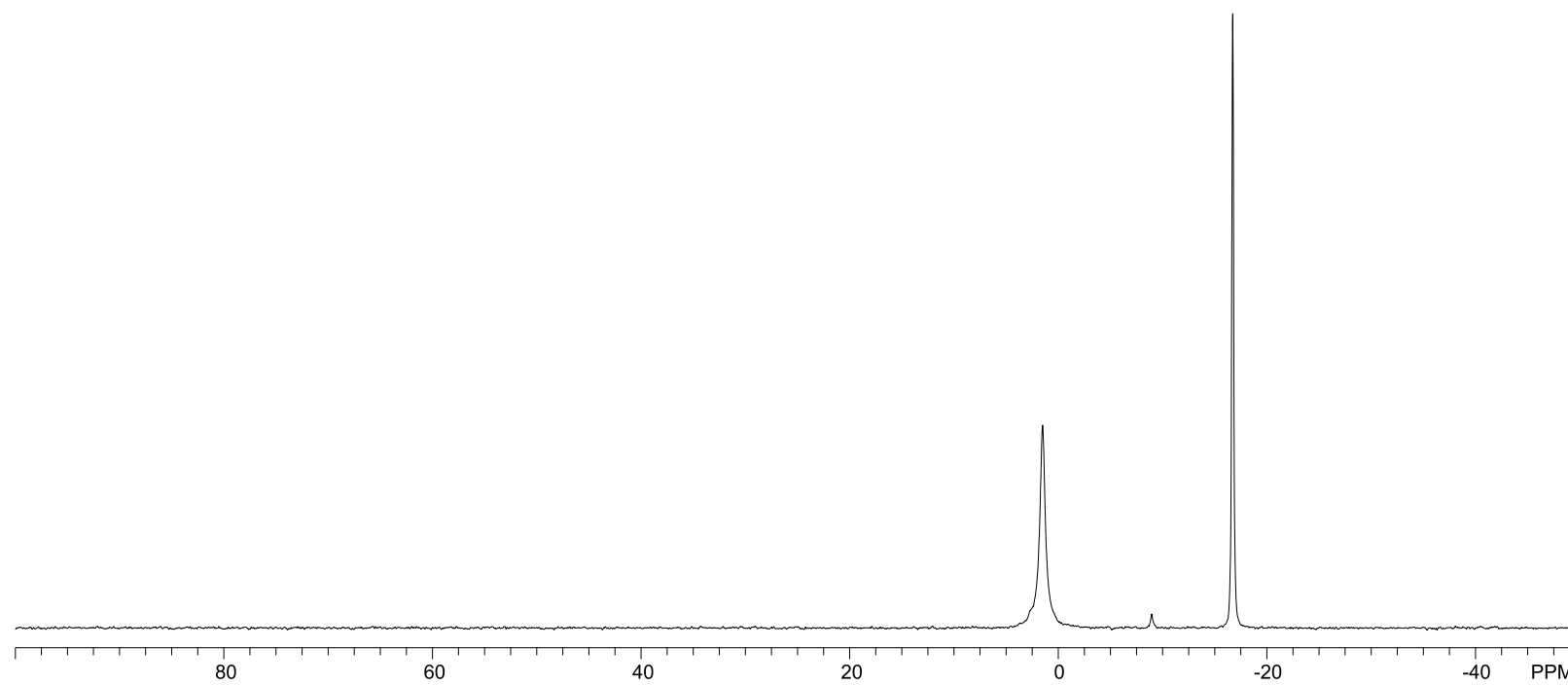
**1-56**



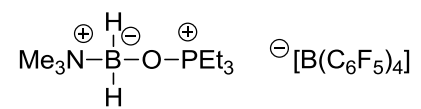
$^{11}\text{B}\{^1\text{H}\}$  NMR (128 MHz),  
 $\text{CD}_2\text{Cl}_2$



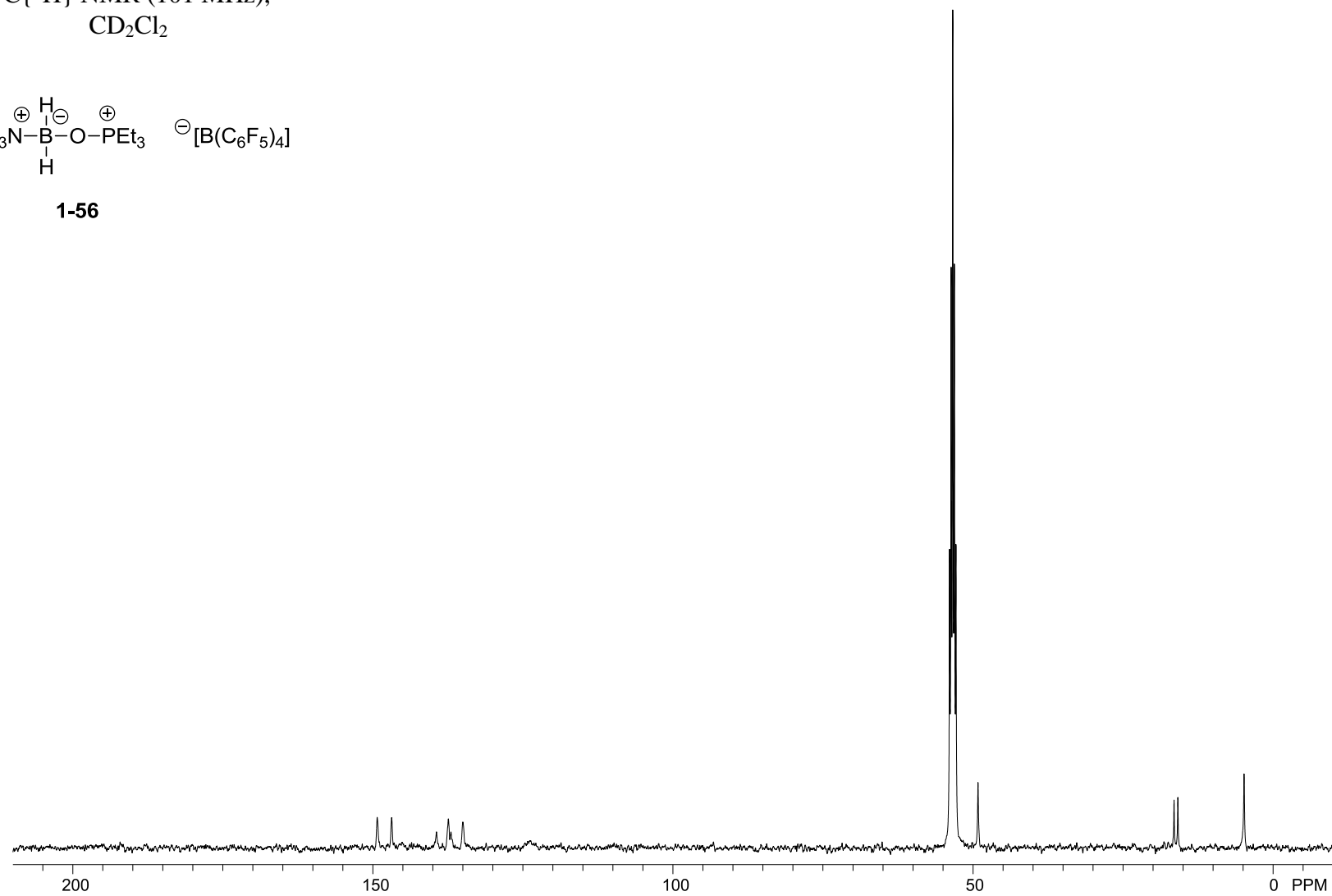
**1-56**



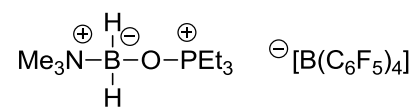
$^{13}\text{C}\{^1\text{H}\}$  NMR (101 MHz),  
 $\text{CD}_2\text{Cl}_2$



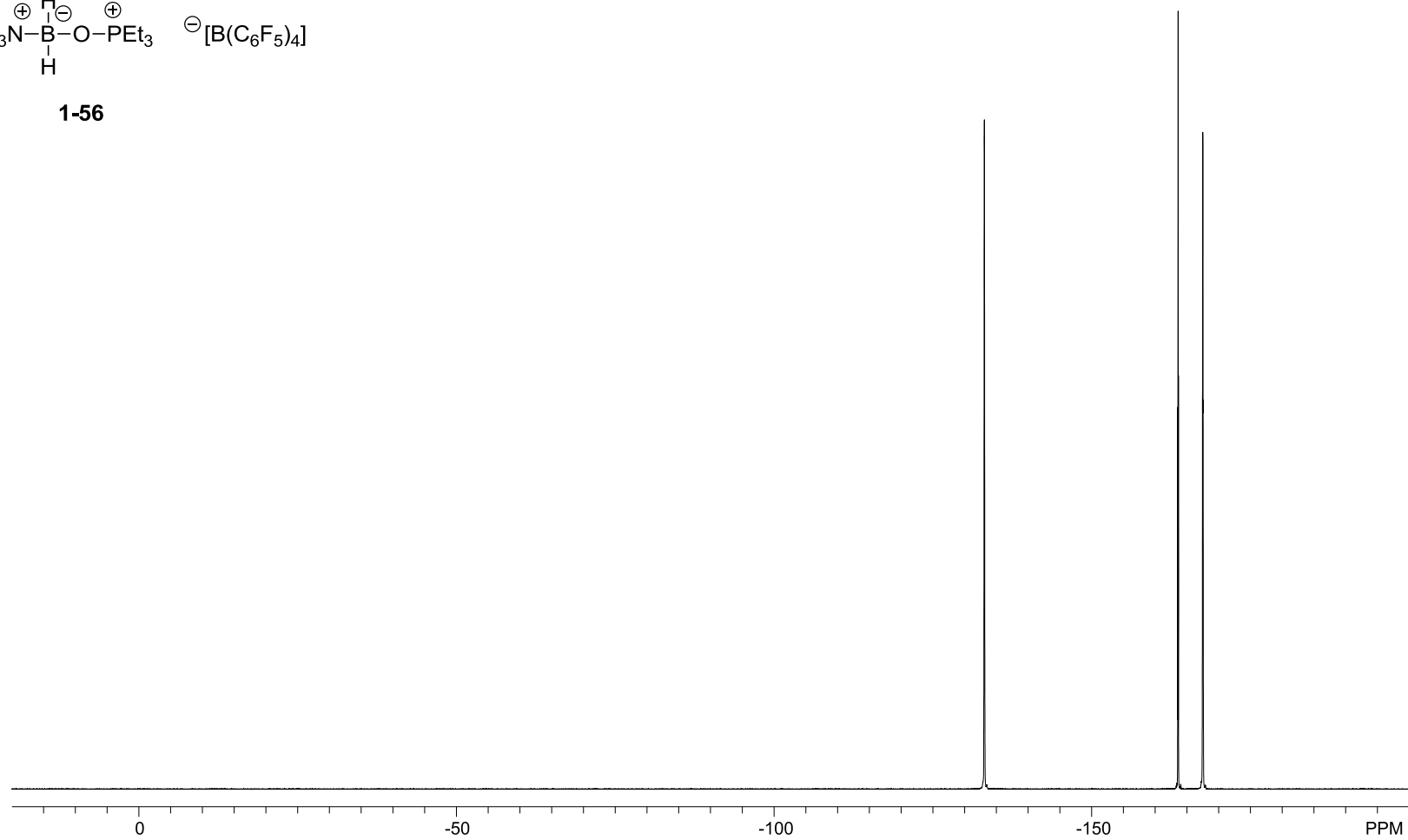
**1-56**



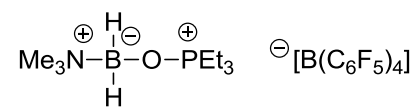
$^{19}\text{F}$  NMR (377 MHz),  
 $\text{CD}_2\text{Cl}_2$



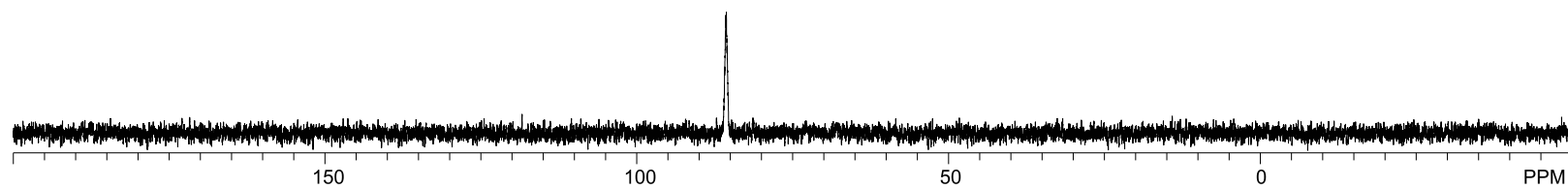
**1-56**



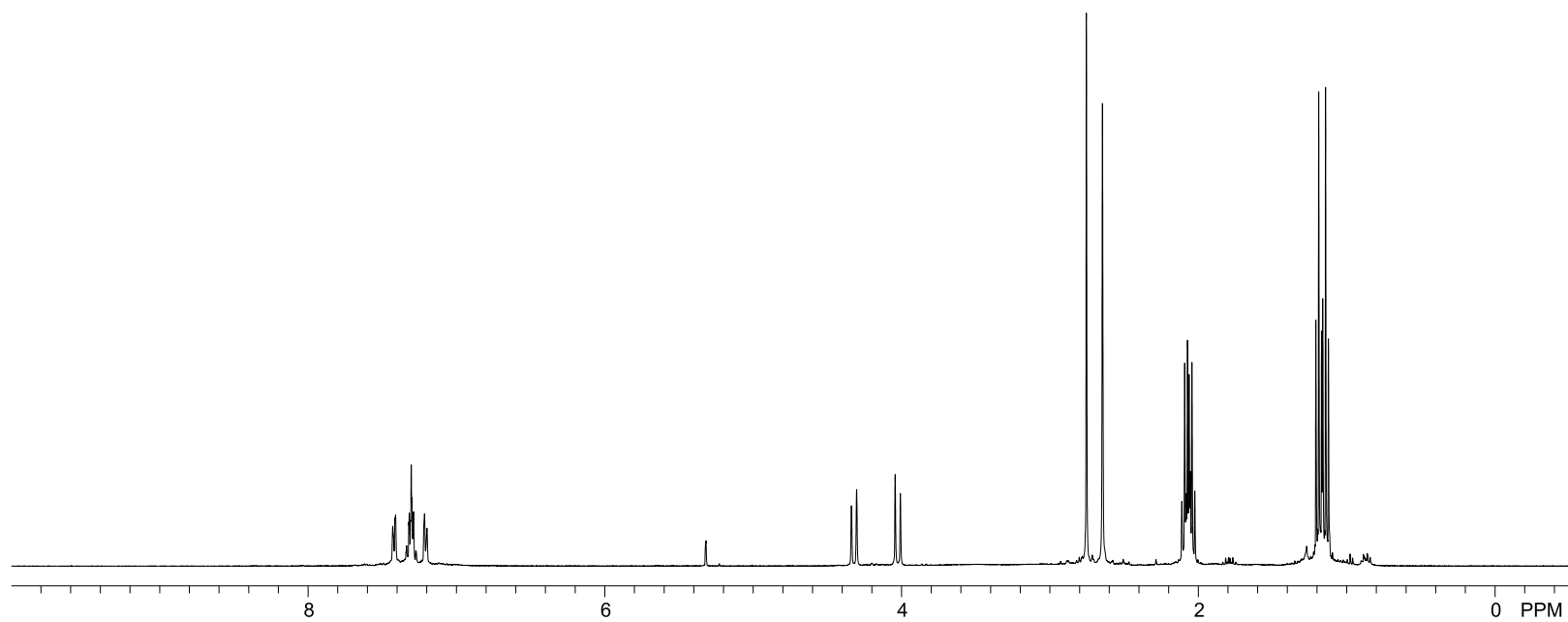
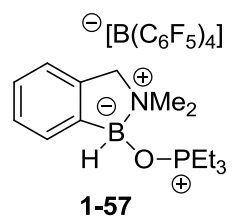
$^{31}\text{P}$  NMR (162 MHz),  
 $\text{CD}_2\text{Cl}_2$



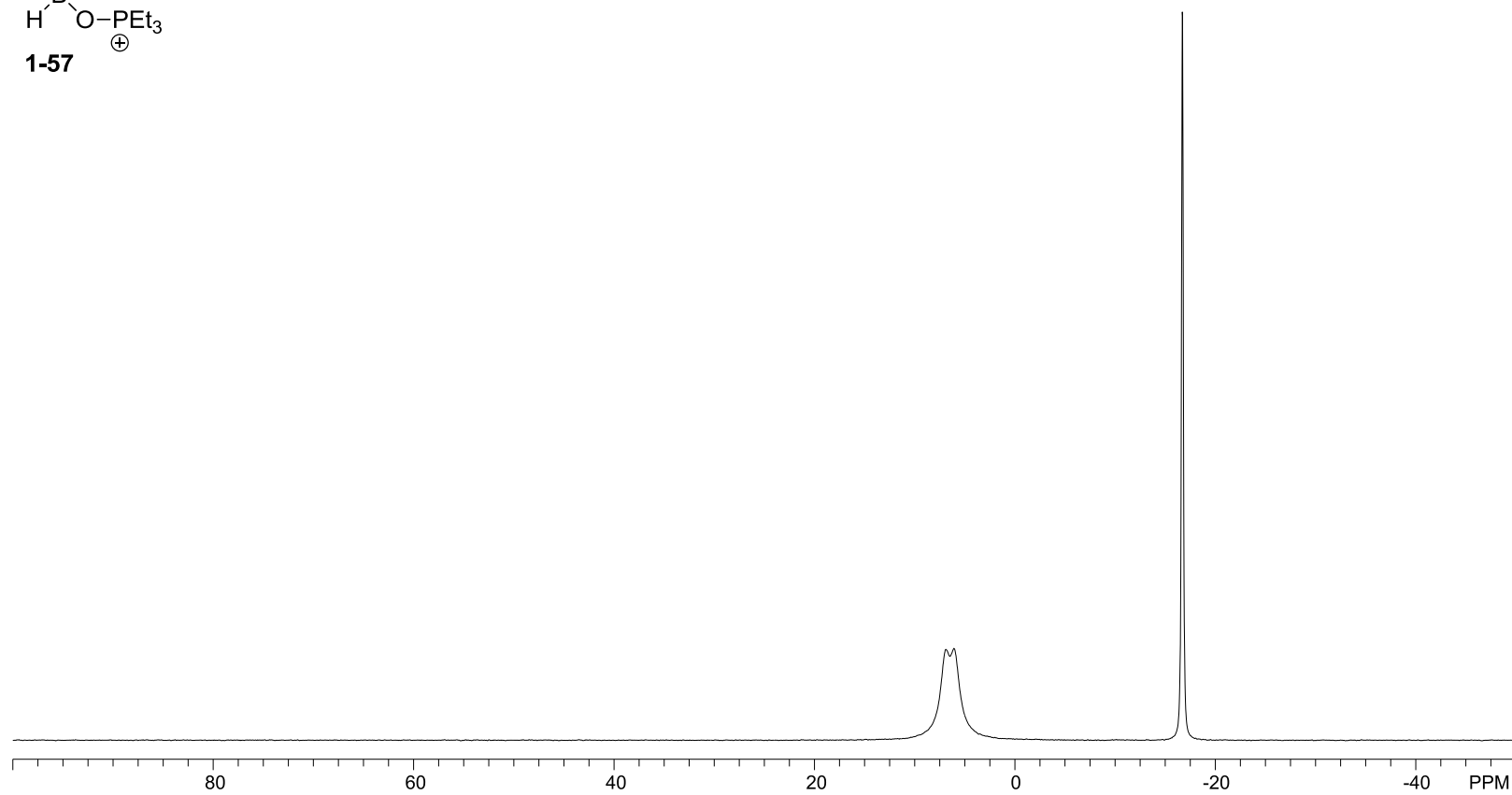
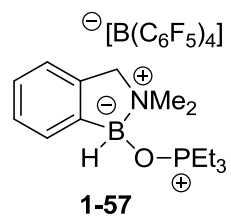
**1-56**



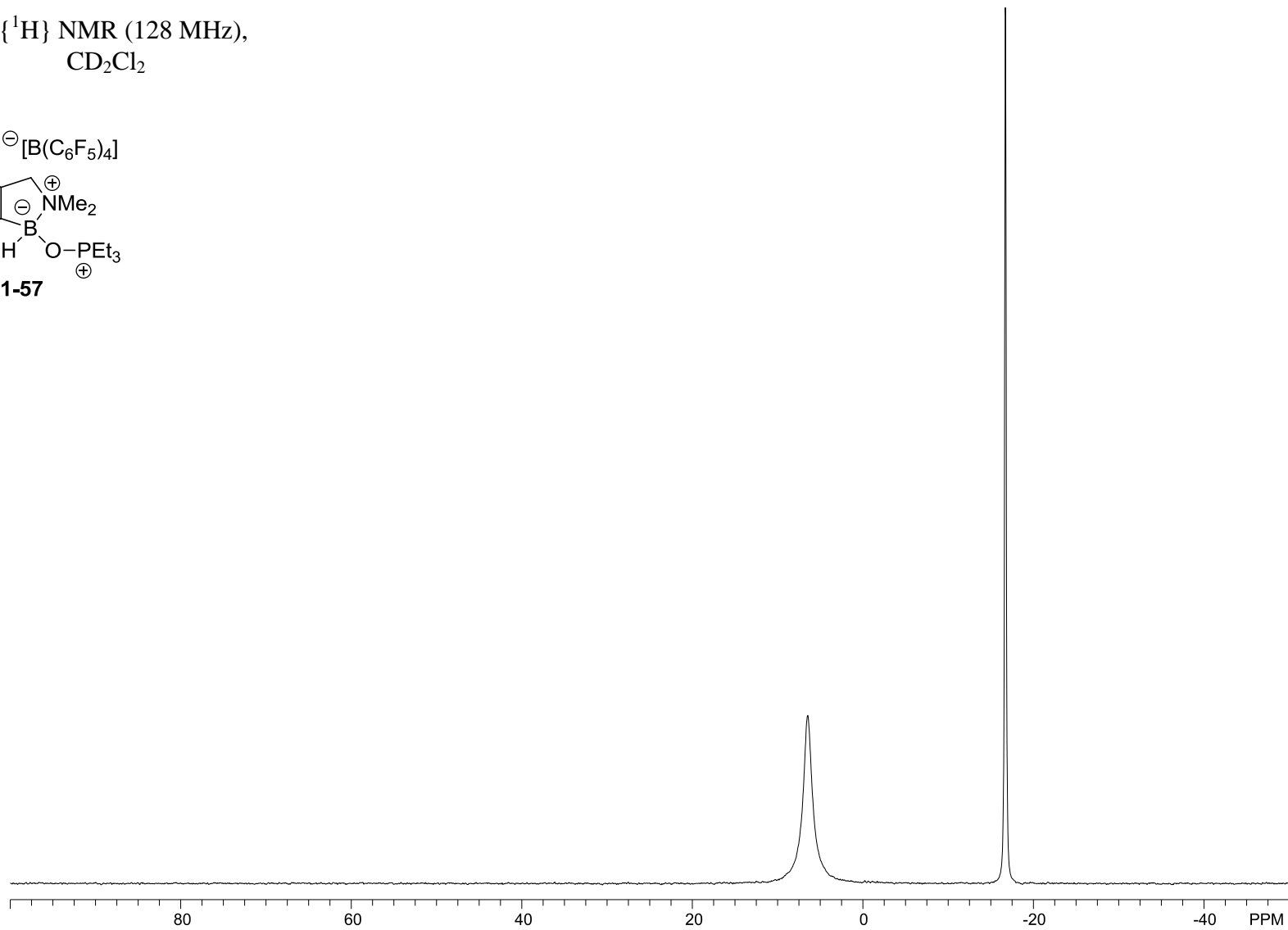
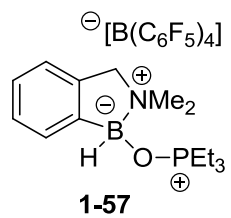
$^1\text{H}$  NMR (400 MHz),  
 $\text{CD}_2\text{Cl}_2$



$^{11}\text{B}$  NMR (128 MHz),  
 $\text{CD}_2\text{Cl}_2$

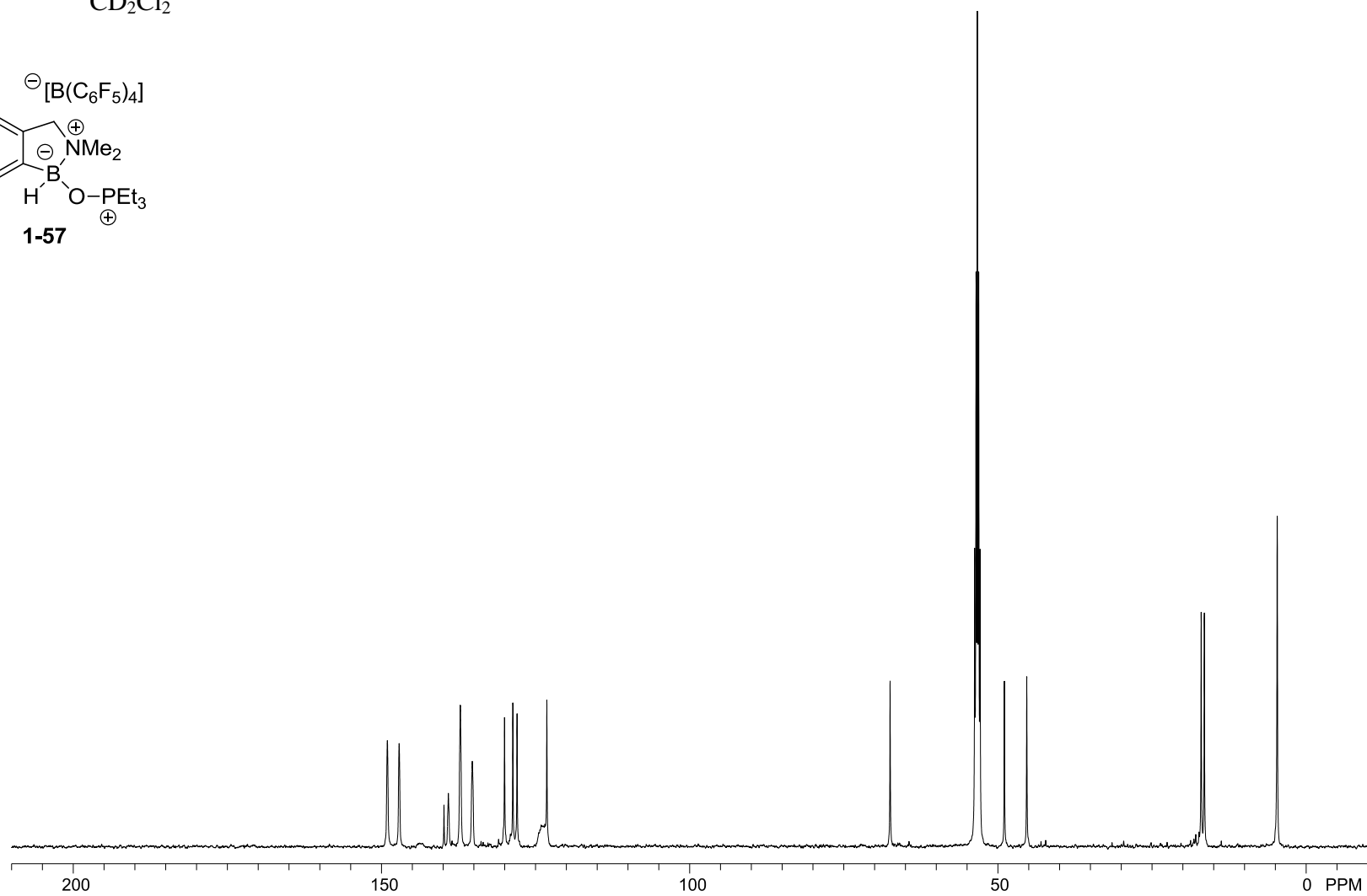
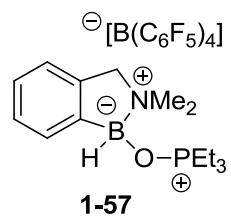


$^{11}\text{B}\{^1\text{H}\}$  NMR (128 MHz),  
 $\text{CD}_2\text{Cl}_2$

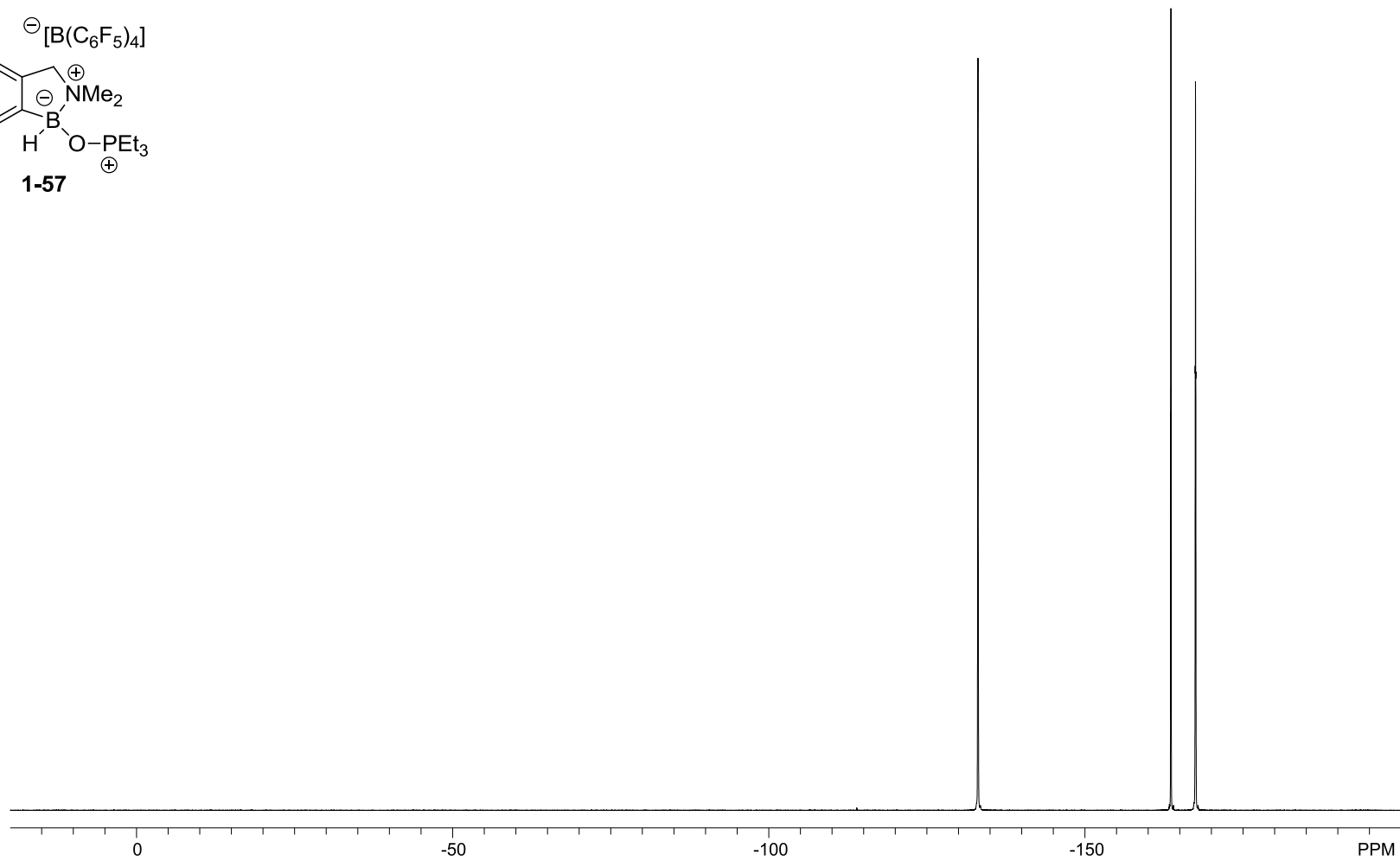
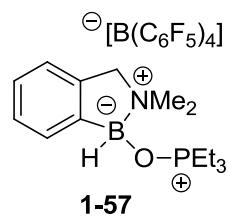




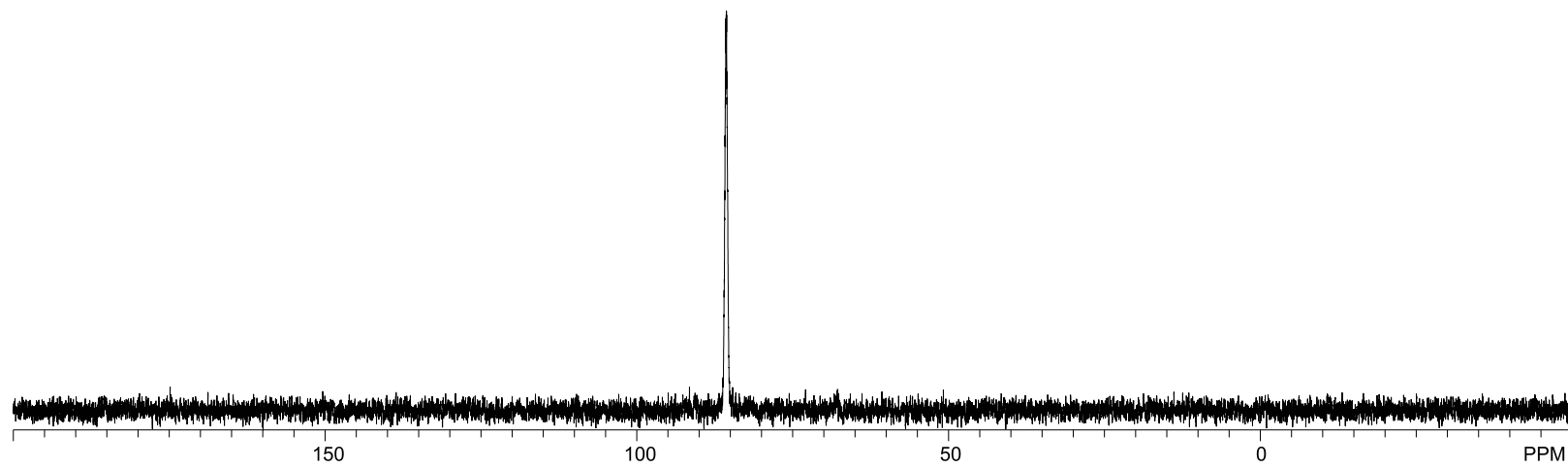
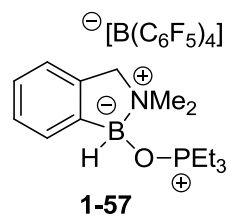
$^{13}\text{C}\{^1\text{H}\}$  NMR (126 MHz),  
 $\text{CD}_2\text{Cl}_2$



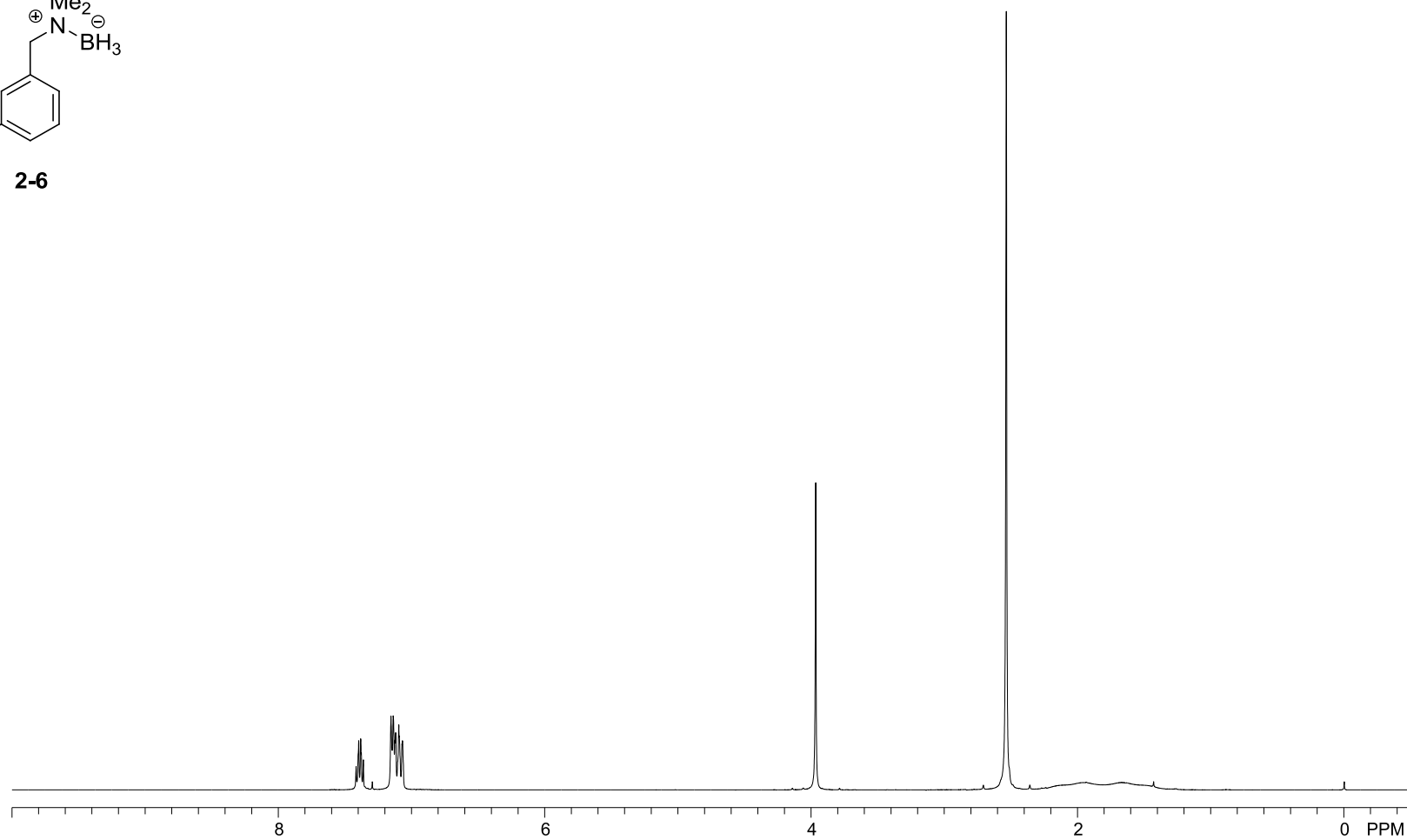
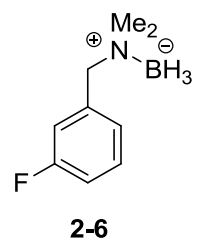
$^{19}\text{F}$  NMR (377 MHz),  
 $\text{CD}_2\text{Cl}_2$



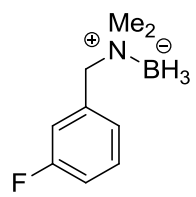
$^{31}\text{P}$  NMR (162 MHz),  
 $\text{CD}_2\text{Cl}_2$



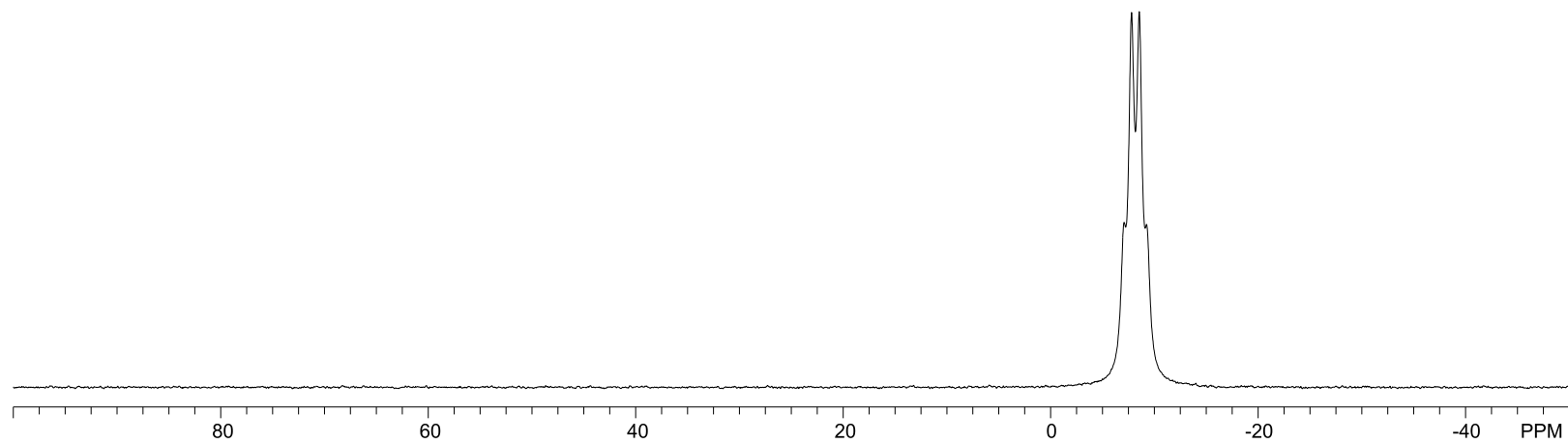
$^1\text{H}$  NMR (400 MHz),  
 $\text{CDCl}_3$



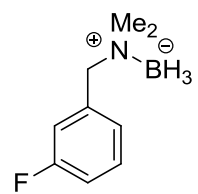
$^{11}\text{B}$  NMR (128 MHz),  
 $\text{CDCl}_3$



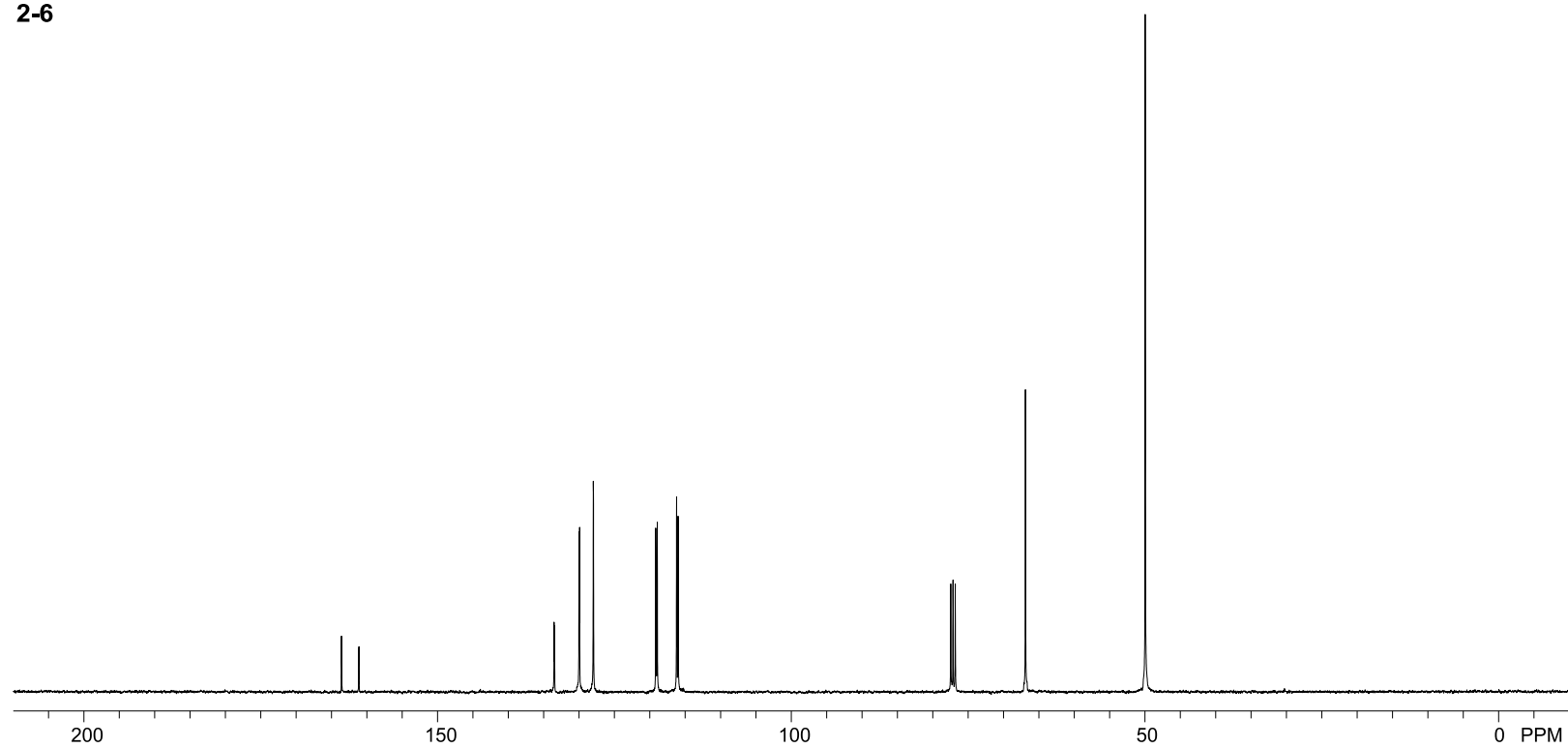
**2-6**



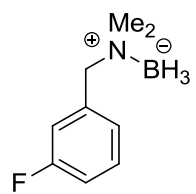
$^{13}\text{C}\{^1\text{H}\}$  NMR (101 MHz),  
 $\text{CDCl}_3$



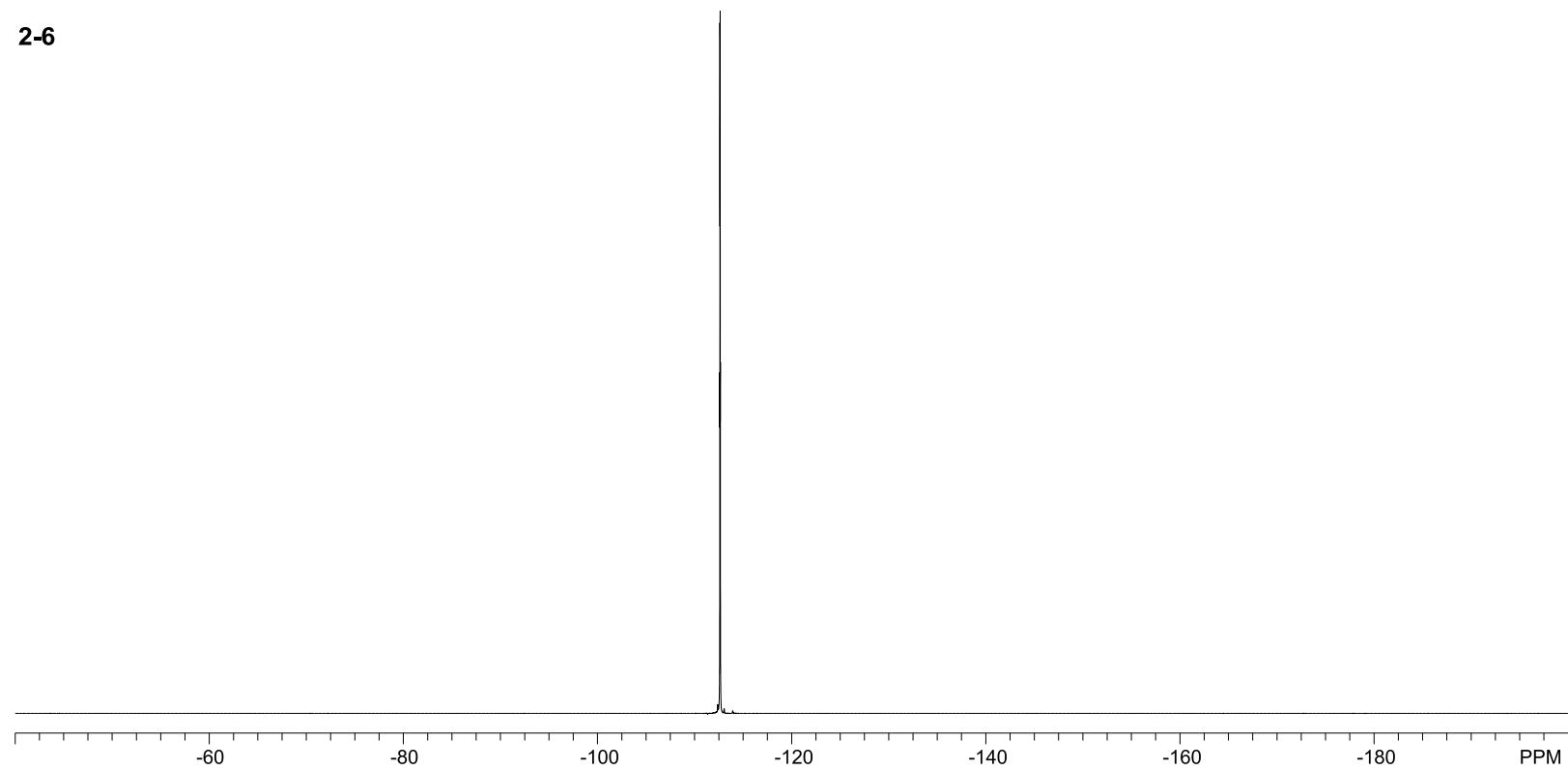
**2-6**



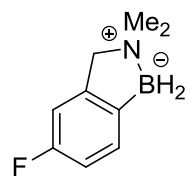
$^{19}\text{F}$  NMR (377 MHz),  
 $\text{CDCl}_3$



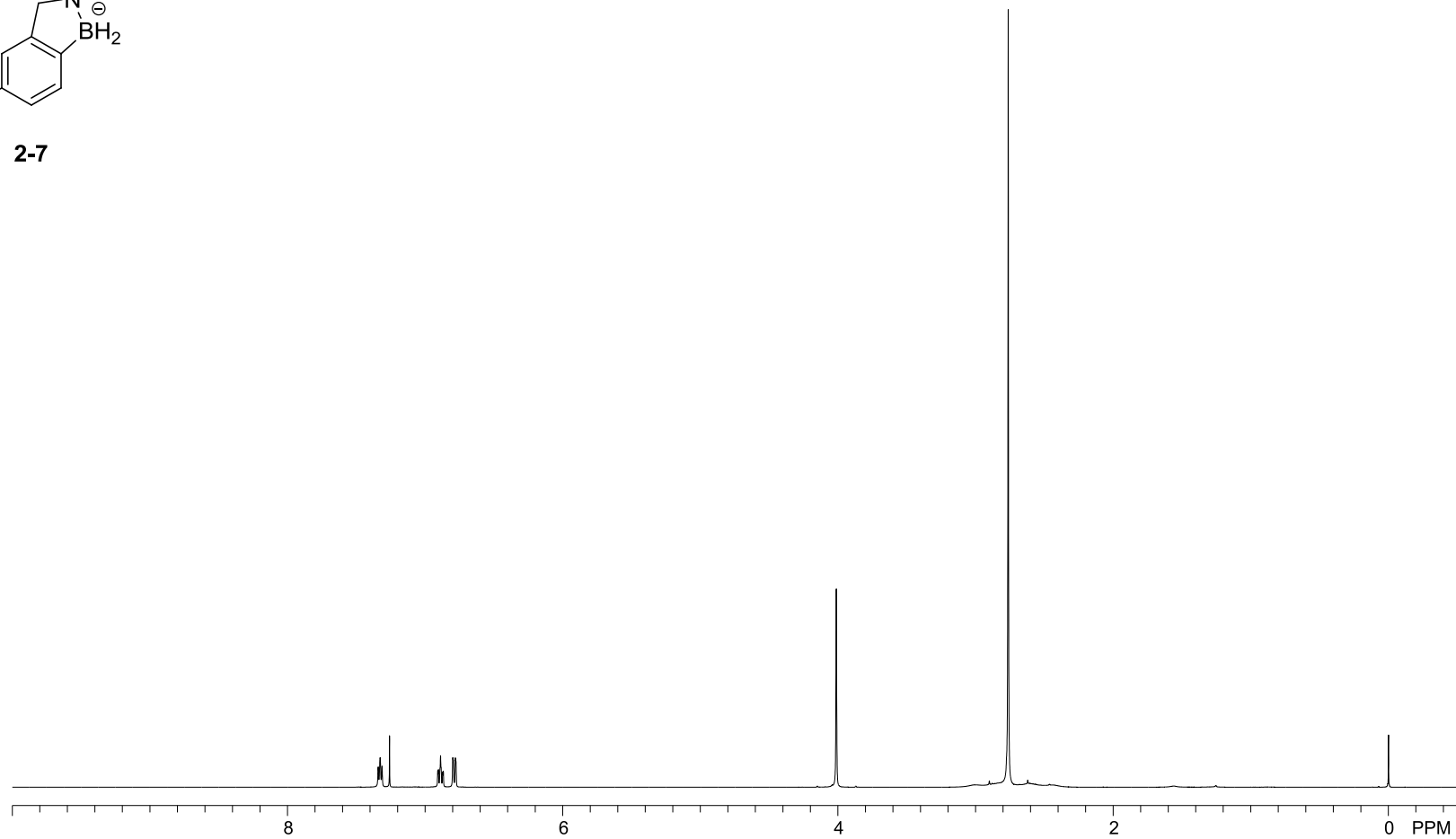
**2-6**



$^1\text{H}$  NMR (500 MHz),  
 $\text{CDCl}_3$

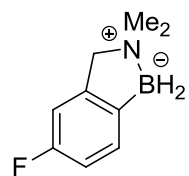


**2-7**

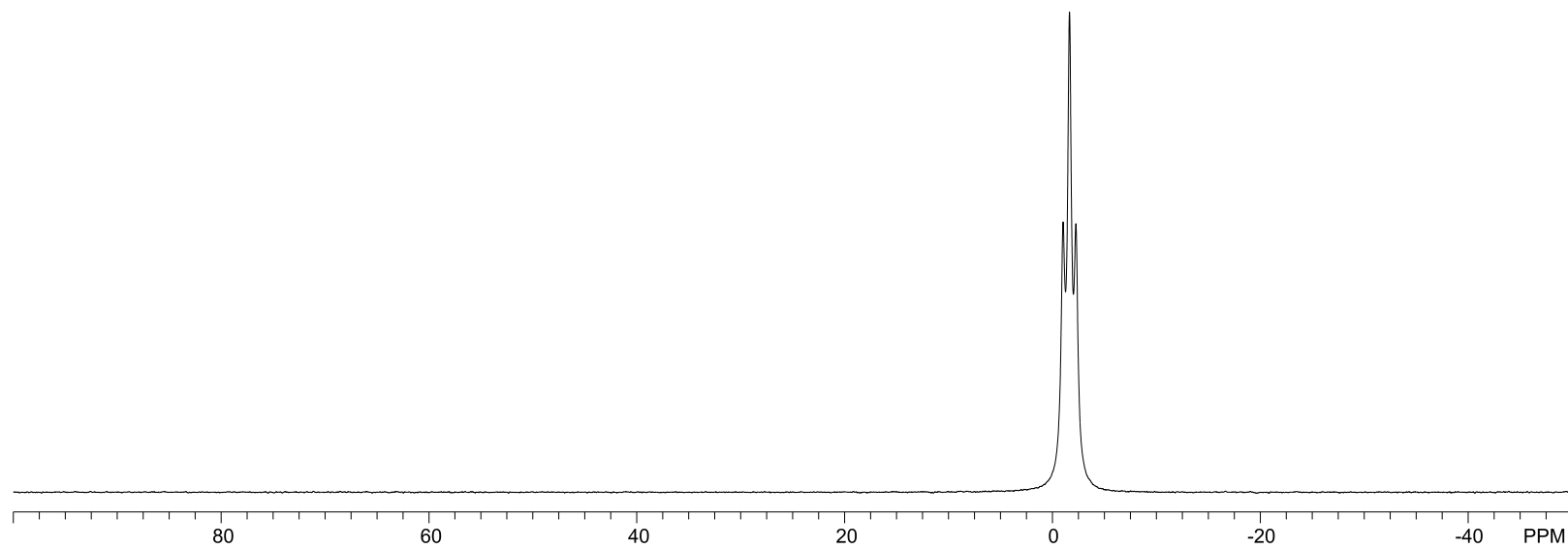




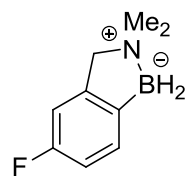
$^{11}\text{B}$  NMR (160 MHz),  
 $\text{CDCl}_3$



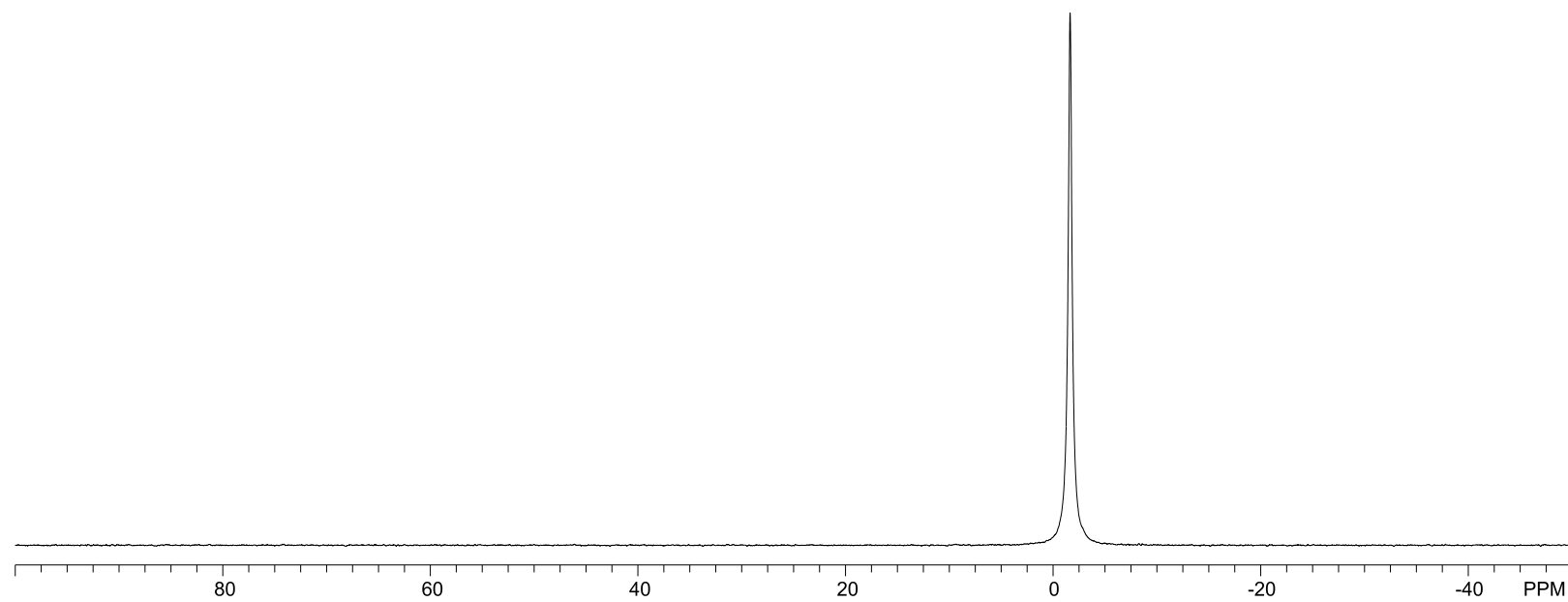
**2-7**



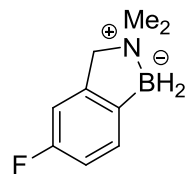
$^{11}\text{B}\{^1\text{H}\}$  NMR (160 MHz),  
 $\text{CDCl}_3$



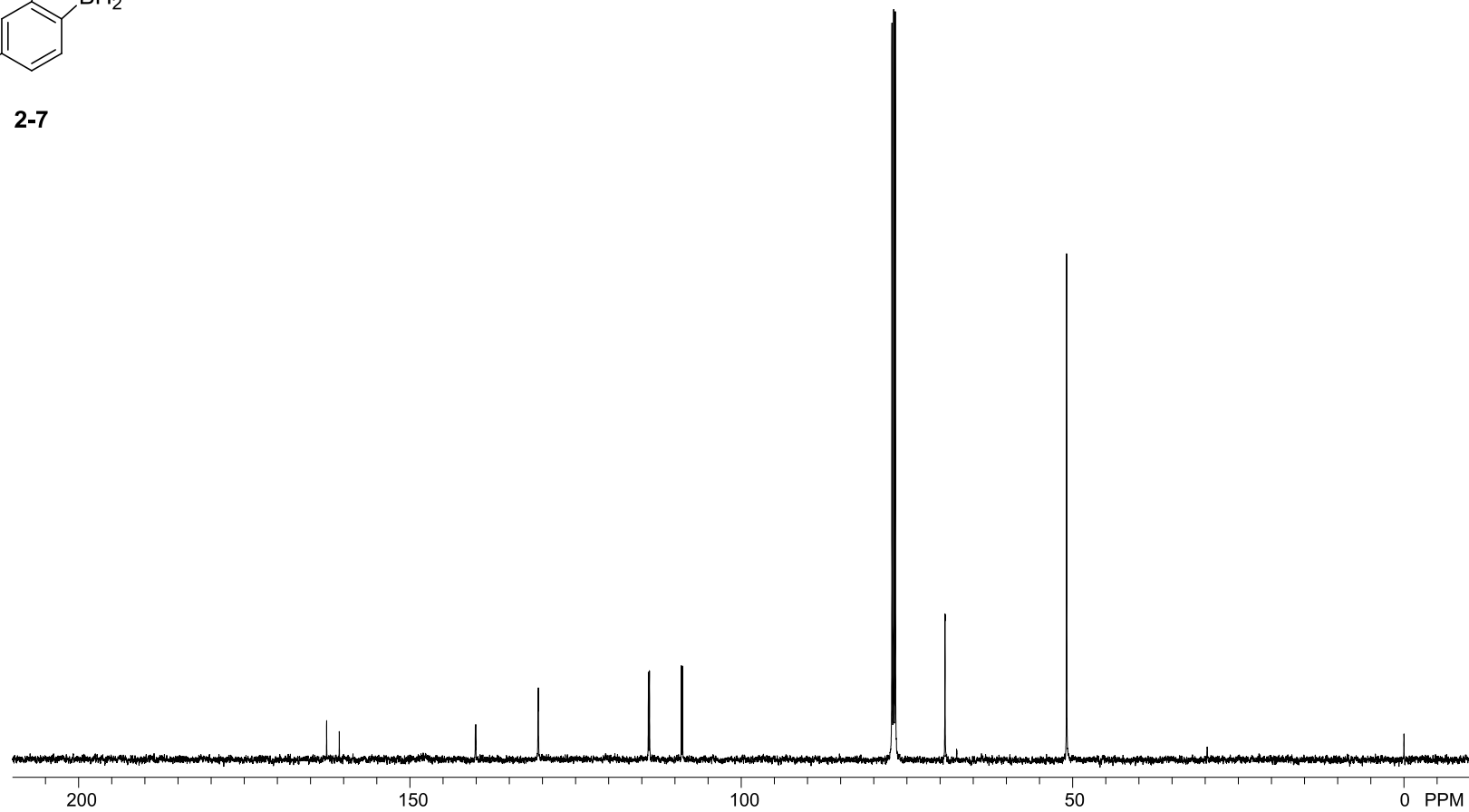
**2-7**



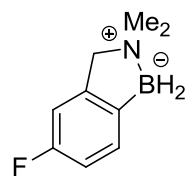
$^{13}\text{C}\{^1\text{H}\}$  NMR (126 MHz),  
 $\text{CDCl}_3$



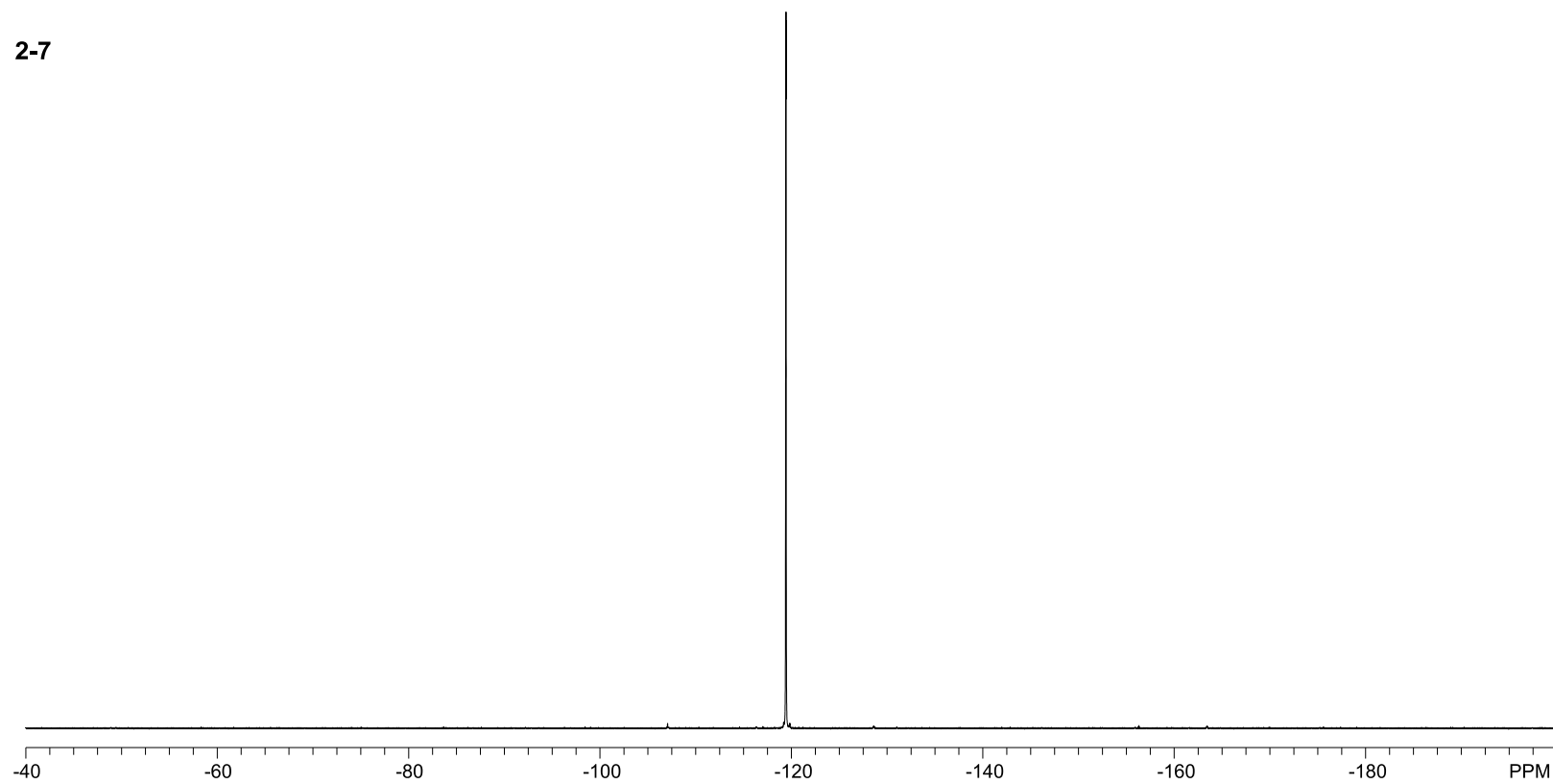
2-7



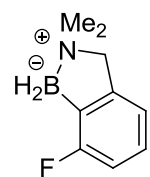
$^{19}\text{F}$  NMR (377 MHz),  
 $\text{CDCl}_3$



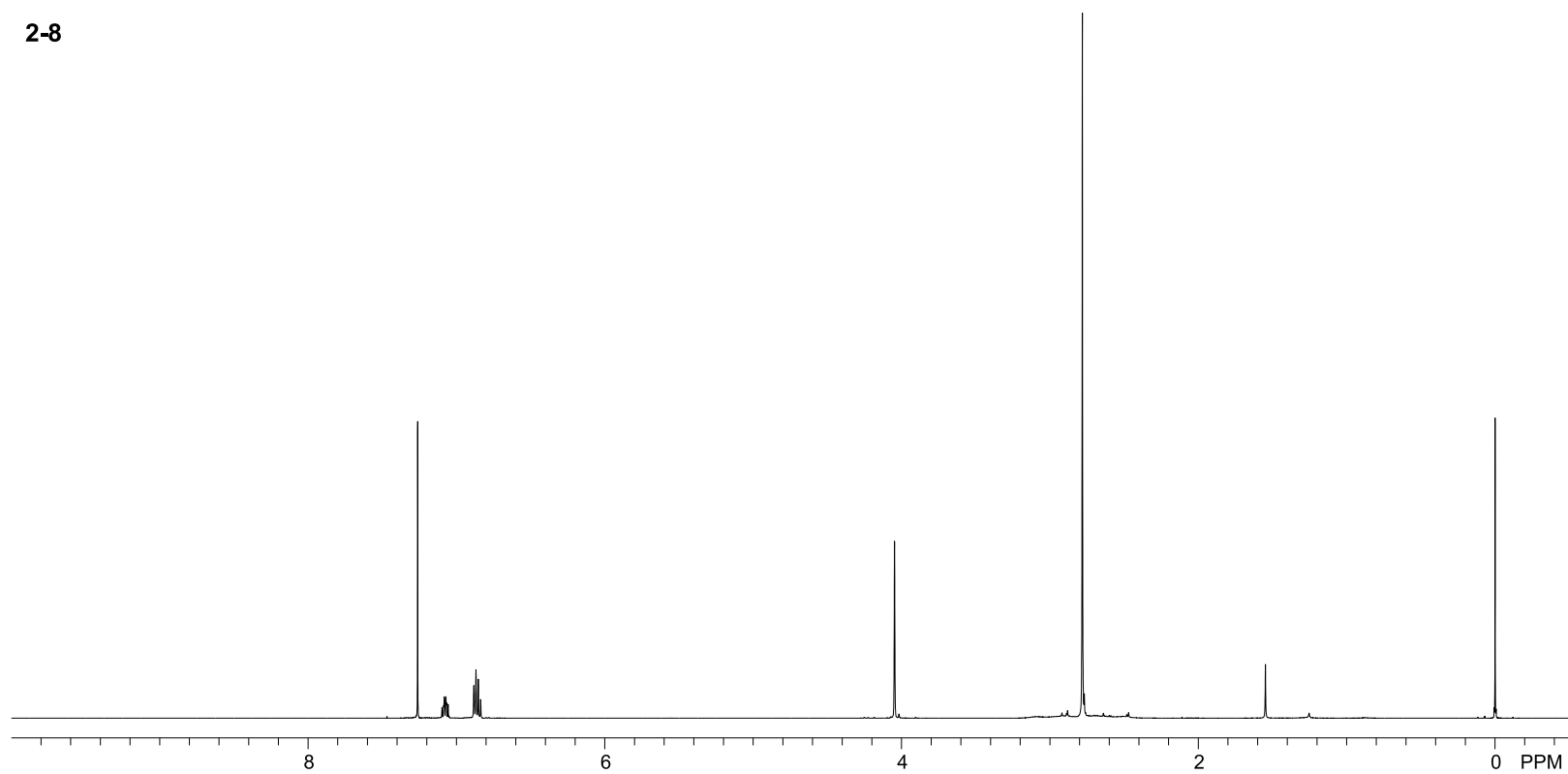
**2-7**



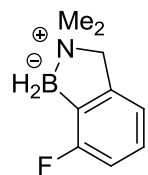
$^1\text{H}$  NMR (500 MHz),  
 $\text{CDCl}_3$



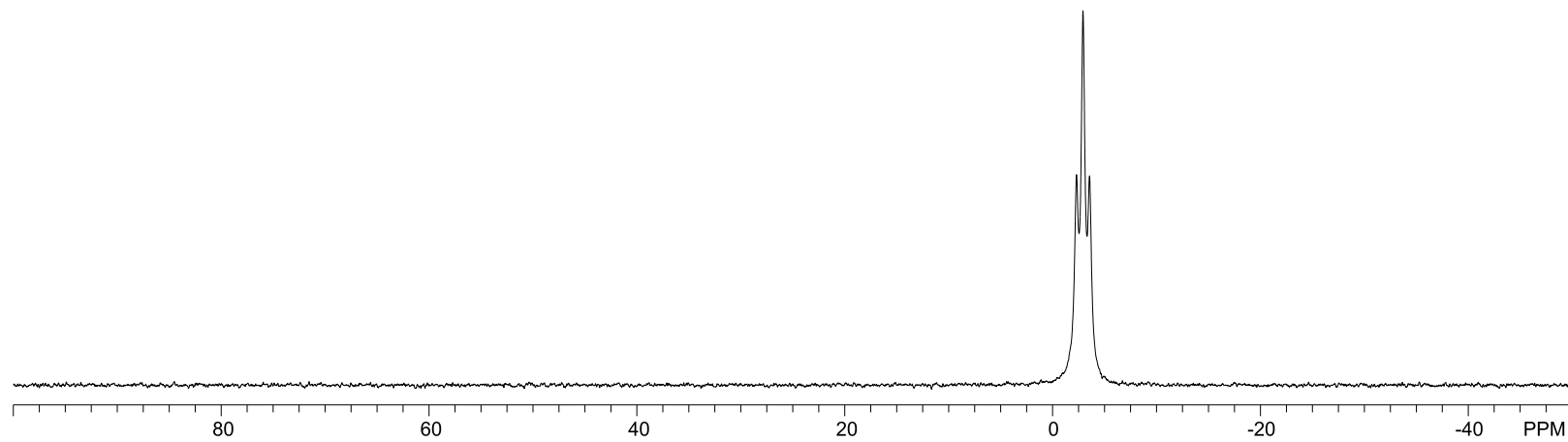
**2-8**



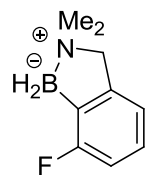
$^{11}\text{B}$  NMR (160 MHz),  
 $\text{CDCl}_3$



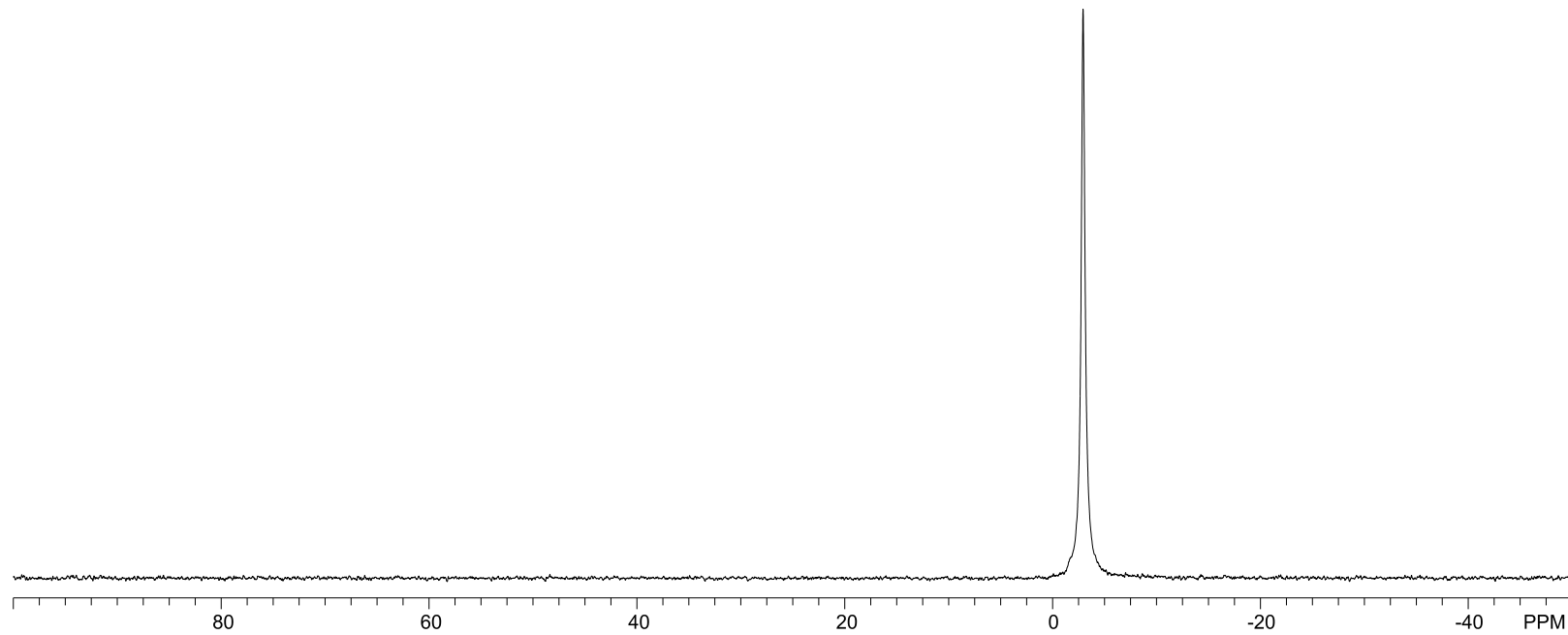
**2-8**



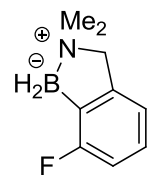
$^{11}\text{B}\{^1\text{H}\}$  NMR (160 MHz),  
 $\text{CDCl}_3$



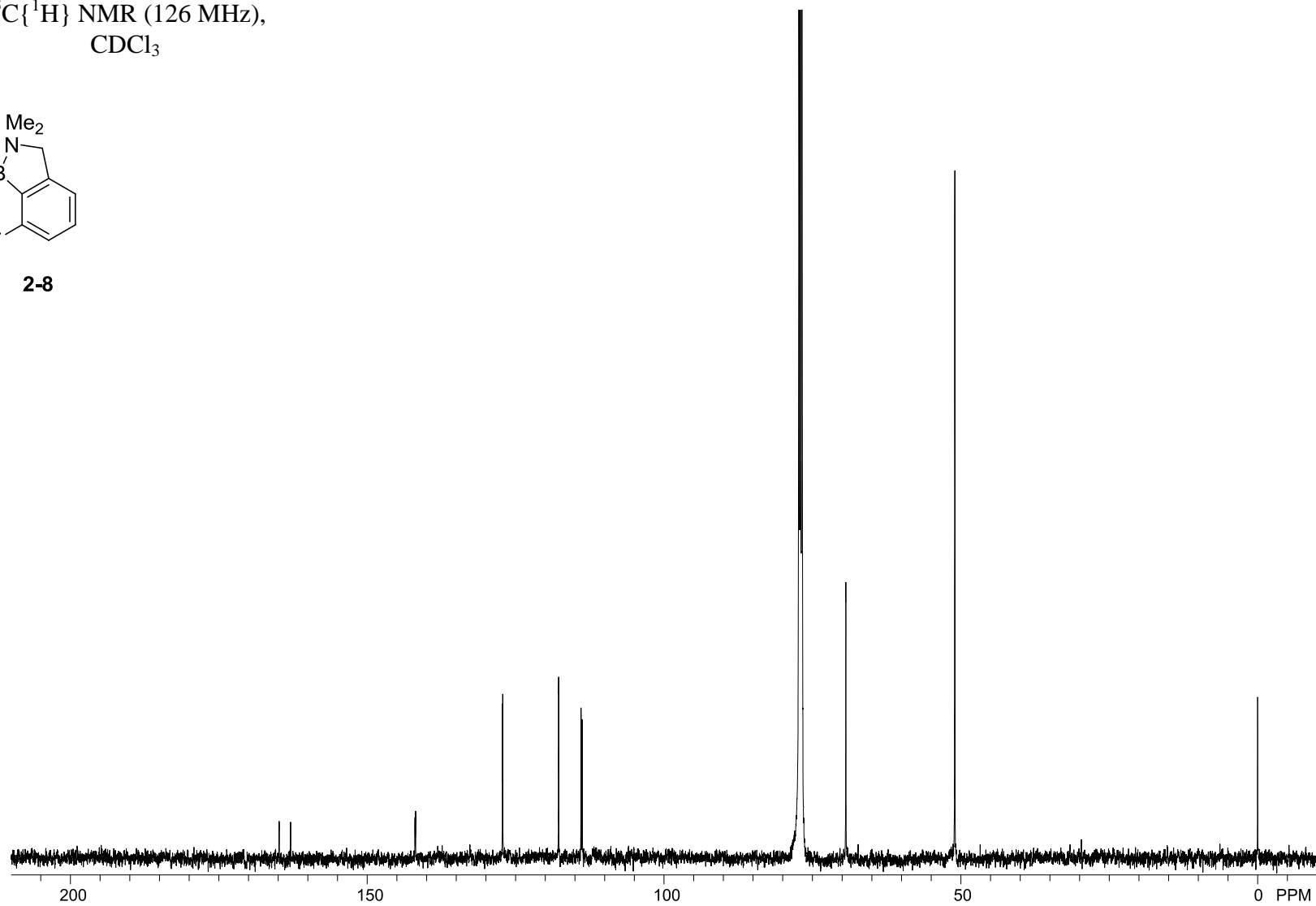
**2-8**



$^{13}\text{C}\{^1\text{H}\}$  NMR (126 MHz),  
 $\text{CDCl}_3$

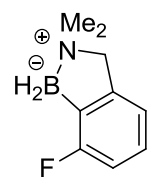


2-8

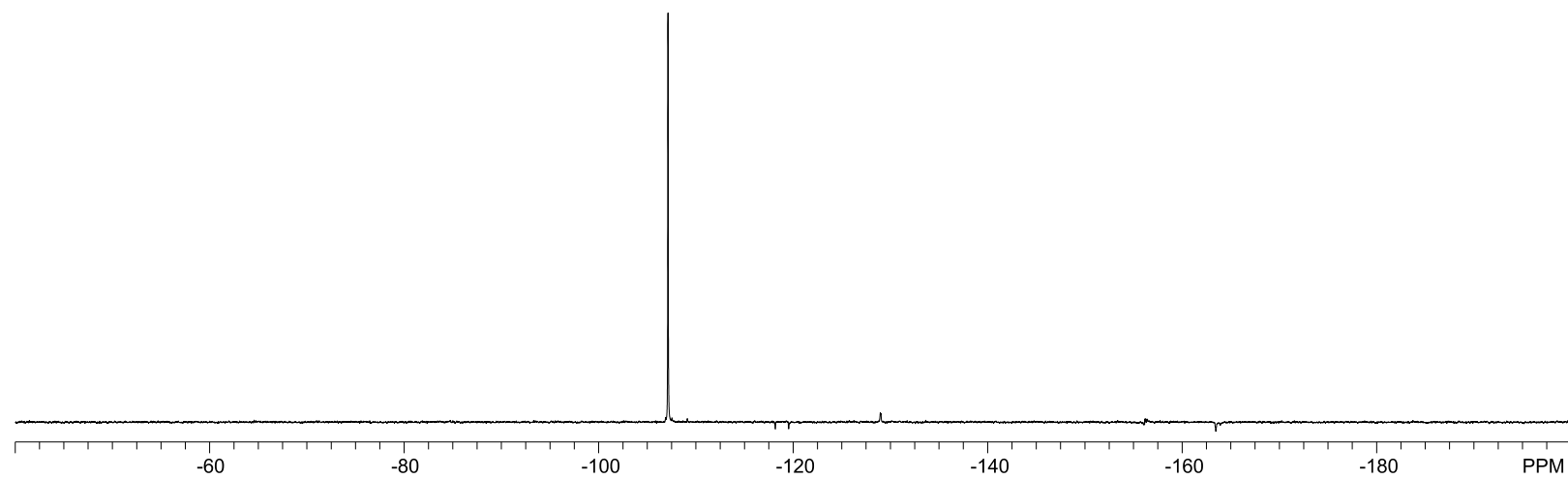




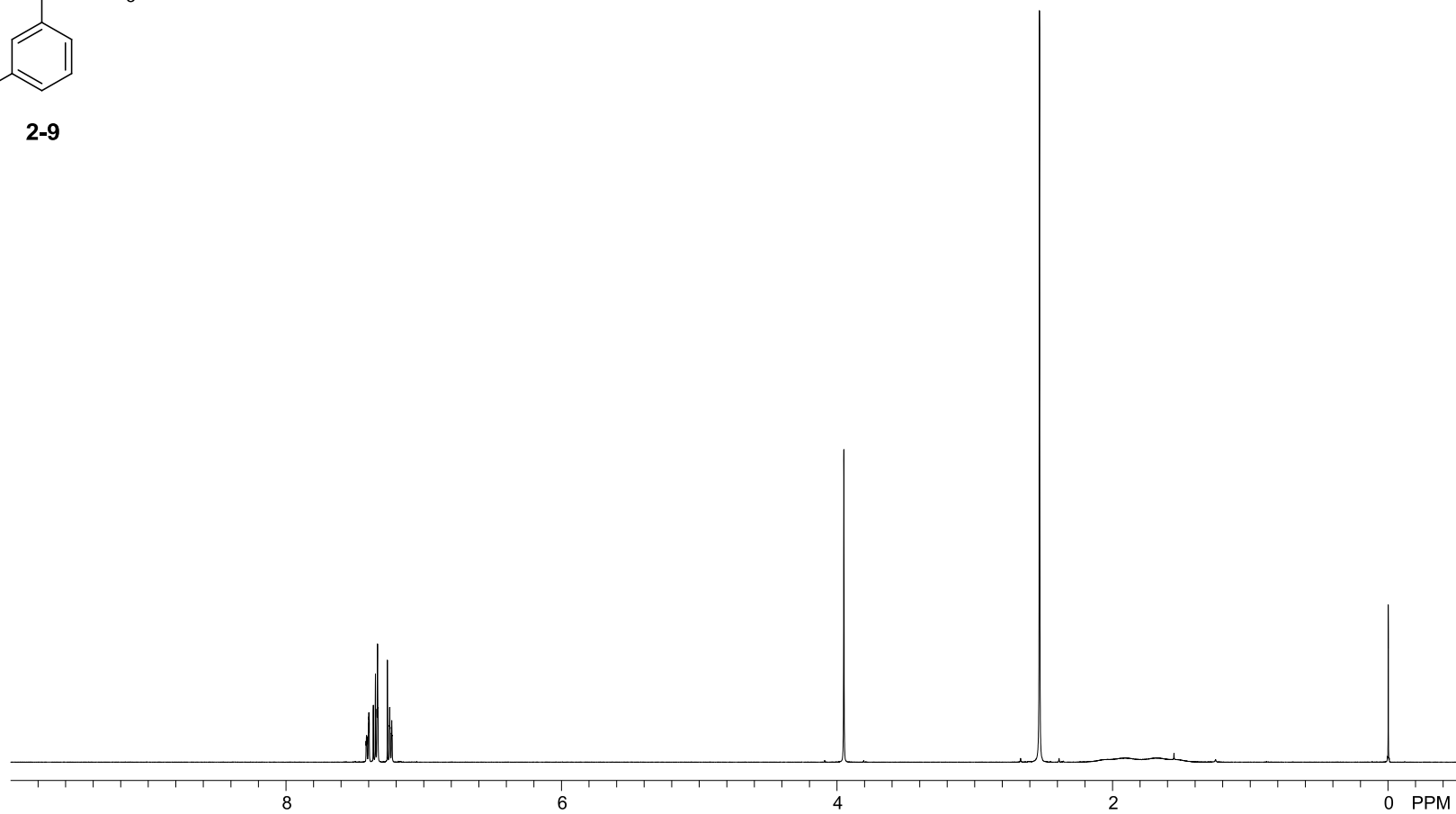
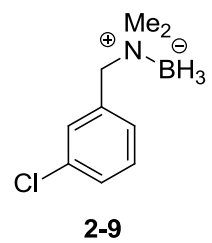
$^{19}\text{F}$  NMR (377 MHz),  
 $\text{CDCl}_3$



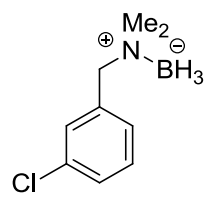
2-8



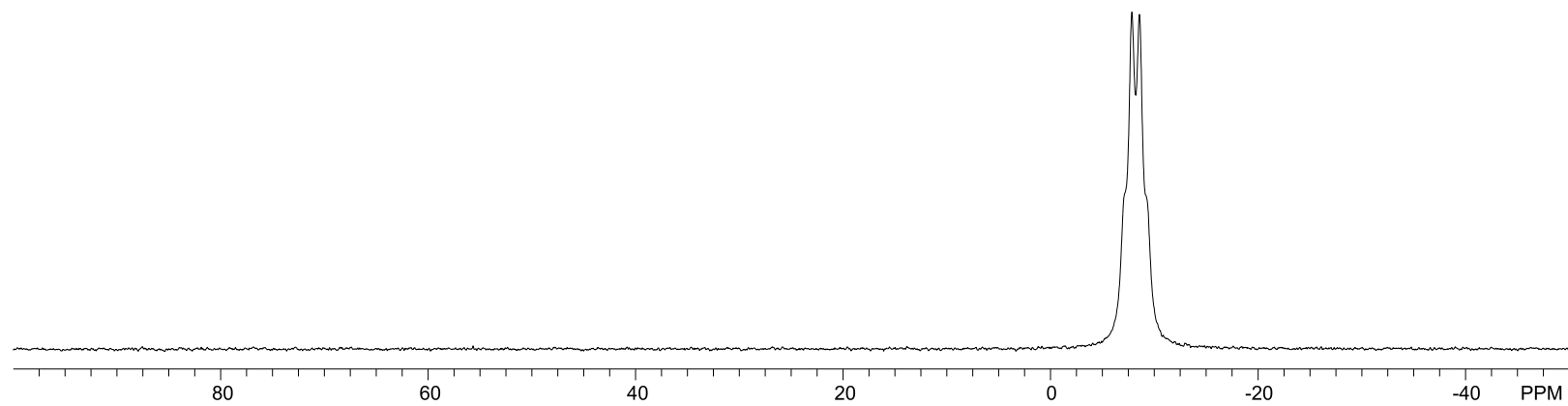
$^1\text{H}$  NMR (500 MHz),  
 $\text{CDCl}_3$



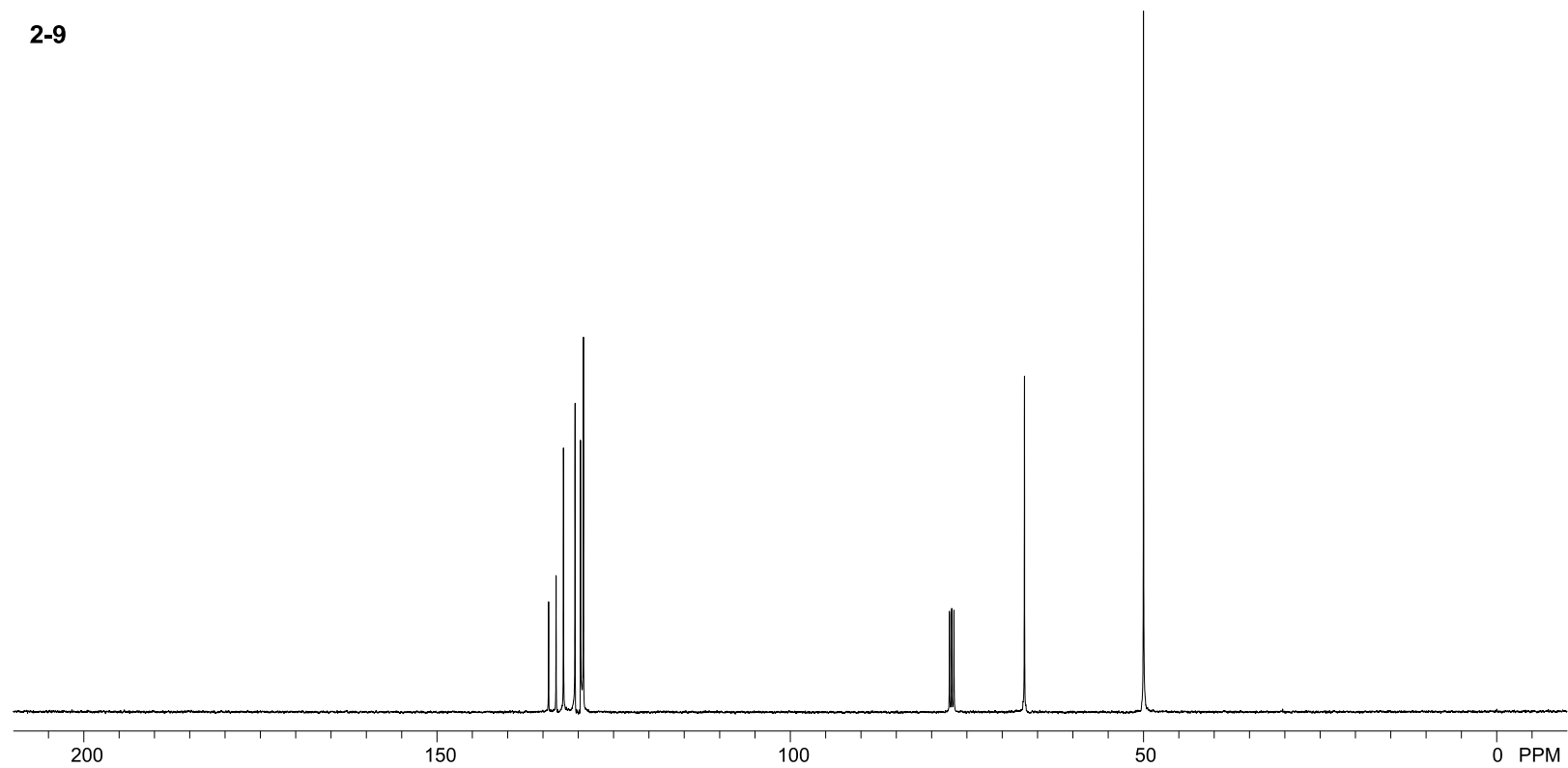
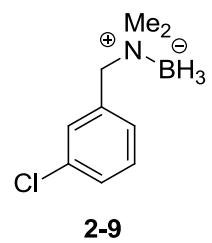
$^{11}\text{B}$  NMR (128 MHz),  
 $\text{CDCl}_3$



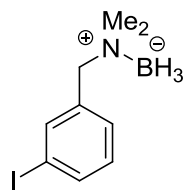
**2-9**



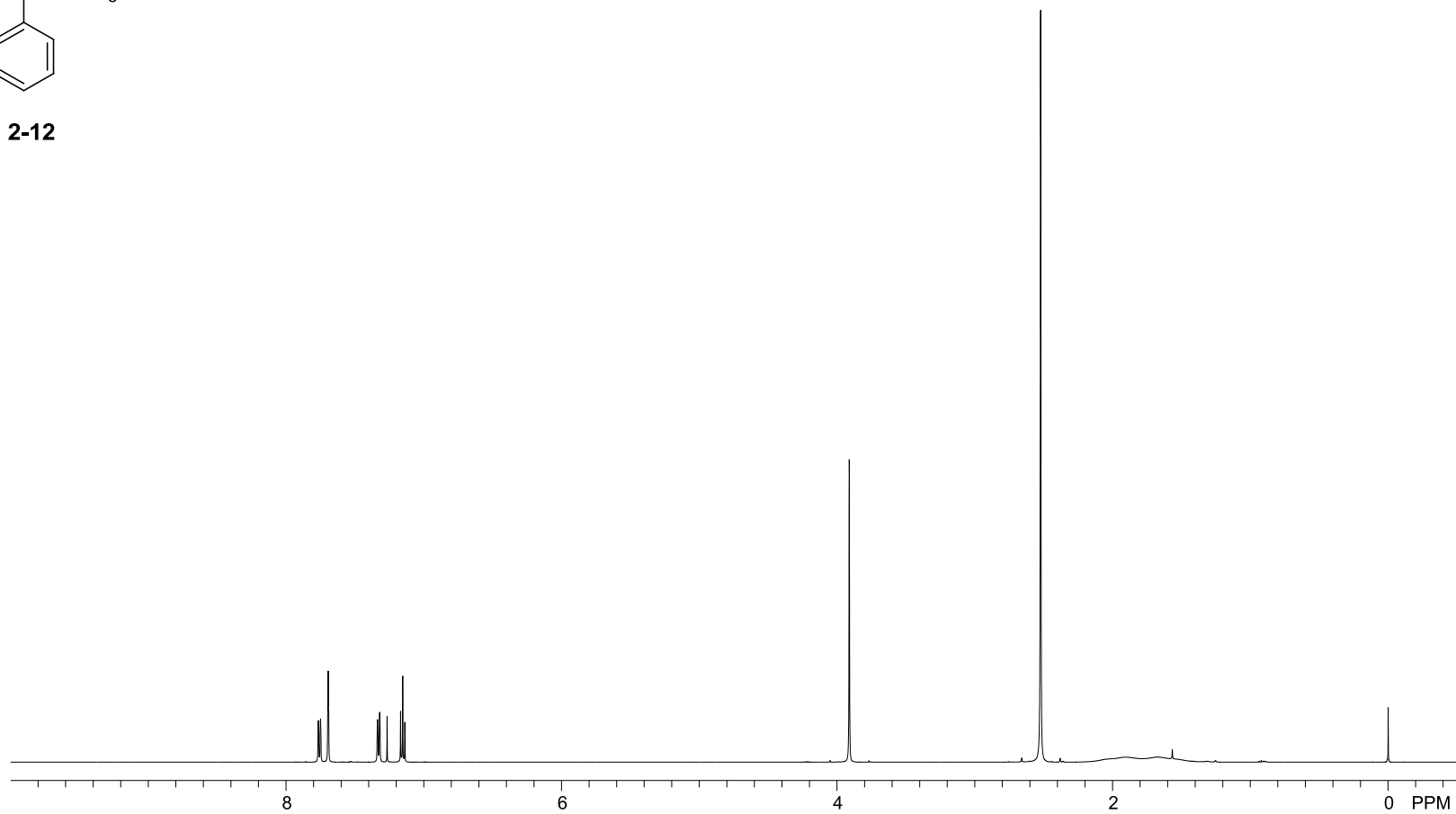
$^{13}\text{C}\{^1\text{H}\}$  NMR (101 MHz),  
 $\text{CDCl}_3$



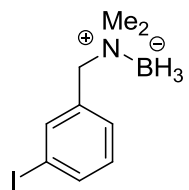
$^1\text{H}$  NMR (500 MHz),  
 $\text{CDCl}_3$



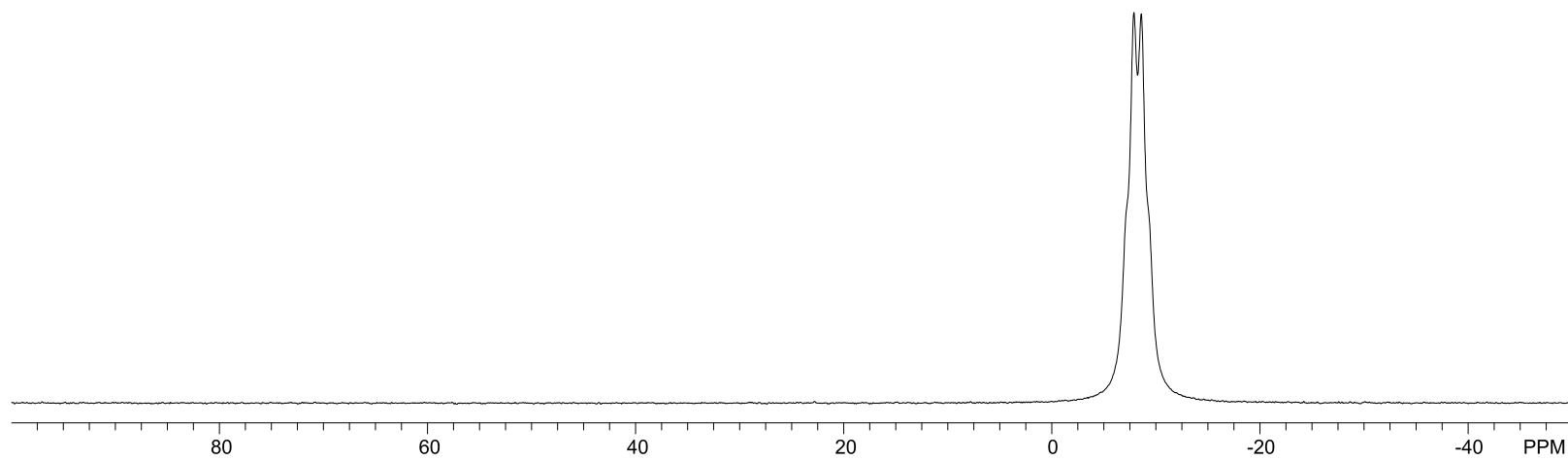
**2-12**



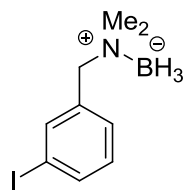
$^{11}\text{B}$  NMR (128 MHz),  
 $\text{CDCl}_3$



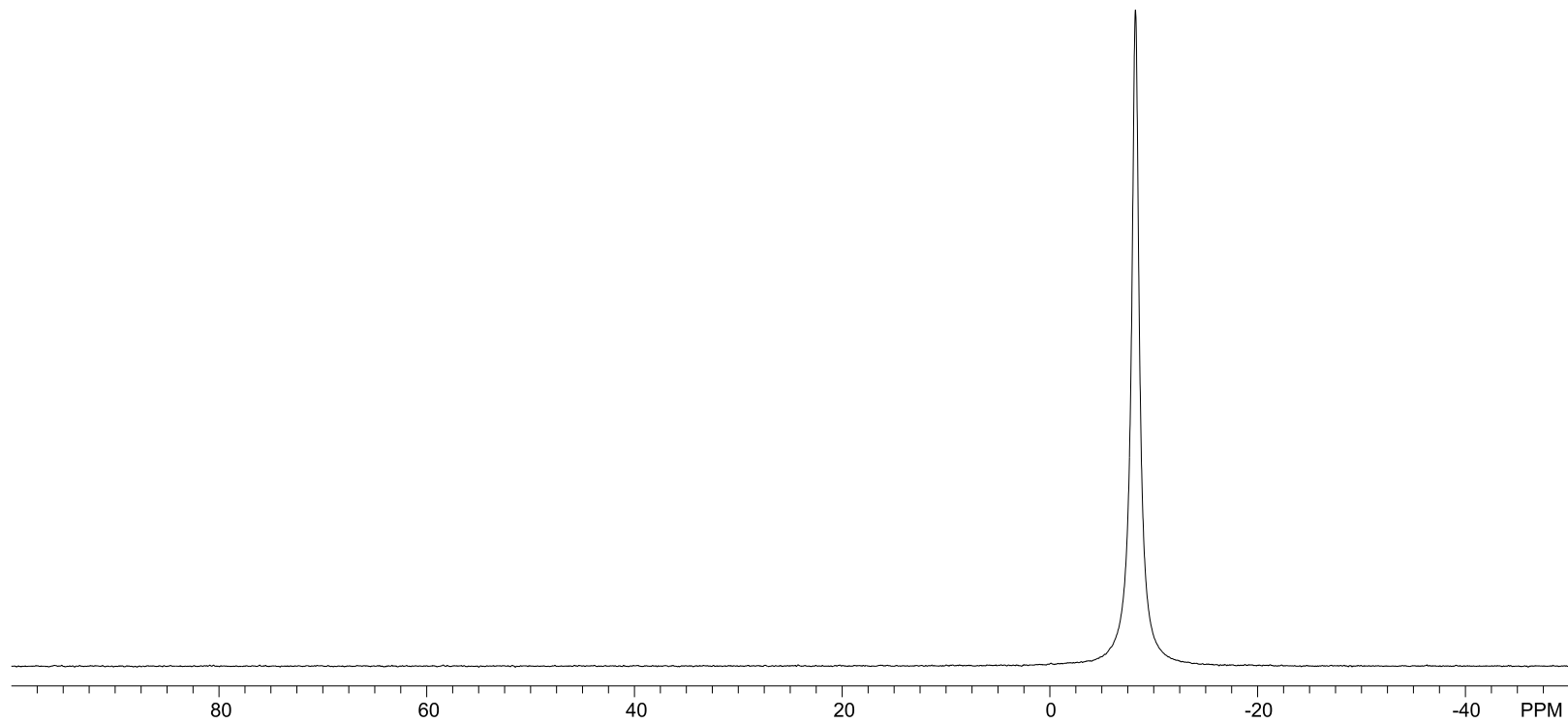
**2-12**



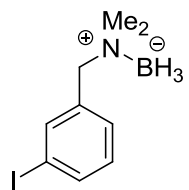
$^{11}\text{B}\{^1\text{H}\}$  NMR (128 MHz),  
 $\text{CDCl}_3$



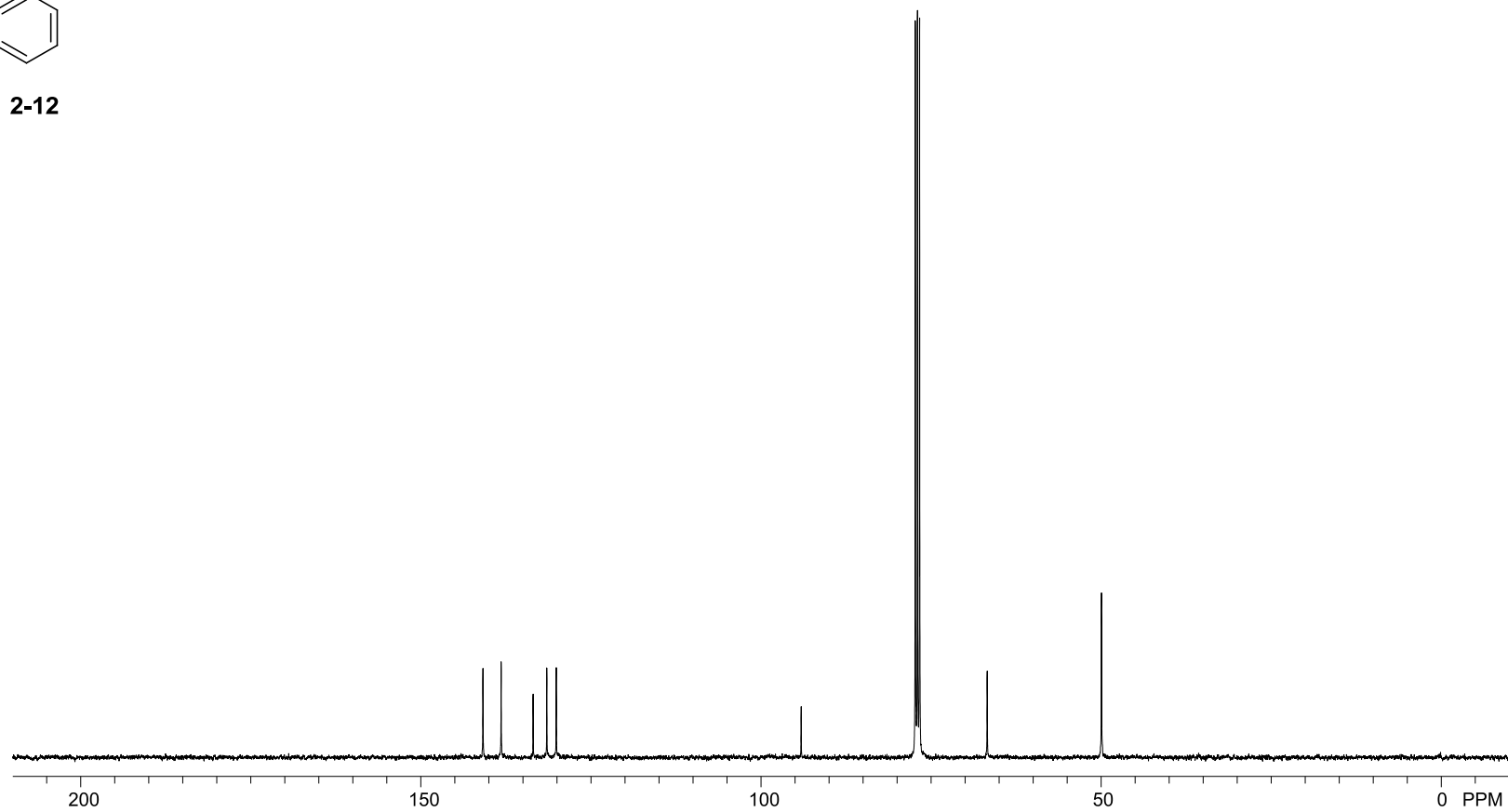
**2-12**



$^{13}\text{C}\{^1\text{H}\}$  NMR (101 MHz),  
 $\text{CDCl}_3$

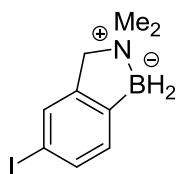


**2-12**

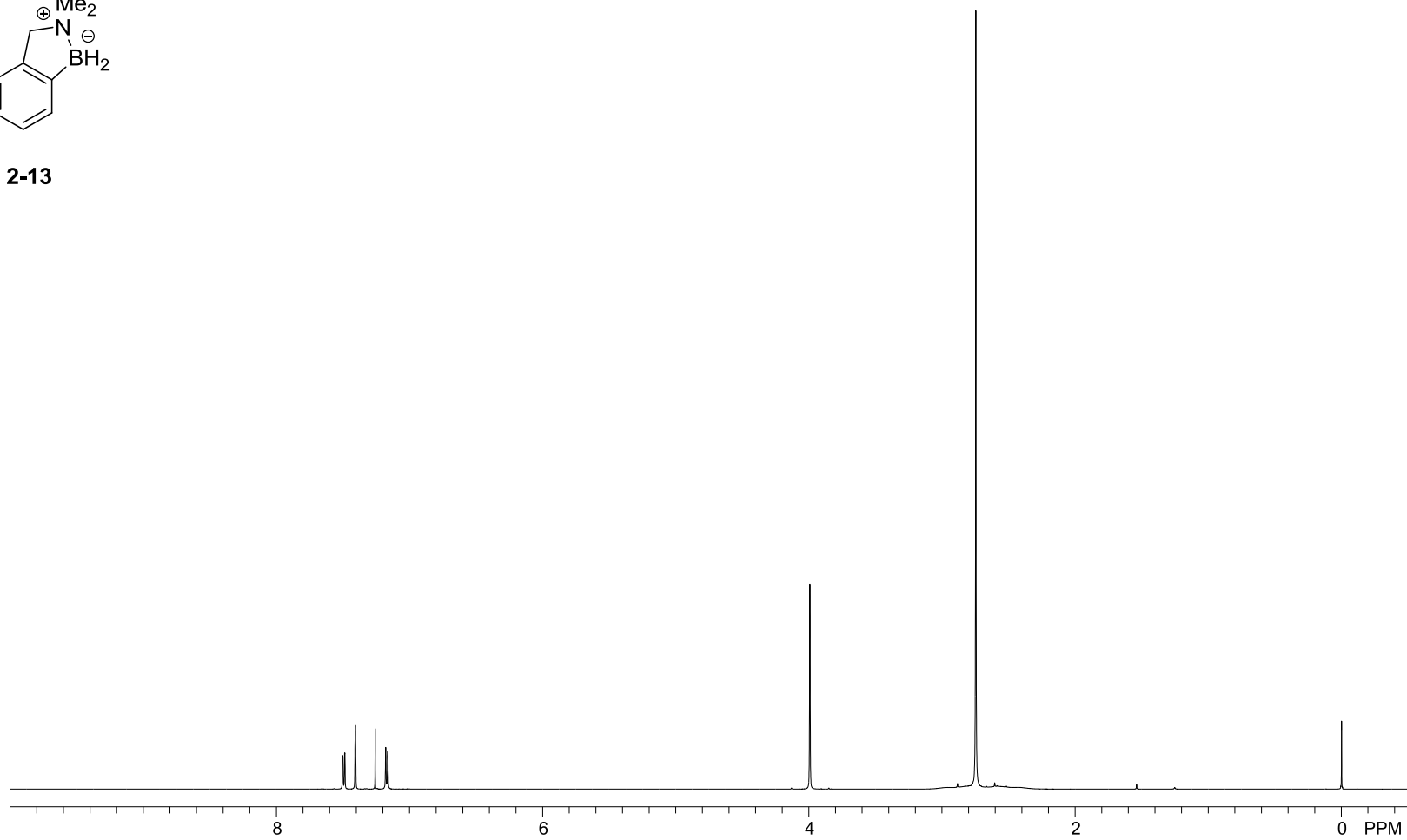




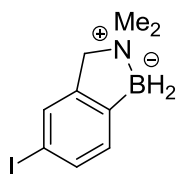
$^1\text{H}$  NMR (500 MHz),  
 $\text{CDCl}_3$



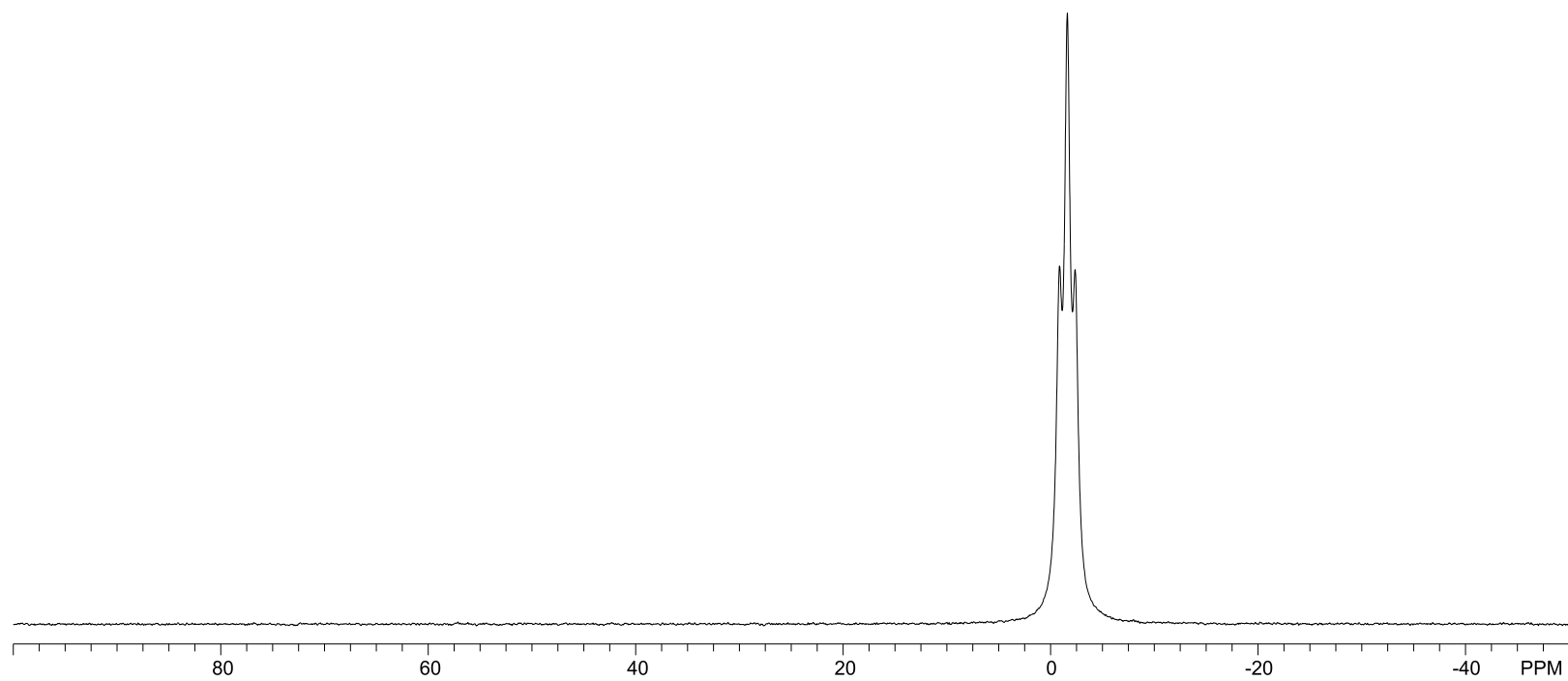
**2-13**



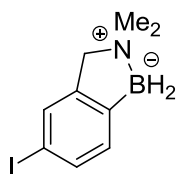
$^{11}\text{B}$  NMR (128 MHz),  
 $\text{CDCl}_3$



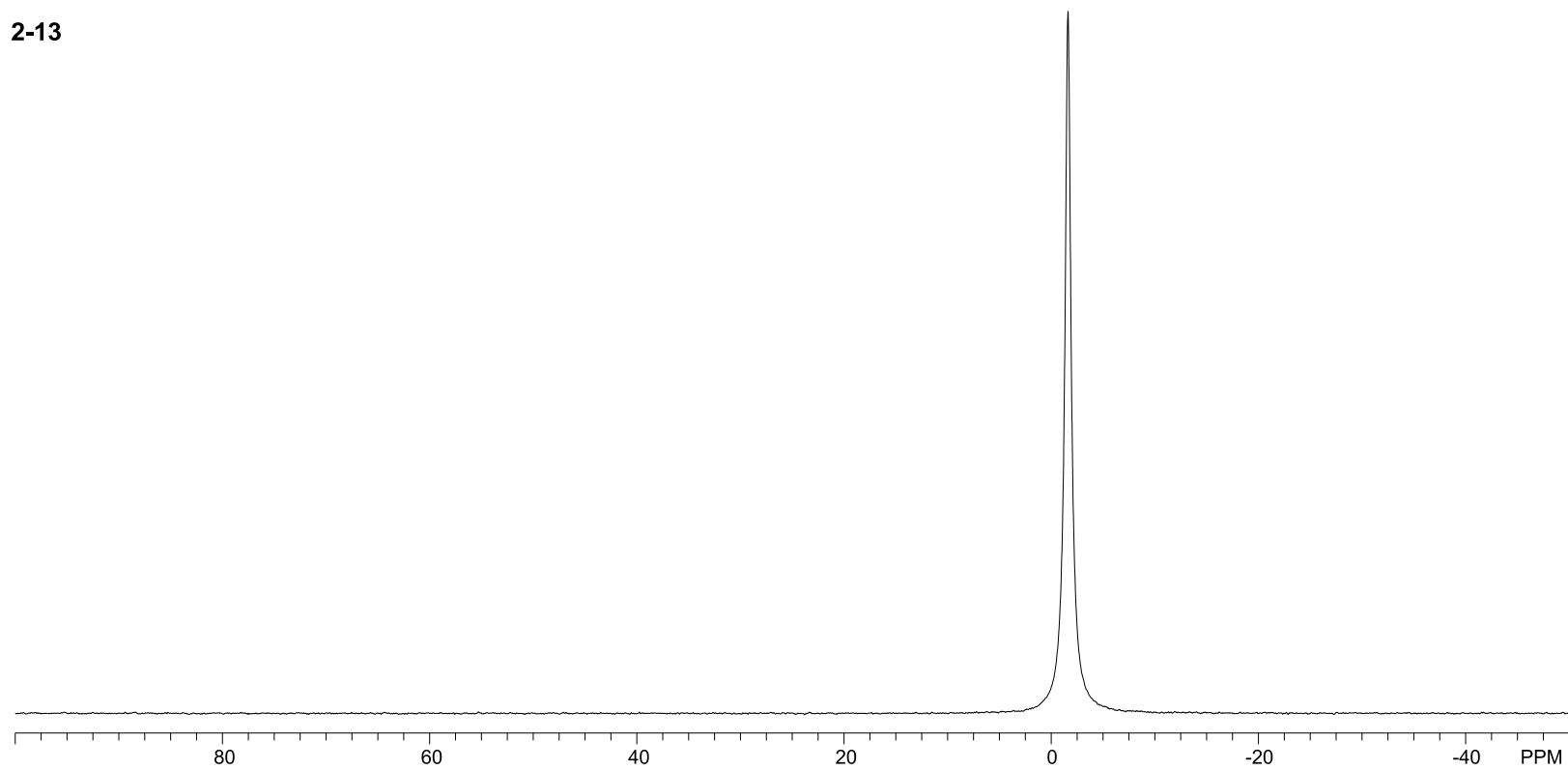
**2-13**



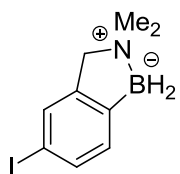
$^{11}\text{B}\{^1\text{H}\}$  NMR (128 MHz),  
 $\text{CDCl}_3$



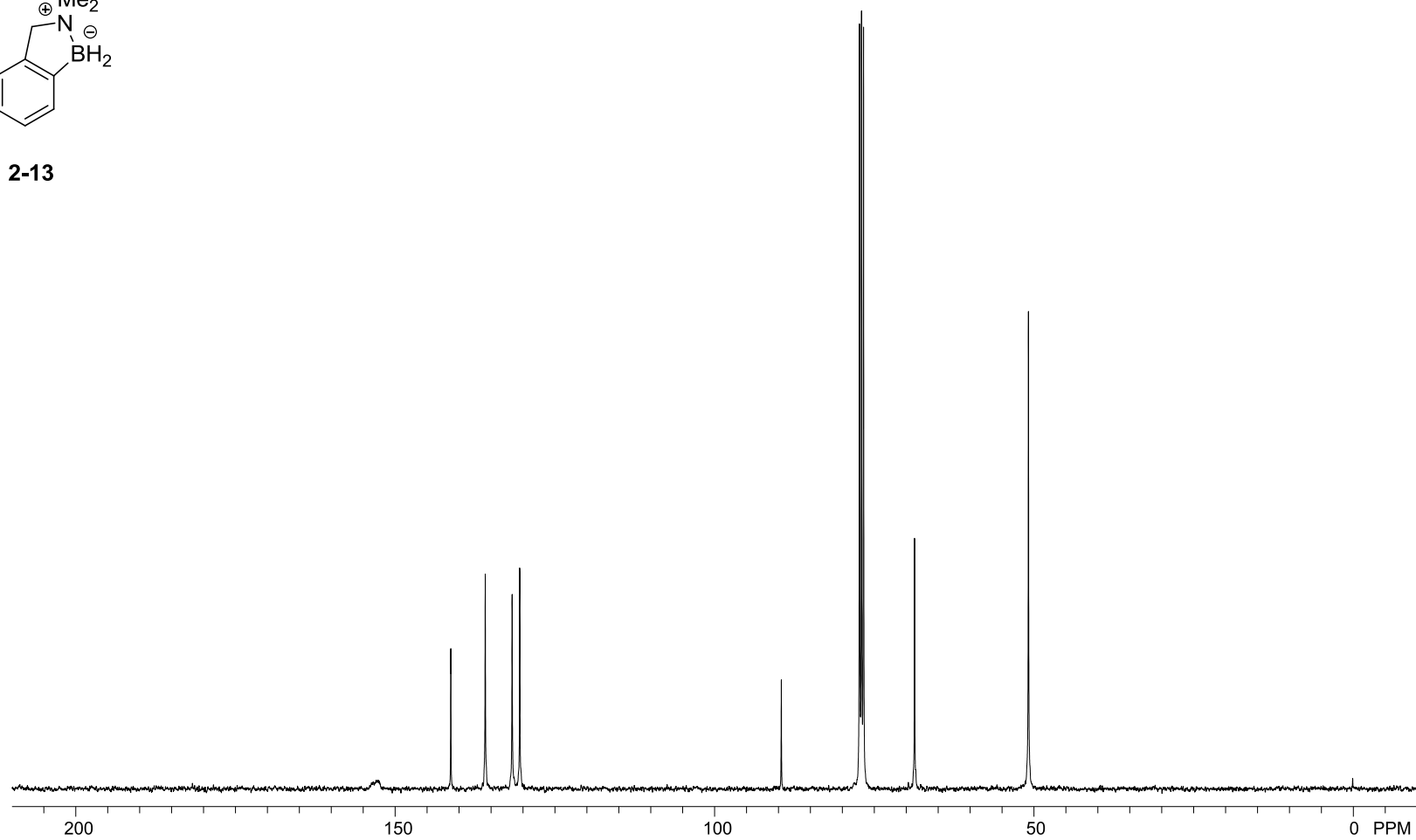
**2-13**



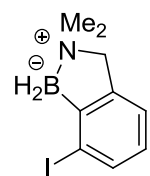
$^{13}\text{C}\{^1\text{H}\}$  NMR (101 MHz),  
 $\text{CDCl}_3$



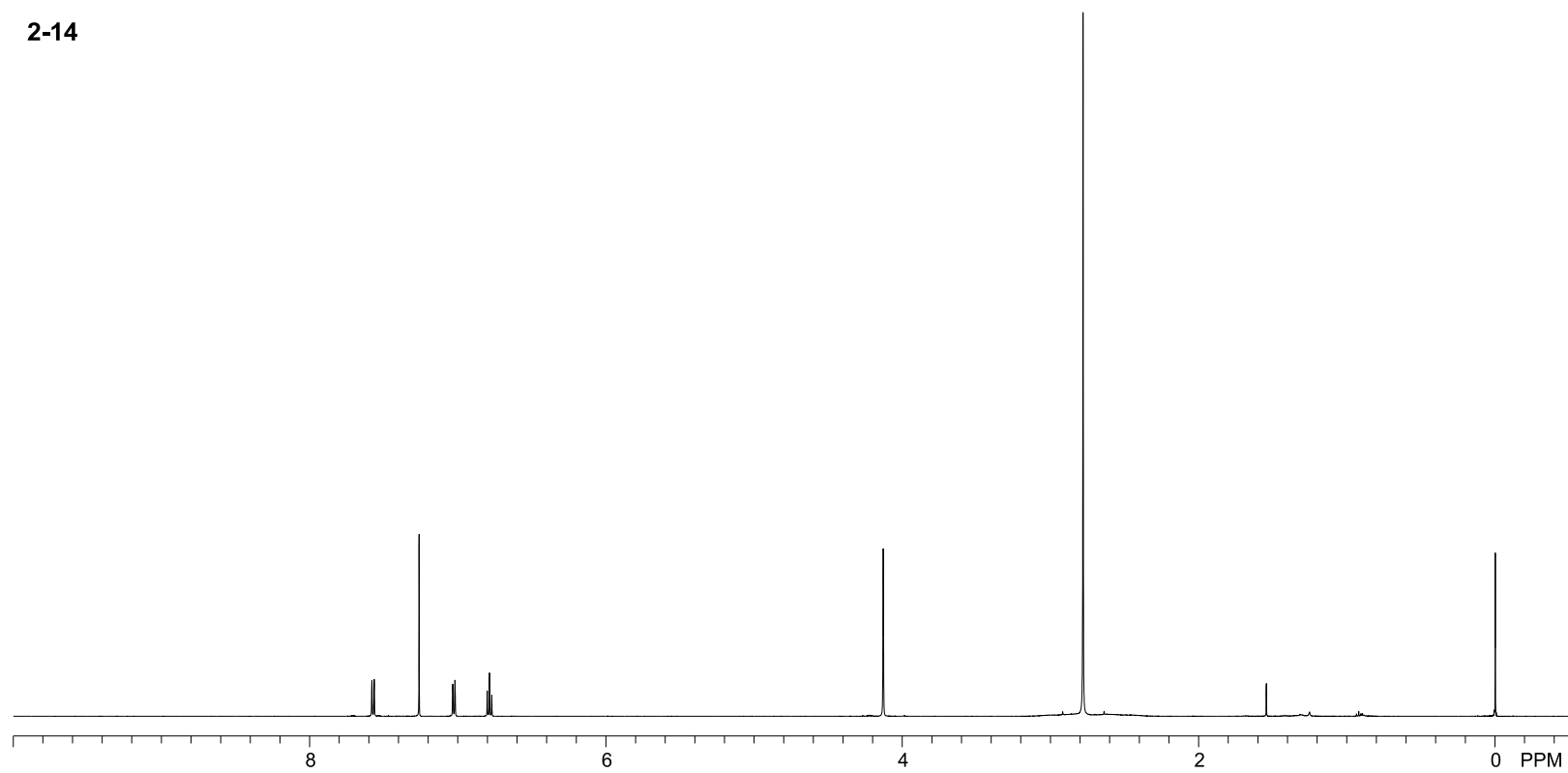
2-13



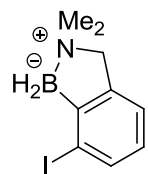
$^1\text{H}$  NMR (500 MHz),  
 $\text{CDCl}_3$



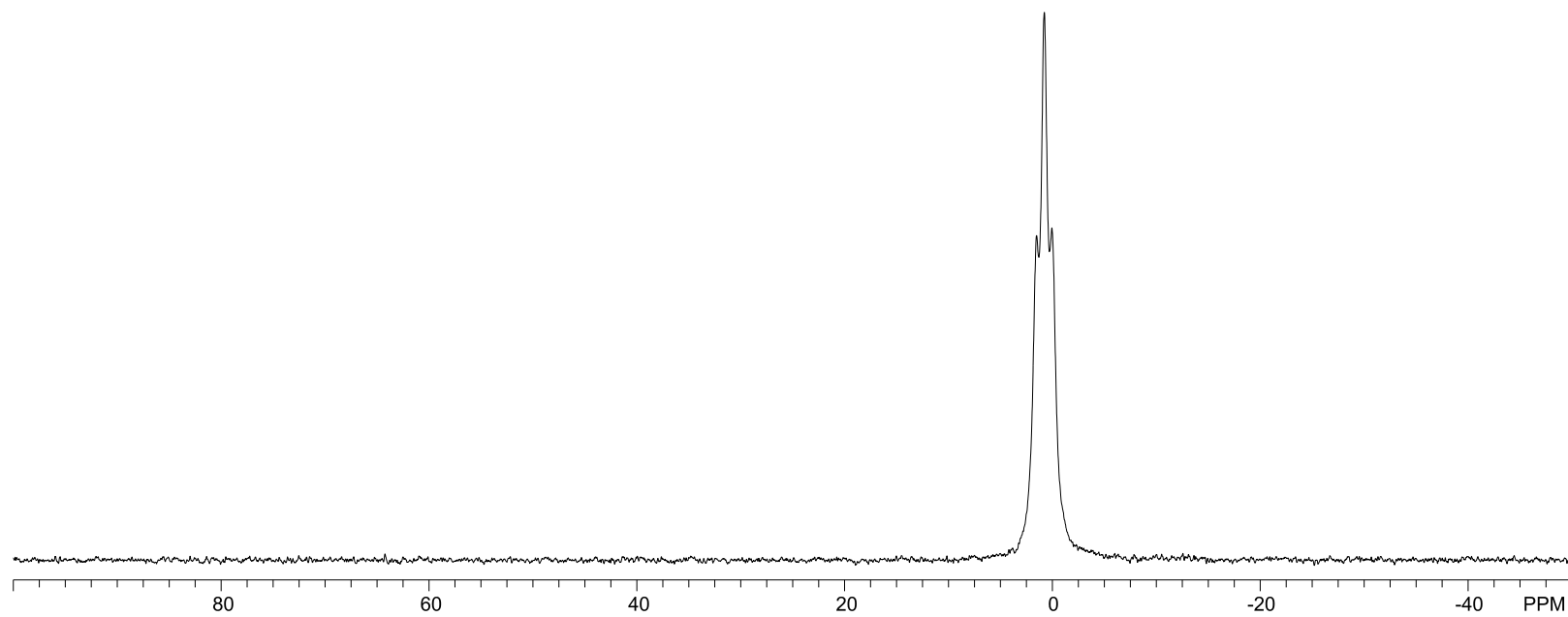
**2-14**



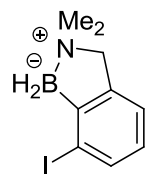
$^{11}\text{B}$  NMR (128 MHz),  
 $\text{CDCl}_3$



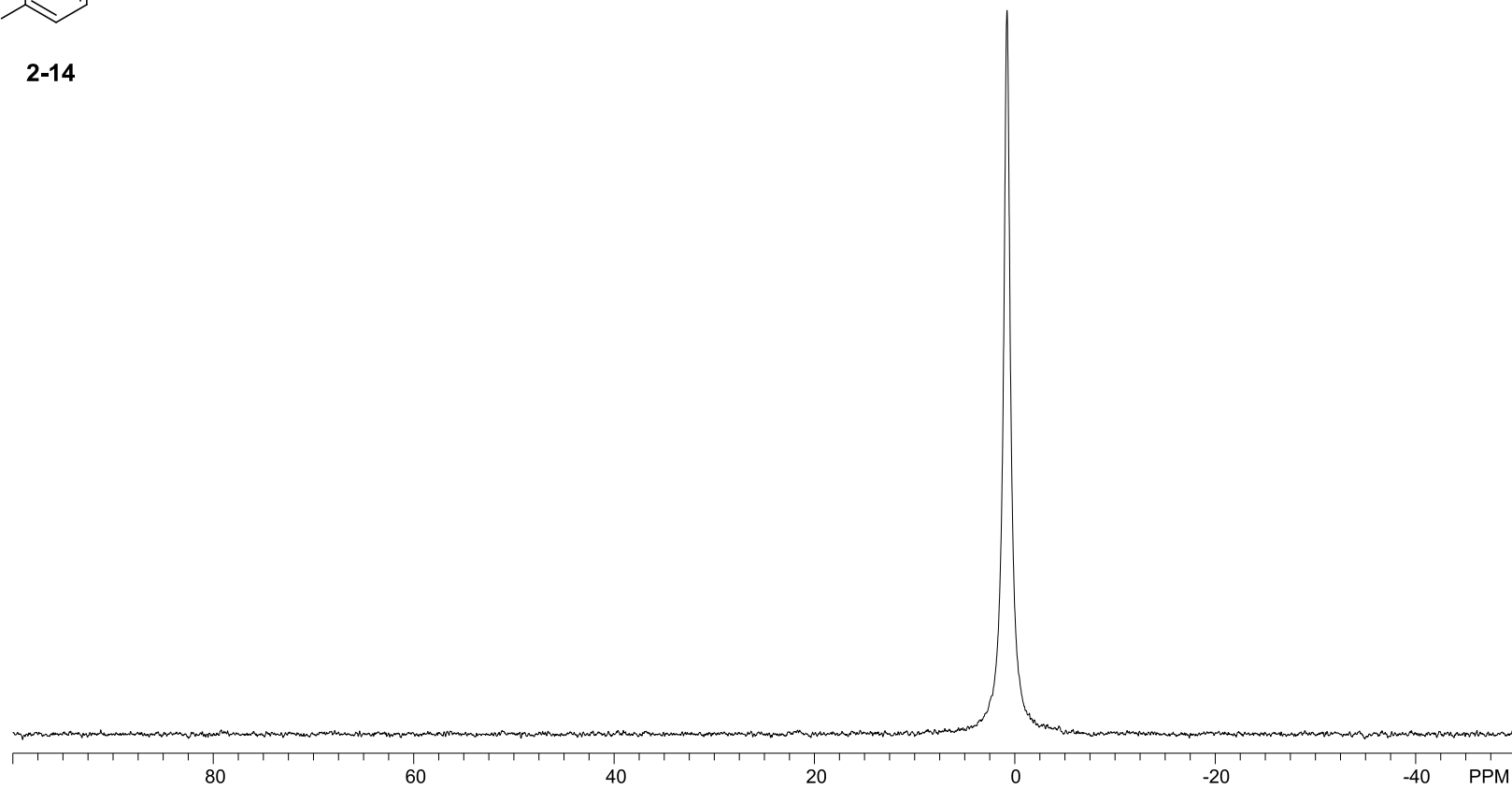
**2-14**



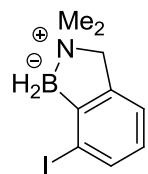
$^{11}\text{B}\{^1\text{H}\}$  NMR (128 MHz),  
 $\text{CDCl}_3$



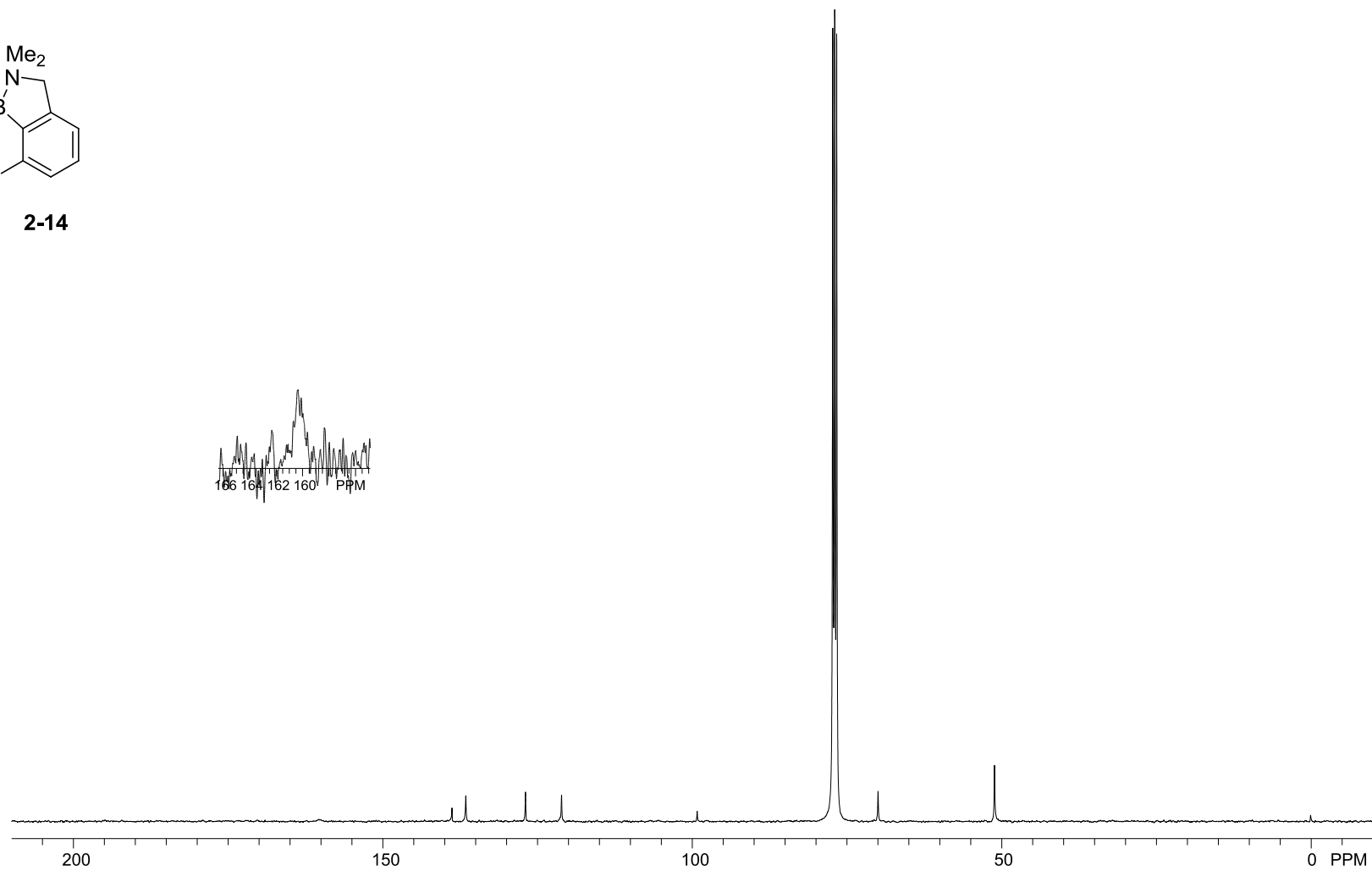
**2-14**



$^{13}\text{C}\{^1\text{H}\}$  NMR (101 MHz),  
 $\text{CDCl}_3$

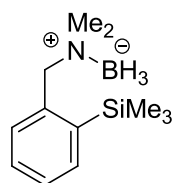


**2-14**

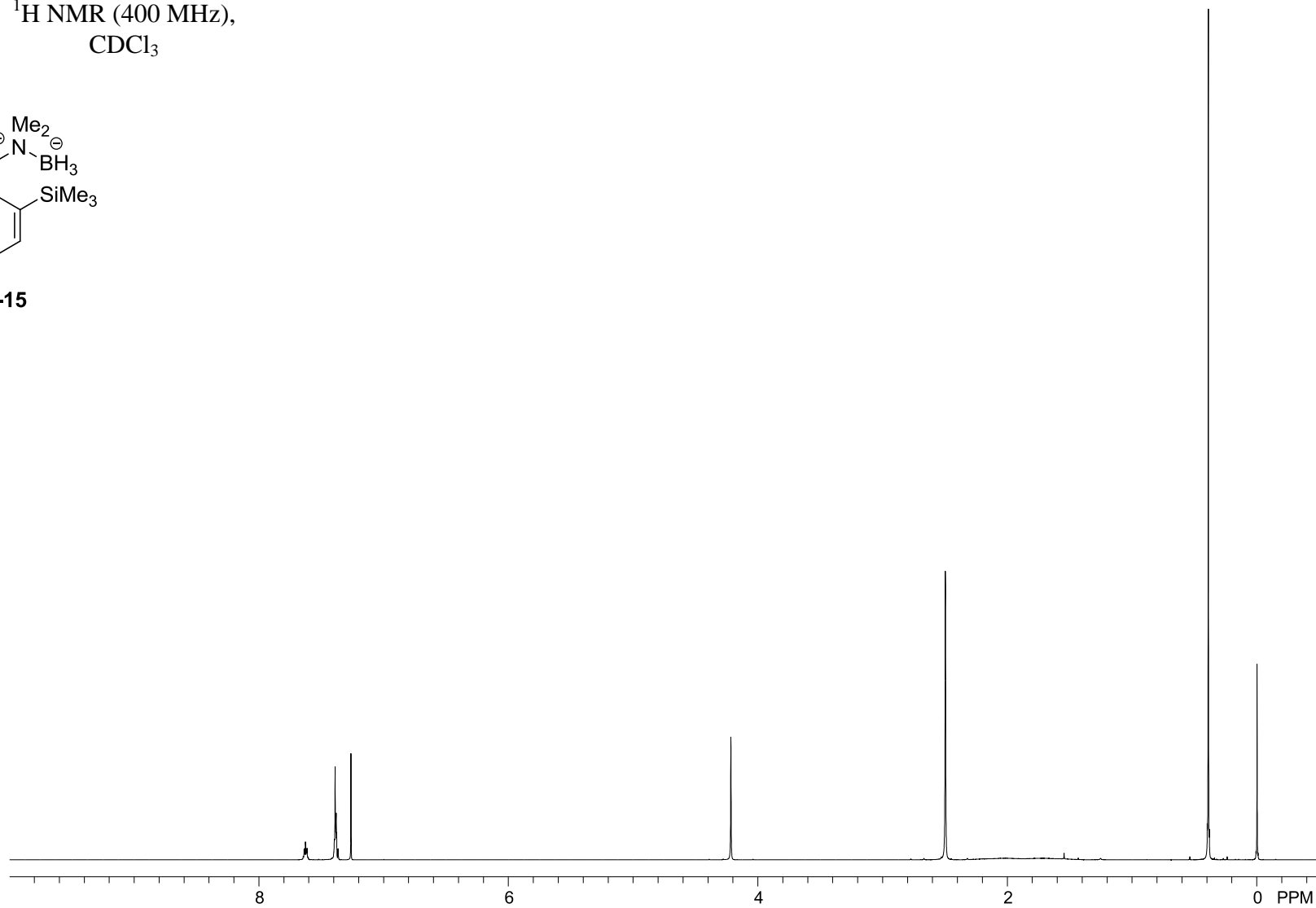




$^1\text{H}$  NMR (400 MHz),  
 $\text{CDCl}_3$



**2-15**

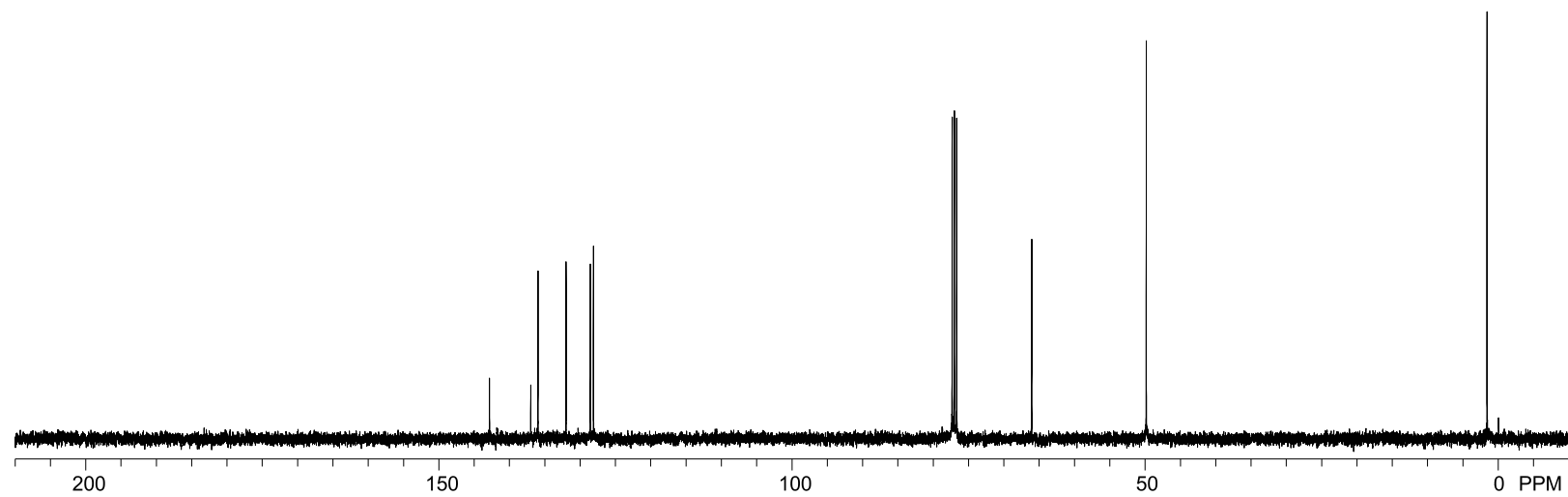




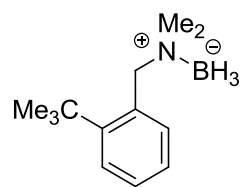
$^{13}\text{C}\{^1\text{H}\}$  NMR (101 MHz),  
 $\text{CDCl}_3$



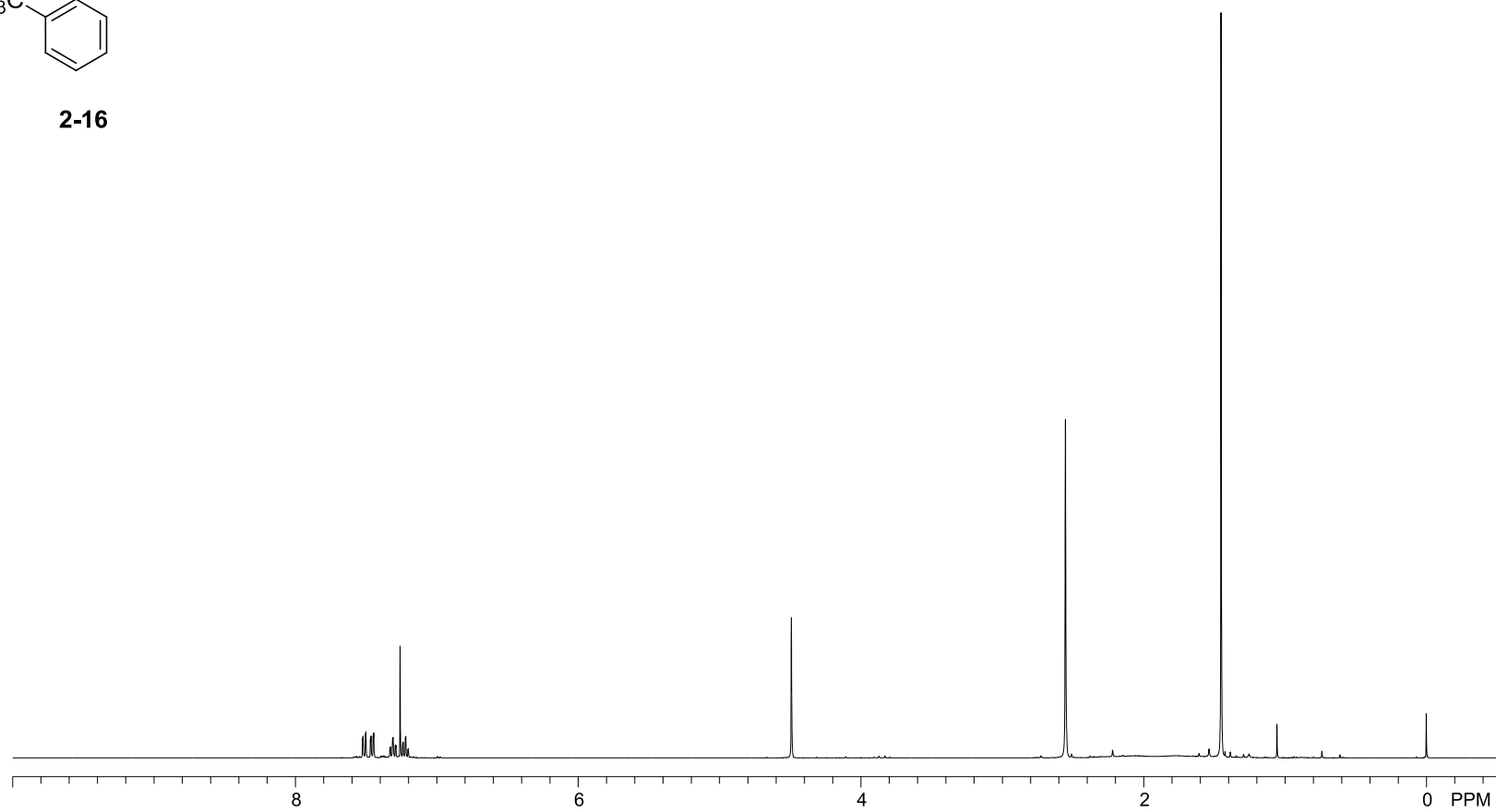
**2-15**



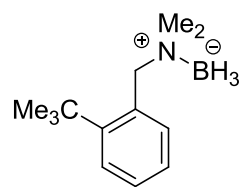
$^1\text{H}$  NMR (400 MHz),  
 $\text{CDCl}_3$



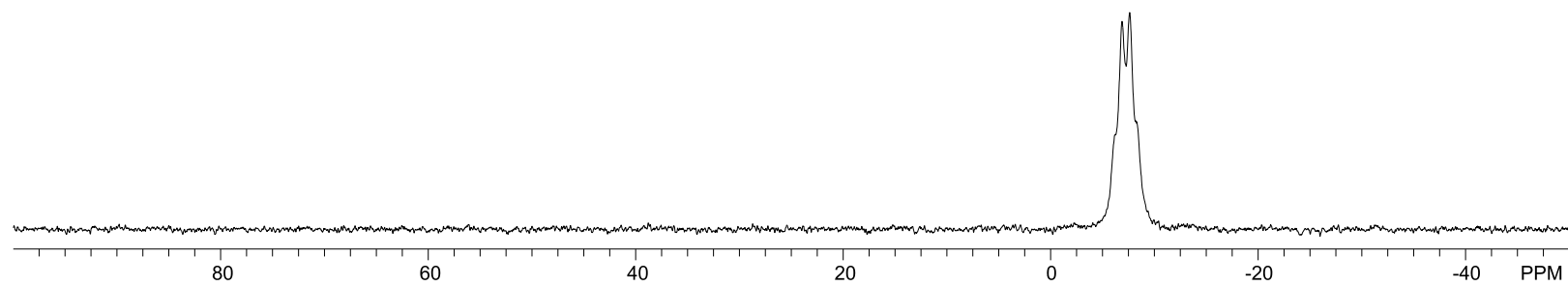
**2-16**



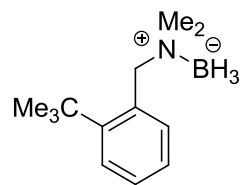
$^{11}\text{B}$  NMR (128 MHz),  
 $\text{CDCl}_3$



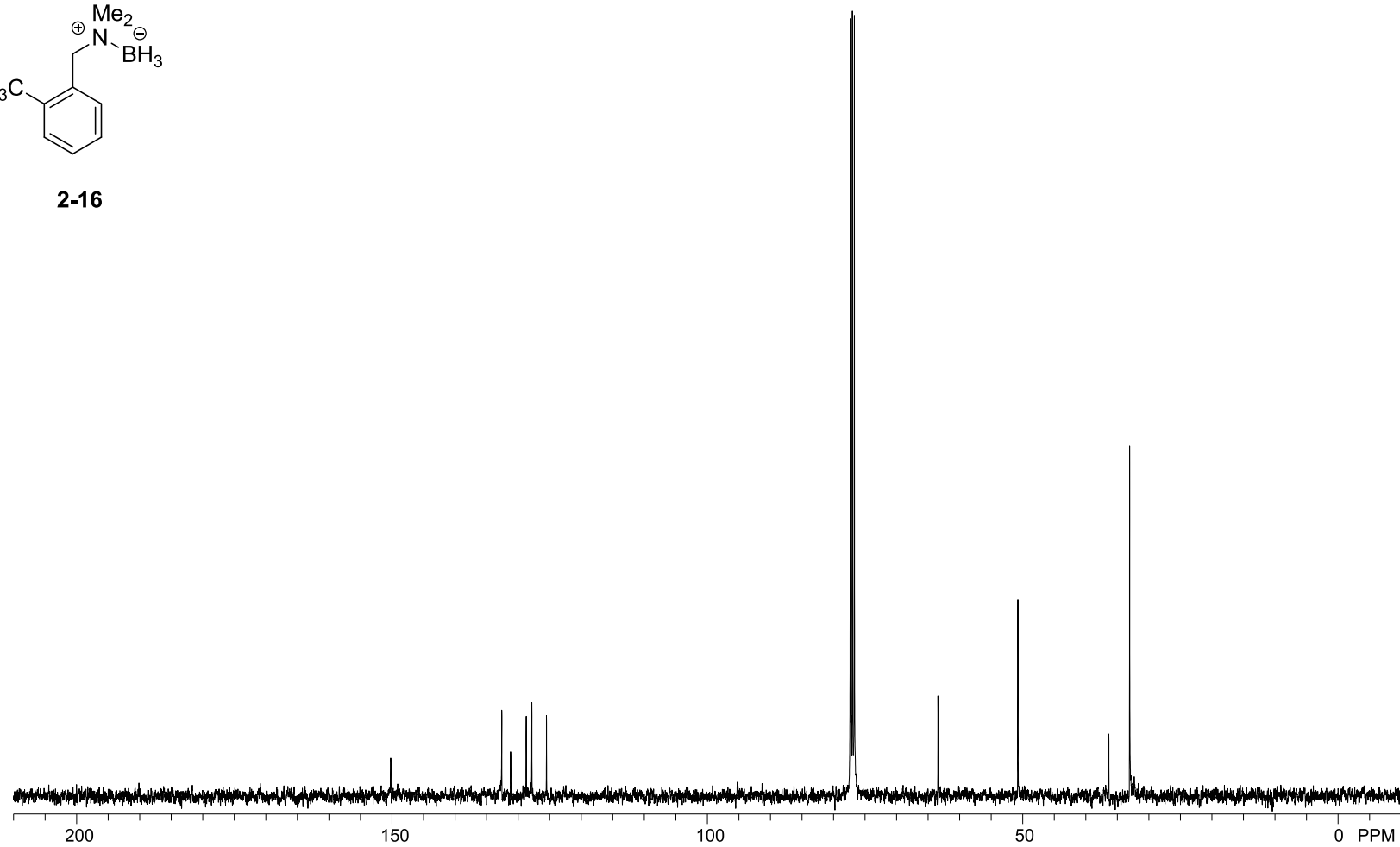
**2-16**



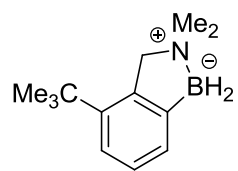
$^{13}\text{C}\{^1\text{H}\}$  NMR (101 MHz),  
 $\text{CDCl}_3$



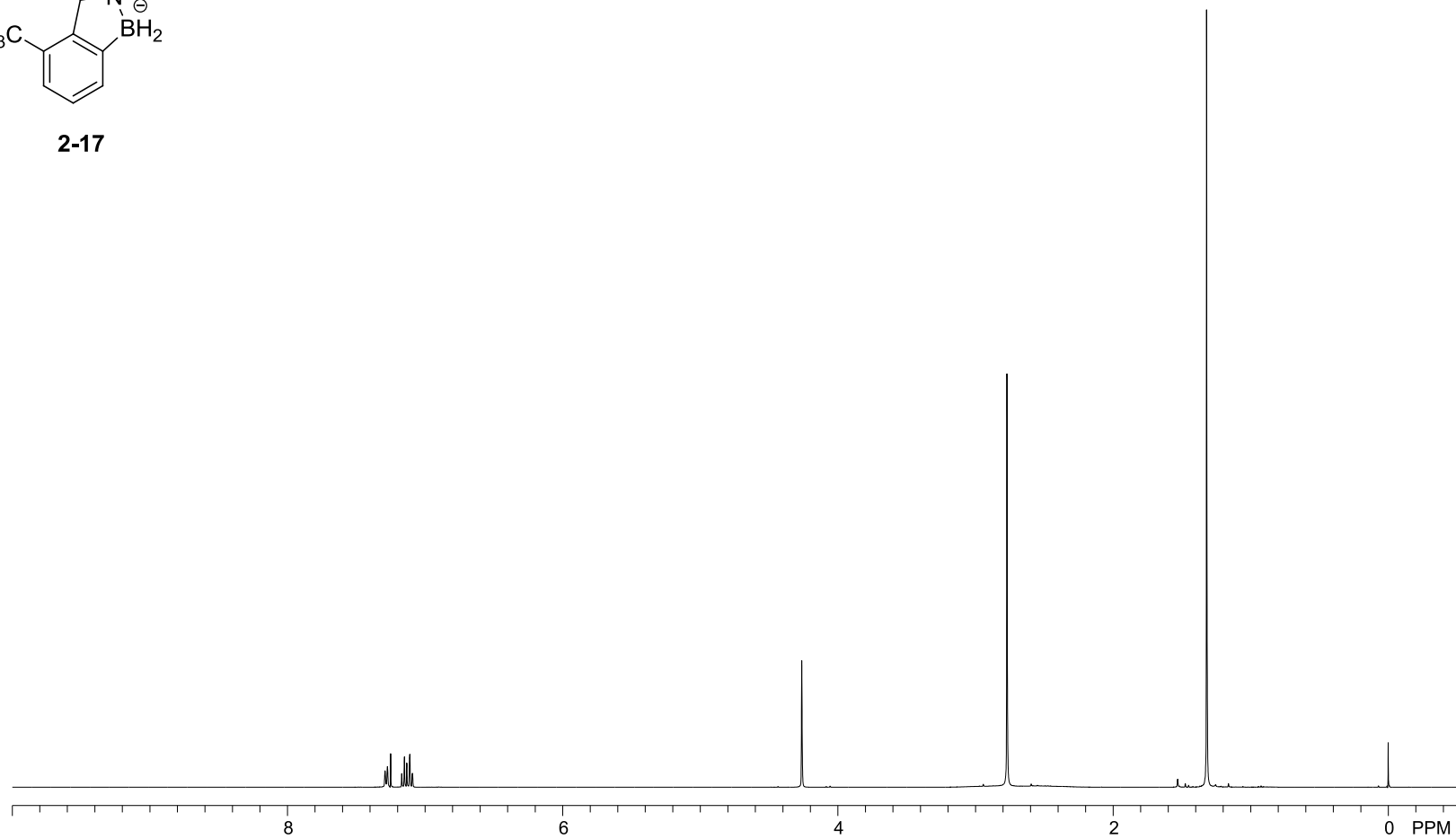
**2-16**



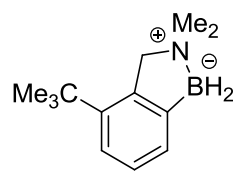
$^1\text{H}$  NMR (400 MHz),  
 $\text{CDCl}_3$



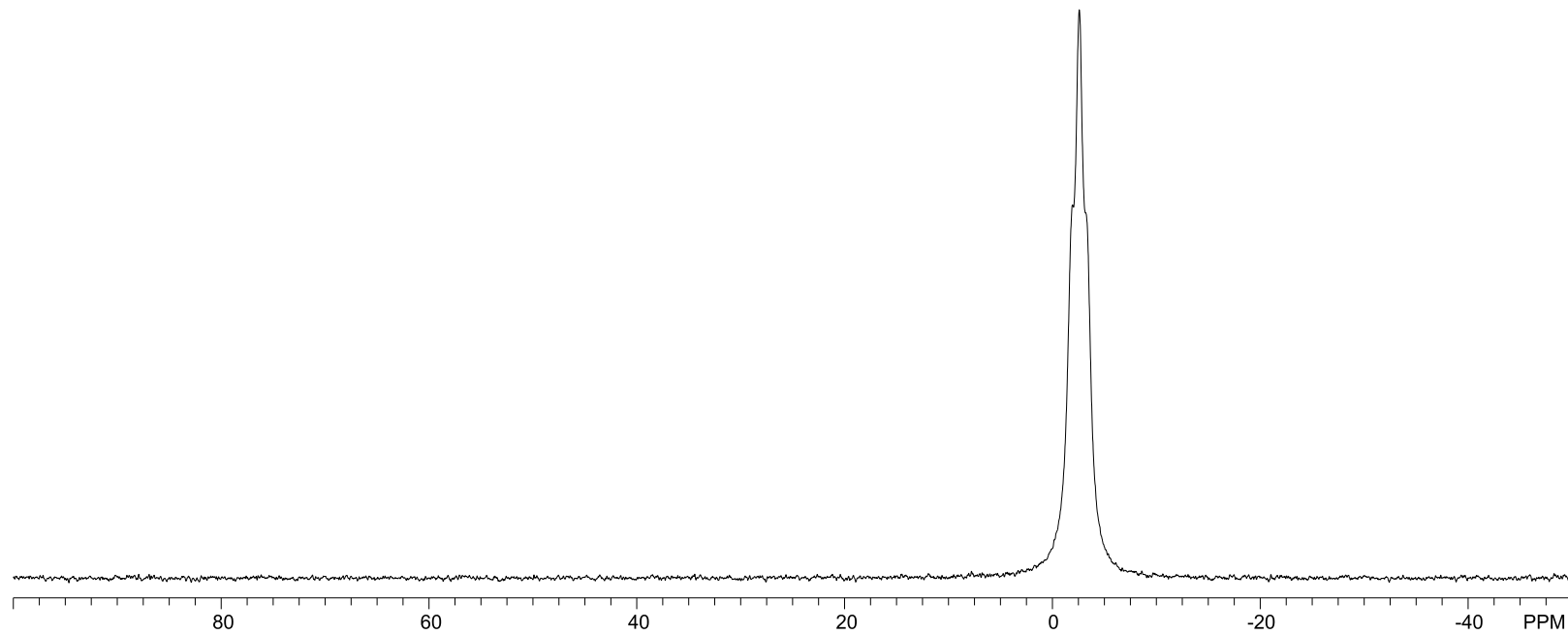
**2-17**



$^{11}\text{B}$  NMR (128 MHz),  
 $\text{CDCl}_3$

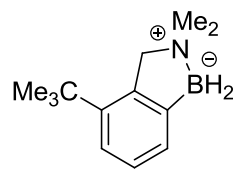


**2-17**

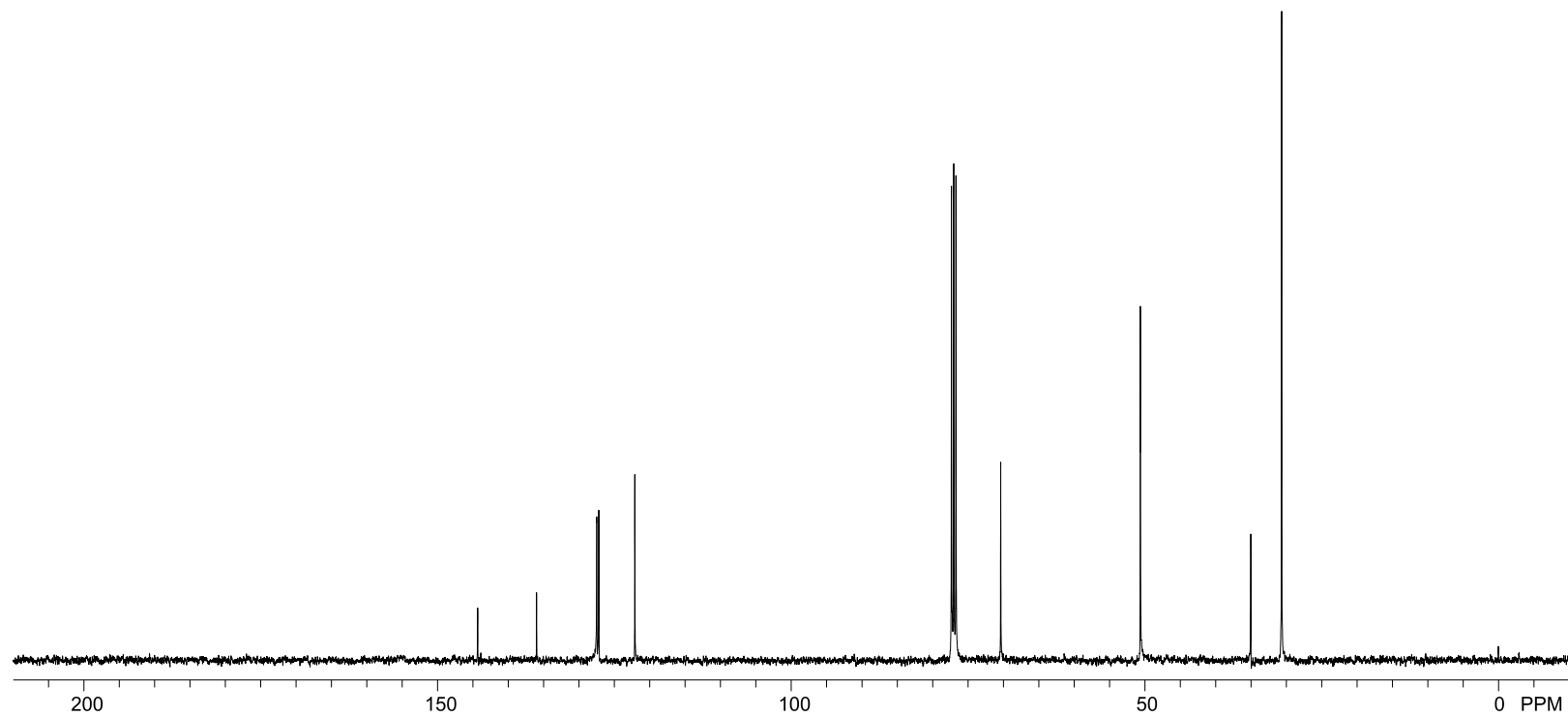




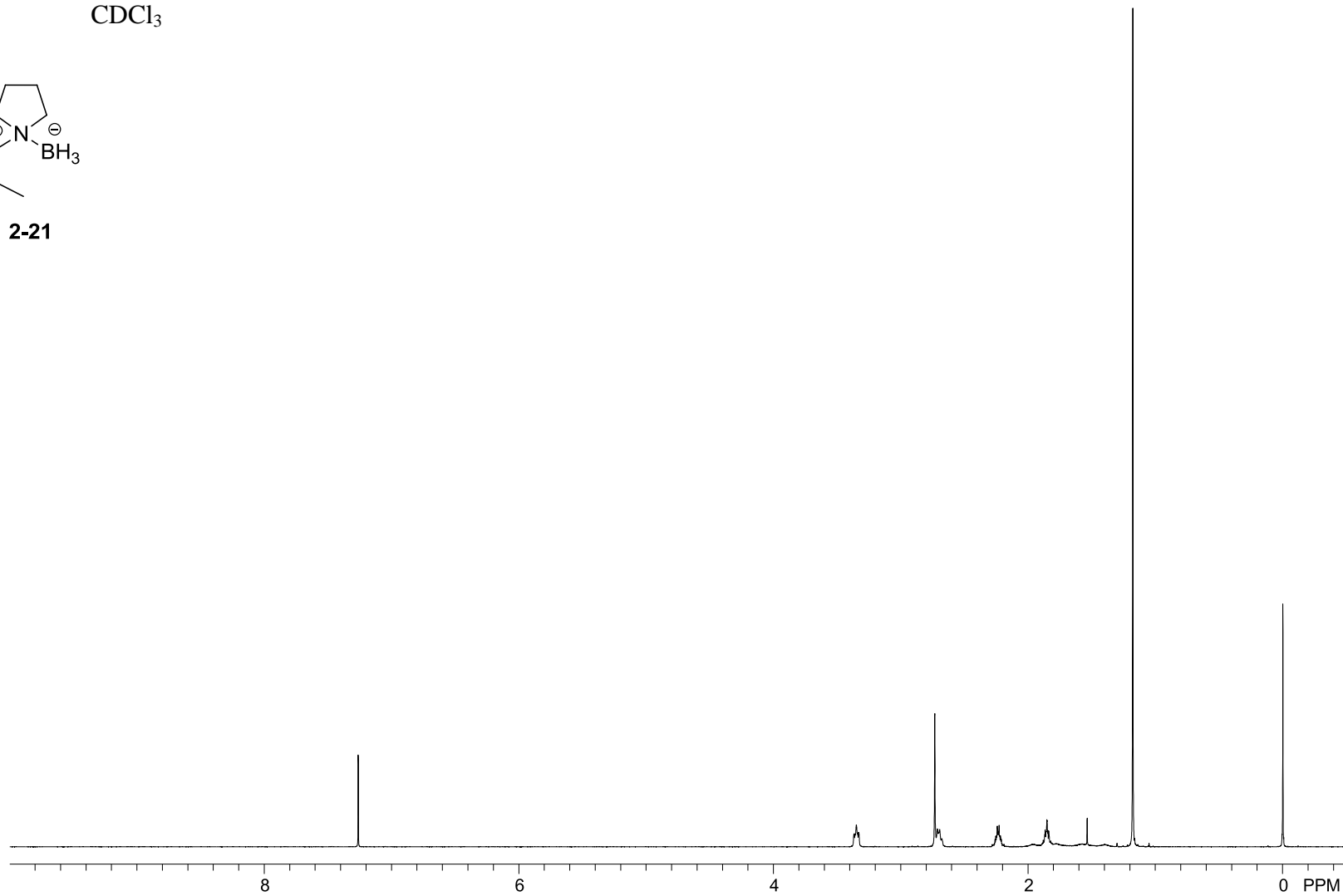
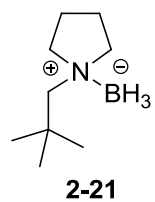
$^{13}\text{C}\{^1\text{H}\}$  NMR (101 MHz),  
 $\text{CDCl}_3$



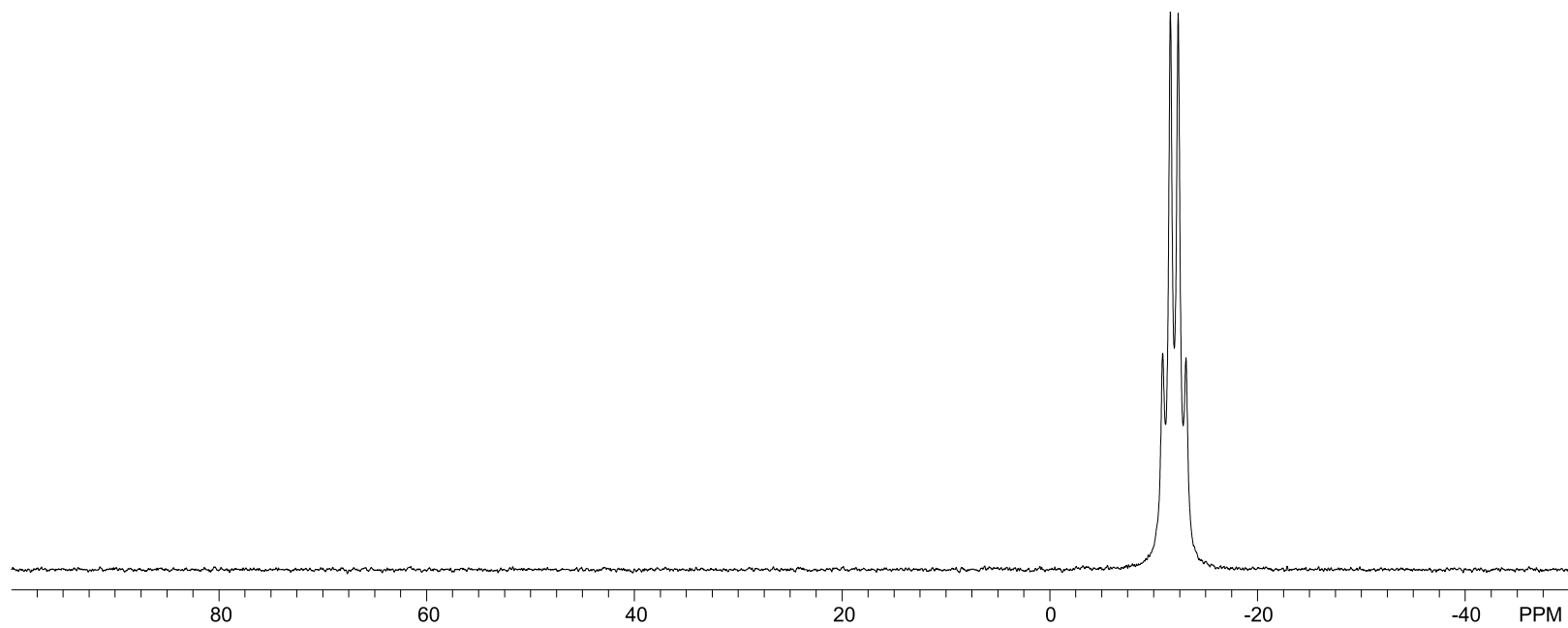
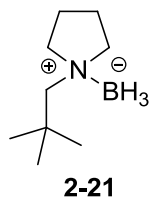
**2-17**



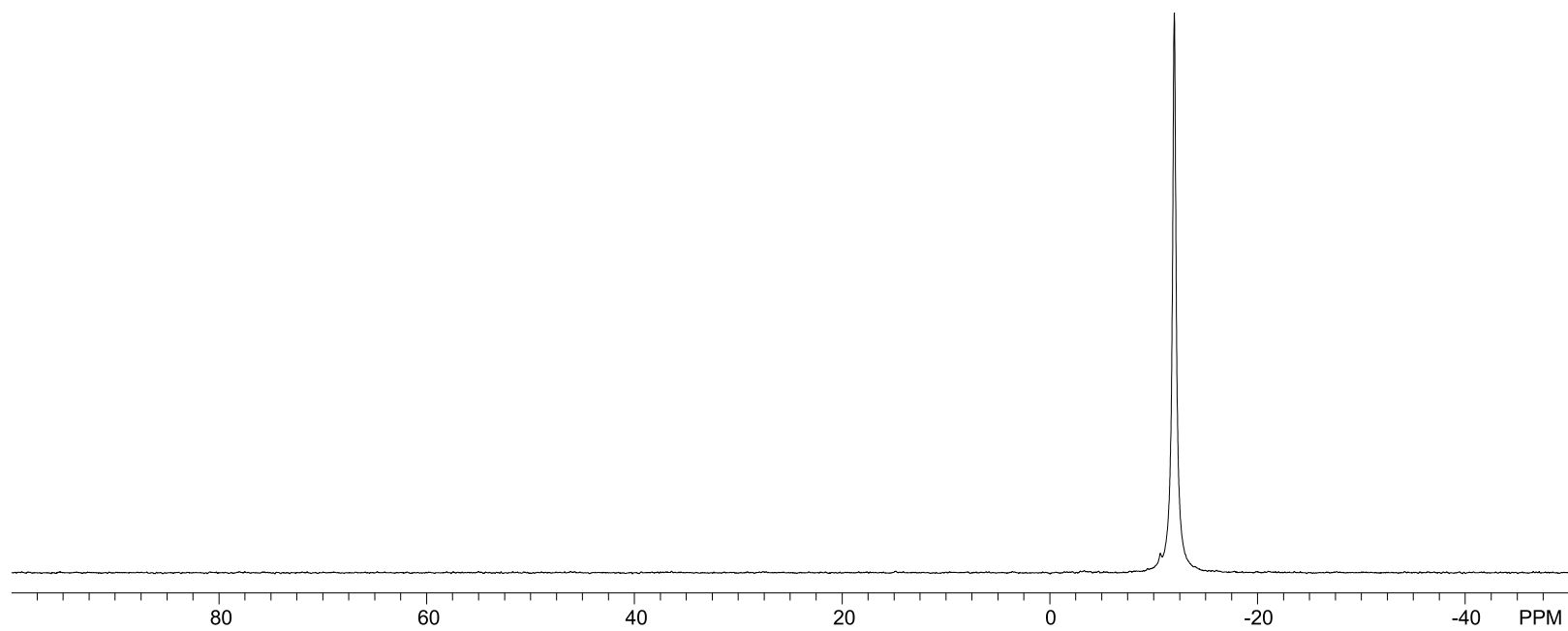
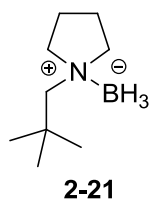
$^1\text{H}$  NMR (500 MHz),  
 $\text{CDCl}_3$



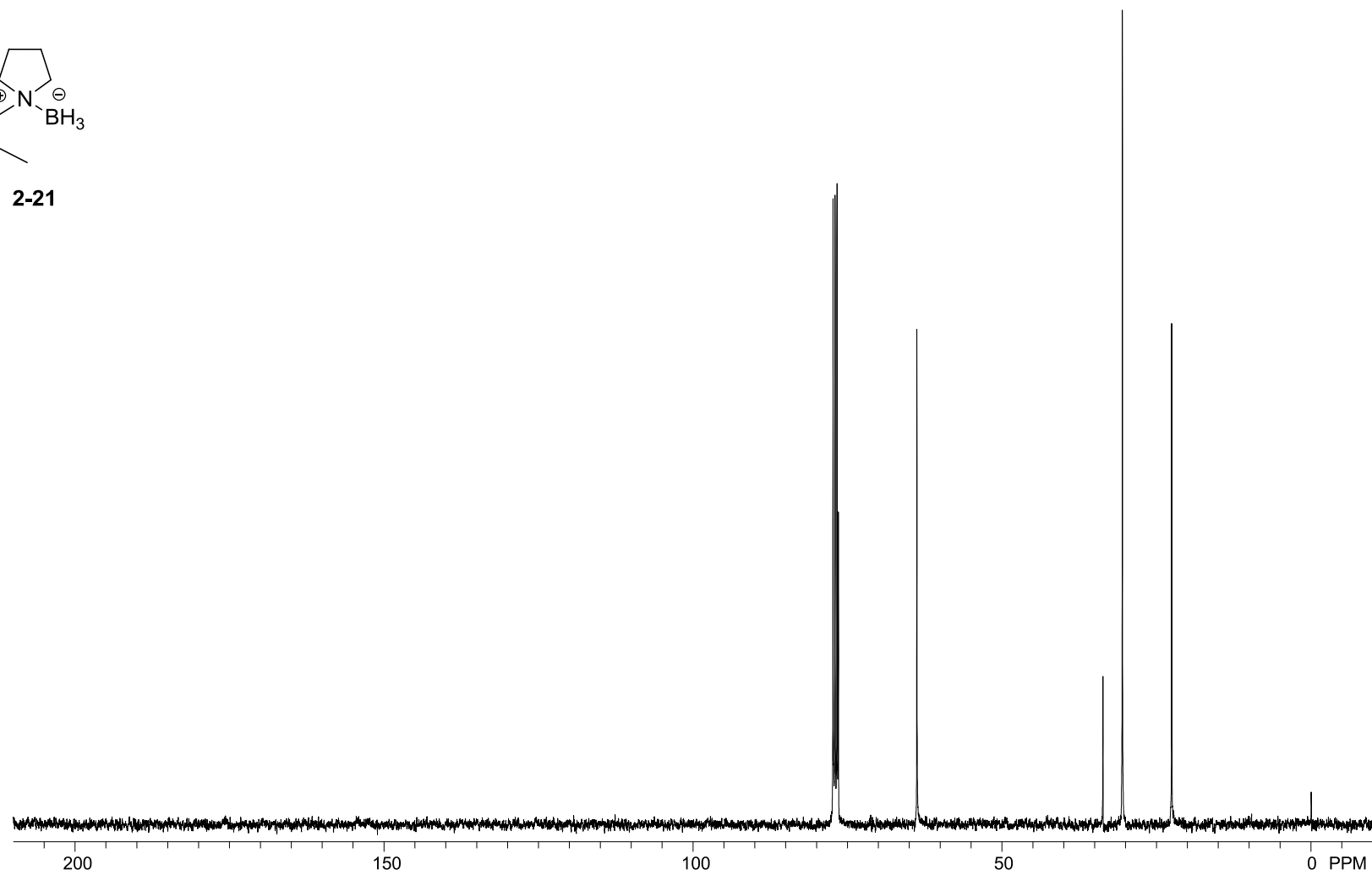
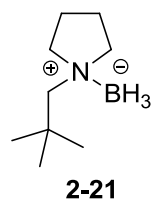
$^{11}\text{B}$  NMR (128 MHz),  
 $\text{CDCl}_3$



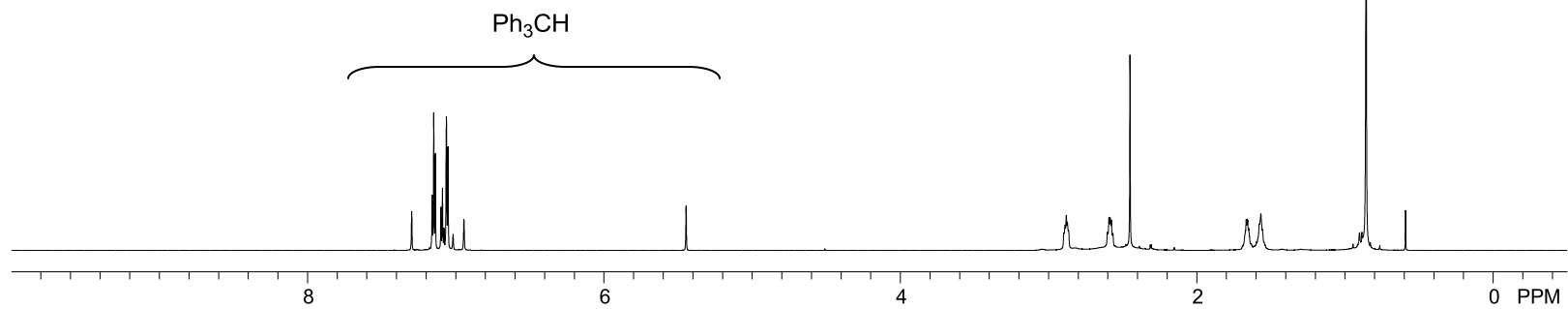
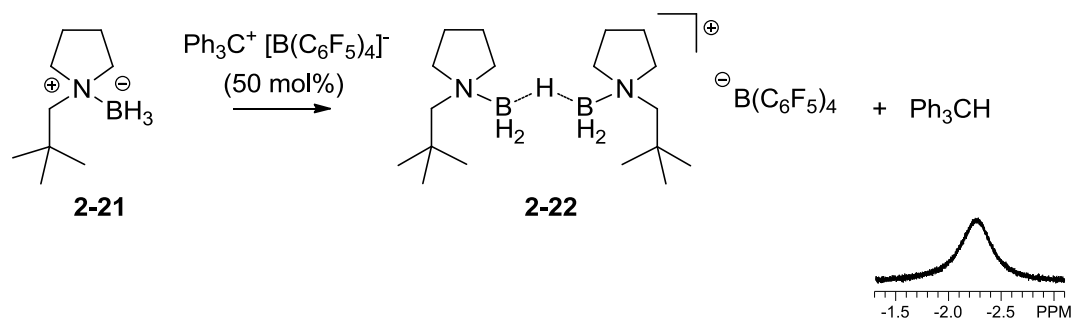
$^{11}\text{B}\{^1\text{H}\}$  NMR (128 MHz),  
 $\text{CDCl}_3$



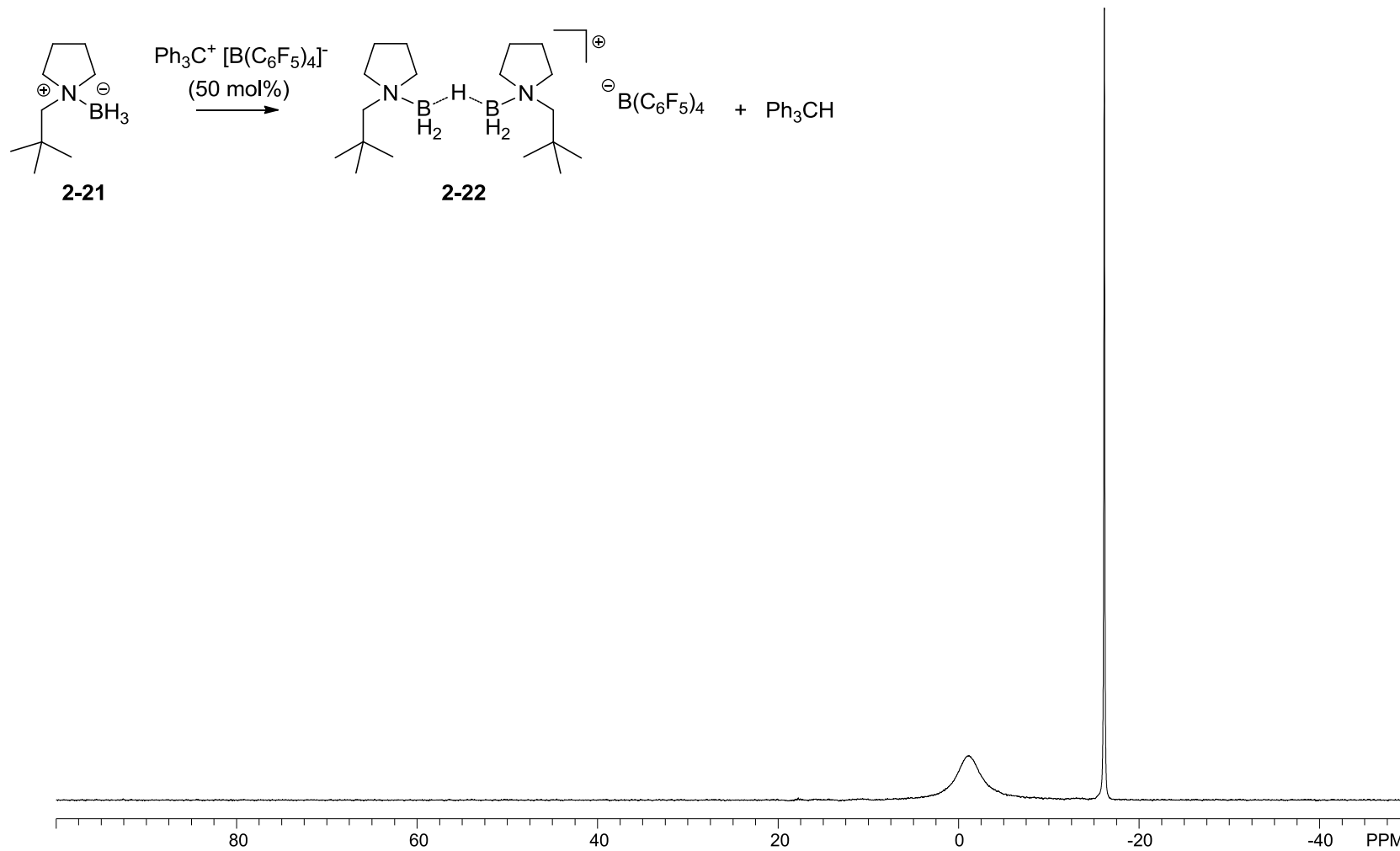
$^{13}\text{C}\{^1\text{H}\}$  NMR (101 MHz),  
 $\text{CDCl}_3$



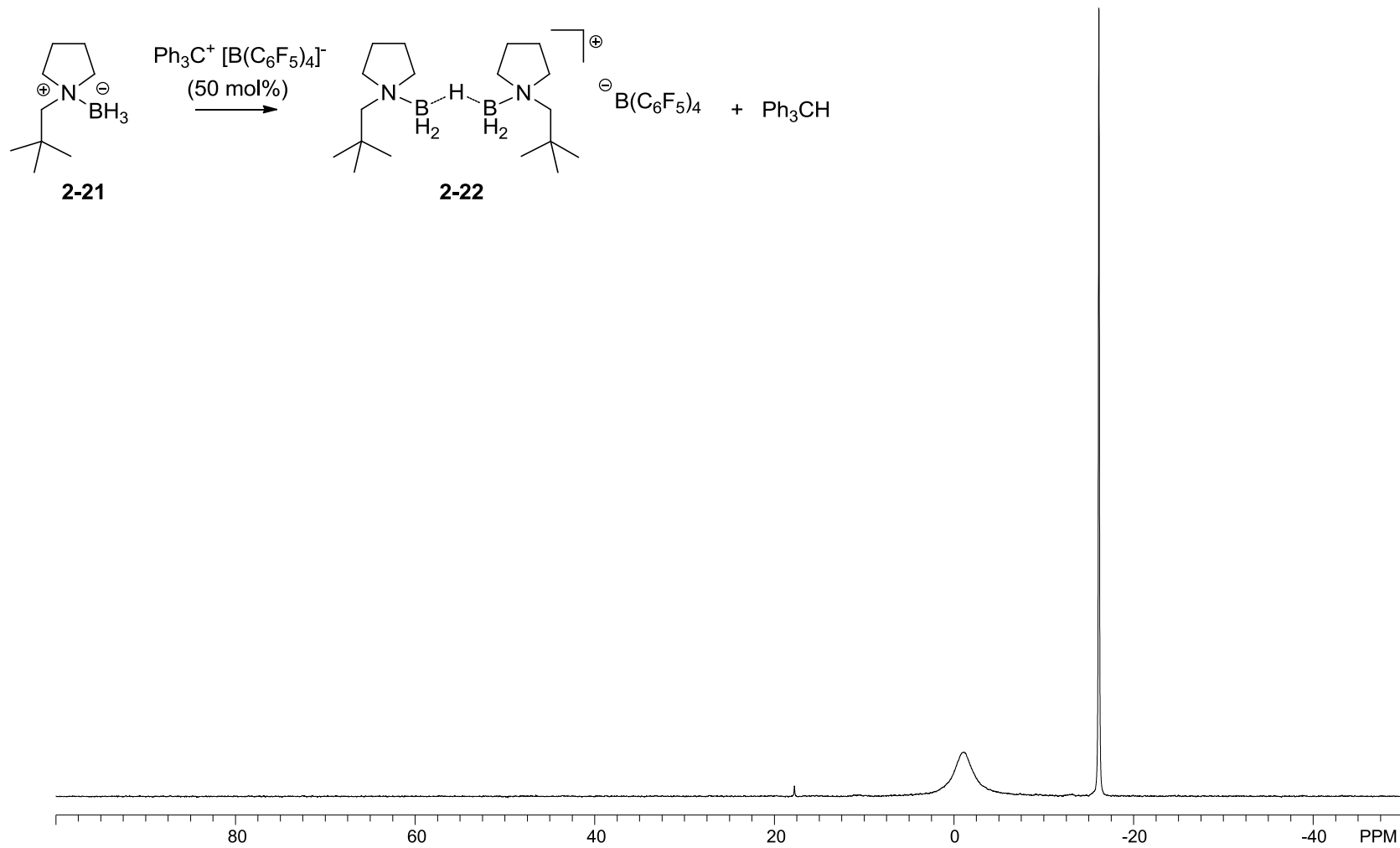
$^1\text{H}$  NMR (700 MHz),  
 $d_5\text{-PhBr}$



$^{11}\text{B}$  NMR (225 MHz),  
 $d_5\text{-PhBr}$

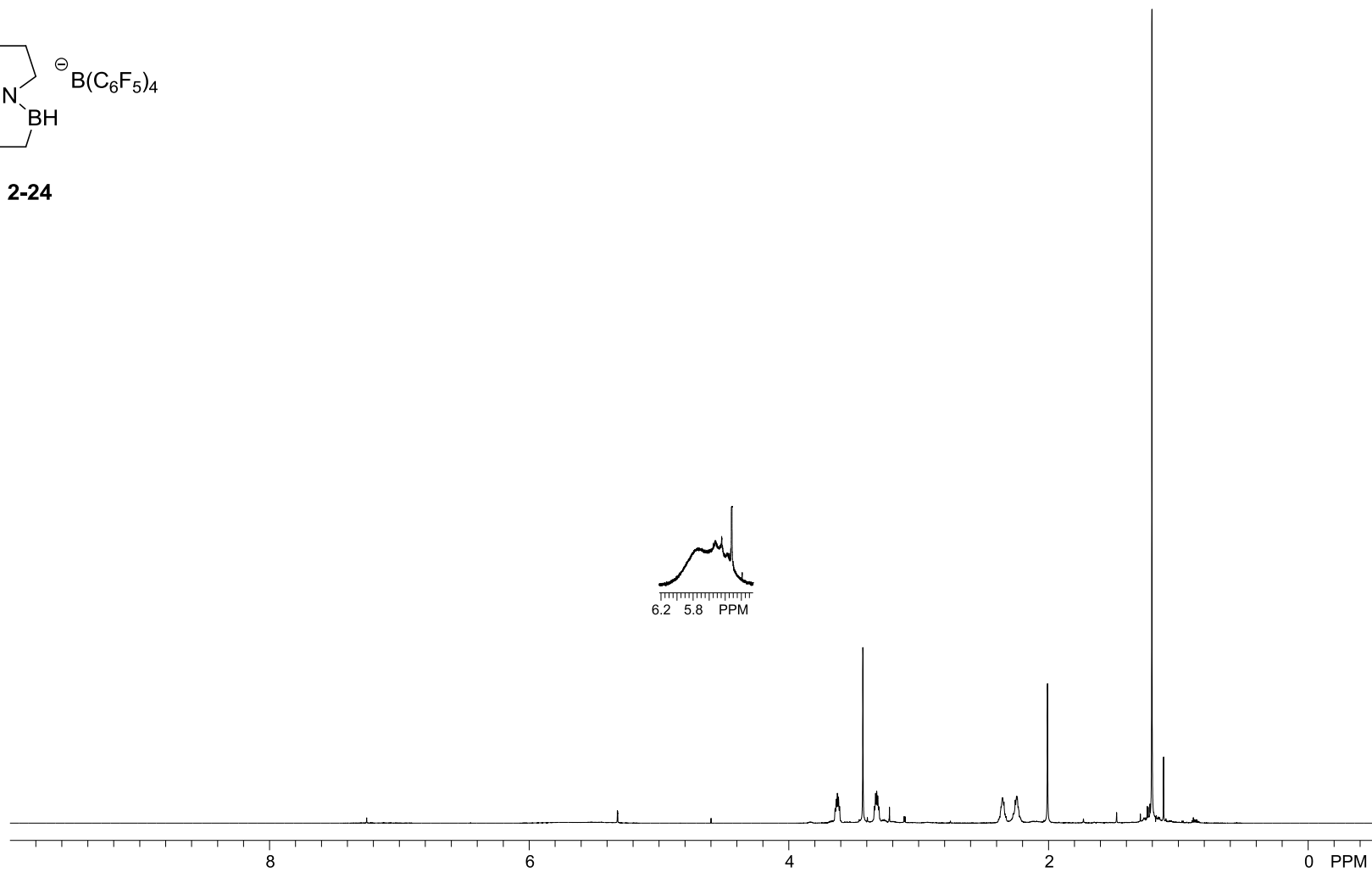
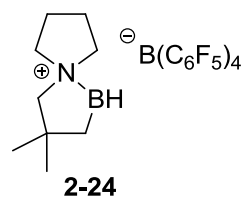


$^{11}\text{B}\{^1\text{H}\}$  NMR (225 MHz),  
 $d_5\text{-PhBr}$

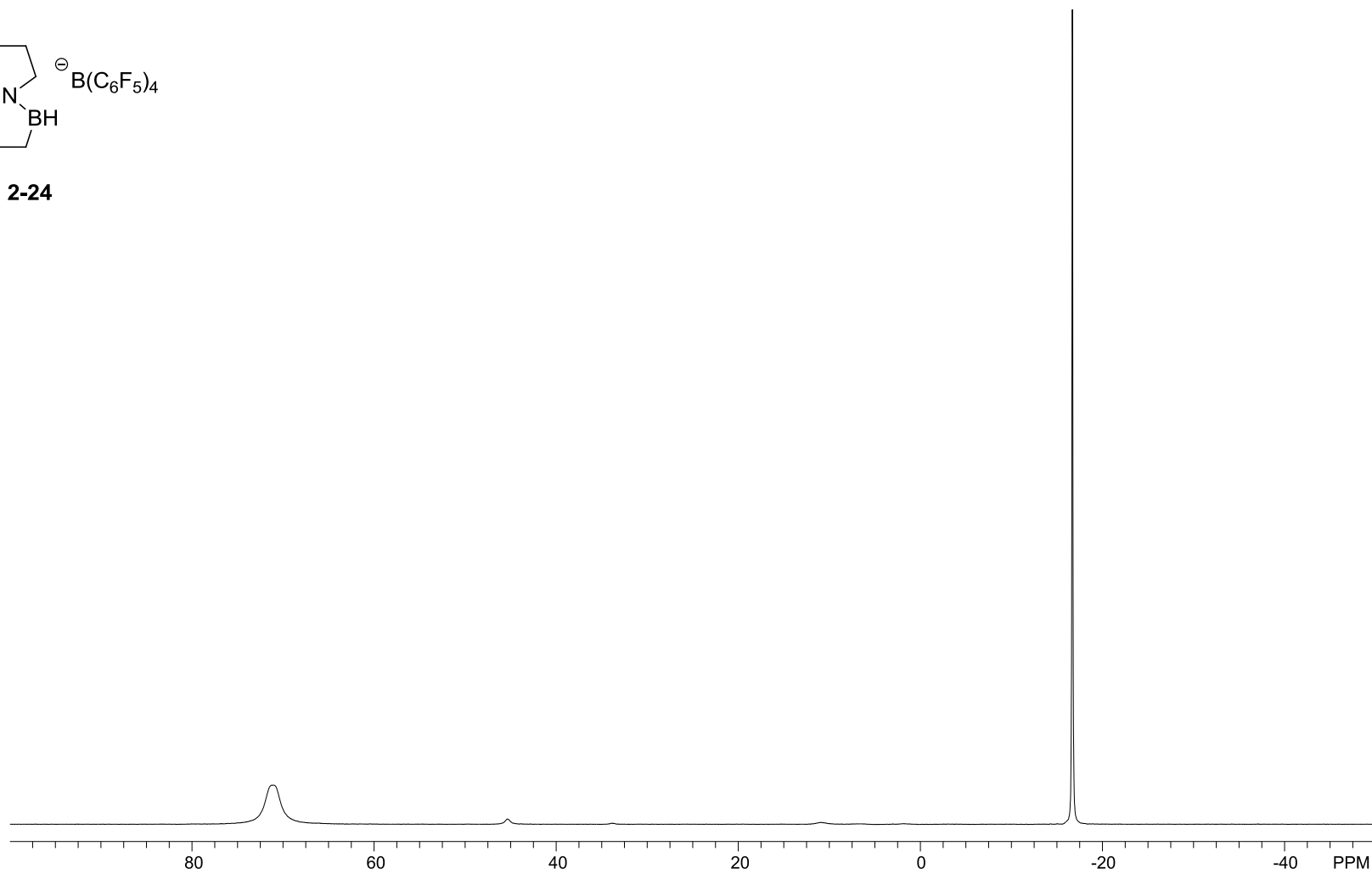
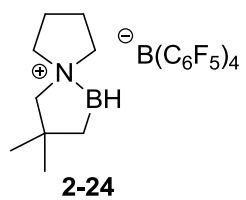




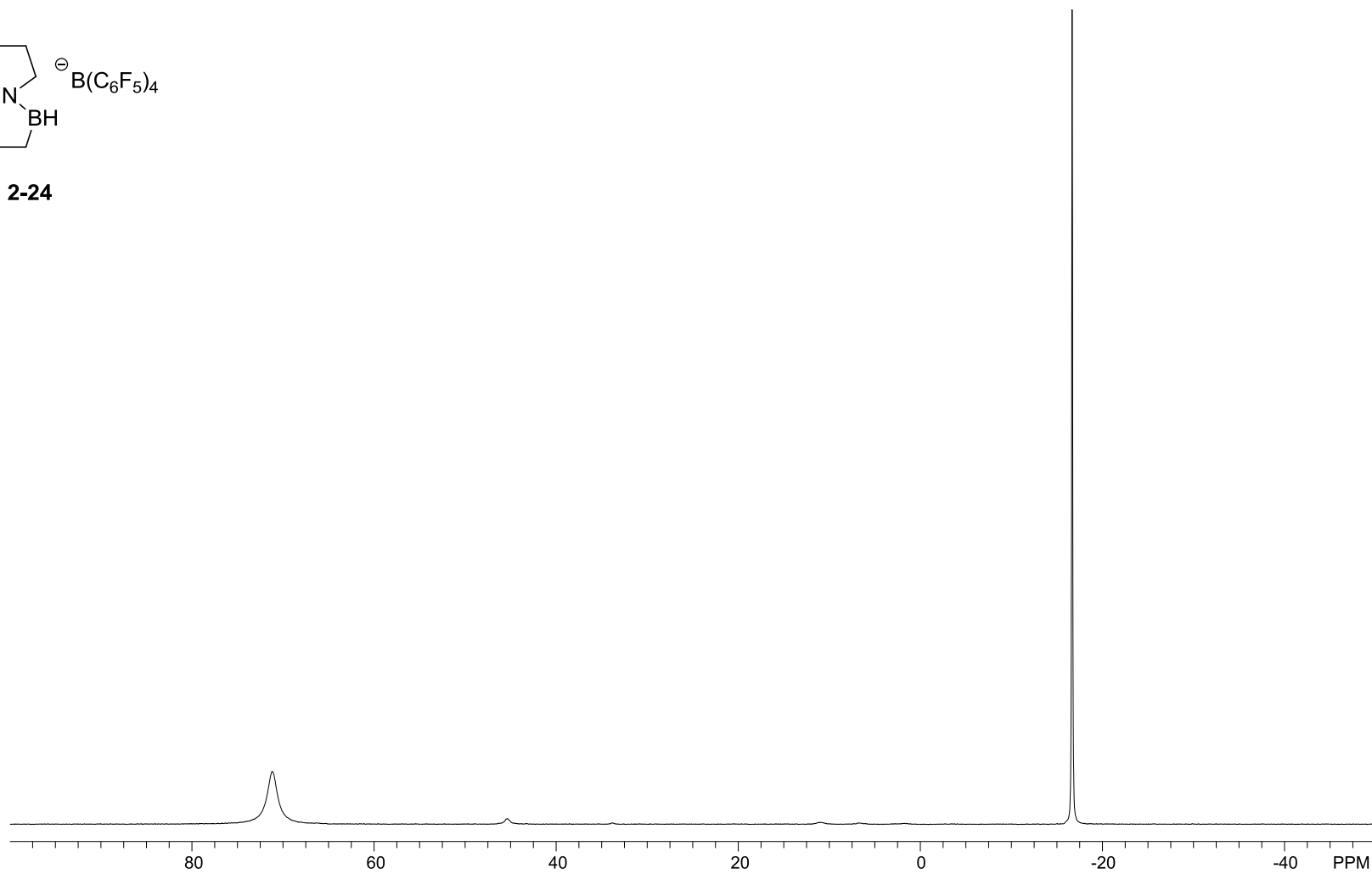
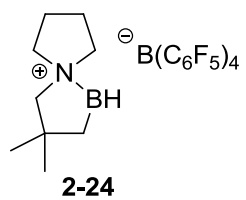
$^1\text{H}$  NMR (700 MHz),  
 $\text{CD}_2\text{Cl}_2$



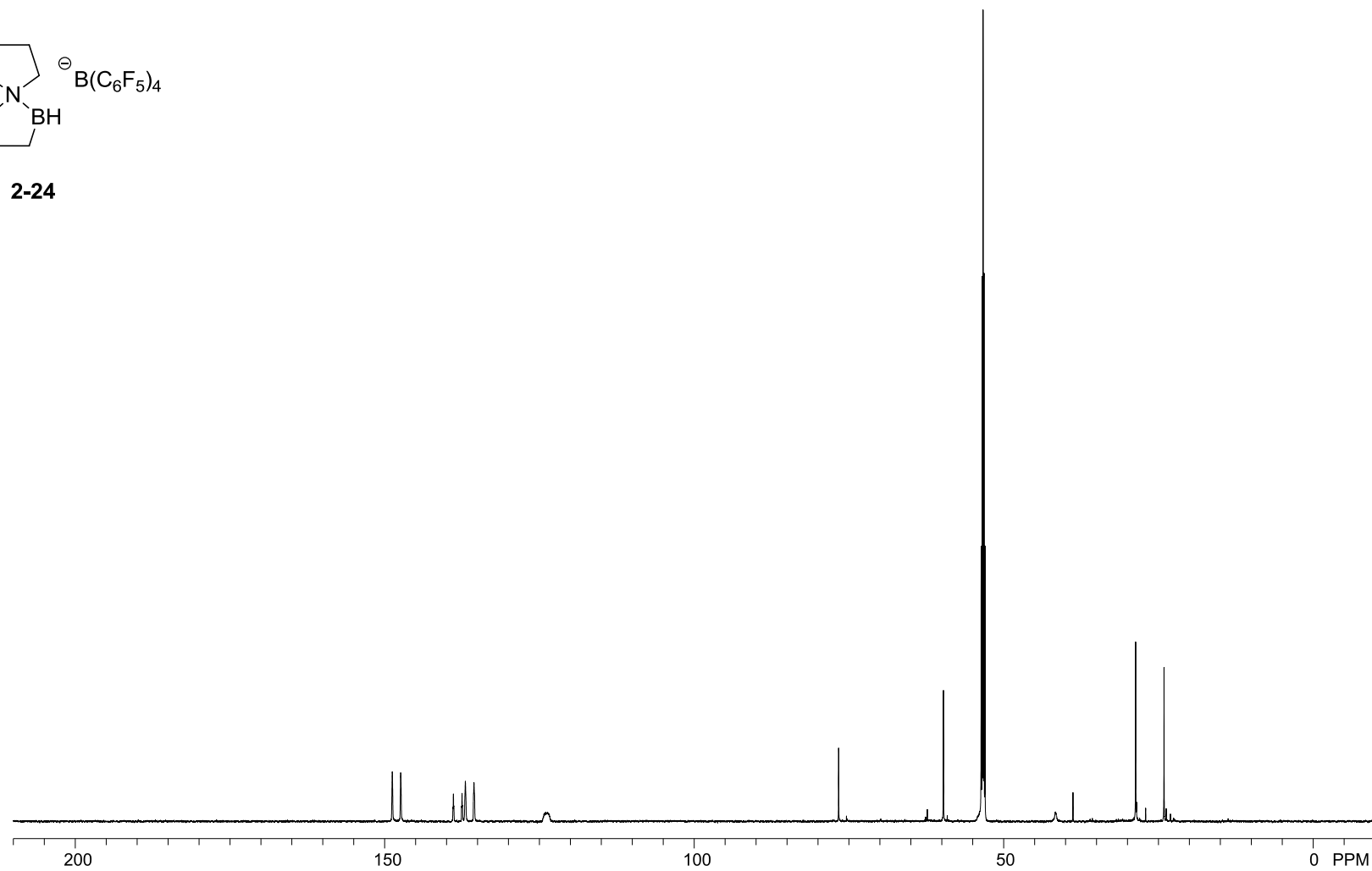
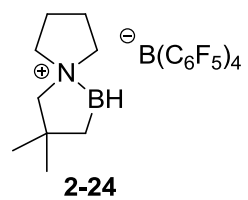
$^{11}\text{B}$  NMR (225 MHz),  
 $\text{CD}_2\text{Cl}_2$



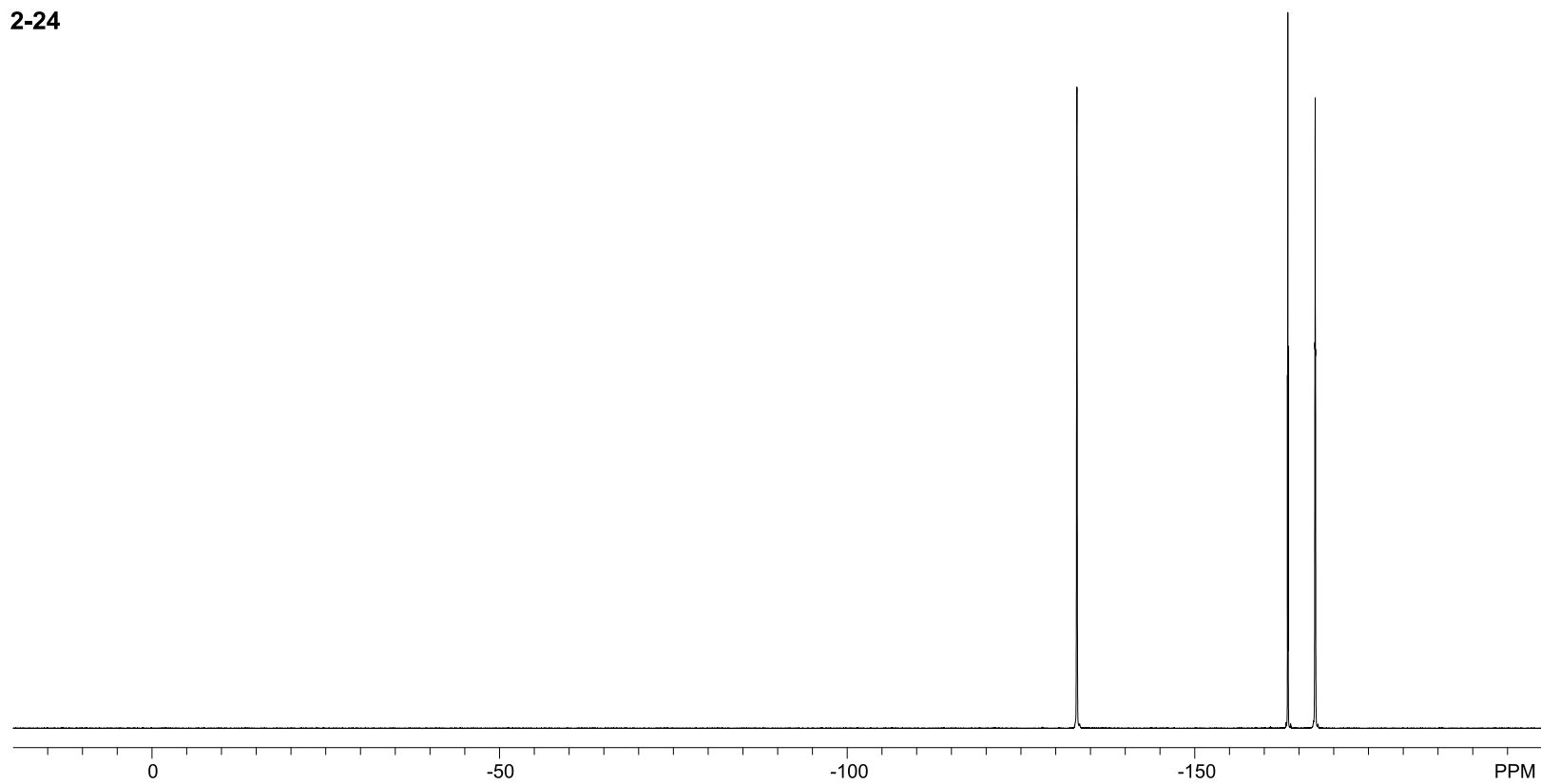
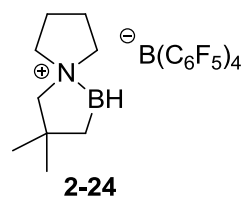
$^{11}\text{B}\{^1\text{H}\}$  NMR (225 MHz),  
 $\text{CD}_2\text{Cl}_2$



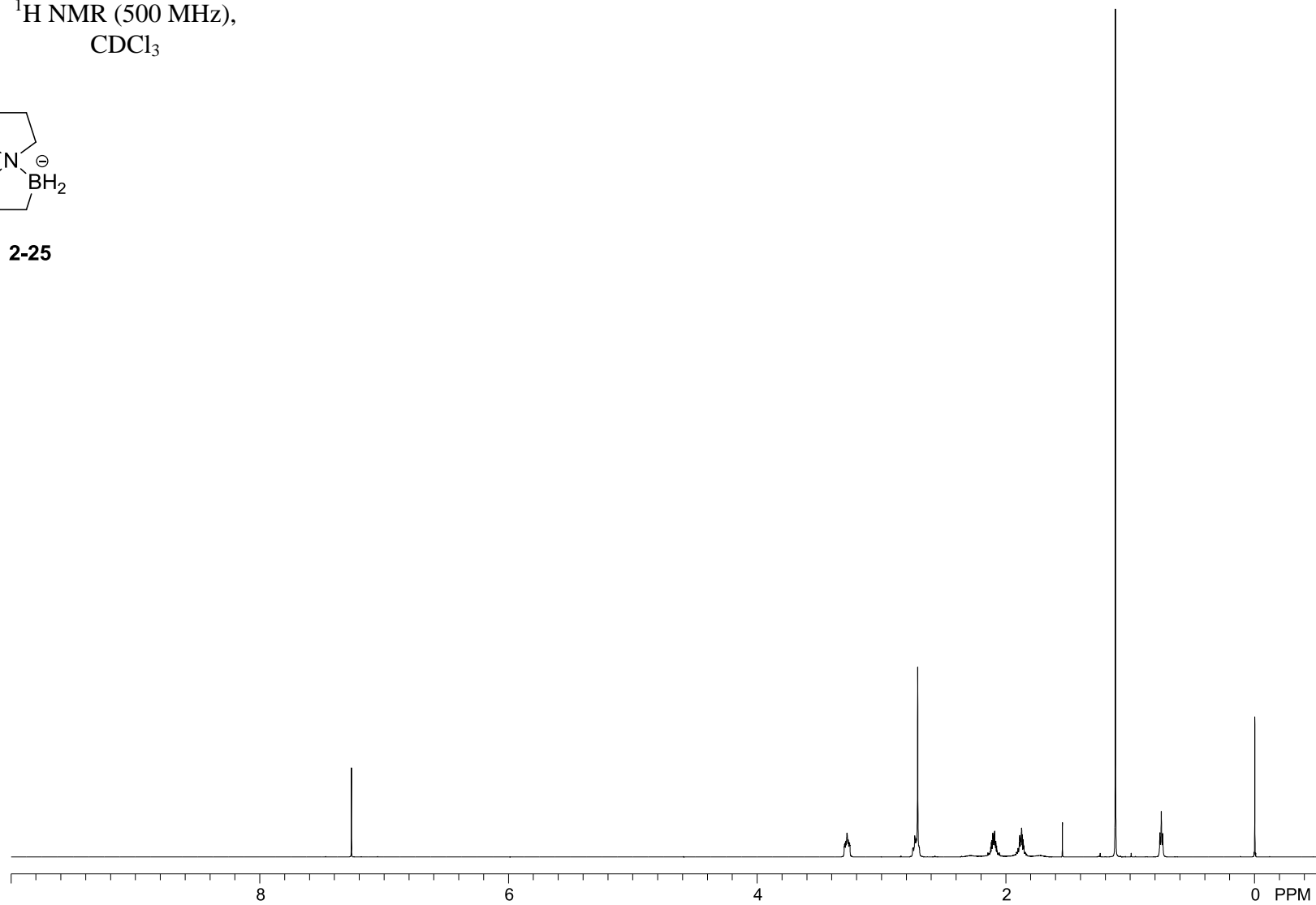
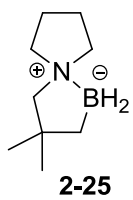
$^{13}\text{C}\{^1\text{H}\}$  NMR (176 MHz),  
 $\text{CD}_2\text{Cl}_2$



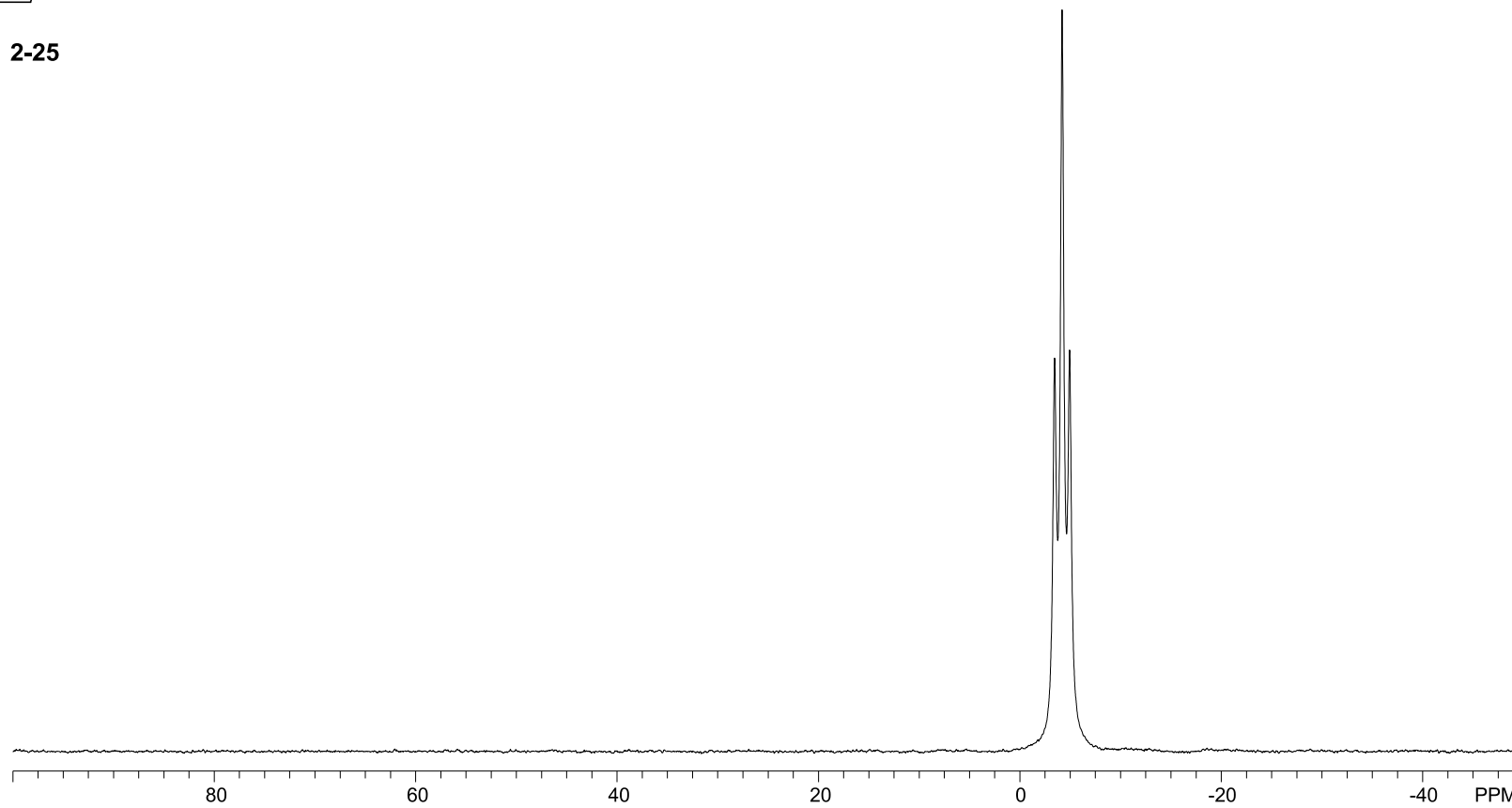
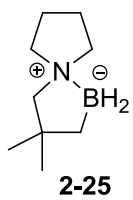
$^{19}\text{F}$  NMR (377 MHz),  
 $\text{CD}_2\text{Cl}_2$



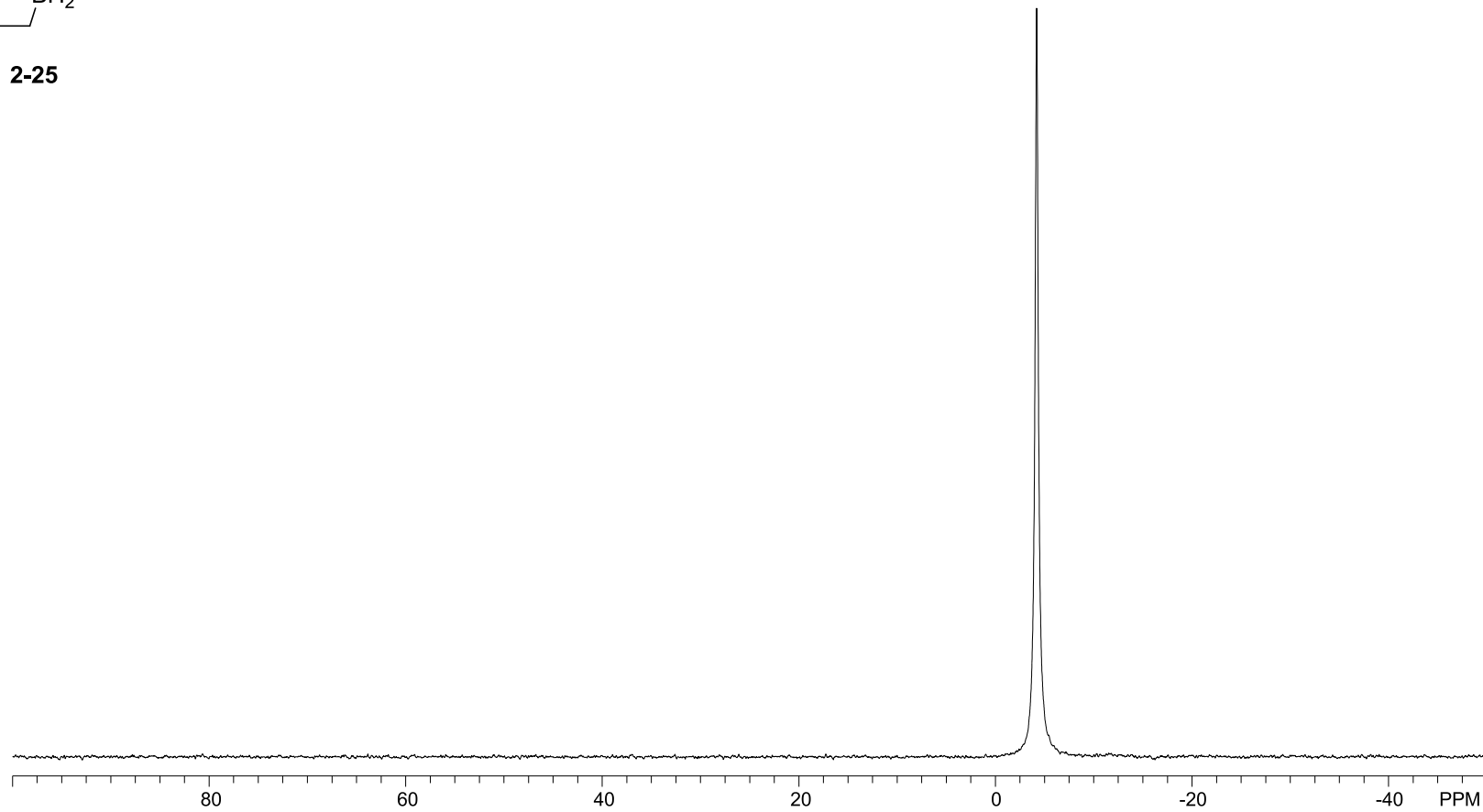
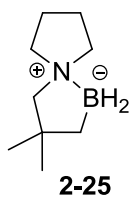
$^1\text{H}$  NMR (500 MHz),  
 $\text{CDCl}_3$



$^{11}\text{B}$  NMR (128 MHz),  
 $\text{CDCl}_3$

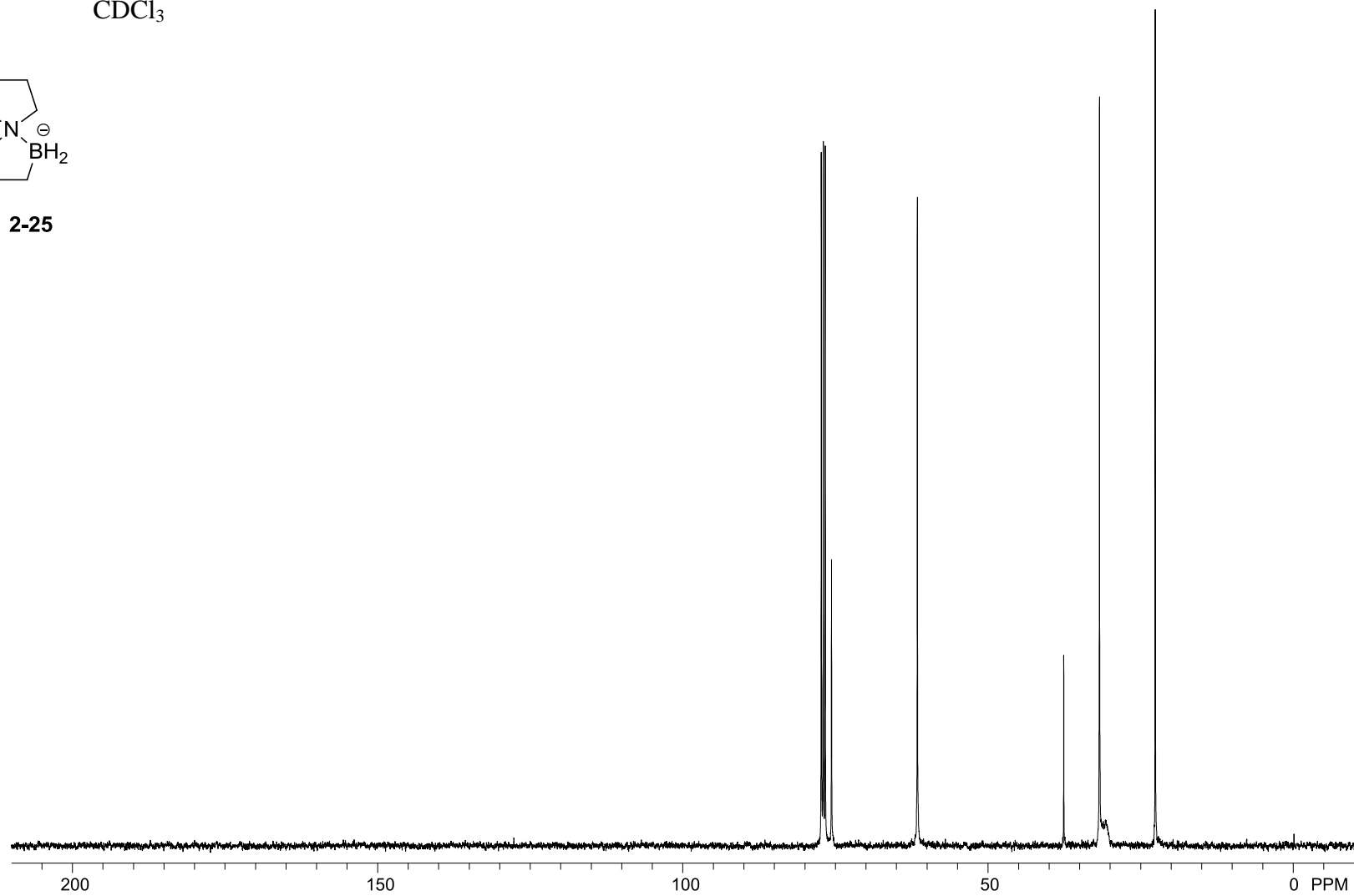
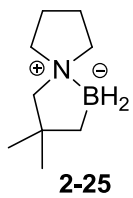


$^{11}\text{B}\{^1\text{H}\}$  NMR (128 MHz),  
 $\text{CDCl}_3$

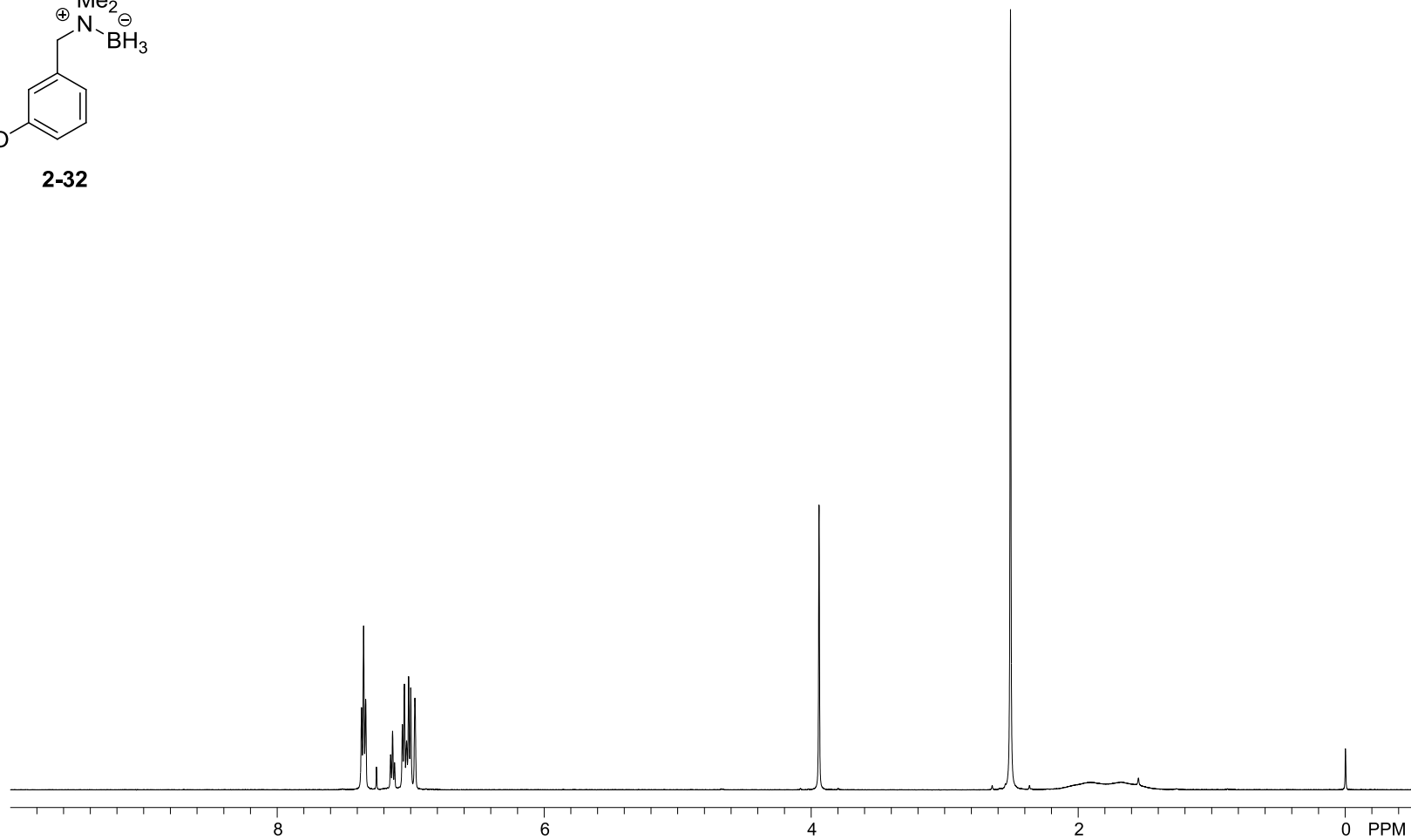
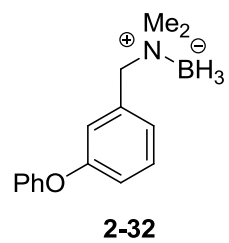




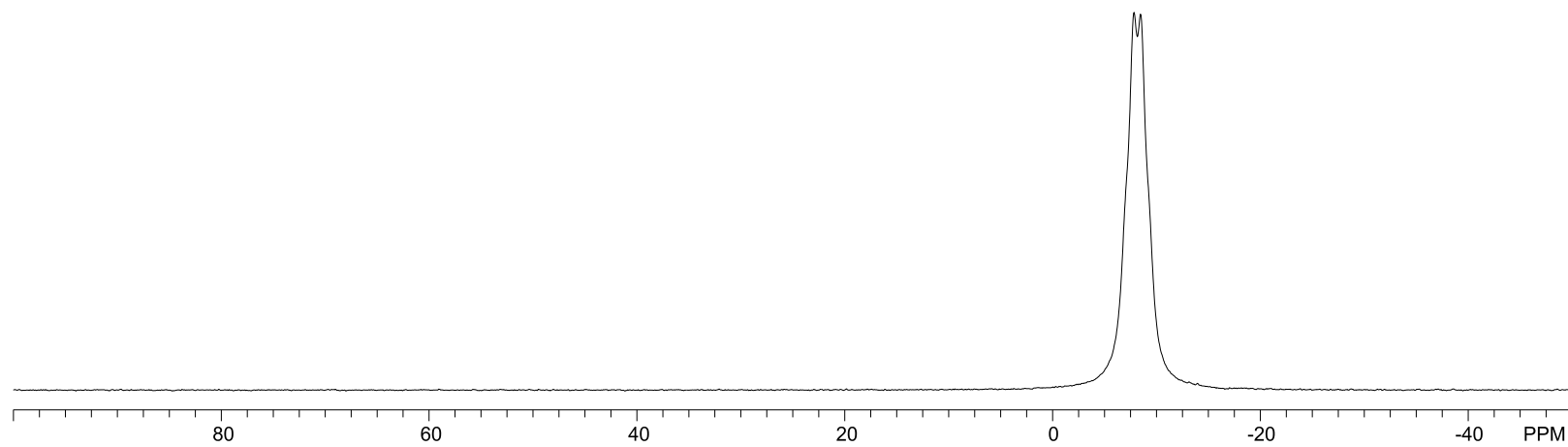
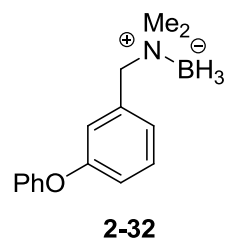
$^{13}\text{C}\{^1\text{H}\}$  NMR (101 MHz),  
 $\text{CDCl}_3$



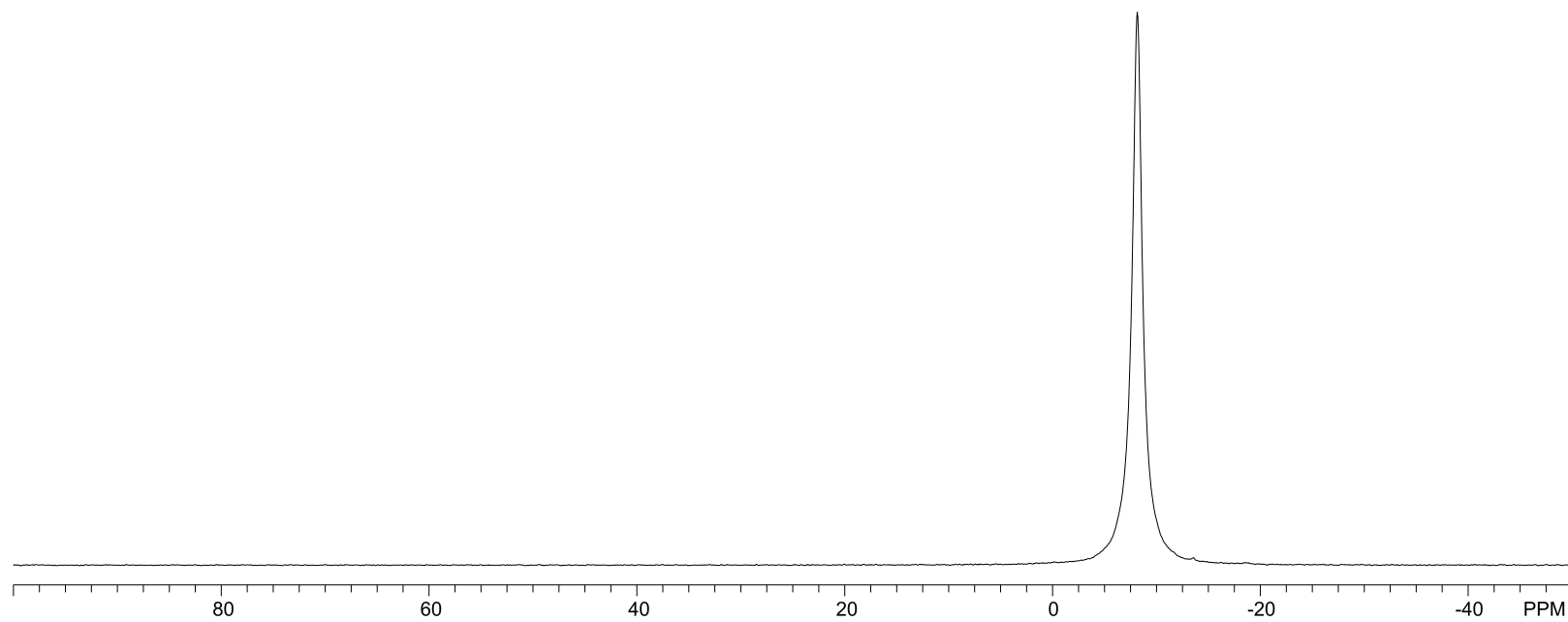
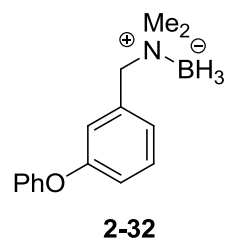
$^1\text{H}$  NMR (500 MHz),  
 $\text{CDCl}_3$



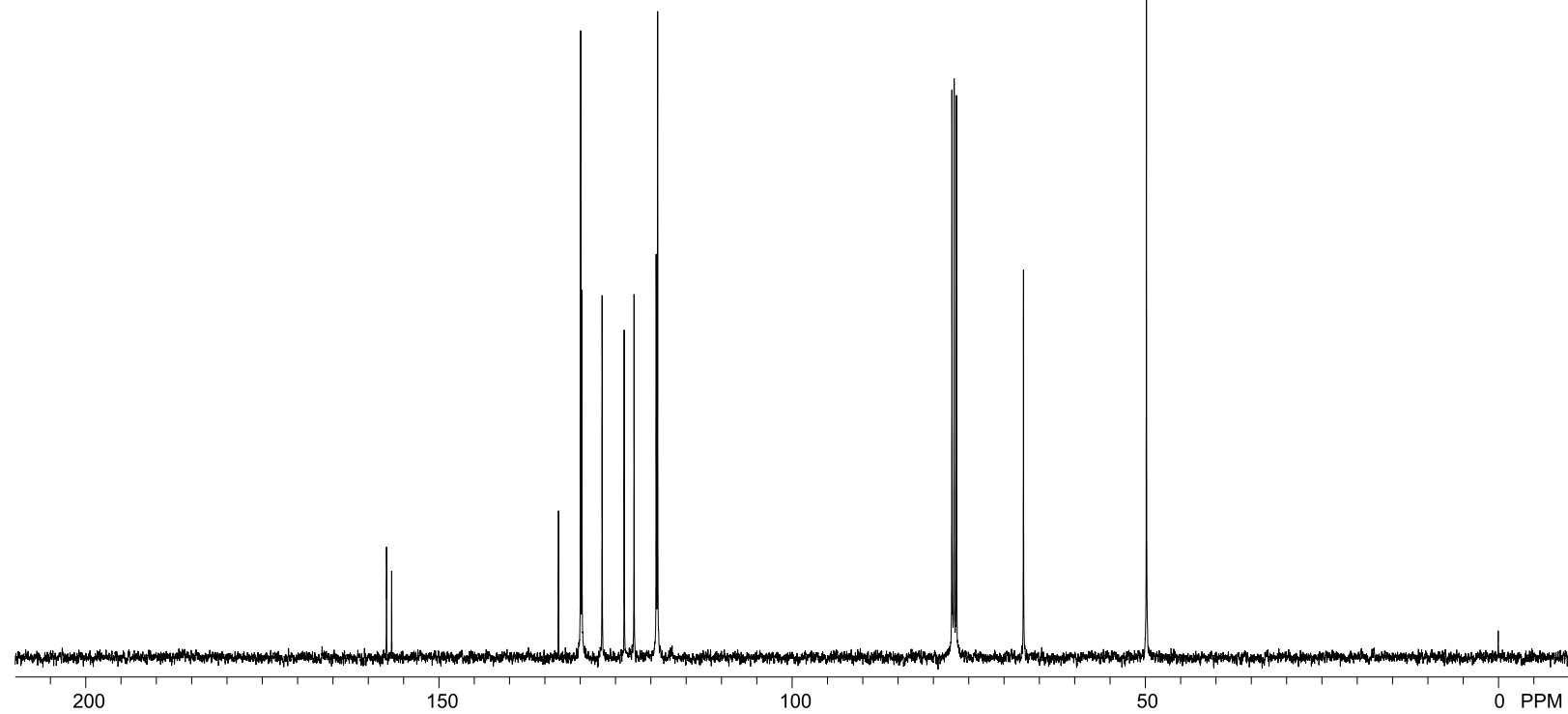
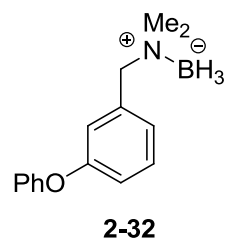
$^{11}\text{B}$  NMR (128 MHz),  
 $\text{CDCl}_3$



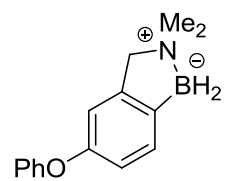
$^{11}\text{B}\{^1\text{H}\}$  NMR (128 MHz),  
 $\text{CDCl}_3$



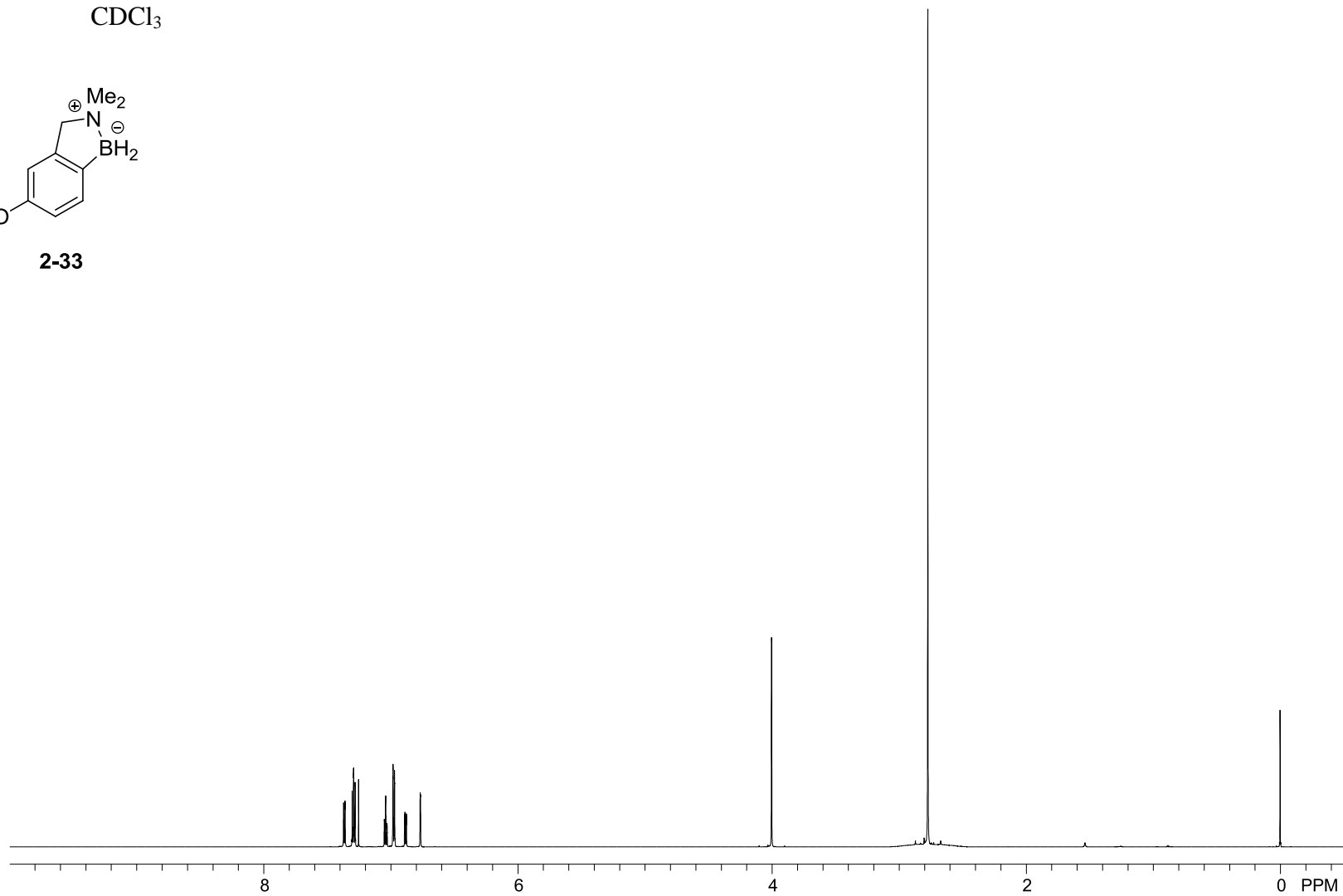
$^{13}\text{C}\{^1\text{H}\}$  NMR (101 MHz),  
 $\text{CDCl}_3$



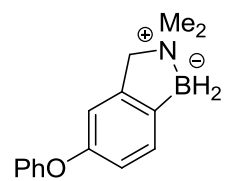
$^1\text{H}$  NMR (700 MHz),  
 $\text{CDCl}_3$



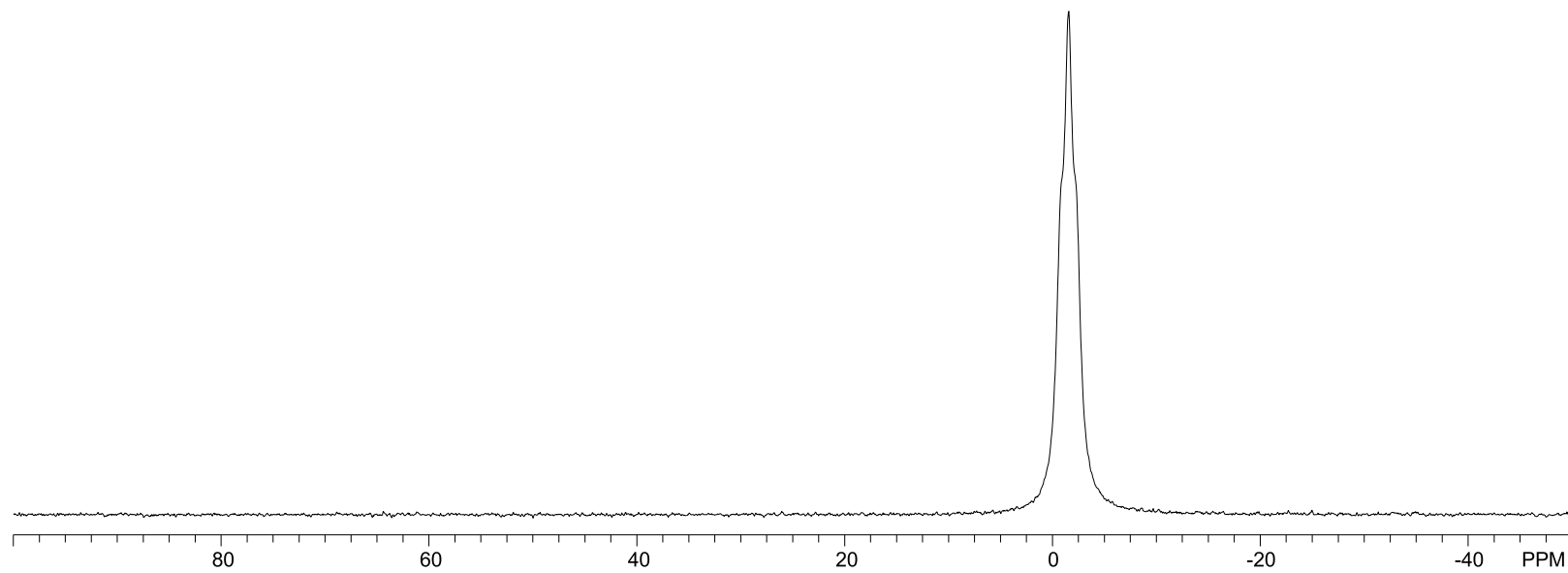
2-33



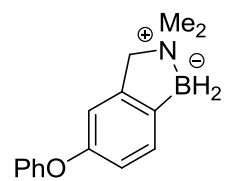
$^{11}\text{B}$  NMR (128 MHz),  
 $\text{CDCl}_3$



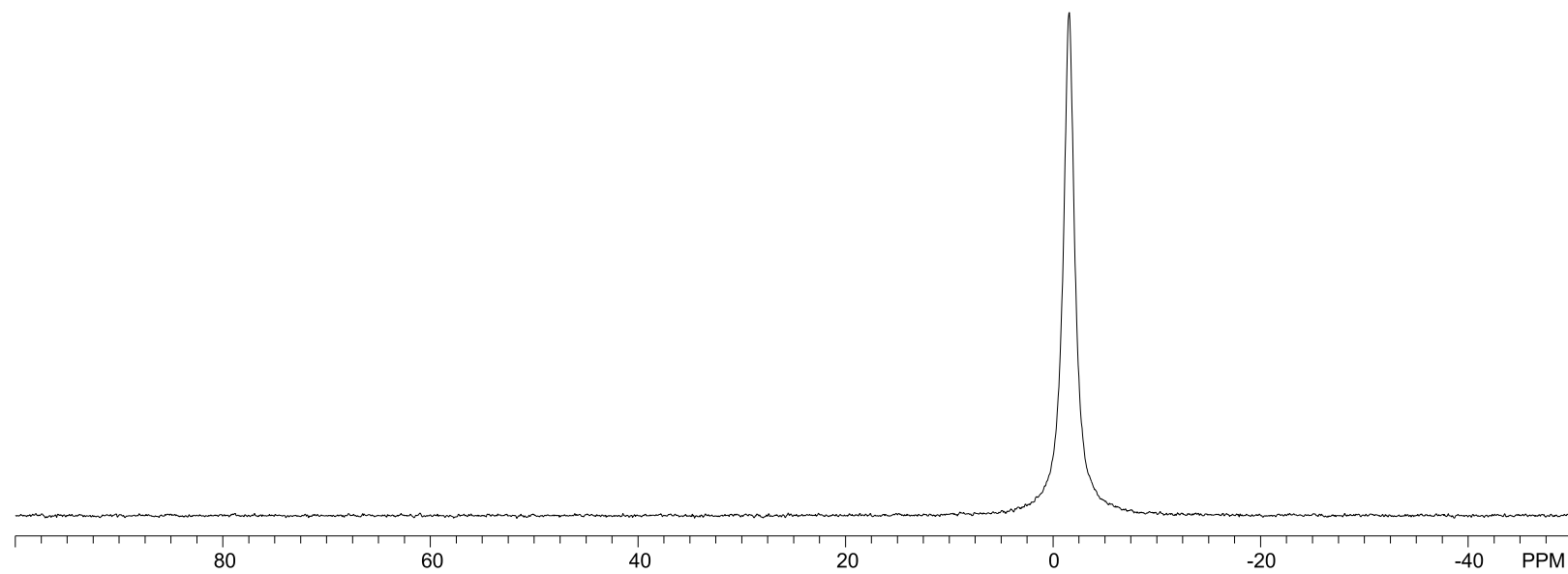
**2-33**



$^{11}\text{B}\{^1\text{H}\}$  NMR (128 MHz),  
 $\text{CDCl}_3$

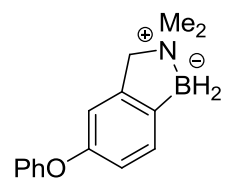


**2-33**

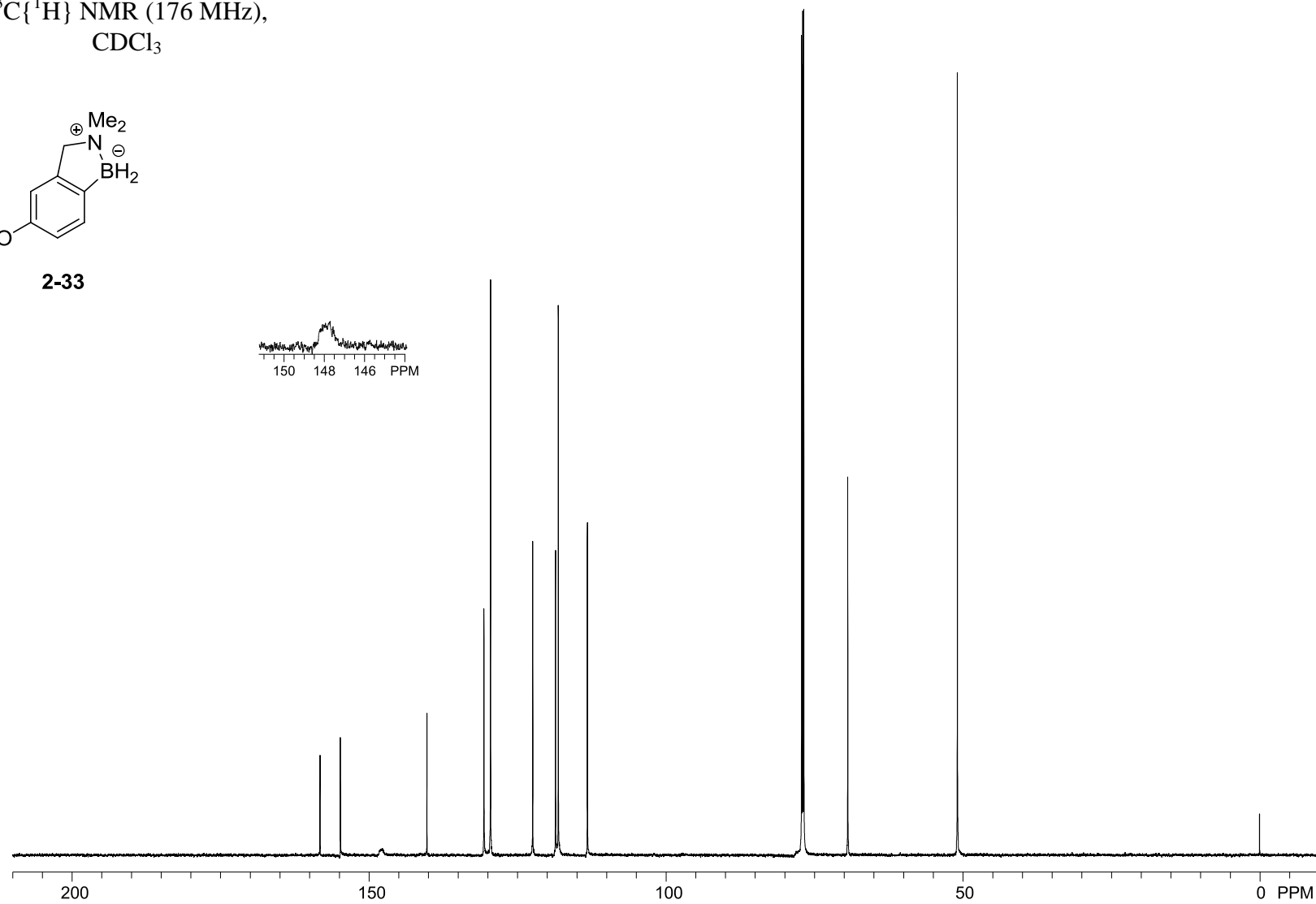




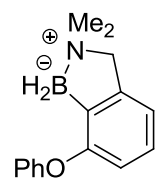
$^{13}\text{C}\{^1\text{H}\}$  NMR (176 MHz),  
 $\text{CDCl}_3$



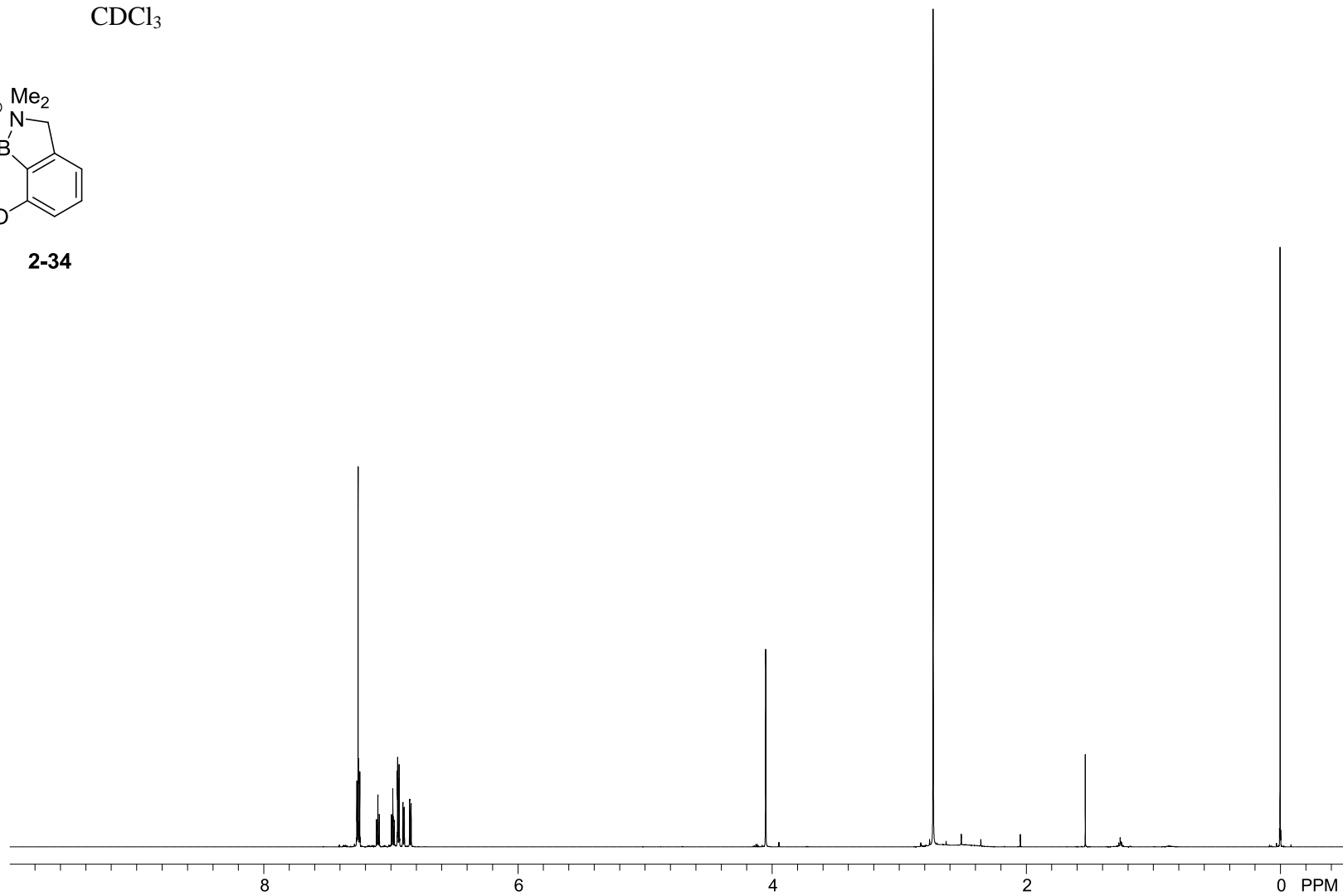
**2-33**



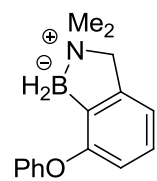
$^1\text{H}$  NMR (700 MHz),  
 $\text{CDCl}_3$



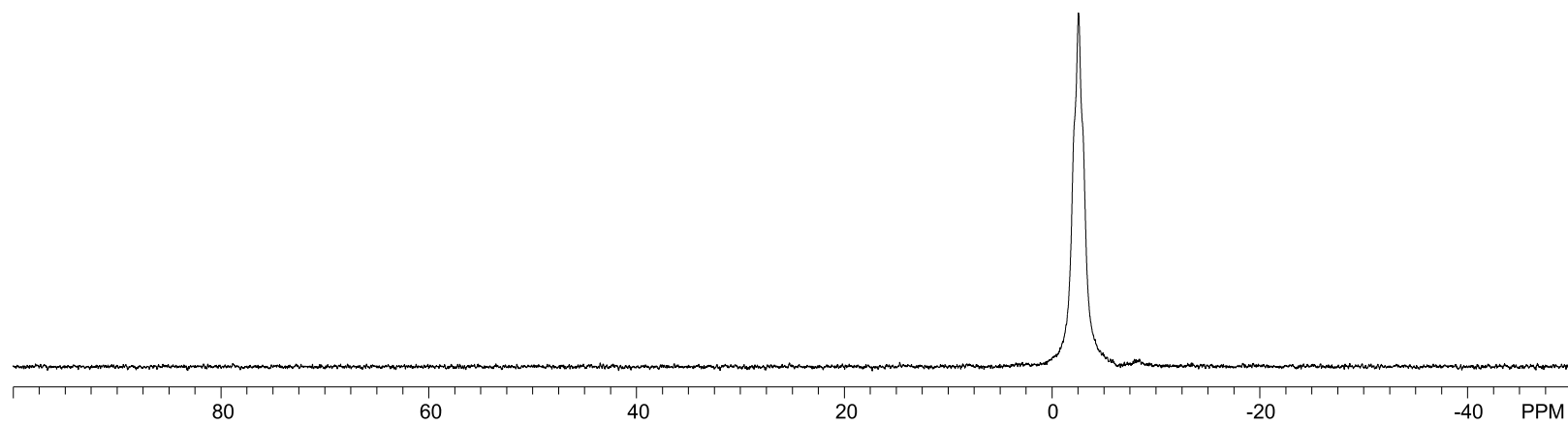
**2-34**



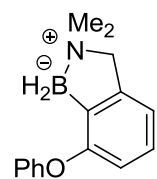
$^{11}\text{B}$  NMR (225 MHz),  
 $\text{CDCl}_3$



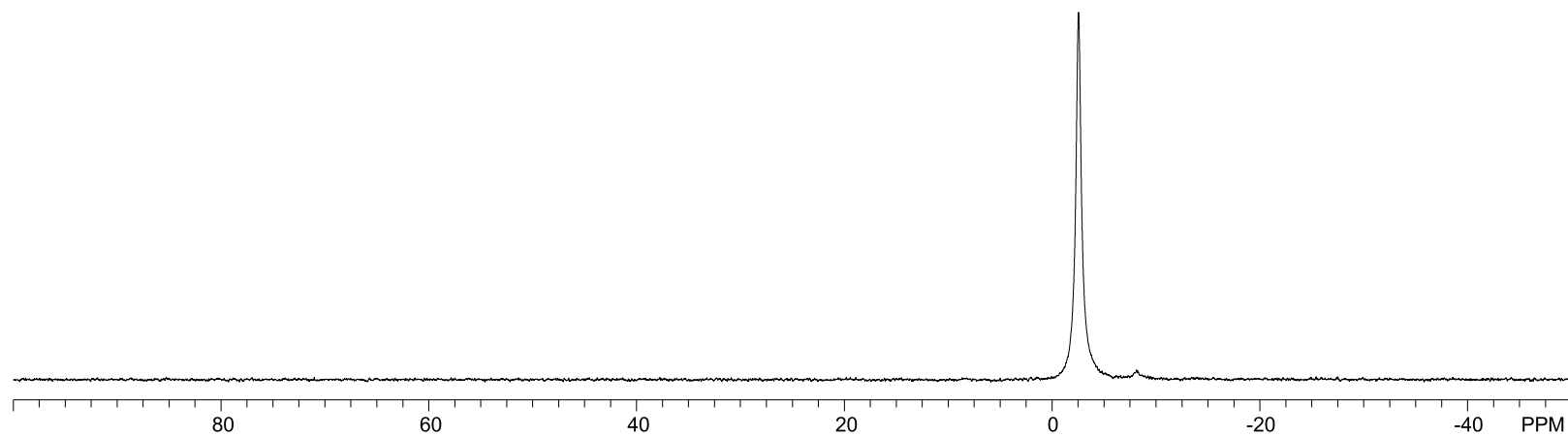
**2-34**



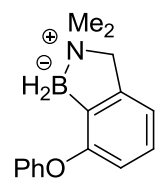
$^{11}\text{B}\{^1\text{H}\}$  NMR (225 MHz),  
 $\text{CDCl}_3$



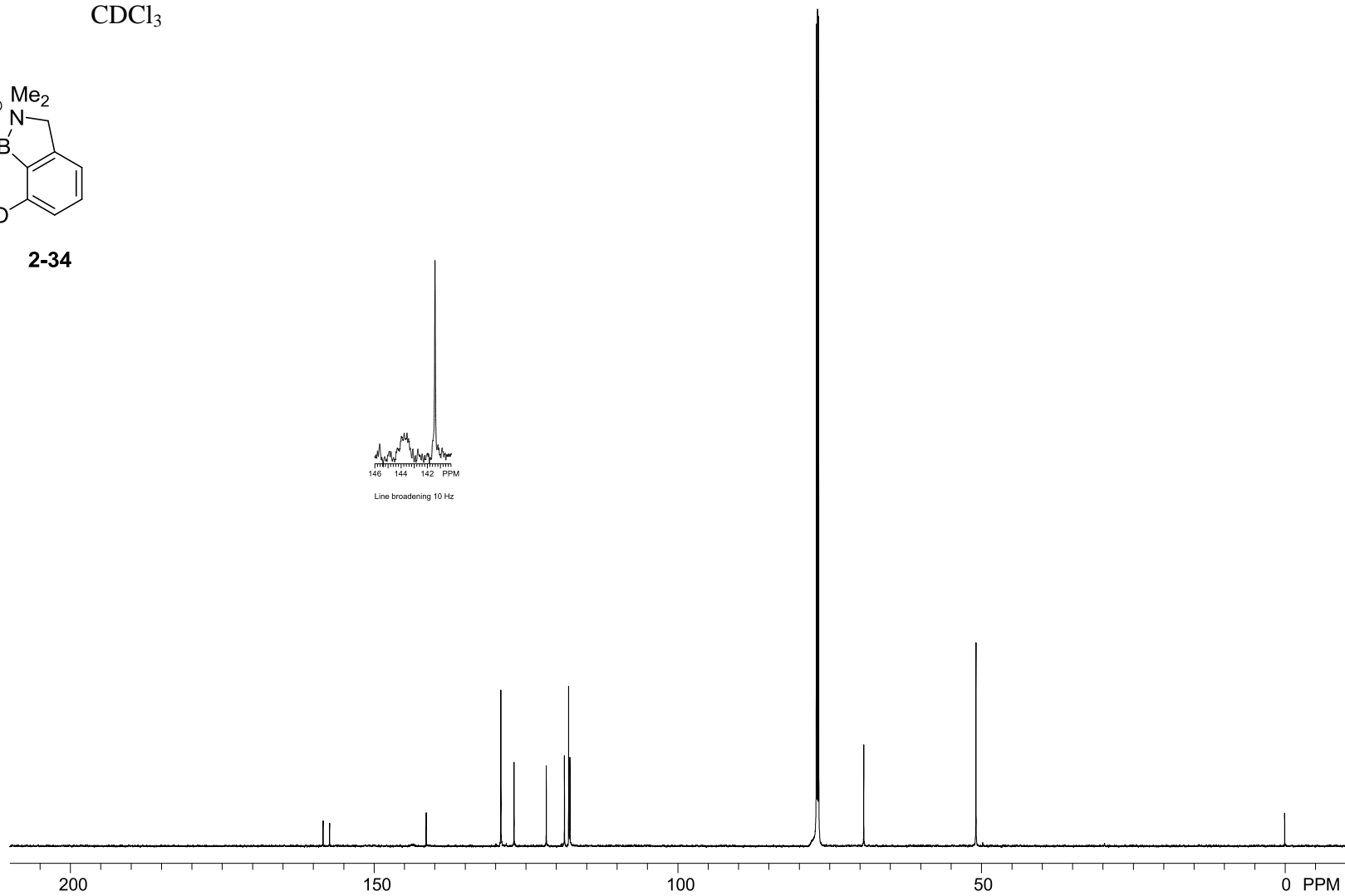
**2-34**



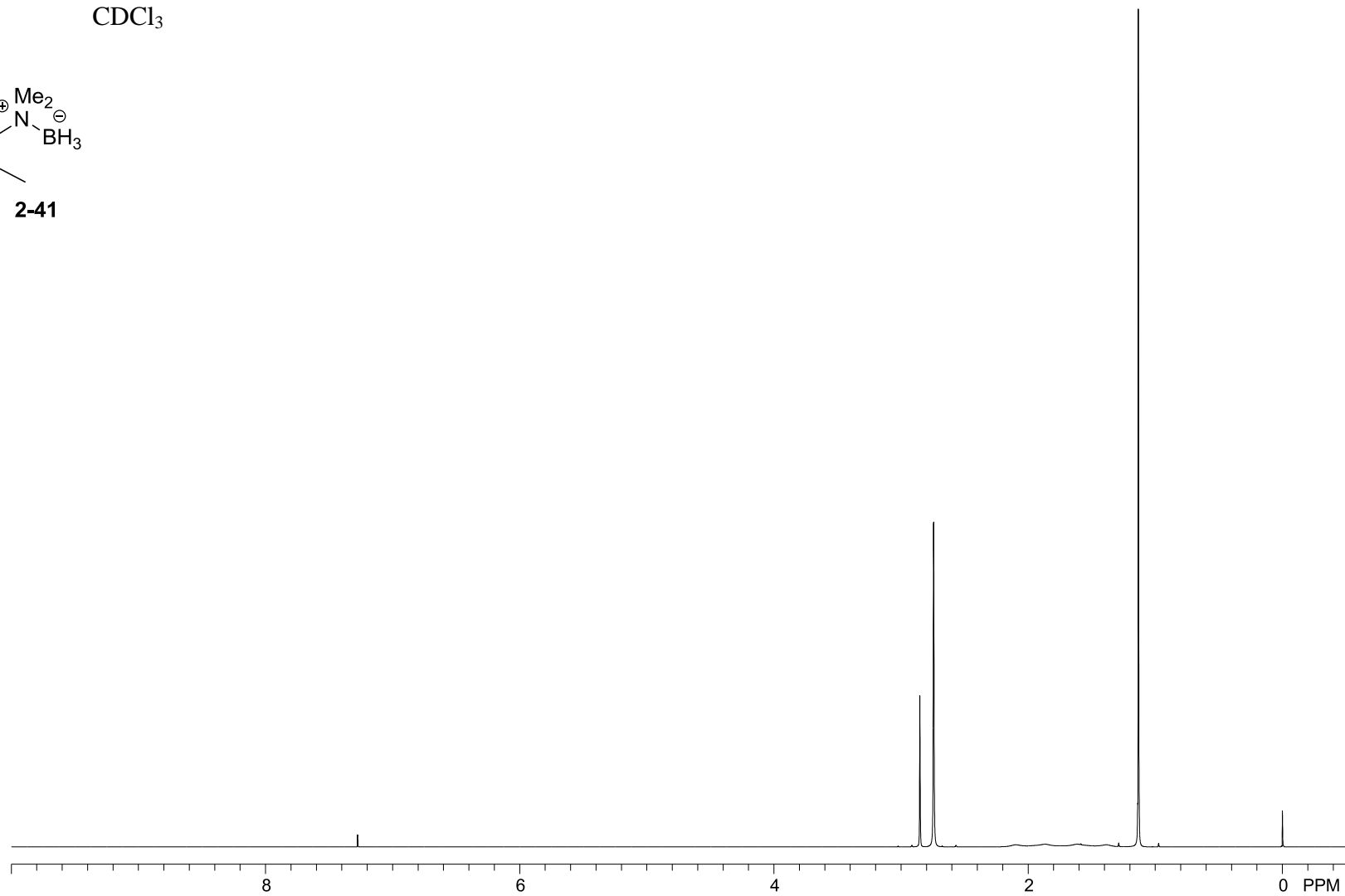
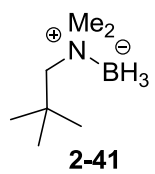
$^{13}\text{C}\{^1\text{H}\}$  NMR (176 MHz),  
 $\text{CDCl}_3$



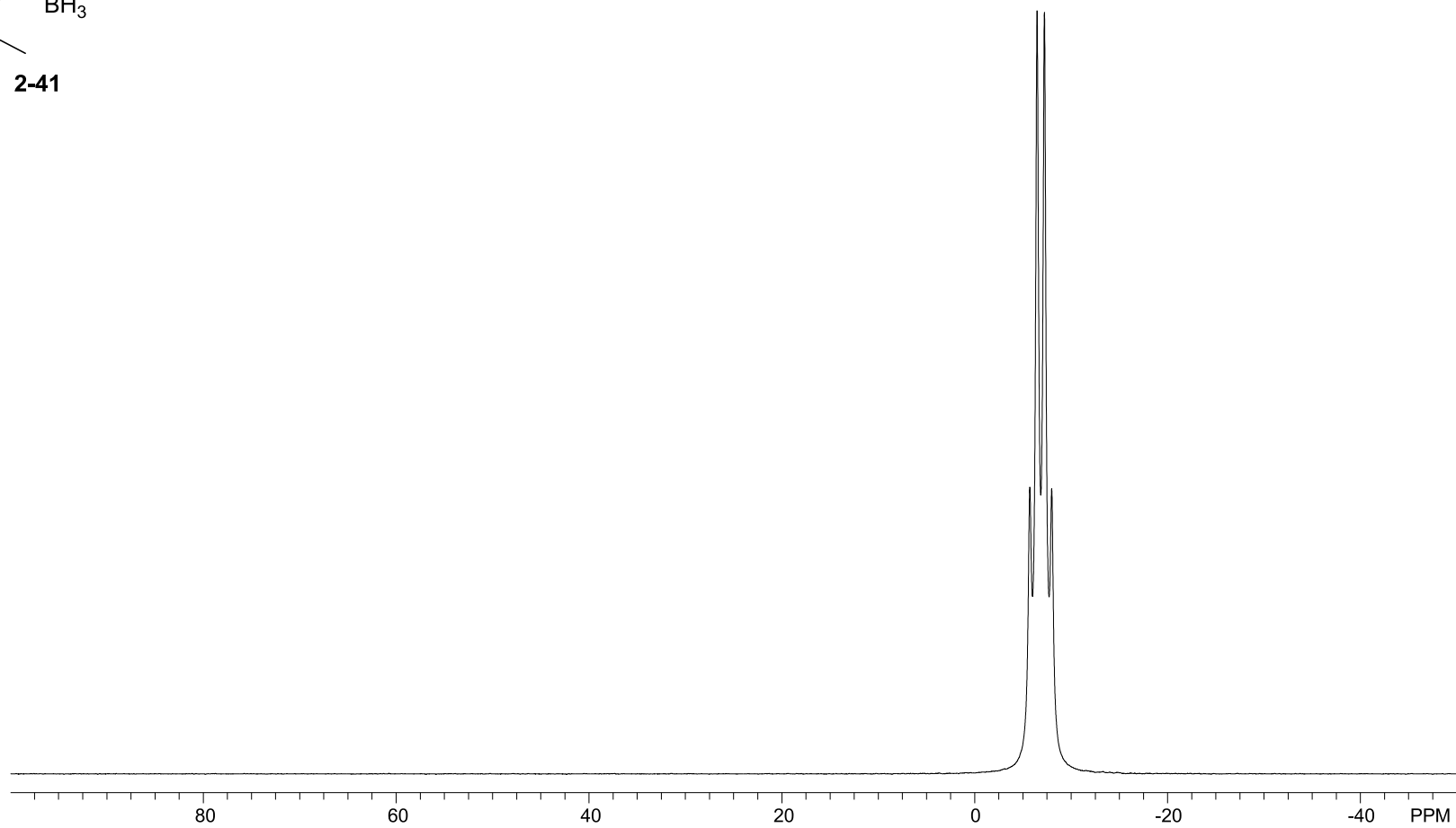
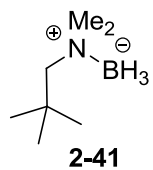
**2-34**



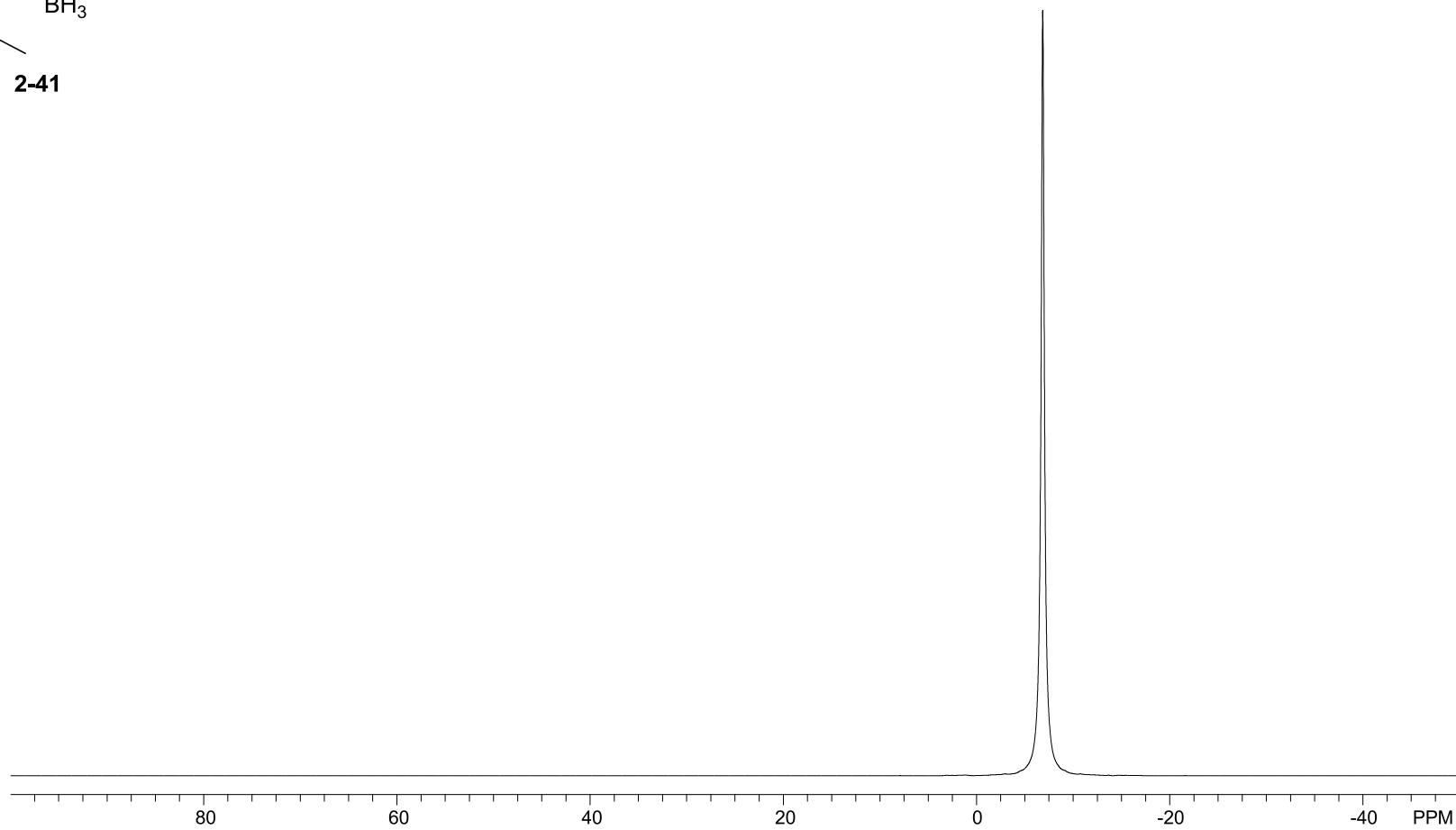
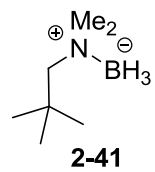
$^1\text{H}$  NMR (400 MHz),  
 $\text{CDCl}_3$



$^{11}\text{B}$  NMR (128 MHz),  
 $\text{CDCl}_3$

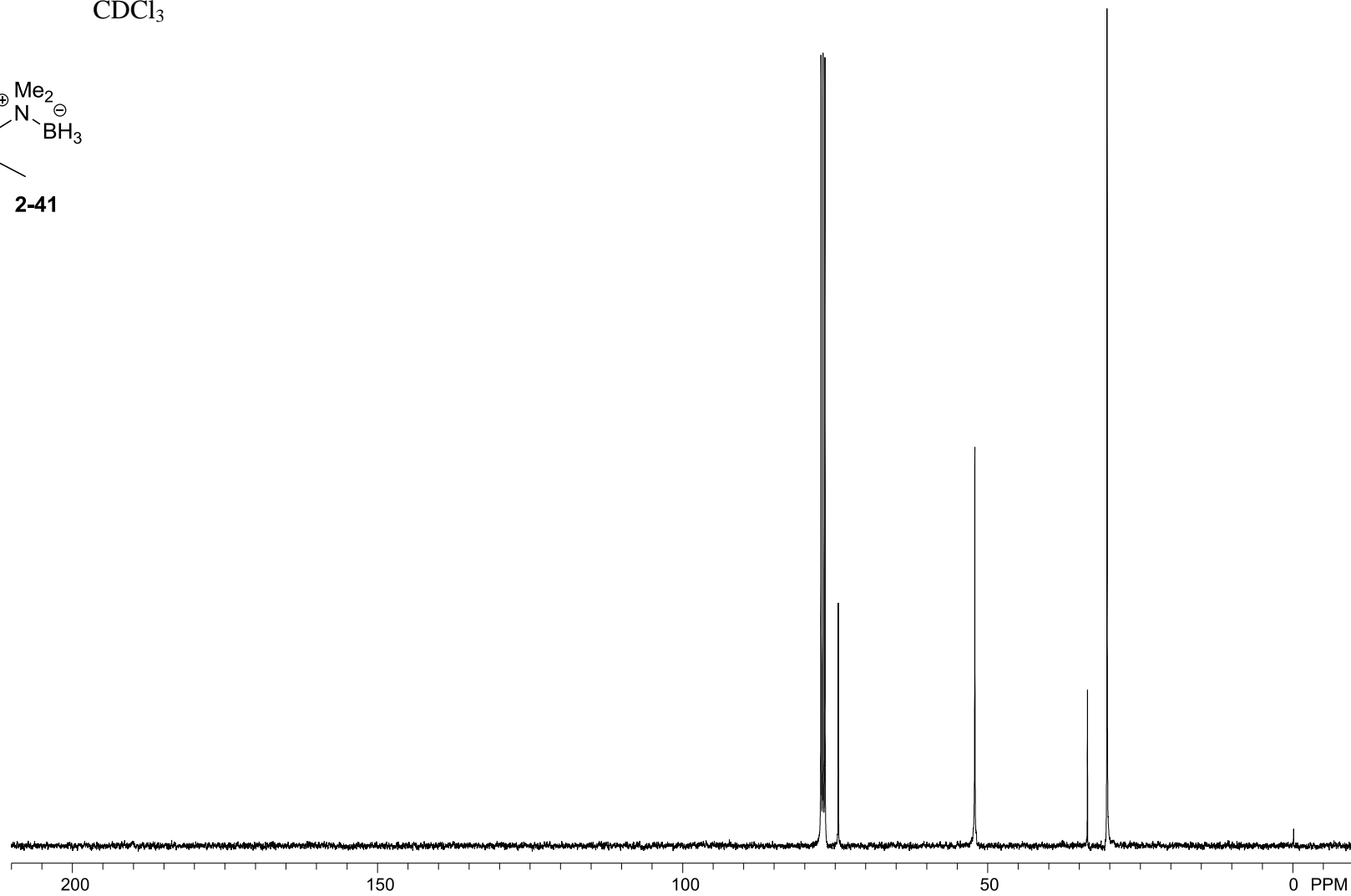
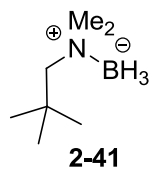


$^{11}\text{B}\{^1\text{H}\}$  NMR (128 MHz),  
 $\text{CDCl}_3$

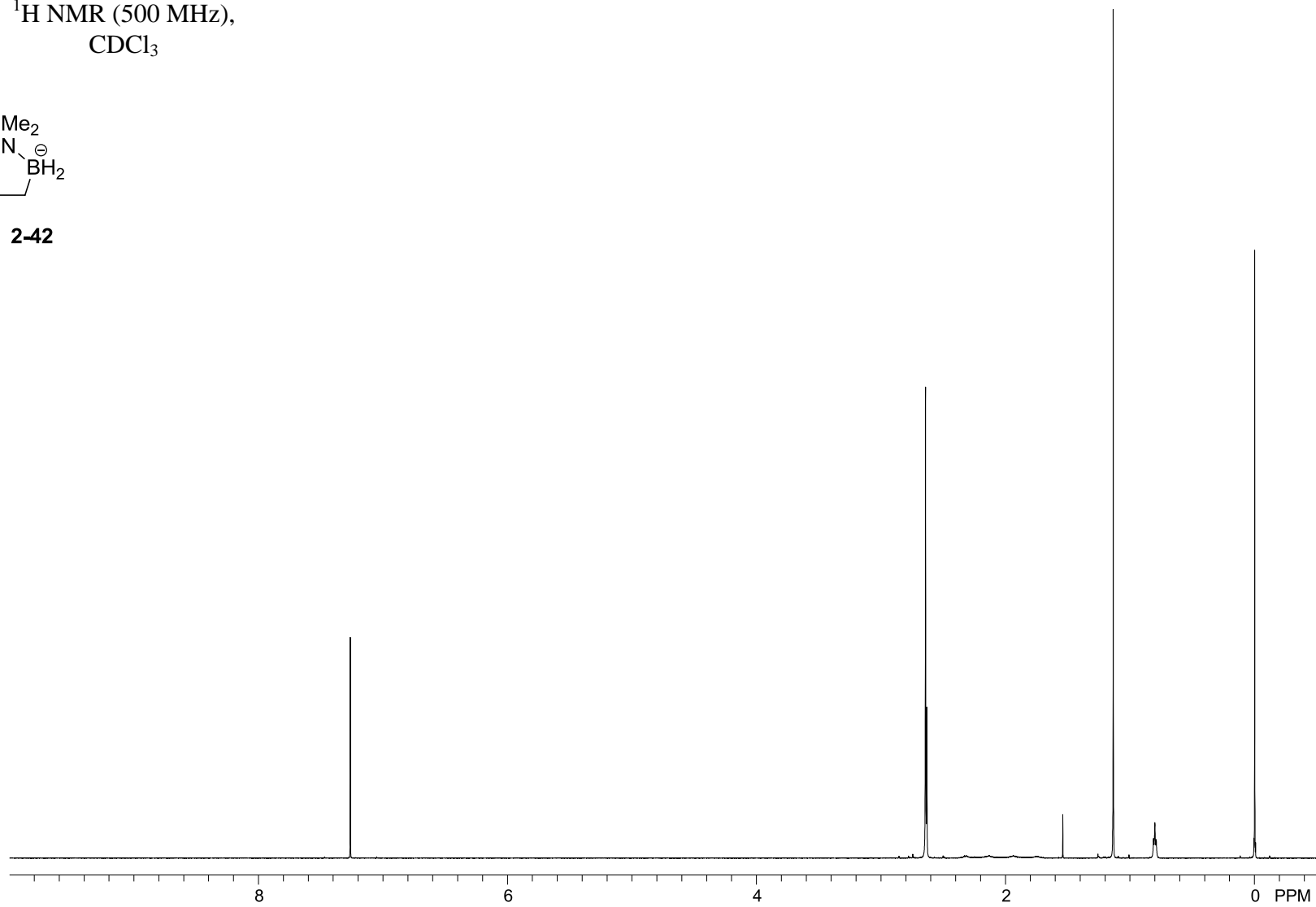
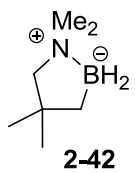




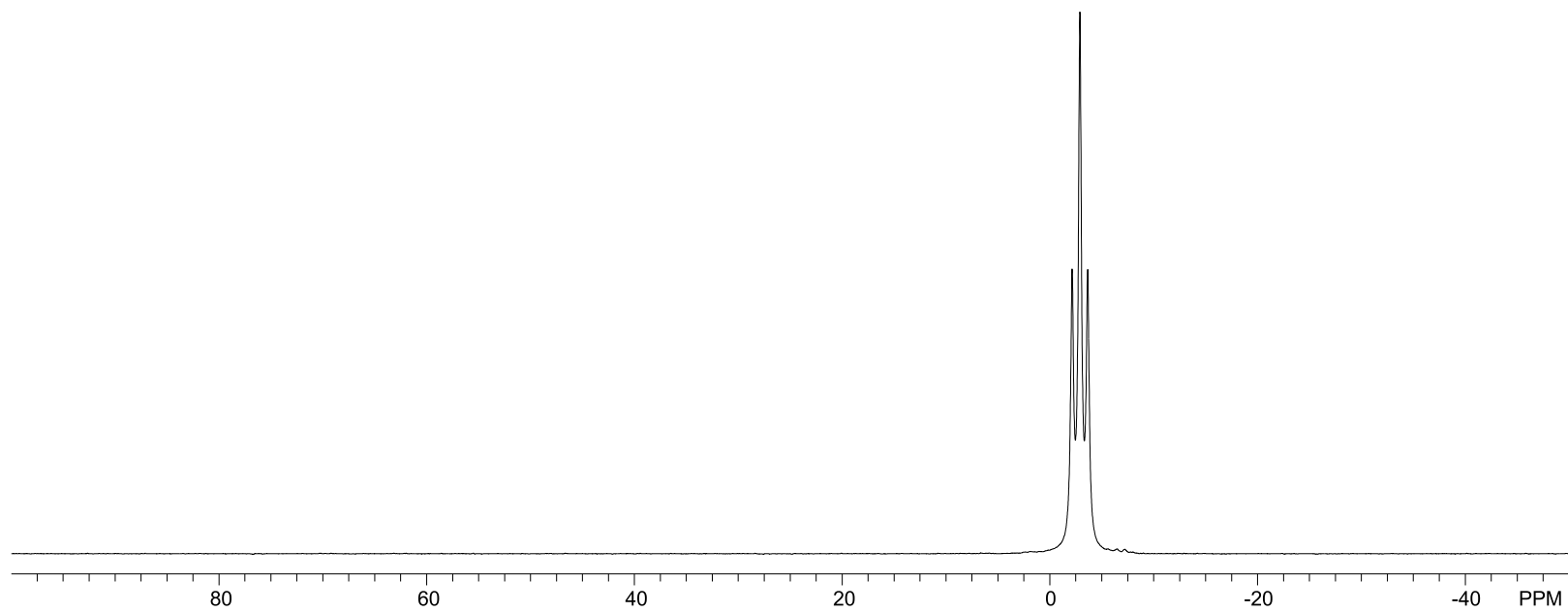
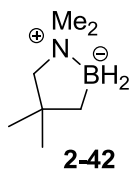
$^{13}\text{C}\{^1\text{H}\}$  NMR (101 MHz),  
 $\text{CDCl}_3$



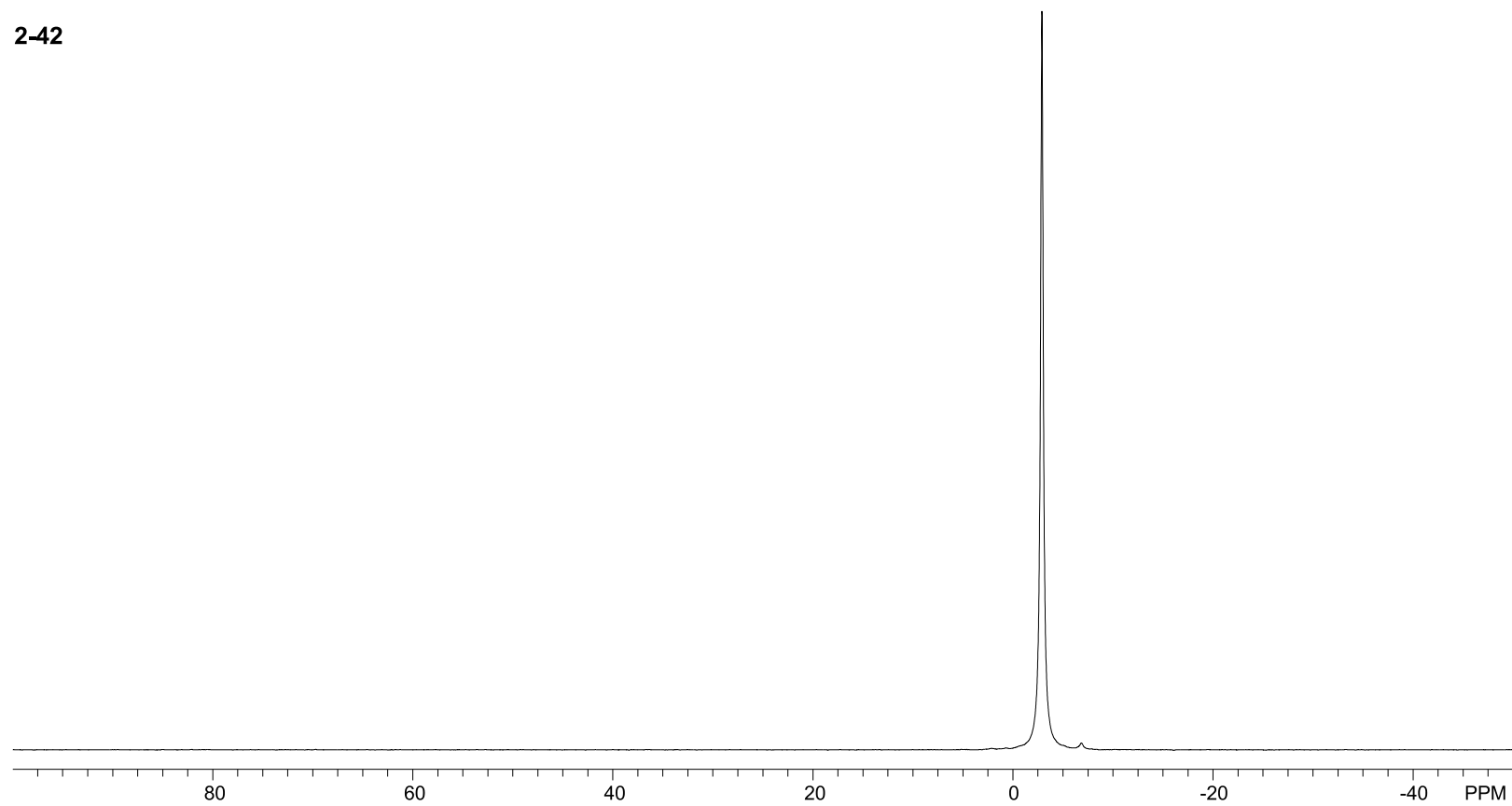
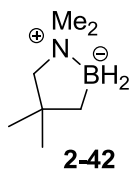
$^1\text{H}$  NMR (500 MHz),  
 $\text{CDCl}_3$



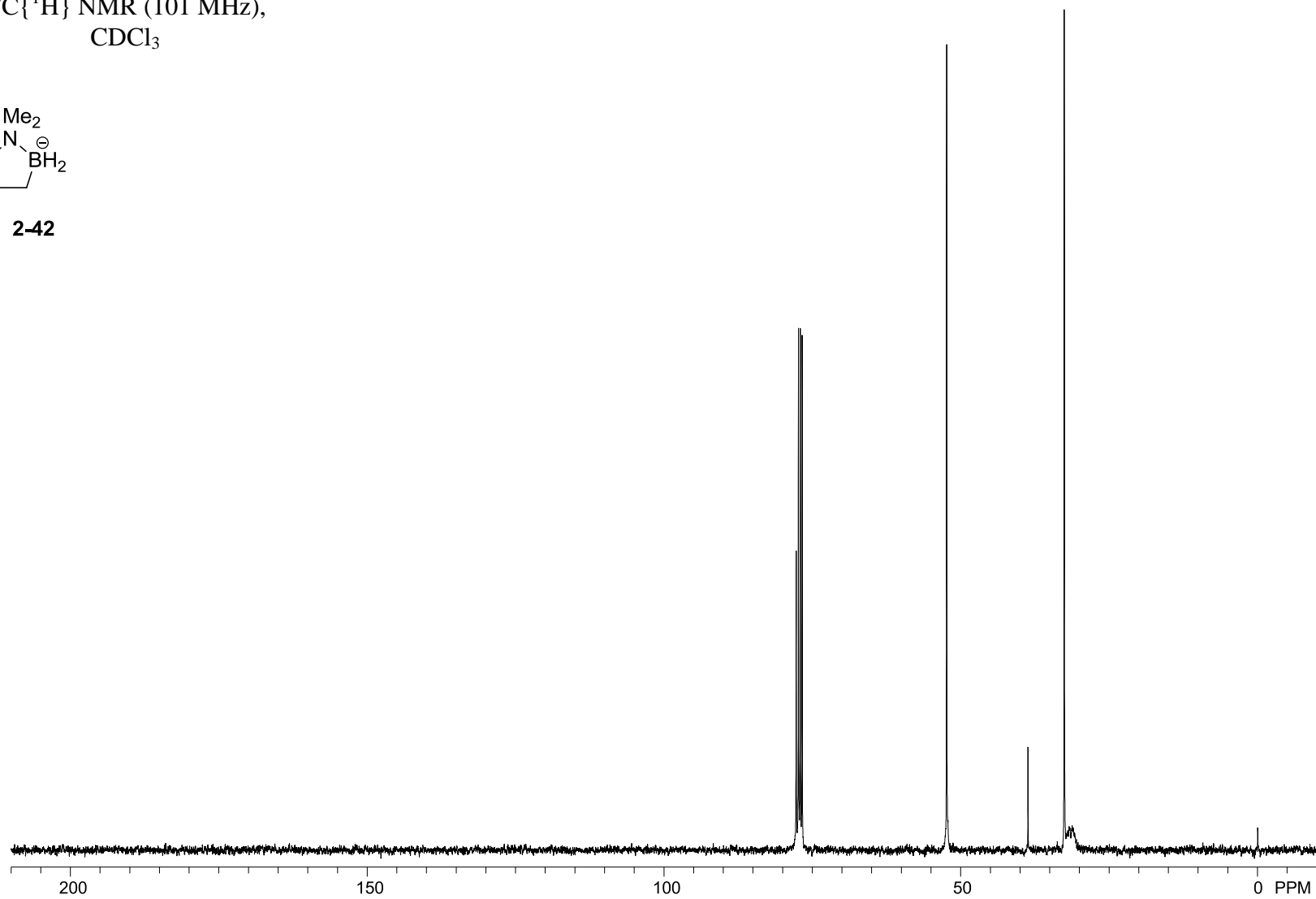
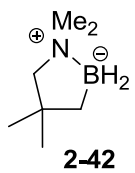
$^{11}\text{B}$  NMR (128 MHz),  
 $\text{CDCl}_3$



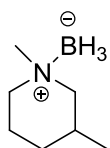
$^{11}\text{B}\{^1\text{H}\}$  NMR (128 MHz),  
 $\text{CDCl}_3$



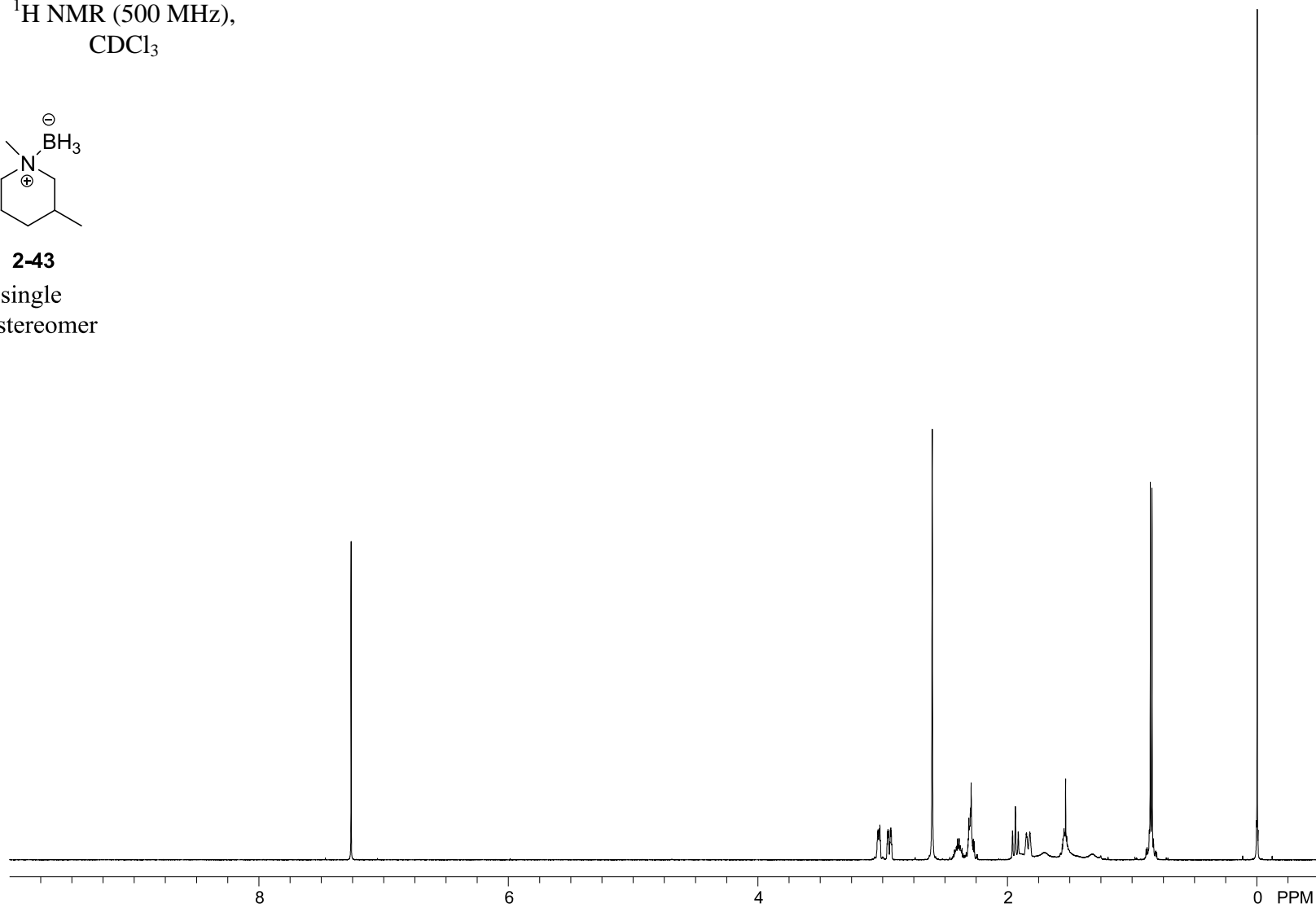
$^{13}\text{C}\{^1\text{H}\}$  NMR (101 MHz),  
 $\text{CDCl}_3$



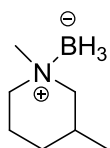
$^1\text{H}$  NMR (500 MHz),  
 $\text{CDCl}_3$



**2-43**  
single  
diastereomer

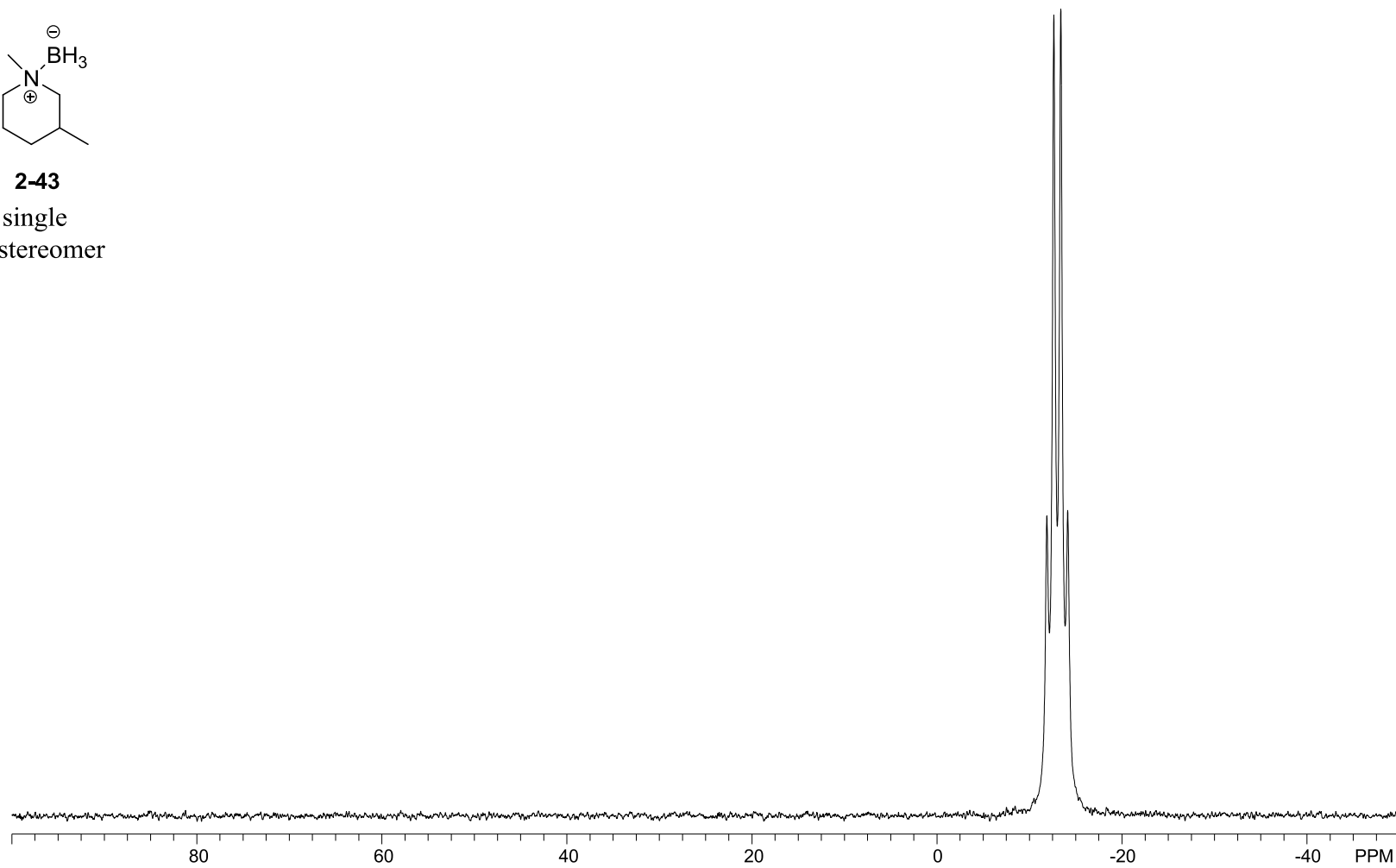


$^{11}\text{B}$  NMR (128 MHz),  
 $\text{CDCl}_3$

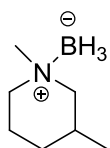


**2-43**

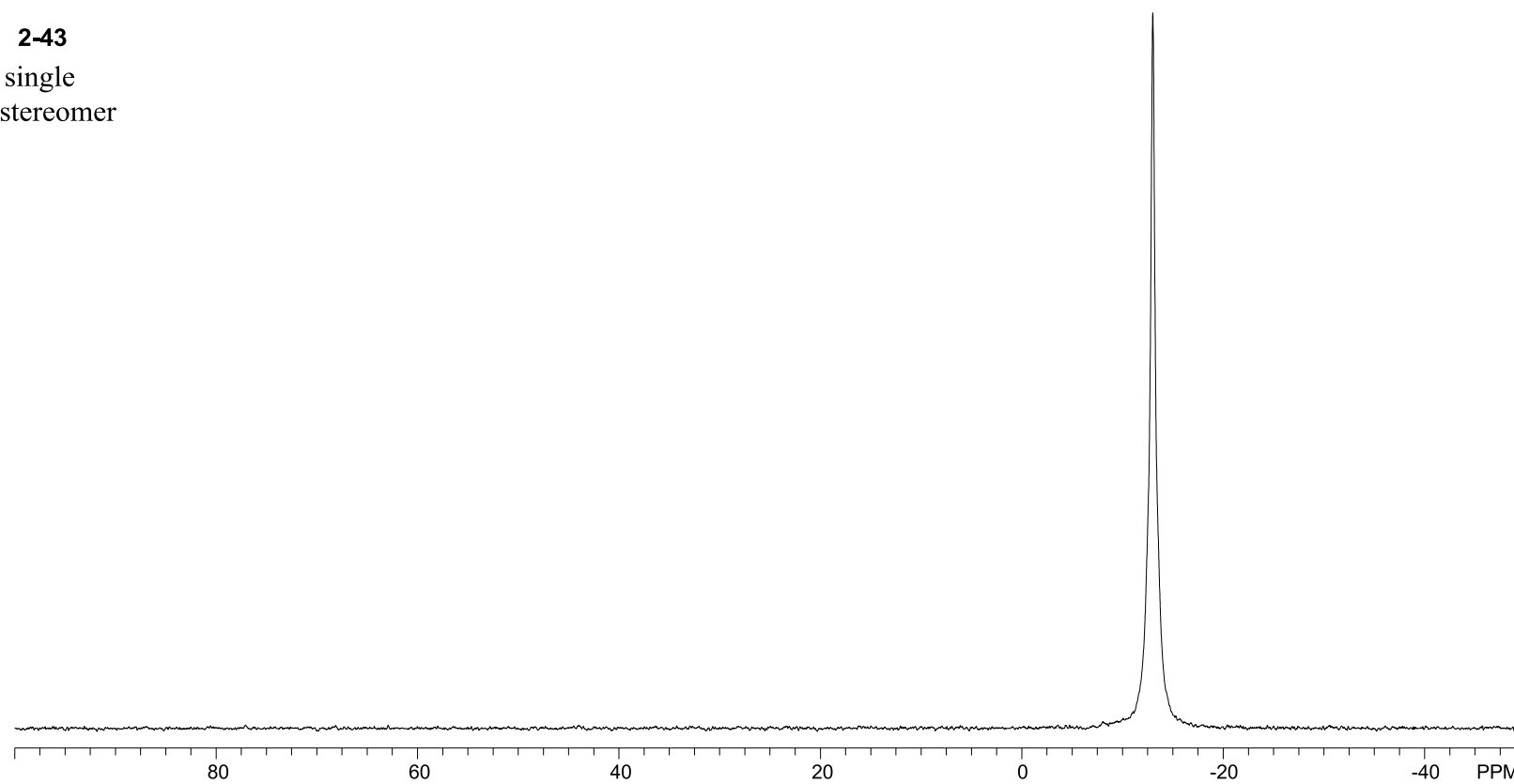
single  
diastereomer



$^{11}\text{B}\{^1\text{H}\}$  NMR (128 MHz),  
 $\text{CDCl}_3$

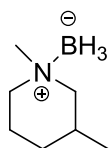


**2-43**  
single  
diastereomer

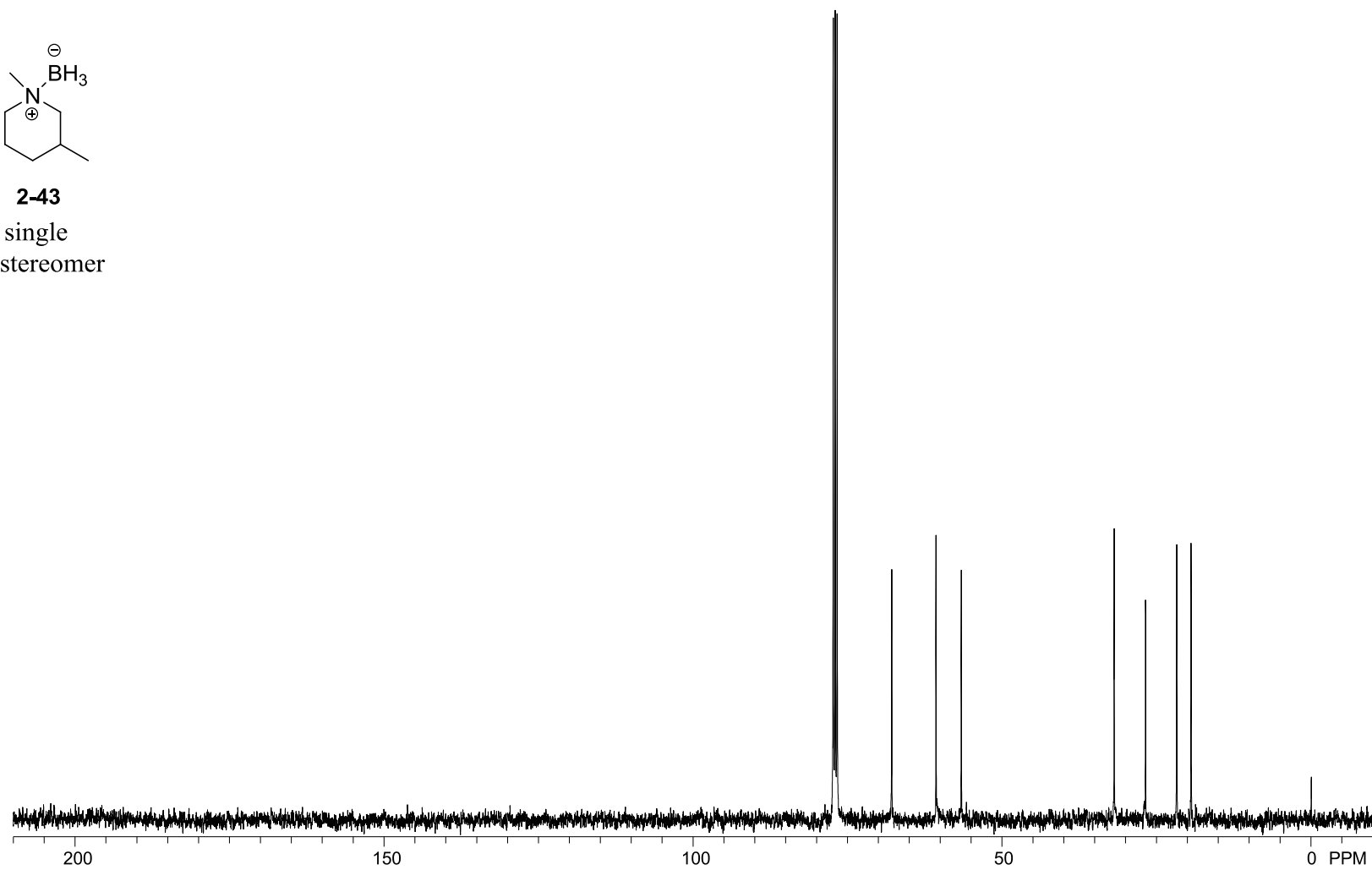




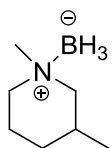
$^{13}\text{C}\{^1\text{H}\}$  NMR (101 MHz),  
 $\text{CDCl}_3$



**2-43**  
single  
diastereomer

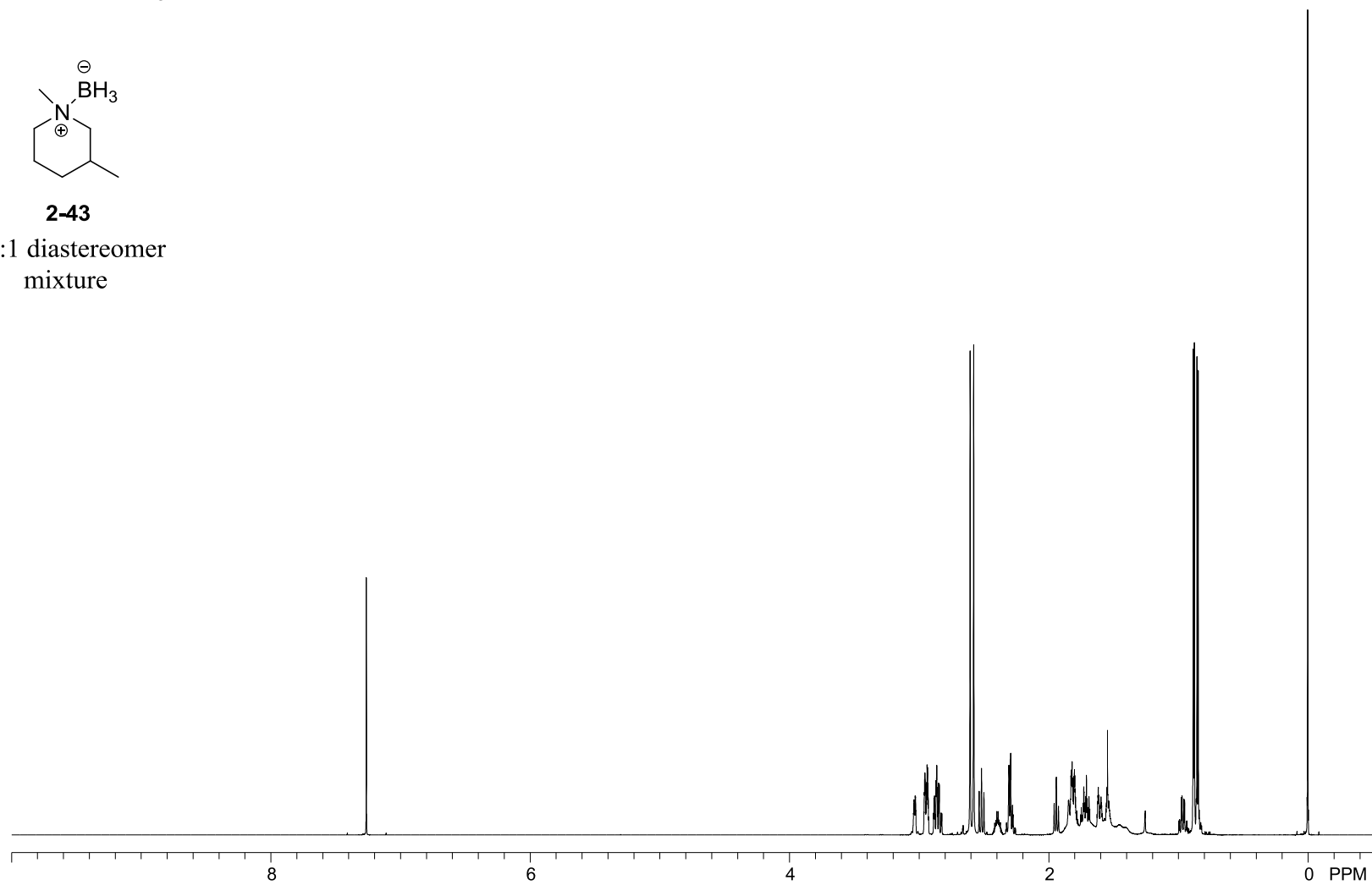


$^1\text{H}$  NMR (700 MHz),  
 $\text{CDCl}_3$

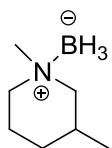


**2-43**

1.1:1 diastereomer  
mixture

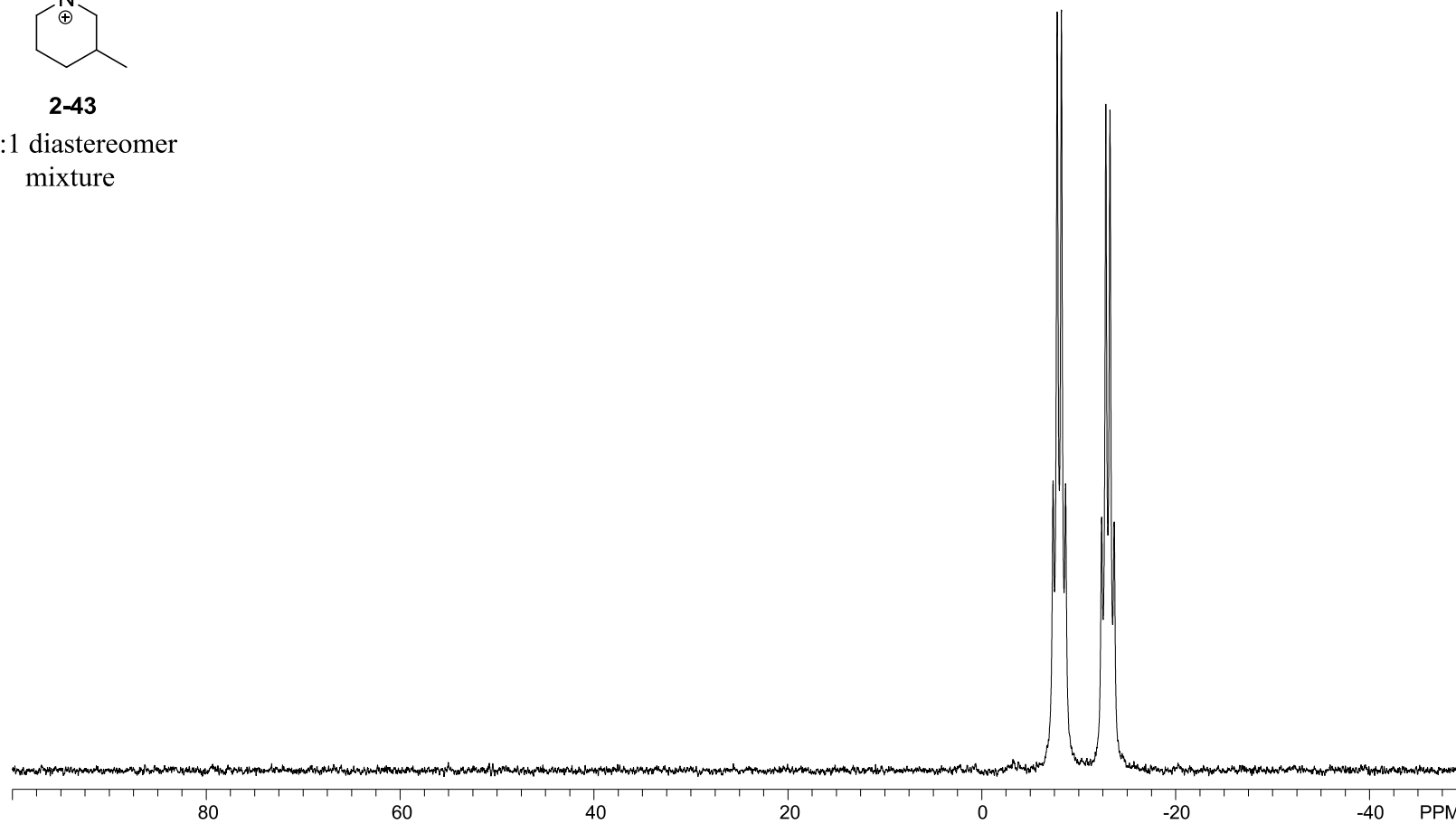


$^{11}\text{B}$  NMR (225 MHz),  
 $\text{CDCl}_3$

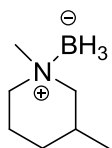


**2-43**

1.1:1 diastereomer  
mixture

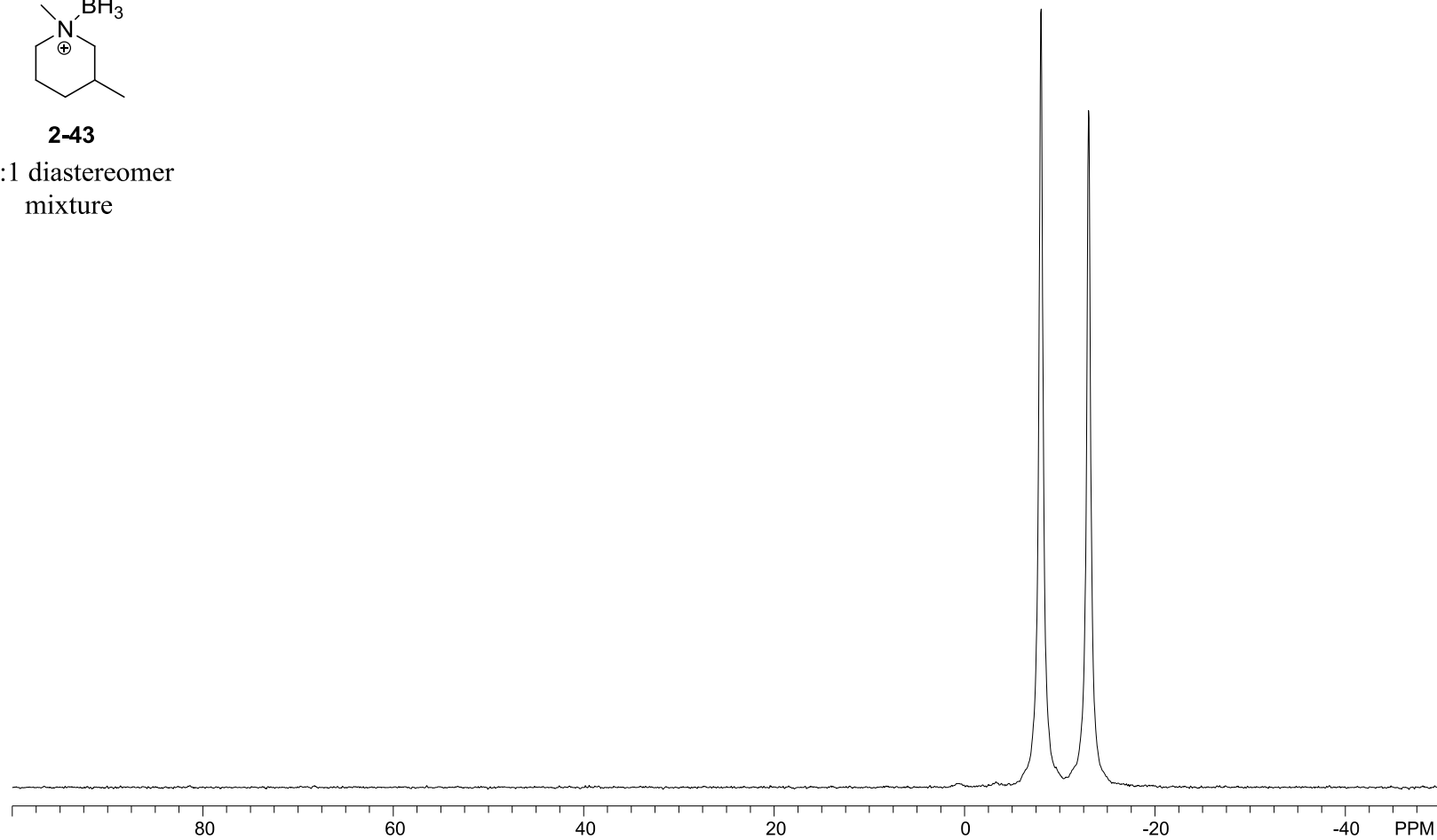


$^{11}\text{B}\{^1\text{H}\}$  NMR (128 MHz),  
 $\text{CDCl}_3$

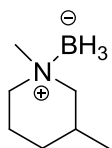


**2-43**

1.1:1 diastereomer  
mixture

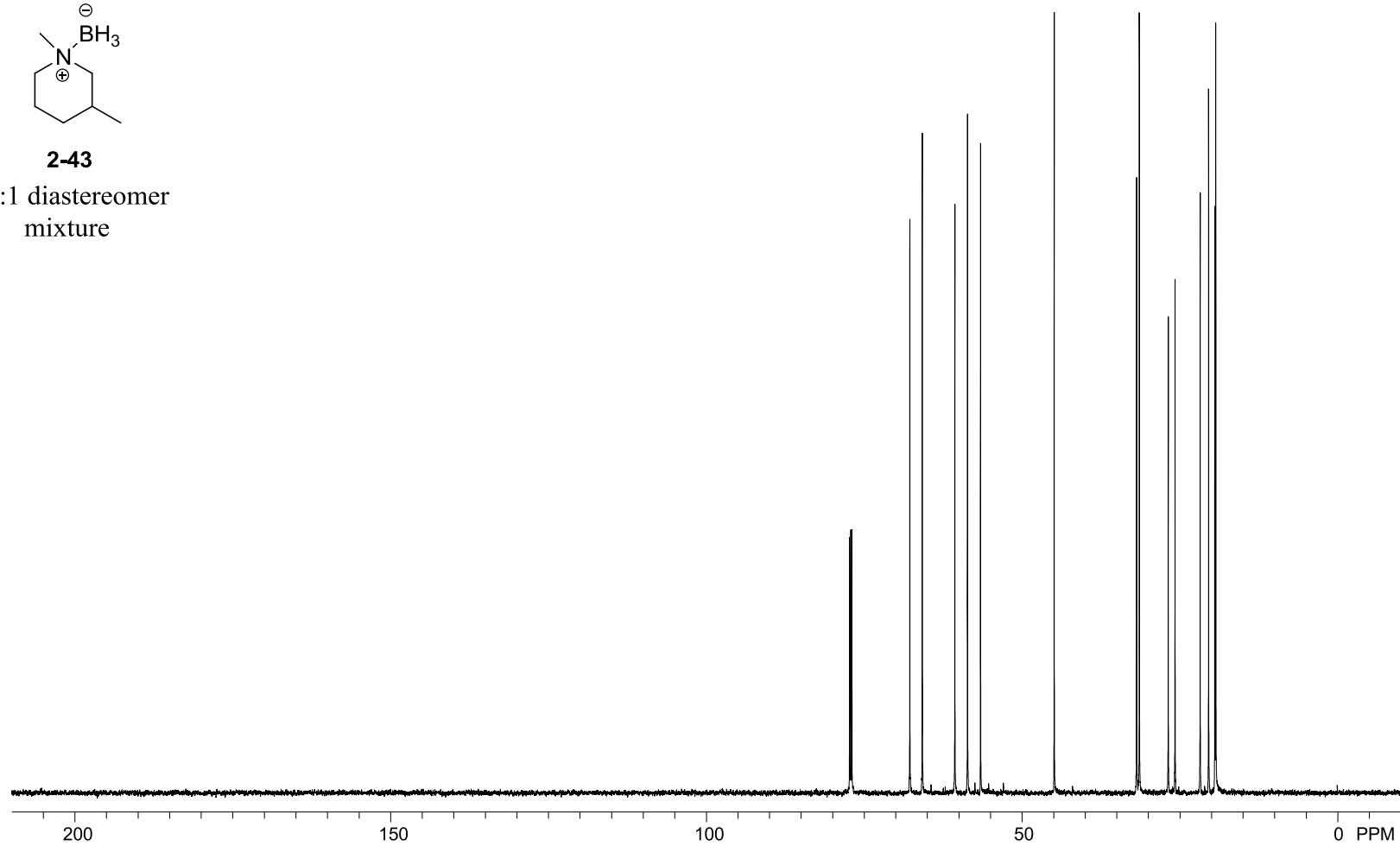


$^{13}\text{C}\{^1\text{H}\}$  NMR (176 MHz),  
 $\text{CDCl}_3$

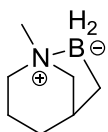


**2-43**

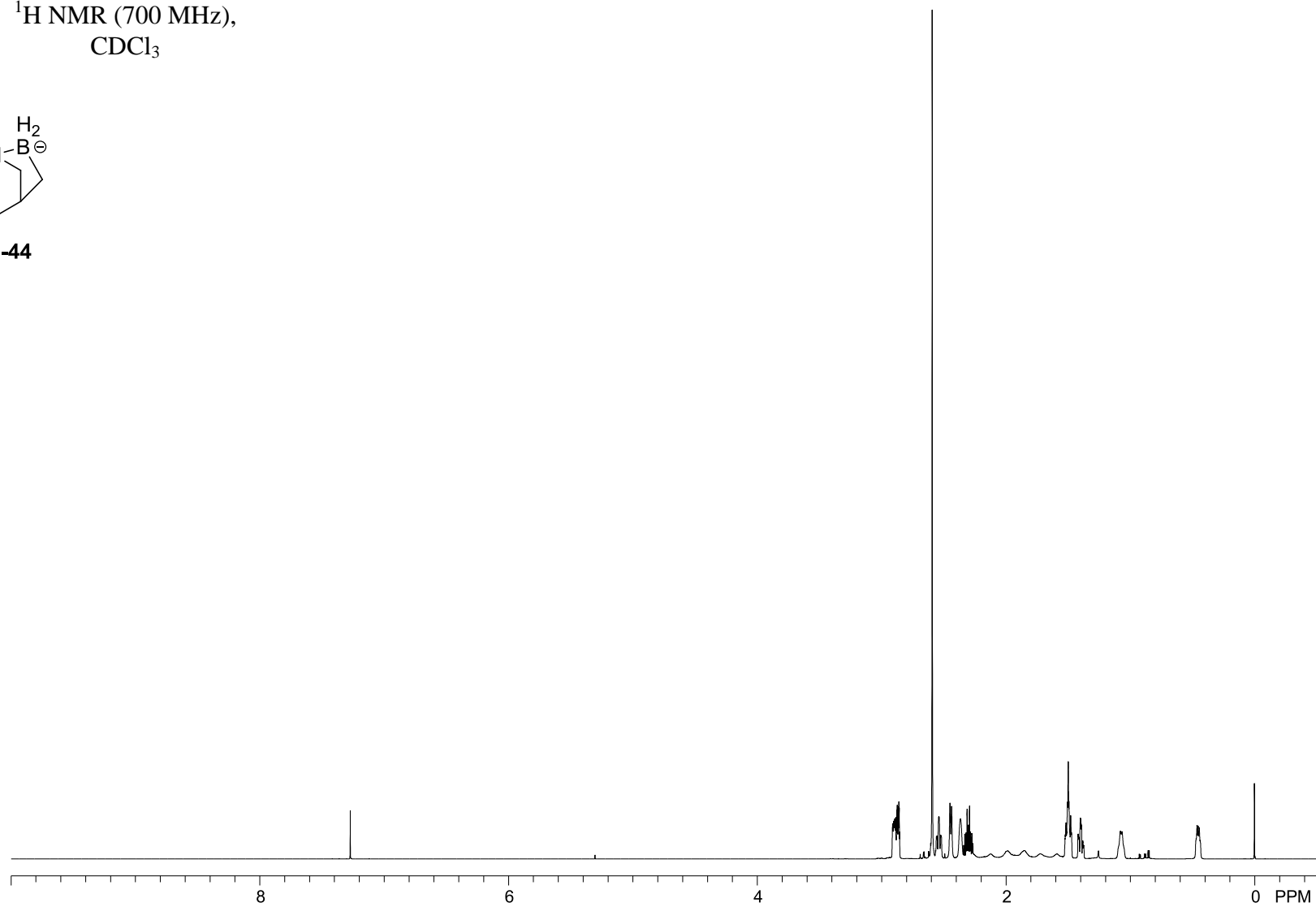
1.1:1 diastereomer  
mixture



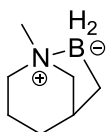
$^1\text{H}$  NMR (700 MHz),  
 $\text{CDCl}_3$



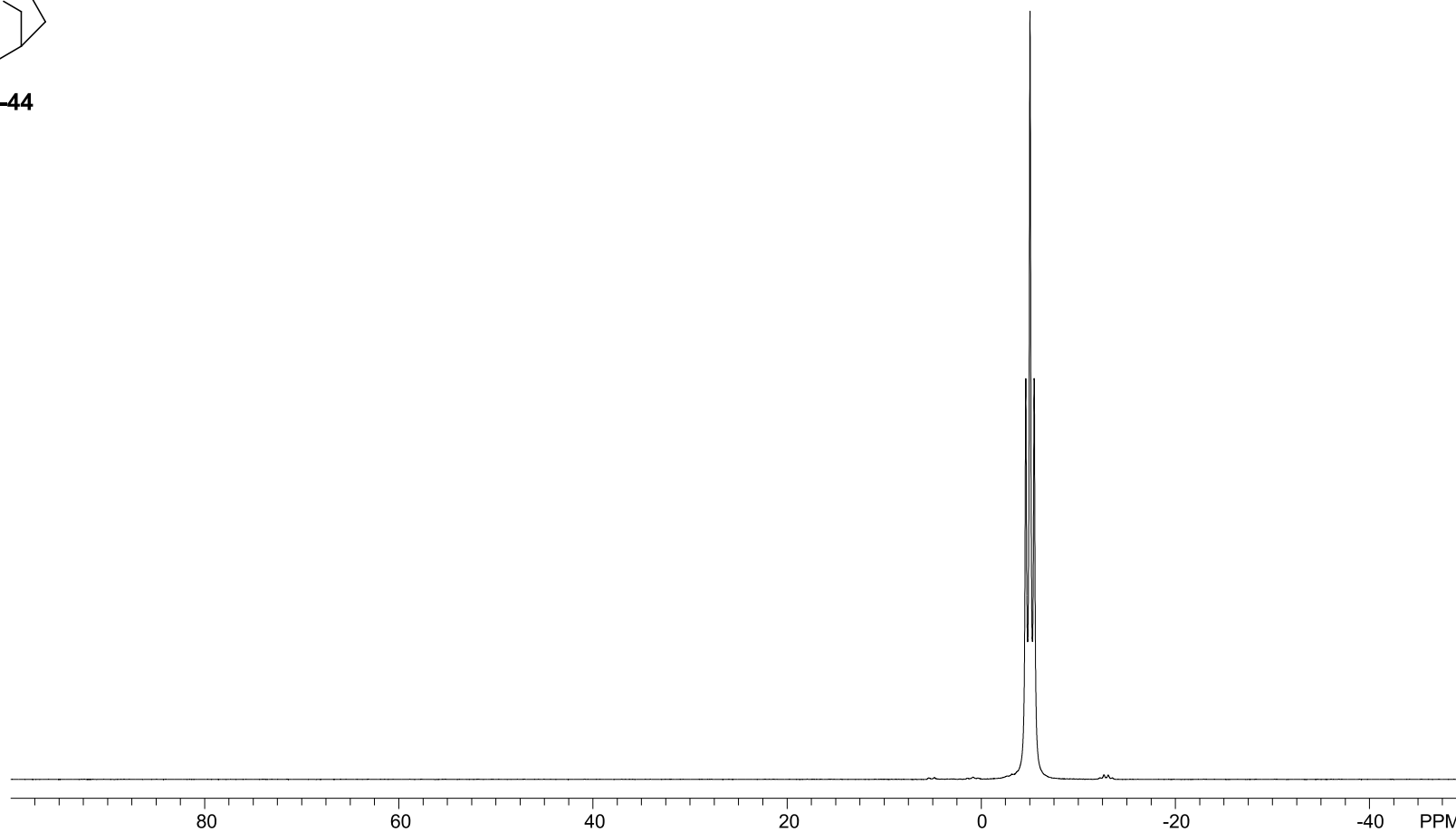
**2-44**



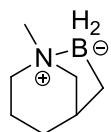
$^{11}\text{B}$  NMR (225 MHz),  
 $\text{CDCl}_3$



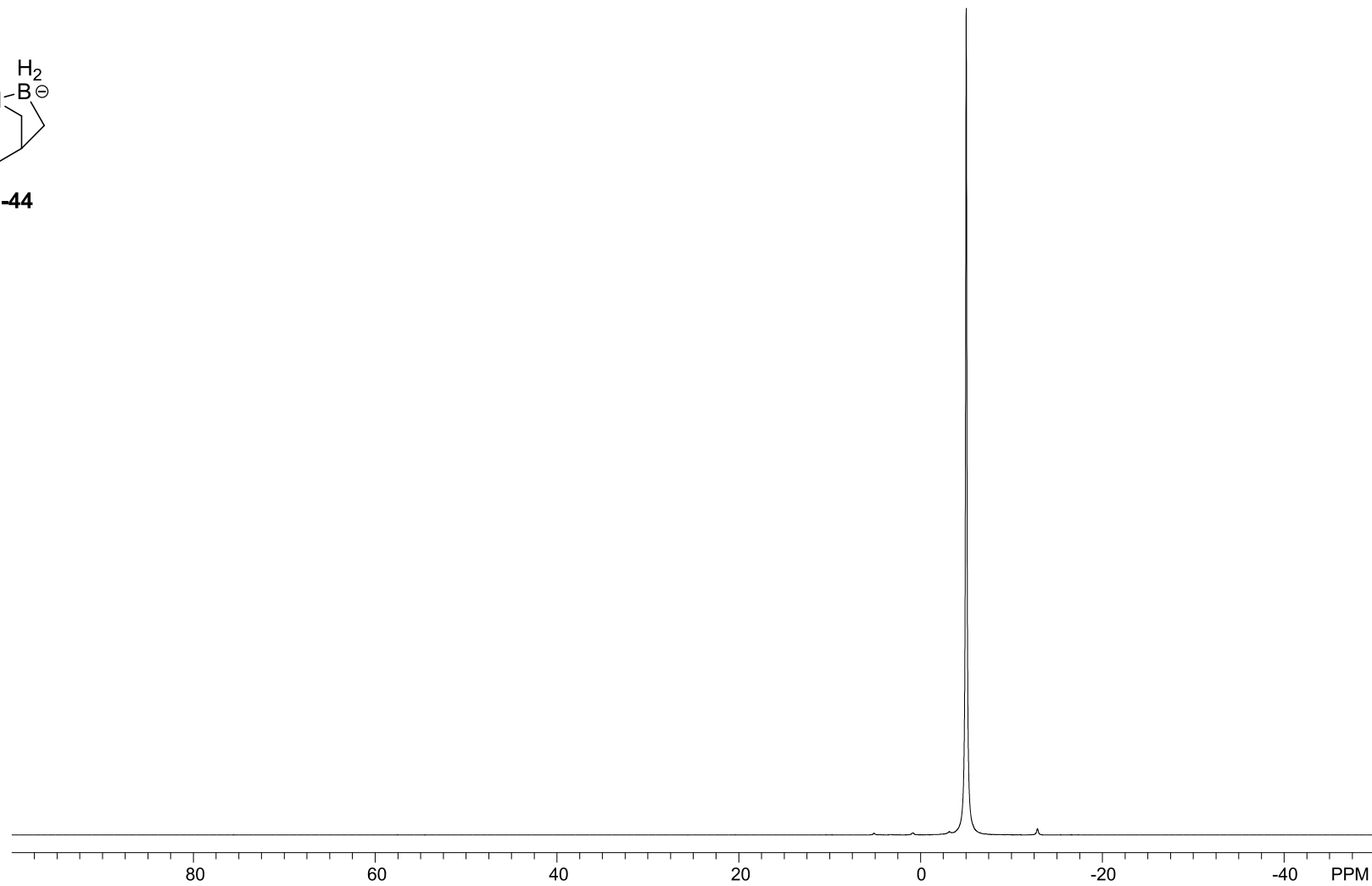
**2-44**



$^{11}\text{B}\{^1\text{H}\}$  NMR (225 MHz),  
 $\text{CDCl}_3$

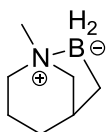


**2-44**

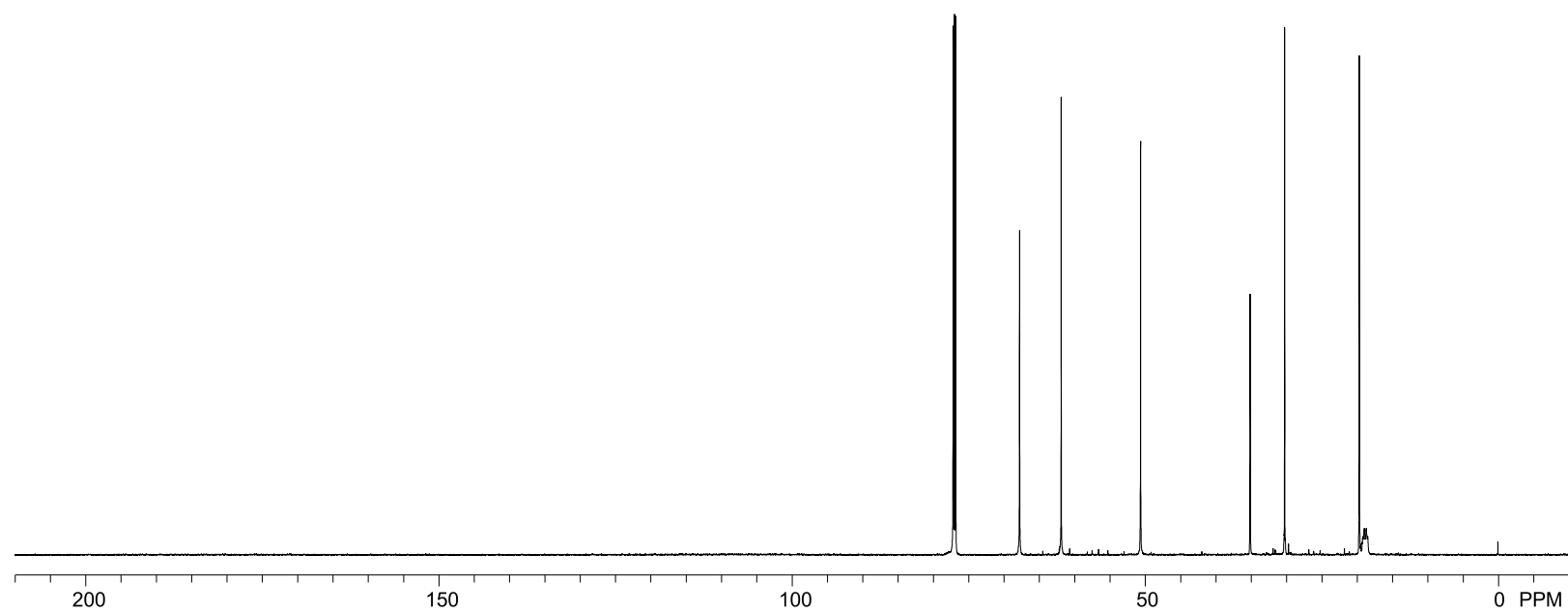




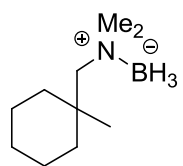
$^{13}\text{C}\{^1\text{H}\}$  NMR (176 MHz),  
 $\text{CDCl}_3$



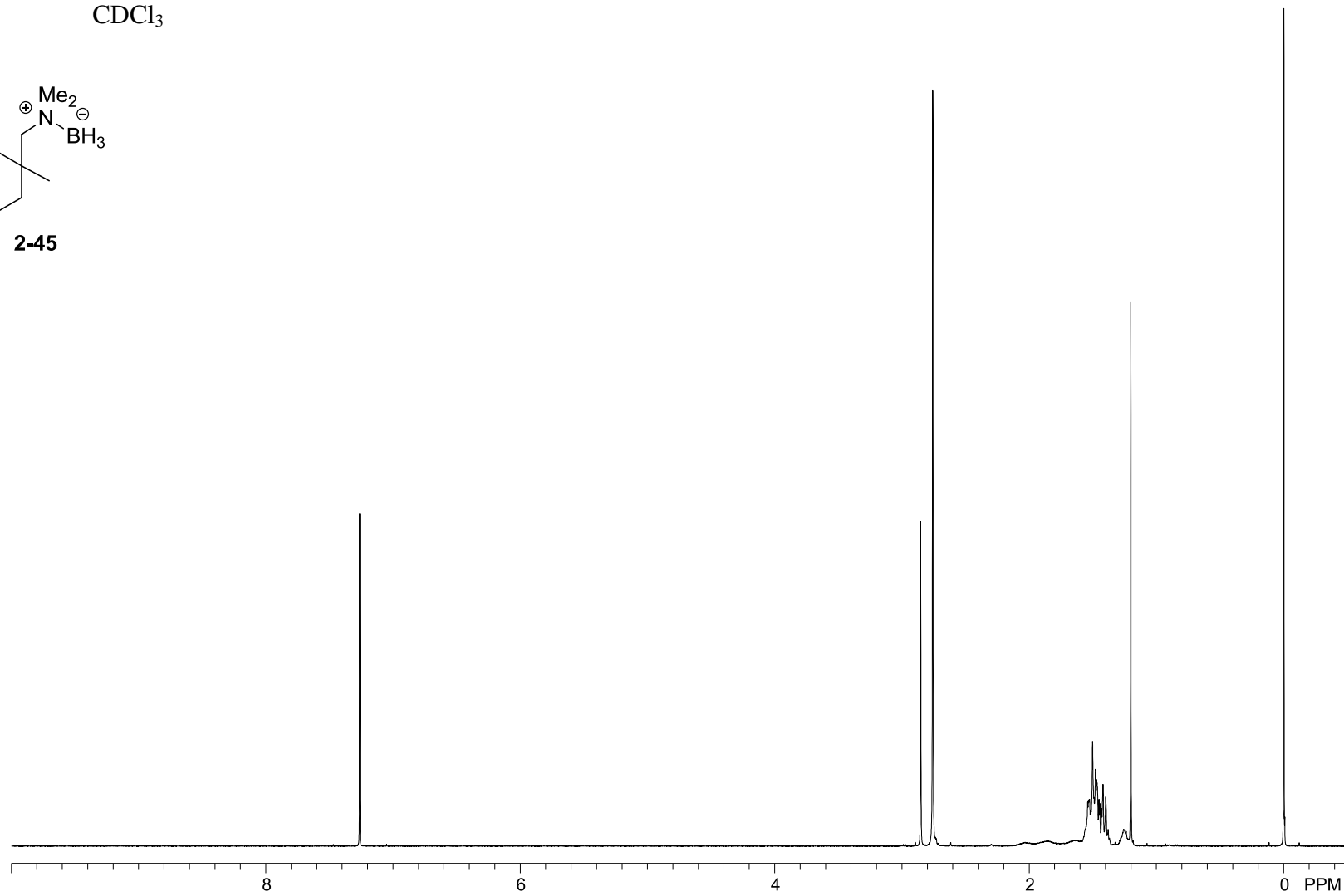
**2-44**



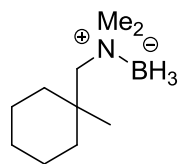
$^1\text{H}$  NMR (500 MHz),  
 $\text{CDCl}_3$



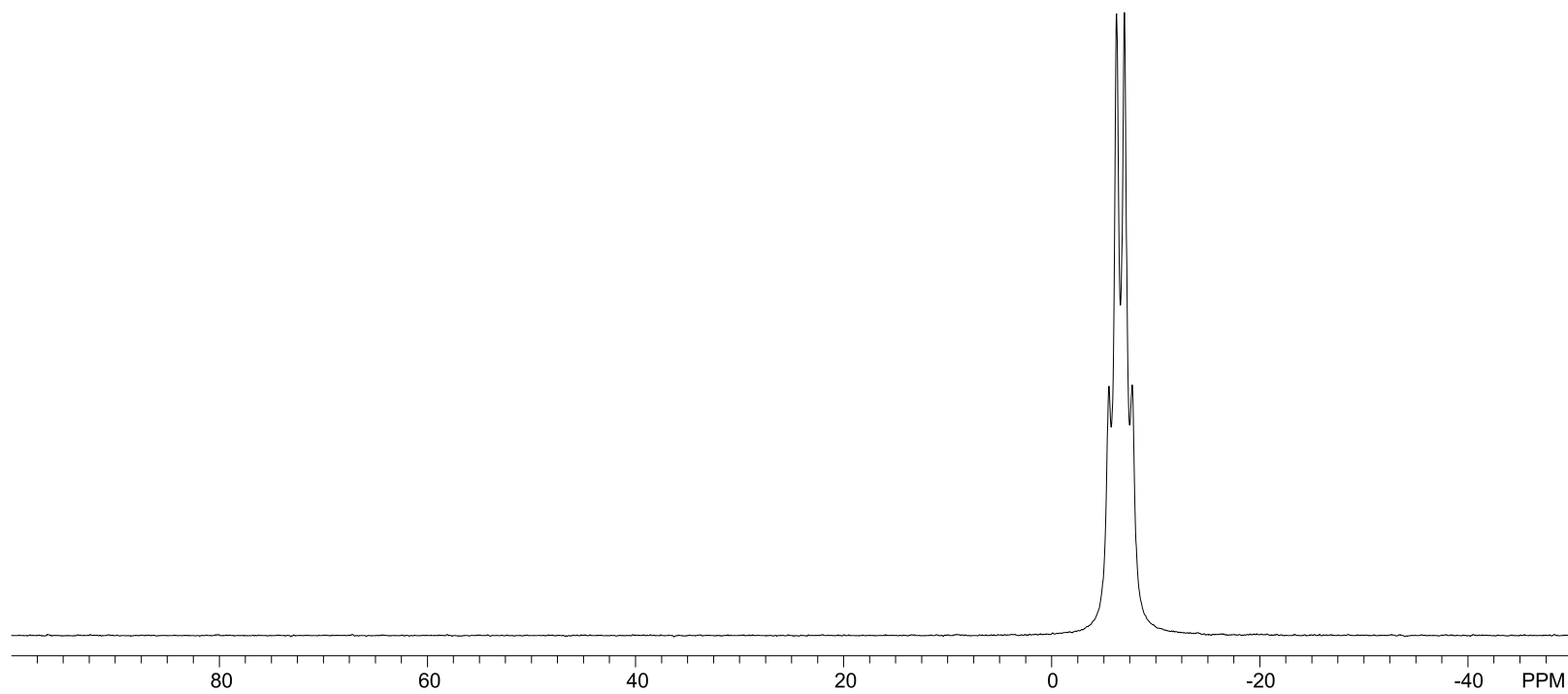
2-45



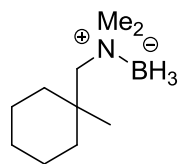
$^{11}\text{B}$  NMR (128 MHz),  
 $\text{CDCl}_3$



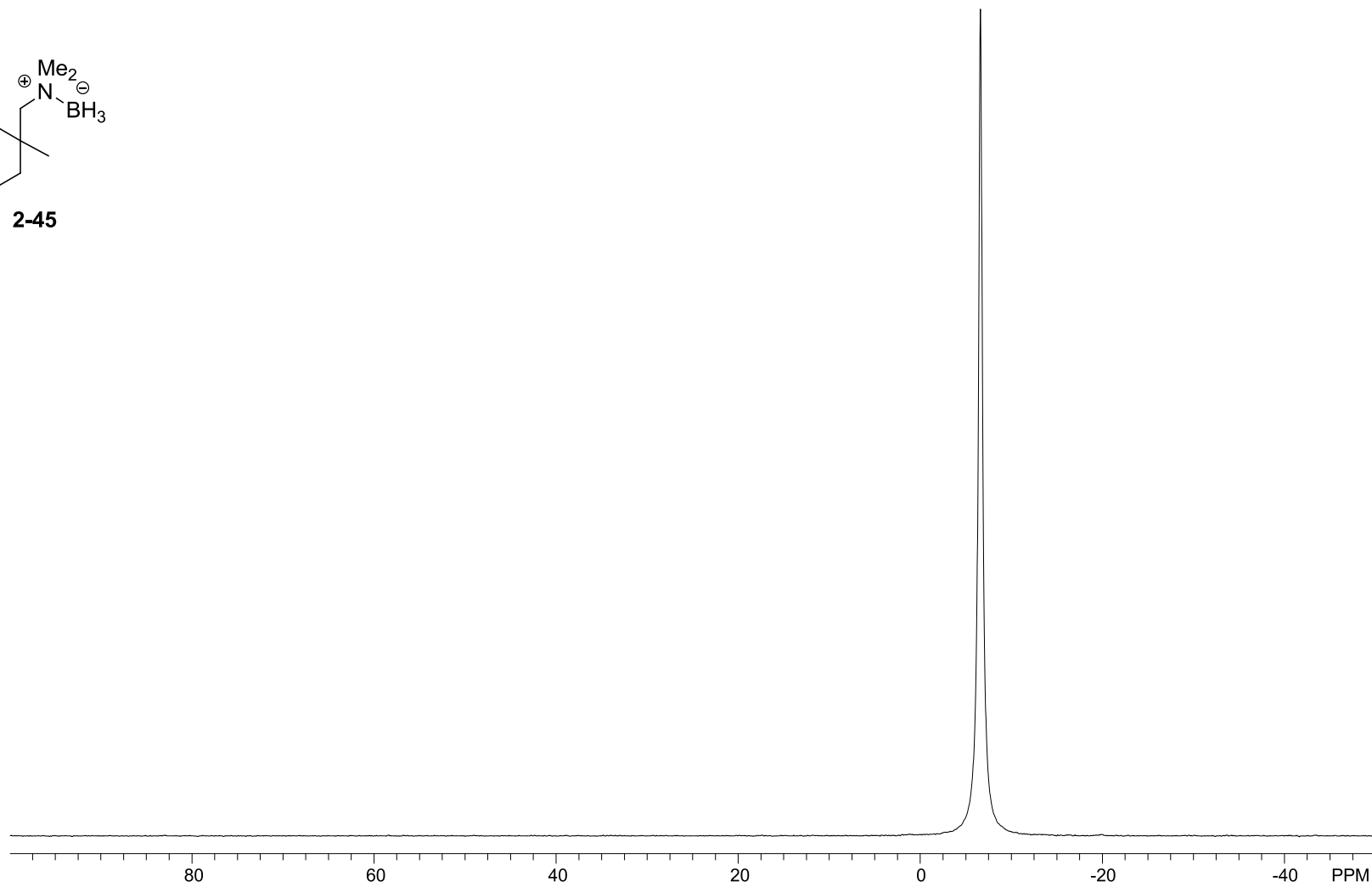
**2-45**



$^{11}\text{B}\{^1\text{H}\}$  NMR (128 MHz),  
 $\text{CDCl}_3$



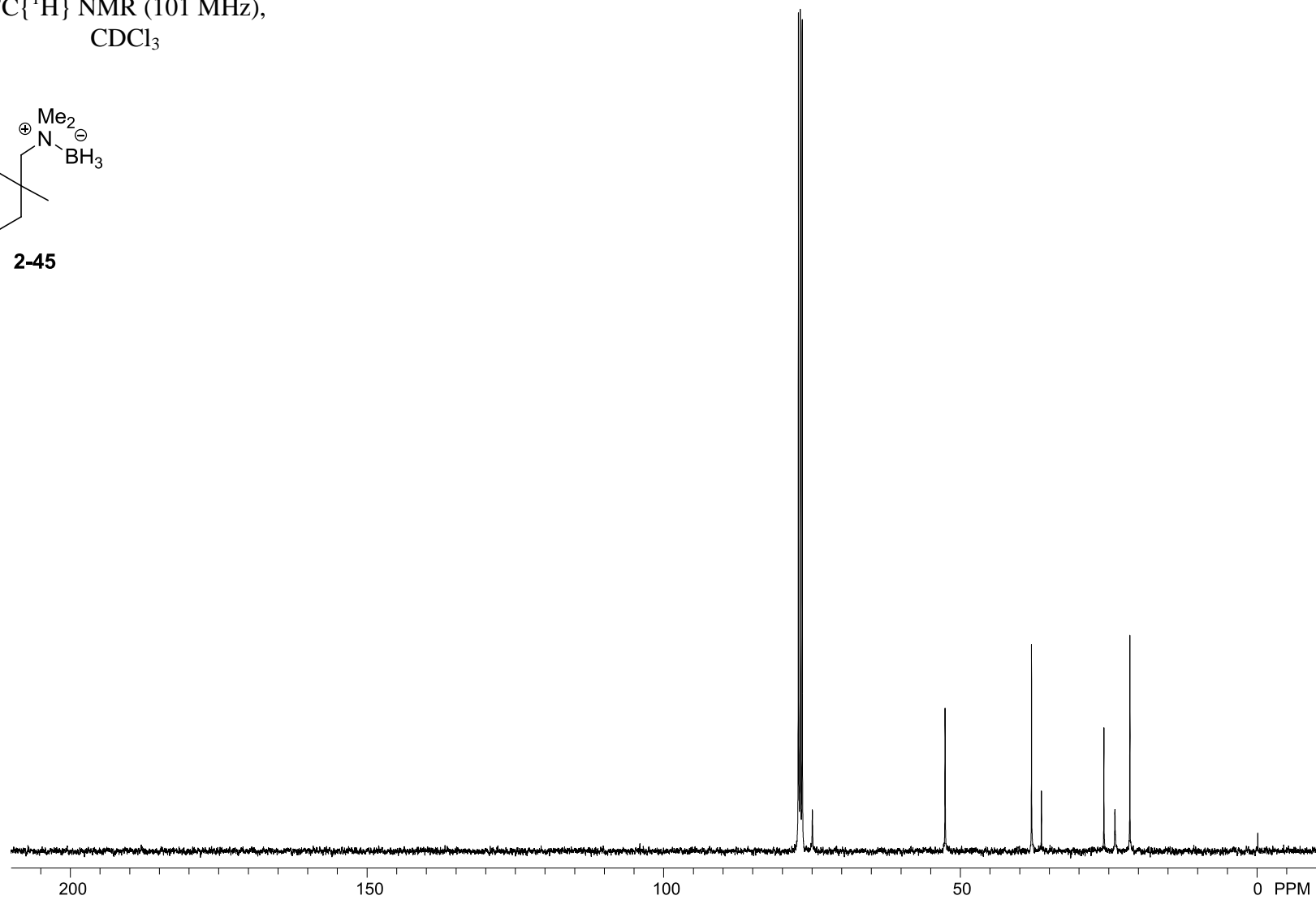
**2-45**



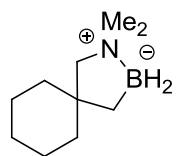
$^{13}\text{C}\{^1\text{H}\}$  NMR (101 MHz),  
 $\text{CDCl}_3$



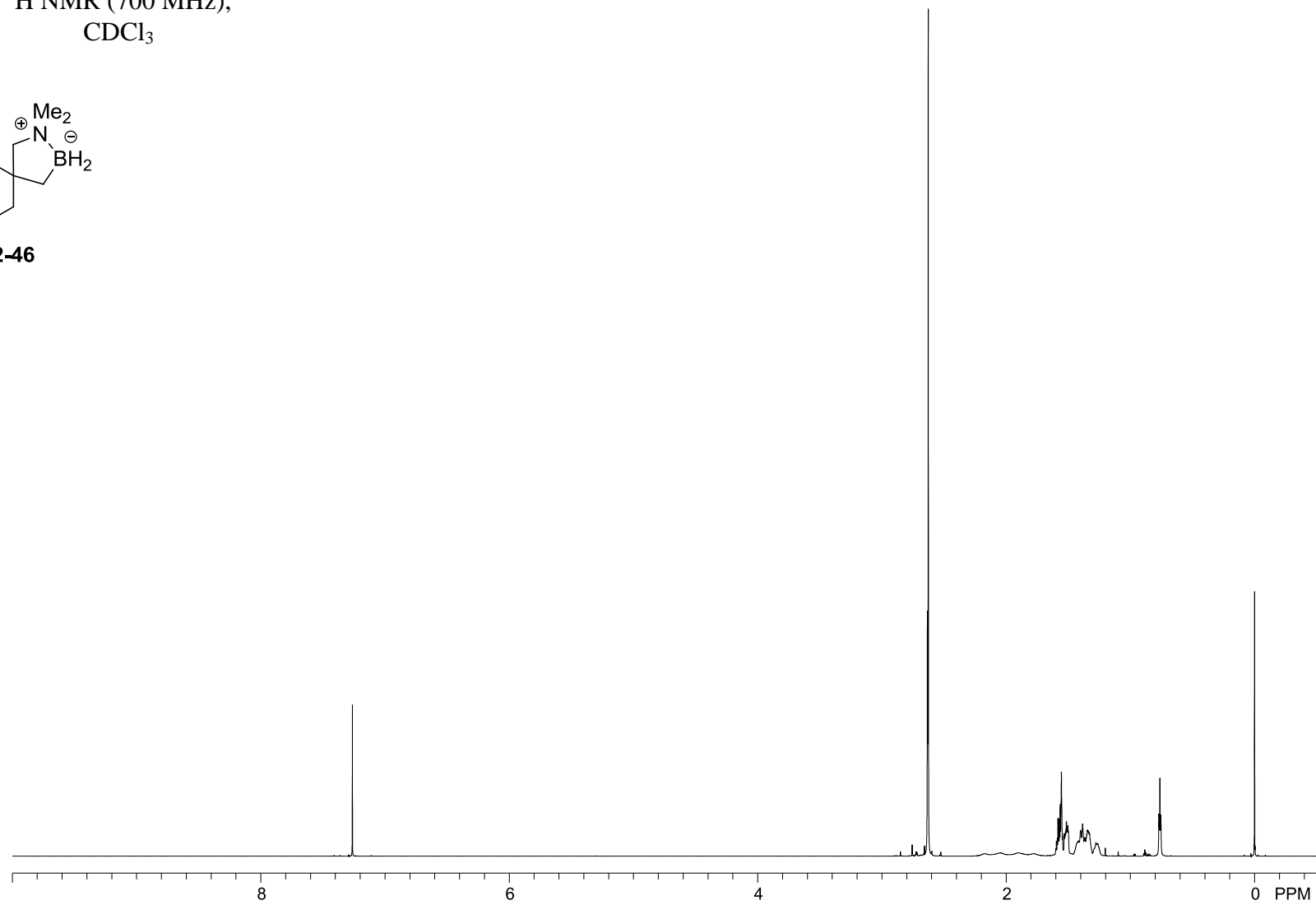
2-45



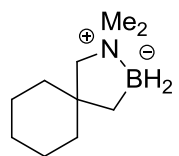
$^1\text{H}$  NMR (700 MHz),  
 $\text{CDCl}_3$



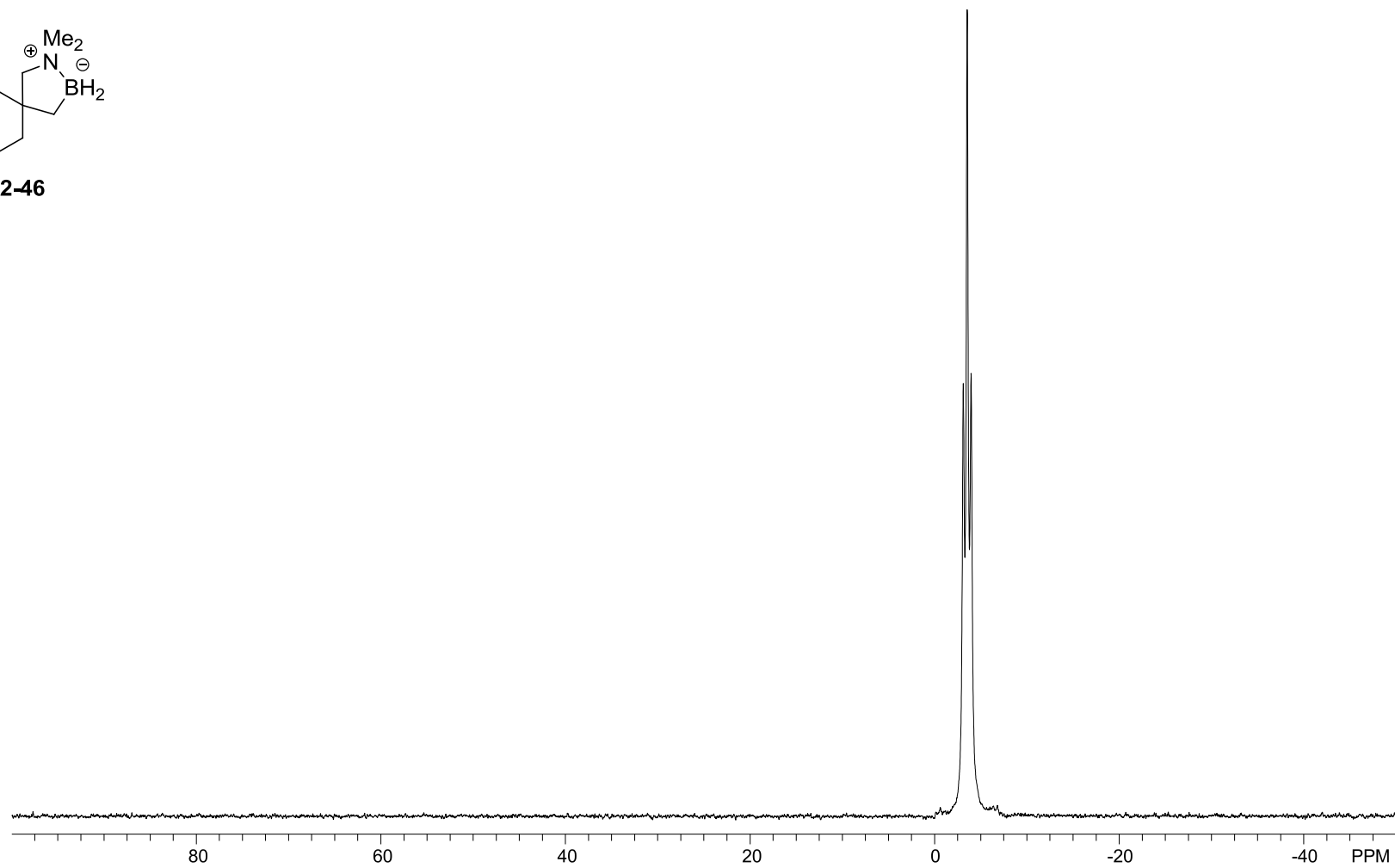
2-46



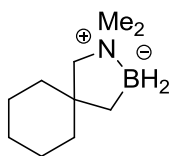
$^{11}\text{B}$  NMR (225 MHz),  
 $\text{CDCl}_3$



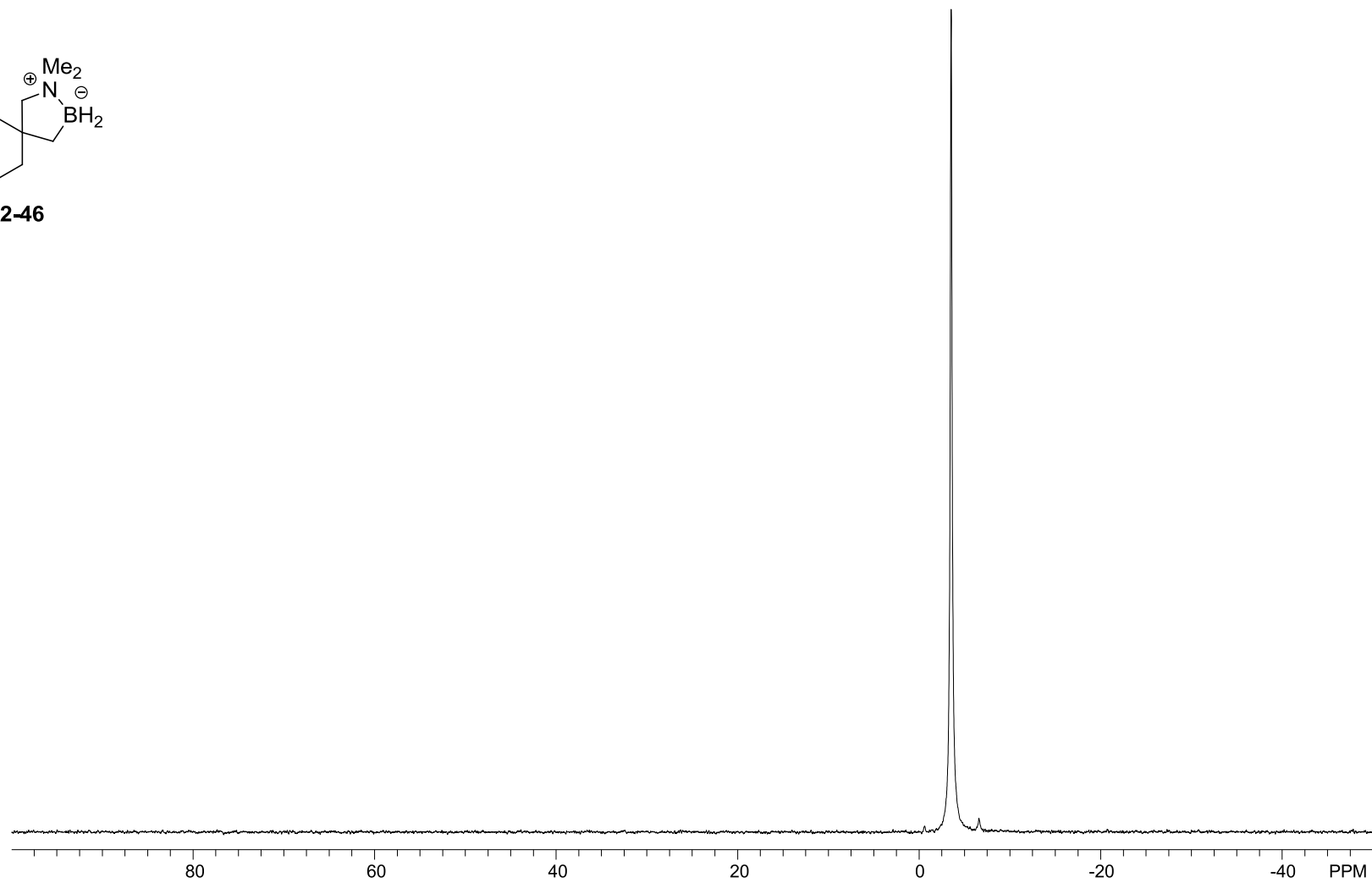
**2-46**



$^{11}\text{B}\{^1\text{H}\}$  NMR (225 MHz),  
 $\text{CDCl}_3$

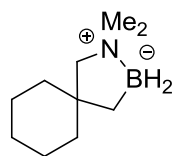


**2-46**

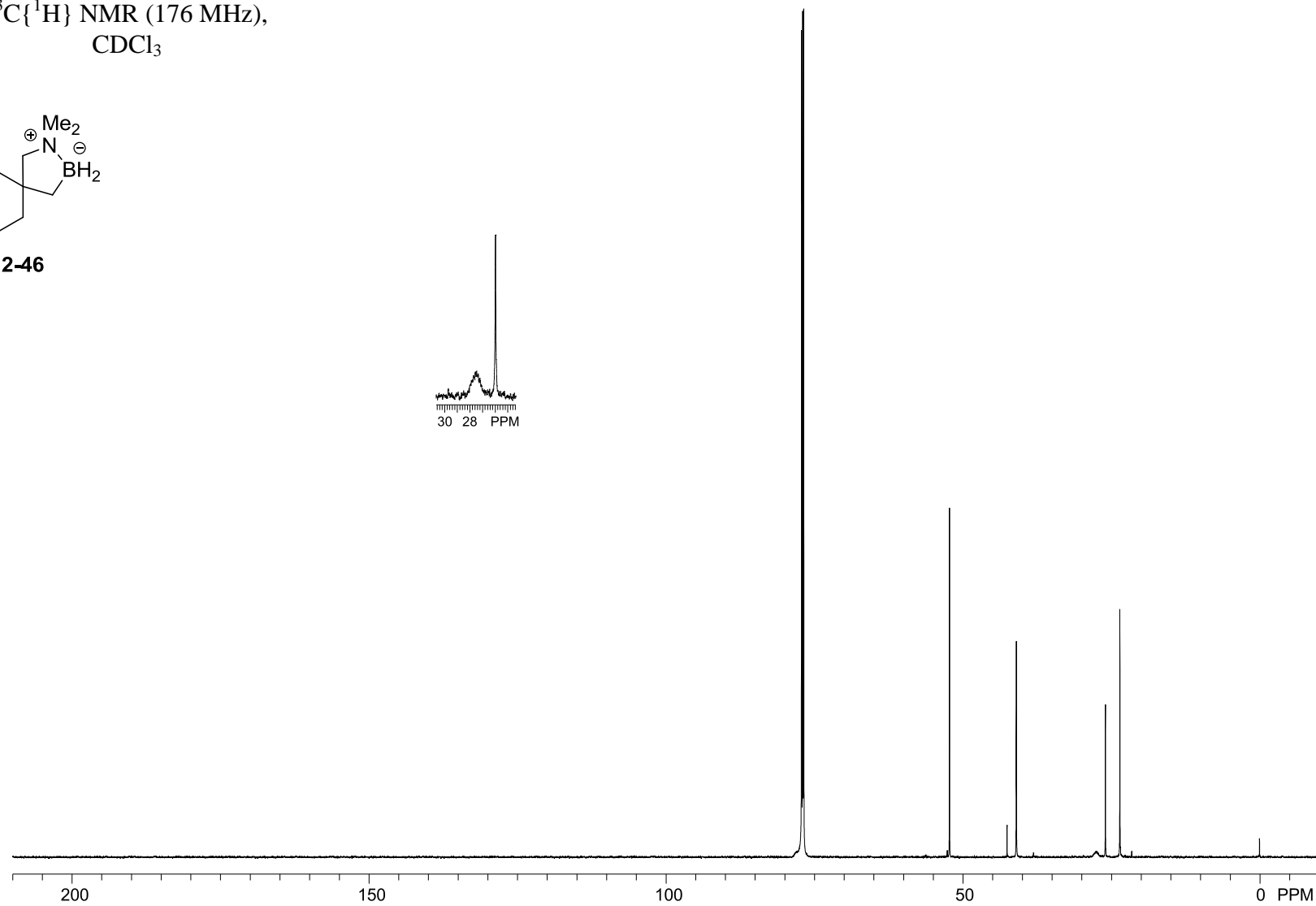




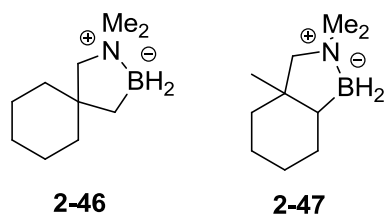
$^{13}\text{C}\{^1\text{H}\}$  NMR (176 MHz),  
 $\text{CDCl}_3$



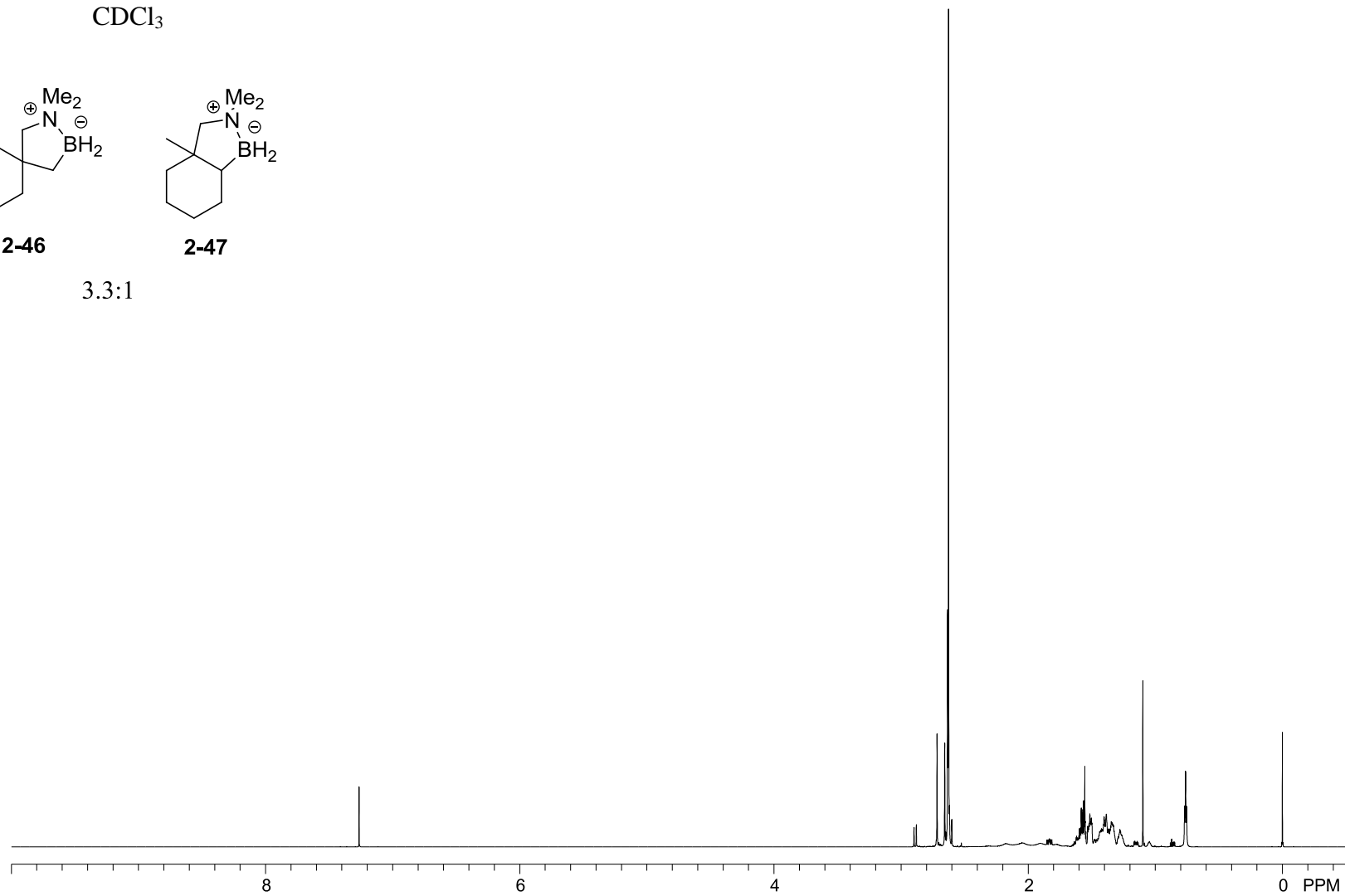
2-46



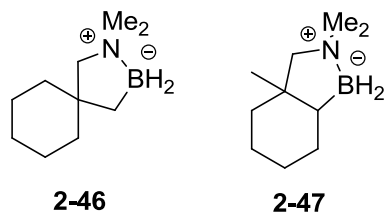
$^1\text{H}$  NMR (700 MHz),  
 $\text{CDCl}_3$



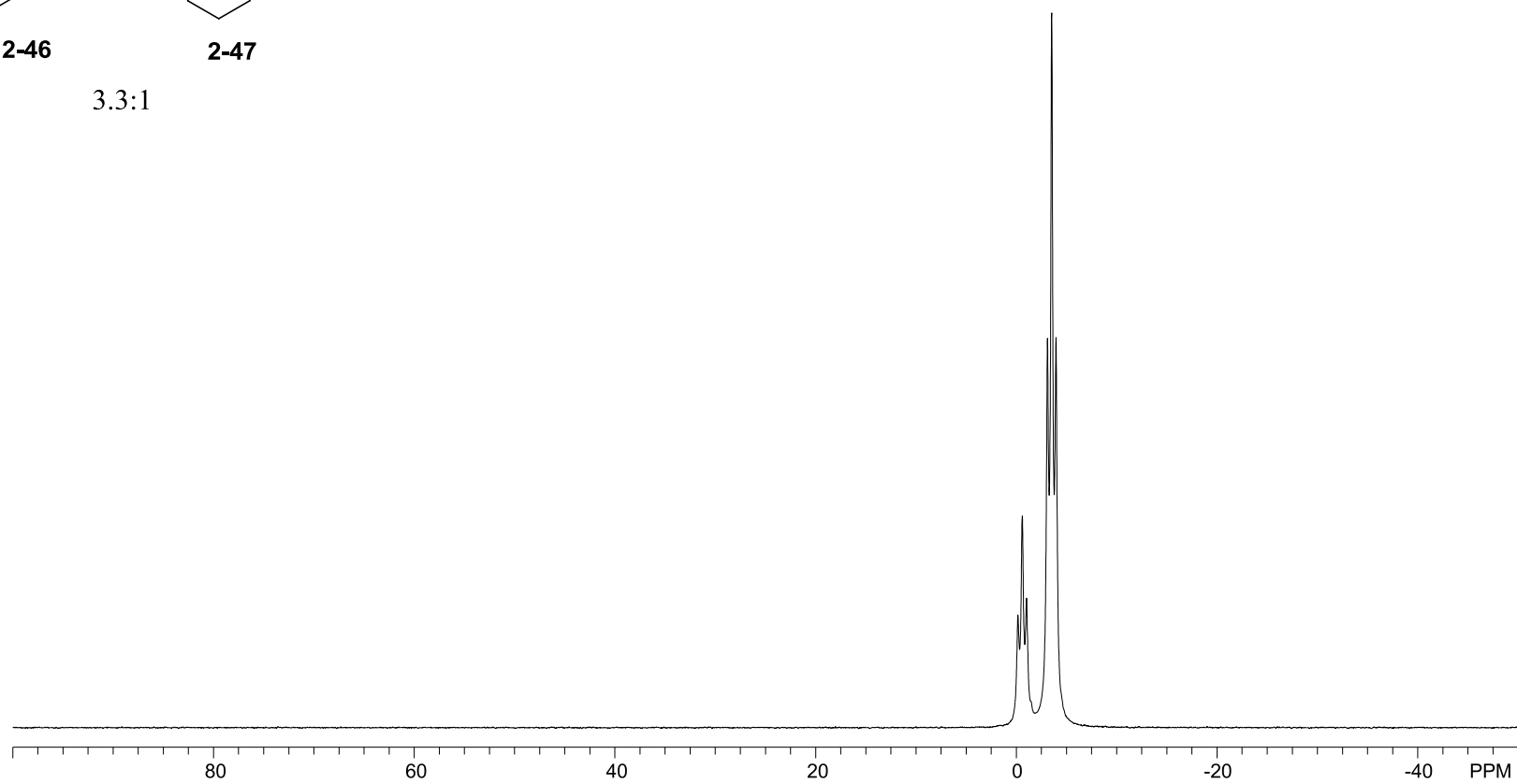
3.3:1



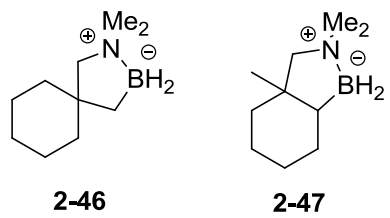
$^{11}\text{B}$  NMR (225 MHz),  
 $\text{CDCl}_3$



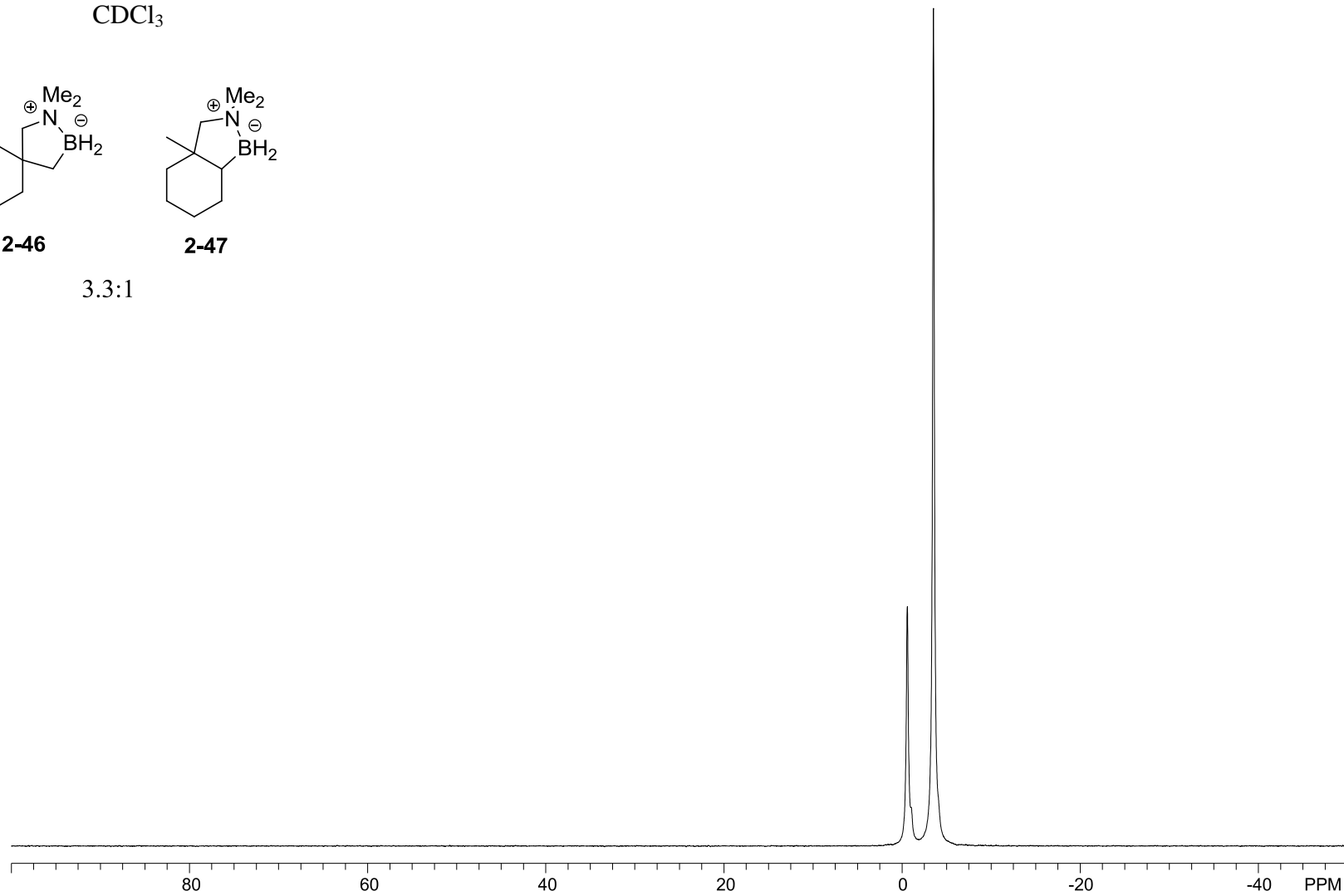
3.3:1



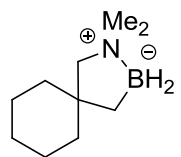
$^{11}\text{B}\{^1\text{H}\}$  NMR (225 MHz),  
 $\text{CDCl}_3$



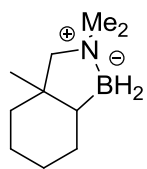
3.3:1



$^{13}\text{C}\{^1\text{H}\}$  NMR (176 MHz),  
 $\text{CDCl}_3$

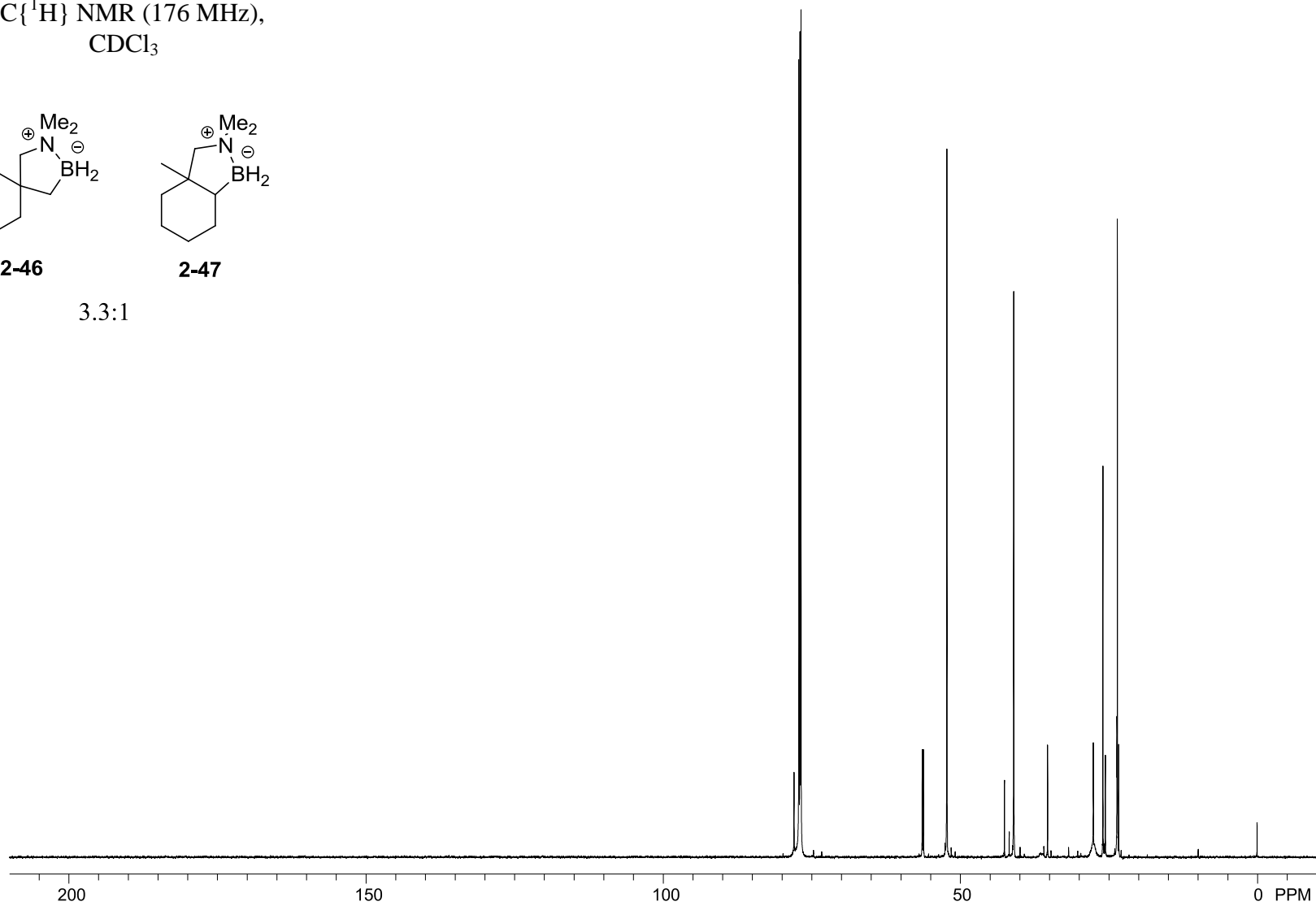


**2-46**

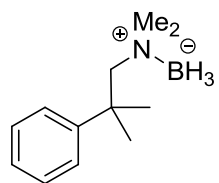


**2-47**

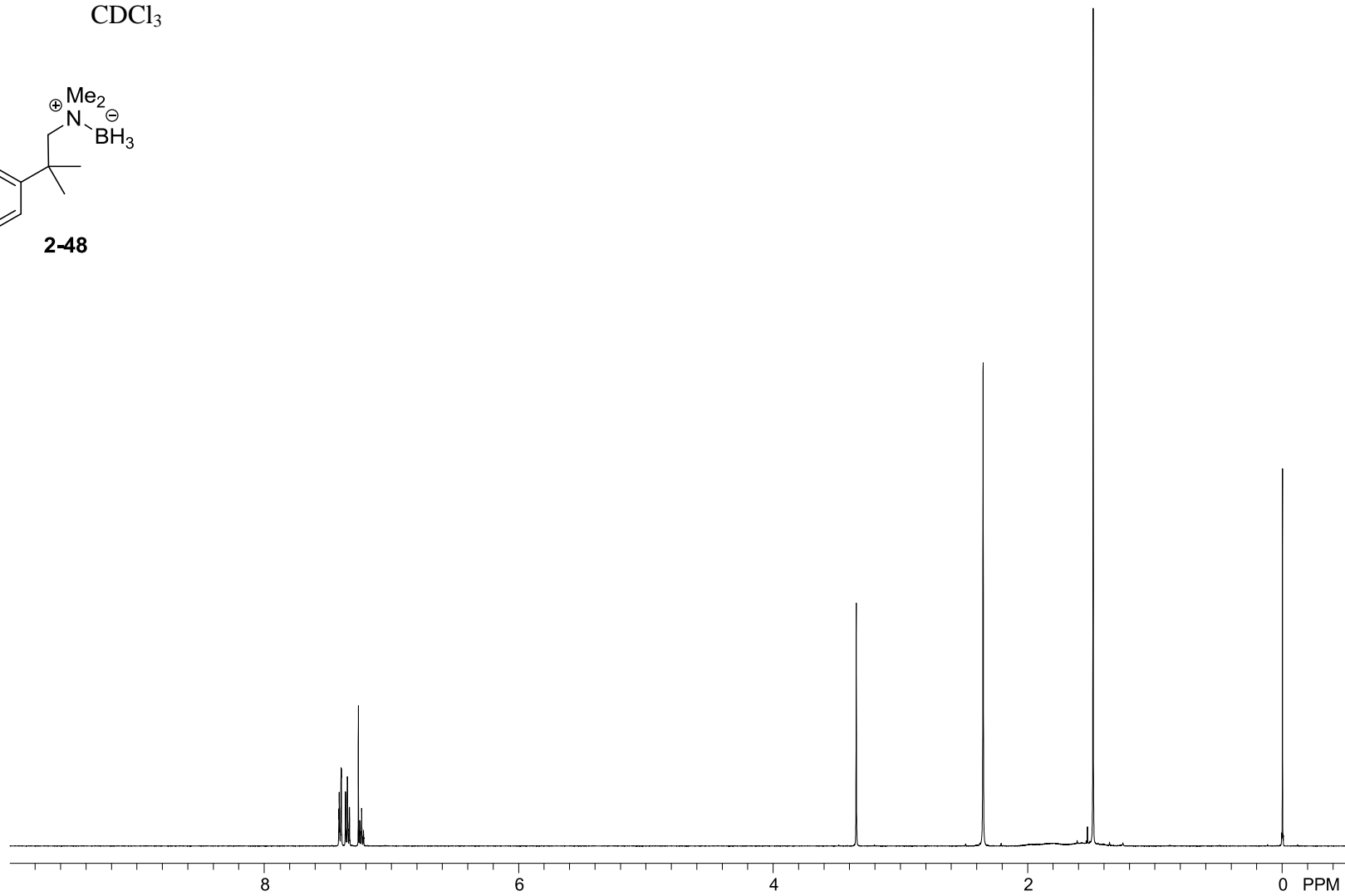
3.3:1



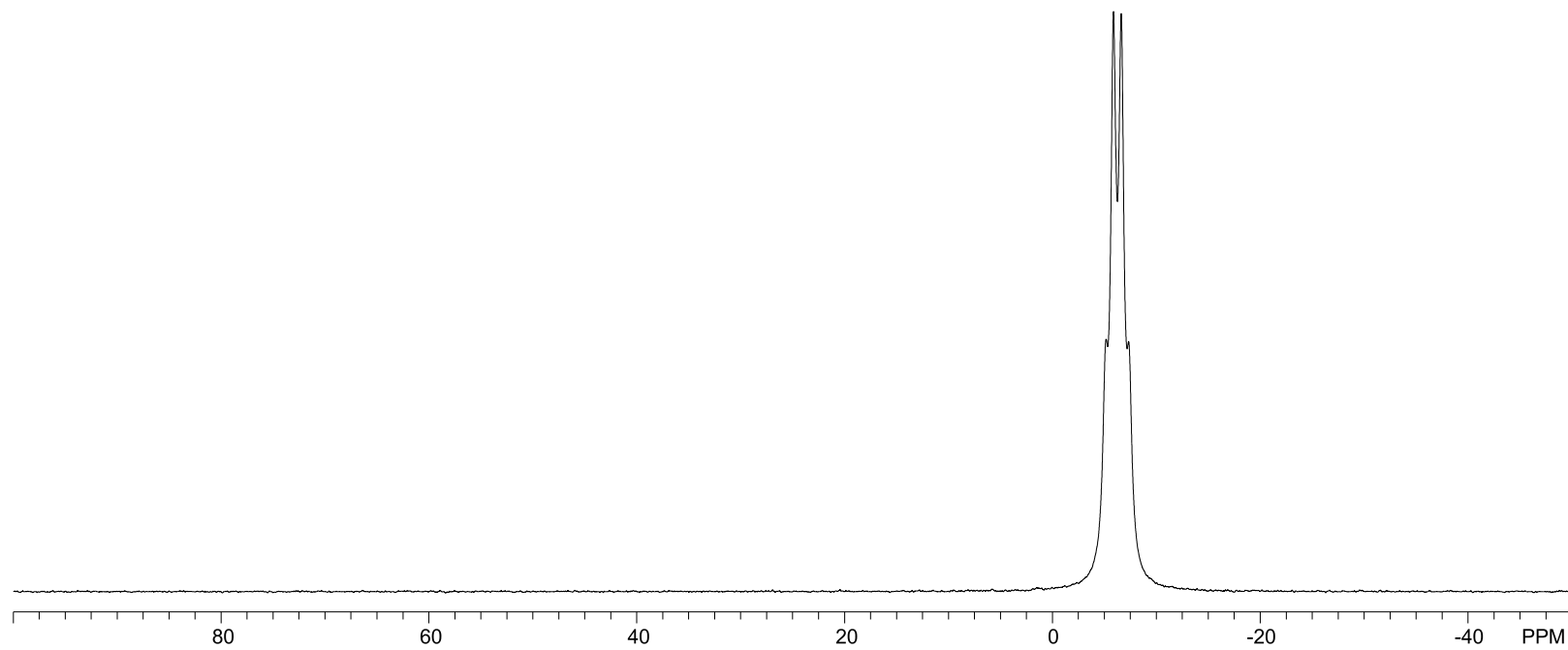
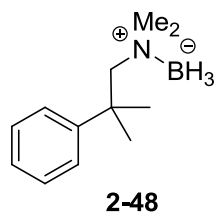
$^1\text{H}$  NMR (500 MHz),  
 $\text{CDCl}_3$



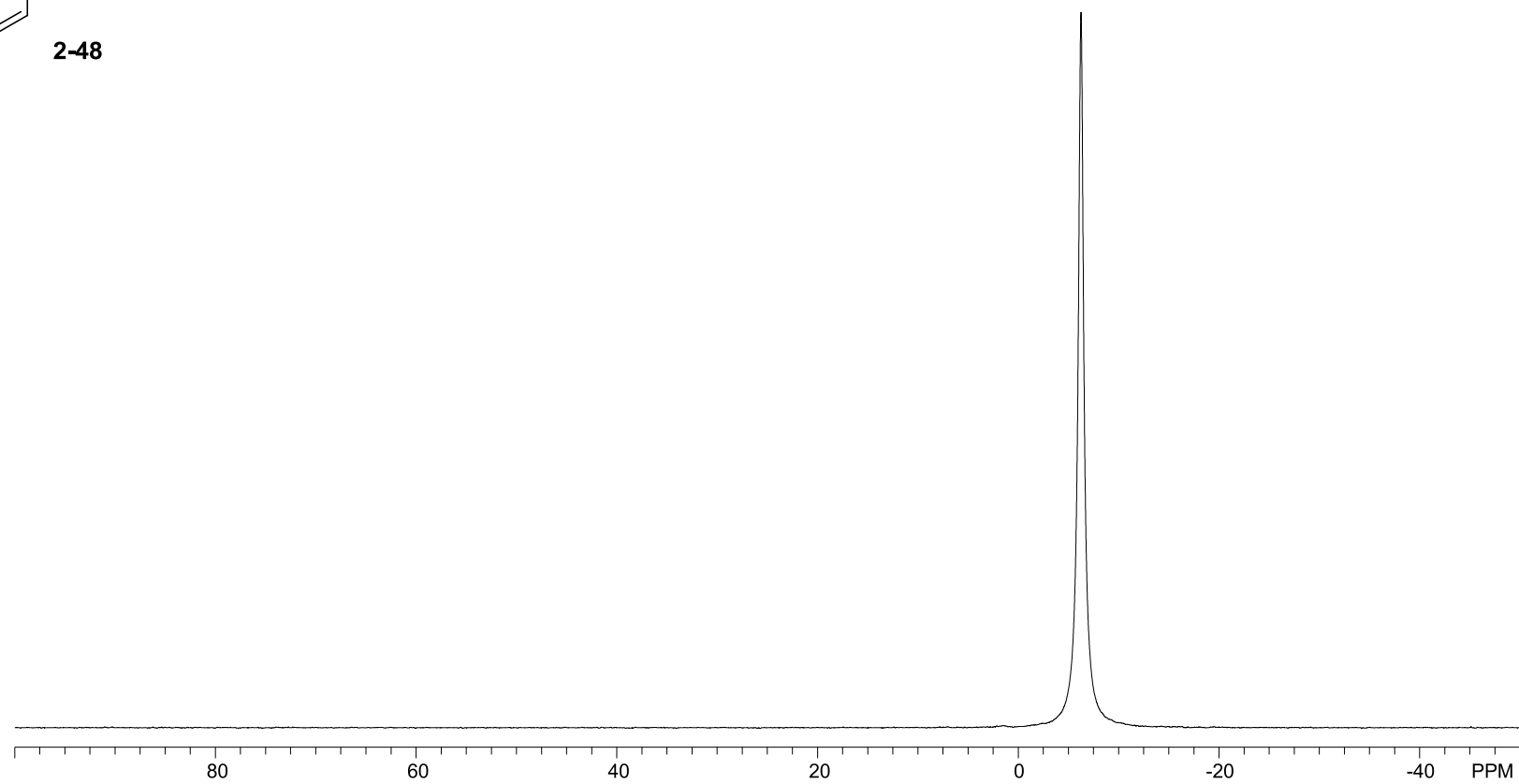
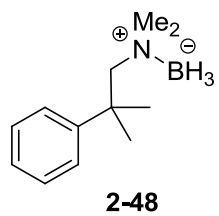
**2-48**



$^{11}\text{B}$  NMR (128 MHz),  
 $\text{CDCl}_3$

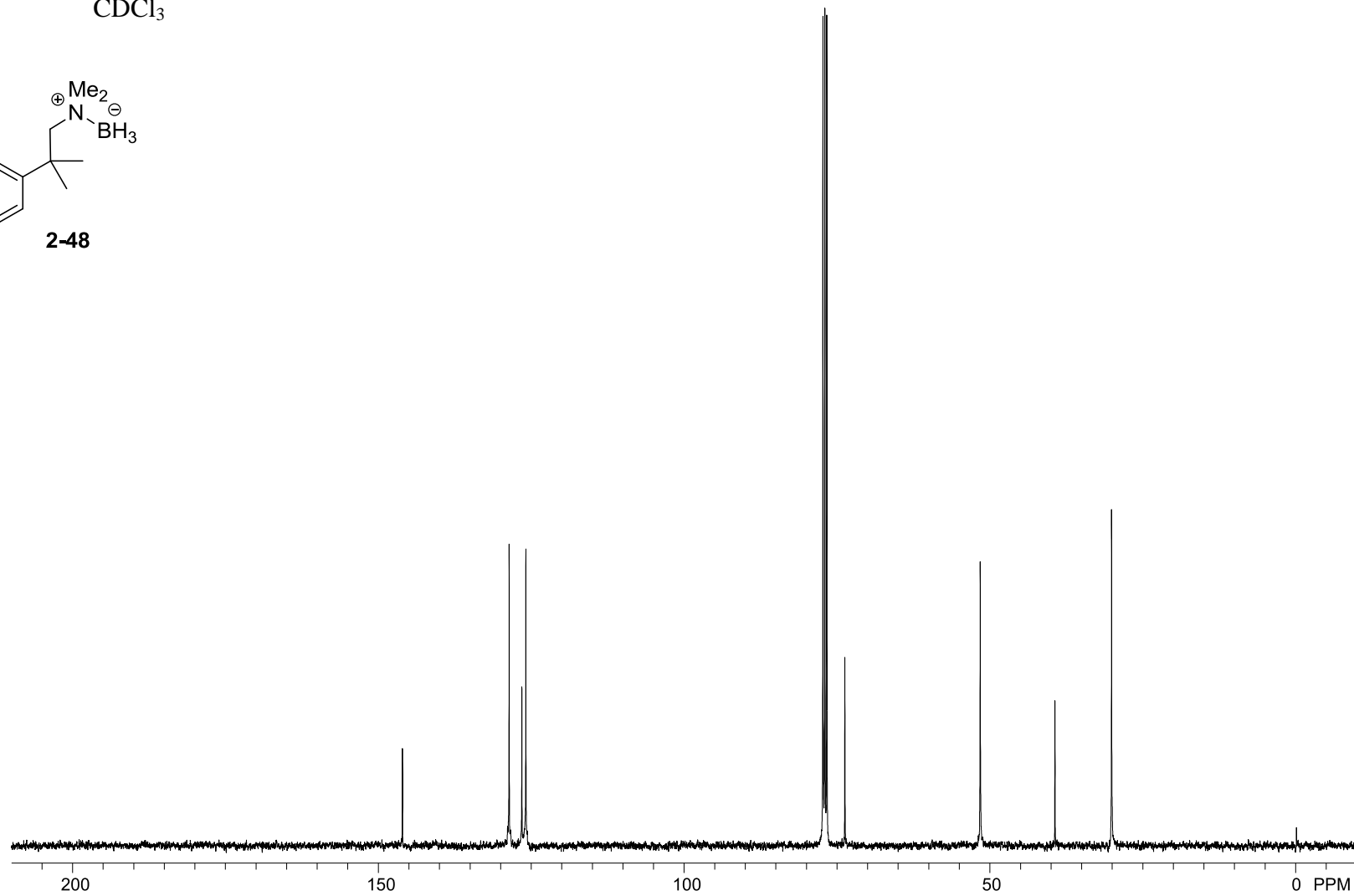
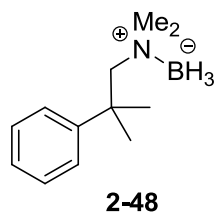


$^{11}\text{B}\{^1\text{H}\}$  NMR (128 MHz),  
 $\text{CDCl}_3$

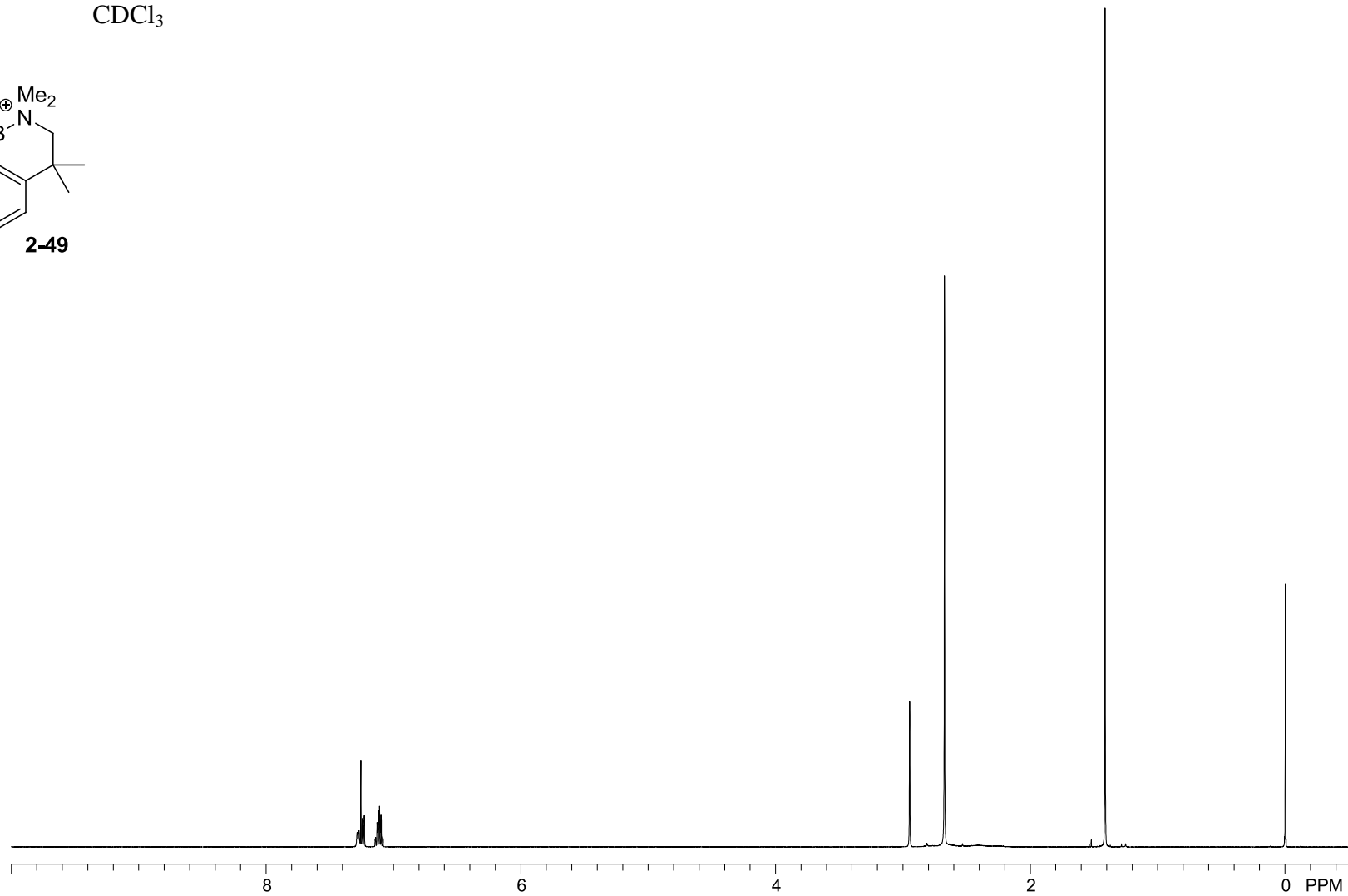
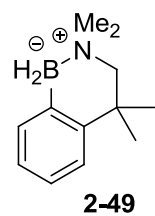




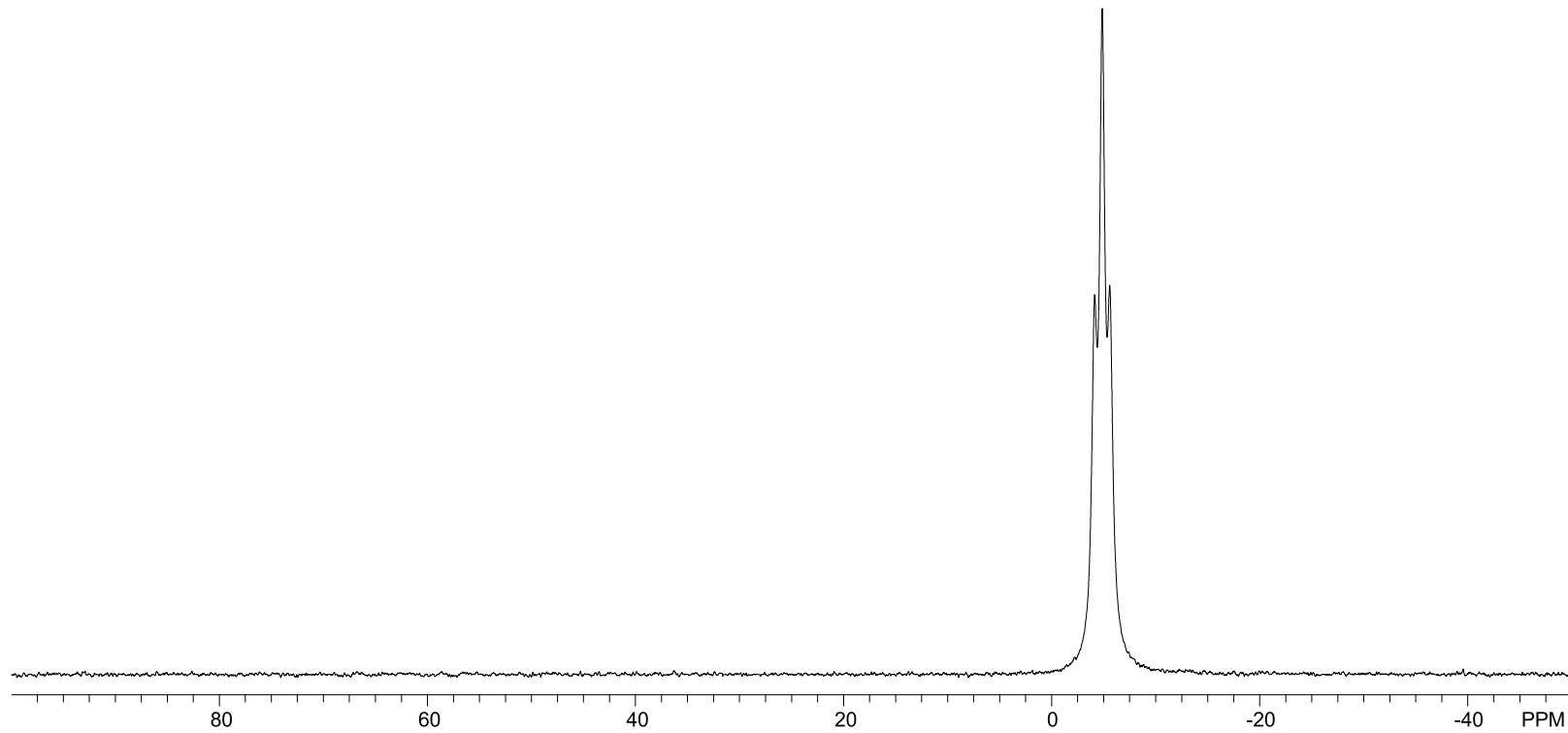
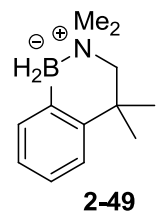
$^{13}\text{C}\{^1\text{H}\}$  NMR (101 MHz),  
 $\text{CDCl}_3$



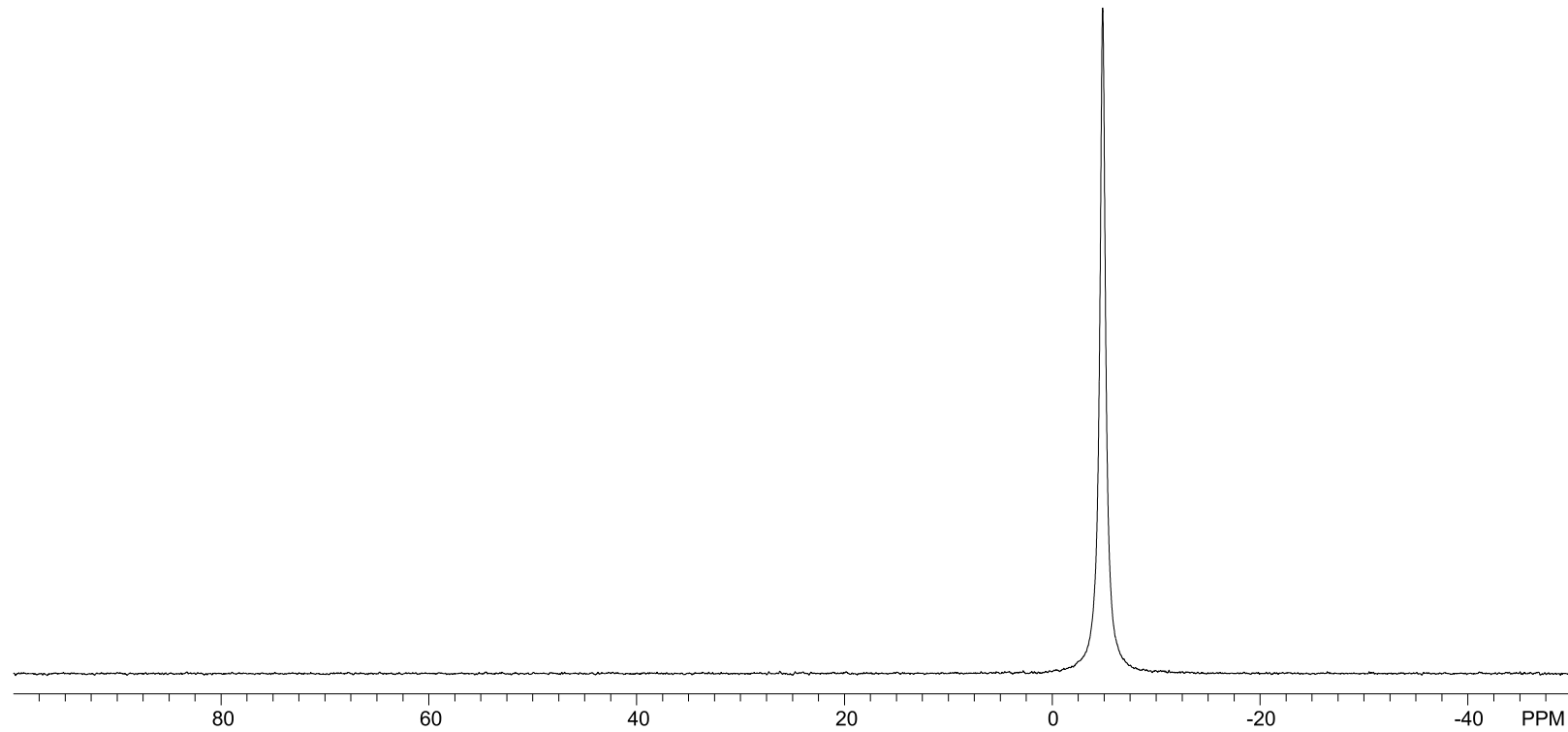
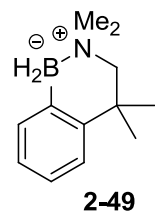
$^1\text{H}$  NMR (500 MHz),  
 $\text{CDCl}_3$



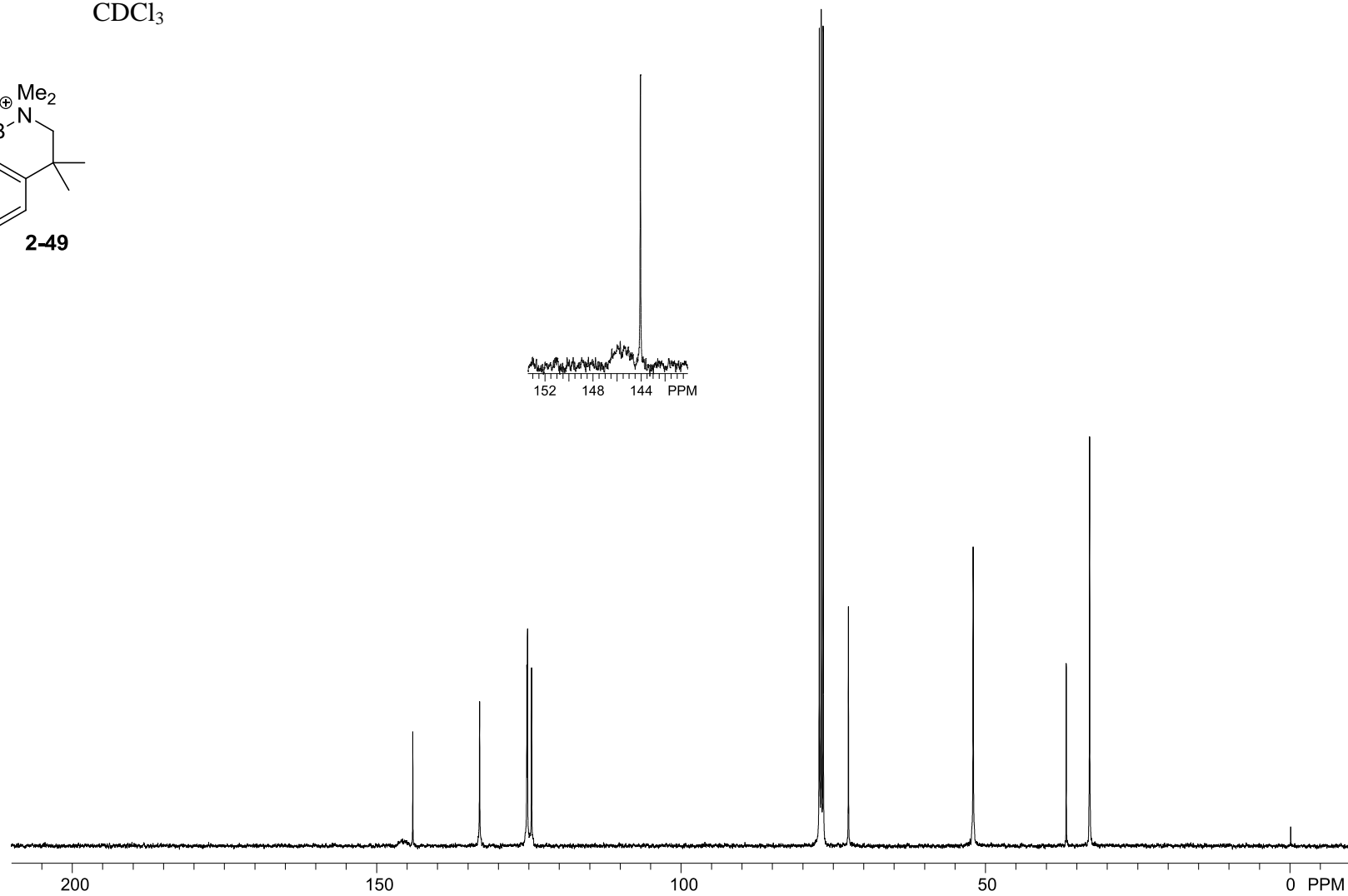
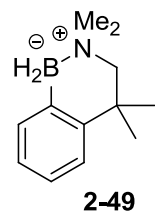
$^{11}\text{B}$  NMR (128 MHz),  
 $\text{CDCl}_3$



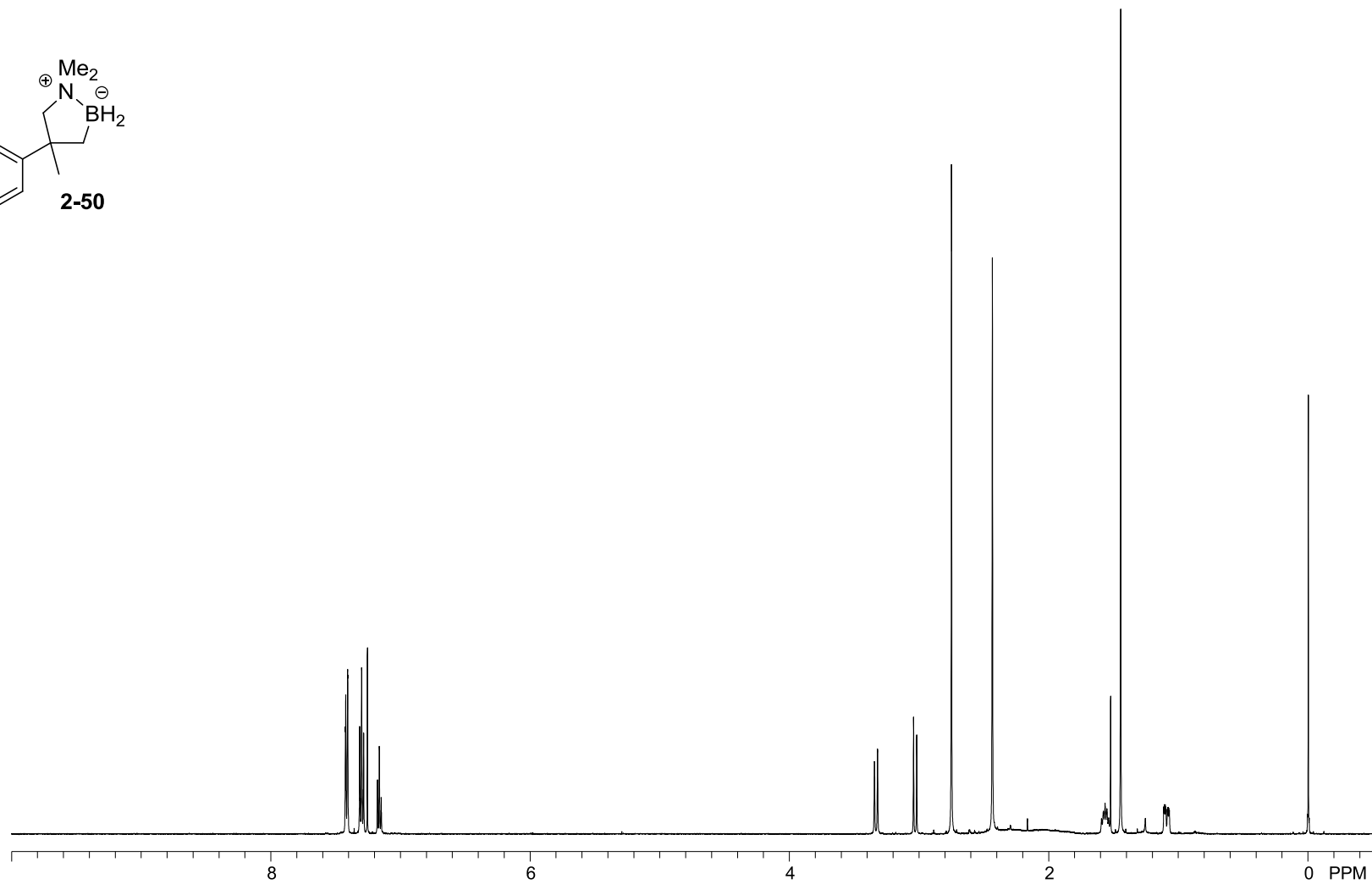
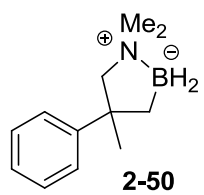
$^{11}\text{B}\{^1\text{H}\}$  NMR (128 MHz),  
 $\text{CDCl}_3$



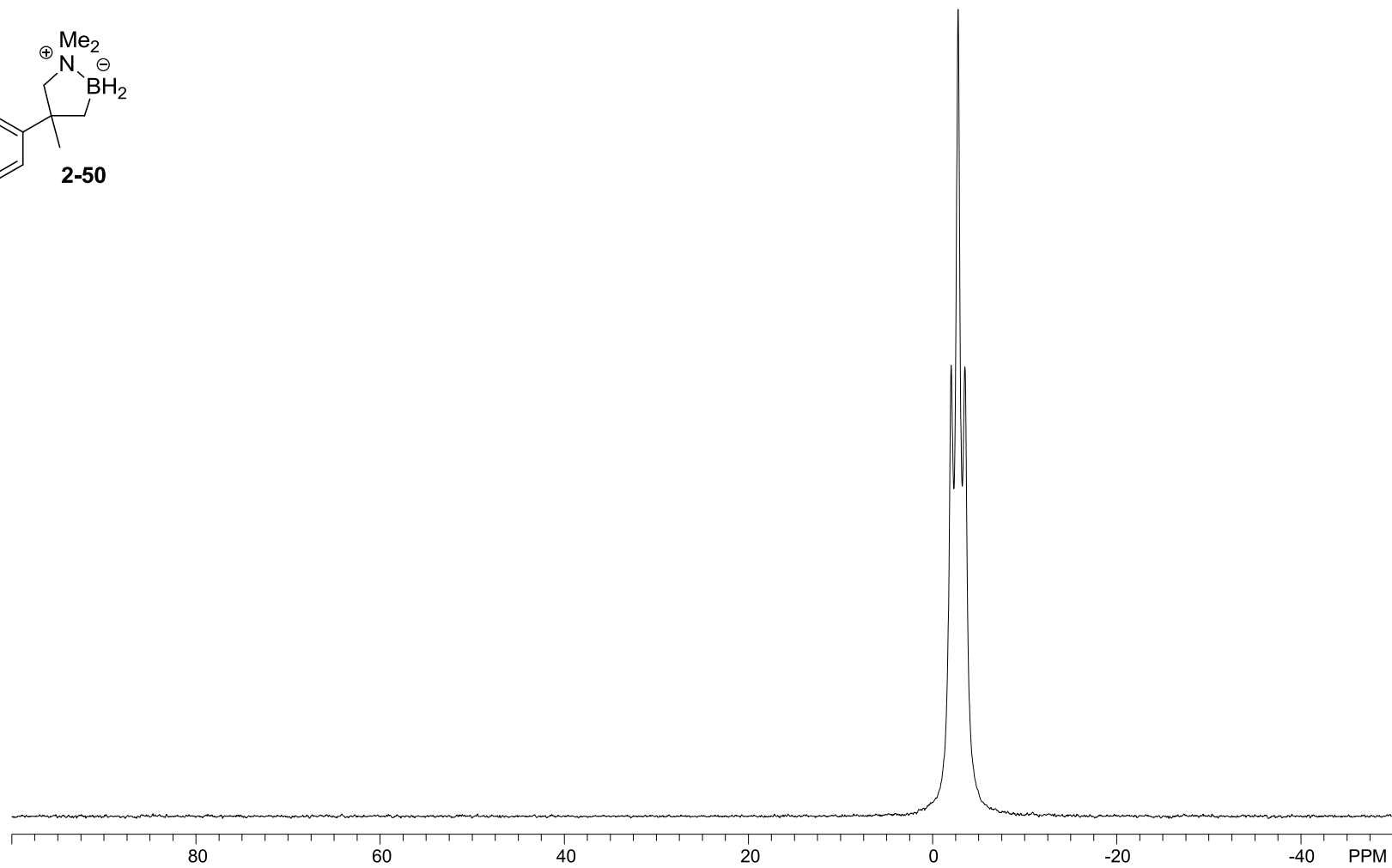
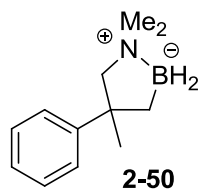
$^{13}\text{C}\{^1\text{H}\}$  NMR (101 MHz),  
 $\text{CDCl}_3$



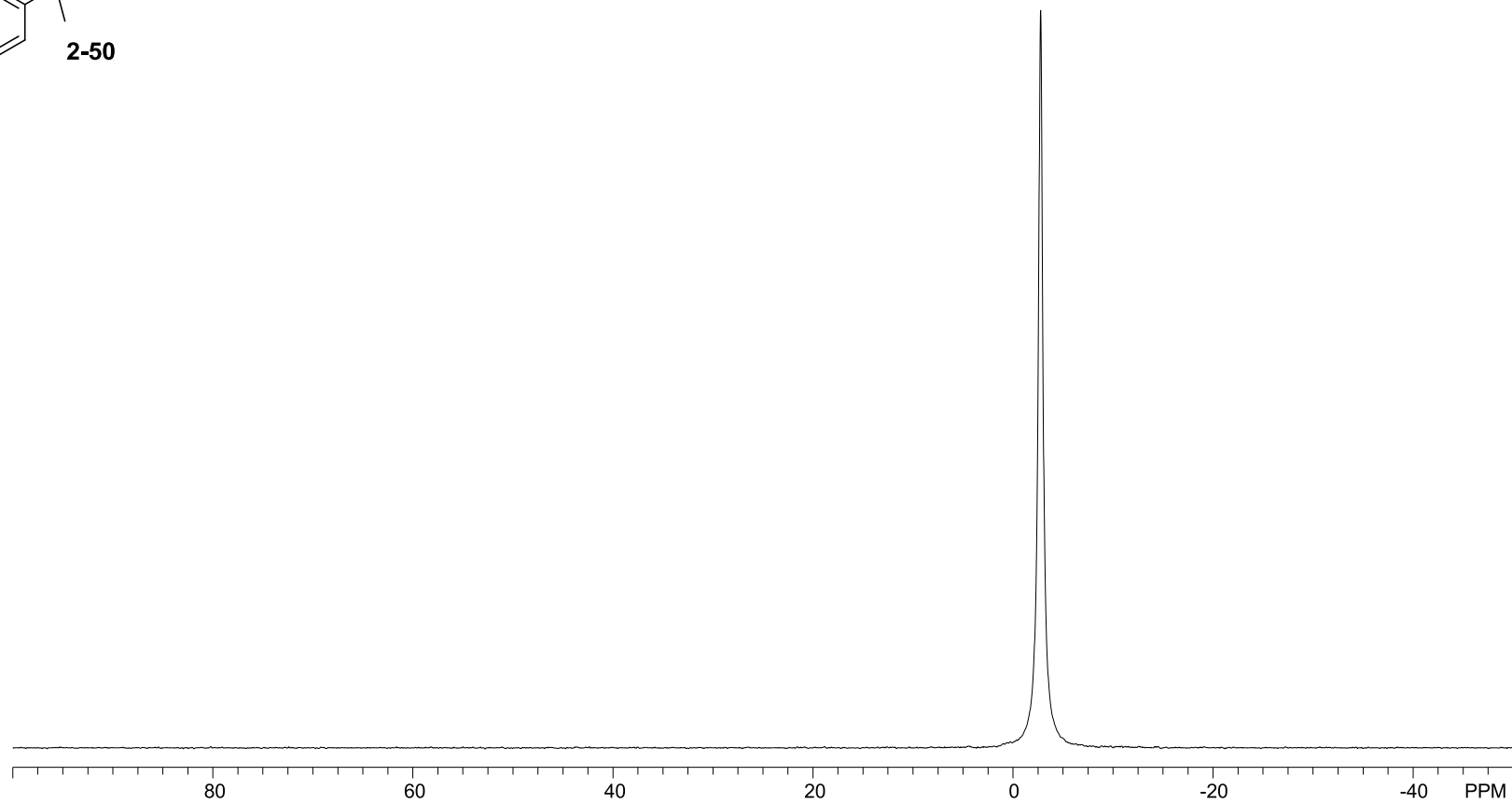
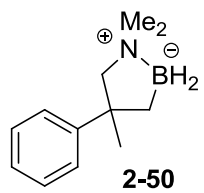
$^1\text{H}$  NMR (500 MHz),  
 $\text{CDCl}_3$



$^{11}\text{B}$  NMR (128 MHz),  
 $\text{CDCl}_3$

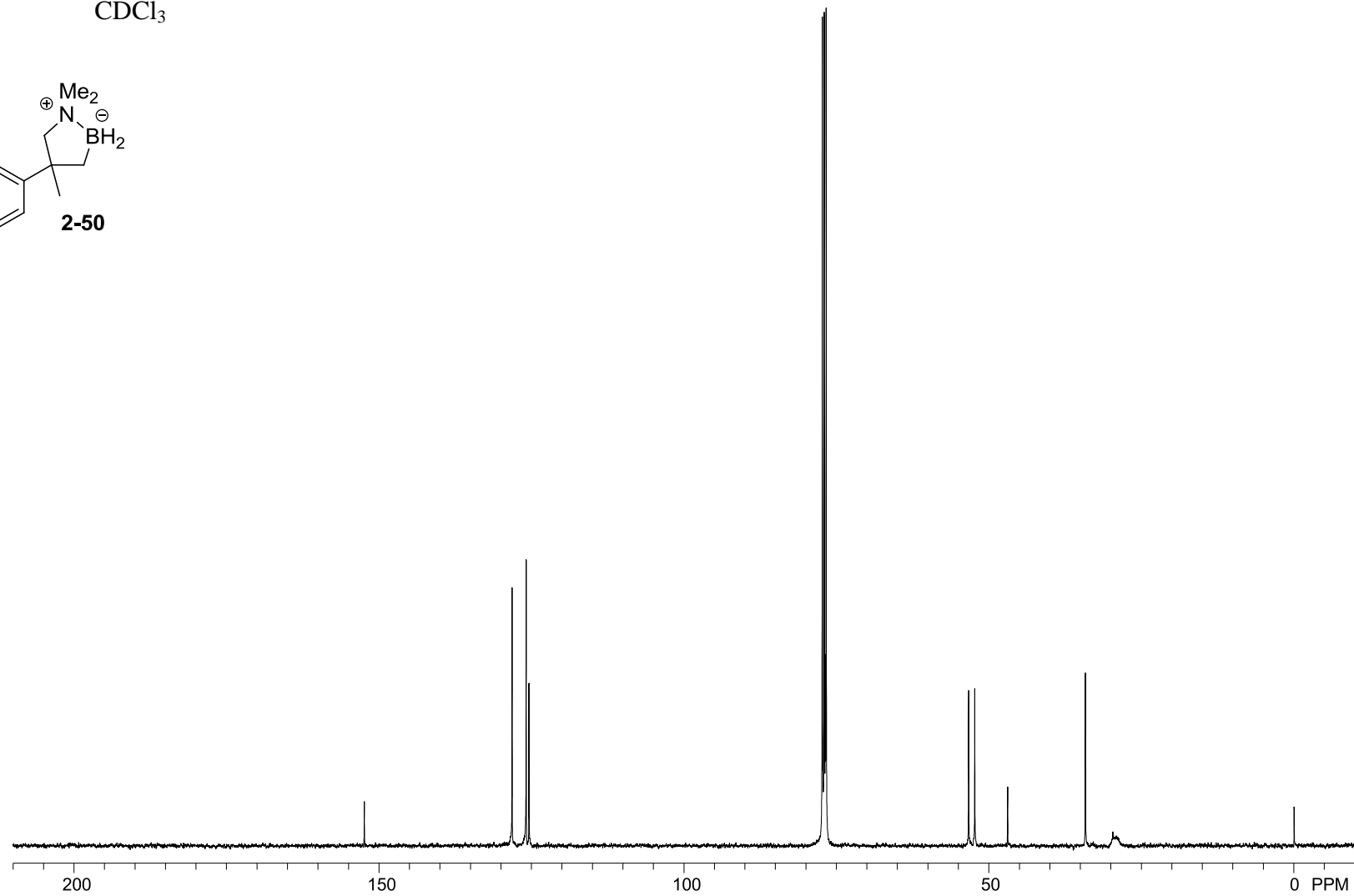
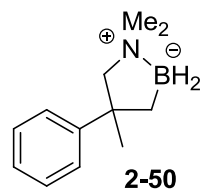


$^{11}\text{B}\{^1\text{H}\}$  NMR (128 MHz),  
 $\text{CDCl}_3$

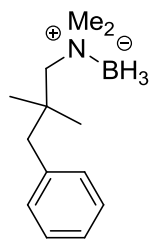




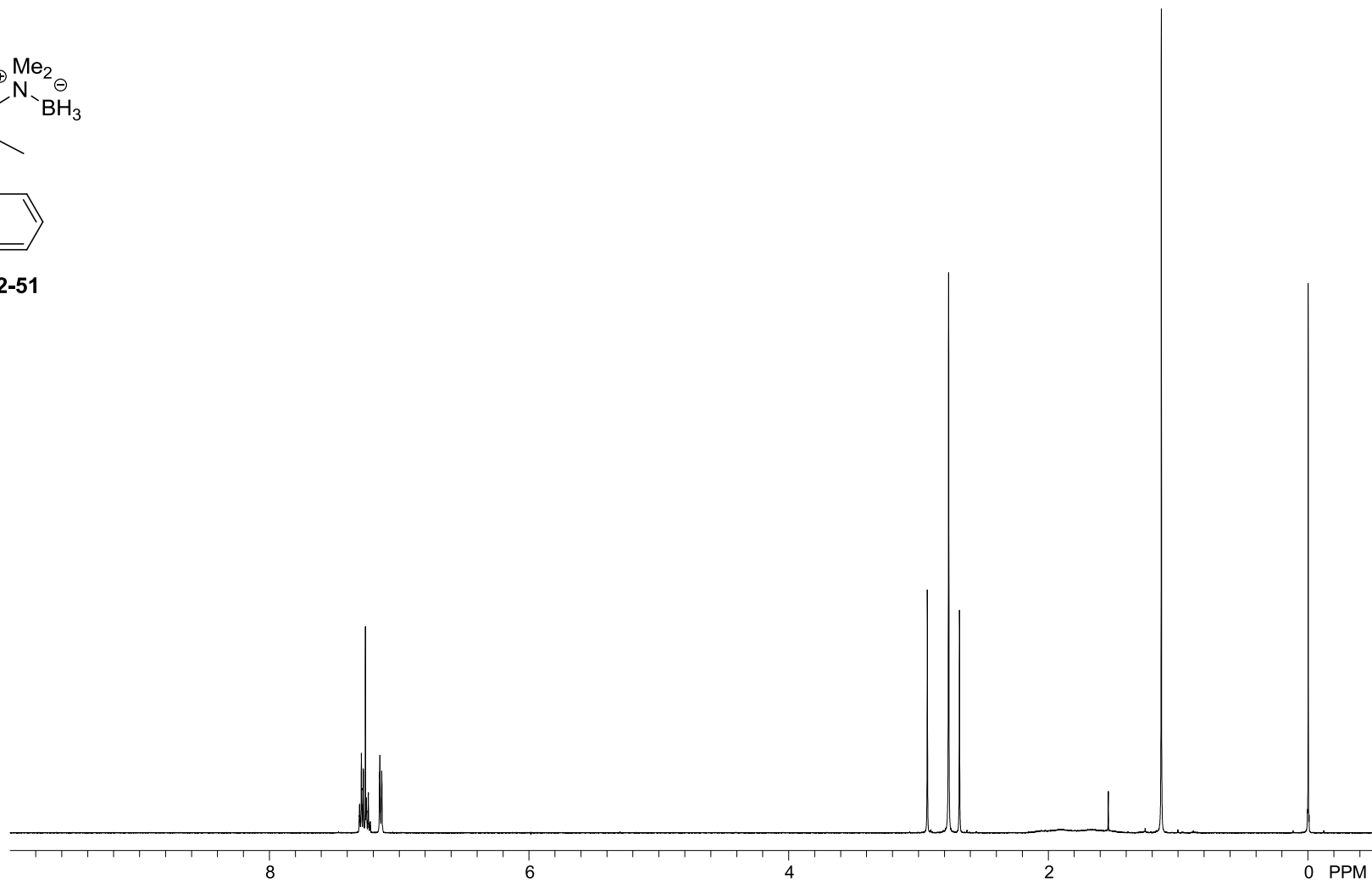
$^{13}\text{C}\{^1\text{H}\}$  NMR (101 MHz),  
 $\text{CDCl}_3$



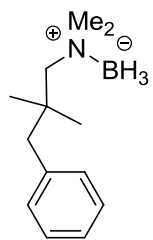
$^1\text{H}$  NMR (500 MHz),  
 $\text{CDCl}_3$



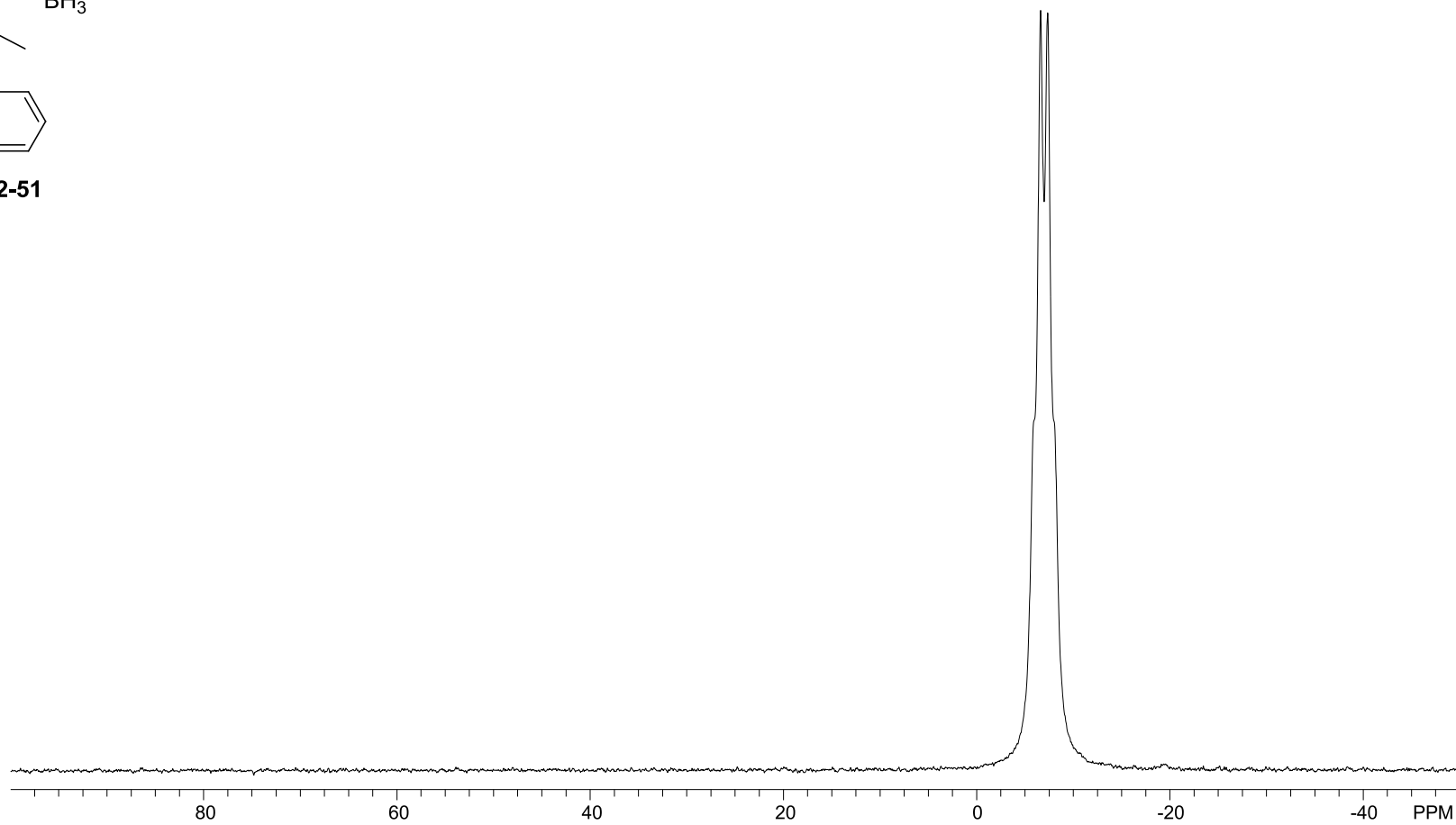
**2-51**



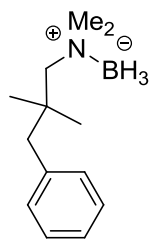
$^{11}\text{B}$  NMR (128 MHz),  
 $\text{CDCl}_3$



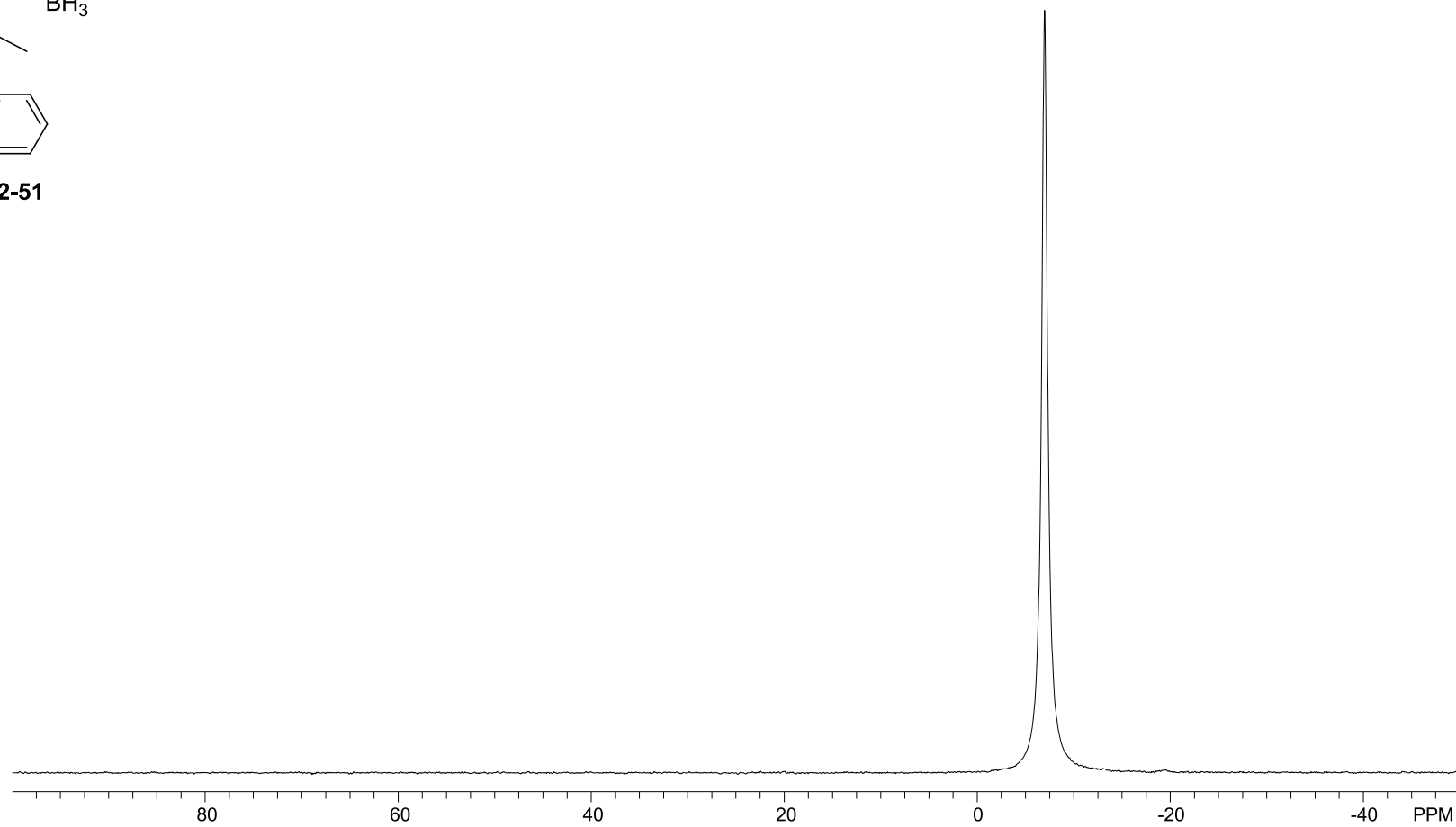
**2-51**



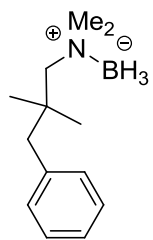
$^{11}\text{B}\{^1\text{H}\}$  NMR (128 MHz),  
 $\text{CDCl}_3$



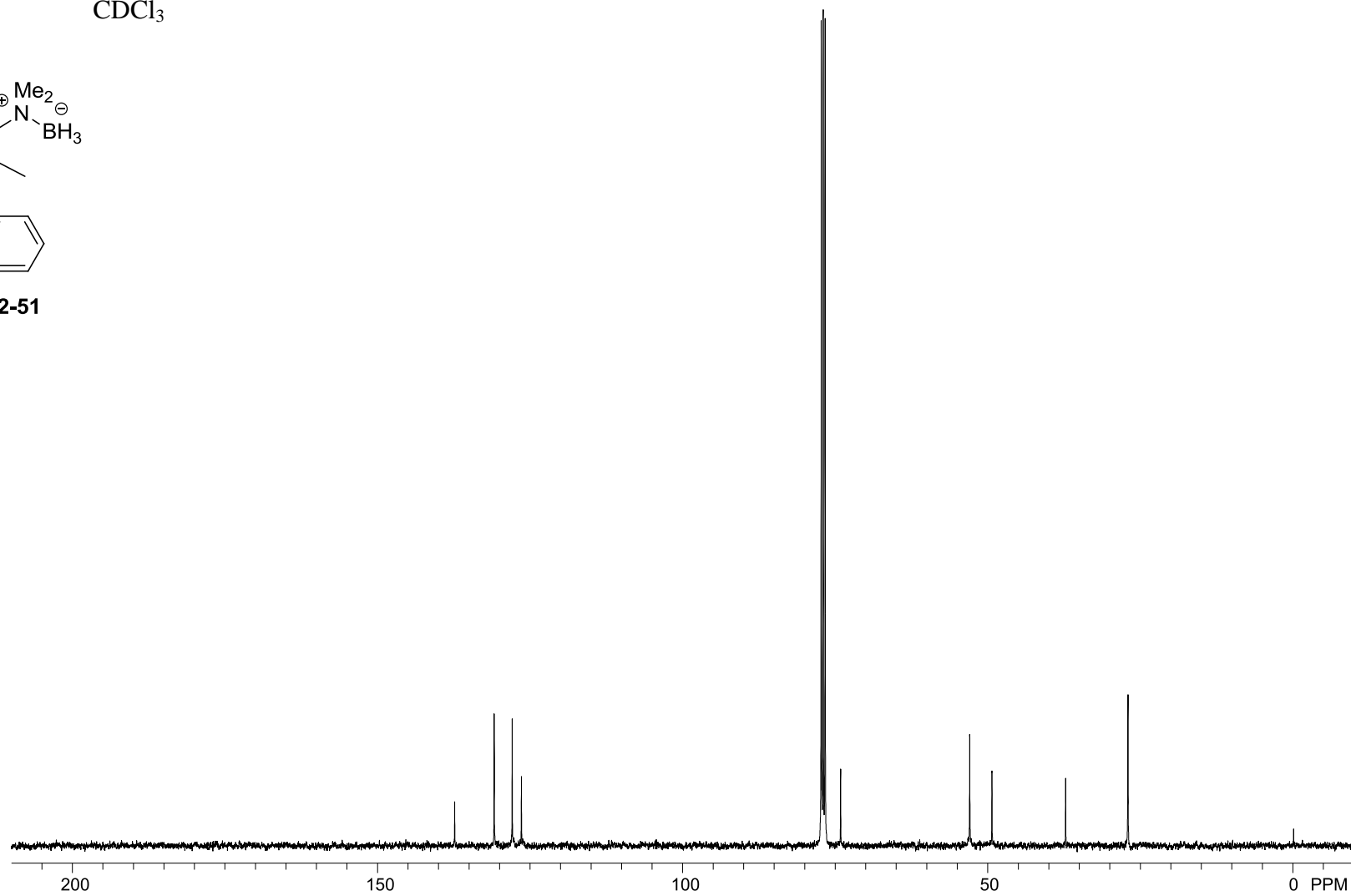
**2-51**



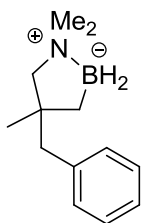
$^{13}\text{C}\{^1\text{H}\}$  NMR (101 MHz),  
 $\text{CDCl}_3$



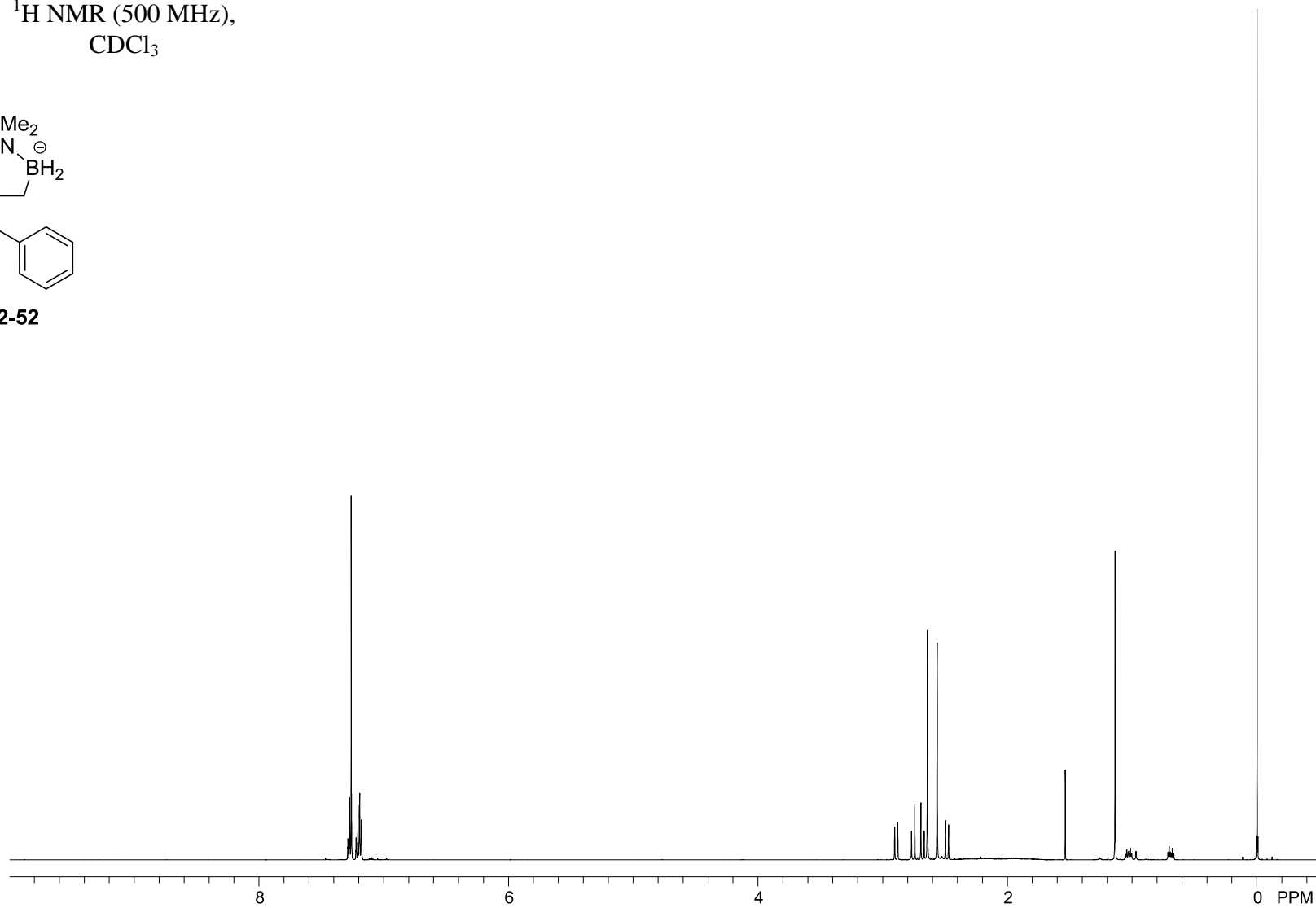
**2-51**



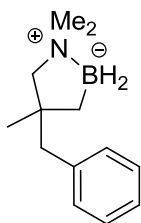
$^1\text{H}$  NMR (500 MHz),  
 $\text{CDCl}_3$



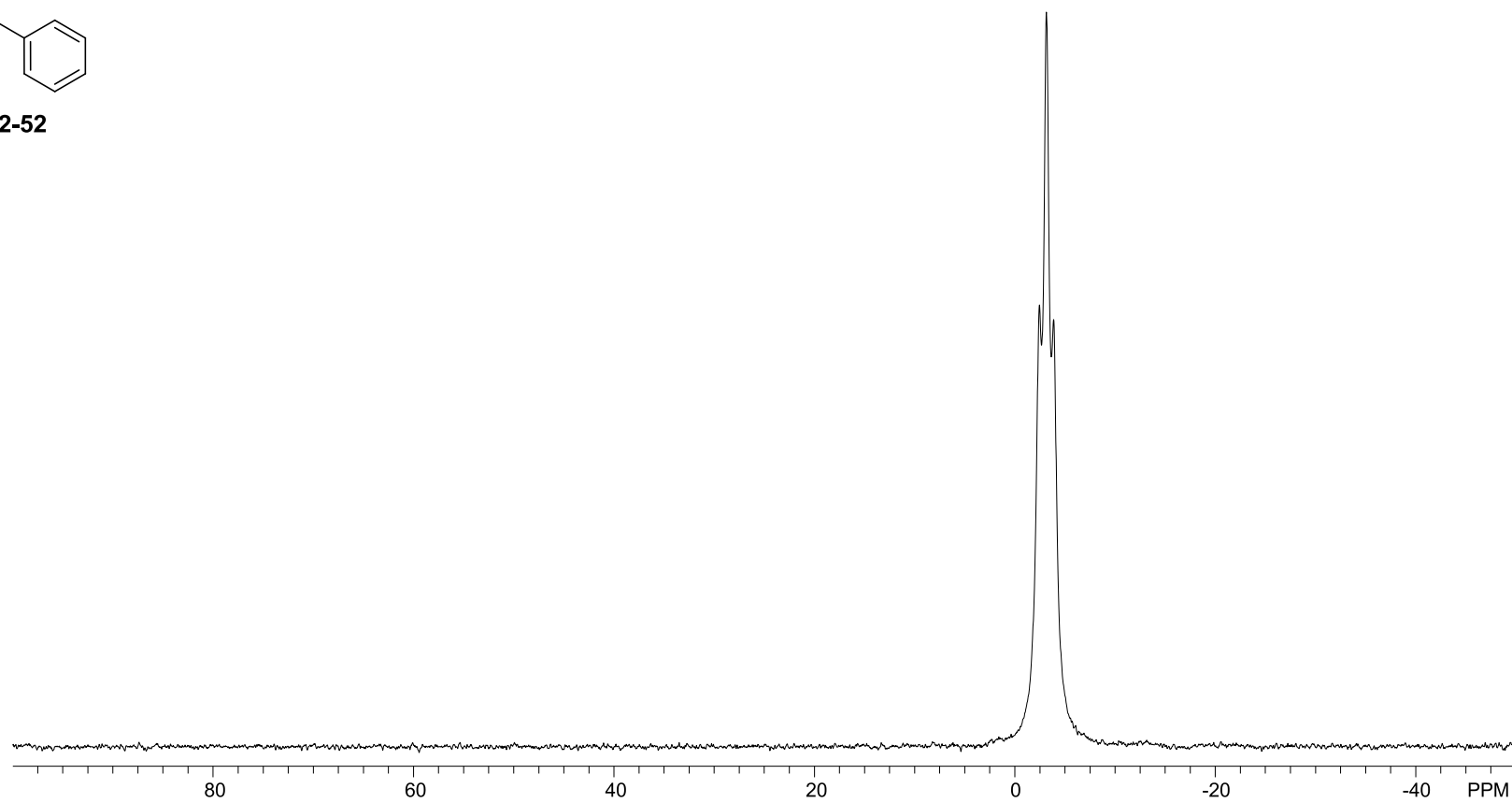
**2-52**



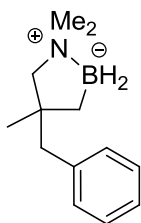
$^{11}\text{B}$  NMR (128 MHz),  
 $\text{CDCl}_3$



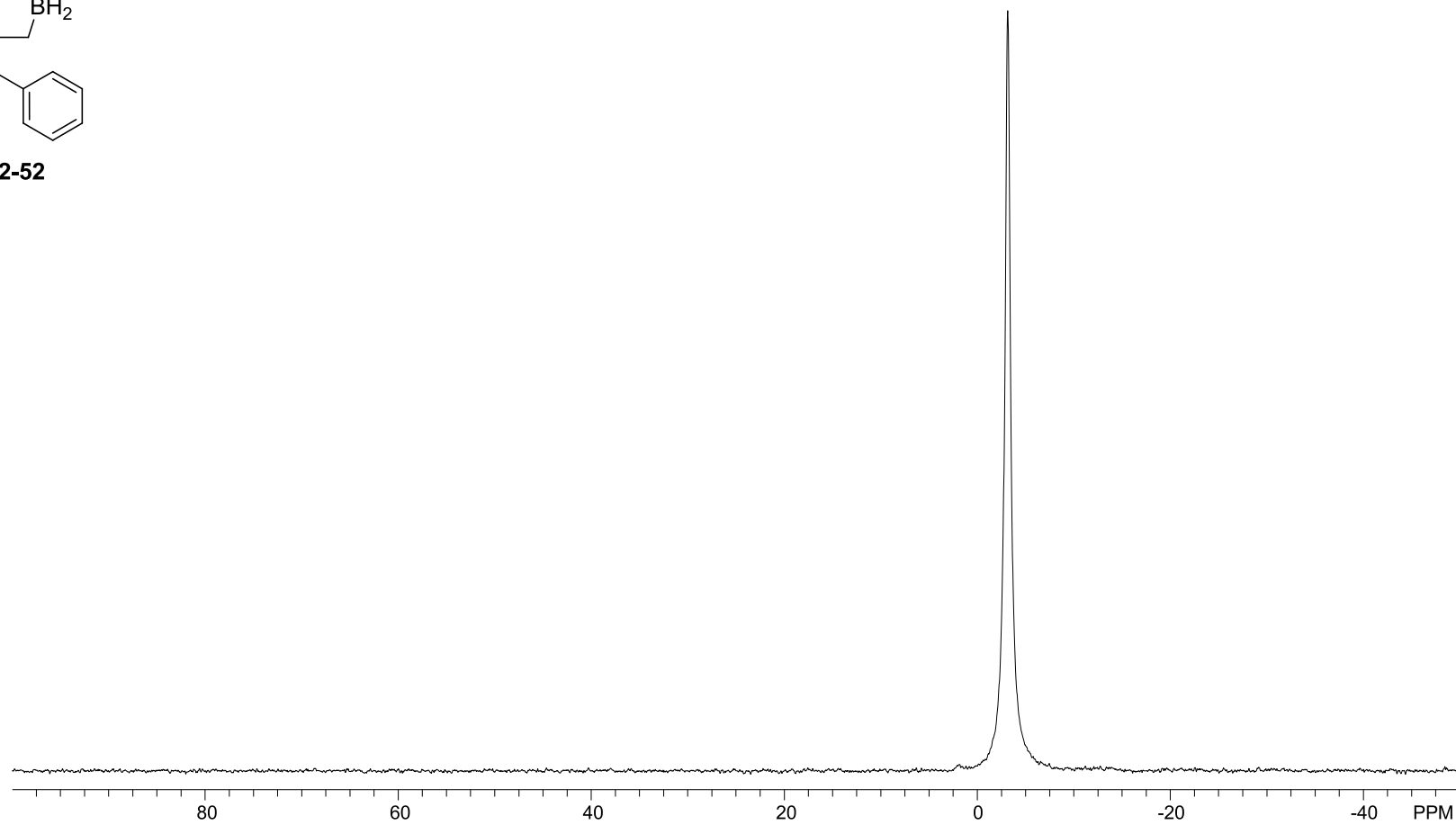
**2-52**



$^{11}\text{B}\{^1\text{H}\}$  NMR (128 MHz),  
 $\text{CDCl}_3$

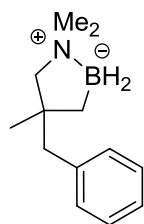


**2-52**

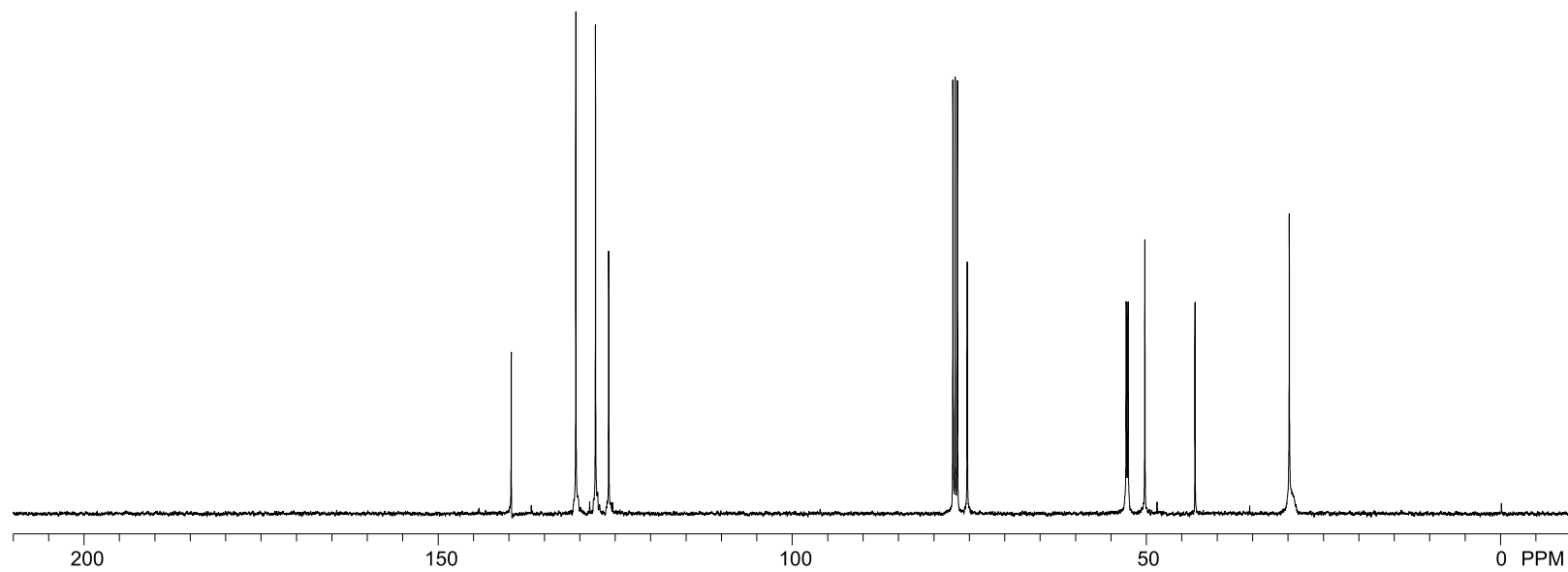
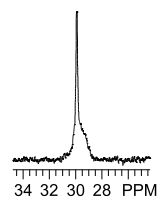




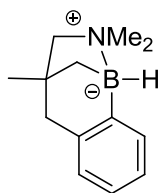
$^{13}\text{C}\{^1\text{H}\}$  NMR (101 MHz),  
 $\text{CDCl}_3$



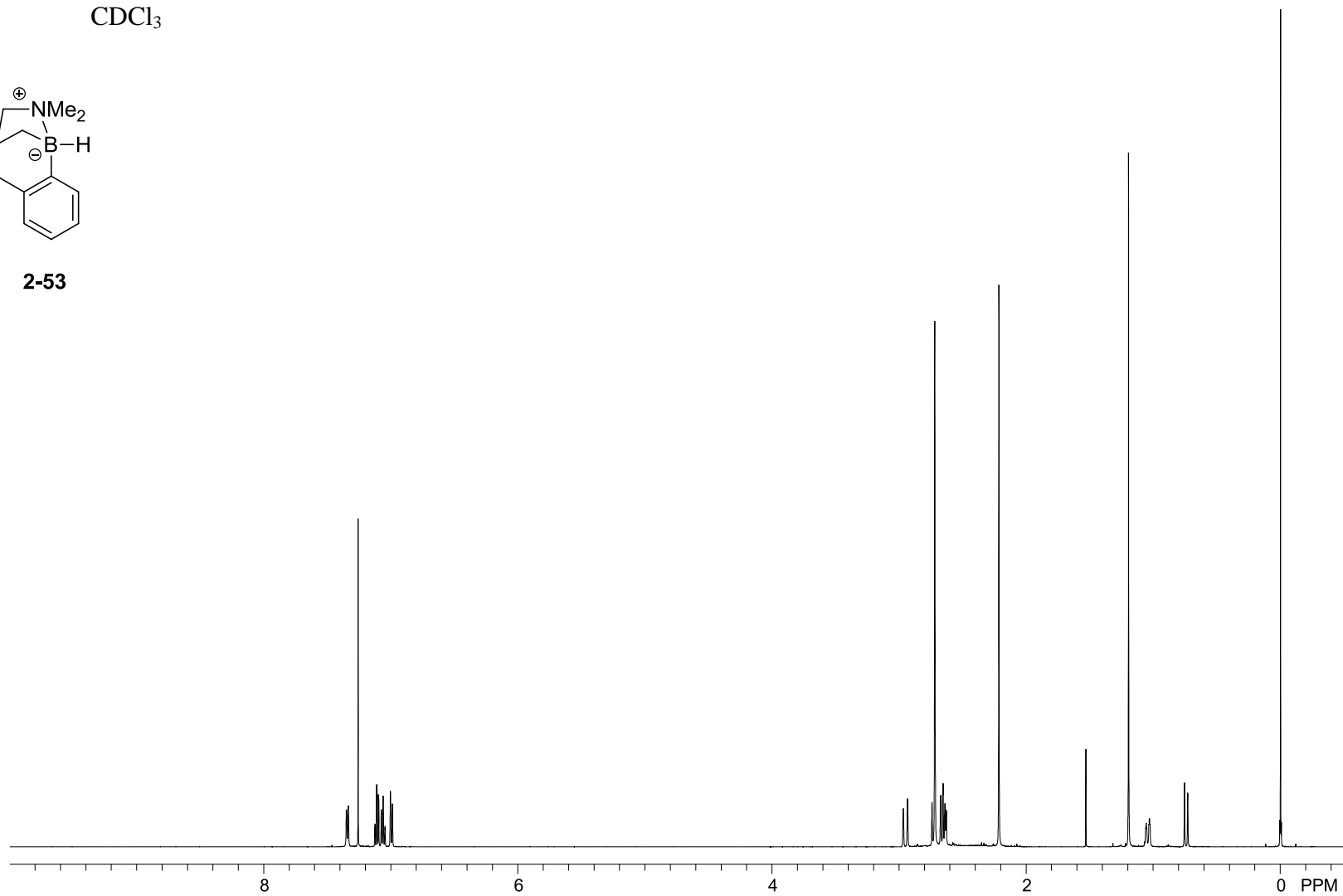
2-52



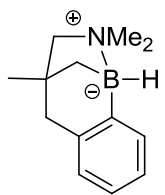
$^1\text{H}$  NMR (500 MHz),  
 $\text{CDCl}_3$



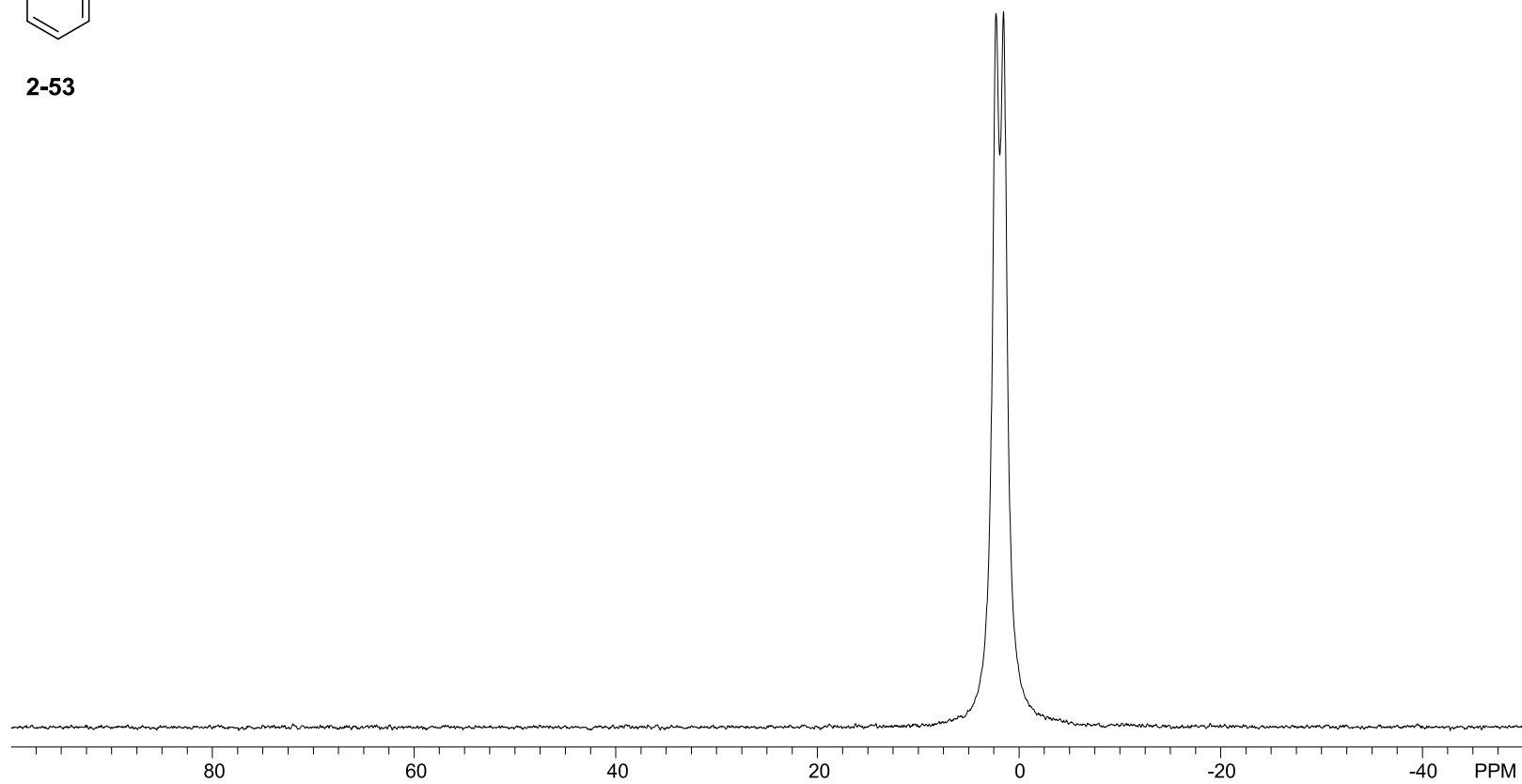
**2-53**



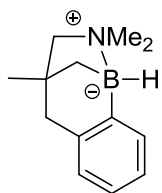
$^{11}\text{B}$  NMR (128 MHz),  
 $\text{CDCl}_3$



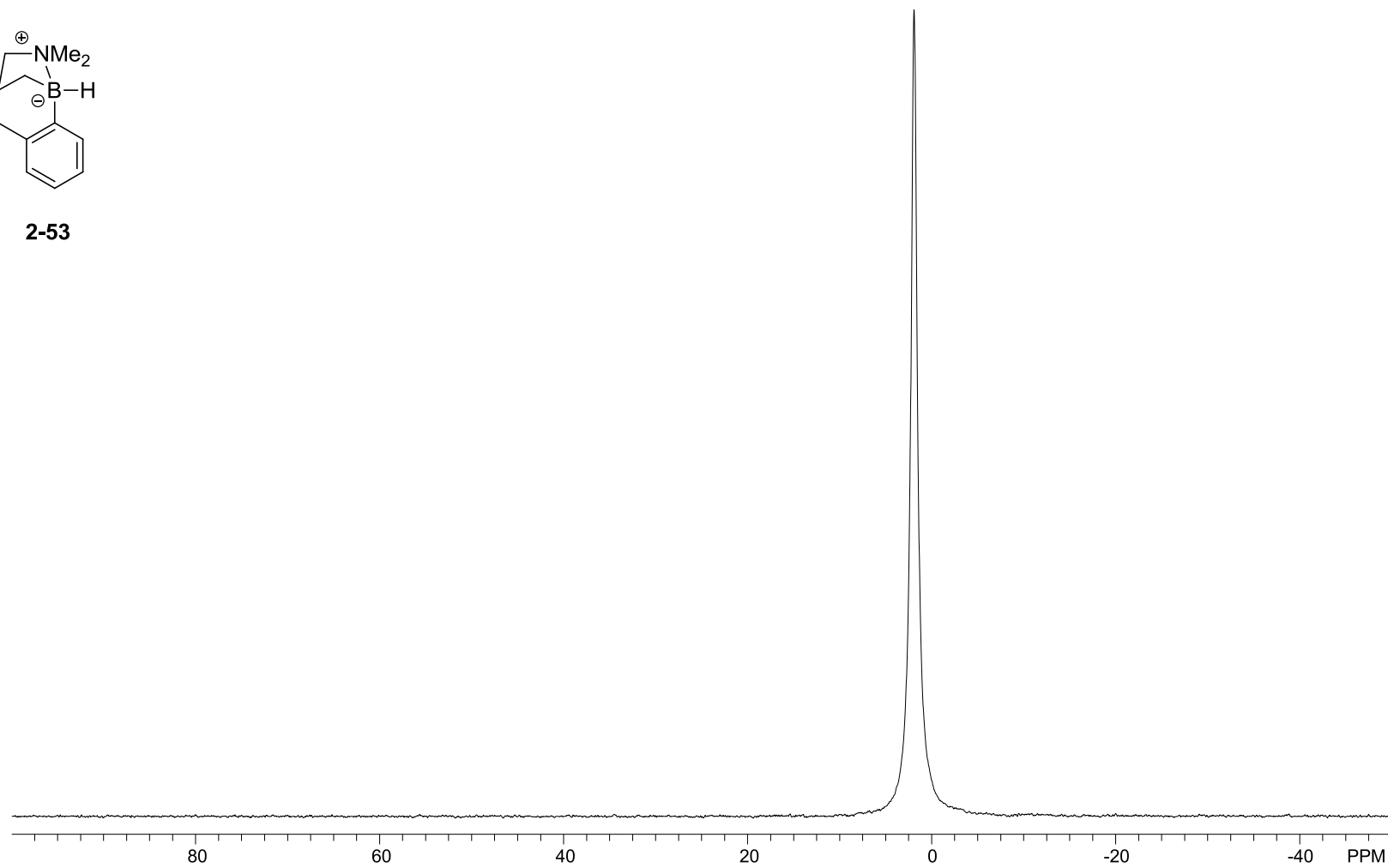
**2-53**



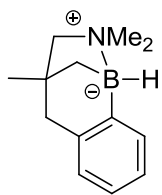
$^{11}\text{B}\{^1\text{H}\}$  NMR (128 MHz),  
 $\text{CDCl}_3$



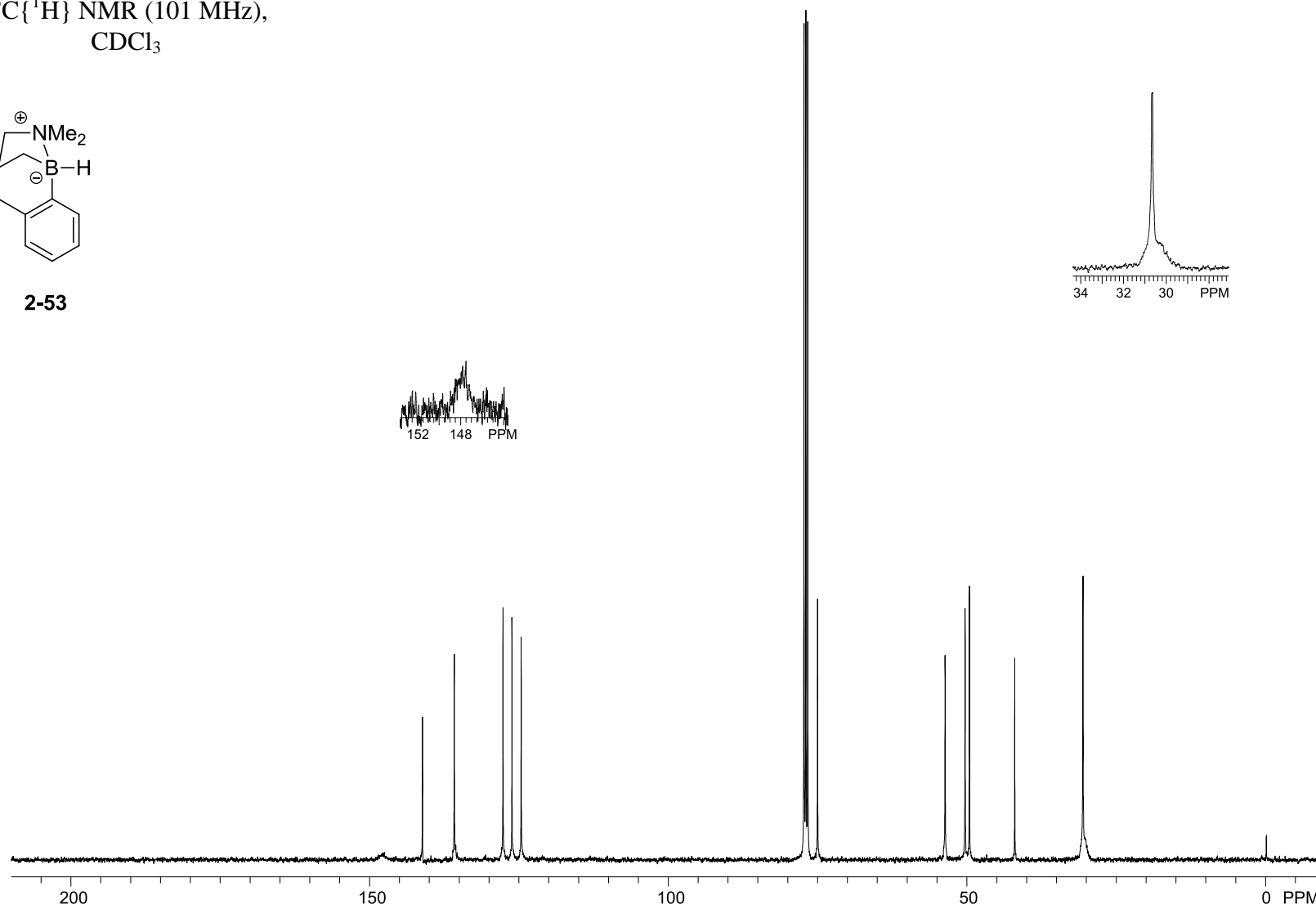
**2-53**



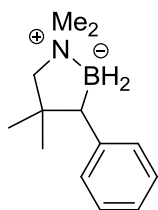
$^{13}\text{C}\{^1\text{H}\}$  NMR (101 MHz),  
 $\text{CDCl}_3$



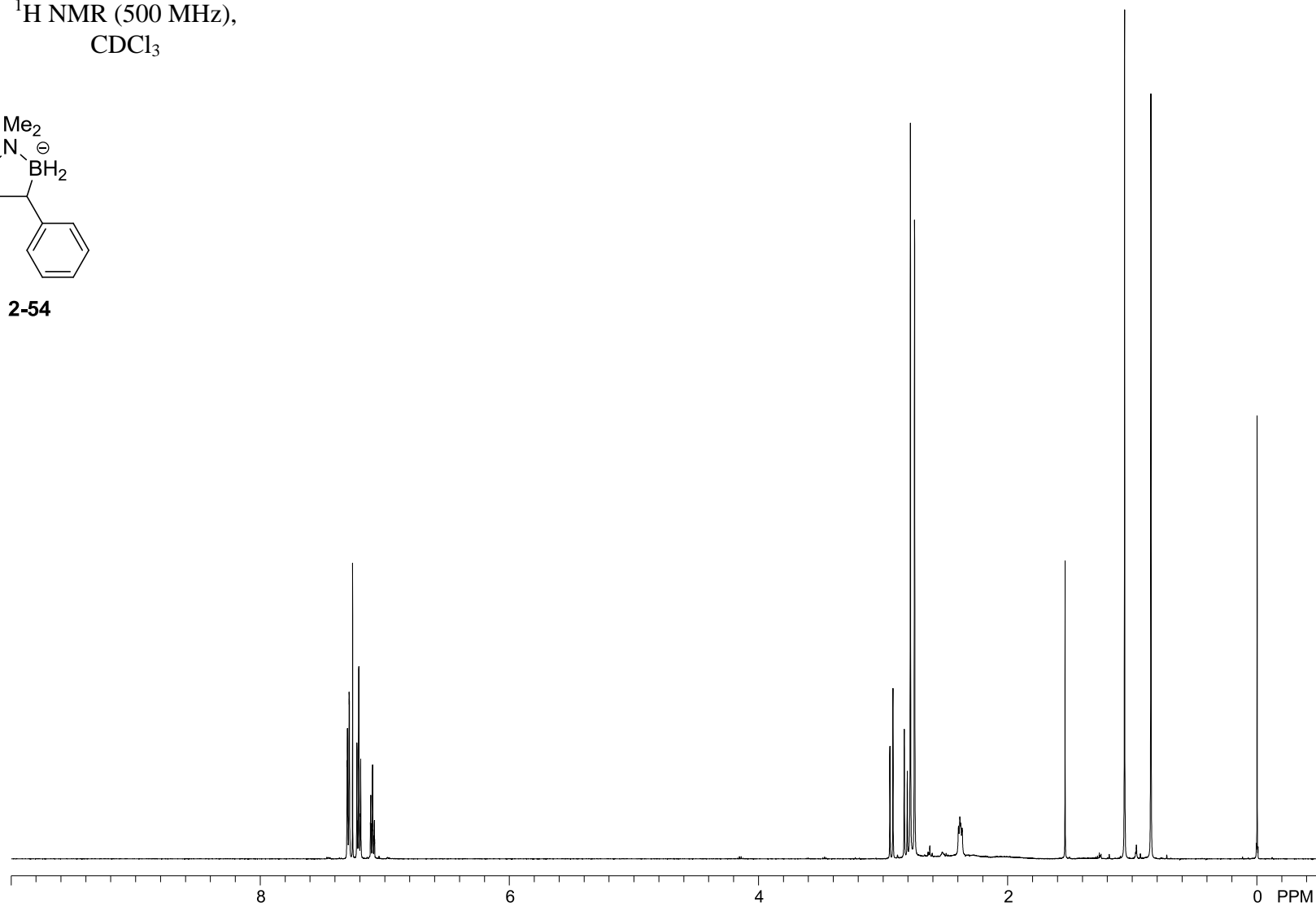
**2-53**



$^1\text{H}$  NMR (500 MHz),  
 $\text{CDCl}_3$



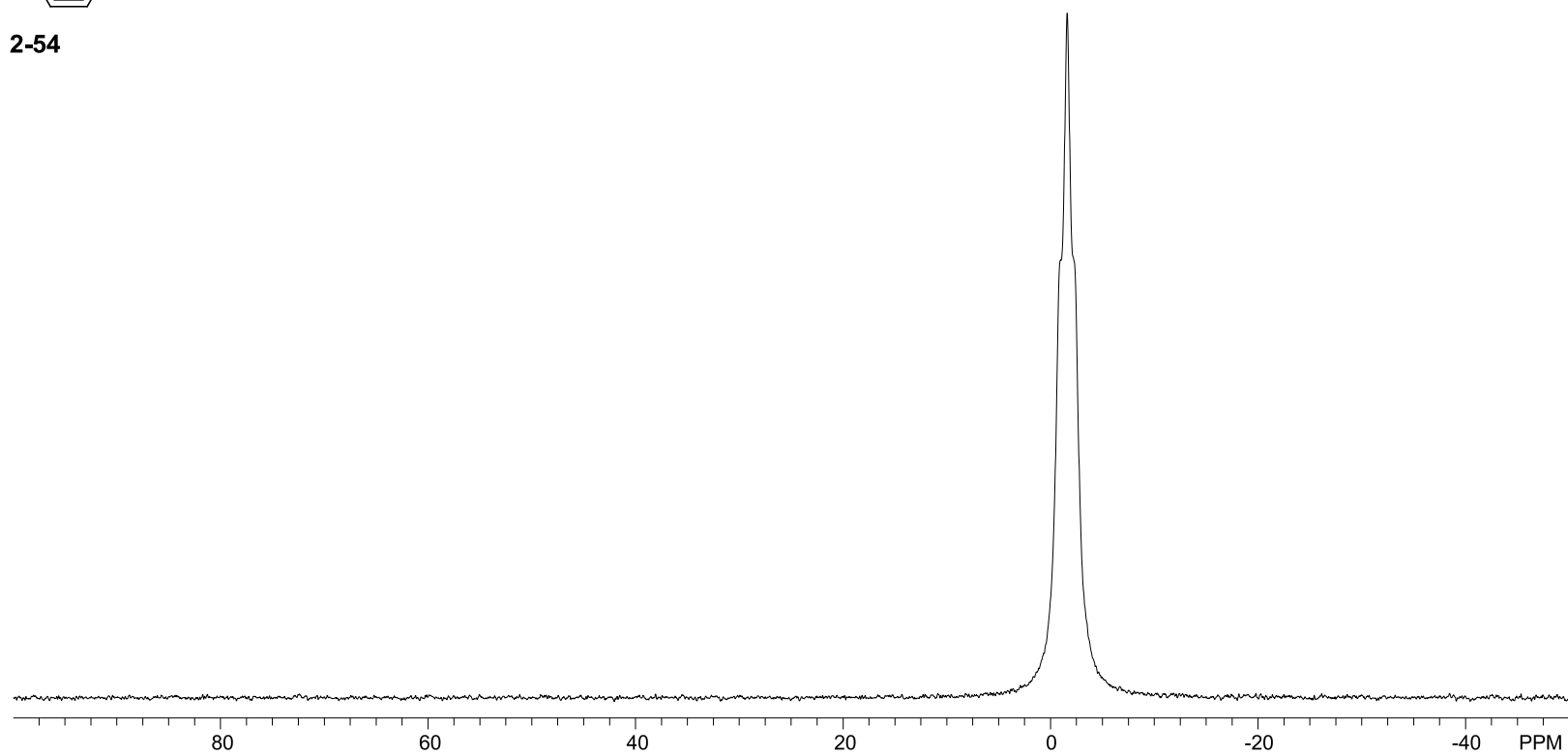
**2-54**



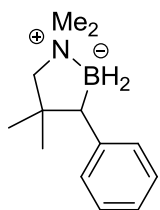
$^{11}\text{B}$  NMR (128 MHz),  
 $\text{CDCl}_3$



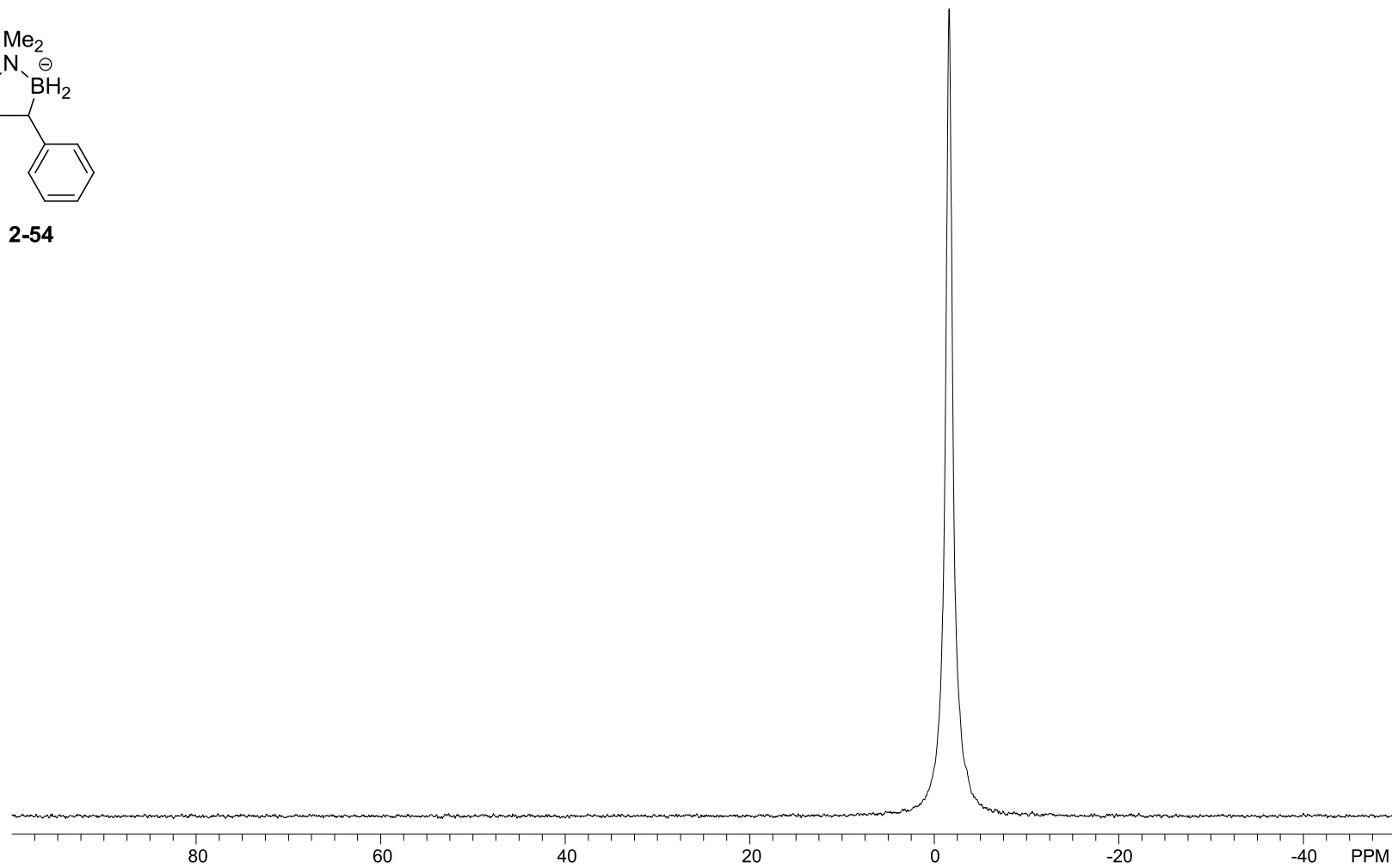
**2-54**



$^{11}\text{B}\{^1\text{H}\}$  NMR (128 MHz),  
 $\text{CDCl}_3$

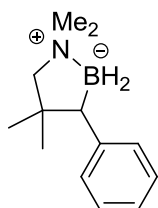


**2-54**

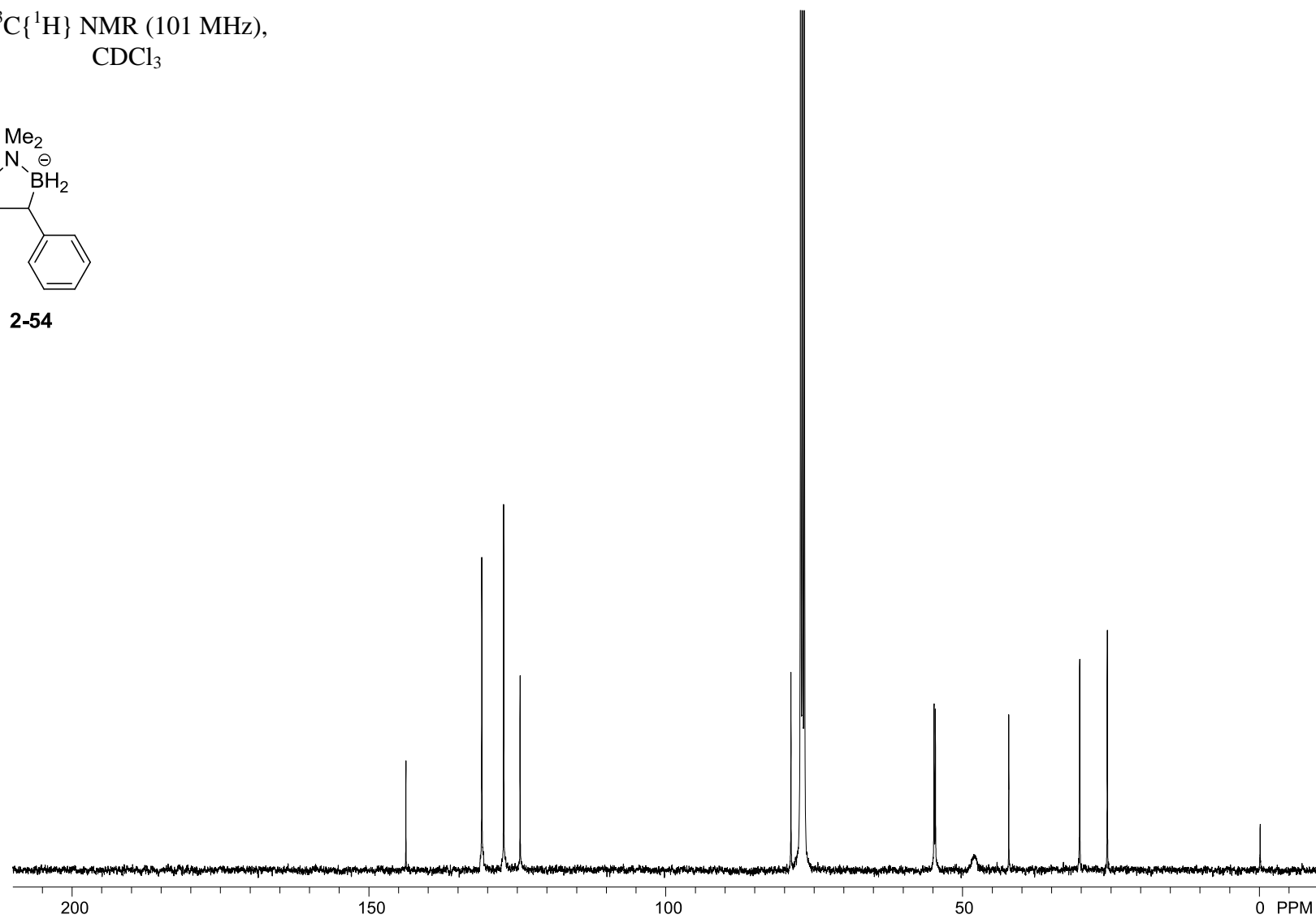




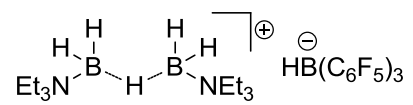
$^{13}\text{C}\{^1\text{H}\}$  NMR (101 MHz),  
 $\text{CDCl}_3$



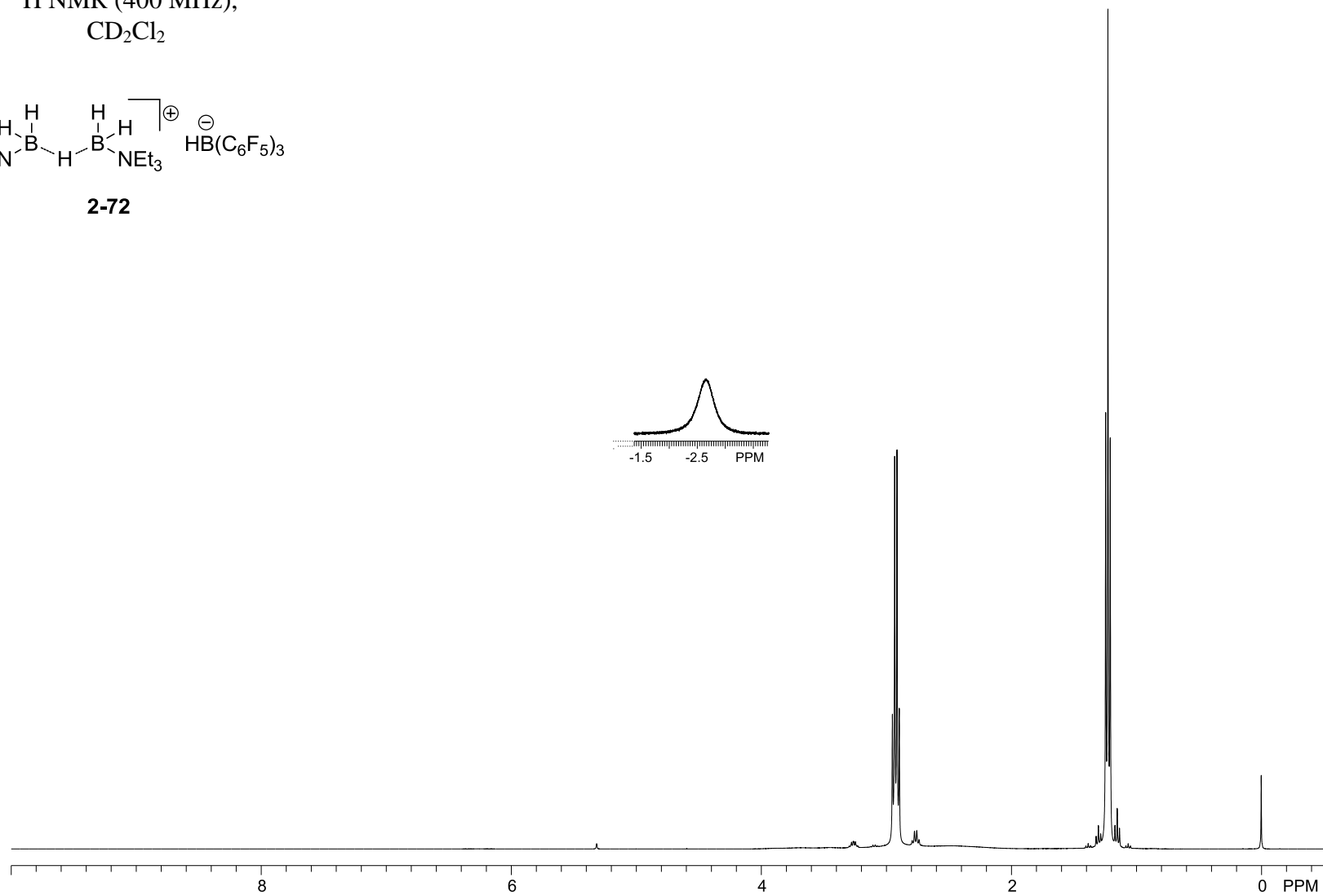
**2-54**



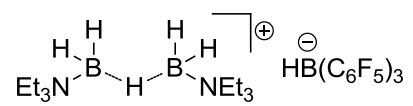
$^1\text{H}$  NMR (400 MHz),  
 $\text{CD}_2\text{Cl}_2$



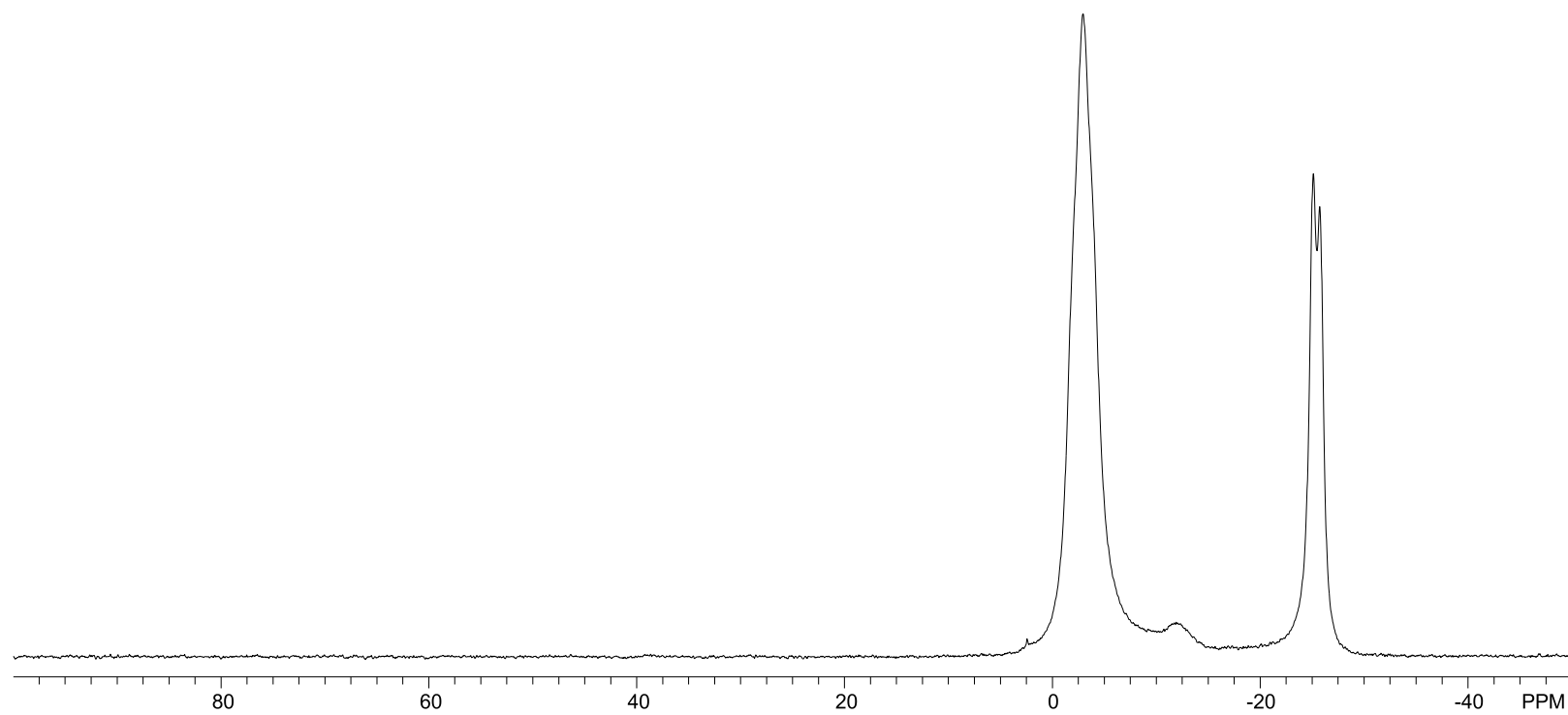
**2-72**



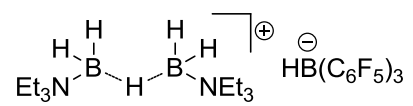
$^{11}\text{B}$  NMR (128 MHz),  
 $\text{CD}_2\text{Cl}_2$



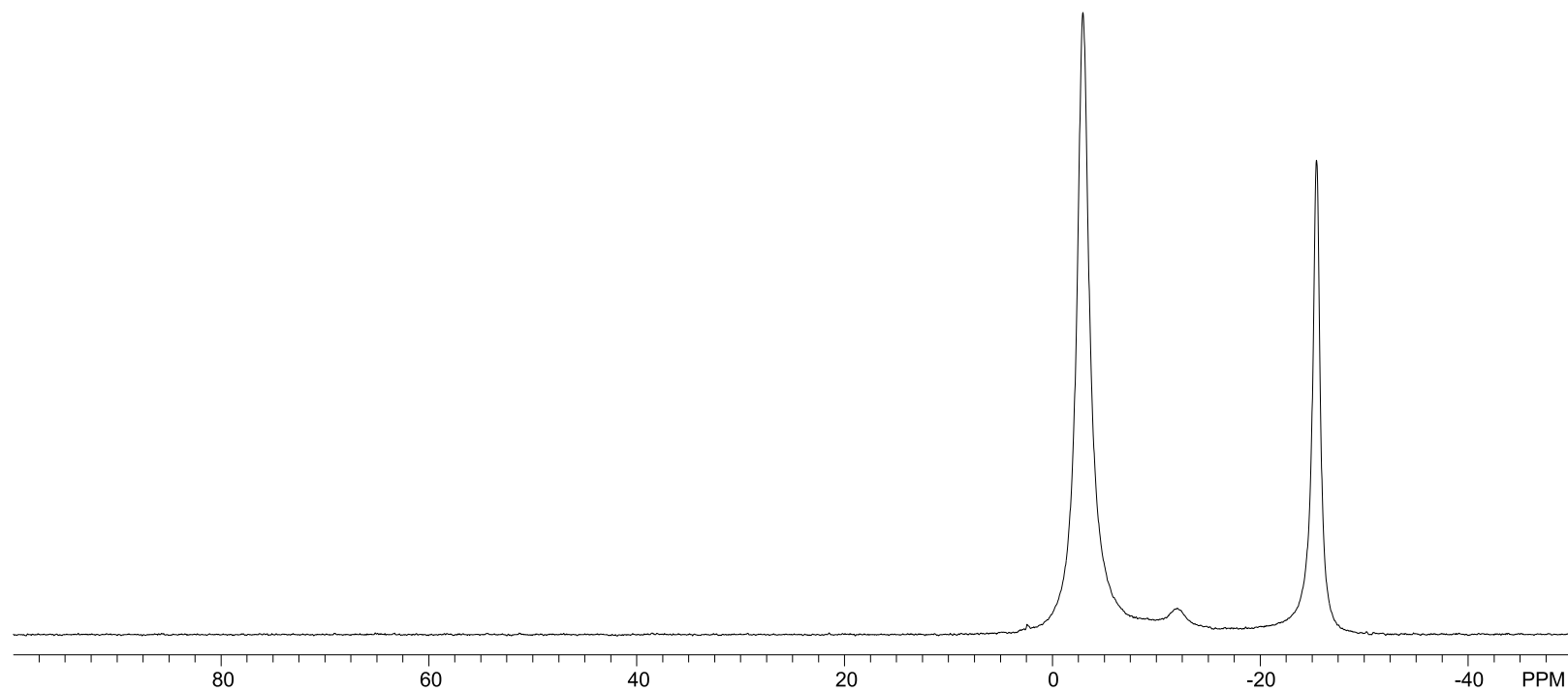
**2-72**



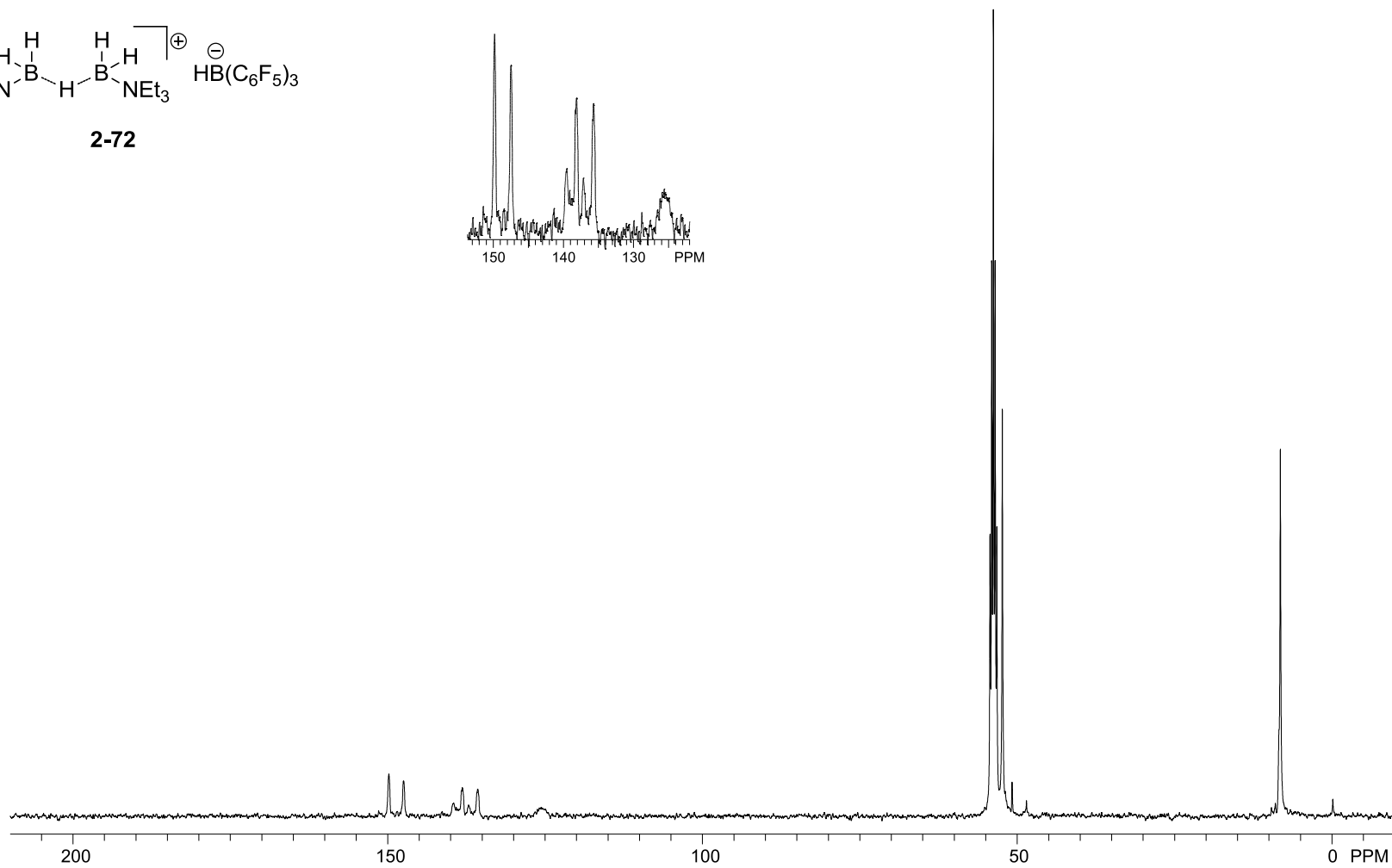
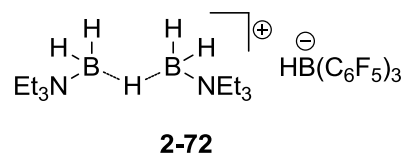
$^{11}\text{B}\{^1\text{H}\}$  NMR (128 MHz),  
 $\text{CD}_2\text{Cl}_2$



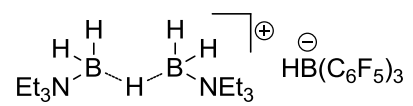
**2-72**



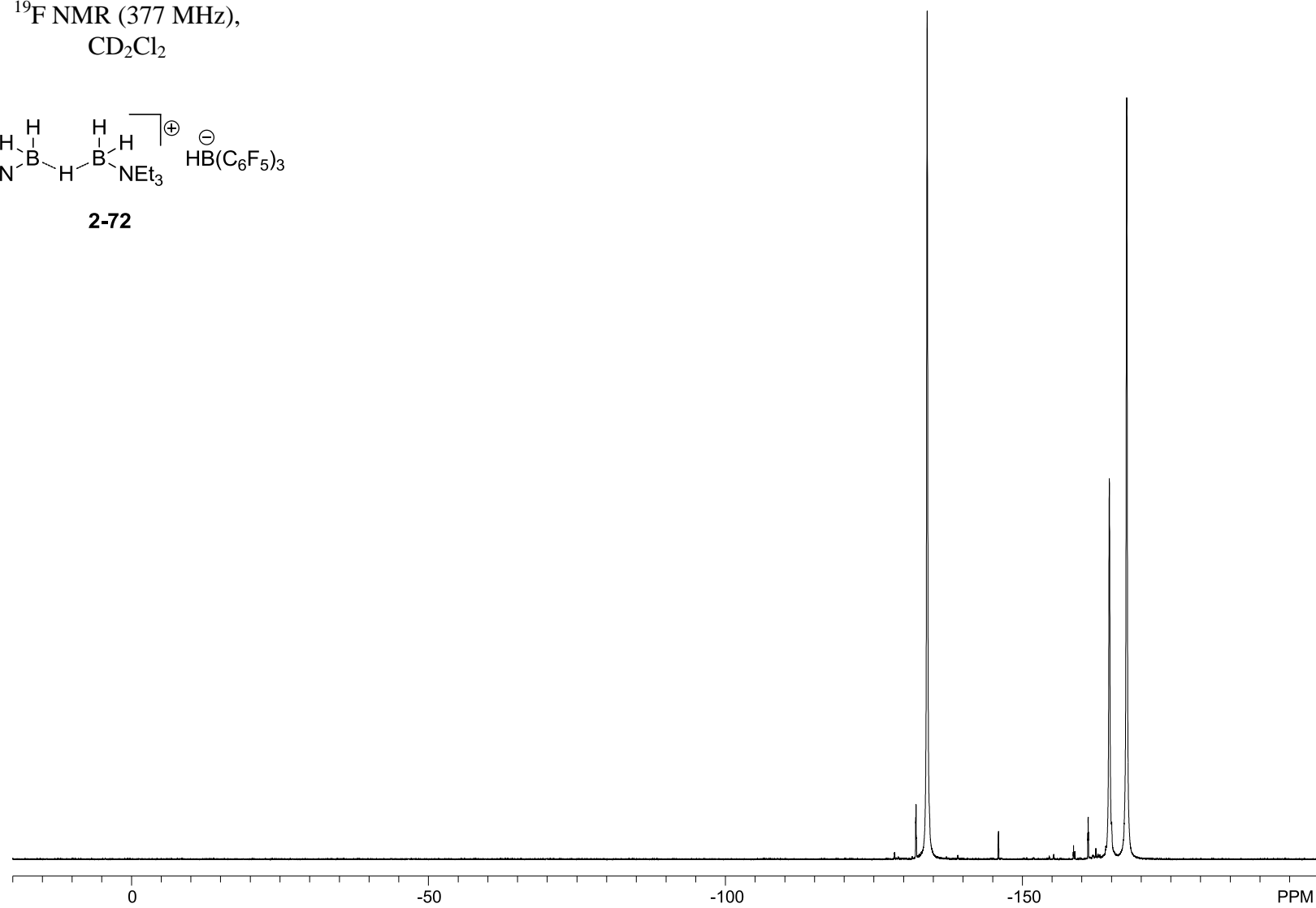
$^{13}\text{C}\{^1\text{H}\}$  NMR (101 MHz),  
 $\text{CD}_2\text{Cl}_2$



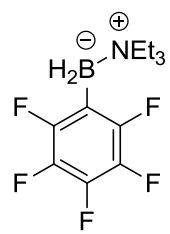
$^{19}\text{F}$  NMR (377 MHz),  
 $\text{CD}_2\text{Cl}_2$



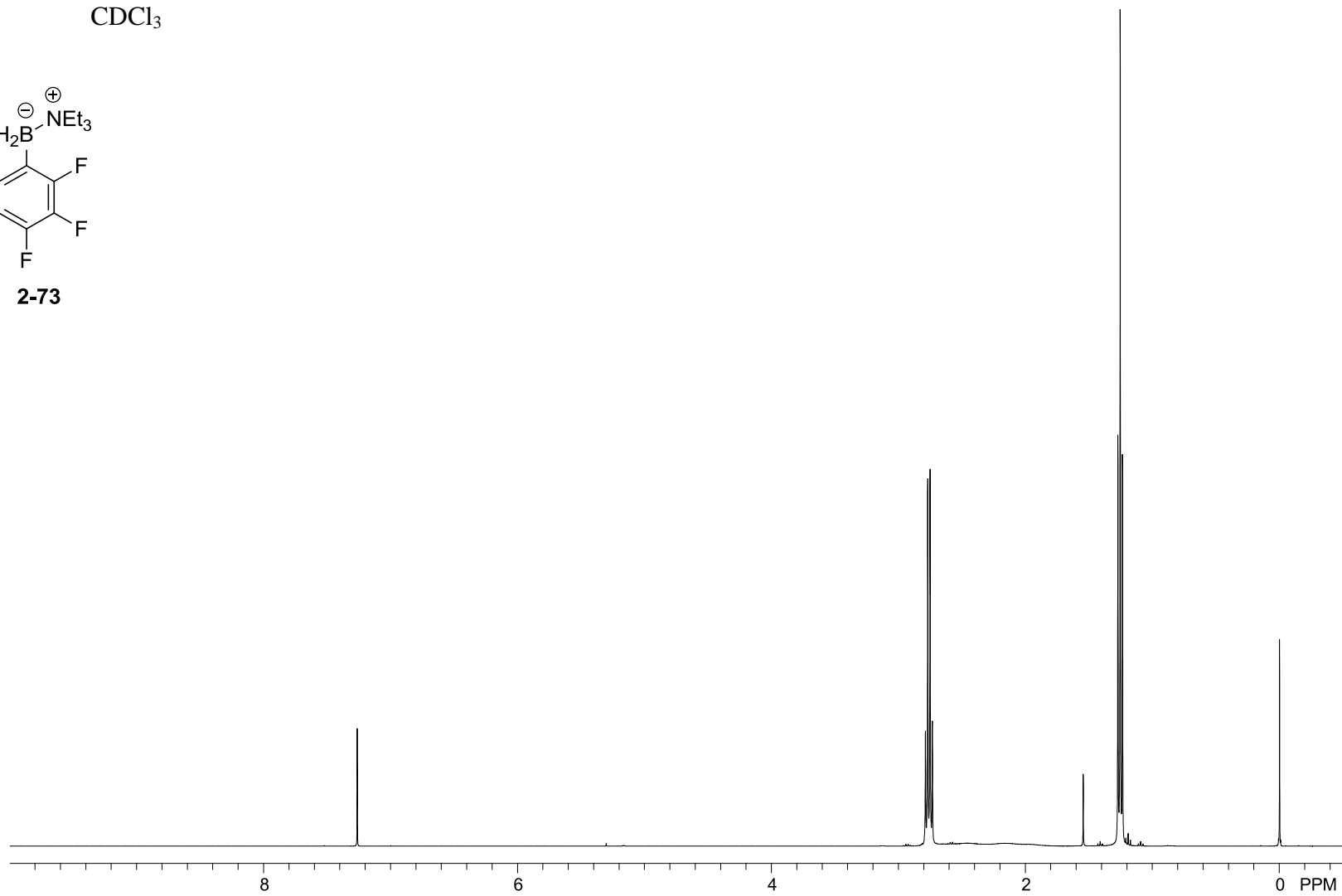
**2-72**



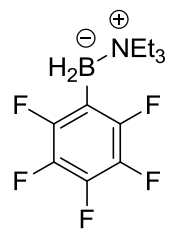
$^1\text{H}$  NMR (400 MHz),  
 $\text{CDCl}_3$



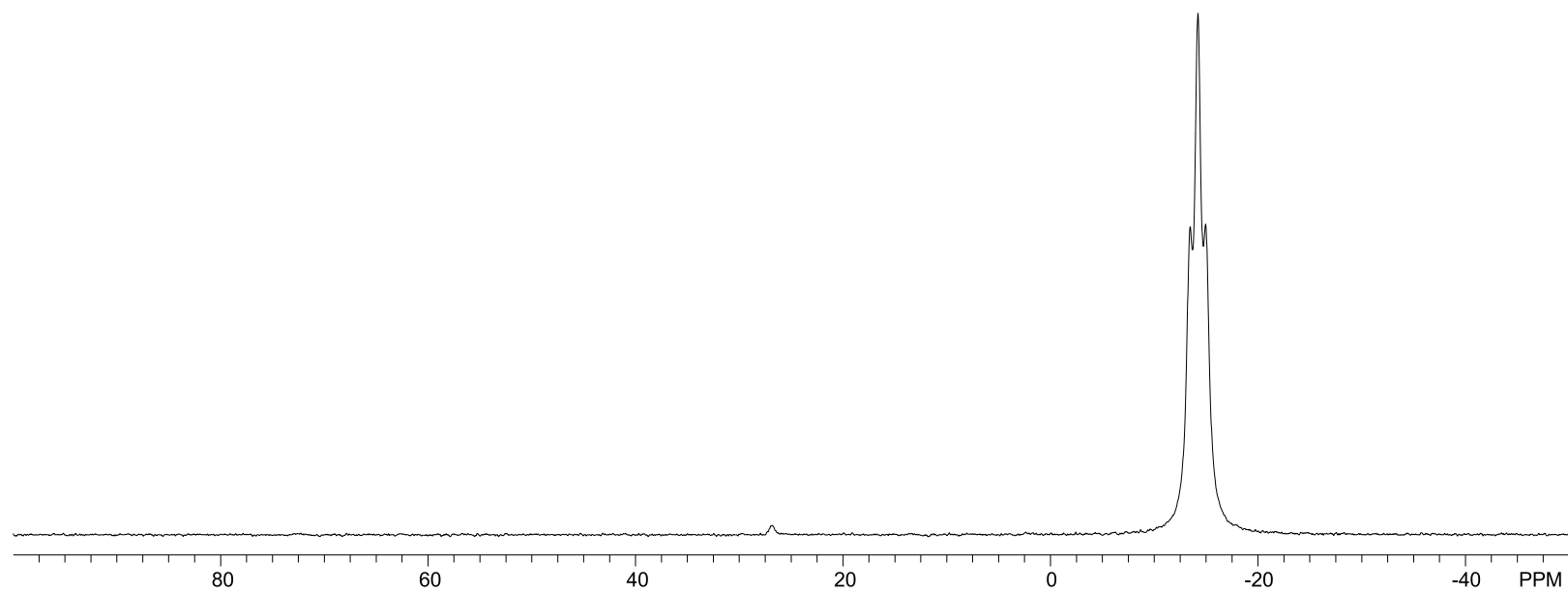
**2-73**



$^{11}\text{B}$  NMR (128 MHz),  
 $\text{CDCl}_3$

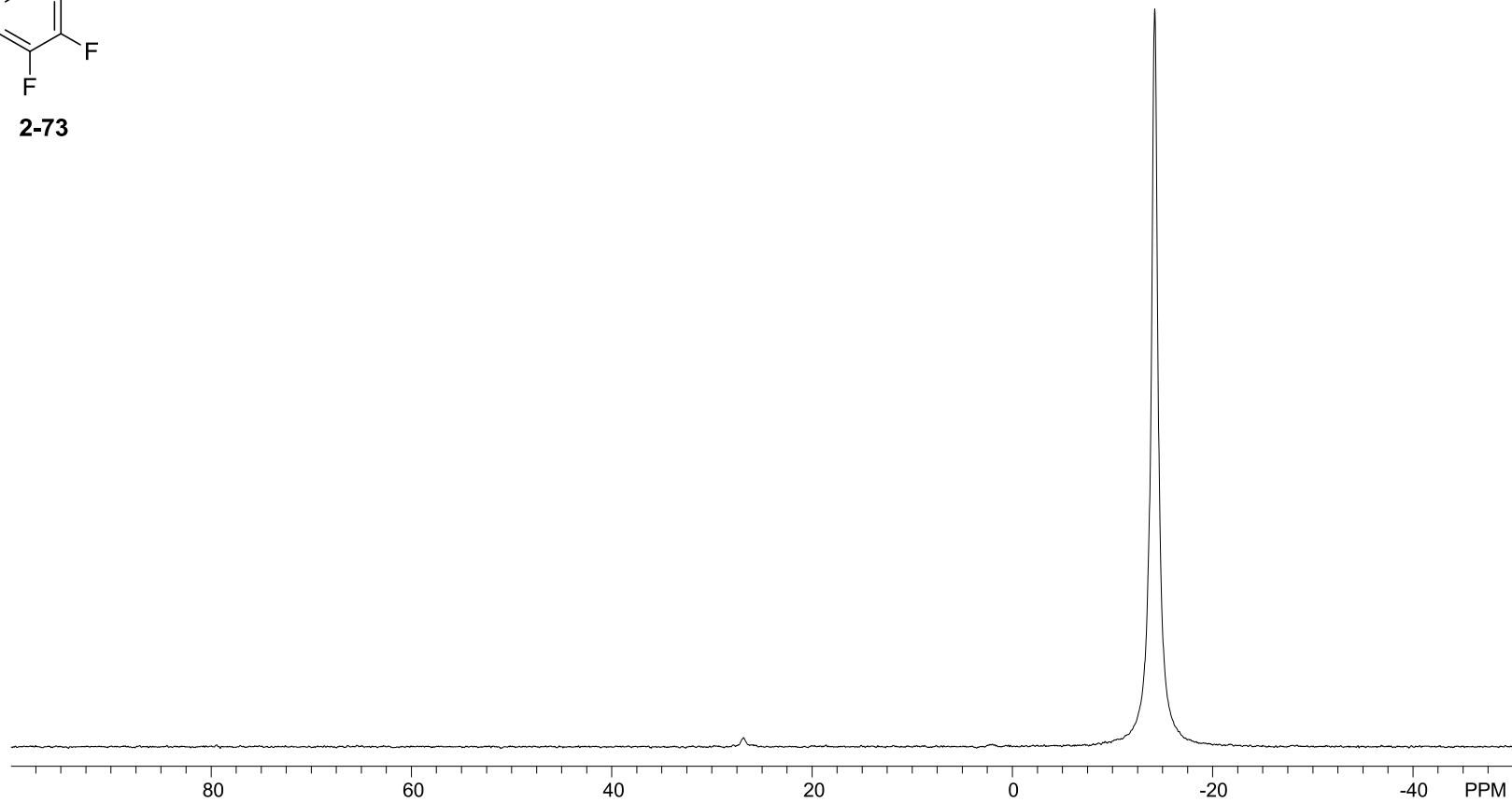
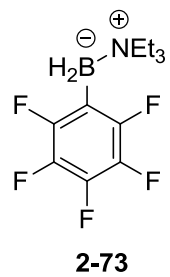


**2-73**

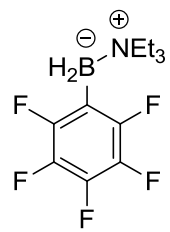




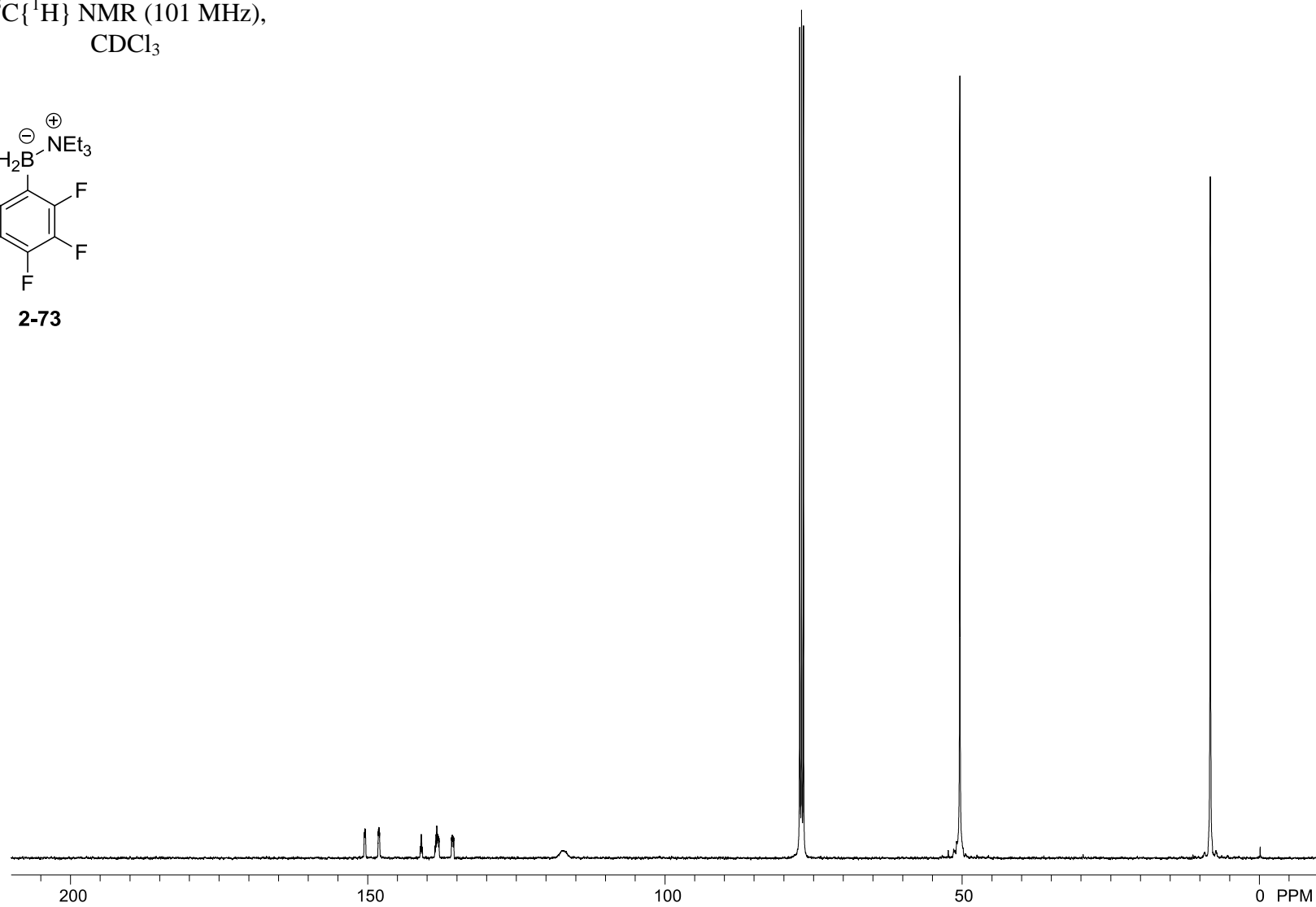
$^{11}\text{B}\{^1\text{H}\}$  NMR (128 MHz),  
 $\text{CDCl}_3$



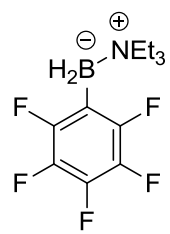
$^{13}\text{C}\{^1\text{H}\}$  NMR (101 MHz),  
 $\text{CDCl}_3$



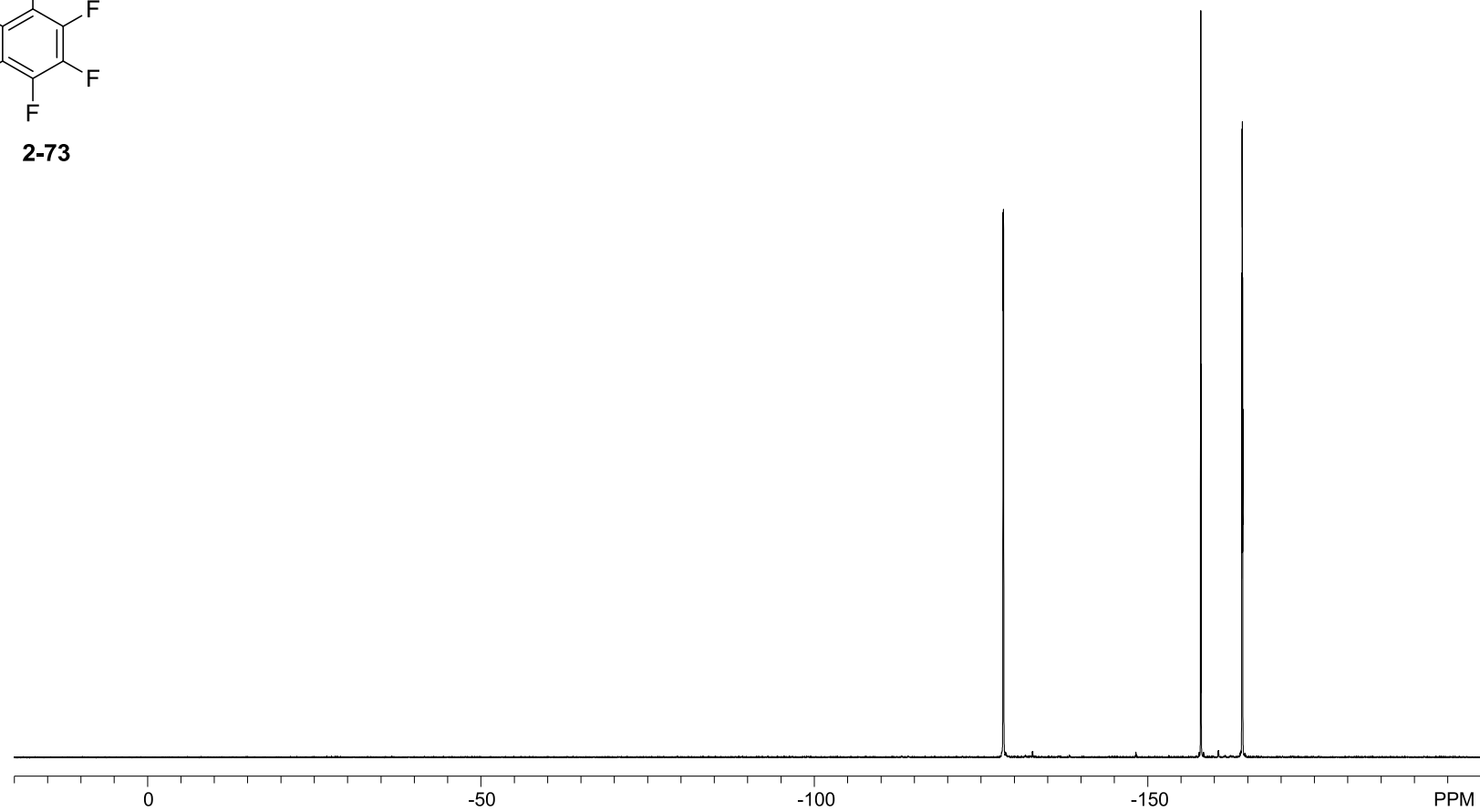
**2-73**



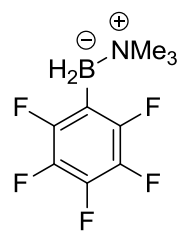
$^{19}\text{F}$  NMR (377 MHz),  
 $\text{CDCl}_3$



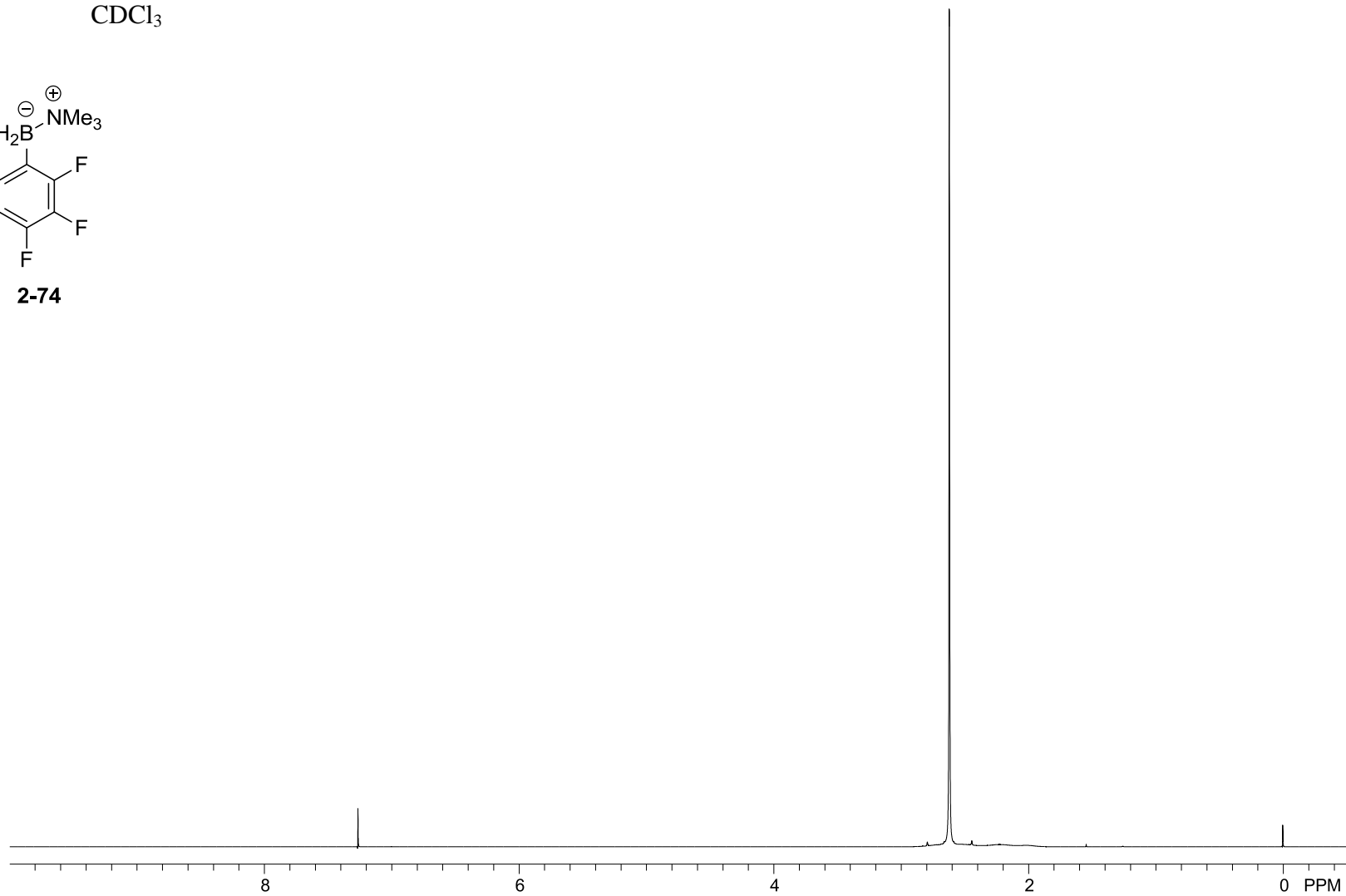
**2-73**



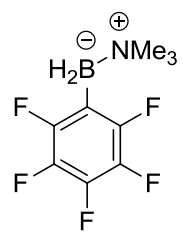
$^1\text{H}$  NMR (400 MHz),  
 $\text{CDCl}_3$



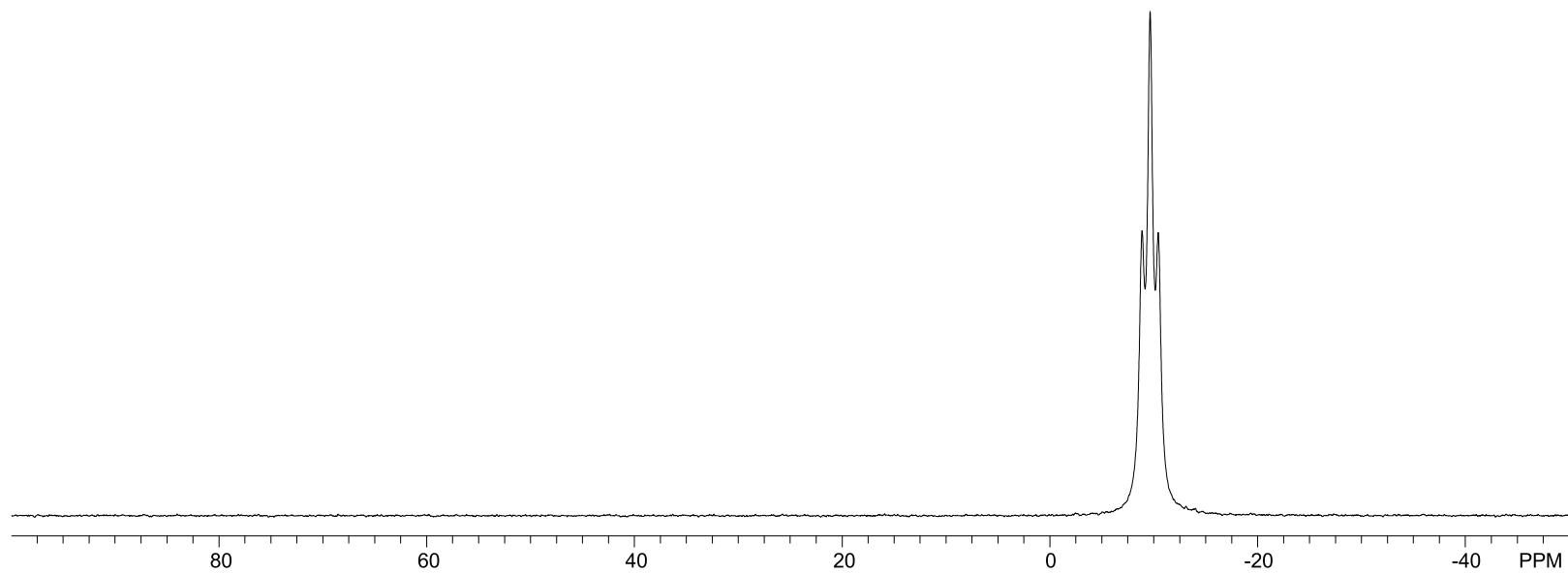
**2-74**



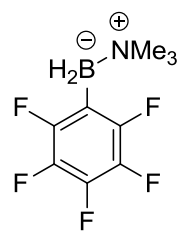
$^{11}\text{B}$  NMR (128 MHz),  
 $\text{CDCl}_3$



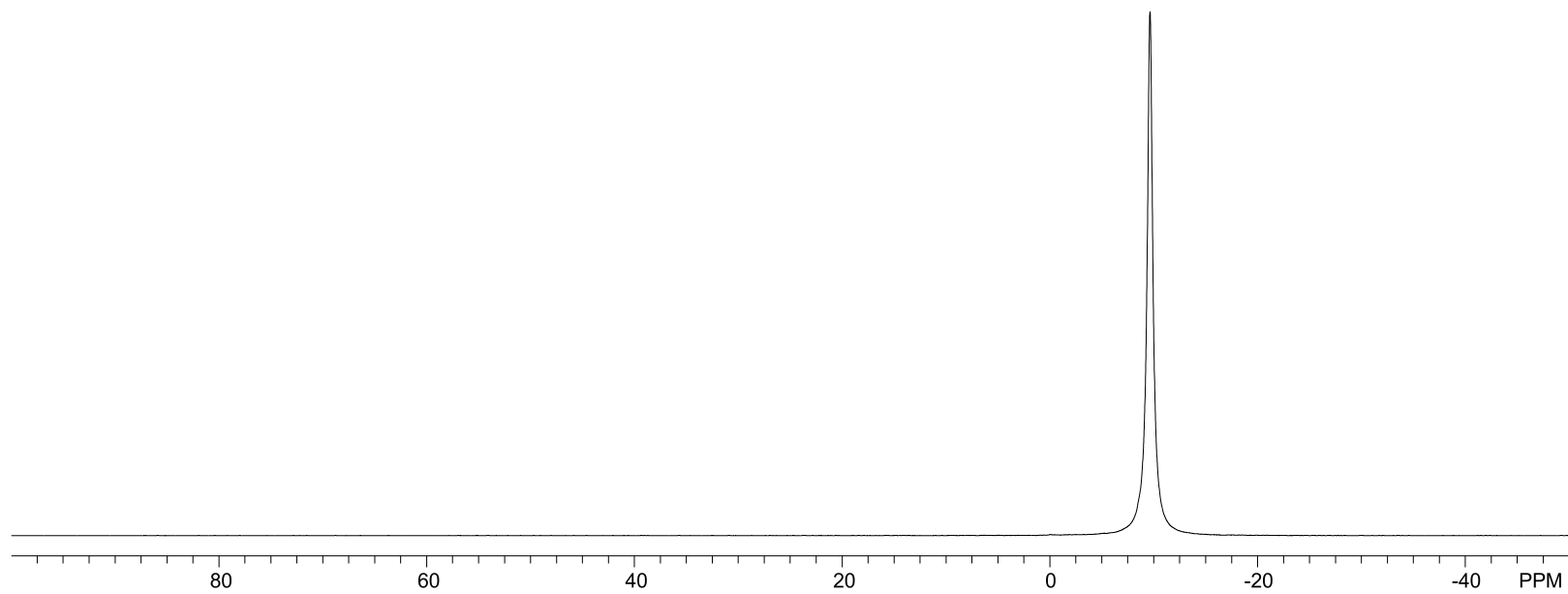
**2-74**



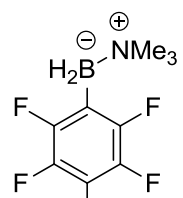
$^{11}\text{B}\{^1\text{H}\}$  NMR (128 MHz),  
 $\text{CDCl}_3$



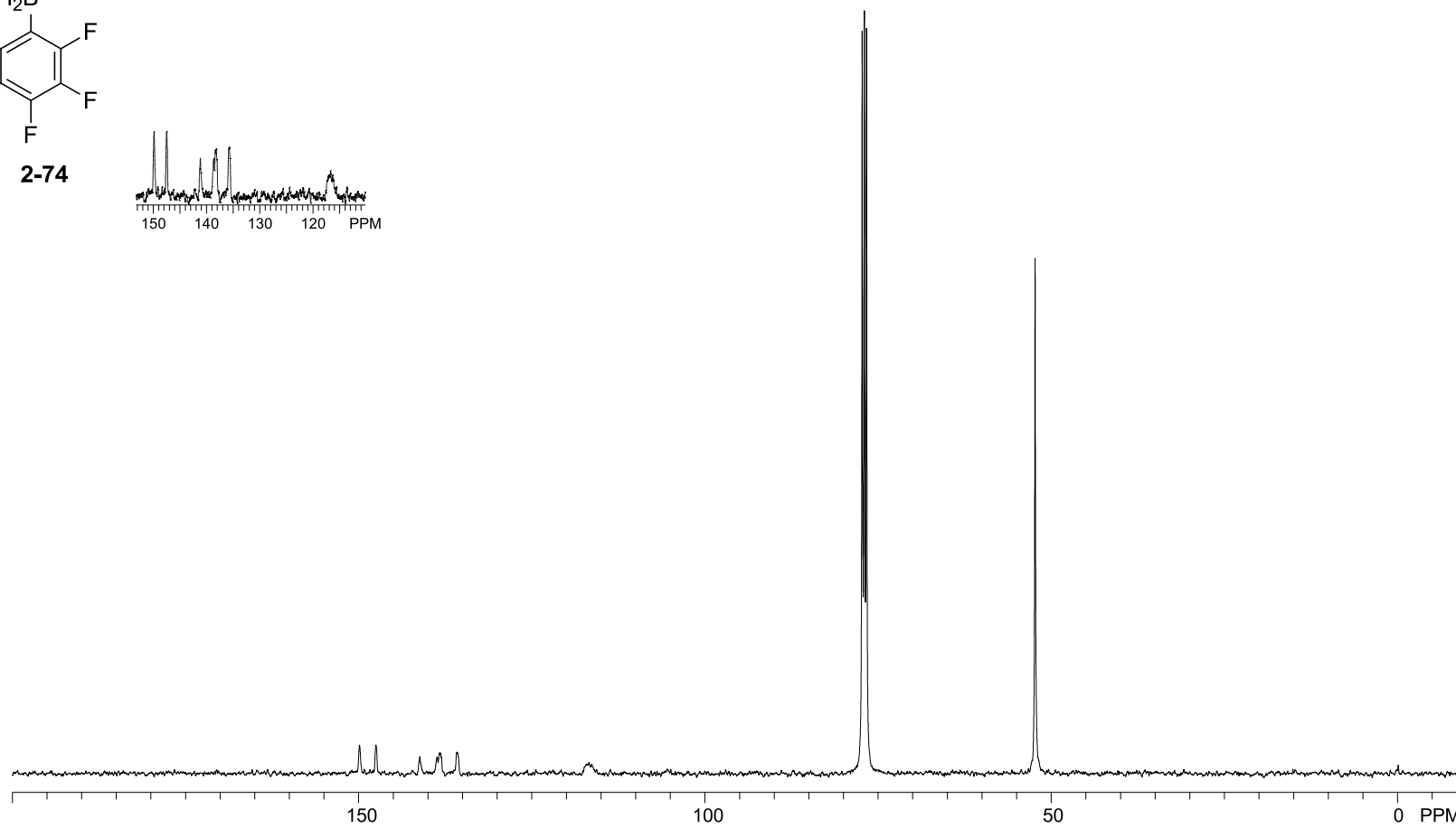
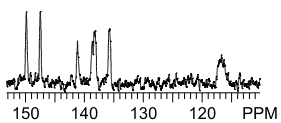
**2-74**



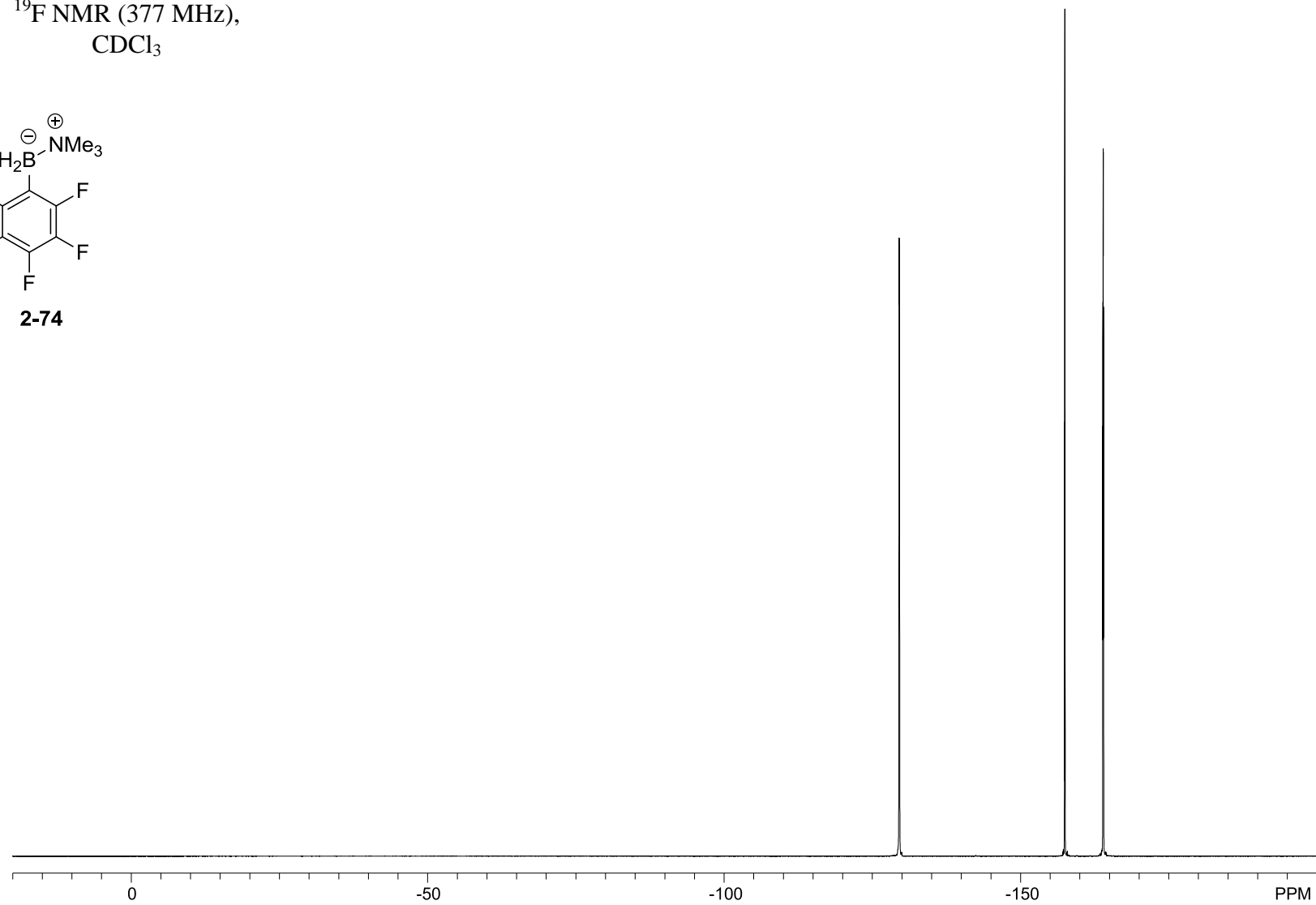
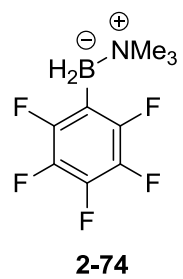
$^{13}\text{C}\{^1\text{H}\}$  NMR (101 MHz),  
 $\text{CDCl}_3$



**2-74**

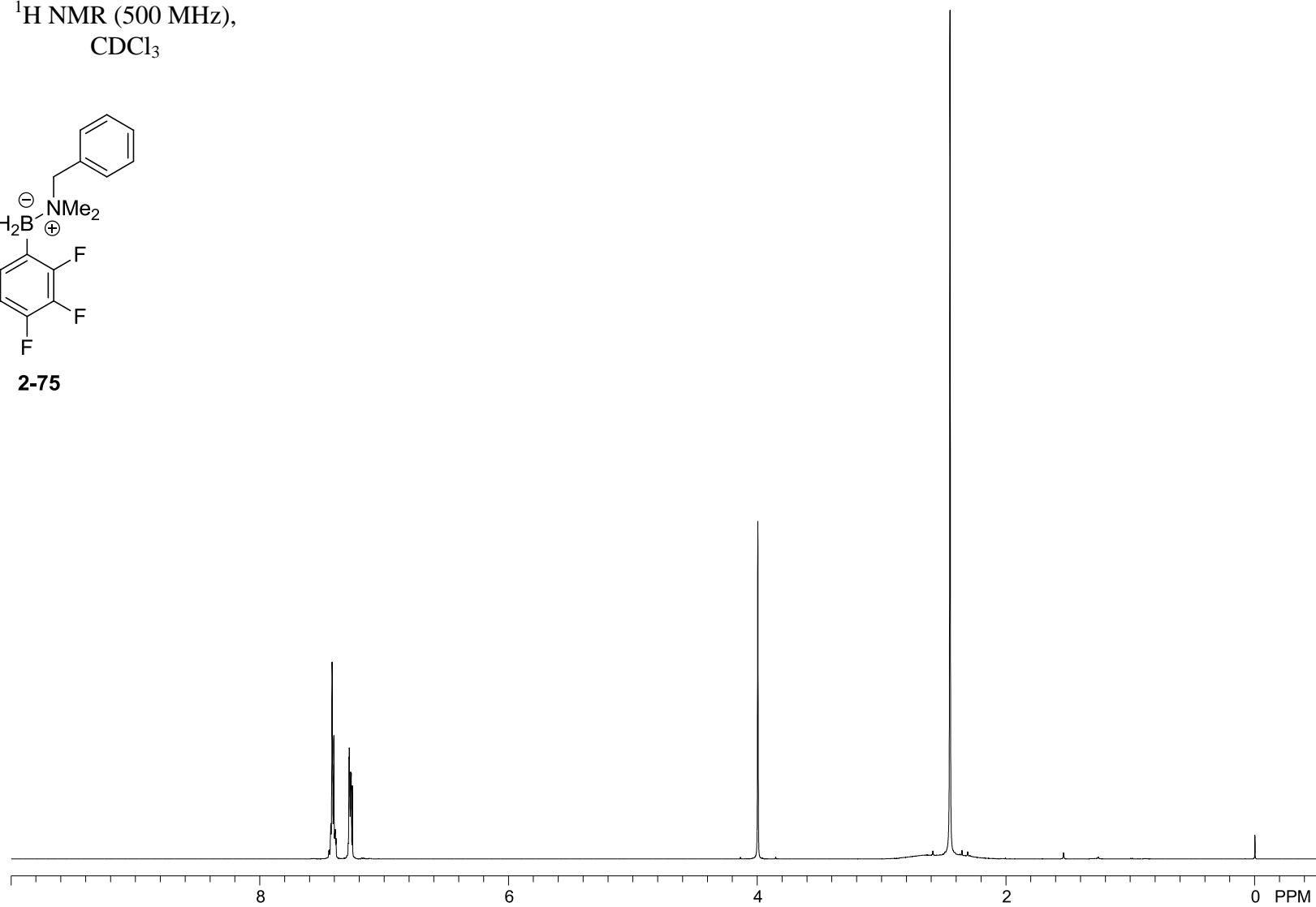
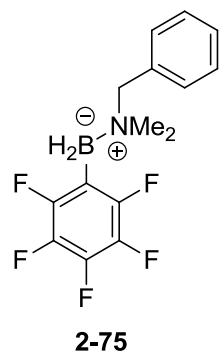


$^{19}\text{F}$  NMR (377 MHz),  
 $\text{CDCl}_3$

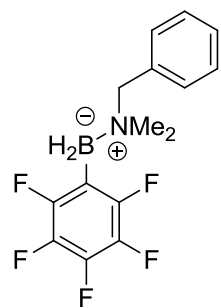




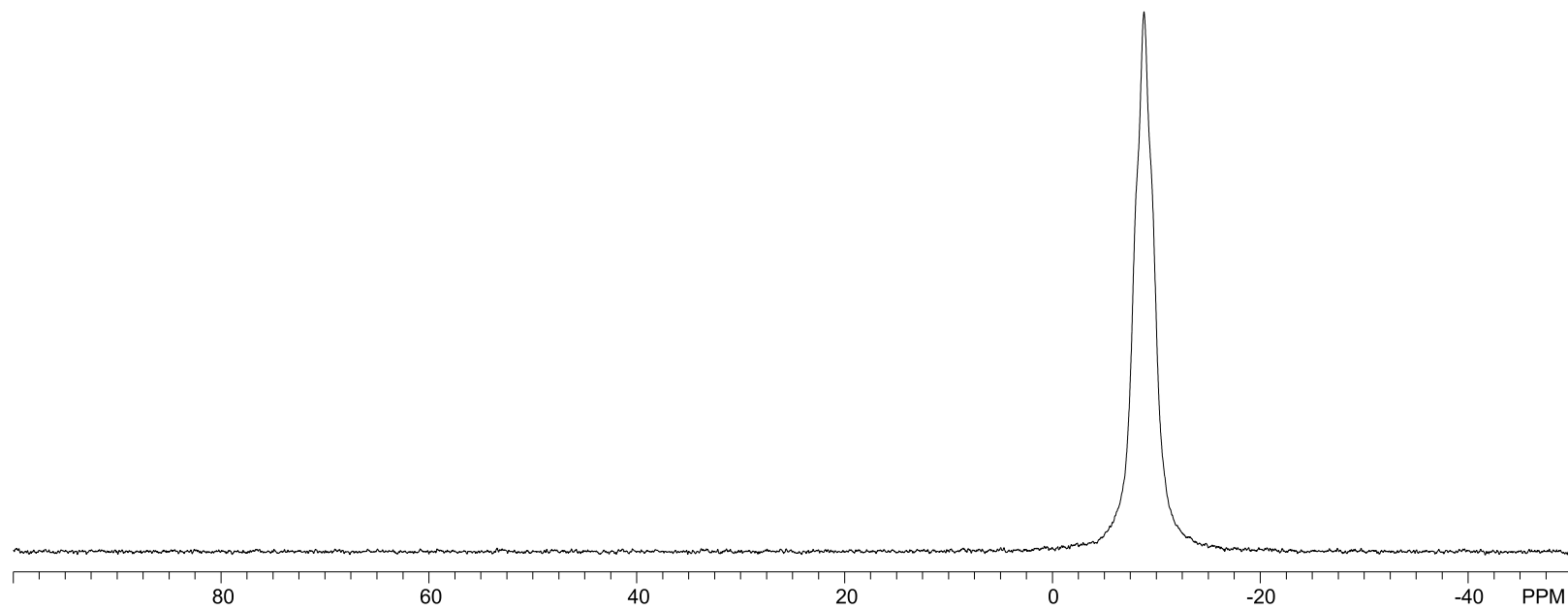
$^1\text{H}$  NMR (500 MHz),  
 $\text{CDCl}_3$



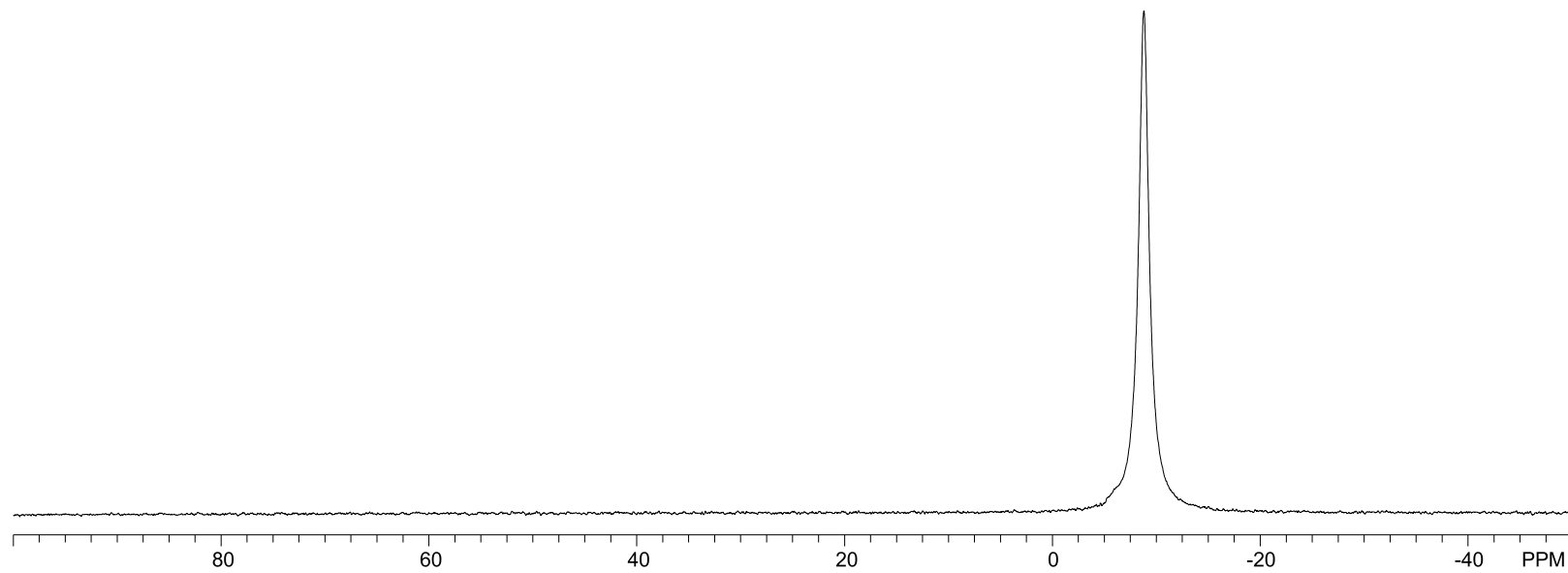
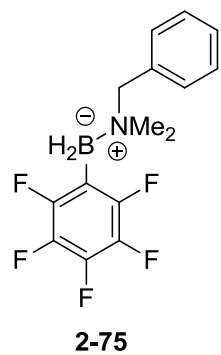
$^{11}\text{B}$  NMR (128 MHz),  
 $\text{CDCl}_3$



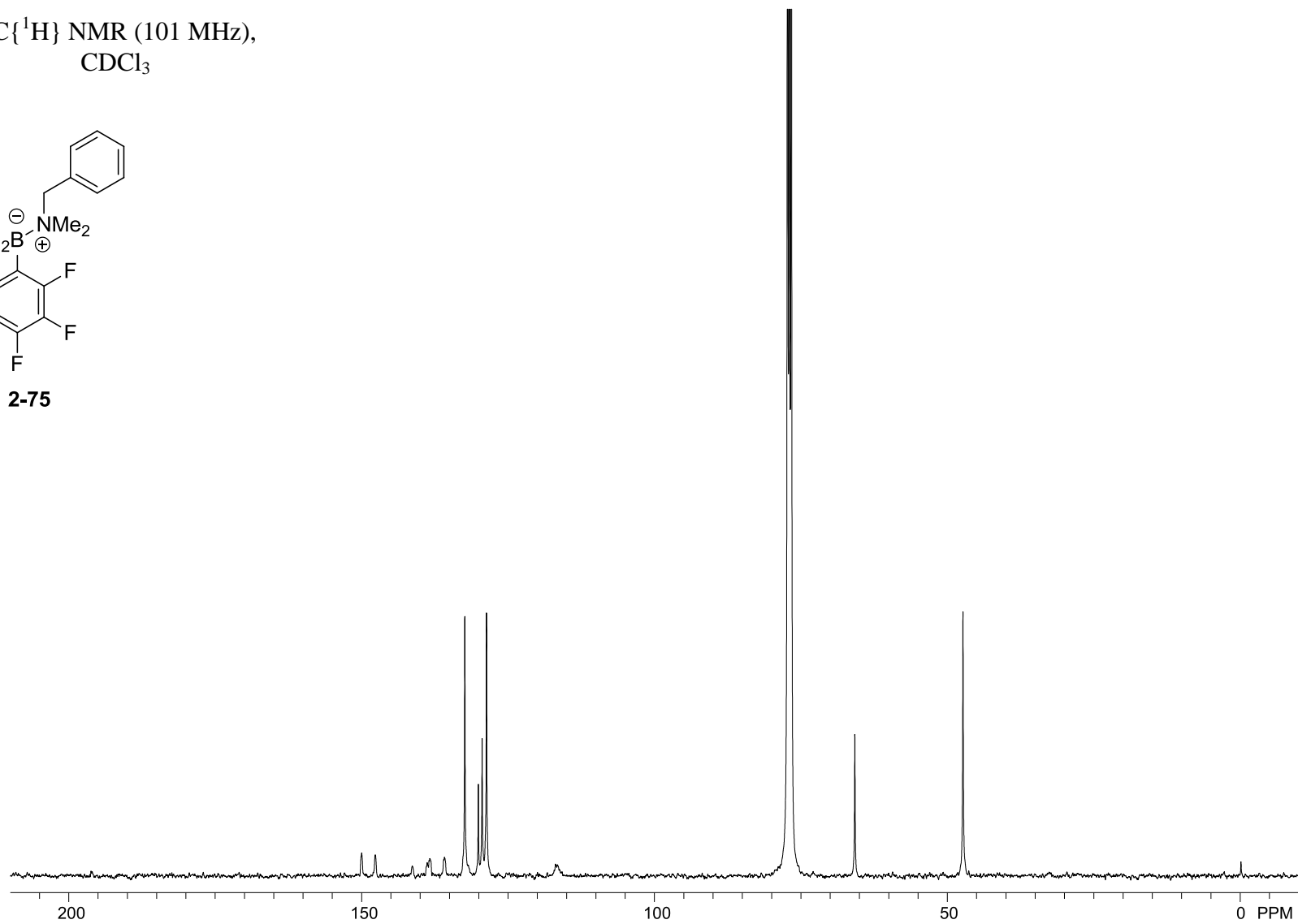
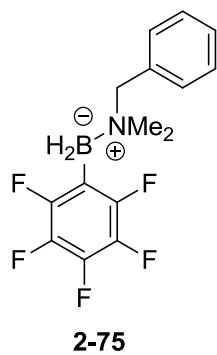
**2-75**



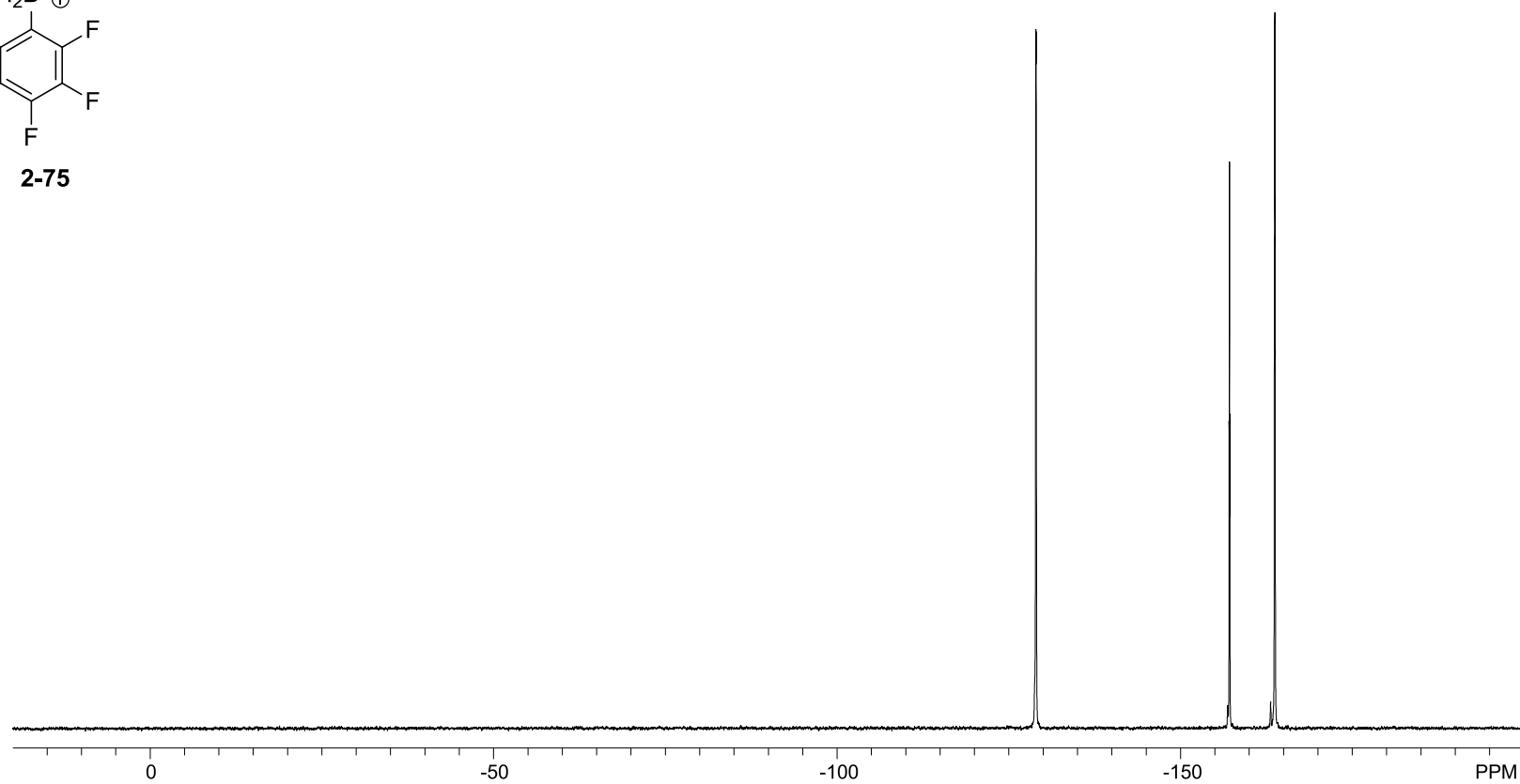
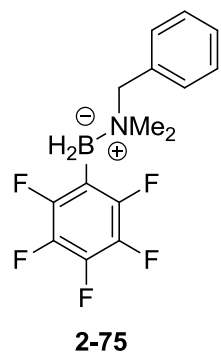
$^{11}\text{B}\{^1\text{H}\}$  NMR (128 MHz),  
 $\text{CDCl}_3$



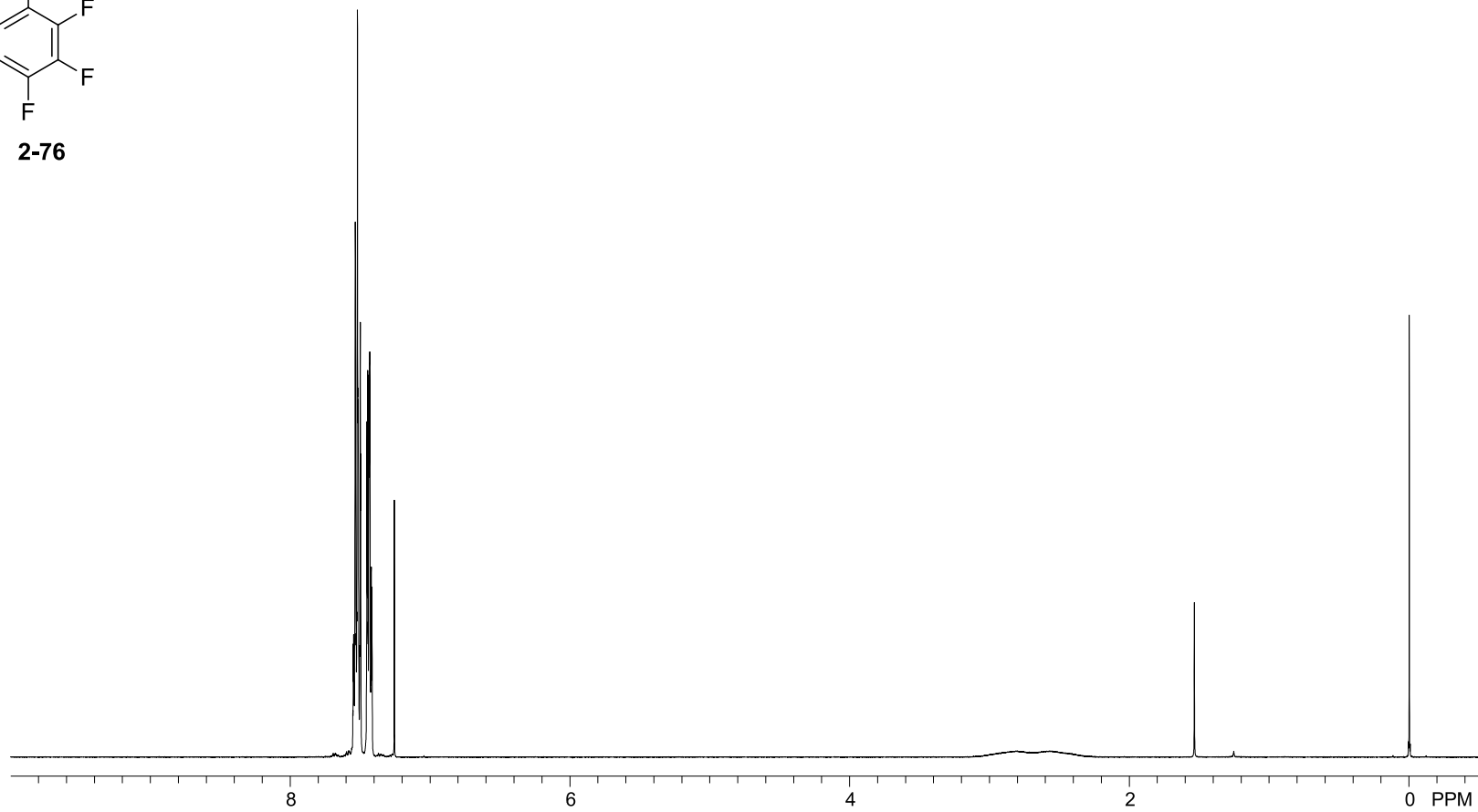
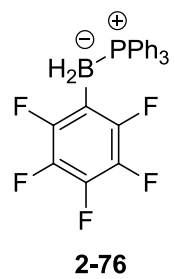
$^{13}\text{C}\{^1\text{H}\}$  NMR (101 MHz),  
 $\text{CDCl}_3$



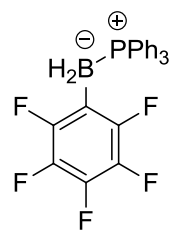
$^{19}\text{F}$  NMR (377 MHz),  
 $\text{CDCl}_3$



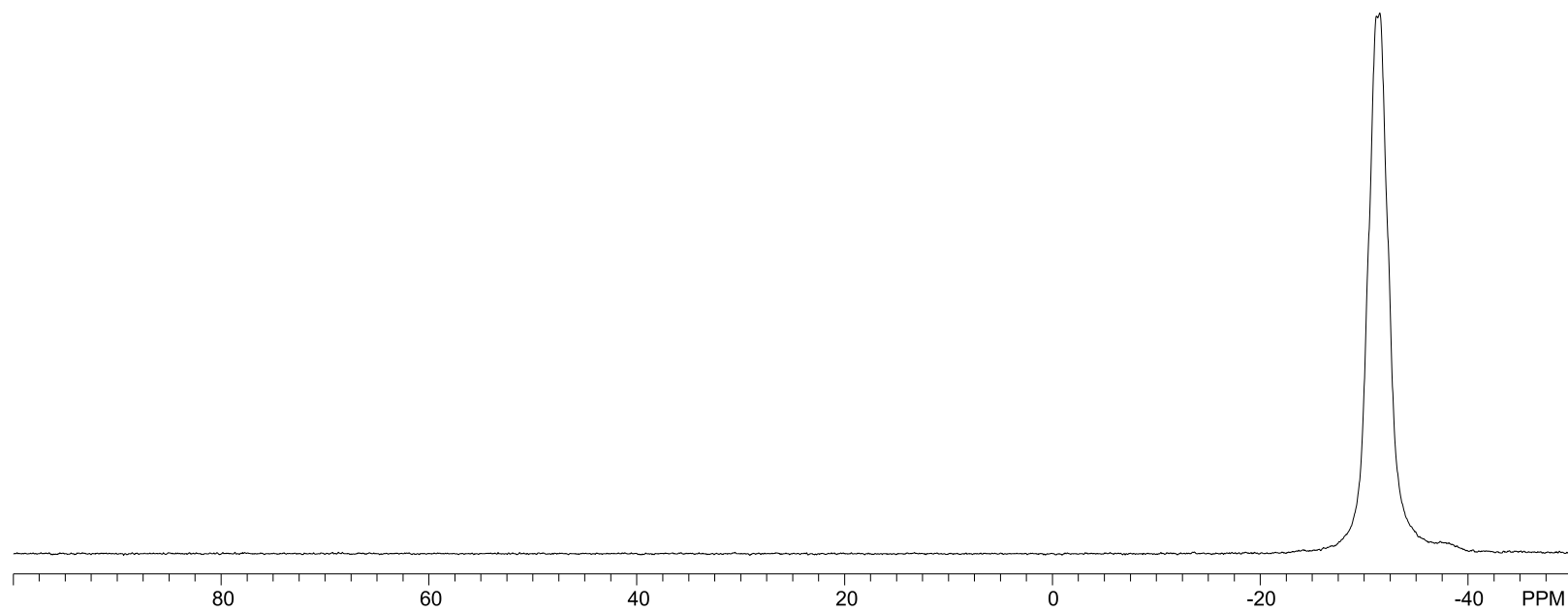
$^1\text{H}$  NMR (500 MHz),  
 $\text{CDCl}_3$



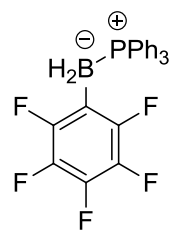
$^{11}\text{B}$  NMR (128 MHz),  
 $\text{CDCl}_3$



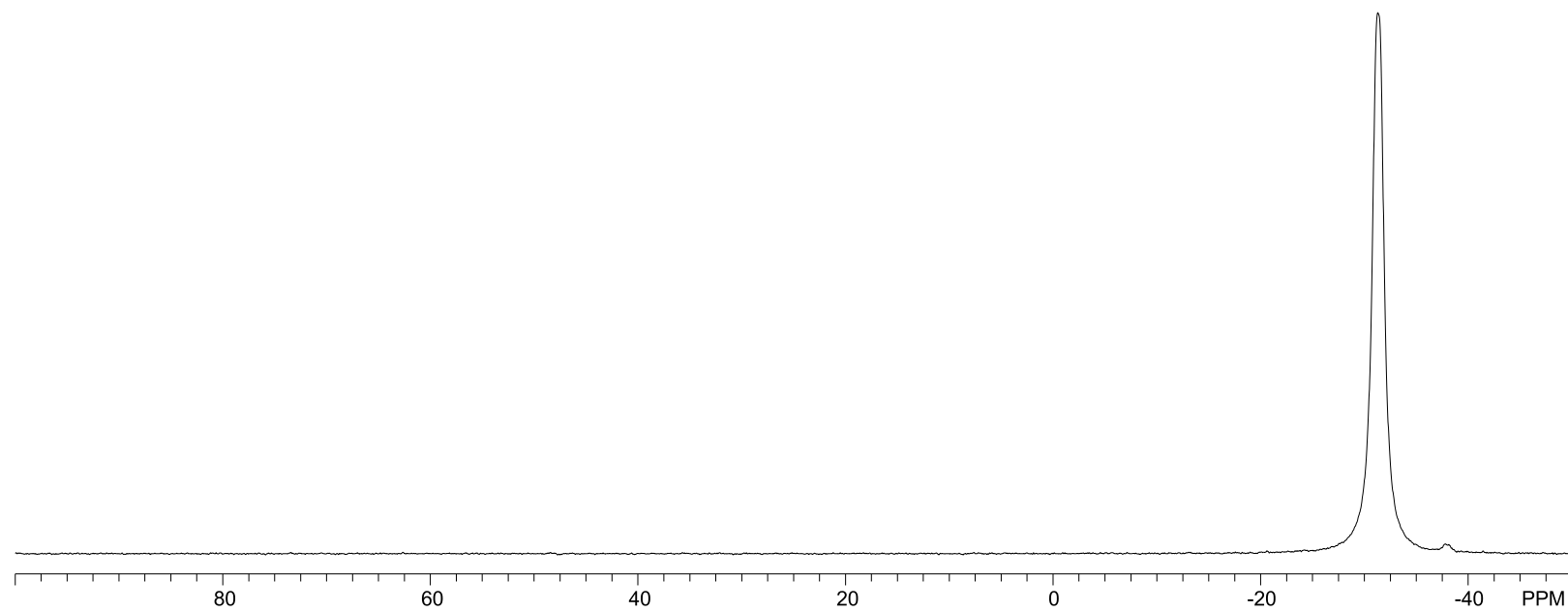
**2-76**



$^{11}\text{B}\{^1\text{H}\}$  NMR (128 MHz),  
 $\text{CDCl}_3$

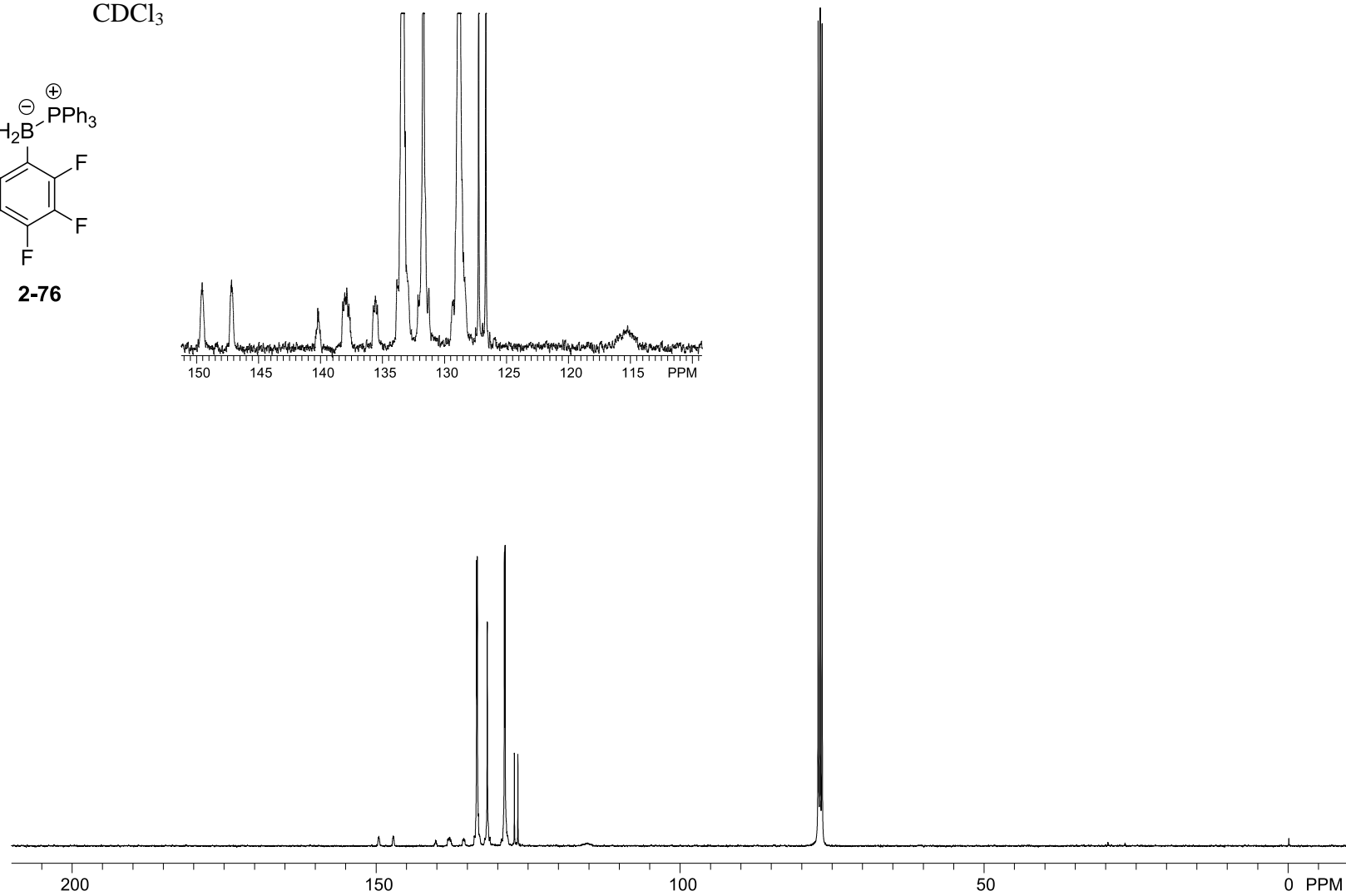
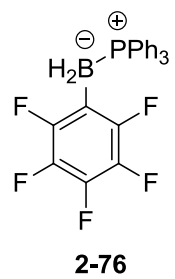


**2-76**

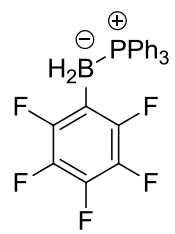




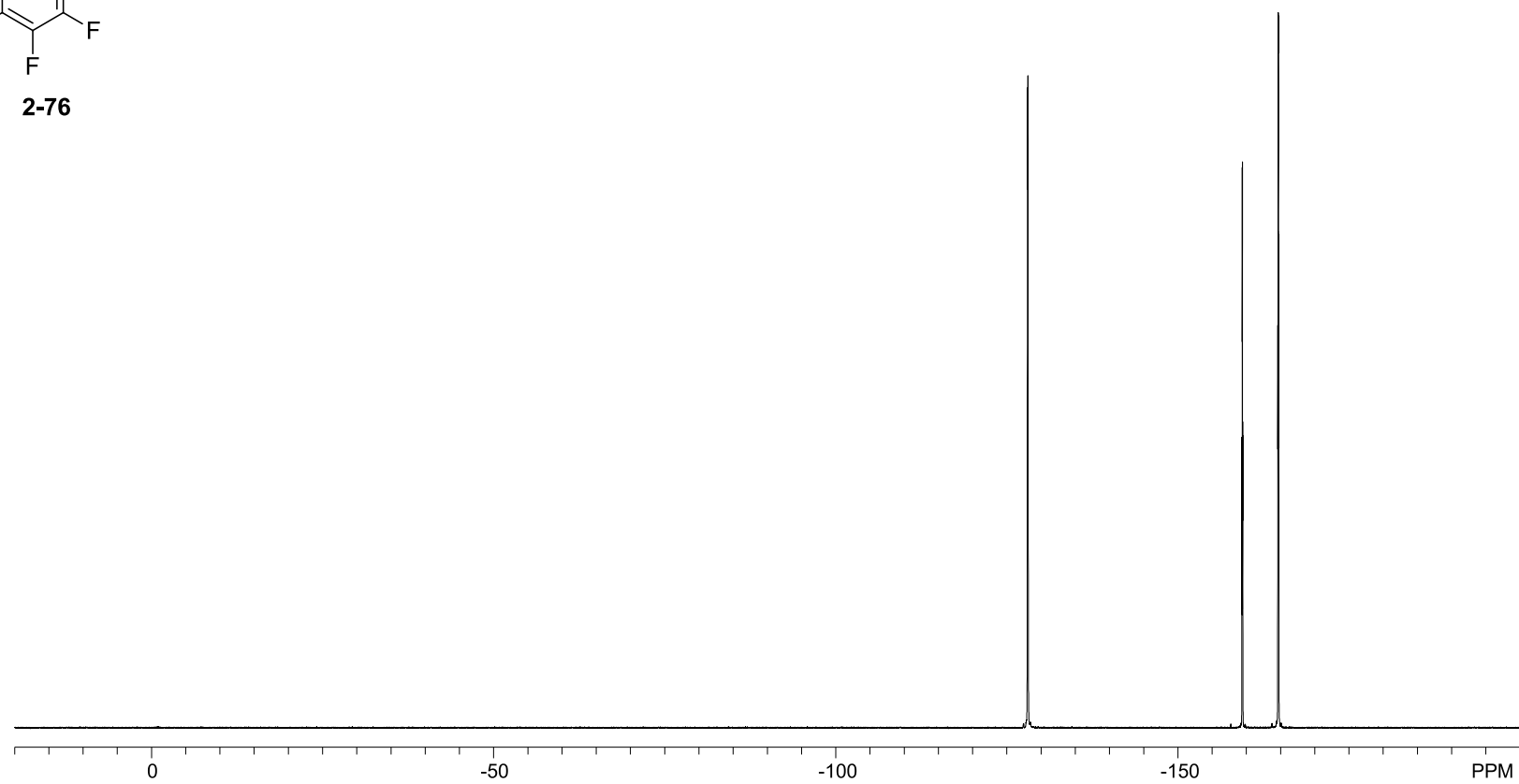
$^{13}\text{C}\{^1\text{H}\}$  NMR (101 MHz),  
 $\text{CDCl}_3$



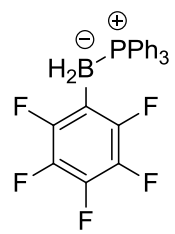
$^{19}\text{F}$  NMR (377 MHz),  
 $\text{CDCl}_3$



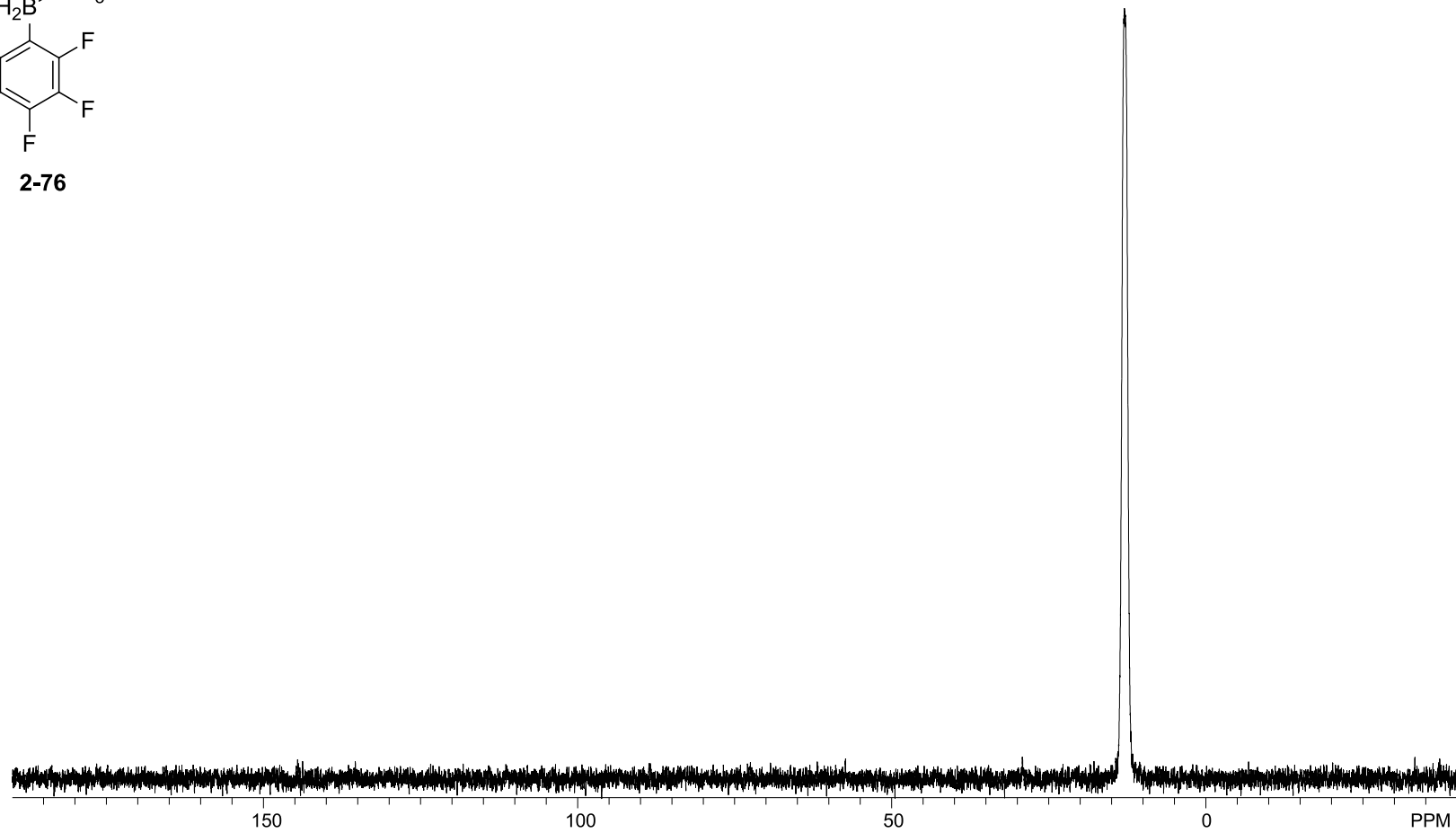
**2-76**



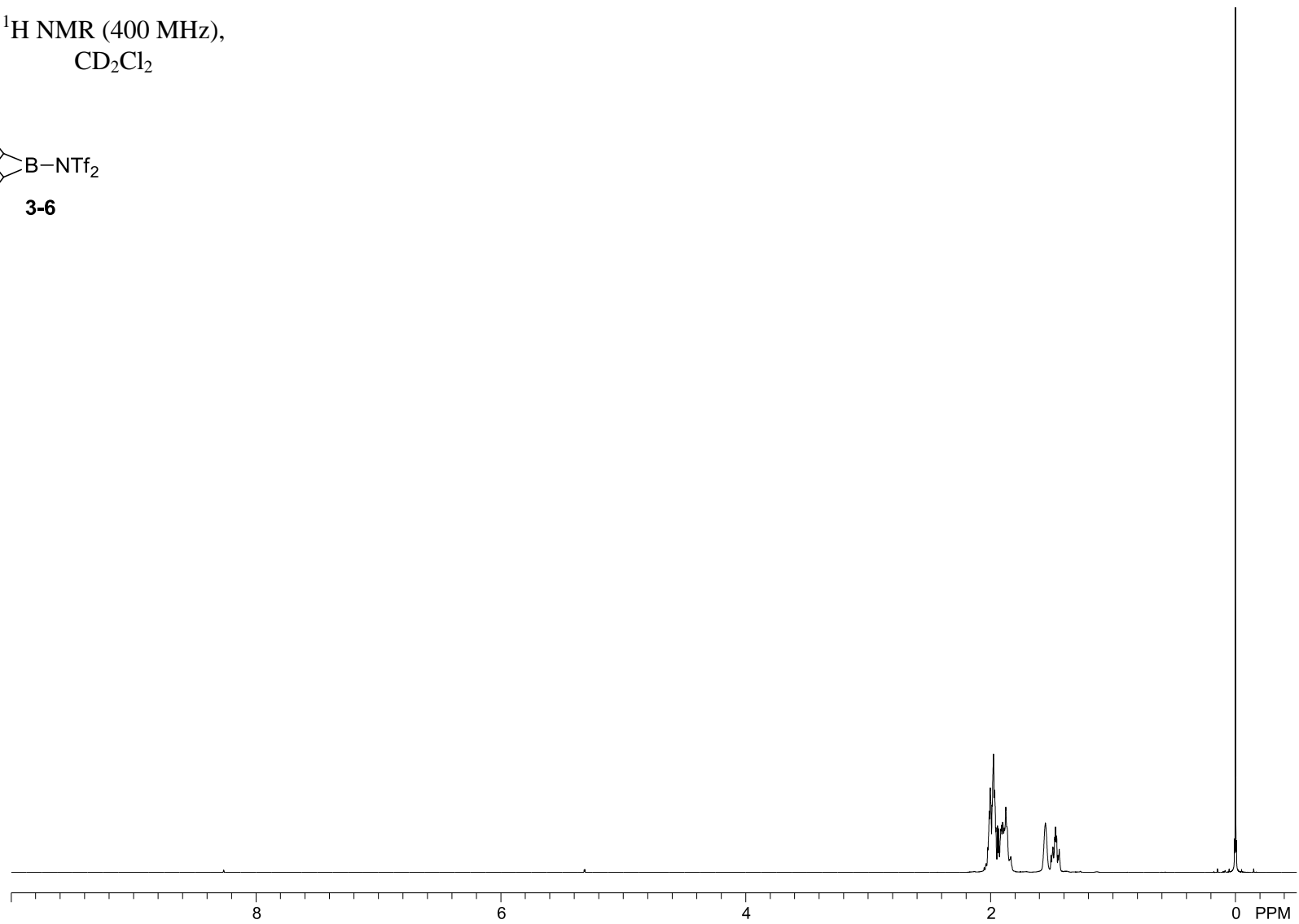
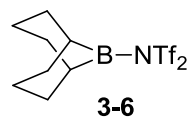
$^{31}\text{P}$  NMR (162 MHz),  
 $\text{CDCl}_3$



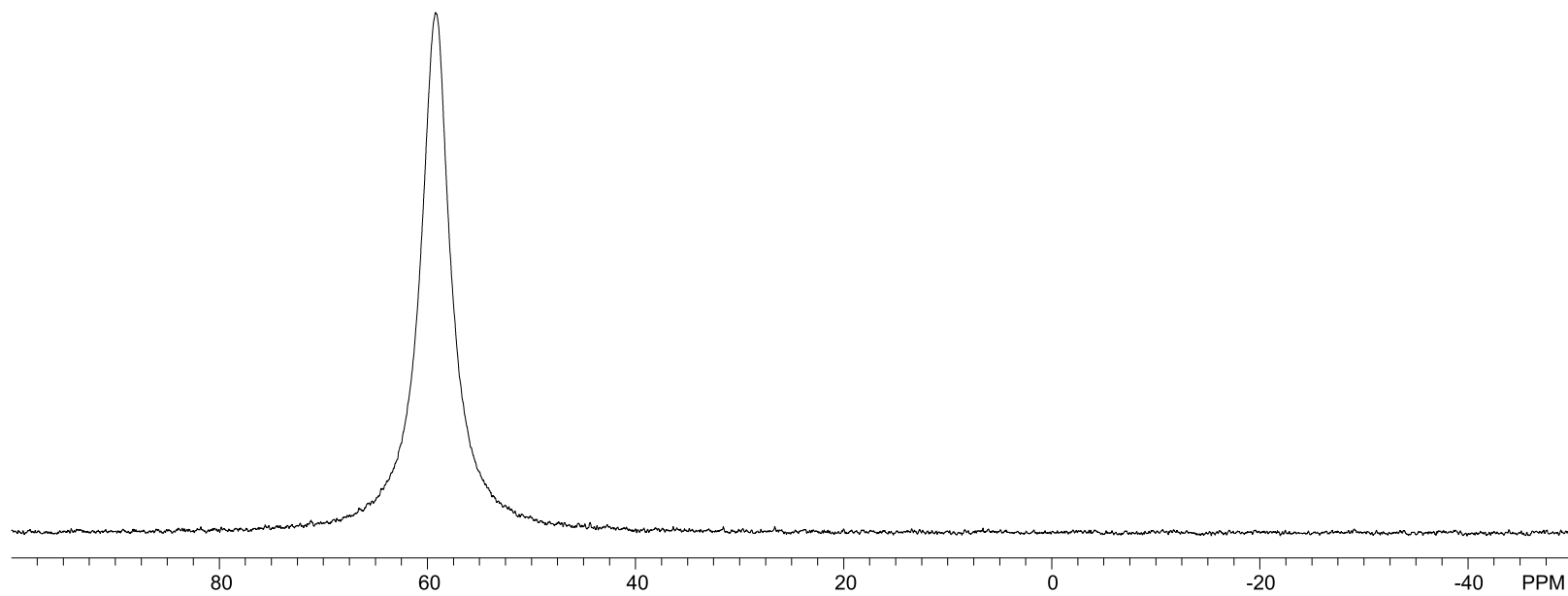
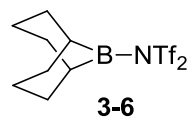
**2-76**



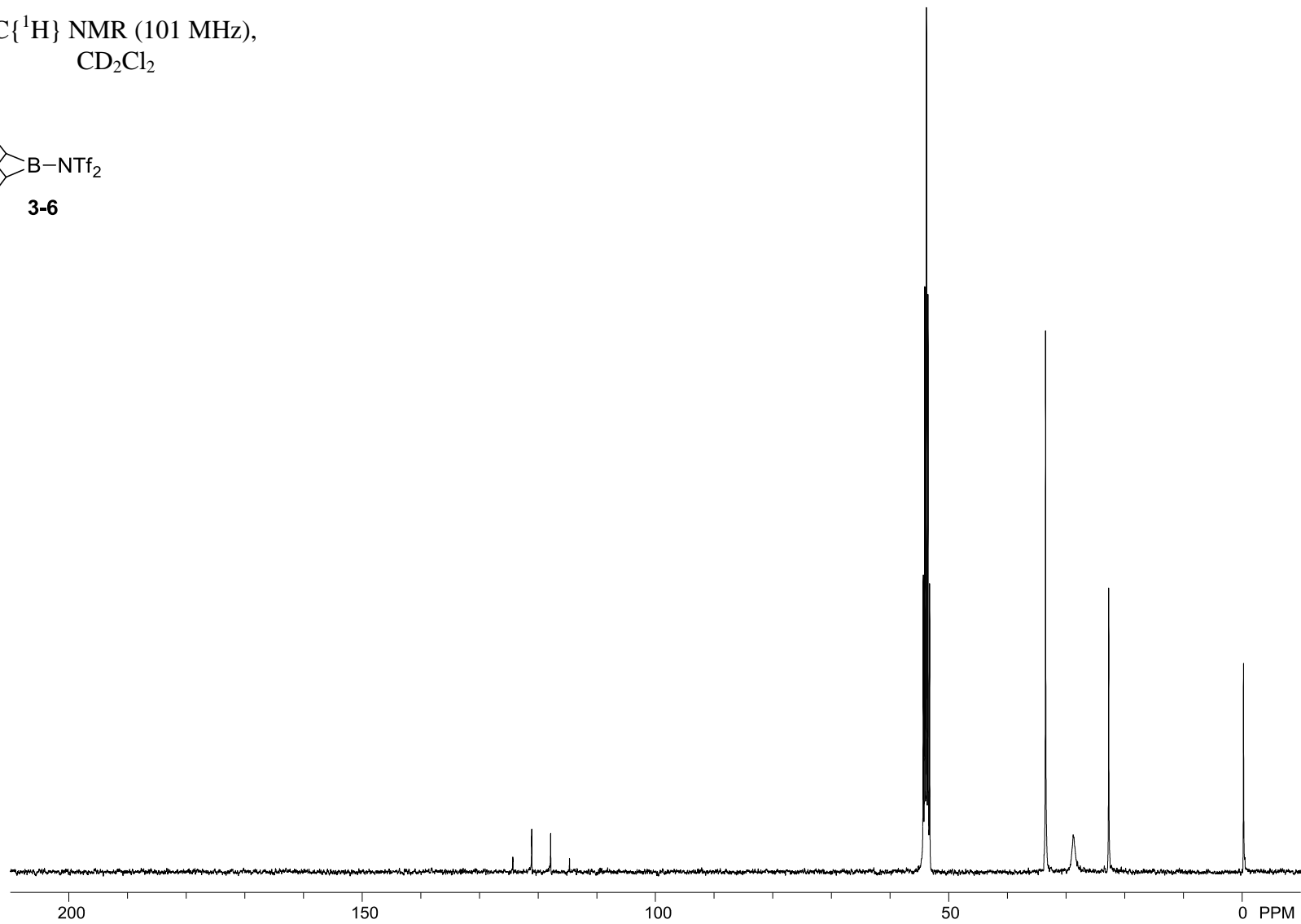
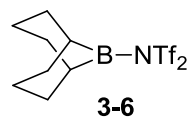
$^1\text{H}$  NMR (400 MHz),  
 $\text{CD}_2\text{Cl}_2$



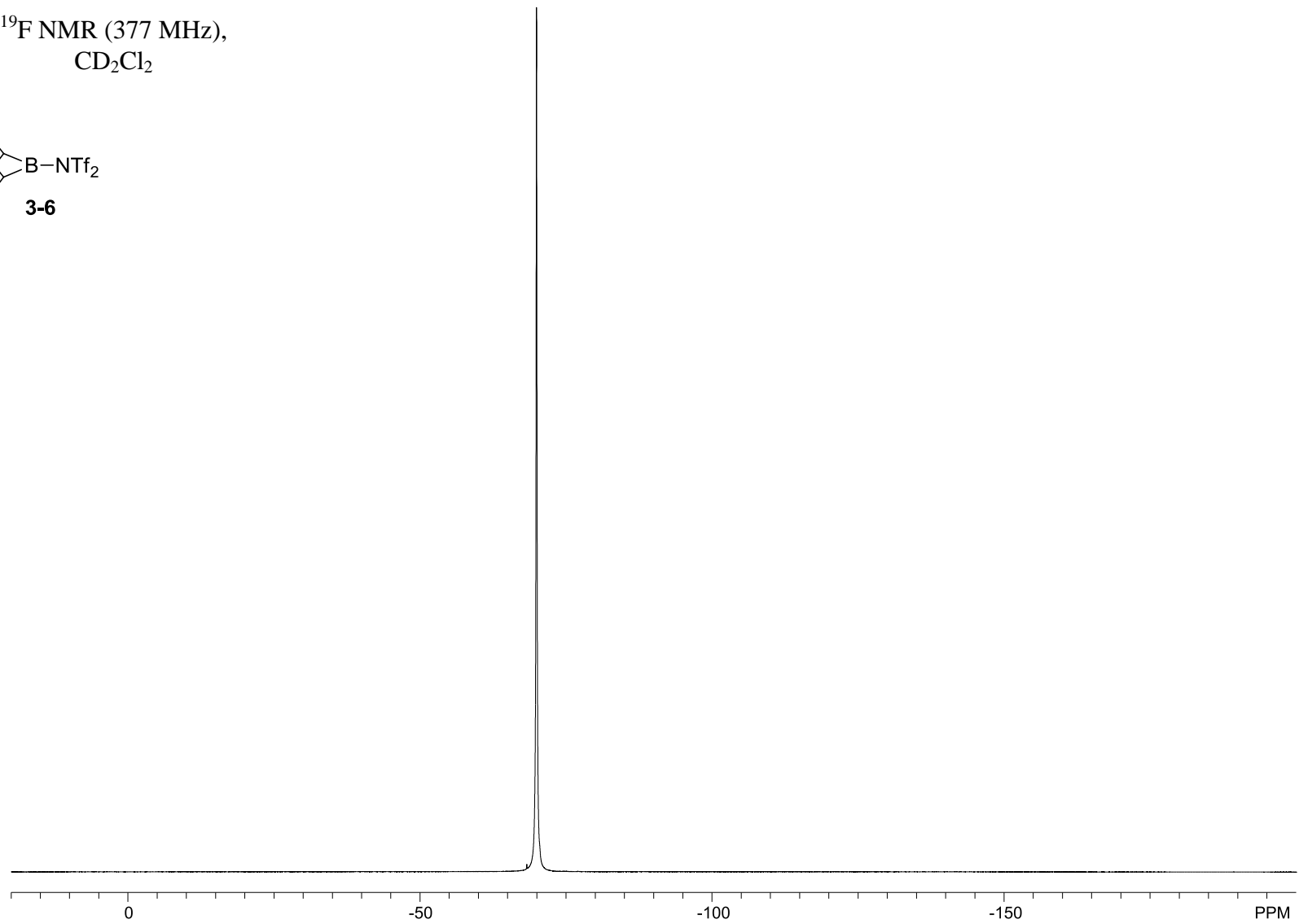
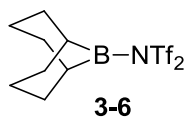
$^{11}\text{B}$  NMR (128 MHz),  
 $\text{CD}_2\text{Cl}_2$



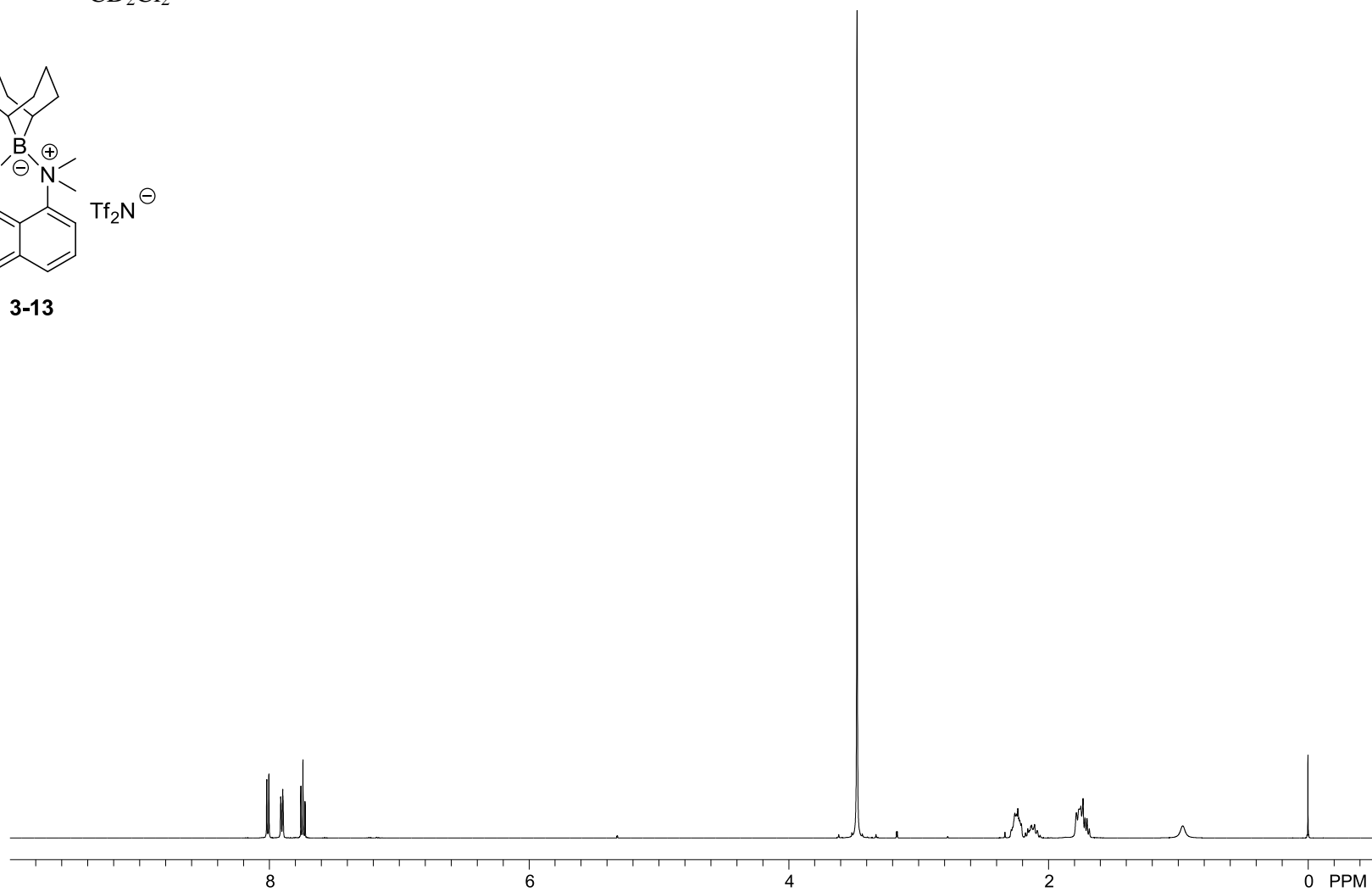
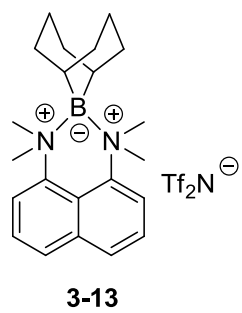
$^{13}\text{C}\{^1\text{H}\}$  NMR (101 MHz),  
 $\text{CD}_2\text{Cl}_2$



$^{19}\text{F}$  NMR (377 MHz),  
 $\text{CD}_2\text{Cl}_2$

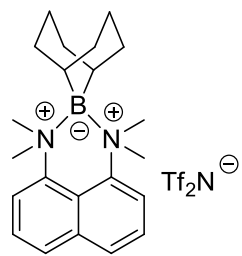


$^1\text{H}$  NMR (500 MHz),  
 $\text{CD}_2\text{Cl}_2$

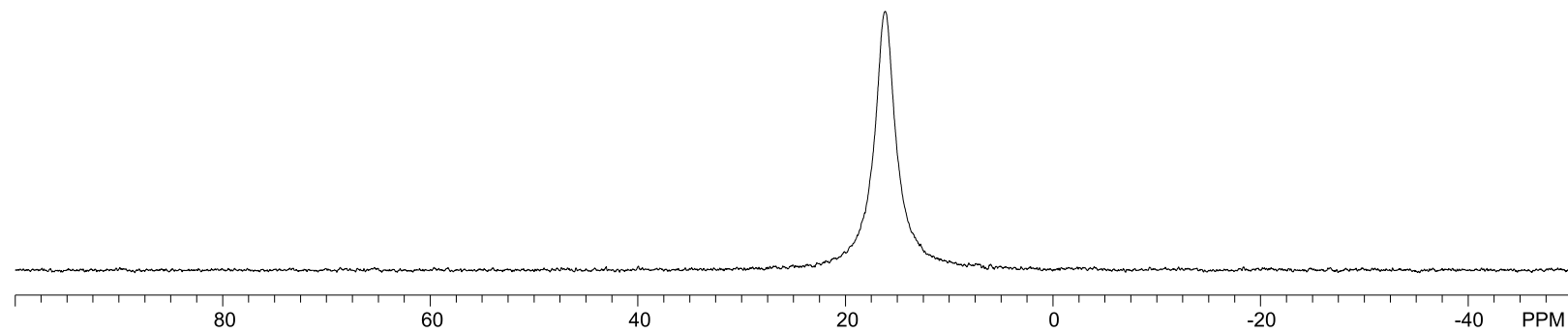




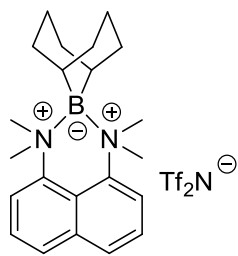
$^{11}\text{B}$  NMR (128 MHz),  
 $\text{CD}_2\text{Cl}_2$



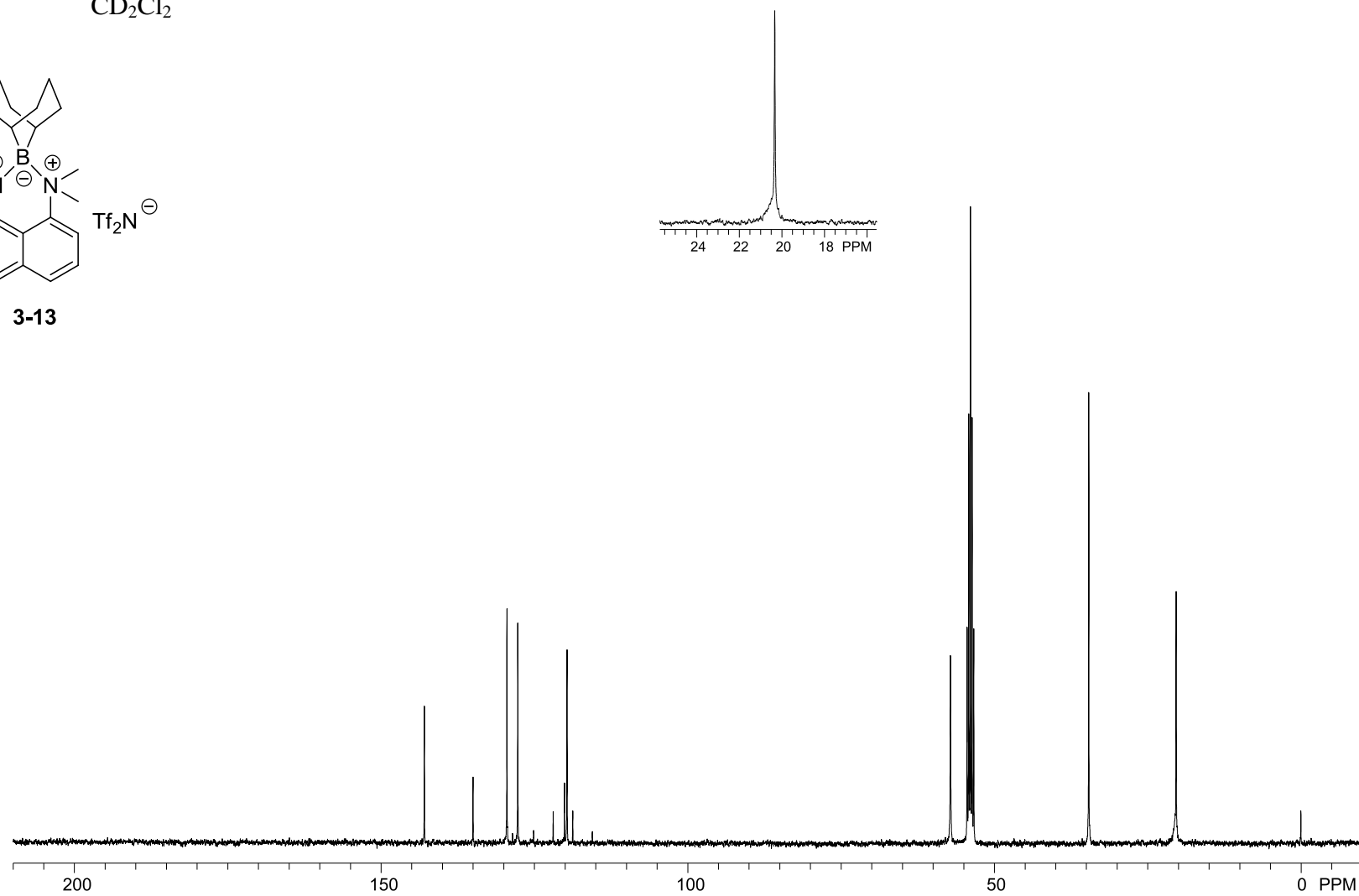
**3-13**



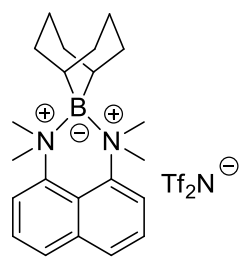
$^{13}\text{C}\{^1\text{H}\}$  NMR (101 MHz),  
 $\text{CD}_2\text{Cl}_2$



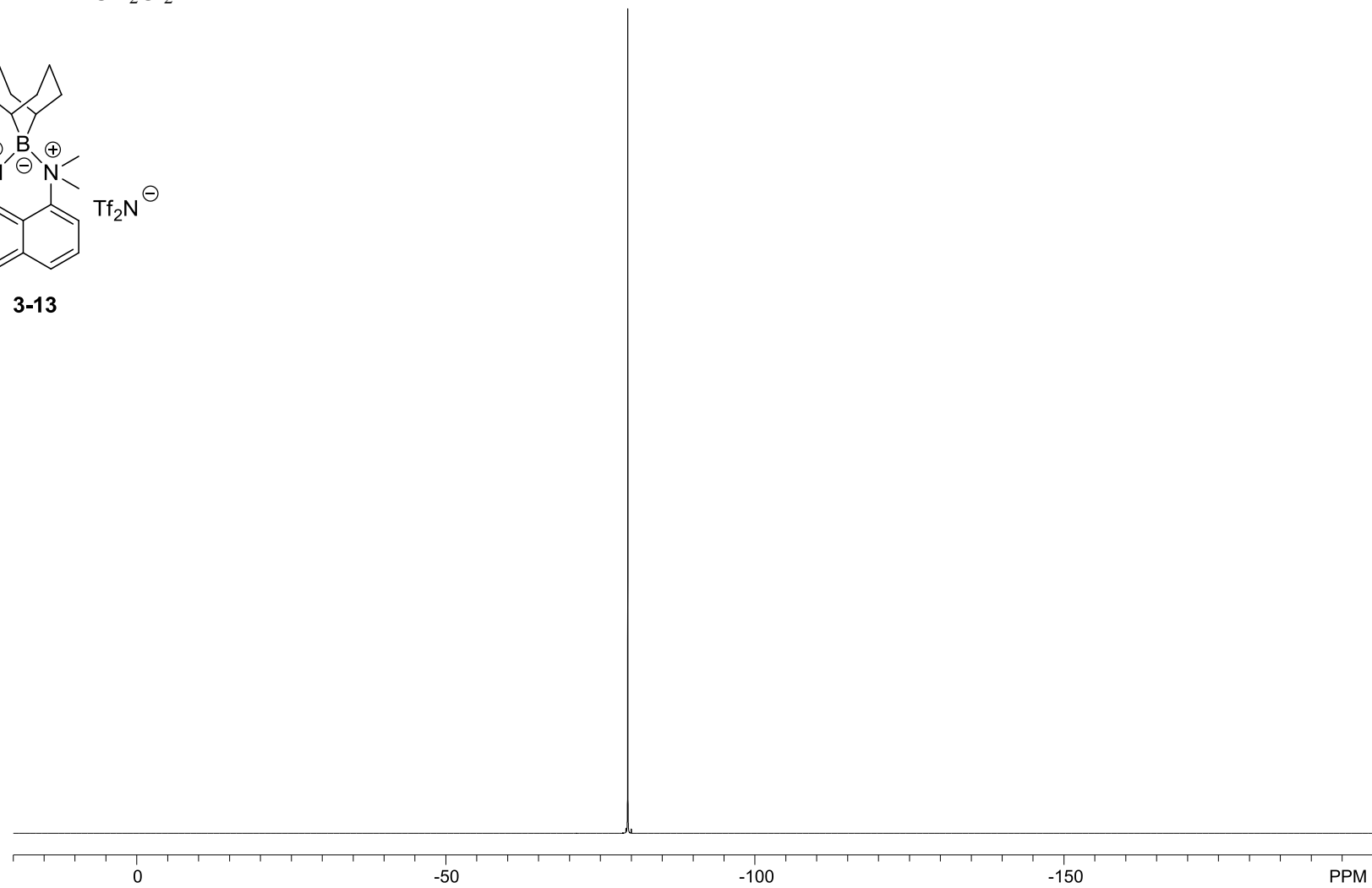
**3-13**



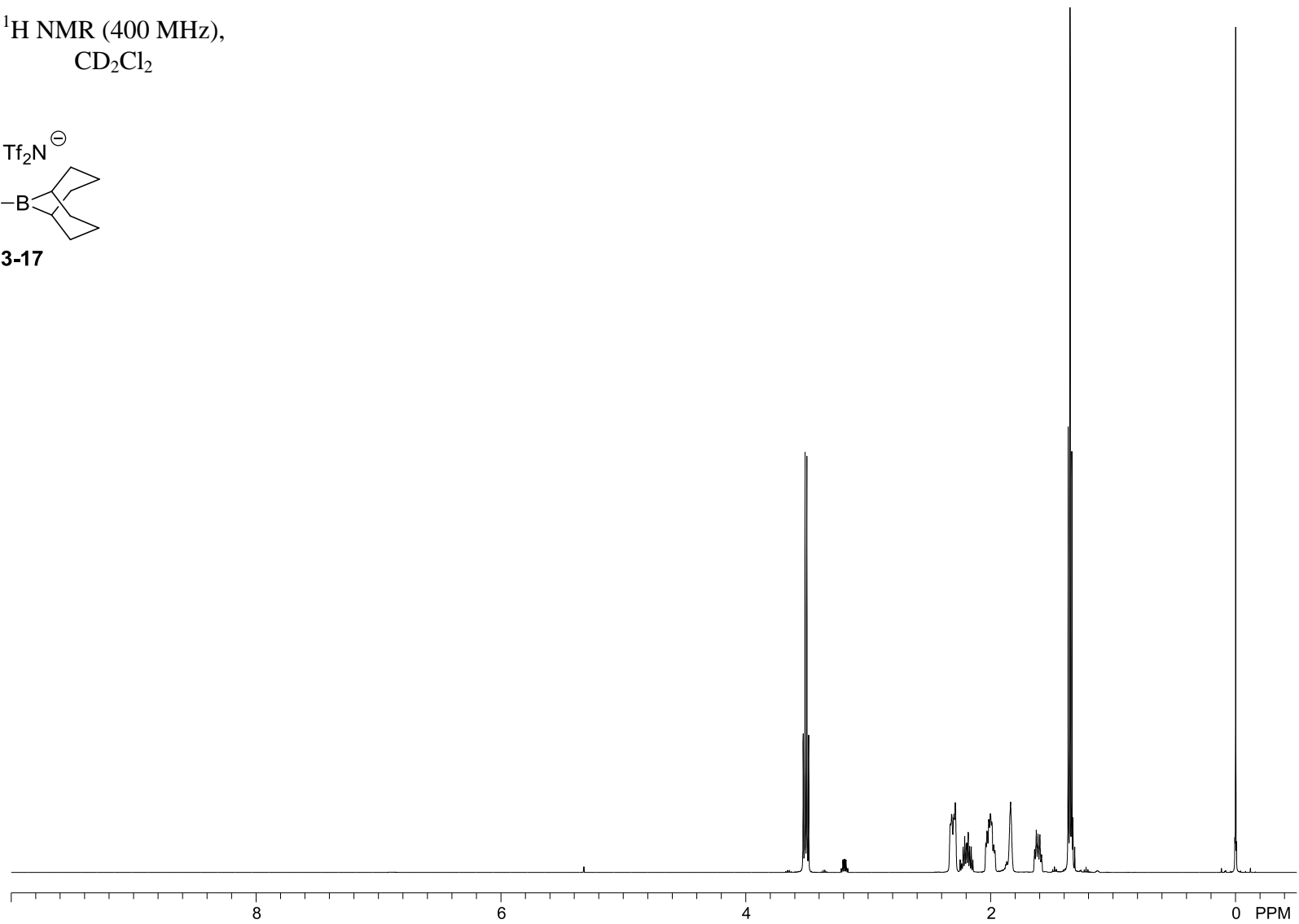
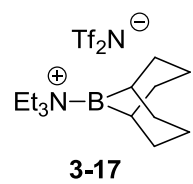
$^{19}\text{F}$  NMR (377 MHz),  
 $\text{CD}_2\text{Cl}_2$



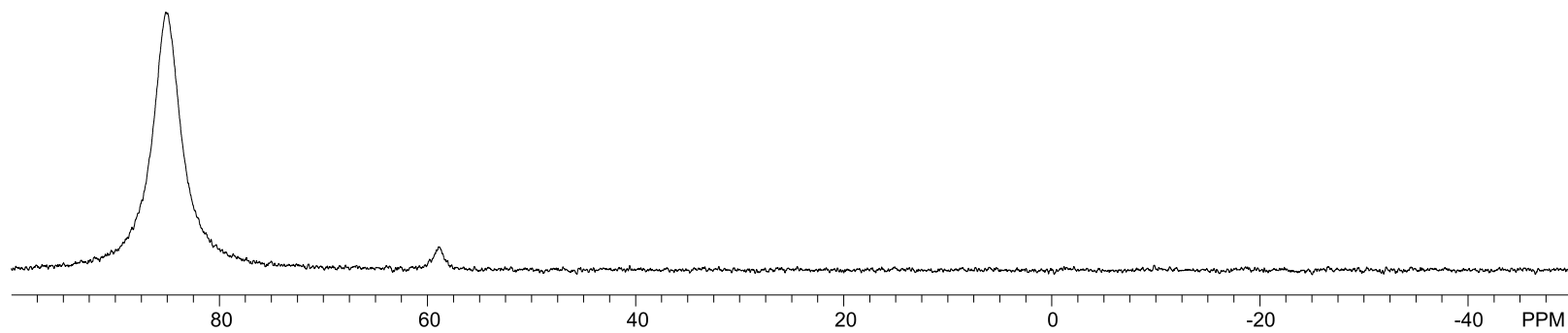
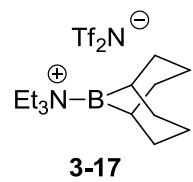
**3-13**



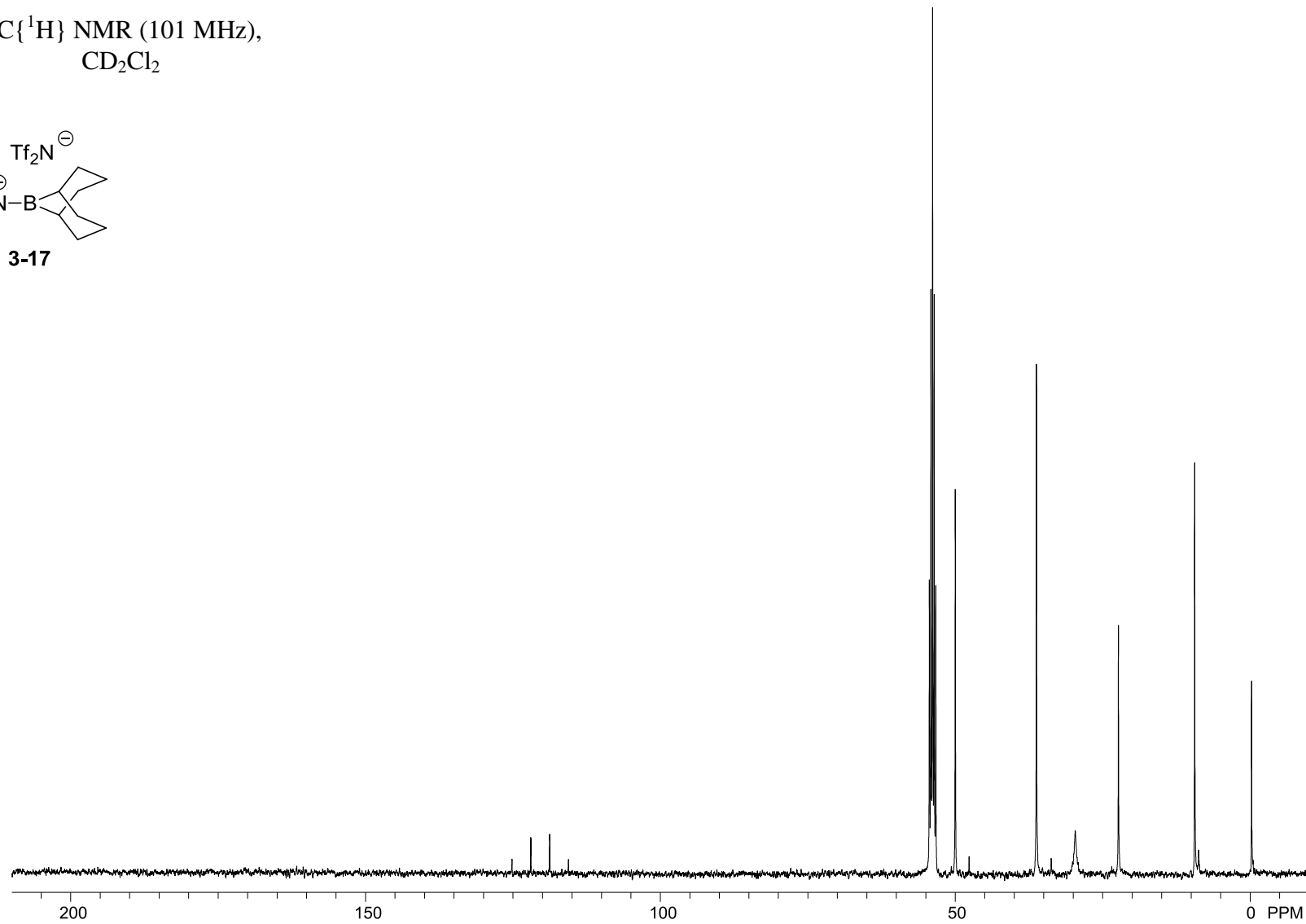
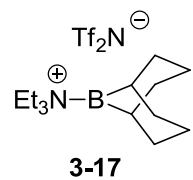
$^1\text{H}$  NMR (400 MHz),  
 $\text{CD}_2\text{Cl}_2$



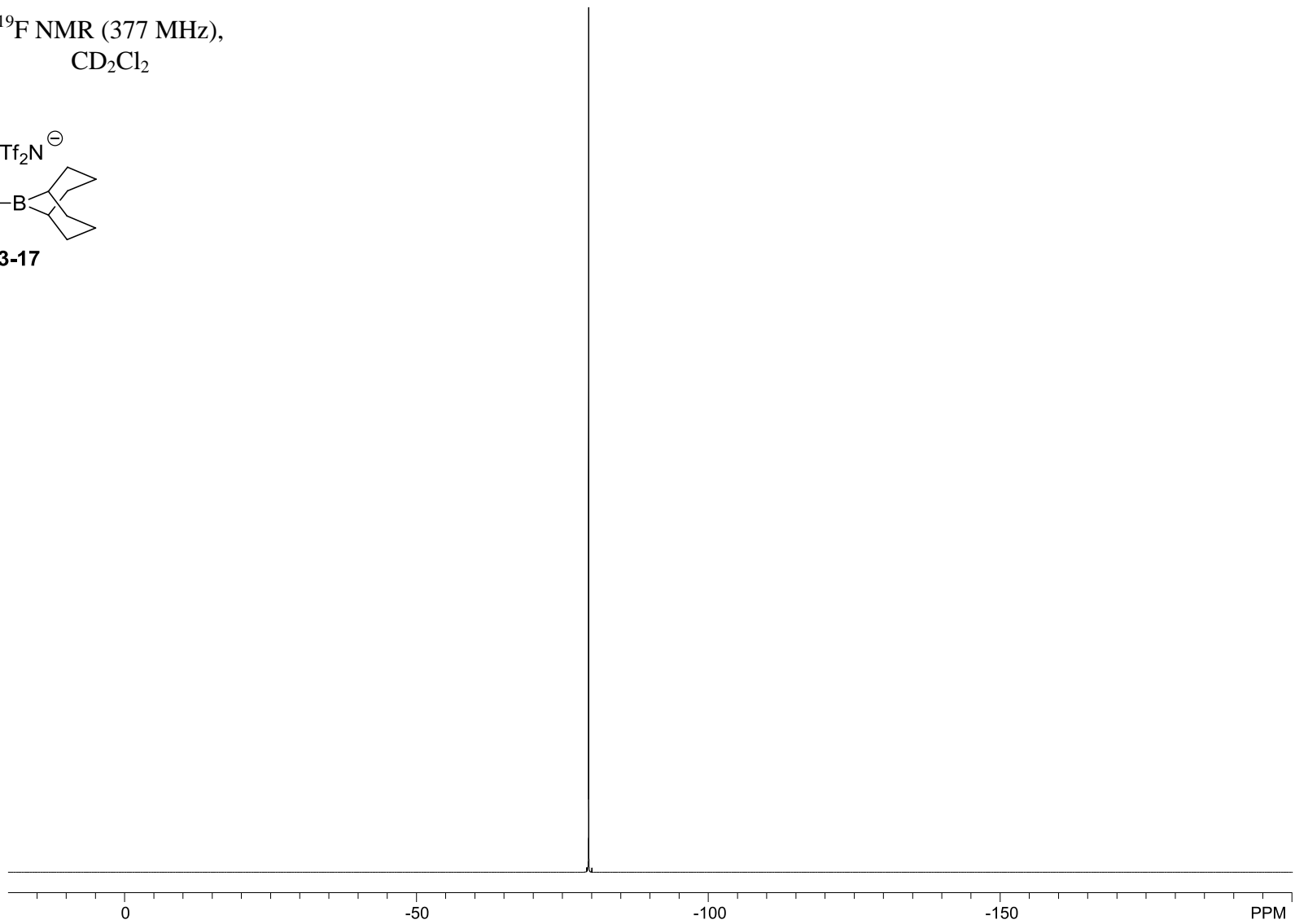
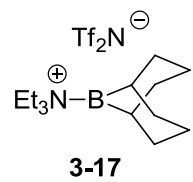
$^{11}\text{B}$  NMR (128 MHz),  
 $\text{CD}_2\text{Cl}_2$



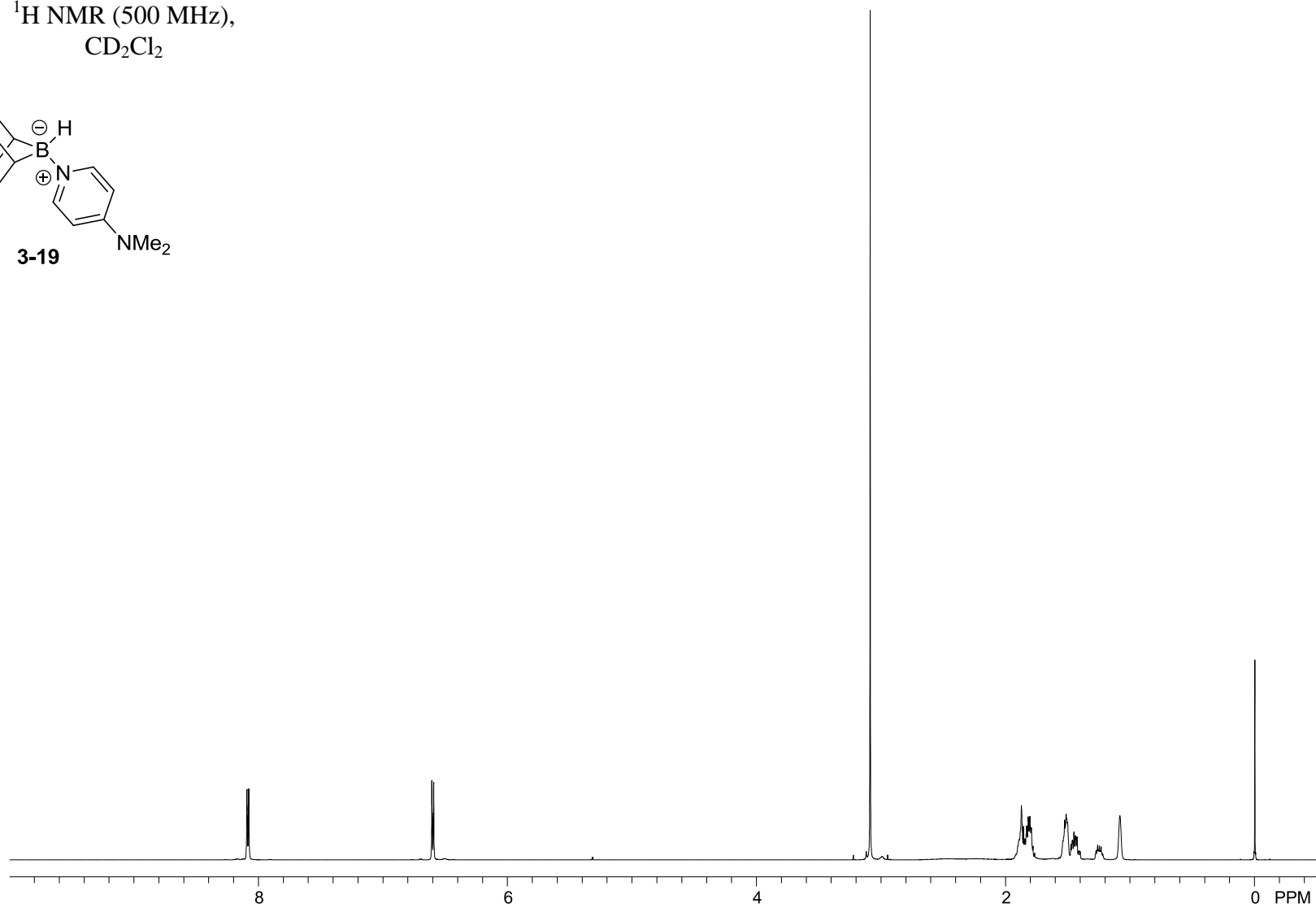
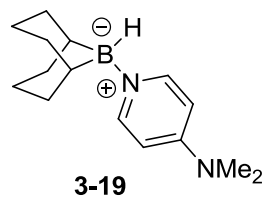
$^{13}\text{C}\{^1\text{H}\}$  NMR (101 MHz),  
 $\text{CD}_2\text{Cl}_2$



$^{19}\text{F}$  NMR (377 MHz),  
 $\text{CD}_2\text{Cl}_2$

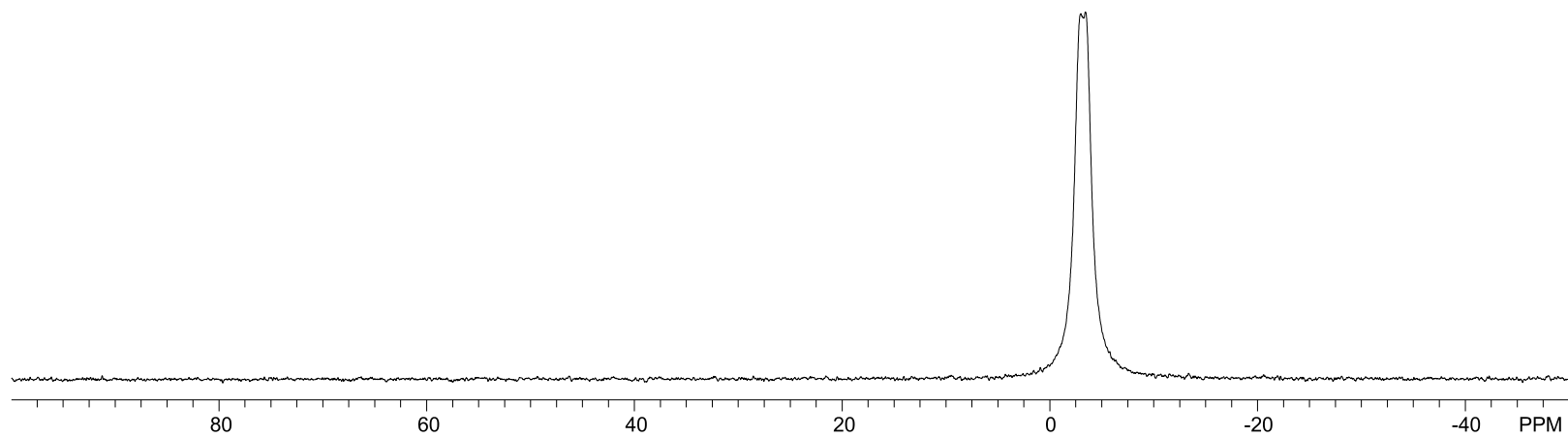
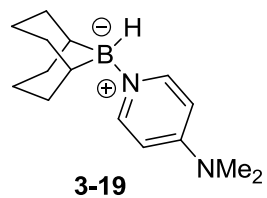


$^1\text{H}$  NMR (500 MHz),  
 $\text{CD}_2\text{Cl}_2$

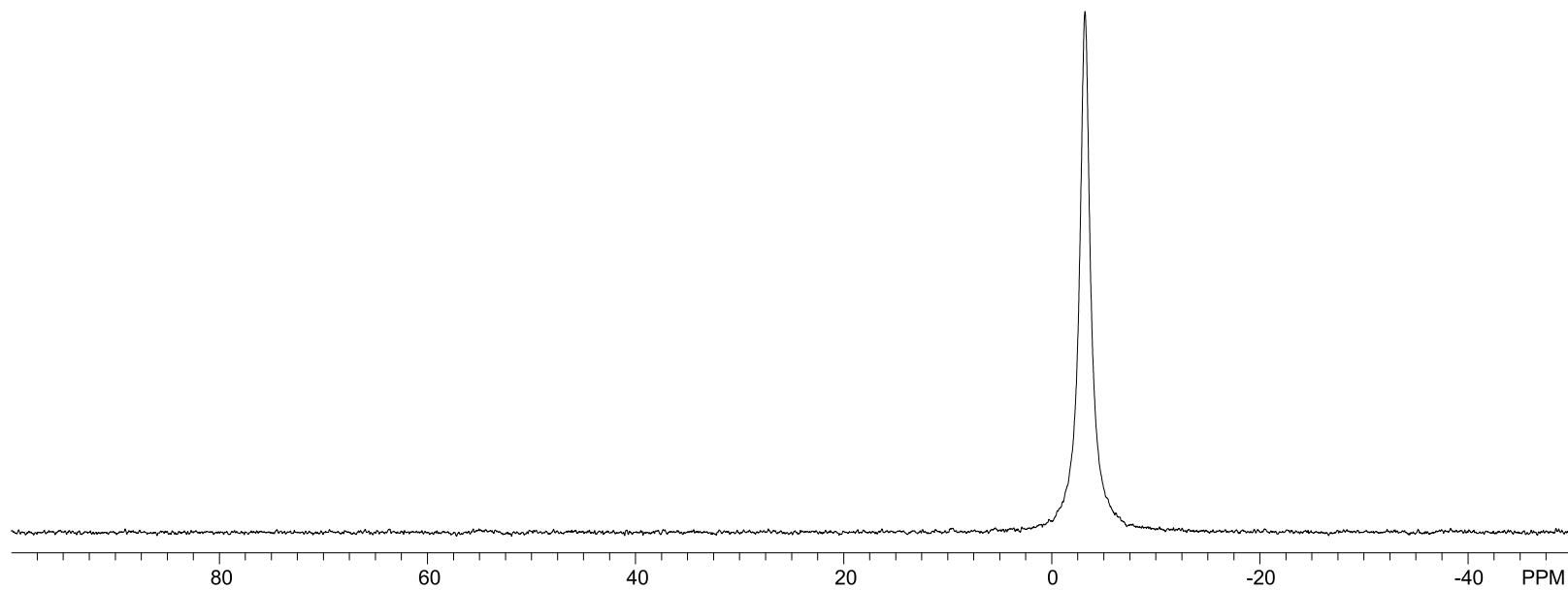
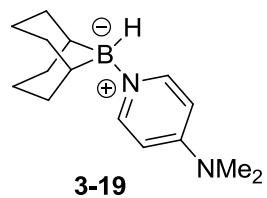




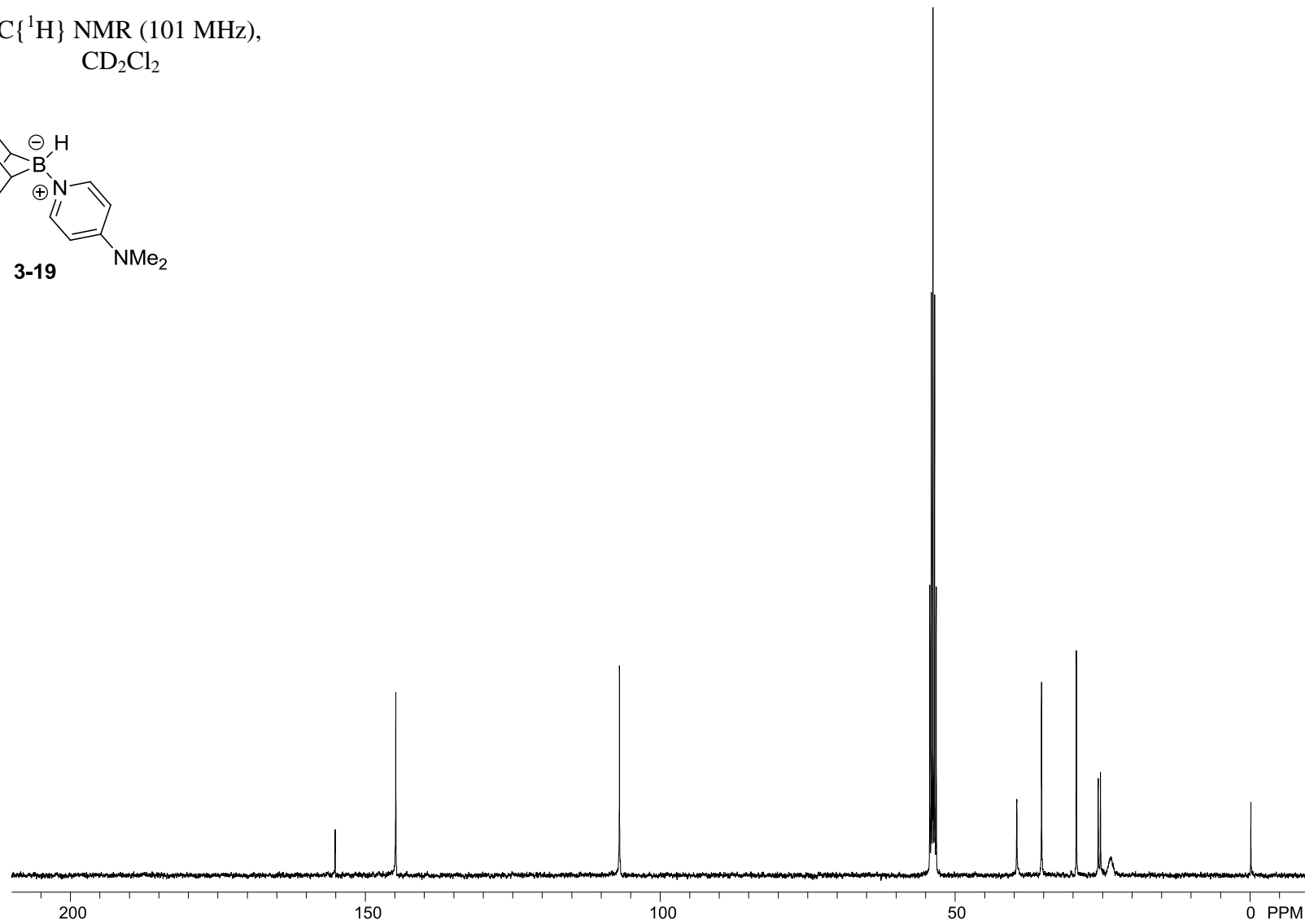
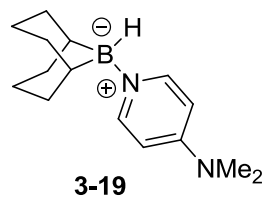
$^{11}\text{B}$  NMR (128 MHz),  
 $\text{CD}_2\text{Cl}_2$



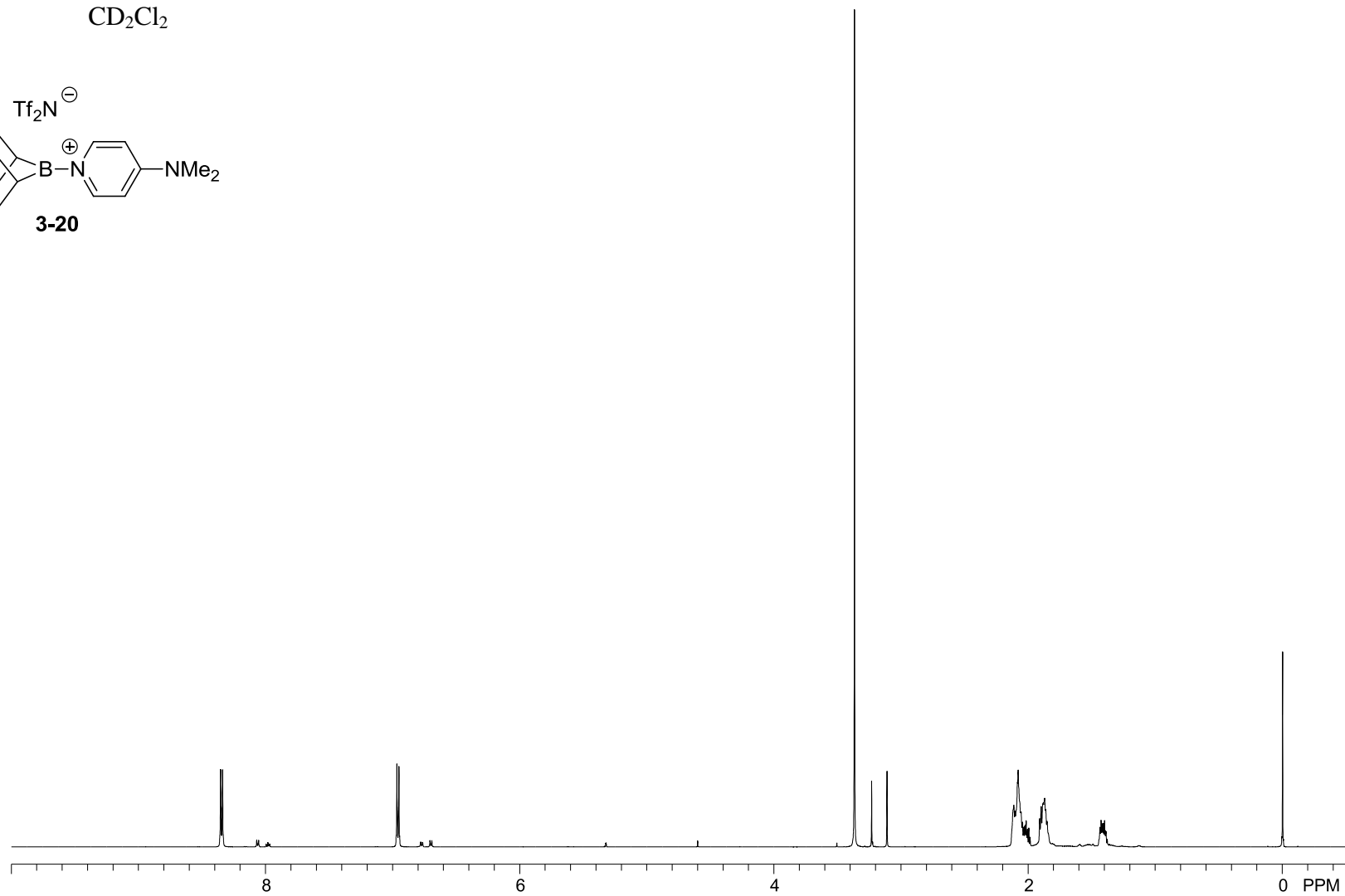
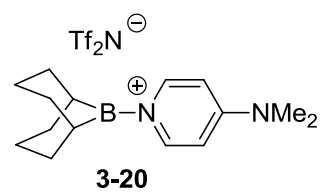
$^{11}\text{B}\{^1\text{H}\}$  NMR (128 MHz),  
 $\text{CD}_2\text{Cl}_2$



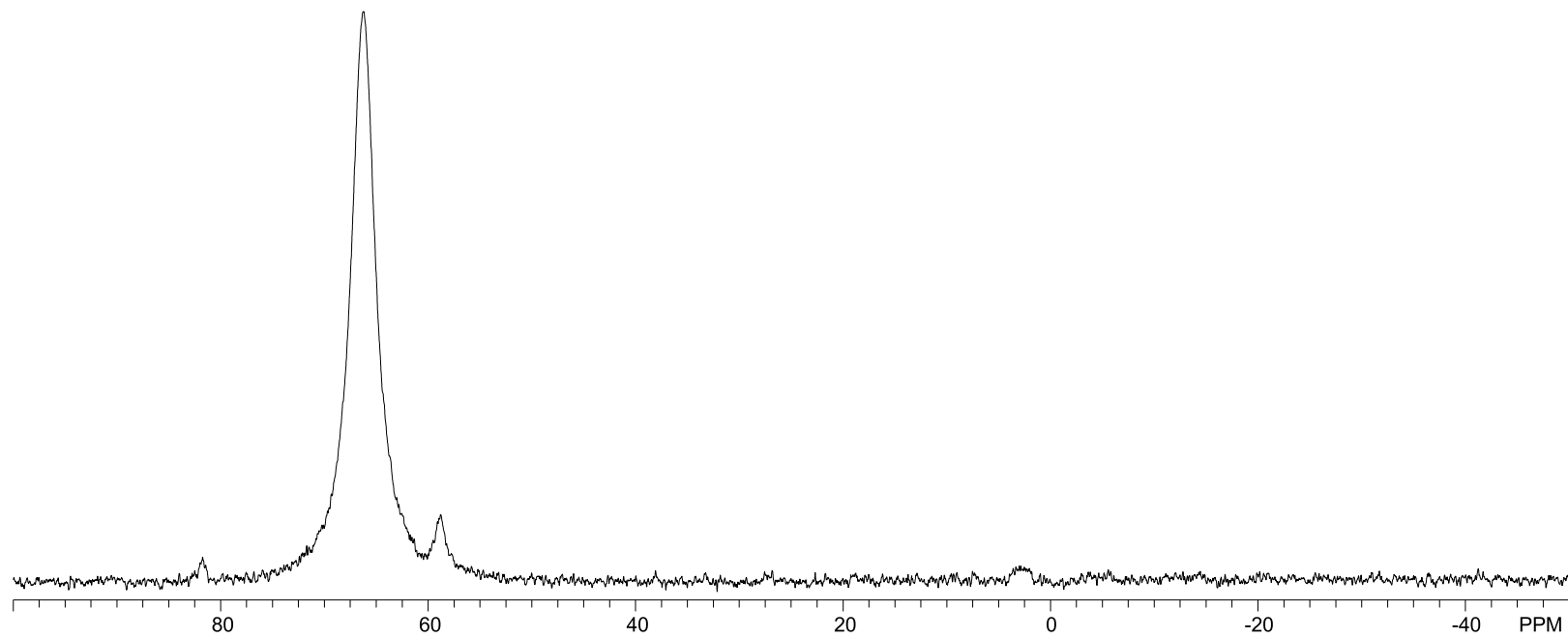
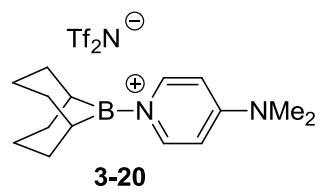
$^{13}\text{C}\{^1\text{H}\}$  NMR (101 MHz),  
 $\text{CD}_2\text{Cl}_2$



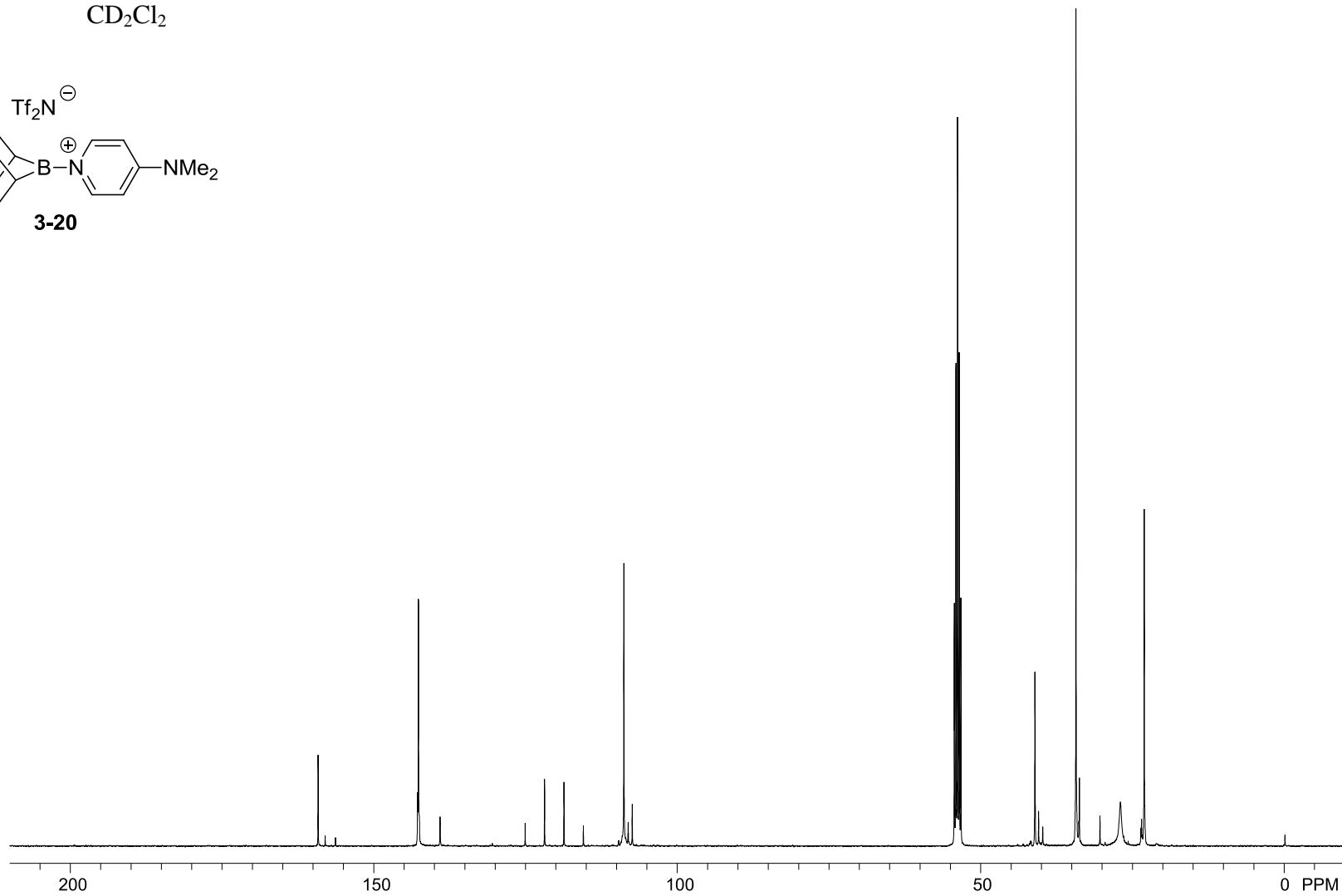
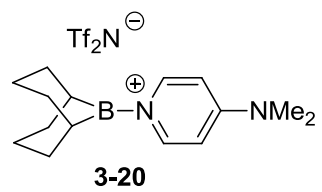
$^1\text{H}$  NMR (500 MHz),  
 $\text{CD}_2\text{Cl}_2$



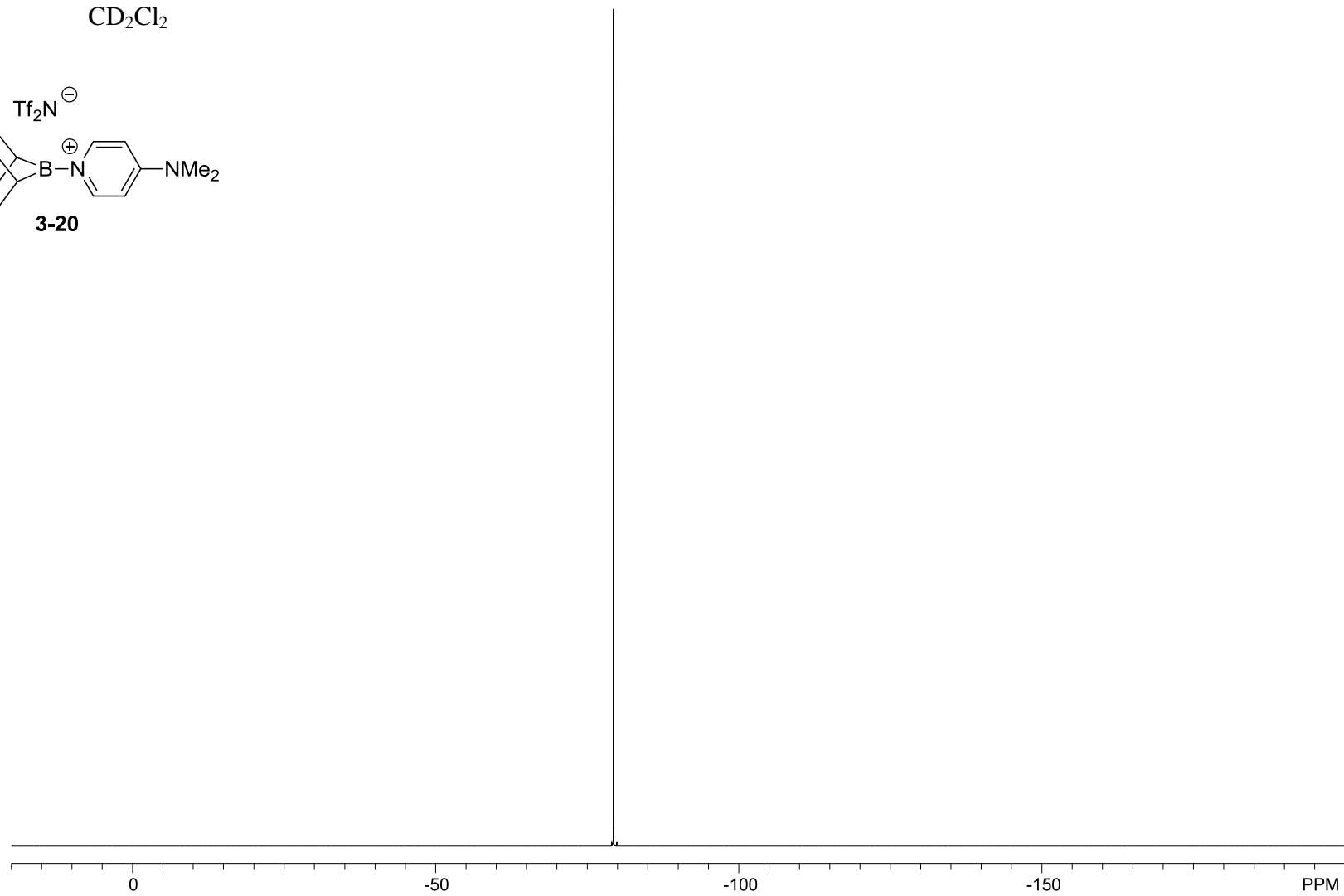
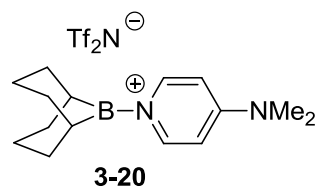
$^{11}\text{B}$  NMR (128 MHz),  
 $\text{CD}_2\text{Cl}_2$



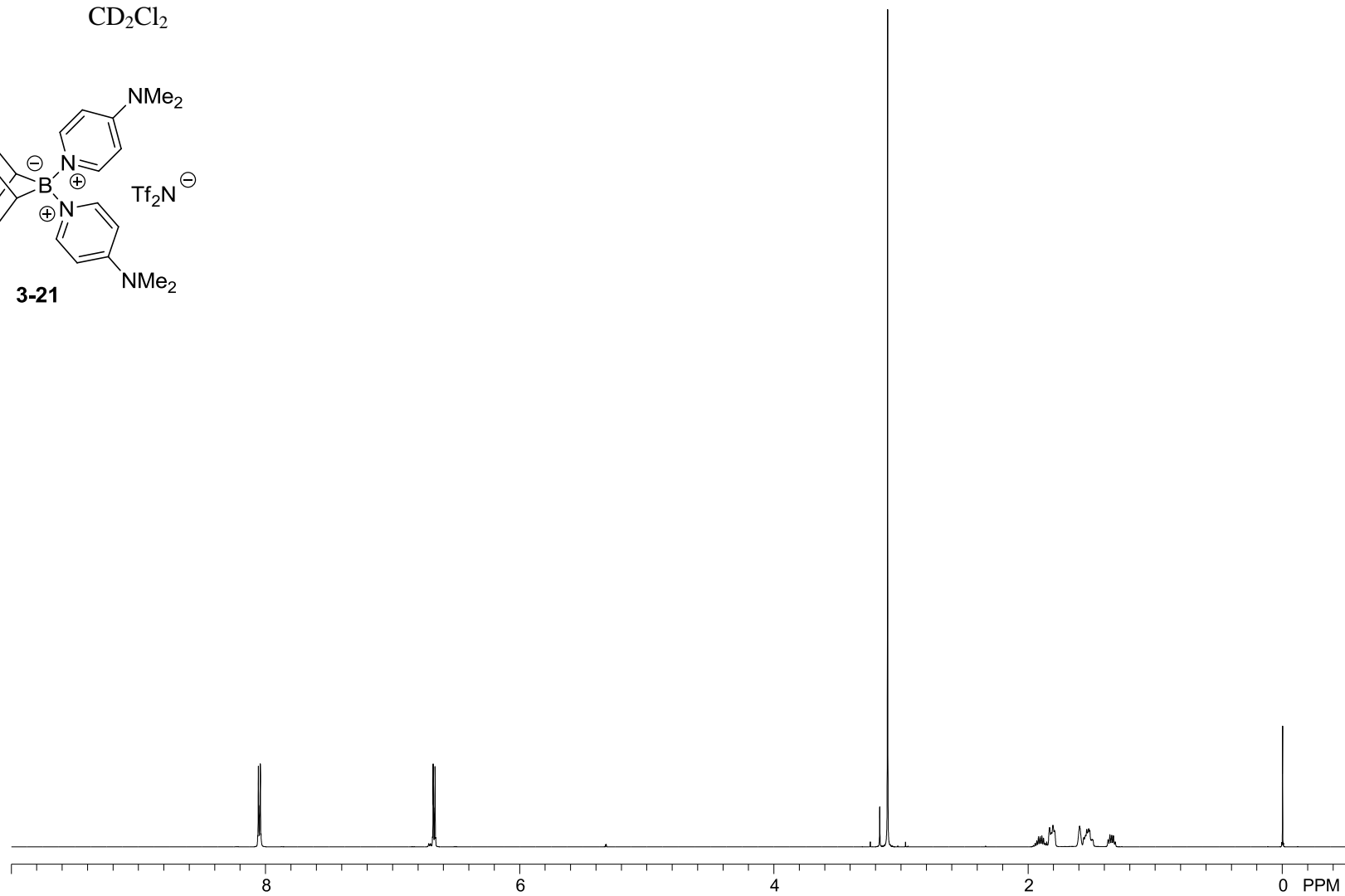
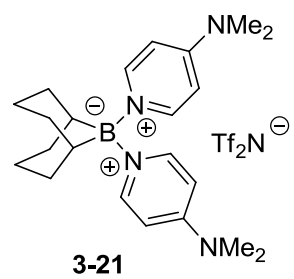
$^{13}\text{C}\{^1\text{H}\}$  NMR (101 MHz),  
 $\text{CD}_2\text{Cl}_2$



$^{19}\text{F}$  NMR (377 MHz),  
 $\text{CD}_2\text{Cl}_2$

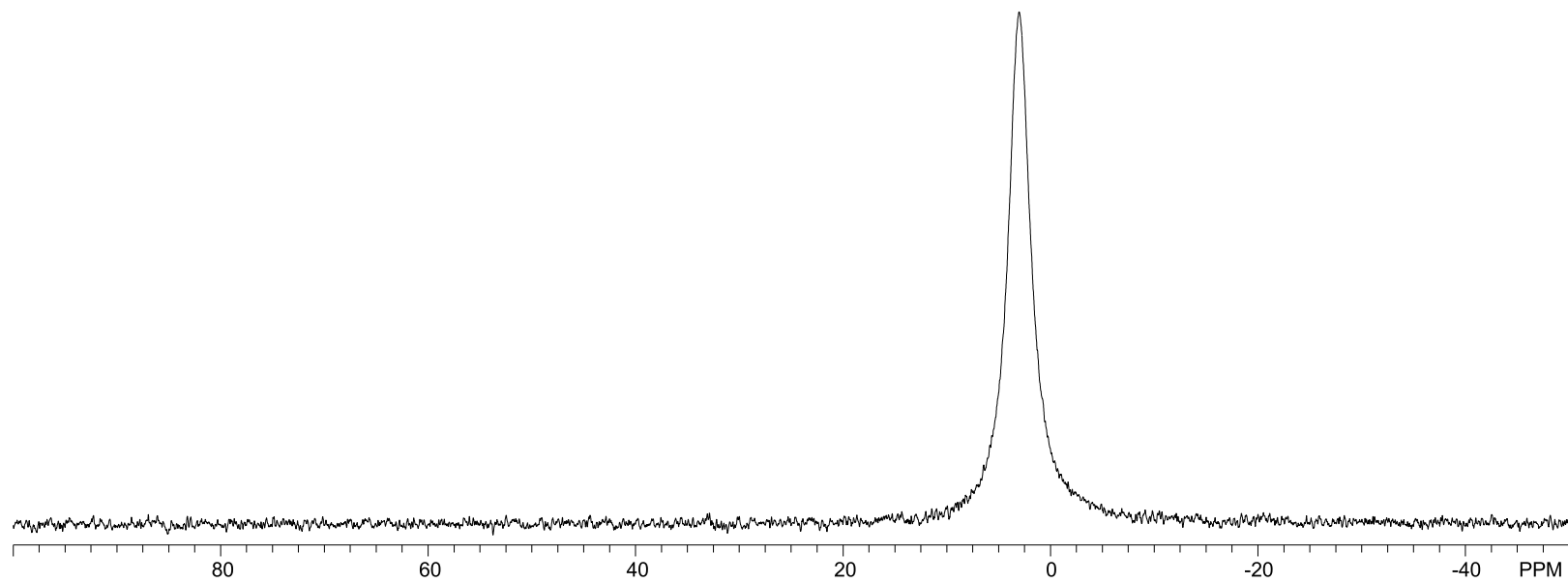
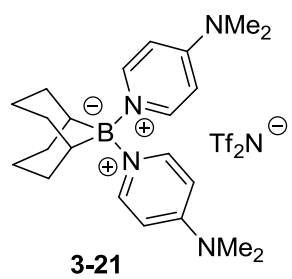


$^1\text{H}$  NMR (500 MHz),  
 $\text{CD}_2\text{Cl}_2$

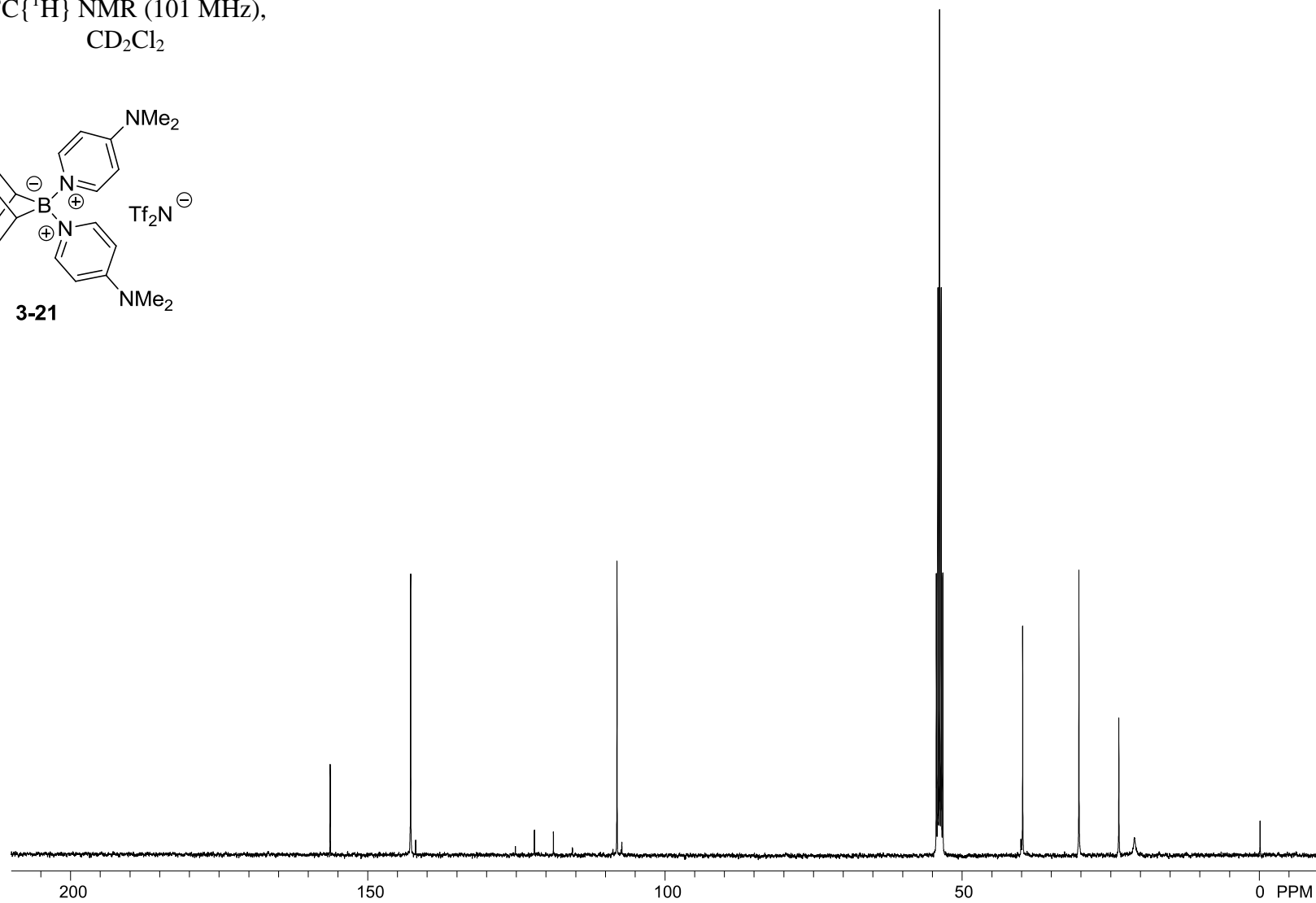
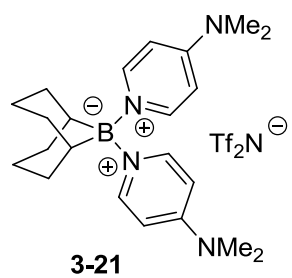




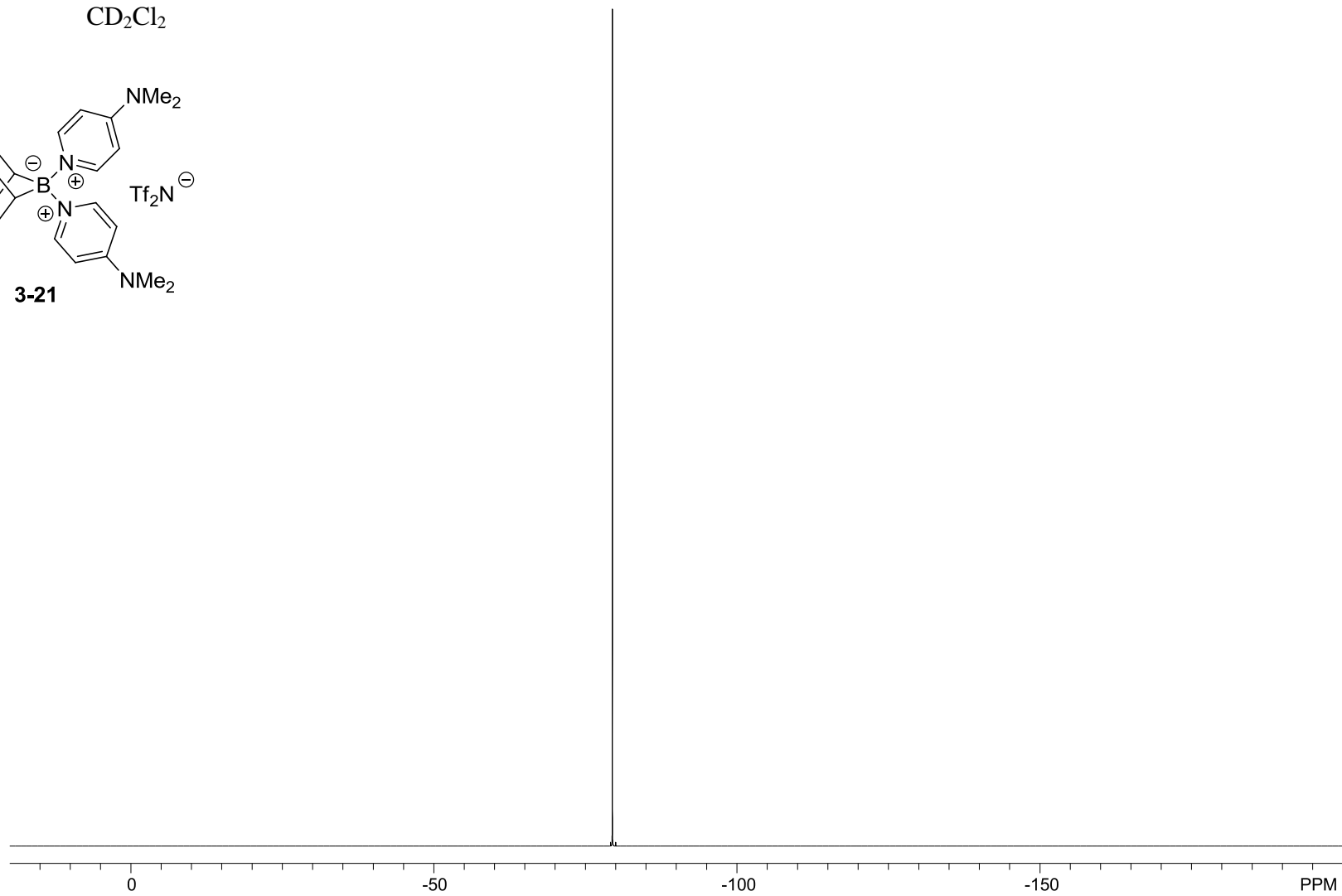
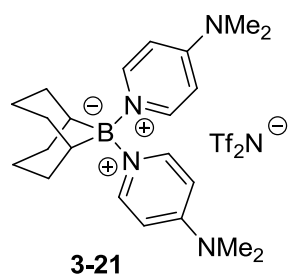
$^{11}\text{B}$  NMR (128 MHz),  
 $\text{CD}_2\text{Cl}_2$



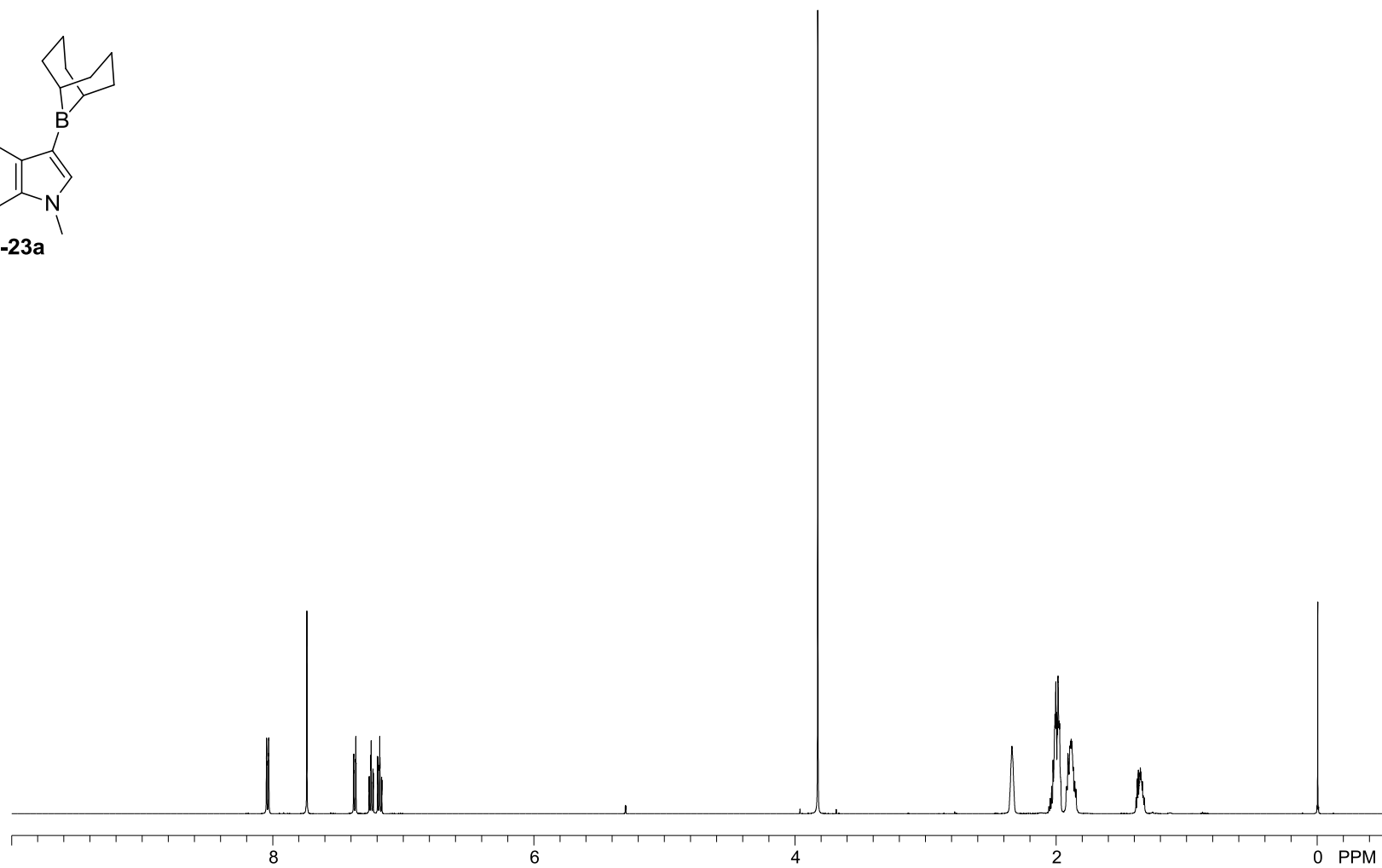
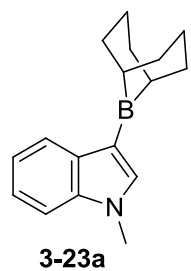
$^{13}\text{C}\{^1\text{H}\}$  NMR (101 MHz),  
 $\text{CD}_2\text{Cl}_2$



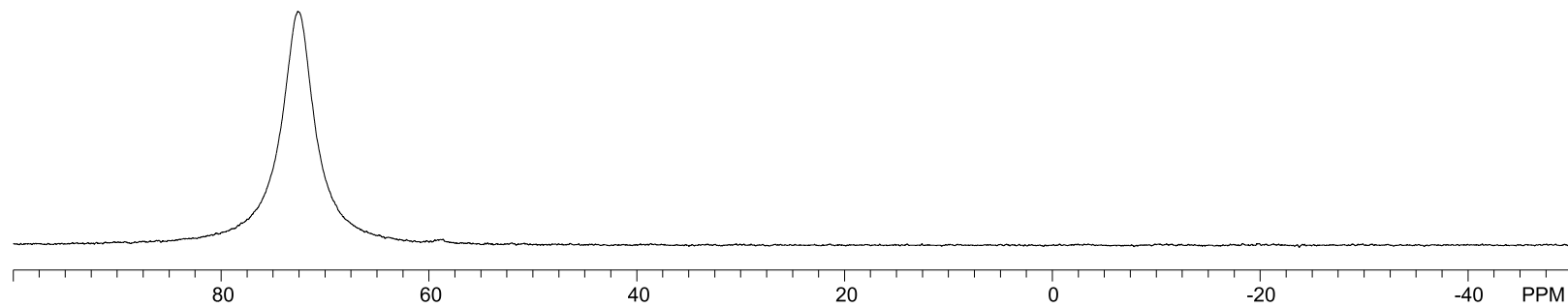
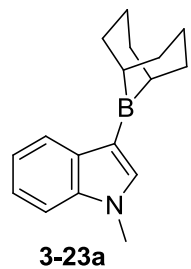
$^{19}\text{F}$  NMR (377 MHz),  
 $\text{CD}_2\text{Cl}_2$



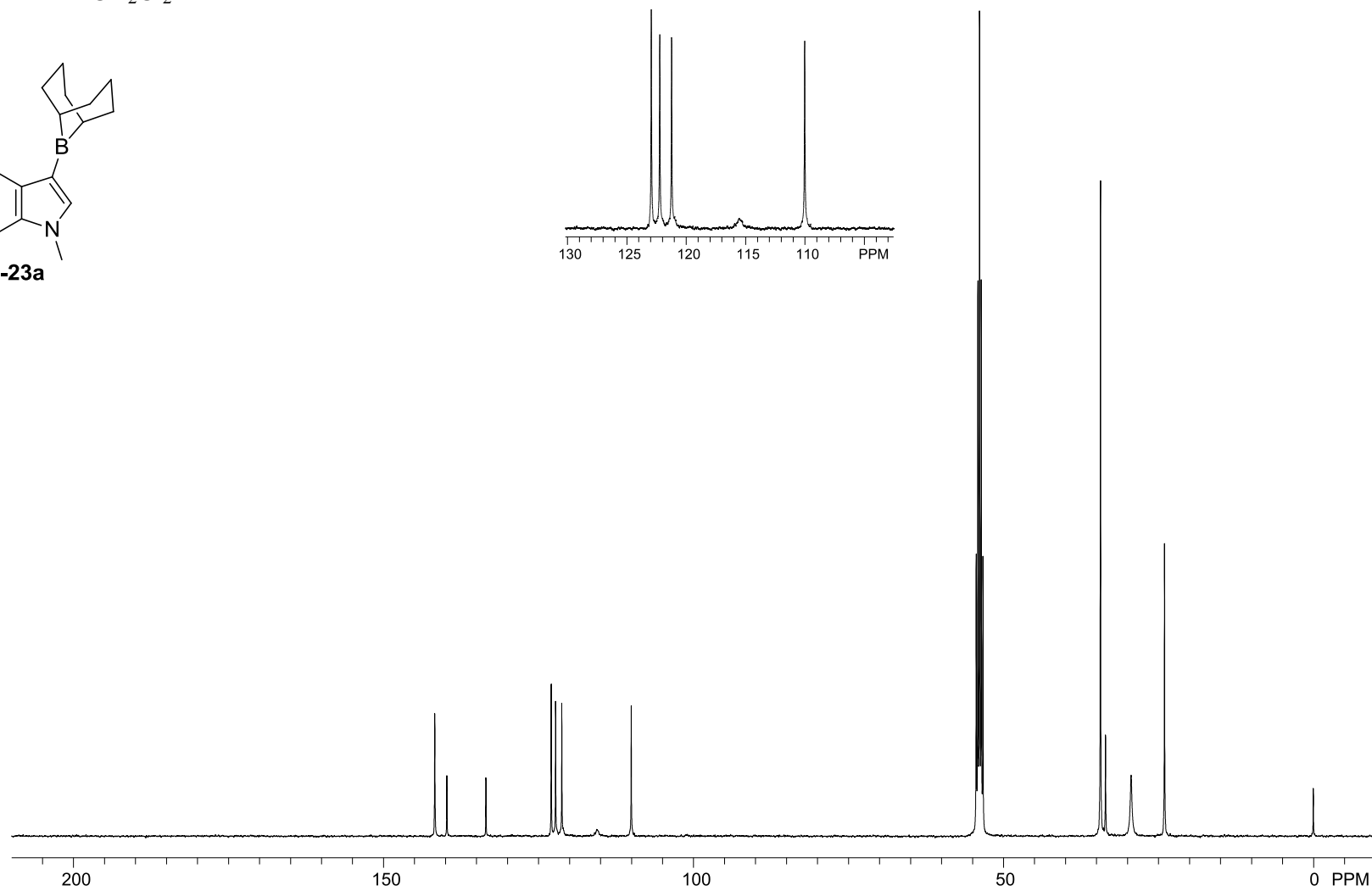
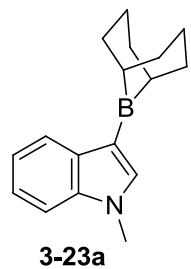
$^1\text{H}$  NMR (500 MHz),  
 $\text{CD}_2\text{Cl}_2$



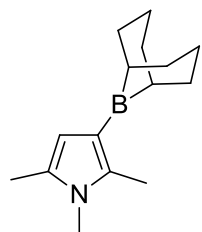
$^{11}\text{B}$  NMR (128 MHz),  
 $\text{CD}_2\text{Cl}_2$



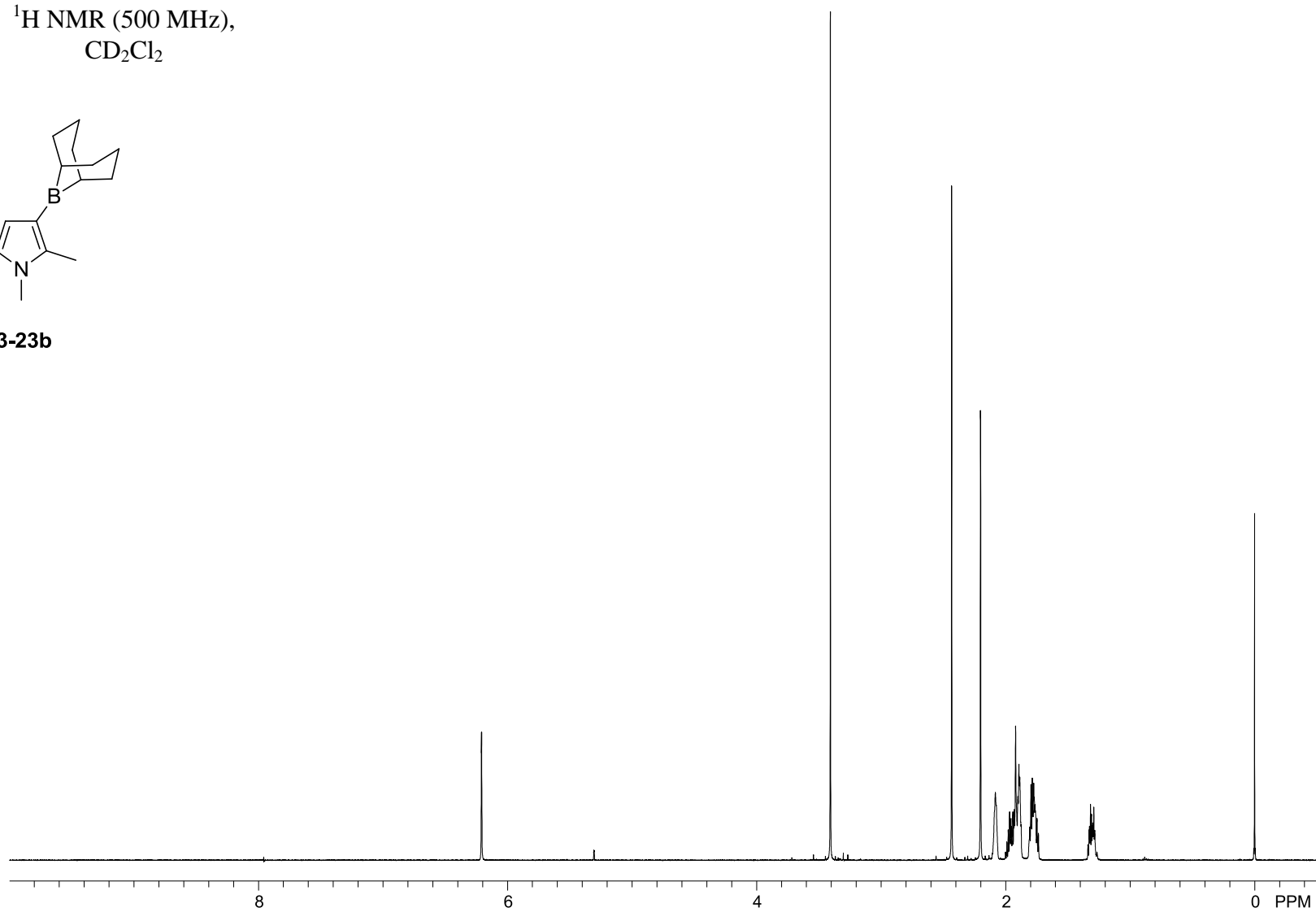
$^{13}\text{C}\{^1\text{H}\}$  NMR (101 MHz),  
 $\text{CD}_2\text{Cl}_2$



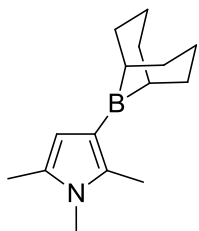
$^1\text{H}$  NMR (500 MHz),  
 $\text{CD}_2\text{Cl}_2$



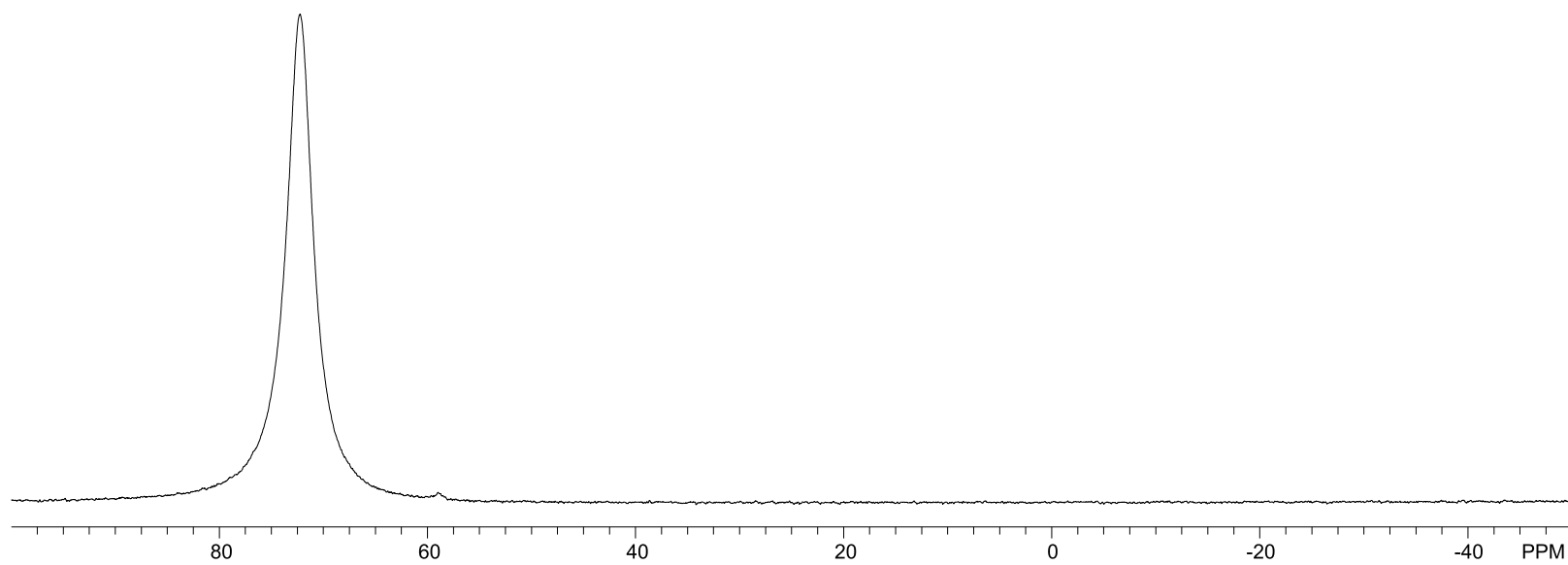
**3-23b**



$^{11}\text{B}$  NMR (128 MHz),  
 $\text{CD}_2\text{Cl}_2$

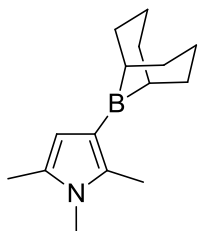


**3-23b**

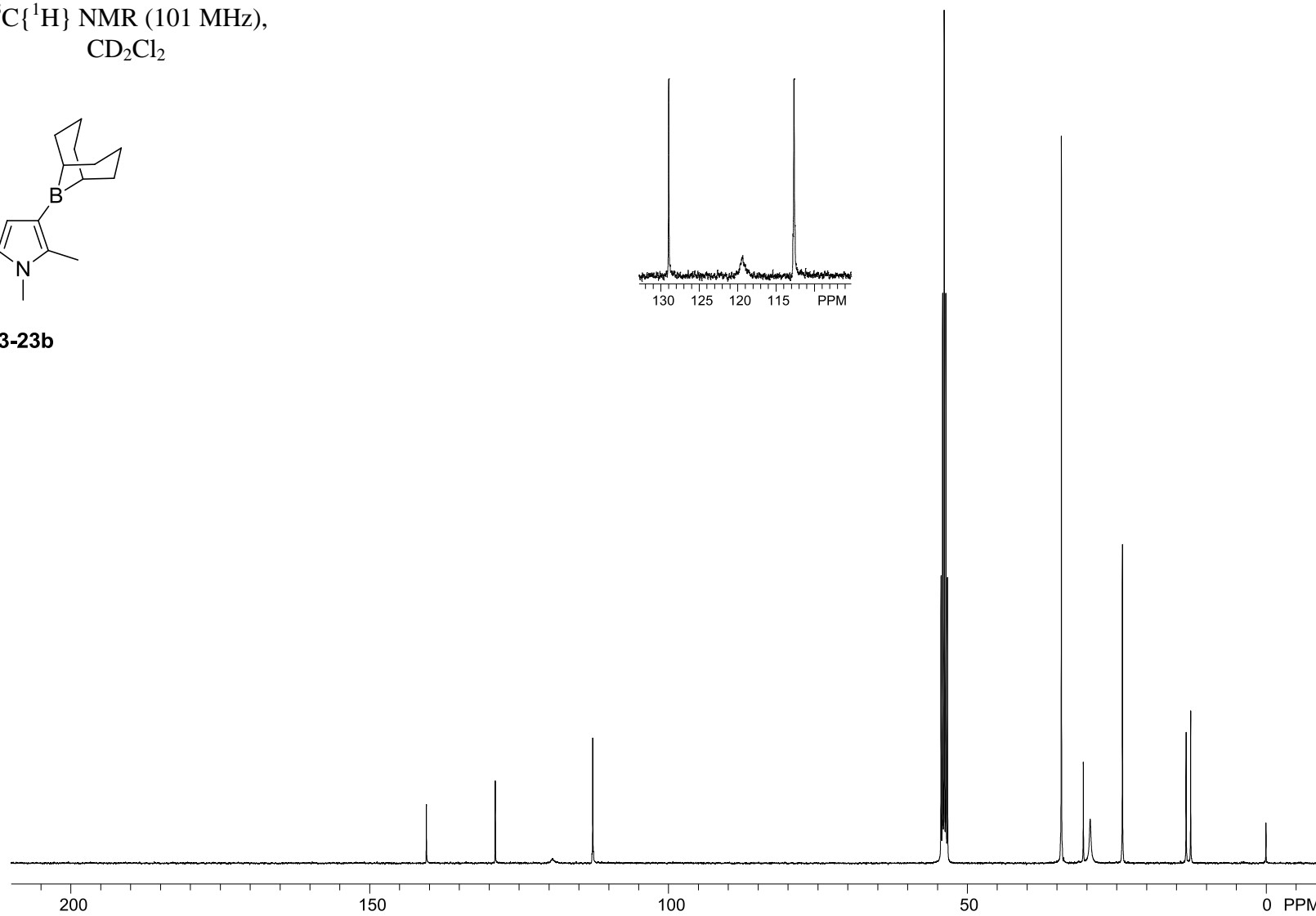




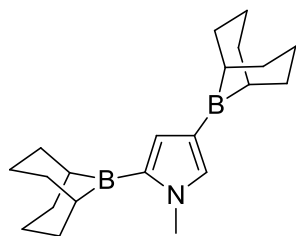
$^{13}\text{C}\{^1\text{H}\}$  NMR (101 MHz),  
 $\text{CD}_2\text{Cl}_2$



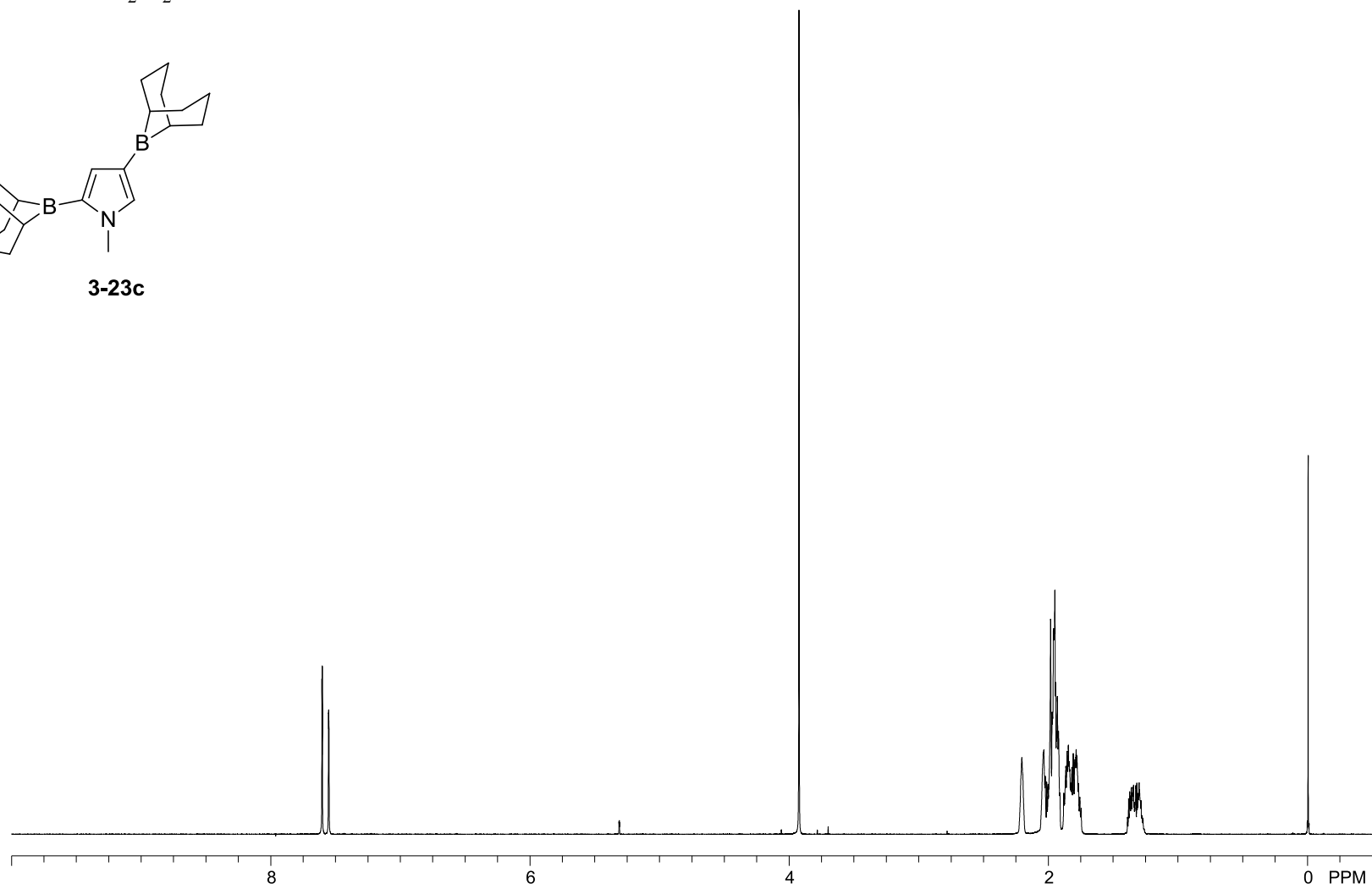
**3-23b**



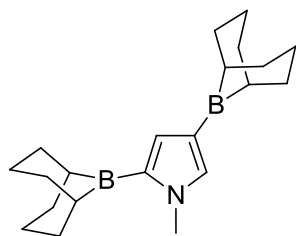
$^1\text{H}$  NMR (500 MHz),  
 $\text{CD}_2\text{Cl}_2$



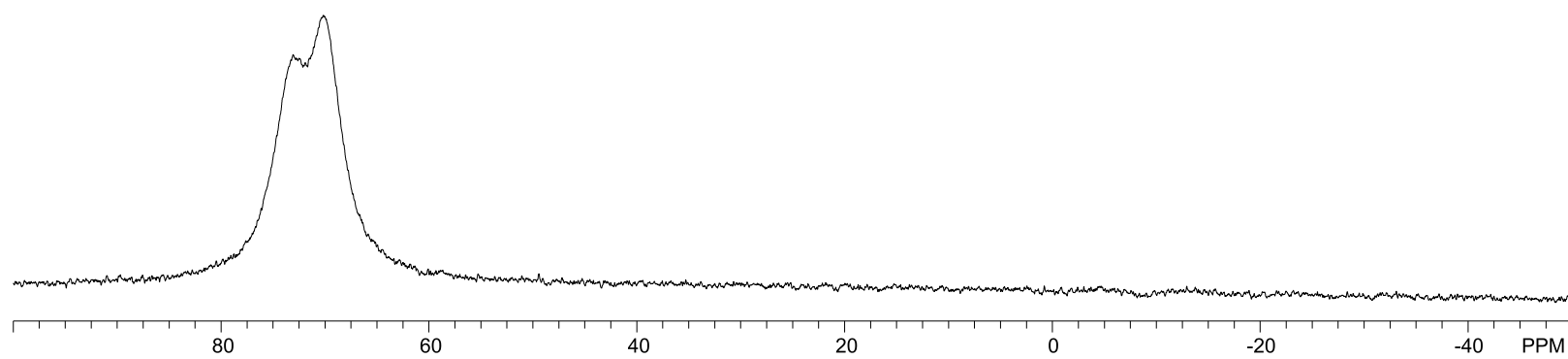
**3-23c**



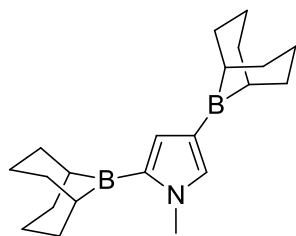
$^{11}\text{B}$  NMR (128 MHz),  
 $\text{CD}_2\text{Cl}_2$



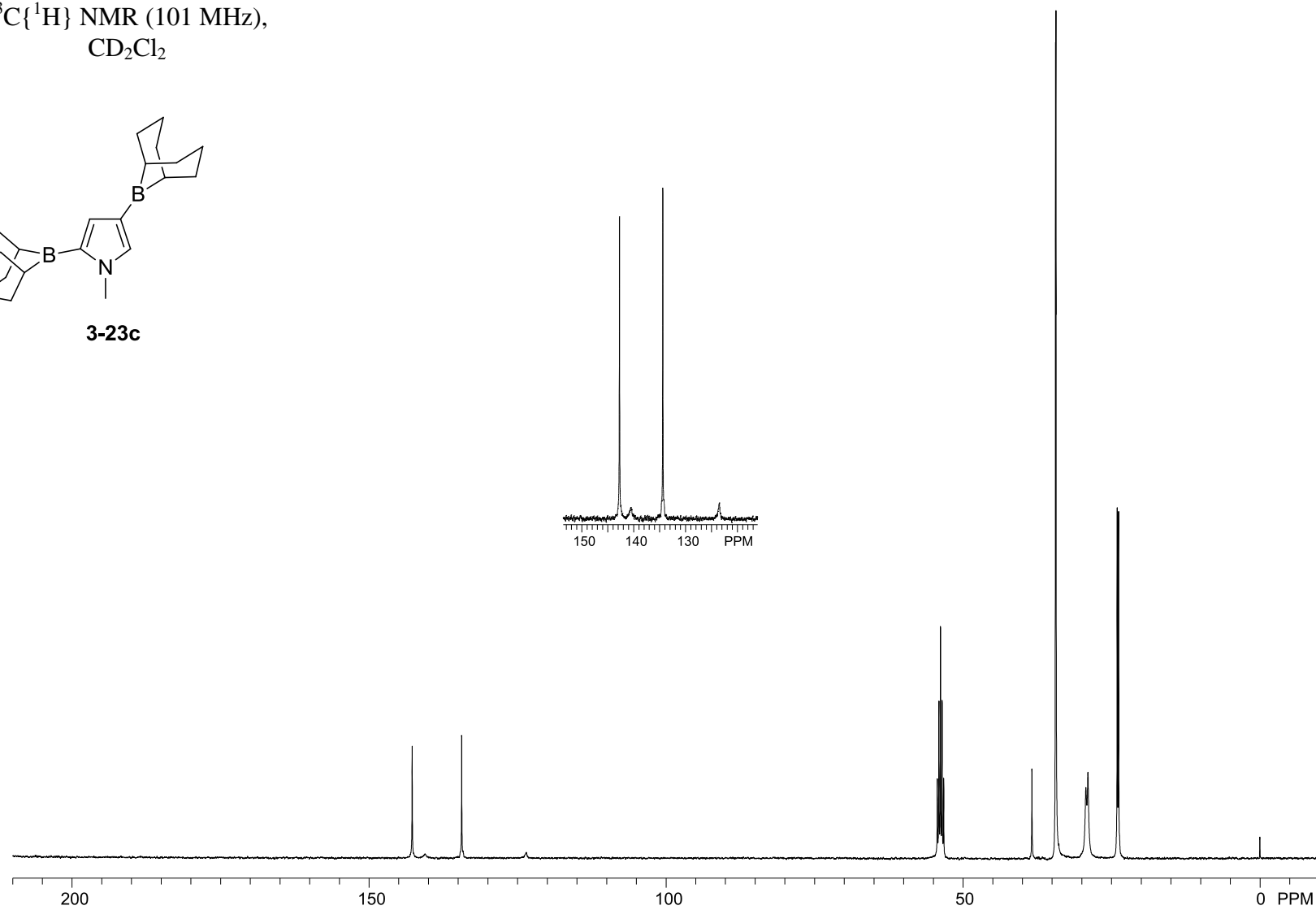
**3-23c**



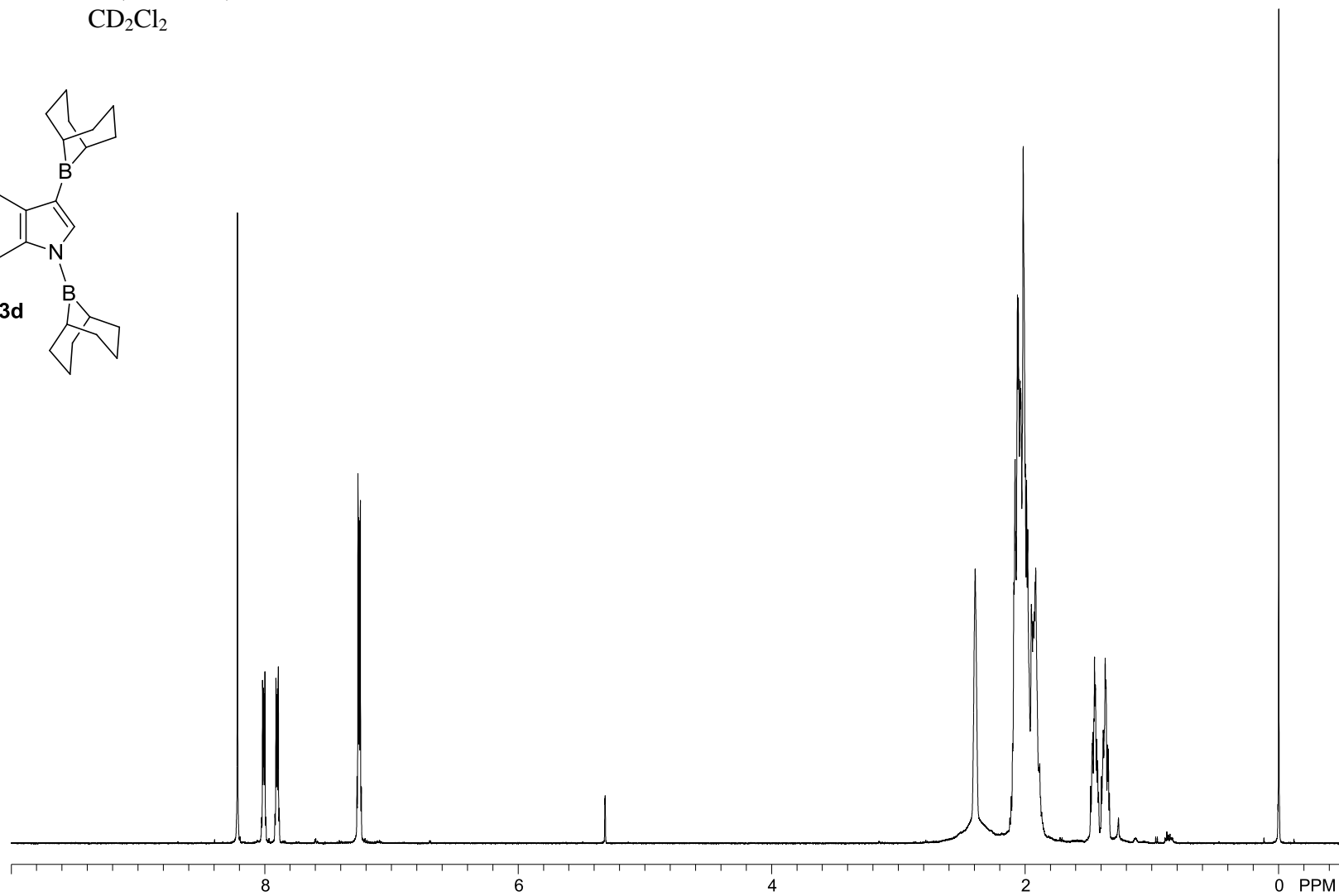
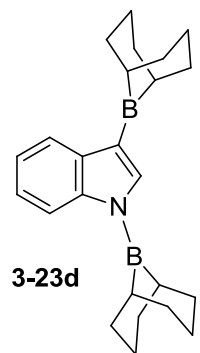
$^{13}\text{C}\{^1\text{H}\}$  NMR (101 MHz),  
 $\text{CD}_2\text{Cl}_2$



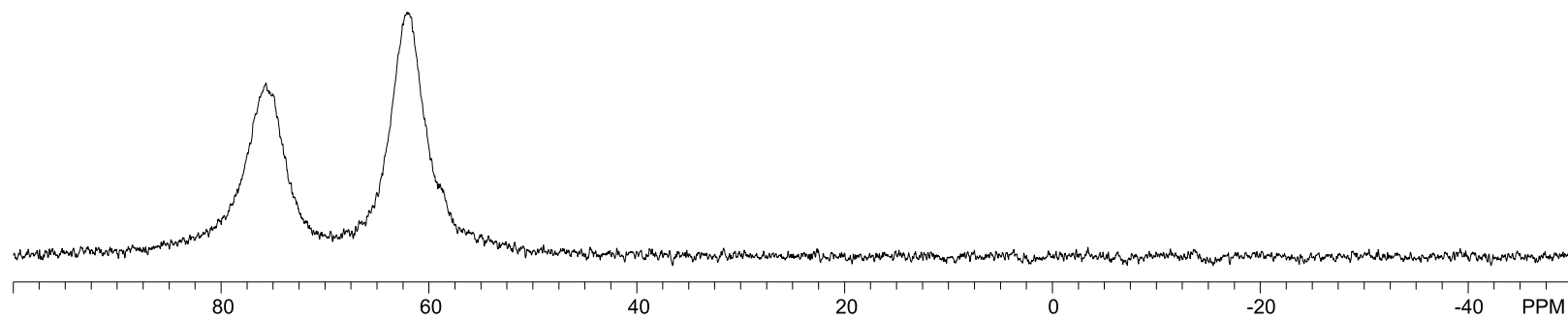
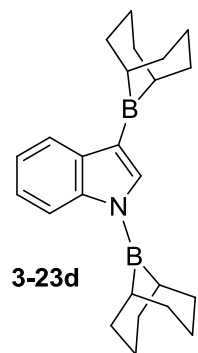
**3-23c**



$^1\text{H}$  NMR (500 MHz),  
 $\text{CD}_2\text{Cl}_2$



$^{11}\text{B}$  NMR (128 MHz),  
 $\text{CD}_2\text{Cl}_2$



$^{13}\text{C}\{^1\text{H}\}$  NMR (101 MHz),  
 $\text{CD}_2\text{Cl}_2$

